Synthesis of D-Glucose Derived Glycoconjugates and Their Application in Molecular Recognition and Catalysis

THESIS

Submitted in partial fulfilment

of the requirements for the degree of

DOCTOR OF PHILOSOPHY

by

SANTOSH KUMAR MISHRA

Under the supervision of

Dr. AJAY KUMAR SAH

BIRLA INSTITUTE OF TECHNOLOGY AND SCIENCE, PILANI

2023

BIRLA INSTITUTE OF TECHNOLOGY AND SCIENCE

PILANI (RAJASTHAN)

CERTIFICATE

This is to certify that the thesis entitled ***Synthesis of D-glucose derived glycoconjugates and their application in molecular recognition and catalysis*** and submitted by **Mr. Santosh Kumar Mishra,** ID No. **2017PHXF0422P** for award of Ph.D. Degree of the Institute embodies the original work done by him under my supervision.

Signature in full of the Supervisor

Prof. AJAY KUMAR SAH

Designation: Professor

Date

Dedicated to my Family

Acknowledgement

I would like to express my sincere gratitude to every supportive individual who helped me directly and indirectly during this wonderful journey of my Ph. D. career.

Firstly, I would like to thank my thesis supervisor *Dr. Ajay Kumar Sah* for his constant support, valuable suggestions and guidance throughout my research tenure. His motivating discussions and kind support helped me a lot. It was indeed a great pleasure working with him.

I take this opportunity to convey my deepest gratitude to members of the Doctoral Advisory Committee; *Dr. Bharti Khungar*, and *Dr. Bibhas* Ranjan Sarkar for their valuable suggestions, intellectual inputs and encouragements during the entire period of doctoral studies.

I am thankful to my teachers Mr Kanhucharan Behera, Mr Sudhakar Behera, Dr. Madhu Sudan Sahu, Dr K. K. Sahoo and Dr. Prakash Mohanty for their motivation and valuable suggestions. I would like to express sincere gratefulness to my previous project leader, Dr Bamaprasad Bad for his guidance.

I respectfully acknowledge to Birla Institute of Technology and Science, Pilani-Pilani campus and DST-SERB for providing me the fellowship and to Department of Chemistry for providing the research and instrumental facilities. I am grateful to all the respectable faculty members, Prof. S. C. Sivasubramanian, Prof. R. K. Roy, Prof. Dalip Kumar, Prof. Anil Kumar, Prof. Saumi Ray, Prof. Bharti Khungar, Prof. I. R. Laskar, Prof. Madhushree Sarkar, Dr. P U Manohar, Dr. Paritosh Shukla, Prof. Indresh Kumar, Prof. Surojit Pande, Prof. Rajeev Sakhuja, Prof. S Chakraborthy, Dr. B R Sarkar, Dr. M Basu, Dr. Avik Kumar Pati, Dr. Partha Sarathi Addy, Dr. Pritam Kumar Jana, Dr. Satyajit Patra, Dr.Amrita Chakraborty, Department of Chemistry, BITS Pilani for their generous help

and fruitful discussions during the different stages of my doctoral study. Thanks to all the office staff (Soni ji, Pushpa ji, Ashok ji, Suresh ji, Nandlal ji) of the Department for their help during PhD tenure.

I am delighted to show my thankfulness to my group member, Vimal bhai, Parmeshthi, and Anuvasita for their contribution in my works and for being a great support during my PhD. I sincerely acknowledge my dear lab mates Prakash, Narshimha, Prakriti, Monika, Nandini, Pragya, Payal and Nidhi for their kind cooperation and valuable suggestions during my PhD.

My special thanks go to my colleagues and friends Subash, Rudra, Raja, Mahesh, Kanhu bhai, Himanshu, Jyoti, Pramod, Amol, Bintu, Sonam, Ram, Pragya, Shivani, Vishakha, Prachi, Aishwarya for their constant help and support in all aspects. I would like to acknowledge my seniors in BITS-Pilani, Santosh bhai, Moyna didi, Pallavi didi, Vicky and Reddy Sir for their valuable suggestions and guide during my Ph. D. tenure.

Finally, my sincere gratitude goes to my parents and my family members for their unflagging love and never-ending support throughout my life. I feel deeply indebted to them for whatever I have achieved so far and I dedicate it to them.

Santosh Kumar Mishra

Abbreviations

Ar	Aryl group	*J*	Coupling Constant
br	Broad	KBr	Potassium bromide
bs	Broad singlet	L	levorotatory
Bu	Butyl	m	Multiplet
CCDC	Cambridge Crystallographic Data Centre	*m*	*meta*
COSY	Correlation spectroscopy	Me	Methyl
^{o}C	Degrees Celsius	mg	Miligram
CH_2Cl_2	Dichloromethane	mL	Millilitre
d	Doublet	mol	Mole
D	dextrorotatory	mp	Melting point
dd	Doublet of doublet	mg	Milli gram
ddd	Doublet of doublet of doublet	mL	Millilitre
ddt	Doublet of doublet of triplet	mol	Mole
dtt	Doublet of triplet of triplet	mp	Melting point
δ	Chemical shift	NMR	Nuclear magnetic resonance
DCE	1,2-Dichloroethane	ORTEP	Oak Ridge Thermal Ellipsoid Plot Program
DCM	Dichloromethane	p	Pentet
de	Diastereomeric excess	Ph	Phenyl
DMF	N,N-Dimethylformamide	ppm	Parts per million
DMSO	Dimethylsulfoxide	q	Quartet
dr	Diastereomeric ratio	qd	Quartet of doublet
EA	Ethyl acetate	rt	Room temperature

ee	Enantiomeric excess	s	Singlet
eq.	Equivalent	t	Triplet
ESI	Electrospray ionization	t_R	Retention time
Et	Ethyl	THF	Tetrahydrofuran
g	Grams	TMS	Tetramethylsilane
h	Hours	Ts	*p*-Toluenesulfonyl
HPLC	High performance liquid chromatography	TLC	thin layer chromatography
HRMS	High Resolution Mass Spectrometry	UV	Ultra violet
Hz	Hertz	XRD	X-ray diffraction

Contents

Abstract

The contents of this thesis entitled **"*Synthesis of D-Glucose Derived Glycoconjugates and Their Application in Molecular Recognition and Catalysis*"** have been divided into seven chapters based on previous research, the results of experimental works performed during the complete course of the PhD research period and its future scope.

Chapter 1 of the dissertation presents a brief review synthetic protocols of glycoconjugates and their applications. This chapter mainly highlighted the interaction of glycoconjugates with amino acids along with metal ions and the catalytic applications of carbohydrate derived metal complexes, since these catalysts were primarily utilized in the works demonstrated in this thesis.

Chapter 2 contains the detail information regarding chemicals, instruments, software and analytical methods used for accomplishing this thesis. This chapter describes procedures followed for the synthesis of commercial unavailable chemicals used in this thesis work.

Chapter 3 describes an efficient protocol of synthesizing nonpolar amino acid moiety containing glycopeptides (Scheme 1) with a detailed structural analysis using NMR, FTIR and UV-visible absorption spectroscopy. Additionally, a comparison between theoretical and experimental aspects of the synthesized *N*-glycoconjugates have also been explored.

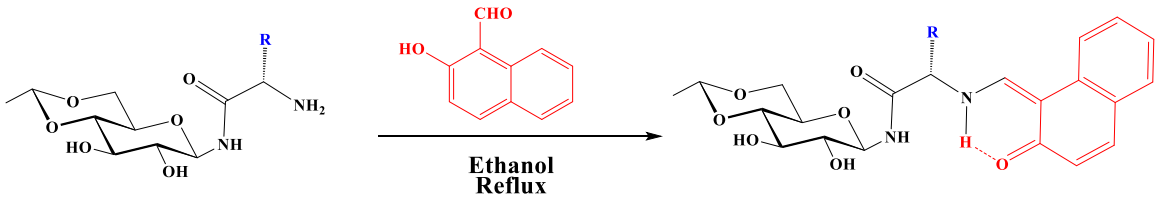

R = CH_2Ph, $CH(CH_3)CH_2CH_3$, CH_3,$CH_2CH_2SCH_3$, $CH(CH_3)_2$,$CH_2CH(CH_3)_2$, $CH_2C_8H_6N$, CH_3

Scheme 1

Chapter 4 demonstrates amino acid binding abilities of the synthesized glycoconjugates. Out of seven *N*-glycoconjugates one selectively interacts with cysteine and four are selectively interactive towards aspartic acid while remaining two show highest order of interaction towards aspartic acid, although it is not selective. In this chapter we have also explored the interactions of *N*-glycoconjugates with aspartic acid using the NMR studies.

It was observed that, the side chain of the amino acid moieties present in sugar derived molecules plays a crucial role in amino acid binding.

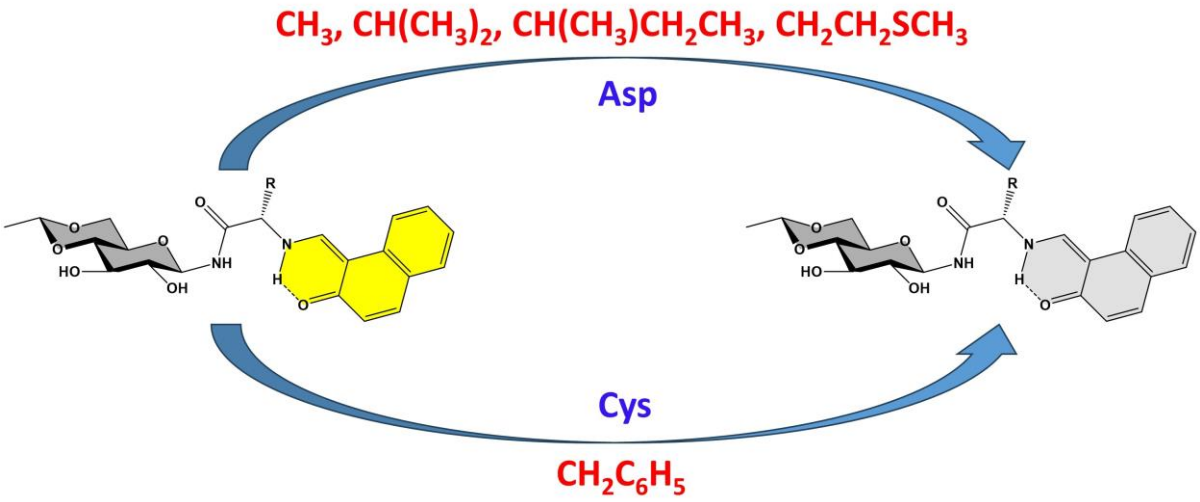

Chapter 5 discloses the complexation abilities of *N*-(2-hydroxynapthylidene)-L-leucienyl-4,6-*O*-ethylidene-β-D-glucopyranosylamine (L_1) with metal ions at different pH. It was observed that the interaction of glycopeptide with Cu(II) ions is immune towards the change in pH of solution. As a continuation we have explored the catalytic application of the *N*-glycoconjugate based copper complex. The copper(II) complex efficiently catalyzes the one pot synthesis of imidazo[1,2-*a*]pyridine under solvent free condition (Scheme 2). The mechanistic aspects and the reusability of the catalyst have also been explored.

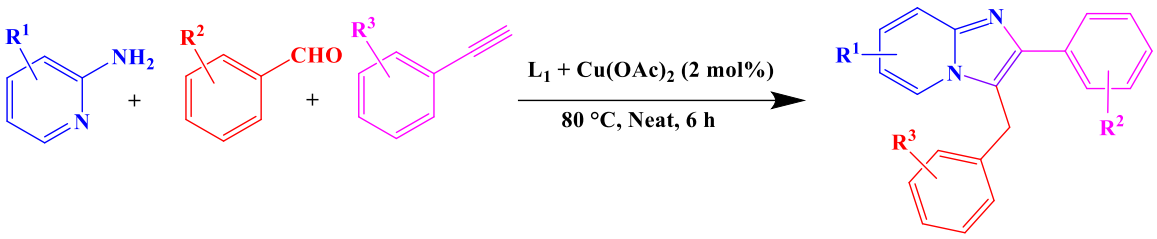

Scheme 2

Chapter 6 presents the synthesis of amphiphilic glycoconjugate and its copper(II) complex. The synthesized complex molecule was characterized by FTIR, UV-visible and XPS spectroscopy whereas the structural details was obtained by X-ray diffraction studies. Further, the complex has been used in catalytic synthesis of asymmetric

propargylamines with a faster rate and higher yield under solvent-free condition using A^3 coupling reaction (Scheme 3). The mechanistic studies of the catalyzed reaction revealed the formation of aminals and iminium ion as intermediates. The reaction is first order with respect to each component like catalyst, cyclic amine, aromatic aldehydes and alkyne. The catalytic system is reusable without any appreciable loss in the enantioselectivity or product yield.

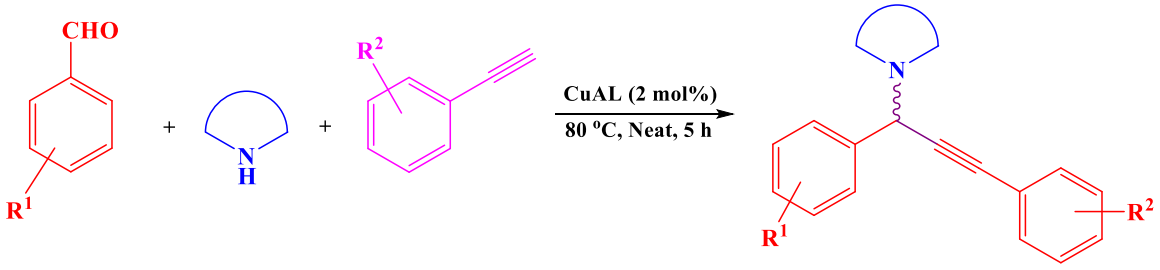

Scheme 3

Chapter 7 is the summary of total work done during the PhD tenure along with future scope of the research outcome in this thesis

Chapter 1

Introduction

Chapter 1

1.1 General introduction to carbohydrates

The word carbohydrate was coined during the nineteenth century, deriving from “carbo” and “hydro”, which means “coal” or “carbon” and “water”, respectively, as on heating carbohydrate degrades into carbon and water. Hence, carbohydrates were also referred as “hydrates of carbon” with the general formula $C_n(H_2O)_n$,[1] however, after the inclusion of polyhydroxy aldehydes, ketones, acids or alcohols into this family, the general formula became irrelevant. Glucose is majorly synthesized by plants from carbon dioxide and water during photosynthesis, which is stored as starch and cellulose in the biological system. Cellulose, the most abundant carbohydrate, is a key component in the cell wall of plants and microorganisms like algae and bacteria whereas, starch fulfils the energy needs required for the cellular process and hence can be regarded as batteries of the living organisms.[2-3] The association of carbohydrates with other biomolecules like proteins, lipids and nucleic acids, facilitate several biological processes.[4-5] Nucleic acids are polymers containing carbohydrate moieties, responsible for the transformation of genetic information to offspring and also act as a controller in the biosynthesis of protein molecules.[6-7] Glycolipids are essential part of cell membrane which ensure their stability and also facilitate several intercellular interactions. In some cases, glycolipids act as receptors, which is important for cell aggregation and dissociation. Proteins attached to sugar are known as glycoproteins, which play a vital role in various cellular functions like cell-cell interaction,[8] cell adhesion,[9] embryonic development,[10] immune response[11] and pathogen recognition[12-13]. Sugar molecules with amino groups, commonly known as aminosugars, have several pharmaceutical applications, like streptomycin and puromycin act as natural antibiotics.[14] Apart from biological functions, carbohydrates have utilization in fertilizers, polymers, textiles, paper, food industries and many more.[15-19]

1.2 Classification of carbohydrates

Carbohydrates can be divided into two main groups like simple carbohydrates and glycoconjugates.[20] Simple carbohydrates are monomers or polymers containing only sugar moieties in their structural units, whereas sugar attached with aglycons through covalent bonds, are known as glycoconjugates.

1.2.1 Simple carbohydrates

Simple carbohydrates can be classified into monosaccharides, oligosaccharides and polysaccharides based on their molecular size. Monosaccharides are the lowest member of the carbohydrate family having polyhydroxy ketone or aldehyde functionality, which can't be further hydrolysed. Oligosaccharides and polysaccharides are polymers of monosaccharides connected through acetal linkage. Oligosaccharides contain two to ten units of monosaccharides, whereas polysaccharides have more than ten monomeric units. Due to the polymeric structures, both oligosaccharide and polysaccharide are susceptible to hydrolysis which can disintegrate them into simple monomeric units.

1.2.1.1 Monosaccharides

Monosaccharides are simplest and smallest carbohydrate units, commonly referred as aldose and ketose depending on the presence of aldehyde and ketone functionality along with hydroxyl groups. All the monosaccharides are chiral and usually exist in many isomeric forms which include both cyclic and acyclic structures (*Fig. 1.1*). Usually, they form either five- or six-member ring systems, which are commonly known as furanose or pyranose, respectively.[21]

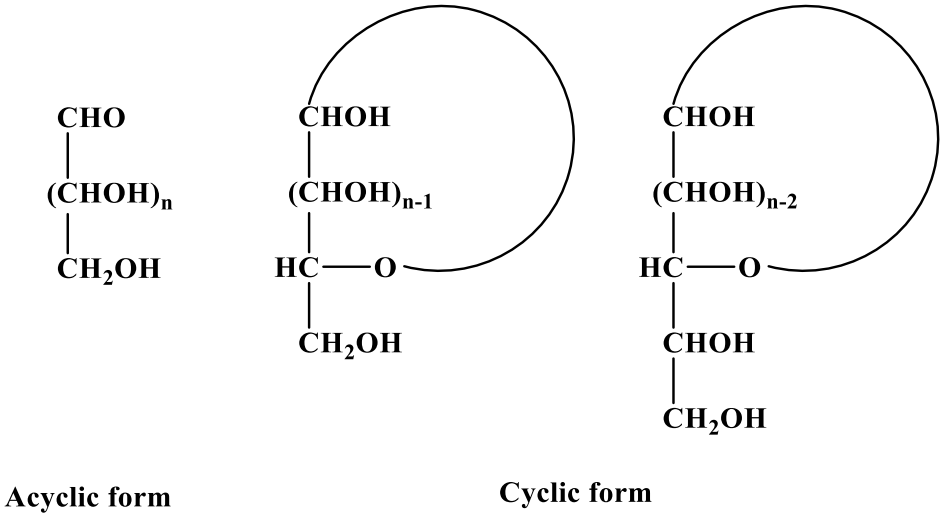

Fig. 1.1 *Acyclic and cyclic forms of monosaccharides*

During the cyclization process, a new chiral centre appears at anomeric carbon (carbon 1) resulting in two stereoisomers called alpha (α) and beta (β) forms. When the hemiacetal -OH is on the opposite side of the plane of the ring, the anomer is denoted as α and if it is on the same side of the plane, the anomer is known as β. An equilibrium between α and β forms exists in the solution via open chain form (*Fig. 1.2*) and this process is known as mutarotation.

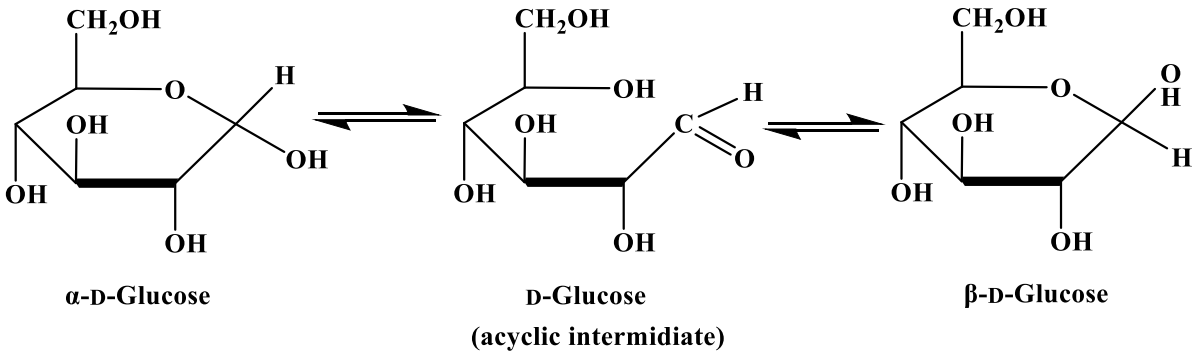

Fig. 1.2 *Mutarotation of glucose anomers*

D and L notations are used to describe the stereochemistry of penultimate carbon (the last stereo genic carbon from most oxidized carbon). Carbohydrates can be denoted as D or L configuration, depending on the -OH group attached to the penultimate carbon is either

positioned at right or left in Fischer projection (*Fig. 1.3*). Though this is an old system, yet used in the modern era as it gives the relative configuration of the carbohydrate molecules. Sometimes + or – notation is also associated with the D or L configurations of the molecules, based on the clockwise or anticlockwise rotation of the plane polarized light, respectively.

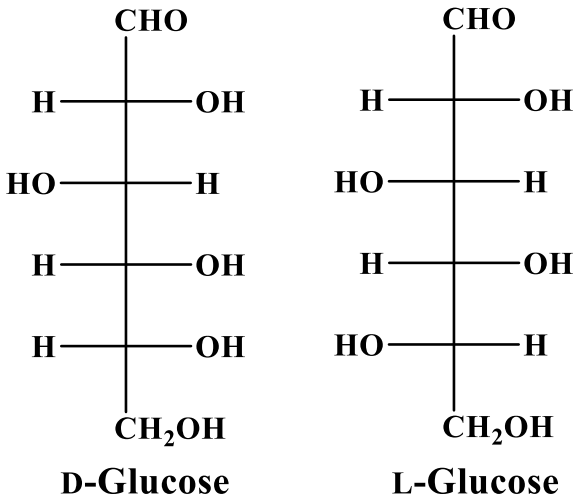

Fig. 1.3 *Fischer projection with D and L configuration of glucose*

1.2.1.2 Oligosaccharides

The term oligo is derived from the Greek word ‘oligos’ which means ‘a few’ and hence, the word oligosaccharide etymologically means a few saccharides. In oligosaccharides, generally two to ten saccharides are linked through an *O*-glycoside bond and hence several glycoside linkages are possible *(Fig. 1.4*). Oligosaccharides consist of same monomeric unit is known as homopolymers. In animal cells, glycogens are the most common homopolymer in which glucose units are linked through α-1,4-glycosidic bonds. Glycogen can also have branching where the glucose is linked through an α-1,6-glycosidic bond. Besides glycogens, some other most popular oligosaccharides include stachyose, raffinose and verbascose.

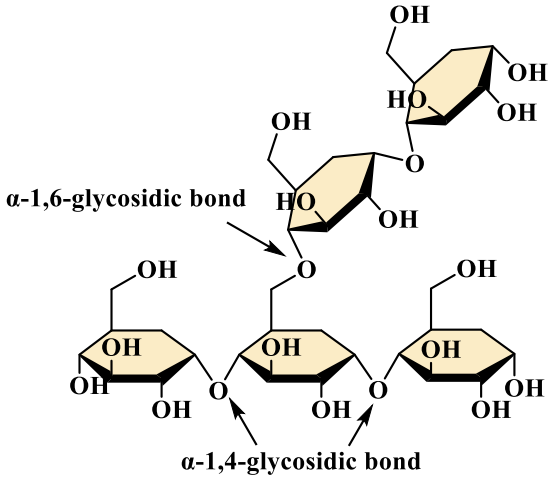

Fig. 1.4 *Structure of glycogen with 1,4-glycosidic and 1,6-glycosidic bonds*

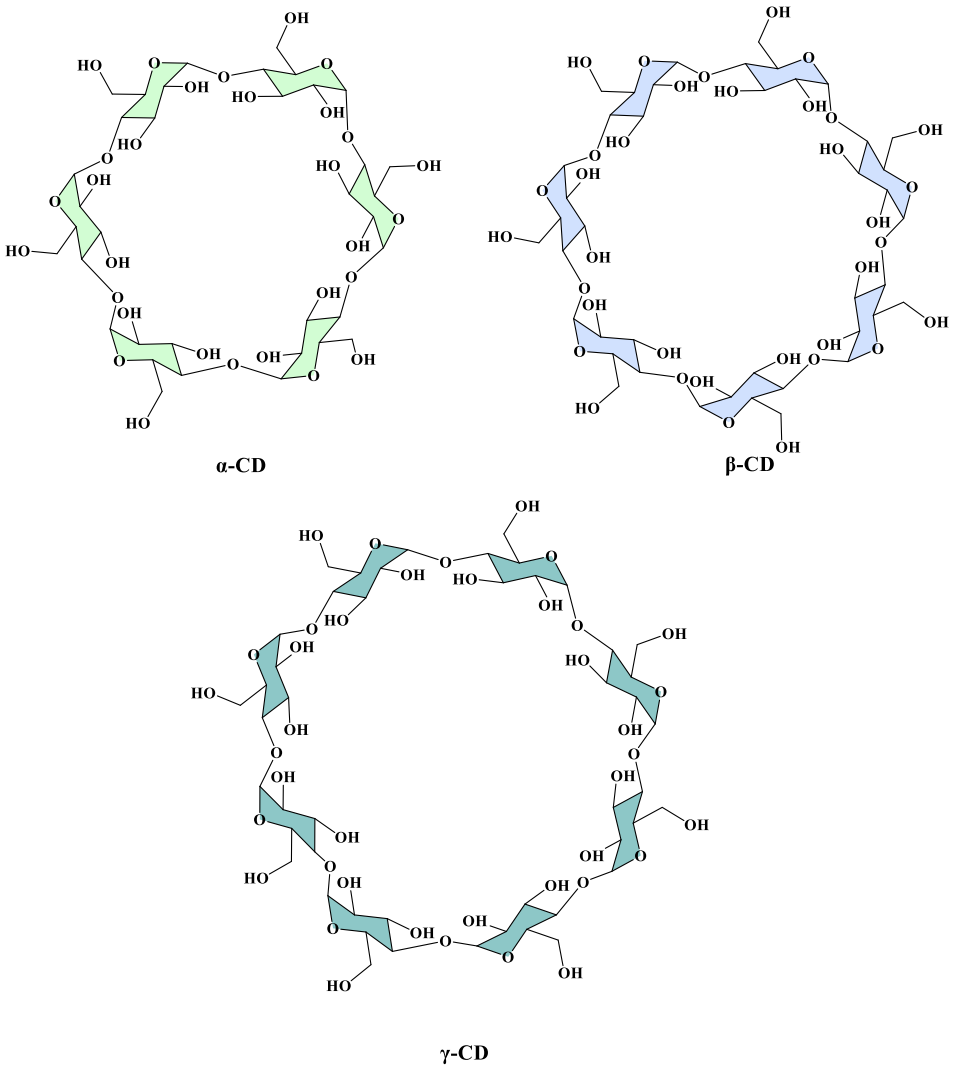

Fig. 1.5 *Chemical structure of α, β and γ Cyclodextrin*

Cyclodextrins (CDs) are another type of oligosaccharides consisting of a macrocyclic ring of α-1,4 linked D-glucose subunits. Biodegradation of starch using glucanotransferase enzyme affords α-, β- and γ-CD (*Fig. 1.5*) containing 6, 7 and 8 glucose subunits, respectively. CDs possess hydrophobic interior and hydrophilic exterior, suitable for a wide range of encapsulation applications. In several approved drugs, CDs are an important ingredient which hosts the active molecules in their internal cavity. This encapsulation of hydrophobic bioactive molecules helps them in body tissue penetration and thus CDs plays a crucial role in drug delivery. Due to their complexation property with hydrophobic molecules, they are used in molecular recognition and also as stationary phase media in HPLC separation.

1.2.1.3 Polysaccharides

Polysaccharides are well known natural polymers in which more than ten monosaccharide units are present. Like oligosaccharides, polysaccharides can also be divided into two subgroups i.e., homopolysaccharides and heteropolysaccharides. Homopolysaccharides contains a single type of monomers, whereas a heteropolysaccharide consists of two or more types of monosaccharide units. Linear polysaccharides like cellulose may contain as many as 10,000-15,000 million D-glucopyranose units coupled through β-glycosidic bonds between their C1 and C4 carbons. Starch is of two types, amylose and amylopectin, which are the polymers of glucose. Amylose is unbranched polysaccharides having α-1,4 glycosidic linkages, while same linkage makes the linear chain in amylopectin with additional α-1,6 linkages at the branching points (*Fig. 1.6*). Agarose is a natural linear heteropolysaccharide made up of 600-700 residues of agarbioses, connected via β-1,3 glycosidic linkages (*Fig. 1.6*). Agarbiose is a disaccharide of D-glalactopyranose and 3,6-anhydro-L-galactopyranose containing β-1,4 glycosidic linkages. Agarose has remarkable gel-forming property and used in the electrophoretic separation of DNA and RNA molecules.

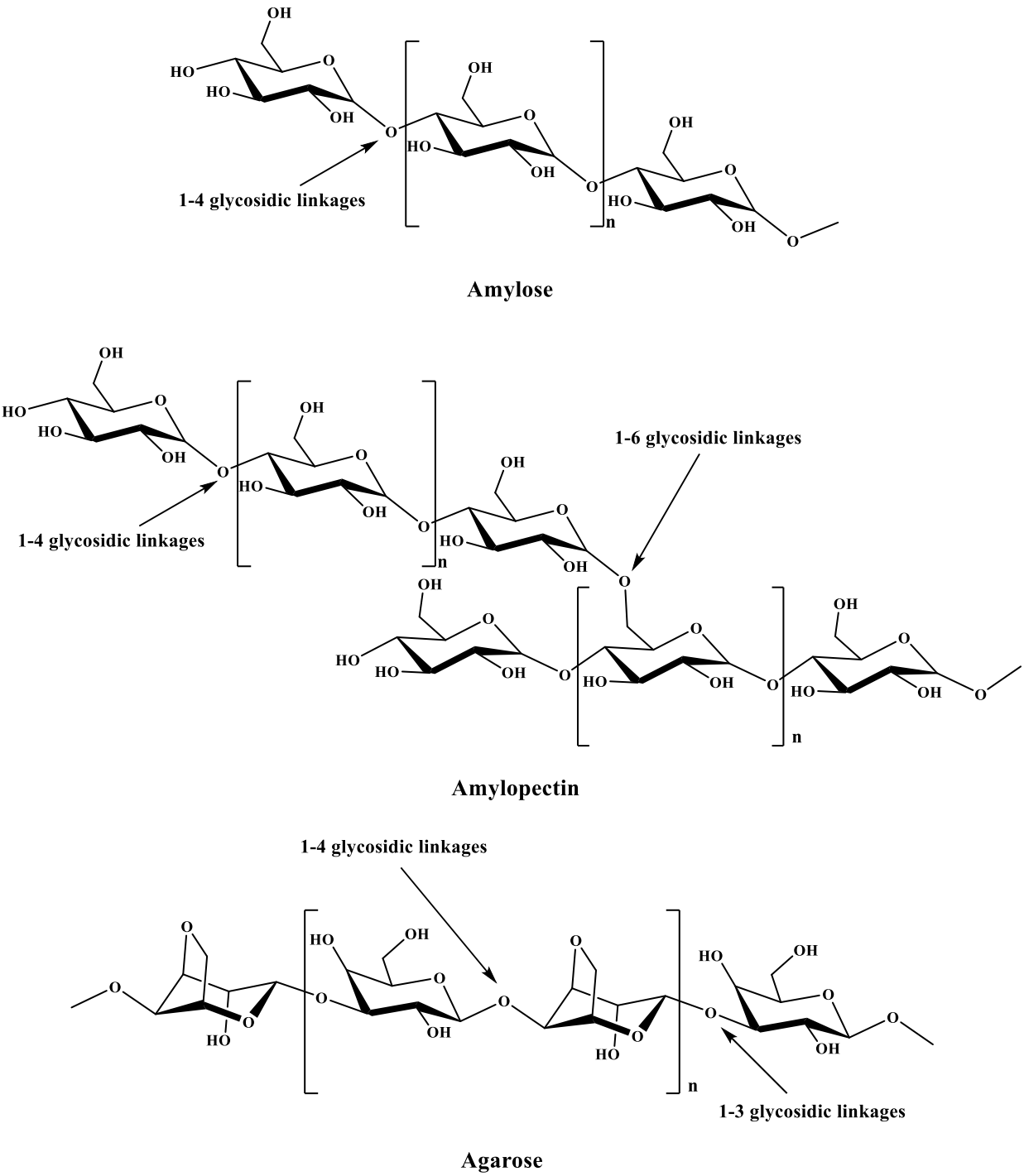

Fig. 1.6 *Chemical structure of amylose, amylopectin and agarose*

Polysaccharides are highly intertwined with human health as without them in our vines and tissues, mankind cannot exist. Traditionally various polysaccharides including starch and cellulose have been used to cure several diseases. The Indian Ayurvedic and Chinese medical traditions are still widely using various polysaccharides in their recipes. Nutraceuticals,

glycosaminoglycans, chitin, mucilage, gums and polysaccharide vaccines are a few examples of polysaccharides, that are well established in modern medical science.

1.2.2 Glycoconjugates

The term "glycoconjugates" includes the molecules in which carbohydrate(s) is/are covalently attached to non-carbohydrate moiety(ies). It includes biological molecules like glycoproteins, glycopeptides, glycans, proteoglycans, glycolipids etc. These molecules are responsible for various biological functions such as cell to cell communication, cross-linkages between proteins, oligo- and polysaccharide biosynthesis etc. Due to the water-binding ability, glycoconjugates also plays a crucial role in maintaining the fluid content in the connective tissues.

In natural glycoconjugates, the carbohydrate linkage can be of three types: glycosylphosphatidylinositol (GPI)-anchored, *O*-glycosidic and *N*-glycosidic linkage. GPI is composed of a phosphatidylinositol group linked through a carbohydrate-containing linker that can be attached to the C-terminus of a proteins during posttranslational modification (*Fig. 1.7*). First characterized approximately 2 decades ago, proteins containing a GPI anchor are well known for their functional diversity and play crucial roles in immune response, prion disease pathogenesis, signal transduction, and the pathobiology of trypanosomal parasites.

In *O*-glycosidic linkage, oxygen acts as the bridging atom between carbohydrate and noncarbohydrate parts whereas in *N*-glycosidic linkage the oxygen atom is replaced by a nitrogen atom (*Fig. 1.7*). Similar to polysaccharides, the *O*-linked glycopeptides can be formed by the condensation reaction between the hydroxyl group of carbohydrates and the carboxylate group of polypeptides. Whereas the *N*-glycosidic bond can be formed by the condensation of carbohydrates with either ammonia or amines in presence/absence of various catalyst and these *N*-glycosides are generally referred as glycosylamines.

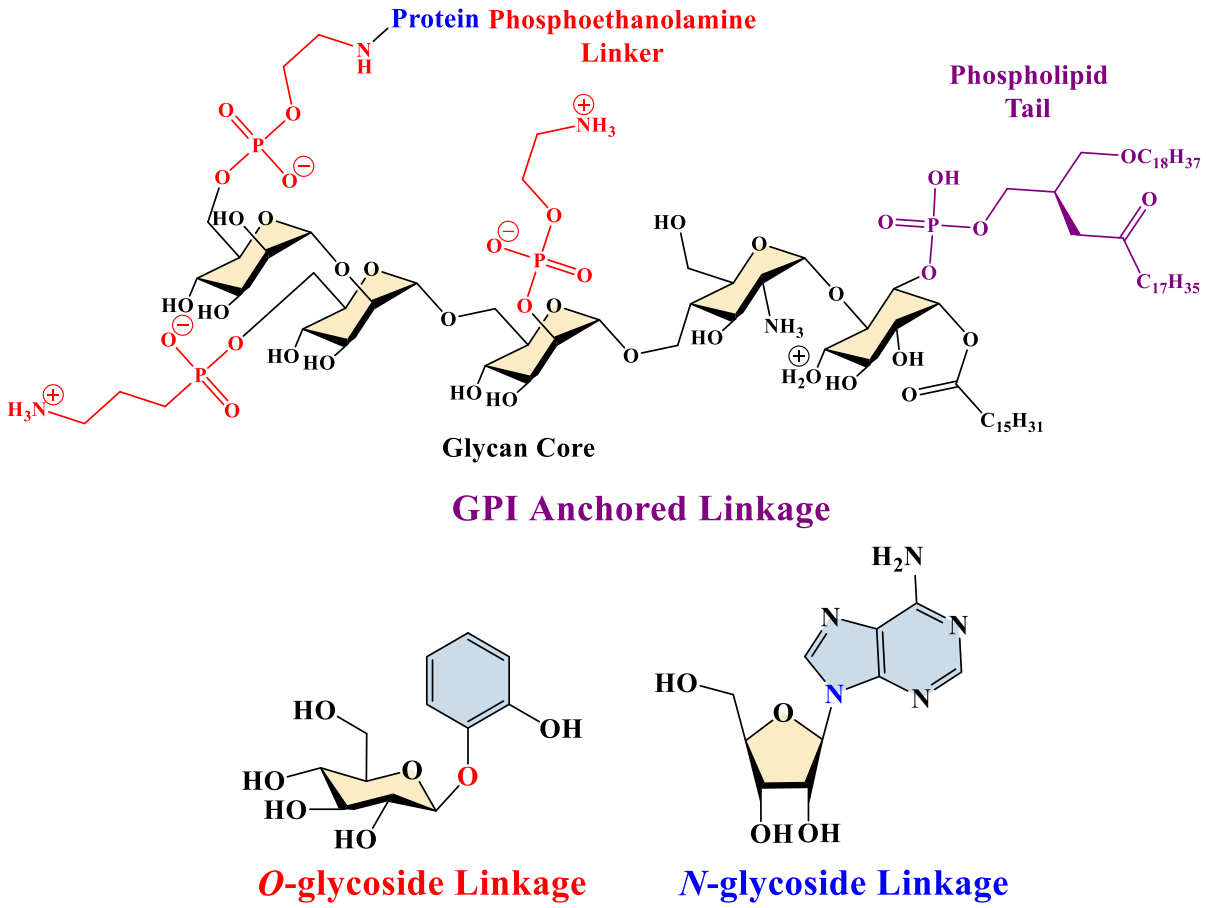

Fig. 1.7 *Structure of Glycoconjugates with GPI-Anchored, O-glycoside and N-glycoside linkage*

1.3 Glycosylamines

Biologically important natural occurring glycosylamines include nucleosides, nucleotides, *N*-glycosyl-amino acids and *N*-glycopeptide derivatives.[22-26] In addition to these, *N*-glycoside linkages are also found in natural products like ansacarbamitocin antibiotics, staurosporine mycorhodin, or anti-carcinogenic akashines A, B, C (*Fig. 1.8*).[27-33] Glycosylamine derivatives have been widely used as antibacterial, antiviral as well as antifungal agents in pharmacological and agrochemical areas.[34-35] Recently these molecules have been used in the preparation of detergents and glycopolymers.[36] Moreover, glycosylamines are also well-established synthetic

intermediates for the preparation of acylated or arylated compounds, which are further used in molecular or metal ions recognition and catalytic reactions.[37-39]

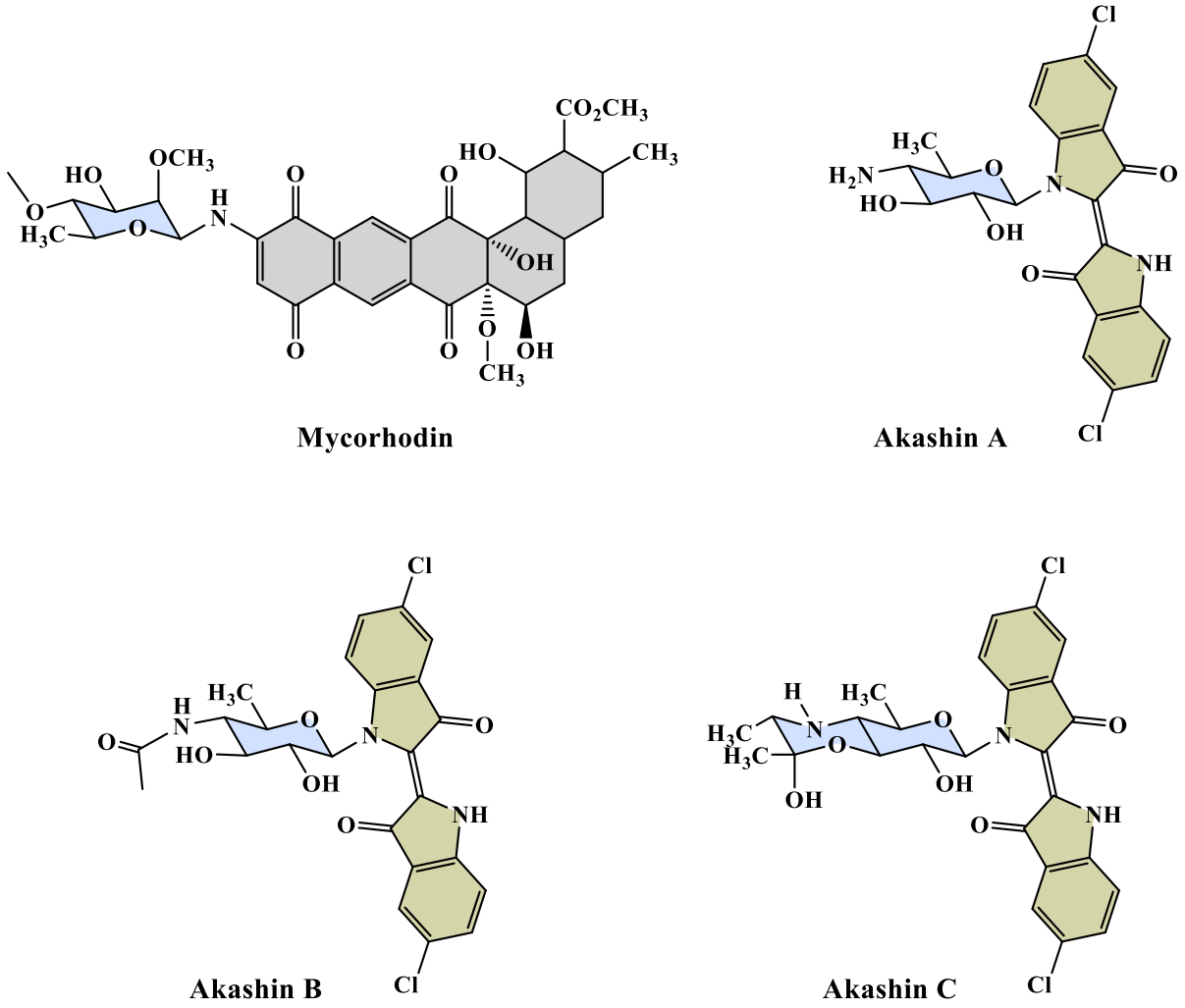

Fig. 1.8 *Structure of Akashin C and Mycorhodin*

1.3.1 Synthesis of glycosylamines

Several protocols have been reported for direct synthesis of glycosylamine using primary or secondary amines and protected or unprotected carbohydrates. Generally, such reactions require protic solvents like methanol or ethanol and some mild acidic or basic conditions for better yield. Reactivity of such starting amines have a strong influence on the rate of the reaction and best results are obtained with aromatic amines with mild basicity. Hugo Schiff

treated D-glucose with aniline and p-toluidine, which yielded a glass like product, later identified as glycosylamines.[40-41] Sorokin improved the yield of the reaction by reacting glucose and aniline in alcoholic medium (methanol or ethanol).[42-44]

Besides the direct condensation, glycosylamine can also be synthesized by the reduction of modified sugars like glycosyl azides (Glu-N_3).[45] Conversion of azides to other *N*-containing functionalities such as amines, imines, amides, ureas, etc., is comparatively easier. Glycosyl azides can be readily converted into amines by using reducing reagents like $NaBH_4$, $LiAlH_4$ or metal-catalyzed hydrogenation using Raney Ni, Pd/C, $Pd(HO)_2$, PtO_2, etc (*Fig. 1.9*).[46-51] Reduction of glycosyl azides using metal-free catalysts such as trimethylphosphine/water and *N*,*N*-diisopropylethylamine/1,3-propanedithiol has also been reported.[52] All these reduction procedures generally are not stereoselective and yields a mixture of α and β anomers of glycosylamines.[53] Selective reduction of glycosyl azides catalyzed by tetrathiomolybdate has been reported by Sridhar et al., to produce corresponding β-glycosylamines.[54]

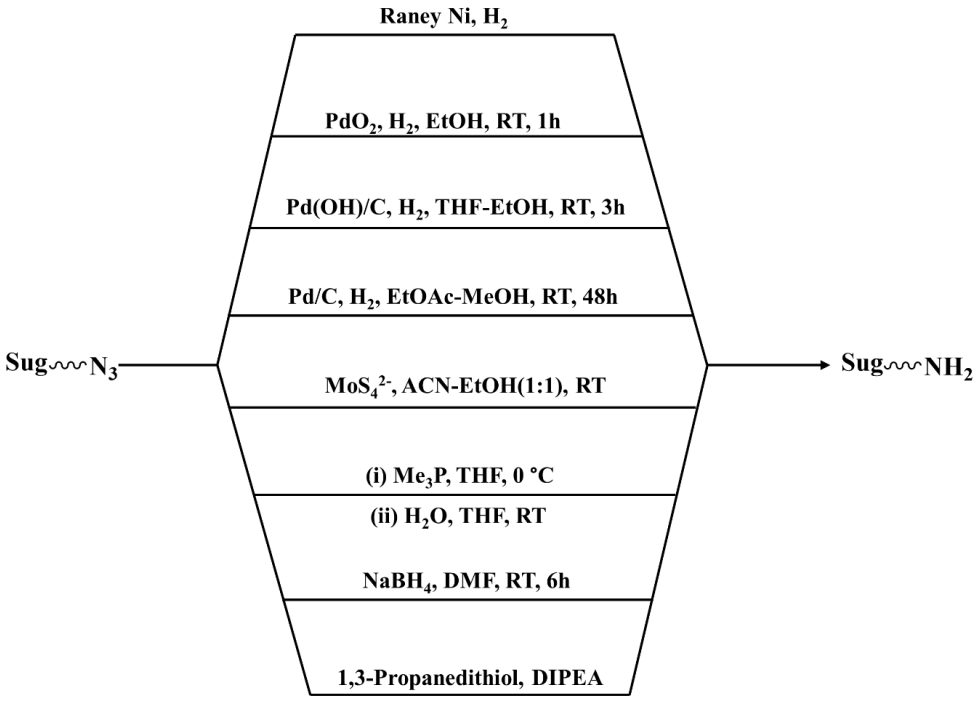

Fig. 1.9 *Reduction procedures of glycosyl azide to glycosylamine*

Lobry de Bruyn reported the synthesis of glycosylamines using reducing sugar in warm water followed by addition of anhydrous methanol saturated with ammonia.[55] In subsequent years, several catalysts like iron carbide,[56] hydrochloric acid,[57] acetic acid[58] etc., were used for better yield and shorter reaction time. Kochetkov's group reported the one-step synthesis of 2-acetamido-2-deoxy-glycopyranosylamines using 2-acetamido-2-deoxy sugar and saturated aqueous solution of ammonium bicarbonate.[59] Later, an alternate protocol was developed by them in which the reducing sugar was heated with 16 M commercial aqueous ammonia at 42 °C for 36 h in presence of ammonium bicarbonate.[60] Lubineau et al. modified Kochetkov condensation by using a saturated aqueous solution of ammonia and a small quantity of ammonium bicarbonate.[60] The main product of this procedure was glycosylcarbamate, which was subjected to cation exchange chromatography and the desired glycosylamine was eluted from methanol–water mixture. Later Likhosherstov and co-workers further improved Kochetkov condensation for synthesis of β-glycopyranosylamines by replacing ammonium bicarbonate with ammonium carbamate and ammonium hydroxide.[61-63] Recently microwave-assisted stereoselective glycosylamine synthesis was explored by Rosencrantz and co-worker (*Fig. 1.10*), which was nothing but the further modification in Likhosherstov's amination method.[64] Microwave assistance not only allow a significant reduction in the reaction time and amount of ammonium salt but also ease the purification process.

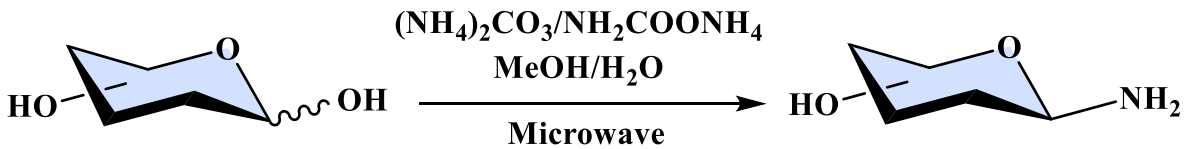

Fig. 1.10 *Synthesis of glycosylamine using microwave*

Santoyo-González and co-workers have reported a simple and efficient synthesis of glucopyranosylamine by reacting glycopyranosyl isothiocyanates with bis(tributyltin)oxide

using a mild one-pot procedure (*Scheme 1.1*).[65] Starting from α-glycopyranosyl derivatives, this procedure afforded both α and β anomers of *N*-acetyl glycopyranosylamines.

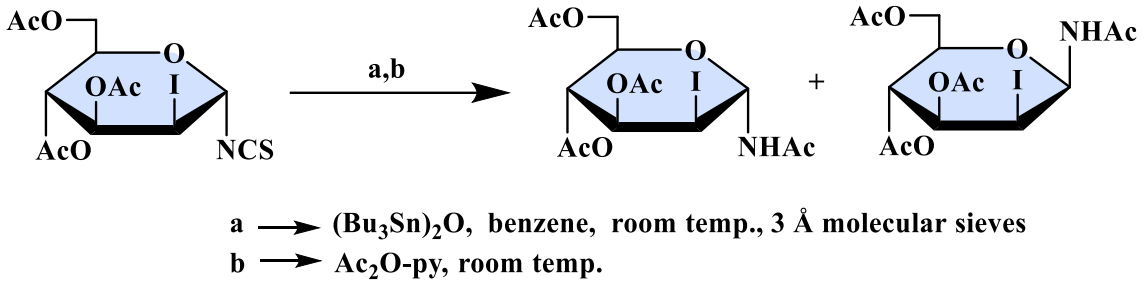

Scheme 1.1 *Synthesis of glycosylamines using glycopyranosyl isothiocynates and bis(tributyltin)oxide.*

Nicolaou and co-workers have developed a methodology for regio- and stereo-selective synthesis of glycosylamines using Burgess reagent along with *O*-protected sugars (*Scheme 1.2*).[66] For carbohydrates bearing free C-2 hydroxy group, the reaction proceeds through sulfamidate intermediates and affords the α-anomers, whereas saccharides with protection at C-2 position directly yields the β-glycosylamines.

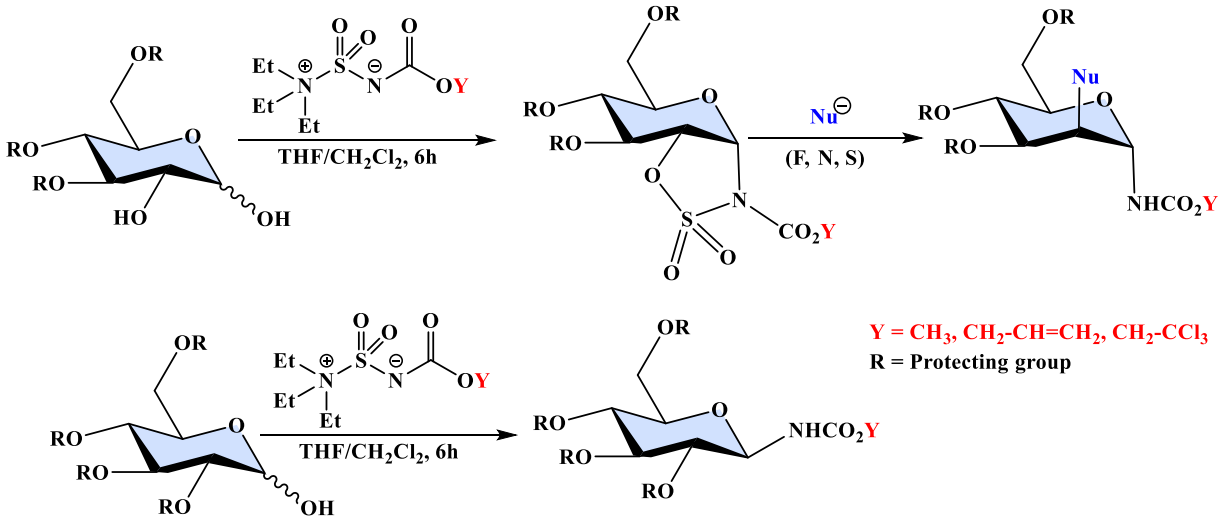

Scheme 1.2 *Synthesis of glycosylamines using Burgess reagent*

1.3.2 Stability of glycosylamines

Despite having a wide range of applications, the major problem with glycosylamines is their stability but *N*-substituted glycosylamines derivatives have comparatively higher stability. Glycosylamine possesses many sugars like properties such as mutarotation (*Fig. 1.11*) and in presence of an acid, they can rearrange themselves into a tautomeric open-chain imine or imonium ion intermediate.[58, 67] The glycosylamines derived from D-sugars usually have the β-configuration as it is more stable compared to α-configuration. The addition of hydroxyl ion to the imonium ion intermediate can yield corresponding amine and saccharide (*Fig. 1.8*).[67] Other glycosylamines can also react with the imonium ion intermediate as a nucleophile, which leads to a transglycosylation reaction (*Fig. 1.11*).[67] Besides the pH of the glycosylamine solution, such reactions also depend on the nature of the amine attached to the carbohydrate moiety.

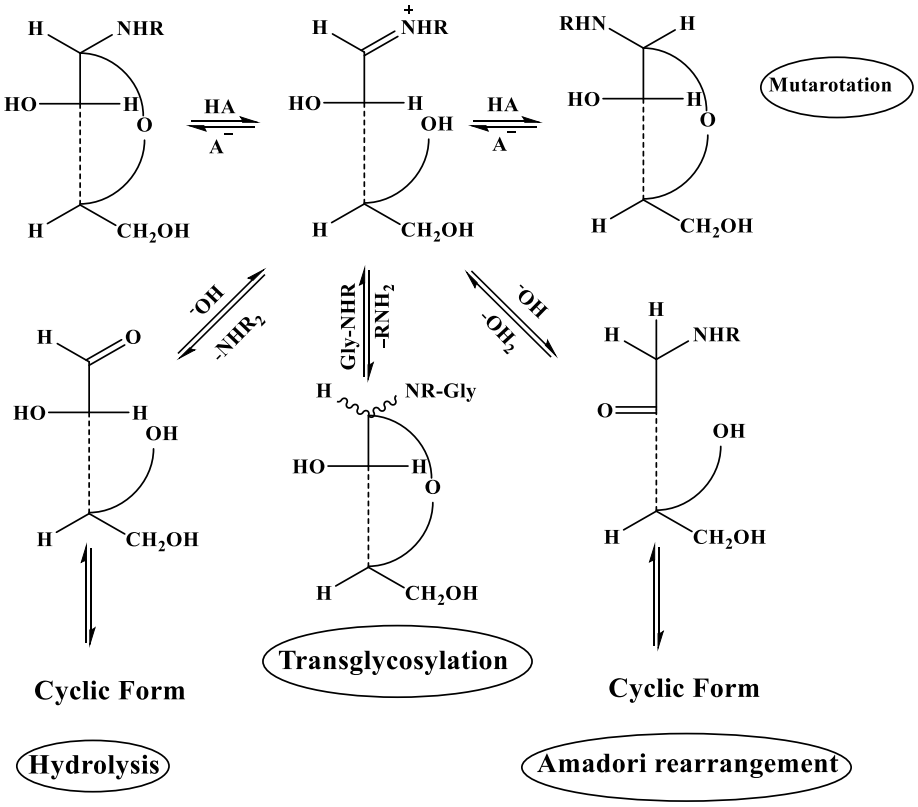

Fig. 1.11 *Mutarotation, hydrolysis, transglycosylation and Amadori rearrangement reactions of glycosylamine via imonium ion intermediate*

Imonium ion intermediate can also go through Amadori rearrangement in which the *N*-glycoside of an aldose or a glycosylamine can rearrange themselves to their corresponding 1-amino-1-deoxy-ketose.[43] The glycosylamine can also go through Amadori rearrangement (*Fig. 1.11*) in which they form the corresponding 1-amino-1-deoxy-ketose. As the reaction proceeds through the imonium ion intermediate, the rate of Amadori rearrangement is highly influenced by the concentration of imonium ion and the nature of the amine group.

1.3.3 Importance of protecting group in glycosylamines

Regio- and stereoselective conversion of sugar into glycosylamines is a challenging task in the chemistry of carbohydrates.[68] However, this problem can be tackled by the introduction of protecting groups that can neutralize specific functional groups and some regioselectively liberated functional groups are allowed to participate in the coupling process. The protecting groups adopted for hydroxyl group protection in carbohydrate chemistry are the same as used in organic chemistry which are commonly divided into three categories i.e., ether, ester and acetal groups.[69] Although the choice of protecting group is highly necessities specific, ethylidene, isopropylidene and benzylidene type acetals are most frequently used cyclic protecting groups as they provide an edge on selective protection to both C-6 and C-4 hydroxyl groups simultaneously in the case of galacto-, manno- and gluco-configurations.[70] In this thesis, the same methodology has been applied for the synthesis of 4,6-*O*-ethylidene-*β*-D-glucopyranosylamine (*Scheme 1.3*),[71-72] which is further modified for metal complexation and molecular sensing.

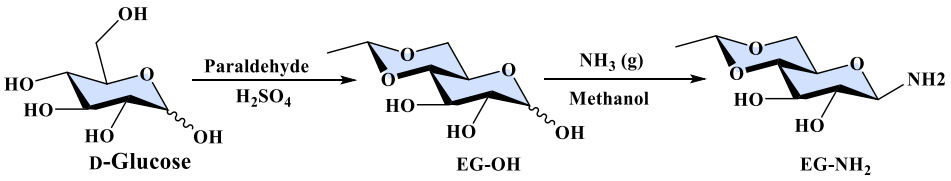

Scheme 1.3 *Synthesis of 4,6-O-ethylidene-β-D-glucopyranosylamine*

Synthesis of 4,6-*O*-ethylidene-*β*-D-glucopyranosylamine from D-glucose is a two-step process. The first step is synthesis of 4,6-*O*-ethylidene-D-glucose using paraldehyde and sulphuric acid reported by Barker and MacDonald.[71] Further, the amination at anomeric carbon afforded corresponding *β*-glycosylamine.[72] However, to provide more resistance to hydrolysis and anomerization, several further modifications has been reported by altering primary amine group at C-1 position into a imines and amides. The presence of two free hydroxyl groups at C-2 and C-3 position provides an additional opportunity for molecular interactions and metal complexation reactions.

1.3.4 Imine derivatives of glycosylamine

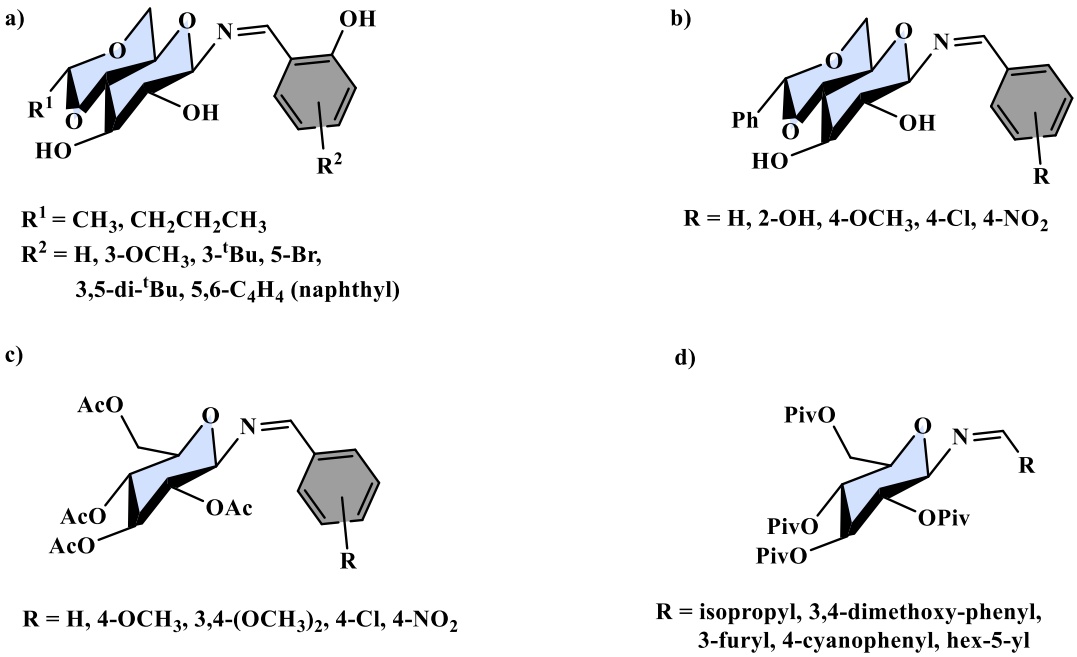

Fig. 1.12 *Schiff base derivatives of glycosylamine*

The stability of glycosylamine can further be increased by substituting the amine group with an imine functionality. Condensation of glycosylamine with aldehydes or ketone in alcoholic medium affords their Schiff base derivatives. Rao et al., have synthesized Schiff bases of 4,6-*O*-butylidene- and 4,6-*O*-ethylidene-*β*-D-glucopyranosylamine with substituted

salicylaldehyde (*Fig. 1.12a*). and these derivatives were used in amino acid sensing and metal complexation reactions.[39, 73-79]. Schiff base derivatives of 4,6-*O*-benzylidene-*β*-D-glucopyranosylamine have also been reported by Shen et al., using benzaldehydes derivatives (*Fig. 1.12b*).[80] Jarrahpour et al., have reported a series of Schiff base derivatives of acylated D-glucopyranosylamine using benzaldehyde derivatives (*Fig. 1.12c*).[81] Knauer et al., have converted 2,3,4,6-tetra-*O*-pivaloyl-β-D-glucopyranosylamine into a series of imines derivatives using aromatic, heteroaromatic and aliphatic aldehydes, which were an intermediate in *N*-glucosyl-dehydropiperidinones synthesis[82](*Fig. 1.12d*).

1.3.5 Amide derivatives of glycosylamine

Several strategies have also been developed for the coupling of glycosylamine with a non-carbohydrate moiety through an amide linkage. Due to the high nucleophilicity of the nitrogen atom attached to the anomeric carbon, direct coupling method is one of the most explored techniques, where the glycosylamine is allowed to react with acyl chloride or acyl anhydride group in presence of reagents like ethyl chloroformate,[81-82] *N*,*N*′-dicyclohexylcarbodiimide (DCC),[83] *N*-(3-dimethylaminopropyl)-*N*'-ethylcarbodiimide hydrochloride (EDCI)/*N*-hydroxybenzo-triazole (HOBT).[84-86] etc. to form a amide linkage.

Our group have developed the protocol to couple 4,6-*O*-ethylidene-*β*-D-glucopyranosylamine with *N*-Fmoc protected nonpolar amino acids through amide linkage in presence of triethylamine (TEA) and ethyl choloroformate (ECF). After the deprotection of Fmoc group glycosylamide is further linked with aromatic acids and aldehydes through amide and imine linkage (*Scheme 1.4*).[81-82, 87-89] The amino acid and metal ion sensing abilities of the synthesized glycosylamide have also been explored by our group and the same has been discussed later in this chapter.

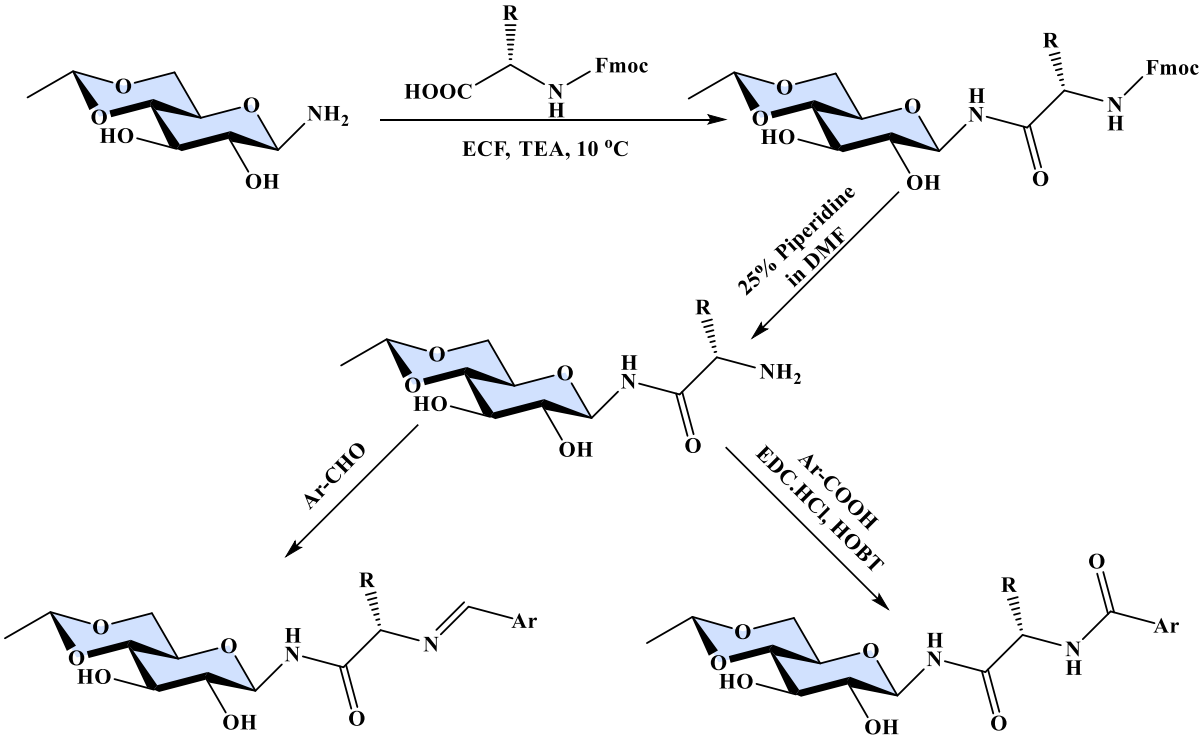

Scheme 1.4 *Glucosylamides synthesised from 4,6-O-ethylidine-β-D-glucopyranosylamine*

1.4 Amino acid recognition using glycoconjugates

Amino acids are building blocks of proteins, in which an amine group along with a carboxylic acid and an organic side chain is attached to the same carbon (α-carbon). Due to these various functional side chains, amino acids play vital roles in different physiological processes.[90] As attention towards human health is increasing and progress in diagnosis and treatment is reaching its new heights, several new methods have been developed for amino acid analysis. Currently electrochemical,[91] chromatographic[92] and spectroscopic[93] techniques are in trend for detection and characterization of amino acid. Amino acid detection using highly selective and sensitive chemosensors is the most elegant approach. Although, development of novel optical chemosensors for recognition of a targeted amino acid have grown significantly, their bio-compatibility is a major concern. Although, nontoxic biorelevant carbohydrate derivatives can address this issue, not much work has been done in this area.

1.4.1 Noncovalent interaction based amino acid sensors

The protein-carbohydrate interaction is a very important process from biological and medical point of view.[94] Proteins like Lectins are well known for their selective carbohydrate recognition and hence they have potentially involved in a verity of applications in pharmacology, immunology and cancer therapy.[78] In general, all these interactions took place at the surface of proteins and after the binding, the carbohydrates are encapsulated in cavities or grooves. In such type of interactions, most of the amino acid moieties participate in carbohydrate binding process, however the strength of interactions is highly governed by their polarity and aromaticity of the side chains. In other words, carbohydrate-amino acid complexation is assumed to be driven by van der Waals forces like π-π or CH-π and hydrogen bonding interaction. These interactions can be investigated using analytical tools like NMR, IR, single crystal XRD etc and also computational model.

1.4.1.1 Hydrogen based amino acid sensing using glycoconjugates

The presence of hydroxyl groups in the carbohydrates facilitate their interaction with amino acids through intermolecular hydrogen bonding and based on this fact several glycoconjugate-based chemosensors have been developed in recent years. In 2007 Rao et al., has reported galactosyl-naphthyl-imine/amine-based receptors for amino acid recognition (*Fig. 1.13*).[78] The imine derivative is found to be responsive towards glutamic acid, histidine, leucine and proline whereas the amine derivative interacts with alanine, cysteine and lysine. The association of imine derivative with glutamic acid was found to be 1:2 ratio while the complexation with histidine, proline and leucine occurred at 1:1 ratio. They have also reported a glucose-based C-2-glycoconjugate, which interacts with the aromatic amino acids, which are phenylalanine, tyrosine, histidine and tryptophan along with two non-aromatic amino acids specifically arginine and alanine.[79] The association constant of C-2-glycoconjugate and aromatic amino

acids were found to be 19400 ± 600 which is 5 to 10 times higher compared to the non-aromatic one. The limit of detection of C-2-glycoconjugate towards aromatic amino acids went down to 1.5-3 ppm. Although all the glycoconjugates interacts quite efficiently with different amino acids, the selectivity still remains an issue.

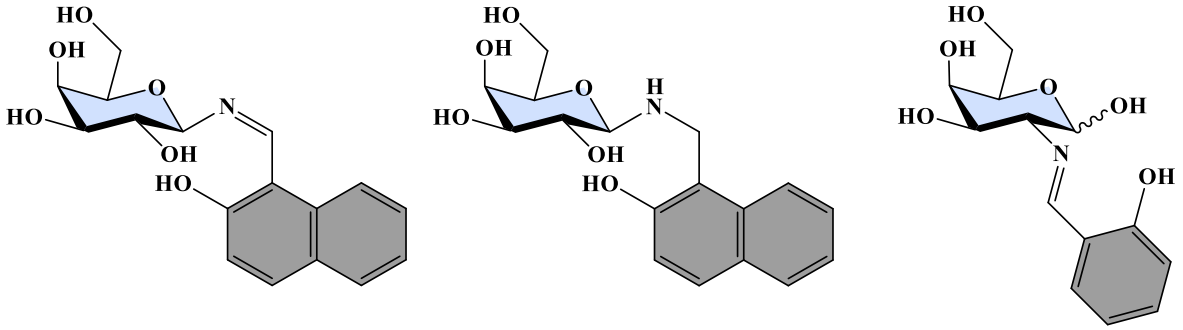

Fig. 1.13 *Galactose based receptors for amino acid recognition*

Our group have reported another glucose derived chemosensors in which protected glucose was conjugated with L-alanine through amide linkage which is further attached to salicylic acid through another amide linkage[86] (*Fig. 1.14*). The glycopeptide solution displayed a bathochromic shift along with the shift in absorbance value whereas fluorescence intensity was quenched in presence of both free and protein bounded tryptophan residue. The quenching rate constants for free and protein bounded residue was found to be 4.76×10^{12} and 1.4×10^{12} L mol^{-1} s^{-1}, respectively, which indicates the formation of non-fluorescent ground state complex between guest and host.

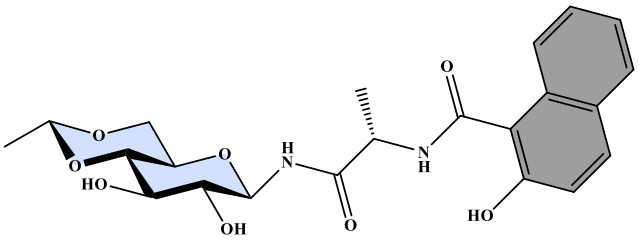

Fig. 1.14 *N-(2-hydroxybenzoyl)-L-alanyl-4,6-O-ethylidene-β-D-glucopyranosylamine used in tryptophan sensing*

1.4.1.2 π-π or CH-π interaction between amino acids and sugar derivatives

The glycoconjugate and aromatic amino acid binding can also be driven by nonpolar forces like π-π or CH-π interaction.[95] The nature of such type of interactions between amino acid and carbohydrate have been explained by Hillier and co-workers using density functional theory (DFT-D) and semi-empirical (PM3-D) methods.[96] According to the theoretical results, the interaction energies are dependent on the stereochemistry of glycoconjugates and amino acids. The interaction energy between carbohydrate and aromatic moieties of amino acids are close to the normal hydrogen bond energy, indicating that the former interaction can also be important in peptide recognition. Although the interaction of peptide backbone with the aromatic moieties of glycoconjugate is not that specific, the unsaturated side chains of both guest and host prefers the stacked orientation.

A quantitative assessment of interactions between protein and monosaccharides have been done by Hudson et al using the high-resolution structure of protein carbohydrate complexes available in the Protein Data Bank.[97] According to their findings the electron-rich aromatic side chain containing tryptophan shows strongest binding with both the plane of carbohydrate moieties. The first-order effect responsible for these binding is the electrostatic interaction between electronegative face of the aromatic side chain of amino acids and electropositive face of carbohydrate moieties. The second-order effect is more specific, which is a CH-π interaction between the polarized C-H bond of carbohydrates and π-electrons of aromatic ring. This model is further supported by theoretical calculation of the electrostatic interaction between carbohydrate and arene rings. Increasing the electropositivity of C-H bonds by electron withdrawing substitutions (*O*-acylated or *O*-sulfated), hydrogen bonding or coordination of key hydroxyl groups with calcium ion can also increase the strength of CH-π interactions. As electropositive characters of C-H bonds vary between carbohydrate isomers, the regions of

carbohydrate with which the arene rings interact also change. This study provides a mechanistic understanding on saccharide and amino acid interaction.

The interactions between different hexopyranoses and amino acids containing aromatic side chain were theoretically and experimentally studied by Spiwok.[98] Due to the axial orientation of C-H hydrogens in β-D-glucopyranose, they can interact with the indole moiety of tryptophan and benzene residue of phenylalanine or tyrosine ring in a parallel stacking geometry at both top and bottom face of aromatic ring (*Fig. 1.15A*). As the anomeric hydroxyl group blocks on the bottom face, α-D-glucopyranose favours only the top face. Some other monosaccharides like α- or β-D-galactopyranose or α-L-fucopyranose interact with the aromatic moieties via a patch of C–H groups attached to C-3, C-4, C-5 and C-6 carbons at the B face (*Fig. 1.15B*). Similarly, C–H groups attached to C-1, C-2 and C-3 carbons of β-D-mannopyranose can also form parallel patch (*Fig. 1.15C*).

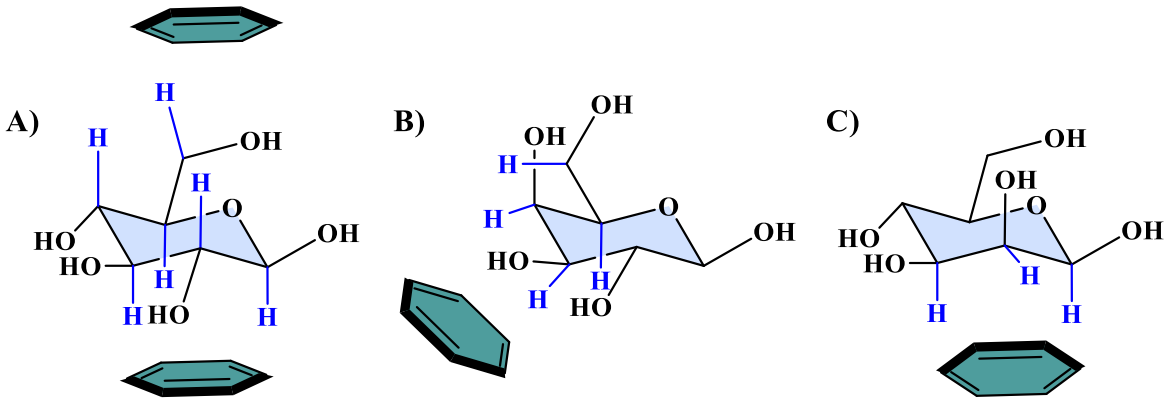

Fig. 1.15 *Carbohydrate aromatic CH-π interaction in A) β-D-glucopyranose, B) α- or β-D-galactopyranose or α-L-fucopyranose and C) β-D-mannopyranose*

1.5 Metal-saccharide interactions

The chemistry between carbohydrate and metal ions interaction is quite important from biological point of view due to the co-existence of saccharides and metal ions in living

organisms.[94, 99] The metal ions-saccharide interaction was first reported in 1825 and most of the work till 1960s were compiled by Rendleman Jr.[100] However, the relationship between structure of carbohydrates and its complexation with metal ions was first explained in 1971 by Angyal and Davies.[101] Afterward, several literatures have reported the interaction of alkali and alkaline earth metal ions with monosaccharides.[102-113] Till 1990, most of the work was confined to the solution-based studies like determination of binding energies, coordination number and stability constants.[114-116] Researchers were able to get the solid-state structure of coordination compounds after substituting simple carbohydrates with sugar derivatives.[117-120] Derivatization of the carbohydrate provides stability to their metal complex. [121-131] Due to the non-toxic nature of sugar, the metal-carbohydrate complexes are subjects of great interests from biological point of view. Several clinical applications of such carbohydrate-based complexes have been established,[132-143] for example Auranofin[144] (acetylthioglucose complex of gold) have been used as oral drug for rheumatoid arthritis treatment (*Fig. 1.16*). The glycoconjugated metal ion complexes are also treated as catalysts in asymmetric synthesis[145-154] due to the chiral centres present in the carbohydrate moieties. A brief literature survey of 4,6-*O*-ethylidene-D-glucose derived ligands and their metal complexes are discussed below.

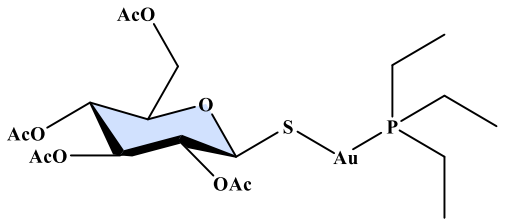

Fig. 1.16 *Structure of Auranofin*

1.5.1 4,6-*O*-Ethylidene-D-glucose derived ligands

Synthetic procedure of 4,6-*O*-ethylidene-D-glucose was established by Barker and MacDonald[71], which can react to ammonia or primary amine to afford corresponding glycosylamines in β-anomeric form.[72, 155] Their imine or amide derivatives was further synthesized by the condensation of 4,6-*O*-Ethylidene-β-D-glucopyranosylamine with aldehyde

or amino acids, respectively. The complexation ability of several *N*-glycosylamine derivatives with alkali, alkaline earth, transition metal ions, lanthanide and actinide ions have been explored. The imine derivatives exhibited excellent complexation abilities and afforded single crystals of V(V),[76] Mo(VI),[76, 156] Ni(II),[157] Cu(II),[77, 158] Zn(II)[159] and U(VI)[76] complexes, which in turn provided clarities on metal binding site.

1.5.1.1 Metal complexes of *N*-(*O*-carboxyphenyl)-4,6-*O*-ethylidene-β-D-glucopyranosylamine

Rao and co-workers used *N*-Glycosylamines of anthranilic acid in complexing several diamagnetic metal ions like Na(I), K(I), Mg(II), Ca(II), Ba(II), Cd(II) and Hg(II).[155] These complexes were characterized by various analytical tools like FTIR, NMR, TGA/DTA and elemental analysis. The crystal structure of potassium complex confirmed the presence of two type of potassium ions in their asymmetric unit (*Fig. 1.17*). The first one has the full occupancy (K^1) whereas other inhabits two positions (K^{2a} and K^{2b}) with the occupancies of 0.5 each. The binding modes of ligand towards the K(I) ion is presented in the *Fig. 1.17* and it clearly shows that almost all the oxygen atoms are participating in the complexation.

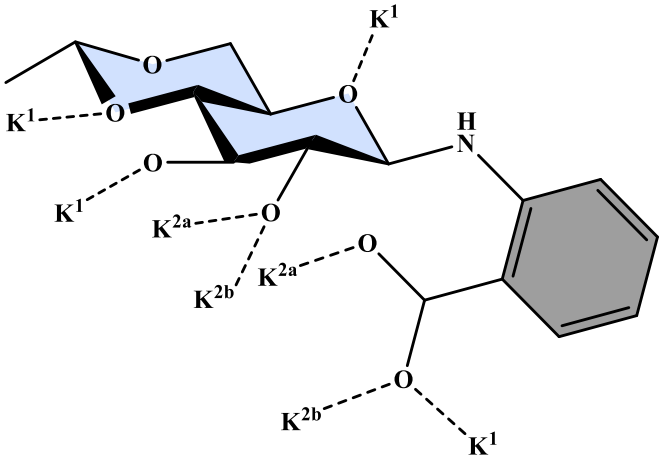

Fig. 1.17 *Binding mode of N-(2-carboxyphenyl)-4,6-O-ethylidene-β-D-glucopyranosylamine with potassium ions*

1.5.1.2 Metal complexes of imine derivatives of 4,6-*O*-ethylidene-β-D-glucopyranosylamine

4,6-*O*-Ethylidene-β-D-glucopyranosylamine based Schiff base ligands (*Fig. 1.18*) have been used for chelating VO^{2+}, MoO_2^{2+}, Ni^{2+}, Cu^{2+}, Zn^{2+}, UO_2^{2+} and Yb^{3+} ions.[39, 77, 120] Regular analytical and spectral techniques have been used to characterize the metal ion complexes and molecular structure of some of the complexes have been established using single crystal X-ray diffraction studies. All the coordination compounds were stable in DMSO solution except the V(V) and Ni(II) complexes. The instability of V(V) complex was confirmed by UV-visible absorption studies, where the complex moiety disintegrated into free ligand and some unidentified compound(s).[76] The preliminary studies of nickel-saccharide complex revealed the stoichiometry of metal and ligand interaction in 1:2 ratio.[157] Slow diffusion of MeOH into concentrated DMSO solution of nickel-saccharide complex yielded green colored crystal of tetrameric compound with metal to ligand ratio 1:1 (*Fig. 1.19*). Transformation of 1:2 product into 1:1 may be attributed to the instability of nickel-saccharide complex in DMSO solution.

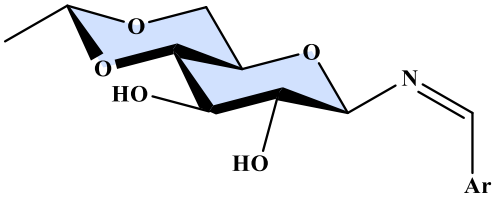

Ar = **2-hydroxy-phenyl (L1)**
2-hydroxy-napthyl (L1a)
2-hydroxy-3methoxyphenyl (L1b)
2-hydroxy-5-bromophenyl (L1c)
2-hydroxy-3-tert-butylphenyl (L1d)
2-hydroxy-3,5-di-tert-butylphenyl (L1e)

Fig. 1.18 *4,6-O-Ethylidene-β-D-glucopyranosylamine derived Schiff base ligands used in metal complexation*

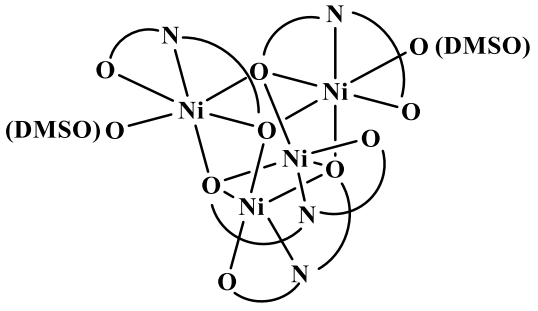

Fig. 1.19 *Tetranuclear Ni(II) complex depicted from literature*

The complexation of di-oxo metal (VO_2^+, MoO_2^{2+} and UO_2^{2+}) with L1 and L1b was reported by Rao and co-workers.[76] The crystal structure revealed the formation of *cis*-dioxo mononuclear complexes for vanadium(V) and molybdenum(VI), while *trans*-dioxo di-nuclear complex for uranium with trigonal bipyramidal, octahedral and pentagonal bipyramidal geometries, respectively. The *trans*-orientation of oxo-groups and large size of uranyl ion might result in the dimeric structure of UO_2^{2+} complex. Few catalytic applications of molybdenum complex in organic synthesis have been reported, which have been discussed later in this chapter.

Chelation of cupric ion with 4,6-*O*-ethylidene-D-glucopyranosylamine derived Schiff base afforded dinuclear complexes with metal to ligand ratio 1:1 (except L1d).[77, 158, 160] The ligands acted as tridentate dianionic and the C2-O of carbohydrate moieties bridges the two copper centers to form a Cu_2O_2 rhomb (*Fig. 1.20*). The metal centres are separated by about 3 Å, which confirms the absence of bonding between them. Depending on the crystallization process, the copper complexes have either square planer or square pyramidal geometry, where the ligand construct the basal plane. In case of square pyramidal geometry, the axial position is occupied by solvent molecules (DMSO, MeOH or pyridine). The hydrogen bonding interactions between C3–OH and phenolate oxygen offer stability to the dinuclear copper complexes.

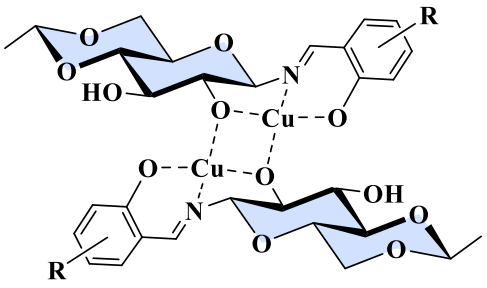

Fig. 1.20 *Dinuclear Cu(II) complex with square planar geometry*

The complexation of *N*-(3-*tert*-butyl-2-hydroxybenzylidene)-4,6-*O*-ethylidene-β-D-glucopyranosylamine (L1d) with cupric ion yielded neutral trinuclear copper(II) complex with metal to ligand stoichiometry of 3:2.[161-162] Recrystallization of the complex in a mixed solvent

($CHCl_3$/MeCN/ROH) resulted in the X-ray quality single crystals with square planar geometry about all the metal centres (*Fig. 1.21a*). However, recrystallization from $CHCl_3$/THF/MeOH yielded square pyramidal geometry (THF occupied the axial positions) about the terminal and square planar about the central metal ion (*Fig. 1.21b*). The fourth basal site is occupied by the alcohol unit and its hydroxyl proton interacts with C3-O through strong intermolecular hydrogen bonding. The **L1d** acts as tetradentate trianionic ligand, where C2-O of carbohydrate moieties bridges the terminal and central copper atoms. The crystal structure of trinuclear copper complex containing ethylamine instead of alcohols at the fourth basal sites of terminal copper has also been reported.[163-164] These amine incorporated molecules are unstable in chloroform and degrade slowly into amine coordinated copper(II) complexes with chloride counter anion.

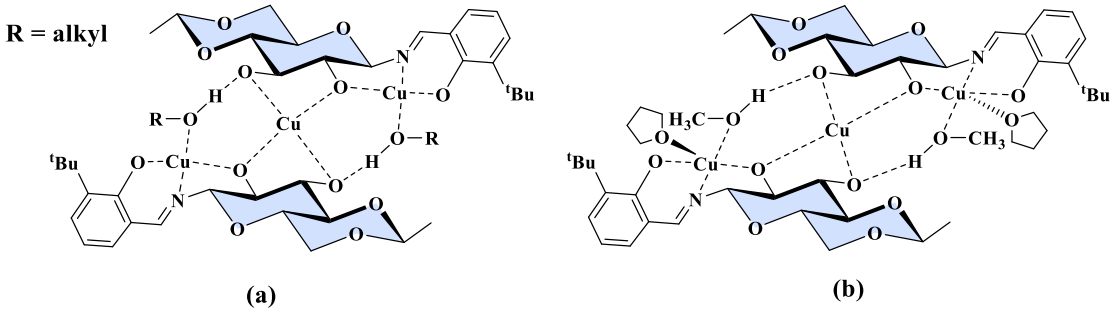

Fig. 1.21 *Trinuclear Cu(II) complex with (a) square planar and (b) square planar and square pyramidal geometry around the central and terminal atom respectively.*

The treatment of trinuclear copper complex of *N*-(3-*tert*-butyl-2-hydroxybenzylidene)-4,6-*O*-ethylidene-β-D-glucopyranosylamine with 4,6-*O*-ethylidene-D-glucopyranose resulted a self-assembled tetranuclear complex via proton transfer reaction (*Fig. 1.22*).[162] In this tetranuclear copper complex each saccharide derivatives act as tetradentate dianionic ligand and the C2-O of sugar moieties bridges two copper(II) ions. Each copper centre has square pyramidal geometry all four basal position are occupied by phenolate oxygen, imine nitrogen

and two bridging C-2 oxygens whereas at axil position a weak interaction by C-3 alkoxy oxygen is present.

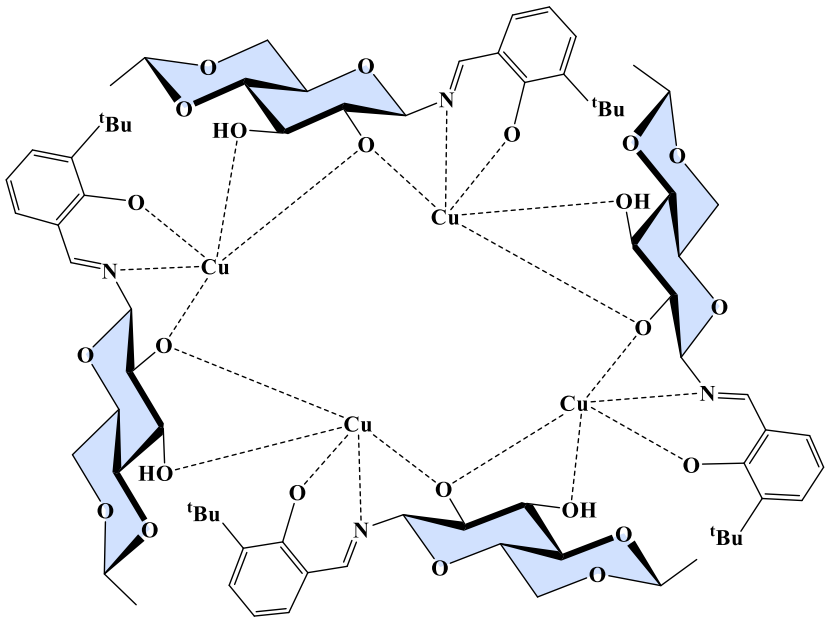

Fig. 1.22 *Structure of tetranuclear copper complex of* ***L1d****.*

The reaction of *N*-(2-hydroxybenzylidene)-4,6-*O*-ethylidene-β-D-glucopyranosylamine (L1) with zinc acetate yields neutral mononuclear complex (*Fig. 1.23*) with metal to ligand stoichiometry of 1:2.[120, 159] The X-ray diffraction studies disclosed the highly distorted trigonal bipyramidal geometry, where the four coordination sites are captured by phenolate oxygen and imine nitrogen of both the ligands. Fifth coordination site is occupied by the pyranose oxygen of one of the saccharide moieties and interacts weakly with the Zn(II) ion.

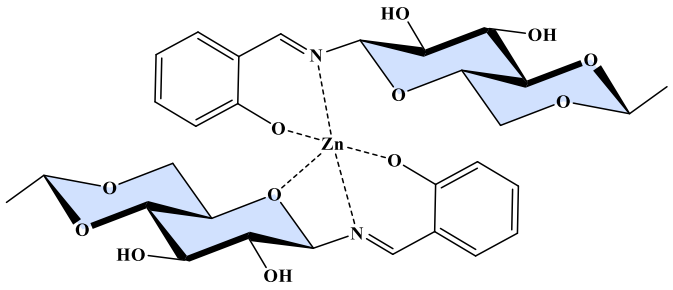

Fig. 1.23 *Glucose derived Zn(II) complex showing*

The reaction between ytterbium acetate and 4,6-*O*-ethylidene-β-D-glucopyranosylamine derived Schiff base afforded a glycoconjugated ytterbium complex,

which has been characterized by FTIR, elemental analysis, HRMS and UV-visible absorption spectroscopy.[165] Using Job's plot, the stoichiometry of complexation was found to be 1:1 which was further conformed by HRMS and elementary analysis. As the crystal structure of the ytterbium complex was not obtained the binding modes of the complexation is unknown.

1.5.1.3 Metal complexes of amide derivatives of 4,6-*O*-ethylidene-β-D-glucopyranosylamine

The selective interaction between cupric acetate and *N*-(2-hydroxybenzoyl)-L-alanyl-4,6-*O*-ethylidene-β-D-glucopyranosylamine (L-DA) has been established using UV-visible and fluorescence spectroscopically.[89] Cupric acetate quenches the fluorescence intensity of diamide ligand with the correlation coefficient, R= 0.978 and Stern Volmer constant, K_{SV} = 38,067 M^{-1}, suggesting the possibilities of quenching via dynamic mode. Replacing the cupric acetate with other copper(II) salt did not result any spectral change for the glycoconjugate, suggesting the complexation between ligand and molecular cupric acetate, not with Cu(II) ion.

1.5.2 Catalytic activities of 4,6-*O*-ethylidene-D-glucose derived metal complexes

Although a range of metal complex have been synthesized, catalytic application of only copper, molybdenum and ytterbium complexes of **L1** have been explored. The dioxo-molybdenum(VI) complex of **L1** has been used for selective oxidation of organic sulfides into corresponding sulfoxides and sulfones under mild reaction condition in ethanolic medium (*Scheme 1.5a*).[156] Selectivity towards sulfoxide and sulfone depends upon the equivalent of UHP added as oxidant. Catalytic conversion of sulfoxides and sulfones form sulfides required one and five equivalents of UHP, respectively. The reusability of the complex was also tested up to five cycles, which confirms no loss in its catalytic activity. Control reaction conforms the formation of an expected molybdenum peroxo complex after the initial reaction between molybdenum complex and UHP, which further transfer oxygen to the sulfide.

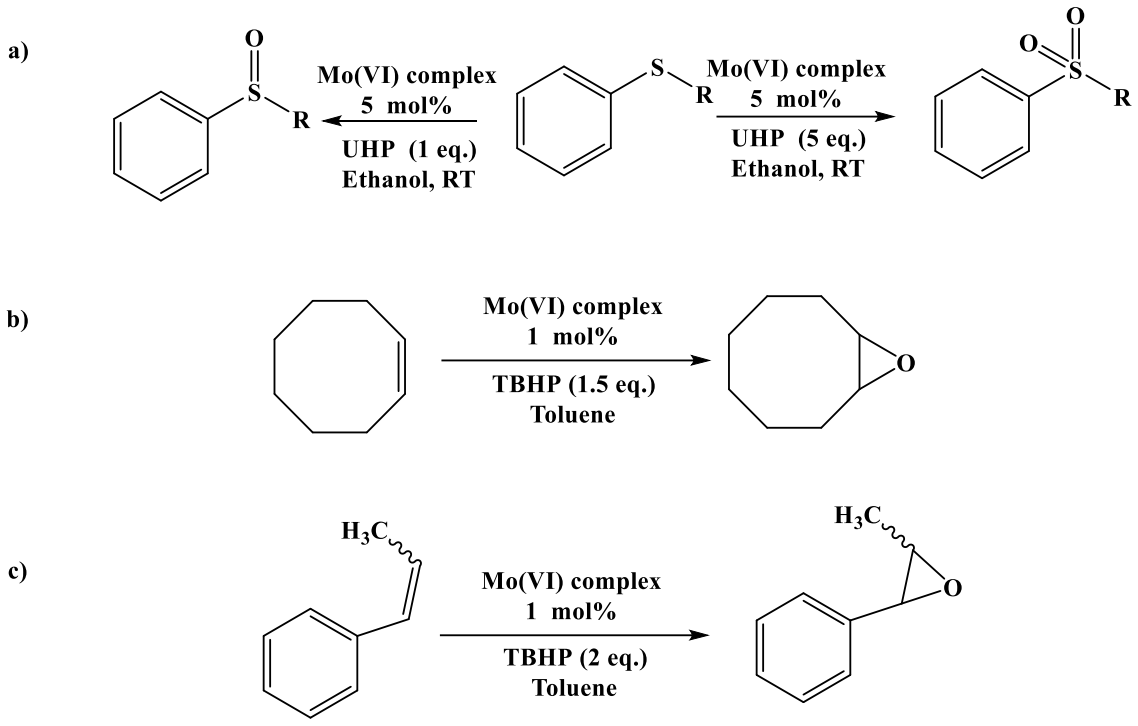

Scheme 1.5 *Oxidation reactions of a) sulfides into sulfoxide and sulfone b) epoxidation of cyclooctene and c) epoxidation of methyl styrene using Mo(VI) complex*

Zhao et al. have reported the oxidation of *cis* and *trans* methyl styrenes as well as cyclooctene to their corresponding epoxides using the Mo(VI) complex of **L1** as catalyst (*Scheme 1.5b*).[166] The catalytic procedure requires mild reaction conditions along with only 1 mol% molybdenum complex and 1.5 equivalent of TBHP, which act as an oxidant. Oxidation of *cis*-methyl styrenes shows better stereoselectivity with 30% enantiomeric excesses (ee) compared to their *trans*-derivatives (12% ee). Baig et al., have reported the synthesis of bis(indolyl)methanes using the same glycoconjugated Mo(VI) complex (5 mol%) under solvent free condition (*Scheme 1.6a*).[167] Recently, glycoconjugated Yb(III) complex (1 mol%) was used in catalysing the Biginelli reaction under solvent free condition (*Scheme 1.6b*).[166] Reaction was performed at 90 °C with good to excellent yields (73-96%) in approximately one hour and the stability of catalyst was established by five times recycling process.

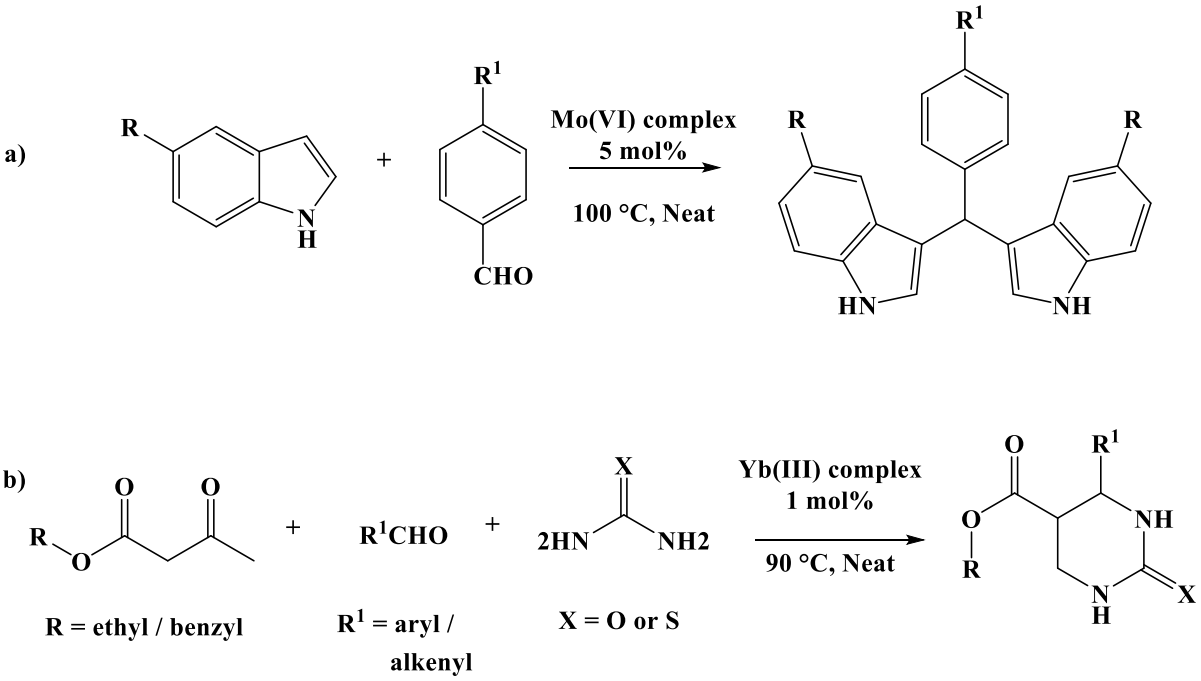

Scheme 1.6 *a) Synthesis of bis(indolyl)methanes using Mo(VI) complex and b) Yb(III) complex catalyzed Biginelli reaction*

Dinuclear copper complex of **L1** has been used as catalyst in selective oxidation of primary and secondary alcohols into corresponding carbonyl compounds (*Scheme 1.7a*).[168] The presence of TEMPO in 1-butyl-3-methyl-3H-imidazol-1-iumtetrafluoroborate (ionic liquid) is required for oxidation reaction and afforded good to excellent yields (65-82%). This complex has also been used as catalyst in arial oxidation of 3,5- di-*tert*-butylcatechol to 3,5-di-*tert*-butyl-*o*-quinone in DMSO-MeOH (mixed solvent) (*Scheme 1.7b*). The arial oxidation of primary and secondary alcohols to corresponding carbonyl compounds was also catalyzed by adduct of cupric acetate and *N*-(2-hydroxybenzoyl)-L-alanyl-4,6-*O*-ethylidene-β-D-glucopyranosylamine (L-DA) (*Scheme 1.7a*).[89]

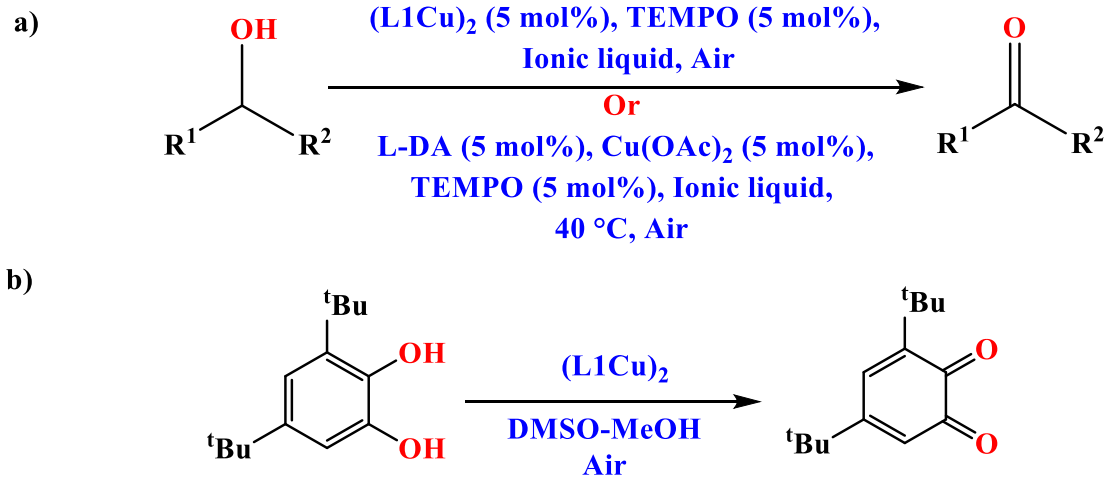

Scheme 1.7 *Application of Cu(II) complexes as catalysts in oxidation reaction*

1.5.3 Glycoconjugated metal complexes in asymmetric synthesis

Since last few decades, the carbohydrate derived chiral ligands have gained significant importance in the field of metal-catalyzed stereoselective reactions. Boysen and co-workers have introduced two D-glucosamine derived ligands containing bis(oxazoline) (*gluco*BOX) and pyridine bis(oxazoline) (*gluco*PyBOX) to replace conventional BOX and PyBOX ligands (*Fig. 1.24*).[169-170] The copper(I) complex of *gluco*BOX gave high enantioselectivity in cyclopropanation of alkenes. During the cyclopropanation of olefins, the yield reached a value of 60–85% with a very good *cis-trans* ratio (above 70%.). On the other hand, the copper(I) complex of *gluco*PyBOX was used in asymmetric synthesis of propargylamines (99% ee).

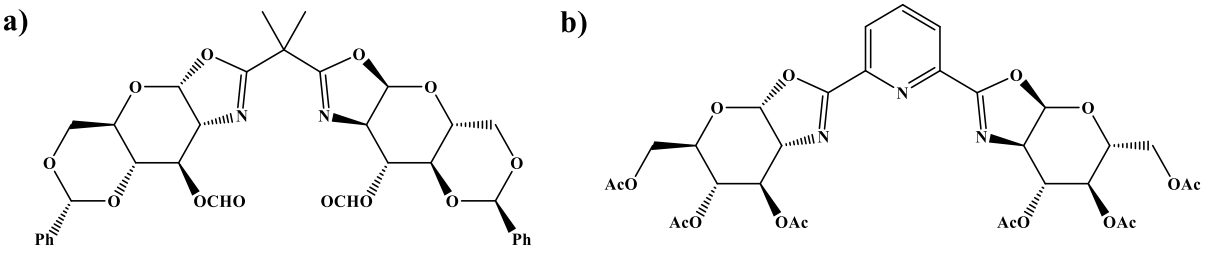

Fig. 1.25 *Glucose derived a) glucoBOX and b) glucoPyBOX ligand*

Ziegler and co-worker have reported a series of thirty carbohydrate derived bi- and tridentate ligands containing triazole- and pyridine moieties.[171] The *in-situ* addition of copper(I)triflate to the reaction mixture containing phenylacetylene, *N*-benzylideneaniline and 10 mol% of triazole containing ligands afforded chiral *N*-(1,3-diphenylprop-2-yn-1-yl)aniline (*Scheme 1.8*). For a comparative evaluation, achiral ligand with similar binding sites were also tested under identical reaction conditions.

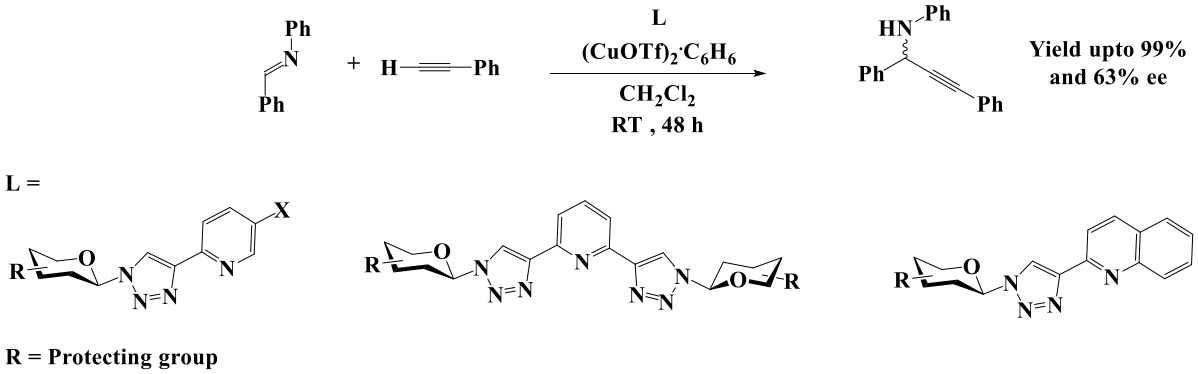

Scheme 1.8 *Synthesis of N-(1,3-diphenylprop-2-yn-1-yl)aniline using glycoconjugated copper(I) complex*

Using D-mannitol, two versions of DUPHOS type ligands, commonly known as ROPHOS and BASPHOS have been introduced by Börner and co-workers (*Fig. 1.25*).[172-173] These types of ligands have additional hemilabile coordinating abilities and also provide secondary interaction sites to substrates. Rhodium complex of such ligands have been used for stereoselective hydrogenation of functionalised alkenes like dehydroamino acids, acetamidocinnamic or itaconic acids and their esters.

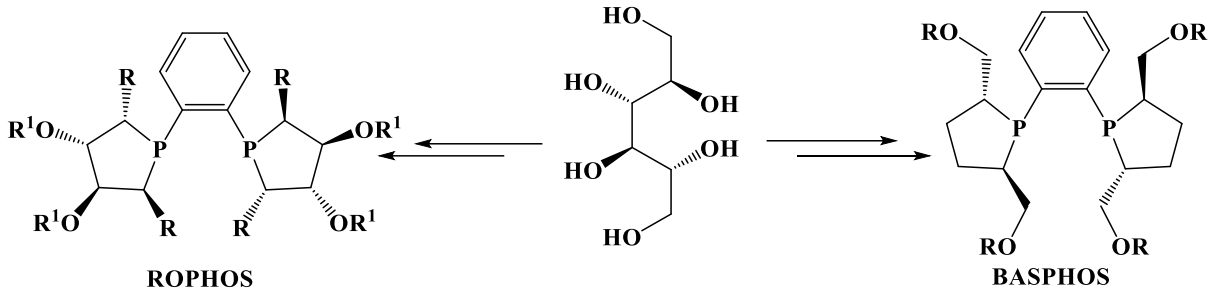

Fig. 1.25 *Structure of* D*-mannitol, ROPHOS and BASPHOS*

1.6 Scope of present thesis

This thesis includes the synthesis, characterization, structural optimization and application of D-glucose derived glycoconjugates. Conversion of D-glucose to 4,6-*O*-ethylidene-β-D-glycosylamine requires the following two steps-

(1) protecting 4- and 6-hydroxy groups of D-glucose using paraldehyde and

(2) replacement of anomeric hydroxy group (C1-OH) with an amine group using ammonia

- A series of glycoconjugates containing amino acid and naphthaldimine moieties have been prepared in two stages. Firstly, 4,6-*O*-ethylidene-β-D-glycosylamine has been condensed with Fmoc protected non-polar amino acids via amide linkages followed by deprotection of Fmoc group to afford corresponding glycopeptide. The resultant glycopeptides has been further condensed with 2-hydroxy-1-naphthaldehyde to form an imine bonded final compound. Structural details of one of the resultant molecules has been studied in details via structural optimization and the results were compared with the crystal data.
- Amino acid sensing abilities through hydrogen bonding of synthesized compounds have been explored.

- Interactions of *N*-(2-hydroxynapthylidene)-L-leucienyl-4,6-*O*-ethylidene-β-D-glucopyranosylamine with transition metal ions have been investigated at three different pH conditions. Further, Cu-complex of *N*-(2-hydroxynapthylidene)-L-leucienyl-4,6-*O*-ethylidene-β-D-glucopyranosylamine has been used in catalytic synthesis of imidazo[1,2-*a*]pyridines.
- An amphiphilic glycoconjugate has been synthesized by condensation of 4,6-*O*-ethylidene-β-D-glycosylamine and 2-hydroxy-4-octyloxy-benzaldehyde. 4,6-*O*-Ethylidene-*N*-(2-hydroxy-4-(octyloxy)benzylidene)-β-D-glucopyranosylamine has been reacted with copper(II) acetate to yield corresponding copper(II) complex, which has been further used in stereoselective synthesis of propargylamines.

References:

1. Lemieux, R.; Lineback, D., Chemistry of the carbohydrates. *Annual Review of Biochemistry* 1963, *32*, 155-184.

2. Handa, N., Carbohydrate metabolism in the marine diatom skeletonema costatum. *Marine Biology* 1969, *4*, 208-214.

3. Tester, R. F.; Debon, S. J., Annealing of starch—a review. *International Journal of Biological Macromolecules* 2000, *27*, 1-12.

4. Allen, H. J.; Kisailus, E. C., *Glycoconjugates: Composition: Structure, and Function*. CRC Press: 1992.

5. Hölemann, A.; Seeberger, P. H., Carbohydrate diversity: synthesis of glycoconjugates and complex carbohydrates. *Current Opinion in Biotechnology* 2004, *15*, 615-622.

6. Crick, F. H. In *On Protein Synthesis*, Symp Soc Exp Biol, 1958; p 8.

7. Lodish, H.; Berk, A.; Zipursky, S. L.; Matsudaira, P.; Baltimore, D.; Darnell, J., Protein glycosylation in the ER and Golgi complex. In *Molecular Cell Biology. 4th edition*, WH Freeman: 2000.

8. Sheen, J.; Zhou, L.; Jang, J.-C., Sugars as signaling molecules. *Current Opinion in Plant Biology* 1999, *2*, 410-418.

9. Albelda, S. M.; Buck, C. A., Integrins and other cell adhesion molecules. *The FASEB Journal* 1990, *4*, 2868-2880.

10. Miller, D. J.; Ax, R. L., Carbohydrates and fertilization in animals. *Molecular Reproduction and Development* 1990, *26*, 184-198.

11. Cobb, B. A.; Kasper, D. L., Coming of age: carbohydrates and immunity. *European Journal of Immunology* 2005, *35*, 352-356.

12. Gwóźdź, M.; Regulska, B.; Ilow, R. I., Dietary carbohydrates in the prevention and treatment of metabolic diseases. *Advances in Clinical and Experimental Medicine* 2007, *16*, 577-588.

13. Bruin, T.; Sturk, A.; Ten Cate, J. W.; Cath, M., The function of the human factor V carbohydrate moiety in blood coagulation. *European Journal of Biochemistry* 1987, *170*, 305-310.

14. Dutcher, J. D., Chemistry of the amino sugars derived from antibiotic substances. *Advances in Carbohydrate Chemistry* 1963, *18*, 259-308.

15. Brode, G. L., Polysaccharides:“Naturals” for cosmetics ad pharmaceuticals. In *Cosmetic and Pharmaceutical Applications of Polymers*, Springer: 1991; pp 105-115.

16. Adams, J., Application of complex carbohydrates in the food industry. *Dietary Fiber in Health and Disease* 1997, 69-78.

17. De Wit, D.; Maat, L.; Kieboom, A., Carbohydrates as industrial raw materials. *Industrial Crops and Products* 1993, *2*, 1-12.

18. Lichtenthaler, F. W.; Peters, S., Carbohydrates as green raw materials for the chemical industry. *Comptes Rendus Chimie* 2004, *7*, 65-90.

19. Chatterjee, C.; Pong, F.; Sen, A., Chemical conversion pathways for carbohydrates. *Green Chemistry* 2015, *17*, 40-71.

20. Tsukise, A.; Yamada, K., The histochemistry of complex carbohydrates in the scrotum of the boar. *Histochemistry* 1981, *72*, 511-521.

21. Hibbert, H.; Timm, J. A., Studies on the reactions relating to carbohydrates and polysaccharides x. Synthesis and relative stability of cyclic acetals from 1, 2-and 1, 3-glycols. *Journal of the American Chemical Society* 1924, *46*, 1283-1290.

22. Spiro, R. G., Protein glycosylation: nature, distribution, enzymatic formation, and disease implications of glycopeptide bonds. *Glycobiology* 2002, *12*, 43R-56R.

23. Gamblin, D. P.; Scanlan, E. M.; Davis, B. G., Glycoprotein synthesis: an update. *Chemical Reviews* 2009, *109*, 131-163.

24. Kan, C.; Danishefsky, S. J., Recent departures in the synthesis of peptides and glycopeptides. *Tetrahedron* 2009, *65*, 9047.

25. Larkin, A.; Imperiali, B., The expanding horizons of asparagine-linked glycosylation. *Biochemistry* 2011, *50*, 4411-4426.

26. Roy, B.; Depaix, A.; Périgaud, C.; Peyrottes, S., Recent trends in nucleotide synthesis. *Chemical Reviews* 2016, *116*, 7854-7897.

27. Snipes, C. E.; Duebelbeis, D. O.; Olson, M.; Hahn, D. R.; Dent Iii, W. H.; Gilbert, J. R.; Werk, T. L.; Davis, G. E.; Lee-Lu, R.; Graupner, P. R., The ansacarbamitocins: polar ansamitocin derivatives. *Journal of Natural Products* 2007, *70*, 1578-1581.

28. Takeda, U.; Okada, T.; Takagi, M.; Gomi, S.; Itoh, J.; Sezaki, M.; Ito, M.; Miyadoh, S.; Shomura, T., SF2446, new benzo[a]naphthacene quinone antibiotics. I. Taxonomy and fermentation of the producing strain, isolation and characterization of antibiotics *The Journal of Antibiotics* 1988, *41*, 417-424.

29. Gomi, S.; Sasaki, T.; Itoh, J.; Sezaki, M., SF2446, new benzo[a]naphthacene quinone antibiotics. II. The structural elucidation. *The Journal of Antibiotics* 1988, *41*, 425-432.

30. Link, J.; Raghavan, S.; Gallant, M.; Danishefsky, S. J.; Chou, T.; Ballas, L. M., Staurosporine and ent-Staurosporine: The first total syntheses, prospects for a regioselective approach, and activity profiles1. *Journal of the American Chemical Society* 1996, *118*, 2825-2842.

31. Belmokhtar, C. A.; Hillion, J.; Ségal-Bendirdjian, E., Staurosporine induces apoptosis through both caspase-dependent and caspase-independent mechanisms. *Oncogene* 2001, *20*, 3354-3362.

32. Antonsson, A.; Persson, J. L., Induction of apoptosis by staurosporine involves the inhibition of expression of the major cell cycle proteins at the G2/M checkpoint accompanied by alterations in Erk and Akt kinase activities. *Anticancer Research* 2009, *29*, 2893-2898.

33. Maskey, R. P.; Grün-Wollny, I.; Fiebig, H. H.; Laatsch, H., Akashins A, B, and C: novel chlorinated indigoglycosides from Streptomyces sp. GW 48/1497. *Angewandte Chemie International Edition* 2002, *41*, 597-599.

34. Barbosa, F.; Pinto, E.; Kijjoa, A.; Pinto, M.; Sousa, E., Targeting antimicrobial drug resistance with marine natural products. *International Journal of Antimicrobial Agents* 2020, *56*, 106005.

35. Lingome, C. E.; Pourceau, G.; Gobert-Deveaux, V.; Wadouachi, A., Efficient synthesis of glycosylamines in solventless conditions promoted by mechanical milling. *RSC Advances* 2014, *4*, 36350-36356.

36. Campa, C.; Donati, I.; Vetere, A.; Gamini, A.; Paoletti, S., Synthesis of glycosylamines: identification and quantification of side products. *Journal of Carbohydrate Chemistry* 2001, *20*, 263-273.

37. Yano, S.; Mikata, Y., Recent progress of functional glycoconjugated metal complexes. *Bulletin of the Chemical Society of Japan* 2002, *75*, 2097-2113.

38. Mitra, A., *C 1-And C 2-based glycoconjugates: synthesis, characterization, ion and molecular recognition studies*. Indian Institute of Technology, Bombay (India), 2010.

39. Madduluri, V. K.; Sah, A. K., Metal complexes of 4, 6-*O*-ethylidene-β-D-glucopyranosylamine derivatives and their application in organic synthesis. *Carbohydrate Research* 2019, *485*, 107798.

40. Schiff, H., Untersuchungen über salicinderivate. *Justus Liebigs Annalen der Chemie* 1870, *154*, 1-39.

41. Schiff, H., Eine neue reihe organischer diamine. *Justus Liebigs Annalen der Chemie* 1866, *140*, 92-137.

42. Sorokin, B., Ueber anilide der glycose. *Berichte der deutschen chemischen Gesellschaft* 1886, *19*, 513-513.

43. Hodge, J. E., The amadori rearrangement. In *Advances in carbohydrate chemistry*, Elsevier: 1955; Vol. 10, pp 169-205.

44. Sorokin, B., 1. Die anilide und toluide der glycosen. *Journal für Praktische Chemie* 1888, *37*, 291-317.

45. Györgydeák, Z.; Thiem, J., Synthesis and transformation of glycosyl azides. *Advances in Carbohydrate Chemistry and Biochemistry* 2006, *60*, 103-182.

46. Shaban, M. A. E.-M.; Jeanloz, R. W., The synthesis of antigenic glycopeptides, 2-acetamido-*N*-(β-L-aspartyl)-2-deoxy-4-*O*-β-(D-galactopyranosyl)-β-D-glucopyranosylamine.(*N*-Acetyllactosaminyl-L-asparagine). *Bulletin of the Chemical Society of Japan* 1981, *54*, 3570-3576.

47. Cudic, M.; Burstein, G. D., Preparation of glycosylated amino acids suitable for Fmoc solid-phase assembly. In *Peptide-Based Drug Design*, Springer: 2008; pp 187-208.

48. Kunz, H.; Unverzagt, C., Protecting-group-dependent stability of intersaccharide bonds—synthesis of a fucosyl-chitobiose glycopeptide. *Angewandte Chemie International Edition in English* 1988, *27*, 1697-1699.

49. Thiering, S.; Sowa, C. E.; Thiem, J., Stereoselective photochemical transformations of hexopyranosyl imides to highly functionalised heterocycles. *Journal of the Chemical Society, Perkin Transactions 1* 2001, 8, 801-806.

50. Shiozaki, M.; Mochizuki, T.; Hanzawa, H.; Haruyama, H., Synthesis of a tetrahydropyrano [2, 3-D] oxazole analogue of trehazolin. *Carbohydrate research* 1996, *288*, 99-108.

51. Spinola, M.; Jeanloz, R. W., The synthesis of disaccharide-L-asparagine compounds: derivatives of *N*-(L-aspart-4-oyl)-4-*O*-β-D-galactopyranosyl-β-D-glucopyranosylamine (lactosyl-L-asparagine), 2-acetamido-*N*-(L-aspart-4-oyl)-2-deoxy-4-*O*-β-D-galactopyranosyl-β-D-glucopyranosylamine (*N*-acetyllactosaminyl-L-asparagine), and 2-acetamido-*N*-(L-aspart-4-oyl)-2-deoxy-6-*O*-β-D-galactopyranosyl-β-D-glucopyranosylamine. *Carbohydrate Research* 1970, *15*, 361-369.

52. Roberge, J. Y.; Beebe, X.; Danishefsky, S. J., A strategy for a convergent synthesis of *N*-linked glycopeptides on a solid support. *Science* 1995, *269*, 202-204.

53. Karban, J.; Kroutil, J., Chemistry of carbohydrate aziridines. *Advances in Carbohydrate Chemistry and Biochemistry* 2006, *60*, 27-101.

54. Sridhar, P. R.; Prabhu, K. R.; Chandrasekaran, S., Selective reduction of anomeric azides to amines with tetrathiomolybdate: Synthesis of β-D-glycosylamines. *The Journal of Organic Chemistry* 2003, *68*, 5261-5264.

55. de Bruyn, C. L., Dérivé ammoniacal de la D-glucose. *Recueil des Travaux Chimiques des Pays-Bas* 1895, *14*, 98-105.

56. Ekstrom, H.; Adcock, W., A new iron carbide in hydrocarbon synthesis catalyst. *J. Am. Chem. Soc.* 1950, *72*, 1042-1051.

57. Kuhn, R.; Birkofer, L., Untersuchungen über *N*-Glykoside und die Amadori-Umlagerung. *Berichte der deutschen chemischen Gesellschaft (A and B Series)* 1938, *71*, 621-633.

58. Eellis, G.; Honeyman, J., Glycosylamines. In *Advances in Carbohydrate Chemistry*, Elsevier: 1955; Vol. 10, pp 95-168.

59. Likhosherstov, L. M.; Novikova, O. S.; Derevitskaja, V. A.; Kochetkov, N. K., A new simple synthesis of amino sugar β-D-glycosylamines. *Carbohydrate Research* 1986, *146*, C1-C5.

60. Lubineau, A.; Augé, J.; Drouillat, B., Improved synthesis of glycosylamines and a straightforward preparation of *N*-acylglycosylamines as carbohydrate-based detergents. *Carbohydrate Research* 1995, *266*, 211-219.

61. Likhosherstov, a. L.; Novikova, O.; Shibaev, V. In *New efficient synthesis of β-glucosylamines of mono-and disaccharides with the use of ammonium carbamate*, Doklady Chemistry, Springer: 2002; pp 89-92.

62. Likhosherstov, L.; Novikova, O.; Shibaev, V. In *New synthesis of β-glycosylamines of D-mannose, 2-and 6-deoxysugars, and D-glucuronic acid with the use of ammonium carbamate*, Doklady Chemistry, Springer: 2003; pp 73-76.

63. Likhosherstov, L.; Novikova, O.; Zheltova, A.; Shibaev, V., An improved procedure for the synthesis of *N*-bromoacetyl-β-glycopyranosylamines, derivatives of mono-and disaccharides. *Russian Chemical Bulletin* 2004, *53*, 709-713.

64. Tang, J. S. J.; Schade, K.; Tepper, L.; Chea, S.; Ziegler, G.; Rosencrantz, R. R., Optimization of the microwave assisted glycosylamines synthesis based on a statistical design of experiments approach. *Molecules* 2020, *25*, 5121.

65. Isac-García, J.; Calvo-Flores, F. G.; Hernández-Mateo, F.; Santoyo-González, F., Synthesis of glycosylamines from glycosyl isothiocyanates and bis (tributyltin) oxide. *European Journal of Organic Chemistry* 2001, *2001*, 383-390.

66. Nicolaou, K.; Snyder, S. A.; Nalbandian, A. Z.; Longbottom, D. A., A new method for the stereoselective synthesis of α-and β-glycosylamines using the Burgess reagent. *Journal of the American Chemical Society* 2004, *126*, 6234-6235.

67. Isbell, H. S.; Frush, H. L., Mutarotation, hydrolysis, and rearrangement reactions of glycosylamines1. *The Journal of Organic Chemistry* 1958, *23*, 1309-1319.

68. Volbeda, A. G.; van der Marel, G. A.; Codée, J. D., Protecting group strategies in carbohydrate chemistry. *Protecting Groups: Strategies and Applications in Carbohydrate Chemistry* 2019, 1-27.

69. Parham, W. E.; Anderson, E., The protection of hydroxyl groups. *Journal of the American Chemical Society* 1948, *70*, 4187-4189.

70. Codee, J. D.; Ali, A.; Overkleeft, H. S.; van der Marel, G. A., Novel protecting groups in carbohydrate chemistry. *Comptes Rendus Chimie* 2011, *14*, 178-193.

71. Barker, R.; MacDonald, D., Some oxidation and reduction products of 2, 4-*O*-Ethylidene-D-erythrose1. *Journal of the American Chemical Society* 1960, *82*, 2301-2303.

72. Linek, K.; Alfoldi, J.; Durindova, M., Glycosylamines. 3. Preparation, structure, and conformation of some glycosylamines. *Chemical Papers-Chemickw Zvesti* 1993, *47*, 247-250.

73. Rajsekhar, G.; Gangadharmath, U. B.; Rao, C. P.; Guionneau, P.; Saarenketo, P. K.; Rissanen, K., Synthesis and characterization of 4, 6-*O*-butylidene-*N*-(2-hydroxybenzylidene)-β-D-glucopyranosylamine: crystal structures of 4, 6-*O*-butylidene-α-D-glucopyranose, 4, 6-*O*-butylidene-β-D-glucopyranosylamine and 4, 6-*O*-butylidene-*N*-(2-hydroxybenzylidene)-β-D-glucopyranosylamine. *Carbohydrate Research* 2002, *337*, 1477-1484.

74. Sah, A. K.; Rao, C. P.; Saarenketo, P. K.; Kolehmainen, E.; Rissanen, K., Synthesis, characterisation and crystal structures of Schiff bases from the reaction of 4, 6-*O*-ethylidene-β-D-glucopyranosylamine with substituted salicylaldehydes. *Carbohydrate Research* 2001, *335*, 33-43.

75. Sah, A. K.; Rao, C. P.; Saarenketo, P. K.; Rissanen, K., Crystal structure of 4, 6-*O*-ethylidene-*N*-(2-hydroxybenzylidene)-β-D-glucopyranosylamine. *Carbohydrate Research* 2002, *337*, 79-82.

76. Sah, A. K.; Rao, C. P.; Saarenketo, P. K.; Wegelius, E. K.; Kolehmainen, E.; Rissanen, K., First crystallographic investigation of complexes of *cis*-VO^{2+}, *cis*-MoO_2^{2+}, and *trans*-UO_2^{2+} species with Schiff-Base molecules derived from 4, 6-*O*-ethylidene-β-D-glucopyranosylamine. *European Journal of Inorganic Chemistry* 2001, *2001*, 2773-2781.

77. Rajsekhar, G.; Sah, A. K.; Rao, C. P.; Guionneau, P.; Bharathy, M.; GuruRow, T., Bis-(μ-saccharide-C-2-oxo) dinuclear Cu (II) complexes of 4, 6-*O*-butylidene/ethylidene-*N*-(α-hydroxynaphthylidene/*O*-hydroxybenzylidene/5-bromo-*O*-hydroxybenzylidene)-β-D-glucopyranosylamine: structural aspects and data correlations. *Dalton Transactions* 2003, 15, 3126-3135.

78. Ahuja, R.; Singhal, N. K.; Ramanujam, B.; Ravikumar, M.; Rao, C. P., Experimental and computational studies of the recognition of amino acids by galactosyl-imine and-amine

derivatives: An Attempt to Understand the Lectin− Carbohydrate Interactions. *The Journal of Organic Chemistry* 2007, *72*, 3430-3442.

79. Mitra, A.; Chinta, J. P.; Rao, C. P., 1-(D-Glucopyranosyl-2′-deoxy-2′-iminomethyl)-2-hydroxybenzene as chemosensor for aromatic amino acids by switch-on fluorescence. *Tetrahedron Letters* 2010, *51*, 139-142.

80. Shen, C.; Zhao, Q.; Zheng, H.; Zhang, P., Synthesis of novel Schiff bases from the reaction of 3-*O*-methyl-4, 6-*O*-benzylidene-β-D-glucopyranosylamine with substituted aldehydes. *Journal of Chemical Research* 2009, *2009*, 317-318.

81. Jarrahpour, A.; Doroodmand, M. M.; Ebrahimi, E., The first report of [2+ 2] ketene–imine cycloaddition reactions (Staudinger) on carbon nanotubes. *Tetrahedron Letters* 2012, *53*, 2797-2801.

82. Knauer, S.; Weymann, M.; Kunz, H., Stereoselective synthesis of bromopiperidinones and their conversion to annulated heterocycles. *Zeitschrift für Naturforschung B* 2009, *64*, 1639-1652.

83. Kónya, B.; Docsa, T.; Gergely, P.; Somsák, L., Synthesis of heterocyclic *N*-(β-D-glucopyranosyl) carboxamides for inhibition of glycogen phosphorylase. *Carbohydrate Research* 2012, *351*, 56-63.

84. Baig, N.; Singh, R. P.; Chander, S.; Jha, P. N.; Murugesan, S.; Sah, A. K., Synthesis, evaluation and molecular docking studies of amino acid derived *N*-glycoconjugates as antibacterial agents. *Bioorganic Chemistry* 2015, *63*, 110-115.

85. Gupta, S. J.; Dutta, S.; Gajbhiye, R. L.; Jaisankar, P.; Sen, A. K., Synthesis, in vitro evaluation and molecular docking studies of novel amide linked triazolyl glycoconjugates as new inhibitors of α-glucosidase. *Bioorganic Chemistry* 2017, *72*, 11-20.

86. Soni, K.; Sah, A. K., Alanyl glycoconjugate: a selective receptor for free and protein-bound tryptophan. *RSC Advances* 2013, *3*, 12096-12099.

87. Baig, N.; Singh, R. P.; Jha, P. N.; Sah, A. K., Synthesis of glucose-derived glycoconjugates and studies on their antimicrobial activities: mechanistic insight. *ChemistrySelect* 2016, *1*, 5281-5285.

88. Soni, K.; Sah, A. K., The synthesis of amino acid derived glycoconjugates and the investigation of their anti-inflammatory and analgesic properties. *RSC Advances* 2014, *4*, 6068-6073.

89. Sah, A. K.; Soni, K., Synthesis of cupric acetate selective receptor derived from alanyl glycoconjugate and their application in selective oxidation of benzylic alcohols. *Catalysis Communications* 2012, *28*, 120-123.

90. Shahrokhian, S., Lead phthalocyanine as a selective carrier for preparation of a cysteine-selective electrode. *Analytical Chemistry* 2001, *73*, 5972-5978.

91. Vardanega, D.; Girardet, C., Nonlinear polarization effects in superchiral nanotube sensors of amino acids. *Chemical Physics Letters* 2009, *469*, 172-176.

92. Wang, J.; Chatrathi, M. P.; Tian, B., Micromachined separation chips with a precolumn reactor and end-column electrochemical detector. *Analytical chemistry* 2000, *72*, 5774-5778.

93. Lee, C.-S.; Teng, P.-F.; Wong, W.-L.; Kwong, H.-L.; Chan, A. S., New C2-symmetric 2, 2′-bipyridine crown macrocycles for enantioselective recognition of amino acid derivatives. *Tetrahedron* 2005, *61*, 7924-7930.

94. Kennedy, J. F.; White, C. A., *Bioactive Carbohydrates: in Chemistry, Biochemistry and Biology*. Ellis Horwood Ltd.: 1983.

95. Fernández-Alonso, M. d. C.; Cañada, F. J.; Jiménez-Barbero, J.; Cuevas, G., Molecular recognition of saccharides by proteins. Insights on the origin of the carbohydrate-aromatic interactions. *Journal of the American Chemical Society* 2005, *127*, 7379-7386.

96. Sharma, R.; McNamara, J. P.; Raju, R. K.; Vincent, M. A.; Hillier, I. H.; Morgado, C. A., The interaction of carbohydrates and amino acids with aromatic systems studied by density functional and semi-empirical molecular orbital calculations with dispersion corrections. *Physical Chemistry Chemical Physics* 2008, *10*, 2767-2774.

97. Hudson, K. L.; Bartlett, G. J.; Diehl, R. C.; Agirre, J.; Gallagher, T.; Kiessling, L. L.; Woolfson, D. N., Carbohydrate–aromatic interactions in proteins. *Journal of the American Chemical Society* 2015, *137*, 15152-15160.

98. Spiwok, V., CH/π interactions in carbohydrate recognition. *Molecules* 2017, *22*, 1038.

99. Berg, J. M., *Principles of bioinorganic chemistry*. University Science Books: 1994.

100. Rendleman Jr, J., Complexes of alkali metals and alkaline-earth metals with carbohydrates. In *Advances in Carbohydrate Chemistry*, Elsevier: 1967; Vol. 21, pp 209-271.

101. Angyal, S.; Davies, K., Complexing of sugars with metal ions. *Journal of the Chemical Society D: Chemical Communications* 1971, 10, 500-501.

102. Angyal, S., Complex formation between sugars and metal ions. In *Carbohydrate Chemistry–VI*, Elsevier: 1973; 131-146.

103. Angyal, S., Haworth memorial lecture. Sugar–cation complexes—structure and applications. *Chemical Society Reviews* 1980, *9*, 415-428.

104. Angyal, S. J., Complexes of metal cations with carbohydrates in solution. In *Advances in Carbohydrate Chemistry and Biochemistry*, Elsevier: 1989; Vol. 47, 1-43.

105. Angyal, S. J., Complexing of carbohydrates with copper ions: a reappraisal. *Carbohydrate Research* 1990, *200*, 181-188.

106. Tajmir-Riahi, H.-A., Sugar complexes with calcium ion: infrared spectra of crystalline D-glucuronic acid and its calcium complexes. *Carbohydrate Research* 1983, *122* (2), 241-248.

107. Tajmir-Riahi, H.-A., Infrared spectra of crystalline β-D-glucuronic acid and its Na^+, K^+, and Rb^+ salts. *Carbohydrate Research* 1984, *125*, 13-20.

108. Tajmir-Riahi, H.-A., Infrared spectra of crystalline L-arabinose and two of its calcium complexes. *Carbohydrate Research* 1984, *127*, 1-8.

109. Tajmir-Riahi, H.-A., Sugar interaction with calcium ion. Synthesis and vibrational spectra of crystalline β-D-fructose and its calcium halide adducts. *Journal of Inorganic Biochemistry* 1986, *27*, 123-131.

110. Tajmir-Riahi, H., Sugar complexation with uranium ion. Synthesis, spectroscopic and structural analysis of UO_2-fructose adducts. *Inorganica Chimica Acta* 1987, *135*, 67-72.

111. Tajmir-Riahi, H.-A., Interaction of D-glucose with alkaline-earth metal ions. Synthesis, spectroscopic, and structural characterization of Mg (II)-and Ca (II)-D-glucose adducts and the

effect of metal-ion binding on anomeric configuration of the sugar. *Carbohydrate Research* 1988, *183*, 35-46.

112. Tajmir-Riahi, H., Carbohydrate complexes with alkaline earth metal ions. Interaction of D-glucono-1, 5-lactone with the Mg (II), Ca (II), Sr (II), and Ba (II) cations in the crystalline solid and aqueous Solution. *Journal of Inorganic Biochemistry* 1990, *39*, 33-41.

113. Oertling, H., Interactions of alkali-and alkaline earth-halides with carbohydrates in the crystalline state–the overlooked salt and sugar cocrystals. *CrystEngComm* 2016, *18*, 1676-1692.

114. Bandwar, R. P.; Rao, C. P., Transition metal–saccharide chemistry and biology: An emerging field of multidisciplinary interest. *Current Science* 1997, 788-796.

115. Alekseev, Y. E.; Garnovskii, A. D.; Zhdanov, Y. A., Complexes of natural carbohydrates with metal cations. *Russian Chemical Reviews* 1998, *67*, 649-669.

116. Gyurcsik, B.; Nagy, L., Carbohydrates as ligands: coordination equilibria and structure of the metal complexes. *Coordination Chemistry Reviews* 2000, *203*, 81-149.

117. Whitfield, D. M.; Stojkovski, S.; Sarkar, B., Metal coordination to carbohydrates. Structures and function. *Coordination Chemistry Reviews* 1993, *122*, 171-225.

118. Piarulli, U.; Floriani, C., Assembling sugars and metals: novel architectures and reactivities in transition metal chemistry. *Progress in Inorganic Chemistry* 1997, *45*, 393-430.

119. Yano, S., Coordination compounds containings sugars and their derivatives. *Coordination Chemistry Reviews* 1988, *92*, 113-156.

120. Rajsekhar, G.; Rao, C. P.; Nättinen, K.; Rissanen, K., Unusual interaction extended between the pyranose ring oxygen and Zn (II) center in the complexes derived from 4, 6-*O*-butylidene/ethylidene-*N*-(α-hydroxynaphthylidene/*O*-hydroxybenzylidene)-β-D-glucopyranosylamine: Evidence for a pseudo-bicapped tetrahedral complex of Zn (II) based on the crystal structure. *Inorganic Chemistry Communications* 2003, *6*, 1156-1160.

121. Diéguez, M.; Pàmies, O.; Claver, C., Ligands derived from carbohydrates for asymmetric catalysis. *Chemical Reviews* 2004, *104*, 3189-3216.

122. Benessere, V.; Del Litto, R.; De Roma, A.; Ruffo, F., Carbohydrates as building blocks of privileged ligands. *Coordination Chemistry Reviews* 2010, *254*, 390-401.

123. Mokhtari, B.; Pourabdollah, K.; Dalali, N., Molecule and ion recognition of nano-baskets of calixarenes since 2005. *Journal of Coordination Chemistry* 2011, *64*, 743-794.

124. Steinborn, D.; Junicke, H., Carbohydrate complexes of platinum-group metals. *Chemical Reviews* 2000, *100*, 4283-4318.

125. Böge, M.; Fowelin, C.; Bednarski, P.; Heck, J. r., Diaminohexopyranosides as ligands in half-sandwich ruthenium (II), rhodium (III), and iridium (III) complexes. *Organometallics* 2015, *34*, 1507-1521.

126. Dumas, C.; Petrig, J.; Frei, L.; Spingler, B.; Schibli, R., Functionalization of glucose at position C-3 for transition metal coordination: organo-rhenium complexes with carbohydrate skeletons. *Bioconjugate Chemistry* 2005, *16*, 421-428.

127. Sreeshailam, A.; Dayaker, G.; Chevallier, F.; Roisnel, T.; Krishna, P. R.; Mongin, F., Diastereoselective deprotonative metalation of sugar-derived ferrocene esters using mixed lithium–cadmium combinations. Wiley Online Library: 2011.

128. Sreeshailam, A.; Dayaker, G.; Ramana, D. V.; Chevallier, F.; Roisnel, T.; Komagawa, S.; Takita, R.; Uchiyama, M.; Krishna, P. R.; Mongin, F., Synthesis of both enantiomers of ferrocene [1, 2-c] 1H-quinoline-2-one by diastereoselective de proto-zincation of sugar-derived ferrocene esters. *RSC Advances* 2012, *2*, 7030-7032.

129. Cucciolito, M. E.; Trinchillo, M.; Iannitti, R.; Palumbo, R.; Tesauro, D.; Tuzi, A.; Ruffo, F.; D'Amora, A., Sugar-incorporated N-heterocyclic-carbene-containing gold (I) complexes: synthesis, characterization, and cytotoxic evaluation. *European Journal of Inorganic Chemistry* 2017, *2017*, 4955-4961.

130. Tsuji, T.; Kuwamura, N.; Yoshinari, N.; Konno, T., Synthesis and coordination behavior of a bipyridine platinum (II) complex with thioglucose. *Inorganic Chemistry* 2013, *52*, 5350-5358.

131. Zhao, W.; Ferro, V.; Baker, M. V., Carbohydrate–*N*-heterocyclic carbene metal complexes: Synthesis, catalysis and biological studies. *Coordination Chemistry Reviews* 2017, *339*, 1-16.

132. Hinckley, C.; Ostenburg, P.; Roth, W., Osmium carbohydrate polymers. *Polyhedron* 1982, *1*, 335-338.

133. Hinckley, C.; Bemiller, J.; Strack, L.; Russell, L., Osmium carbohydrate polymers as potential antiarthritic drugs. ACS Publications: 1983.

134. Zasukhina, G.; Chopikashvili, L.; Bobyleva, L.; Alekhina, N.; Vasil'Eva, I.; L'vova, G., Ascorbic acid reduces mutational transformations in workers exposed to heavy metals. *Doklady Akademii Nauk SSSR* 1991, *316*, 739-743.

135. Barker, S. A.; Somers, P. J.; Stevenson, J., Redissolvable ferric-D-fructose and ferric-D-glucose-D-fructose complexes. *Carbohydrate Research* 1974, *36*, 331-337.

136. Kohn, R., Binding of toxic cations to pectin, its oligomeric fragments and plant tissues. *Carbohydrate Polymers* 1982, *2*, 273-275.

137. Hartinger, C. G.; Nazarov, A. A.; Ashraf, S. M.; Dyson, P. J.; Keppler, B. K., Carbohydrate-metal complexes and their potential as anticancer agents. *Current Medicinal Chemistry* 2008, *15*, 2574-2591.

138. Gottschaldt, M.; Schubert, U. S., Prospects of metal complexes peripherally substituted with sugars in biomedicinal applications. *Chemistry–A European Journal* 2009, *15*, 1548-1557.

139. Mikata, Y.; Yano, S., Development of sugar-based materials for biological devices. *Current Topics in Medicinal Chemistry* 2012, *12*, 145-157.

140. Lo, K. K.-W., Luminescent rhenium (I) and iridium (III) polypyridine complexes as biological probes, imaging reagents, and photocytotoxic agents. *Accounts of chemical research* 2015, *48*, 2985-2995.

141. Hanack, M.; Crucius, G.; JF Calvete, M.; Ziegler, T., Glycosylated metal phthalocyanines. *Current Organic Synthesis* 2014, *11*, 59-66.

142. Florindo, P. R.; Pereira, D. M.; Borralho, P. M.; Rodrigues, C. M.; Piedade, M.; Fernandes, A. C., Cyclopentadienyl–ruthenium (II) and iron (II) organometallic compounds with carbohydrate derivative ligands as good colorectal anticancer agents. *Journal of Medicinal Chemistry* 2015, *58*, 4339-4347.

143. Mikata, Y.; Gottschaldt, M., Metal complexes of carbohydratetargeted ligands in medicinal inorganic chemistry. *Ligand Design in Medicinal Inorganic Chemistry, John Wiley & Sons Ltd., Chichester* 2014.

144. Finkelstein, A.; Walz, D.; Batista, V.; Mizraji, M.; Roisman, F.; Misher, A., Auranofin. New oral gold compound for treatment of rheumatoid arthritis. *Annals of the rheumatic diseases* 1976, *35*, 251-257.

145. Cullen, W. R., Asymmetric hydrogenation catalyzed by diphosphiniti rhodium complex derived from a sugar. *Tetrahedron Letters*, 1978, 19,1635-1636

146. Riediker, M.; Duthaler, R. O., Enantioselective allylation of carbonyl compounds with titanium-carbohydrate complexes. *Angewandte Chemie International Edition in English* 1989, *28*, 494-495.

147. Duthaler, R. O.; Herold, P.; Lottenbach, W.; Oertle, K.; Riediker, M., Enantioselective aldol reaction of tert-butyl acetate using titanium-carbohydrate complexes. *Angewandte Chemie International Edition in English* 1989, *28*, 495-497.

148. Bold, G.; Duthaler, R. O.; Riediker, M., Enantioselective synthesis of D-threo-β-hydroxy-α-amino acids with titanium-carbohydrate complexes. *Angewandte Chemie International Edition in English* 1989, *28*, 497-498.

149. Riediker, M.; Hafner, A.; Piantini, U.; Rihs, G.; Togni, A., Structure of chloro (cyclopentadienyl) bis (1,2,5,6-di-*O*-isopropylidene-α-D-glucofuranos-3-*O*-yl) titanate, a novel titanium-carbohydrate complex. *Angewandte Chemie International Edition in English* 1989, *28*, 499-500.

150. Kitaev, P.; Zeysing, D.; Heck, J., Monosaccharide ligands in organotitanium and organozirconium chemistry. *Activating Unreactive Substrates: The Role of Secondary Interactions* 2009, 147-164.

151. Zamojski, A.; Jarosz, S., Iron complexes in carbohydrate chemistry. *Current Organic Chemistry* 2003, *7*, 1-12.

152. Kraft, J.; Mill, K.; Ziegler, T., Sugar-annulated oxazoline ligands: a novel Pd (II) Complex and its application in allylic substitution. *Molecules* 2016, *21*, 1704.

153. Diéguez, M.; Pàmies, O.; Ruiz, A.; Díaz, Y.; Castillón, S.; Claver, C., Carbohydrate derivative ligands in asymmetric catalysis. *Coordination Chemistry Reviews* 2004, *248*, 2165-2192.

154. Annunziata, A.; Cucciolito, M. E.; Imbimbo, P.; Silipo, A.; Ruffo, F., A hydrophilic olefin Pt (0) complex containing a glucoconjugated 2-iminopyridine ligand: Synthesis, characterization, stereochemistry and biological activity. *Inorganica Chimica Acta* 2021, *516*, 120092.

155. Sah, A. K.; Rao, C. P.; Saarenketo, P. K.; Wegelius, E. K.; Rissanen, K.; Kolehmainen, E., *N*-Glycosylamines of 4, 6-*O*-ethylidene-α-D-glucopyranose: synthesis, characterisation and structure of CO_2H, Cl and F ortho-substituted phenyl derivatives and metal ion complexes of the CO_2H derivative. *Journal of the Chemical Society, Dalton Transactions* 2000, 20, 3681-3687.

156. Sah, A. K.; Baig, N., Synthesis and characterization of glucose derived dioxo-molybdenum (VI) complexes and their application in sulphide oxidation. *Catalysis Letters* 2015, *145*, 905-909.

157. Sah, A. K.; Rao, C. P.; Saarenketo, P. K.; Rissanen, K., Structure of the First Tetranuclear Ni (II) complex derived from *N*-(2-hydroxybenzylidene)-4, 6-*O*-ethylidene-β-D-glucopyranosylamine. *Chemistry Letters* 2001, *30*, 1296-1297.

158. Sah, A. K.; Rao, C. P.; Saarenketo, P. K.; Rissanen, K.; Albada, G. v.; Reedijk, J., Dinuclear copper complexes of *N*-(2-hydroxybenzylidene or 5-bromo-2-hydroxybenzylidene)-4, 6-*O*-ethylidene-β-D-glucopyranosylamine: coordination variation and structural diversity. *Chemistry Letters* 2002, *31*, 348-349.

159. Sah, A. K.; Rao, C. P.; Wegelius, E. K.; Kolehmainen, E.; Rissanen, K., Synthesis, characterization and the first crystal structure of the Zn (II) complex of 4, 6-*O*-ethylidine-*N*-(2-hydroxybenzylidene)-β-D-glucopyranosylamine. *Carbohydrate Research* 2001, *336*, 249-255.

160. Nagarajan, S.; Kumbhar, A.; Varghese, B.; Das, T. M., Structural and DNA cleavage of sugar-derived Schiff base ligands and their dinuclear Cu (II) complexes. *Carbohydrate Research* 2010, *345*, 1077-1083.

161. Sah, A. K.; Kato, M.; Tanase, T., Trinuclear coordinatively labile Cu (II) complex of 4, 6-*O*-ethylidene-β-D-glucopyranosylamine derived Schiff base ligand and its reactivity towards primary alcohols and amines. *Chemical Communications* 2005, 5, 675-677.

162. Sah, A. K.; Tanase, T.; Mikuriya, M., Tri-and tetranuclear copper (II) complexes consisting of mononuclear Cu (II) chiral building blocks with a sugar-derived Schiff's base ligand. *Inorganic Chemistry* 2006, *45*, 2083-2092.

163. Sah, A. K.; Tanase, T., Crystal-to-crystal transformation from tri-to mononuclear Cu (II) complex with a sugar-derived ligand via proton transfer reaction and rearrangement of hydrogen bonding networks. *Chemical Communications* 2005, 48, 5980-5981.

164. Sah, A. K.; Tanase, T., Amine mediated proton transfer reaction and C–Cl bond activation of solvent chloroform by a trinuclear copper (II) complex of a glucopyranosylamine derived ligand. *Dalton Transactions* 2006, 31, 3742-3751.

165. Madduluri, V. K.; Mishra, S. K.; Sah, A. K., Synthesis and catalytic application of D-glucose derived ytterbium (III) complex in Biginelli reaction. *Inorganic Chemistry Communications* 2020, *120*, 108165.

166. Zhao, J.; Zhou, X.; Santos, A. M.; Herdtweck, E.; Romão, C. C.; Kühn, F. E., Molybdenum (VI) cis-dioxo complexes bearing sugar derived chiral Schiff-base ligands: synthesis, characterization, and catalytic applications. *Dalton Transactions* 2003, 19, 3736-3742.

167. Baig, N.; Shelke, G. M.; Kumar, A.; Sah, A. K., Selective synthesis of bis (indolyl) methanes under solvent free condition using glucopyranosylamine derived cis-dioxo Mo (VI) complex as an efficient catalyst. *Catalysis Letters* 2016, *146*, 333-337.

168. Soni, K.; Kumar, A.; Sah, A. K., Saccharide derived dinuclear Cu (II) complex: An efficient catalyst for oxidation of catechol and benzylic alcohols. *Catalysis Communications* 2012, *17*, 95-98.

169. Irmak, M.; Groschner, A.; Boysen, M. M., GlucoBox ligand—a new carbohydrate-based bis (oxazoline) ligand. Synthesis and first application. *Chemical communications* 2007, 2, 177-179.

170. Irmak, M.; Boysen, M. M., A new pyridyl bis (oxazoline) ligand prepared from D-glucosamine for asymmetric alkynylation of imines. *Advanced Synthesis & Catalysis* 2008, *350*, 403-405.

171. Kraft, J.; Schmollinger, D.; Maudrich, J.; Ziegler, T., Synthesis of sugar-derived triazole-and pyridine-based metal complex ligands. *Synthesis* 2015, *47*, 199-208.

172. Li, W.; Zhang, Z.; Xiao, D.; Zhang, X., Synthesis of chiral hydroxyl phospholanes from D-mannitol and their use in asymmetric catalytic reactions. *The Journal of Organic Chemistry* 2000, *65*, 3489-3496.

173. Holz, J.; Heller, D.; Stürmer, R.; Börner, A., Synthesis of the first water-soluble chiral tetrahydroxy diphosphine Rh (I) catalyst for enantioselective hydrogenation. *Tetrahedron Letters* 1999, *40*, 7059-7062

Chapter 2

Materials and Methods

Chapter 2

This chapter provides information regarding several chemicals, instruments and software used during the PhD tenure. The methodologies and experimental details for the preparation of reported molecules along with the mathematical formulas used in quantitative analysis have also been provided.

2.1 Chemicals

2.1.1 Purchased chemicals

D-Glucose, Fmoc-L-alanine, Fmoc-L-phenylalanine, Fmoc-L-leucine, Fmoc-L-isoleucine, Fmoc-L-valine, Fmoc-L-methionine, Fmoc-L-tryptophan, ethyl chloroformate (ECF), Triethylamine (TEA), L-alanine, L-arginine, L-asparagine, L-aspartic acid, L-cysteine, L-glutamic acid, L-glutamine, L-glycine, L-histidine, L-isoleucine, L-leucine, L-lysine, L-methionine, L-phenylalanine, L-proline, L-serine, L-threonine, L-tryptophan, L-tyrosine, L-valine, phenylacetylene, 1-ethynyl-4-methylbenzene, 1-ethynyl-4-fluorobenzene, 1-(*tert*-butyl)-4-ethynylbenzene, 2-aminopyridine, 5-chloro-2-aminopyridine, benzaldehyde, 3-nitrobenzaldehyde, 4-methoxybenzaldehyde, cinnamaldehyde, 4-methylbenzaldehyde, 2-chlorobenzaldehyde, 2-hydroxy-3-methoxybenzaldehyde, 1-naphthaldehyde, 2-hydroxy-1-naphthaldehyde, 4-fluorobenzaldehyde, 4-bromobenzaldehyde, 4-cyanobenzaldehyde, terephthalaldehyde, thiophene-2-carbaldehyde, furan-2-carbaldehyde, 4-bromo-2-fluorobenzaldehyde, 2,4-dihydroxybenzaldehyde, 4-chlorobenzaldehyde, 3,4-dimethoxybenzaldehyde, pyrene-1-carbaldehyde, indoline-3-carbaldehyde, piperidine, 3-methylpiperidine, 4-cyanopiperidine, 1-methylpiperazine, morpholine, pyrrolidine, 1-bromooctane, silver(I) acetate, aluminium(III) acetate, calcium(II) acetate, cadmium(II) acetate, chromium(III) acetate hydroxide, copper(II) acetate, stannous(I) acetate, iron(II) acetate, mercury(II) acetate, magnesium(II) acetate tetrahydrate, manganese(II) acetate, sodium(I) acetate, nickel(II) acetate tetrahydrate, lead(II) acetate, zinc(II) acetate, sodium

bicarbonate, potassium iodide, zinc chloride, sulfuric acid, hydrochloric acid, ethanol, methanol, dioxane, acetone, acetonitrile, dichloromethane, hexane, chloroform, ethyl acetate, dimethyl formamide, chloroform-*d*, dimethyl sulfoxide-d_6, D_2O, ammonia gas, silica gel (60-120 and 100-200 mesh), were purchased from different vendors like Sigma-Aldrich, Alfa-Aesar, Merck chemicals India, SRL, Fischer-Scientific, Spectrochem, TCI chemicals etc. The commercial solvents were purified and dried following the standard literature procedures prior to use. HPLC grade (methanol, acetonitrile, water), spectroscopy grade (methanol, dimethyl sulfoxide) and LC-MS grade solvents (methanol, acetonitrile and water) were used as received for analytical purposes with respective instruments.

2.1.2 Synthesized chemicals

Several commercially unavailable or costly chemicals were synthesized following the previously reported methods.

2.1.2.1 Synthesis of 4,6-*O*-ethylidene-β-D-glucopyranosylamine (**EGNH$_2$**)

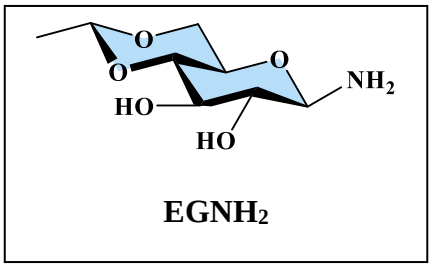

EGNH$_2$

The reaction between D-glucose with paraldehyde in presence of a catalytic amount of sulfuric acid afforded 4,6-*O*-ethylidene-D-glucopyranose (EG-OH).[1] In a two-necked round bottom flask, methanolic solution of EG-OH (15.0 g, 72 mmol) was reacted with ammonia gas in presence of $ZnCl_2$ (0.2 g, 1.5 mmol) at 0 °C. The low temperature was maintained until formation of white precipitate started, thereafter reaction mixture was stirred at room temperature for another 8 hours under ammonia atmosphere. After completion of the reaction, the white precipitate was filtered and washed with methanol.[2-3] Yield: 4.5 g (97%). ^{1}H NMR (400 MHz, DMSO-d_6) δ 5.13 (1H, d, *J* = 5.1 Hz, Glu-OH3), 4.76 (1H, d, *J* = 4.3 Hz, Glu-OH2), 4.69 (1H, q, *J* = 5.0 Hz, ethylidene CH), 3.96 (1H, dd, *J* = 10.2, 4.7 Hz, Glu-H6b), 3.88 (1H, d, *J* = 8.5 Hz,Glu-H1), 3.42 – 3.34 (1H, m, Glu-H6a), 3.31 (1H,

td, *J* = 8.9, 4.8 Hz, Glu-H3), 3.15 (1H, dt, *J* = 9.7, 4.9 Hz, Glu-H5), 3.08 (1H, t, *J* = 9.1 Hz, Glu-H4), 2.88 (1H, td, *J* = 8.5, 3.4 Hz, Glu-H2), 2.39 (2H, br, s, NH_2), 1.22 (3H, d, *J* = 5.0 Hz, ethylidene CH_3); ^{13}C NMR (100 MHz, DMSO-d_6) δ 98.95, 87.75, 81.15, 76.49, 73.83, 68.10, 67.39, 20.84.

2.1.2.2 Synthesis of 2-hydroxy-4-(octyloxy)benzaldehyde

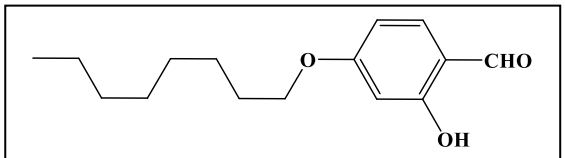

2-Hydroxy-4-(octyloxy)benzaldehyde

A mixture of 2,4-dihydroxybenzaldehyde (5 g, 36.2 mmol), 1-bromo-n-octane (8.3 mL, 37.5 mmol), sodium bicarbonate (3.15 g, 37.5 mmol) and potassium iodide (catalytic amount) in dry acetone (120 mL) was refluxed for 48 hours and the content was filtered while hot to remove the insoluble solid.[4] The filtrate was neutralized with HCl and extracted with dichloromethane (50 mL x 3). The combined organic layer was concentrated and purified by column chromatography using silica gel (100-200 mesh) as solid support and chloroform/hexane (3:7 v/v) as eluent. Yield: 4.75 g (52%). Pale yellow liquid; ^{1}H NMR (400 MHz, DMSO-d_6) δ 11.01 (s, 1H), 10.00 (s, 1H), 7.61 (d, *J* = 8.7 Hz, 1H), 6.54 (dd, *J* = 8.7, 2.3 Hz, 1H), 6.46 (d, *J* = 2.3 Hz, 1H), 4.01 (s, 2H), 1.70 (dd, *J* = 8.2, 6.3 Hz, 2H), 1.42 – 1.22 (m, 11H), 0.89 – 0.82 (m, 3H). ^{13}C NMR (100 MHz, DMSO-d_6) δ 194.00, 164.91, 164.39, 134.44, 115.72, 108.41, 103.95, 68.21, 31.79, 30.11, 29.45, 29.34, 26.18, 22.72, 14.09.

2.1.2.3 Synthesis of *N*-Fmoc-L-phenylalanyl-4-6-*O*-ethylidiene-β-D-glucopyranosylamine (**F1**)

A mixture of Fmoc-L-phenylalanine (6 g, 15.5 mmol), ethyl chloroformate (1.48 mL, 15.55 mmol) and triethylamine (2.16 mL, 15.52 mmol) in dioxane (50 ml) was stirred at 0 °C. After 10 minutes, a suspension of **EGNH$_2$** (3.18 g, 15.5 mmol) in dioxane (150 ml) was added to it and the stirring was continued overnight at room temperature.[5] The removal of solvents under

vacuum resulted in a pasty mass and addition of ice-cold water to that yielded the solid product. The product was filtered, washed with the cold dilute sulphuric acid (3%, 30 ml) followed by sodium bicarbonate (1M, 30 ml) and recrystallised from ethanol. Yield: 5 g (56%), ^{1}H NMR (400 MHz, DMSO-d_6) δ; 8.81 (1H, s, NH), 8.53 (1H, s, NH), 7.85 (2H, d, *J* = 7.6 Hz), 7.63-7.62 (2H, m), 7.41-7.13 (10H, m), 5.38 (1H, d, *J* = 5.2 Hz), 5.15 (1H, d, *J* = 5.5 Hz), 4.85 (1H, t, *J*, = 8.9 Hz), 4.69 (1H, q, *J* = 5.1, Hz), 4.27 (1H, m), 4.09 (2H, m), 3.99 (1H, m), 3.4 – 3.09 (m, 6H), 3.13 (t, *J* = 9.3 Hz, 1H), 2.89-2.75 (2H, m), 1.21 (3H, d, *J* = 4.9 Hz); ^{13}C NMR (100 MHz, DMSO-d_6) δ 175.88, 143.22, 140.08, 138.08, 130.05, 130.01, 129.60, 128.72, 128.60, 127.97, 126.70, 122.06, 120.71, 110.47, 99.22, 80.92, 74.03, 68.24, 68.05, 57.10, 56.70, 20.99, 19.25.

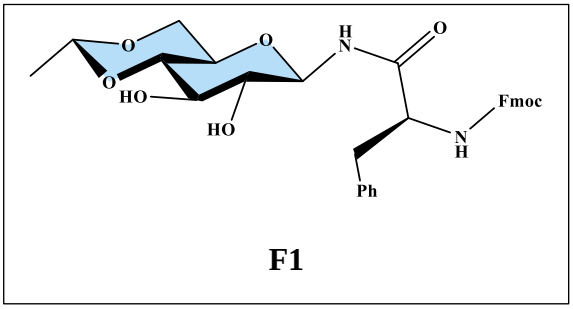

F1

2.1.2.4 Synthesis of *N*-Fmoc-L-leucyl-4-6-*O*-ethylidiene-β-D-glucopyranosylamine (**F2**)

This compound was synthesised following the procedure mentioned above (2.1.2.3) but using **EGNH$_2$** (3.62 g, 16.97 mmol), Fmoc-L-leucine (6 g, 16.97 mmol), triethylamine (2.35 mL, 16.97 mmol) and ethyl chloroformate (1.62 mL, 16.97 mmol). Yield: 5 g (53.7%), ^{1}H NMR (400 MHz, DMSO-d_6) δ; 8.58 (1H, s), 8.49 (1H, s), 7.87 (2H, d, *J* = 7.6 Hz), 7.72 (2H, t, *J* = 7.6 Hz), 7.48-7.35 (2H, m), 7.37-7.27 (2H, m), 5.34 (1H, d, *J* = 5.2 Hz), 5.21 (1H, d, *J* = 5.5 Hz), 4.80 (1H, t, *J*, = 8.9 Hz), 4.69 (1H, q, *J* = 4.8, Hz), 4.29-4.17 (3H, m), 4.09 (1H, m), 3.96 (1H, m), 3.4 – 3.06 (5H, m), 1.57 (1H, m), 1.45 (1H, m), 1.34 (1H, m) 1.21 (3H, d, *J* = 4.9 Hz), 0.84 (1H, m); ^{13}C NMR (100 MHz, DMSO-d_6) δ 174.27, 143.22,

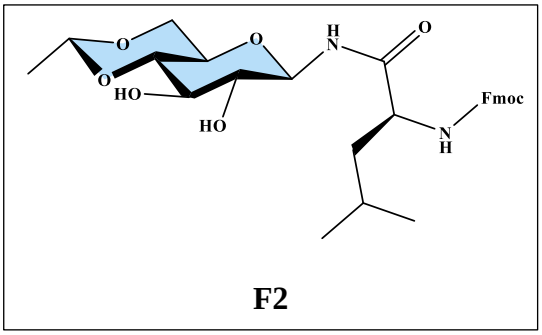

F2

140.08, 138.08, 129.60, 128.72, 127.97, 122.06, 120.71, 110.47, 99.22, 80.92, 74.18, 74.04, 68.24, 68.05, 53.70, 24.85, 23.97, 23.84, 22.06, 20.99.

2.1.2.5 Synthesis of *N*-Fmoc-L-alanyl-4-6-*O*-ethylidiene-β-D-glucopyranosylamine (**F3**)

This compound was synthesised following the procedure mentioned above (2.1.2.3) but using **EGNH$_2$** (3.29 g, 16 mmol), Fmoc-L-alanine (5g, 16 mmol), triethylamine (2.23 ml, 16 mmol) and ethyl chloroformate (1.53 ml, 16 mmol). Yield: 4.02 g (50%), ^{1}H NMR (400 MHz, DMSO-d_6) δ; 8.67 (1H, s, NH), 8.49 (1H, s, NH), 7.85 (2H, d, *J* = 7.6 Hz), 7.76-7.66 (2H, m), 7.49-7.36 (2H, m), 7.35-7.26 (2H, m), 5.32 (1H, d, *J* = 5.3 Hz), 5.10 (1H, d, *J* = 5.8 Hz), 4.81 (1H, t, *J*, = 9 Hz), 4.67 (1H, q, *J* = 4.9, Hz), 4.32-4.15 (3H, m), 4.15-4.03 (1H, m), 3.97 (1H, m), 3.88 (1H, d, *J* = 8.5 Hz), 3.47 – 3.36 (2H, m), 3.31 – 3.20 (2H, m), 3.13 (1H, t, *J* = 9.3 Hz), 1.31 (3H, d, *J* = 6.8 Hz), 1.24 (3H, d, *J* = 4.9 Hz); ^{13}C NMR (100 MHz, DMSO-d_6) δ 174.07, 157.58, 143.22, 140.08, 138.08, 129.60, 127.97,122.06, 120.71, 110.47, 99.22, 80.88, 74.13, 73.82, 68.27, 50.55, 40.78, 20.98, 19.36.

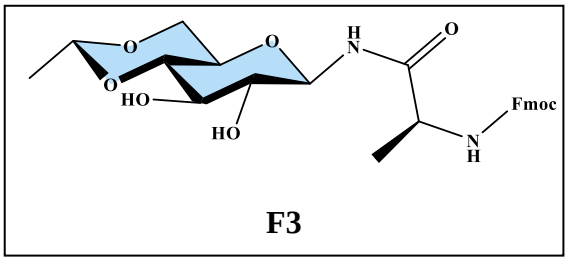

F3

2.1.2.6 Synthesis of *N*-Fmoc-L-methionyl-4-6-*O*-ethylidiene-β-D-glucopyranosylamine (**F4**)

This compound was synthesised following the procedure mentioned above (2.1.2.3) but using **EGNH$_2$** (2 g, 10 mmol), Fmoc-L- methionine (3.7 g, 10 mmol), triethylamine (1.3 mL, 10 mmol) and ethyl chloroformate (0.95 mL, 10 mmol). Yield: 4 g (71%), ^{1}H NMR (400 MHz, DMSO-d_6) δ; 8.94 (1H, d, *J* = 8.8 Hz), δ 7.95 (d, *J* = 8.1 Hz, 1H), 7.83 – 7.78 (m, 2H), 7.64 (m, 2H), 7.54 (m, 2H), 7.45 – 7.38 (m, 2H), 5.08 (d, *J* = 6.2 Hz, 1H), 4.84 (d, *J* = 6.2 Hz, 1H), 4.65 (m, 2H), 4.42 (d, *J* = 4.9 Hz, 3H), 4.03 (m,

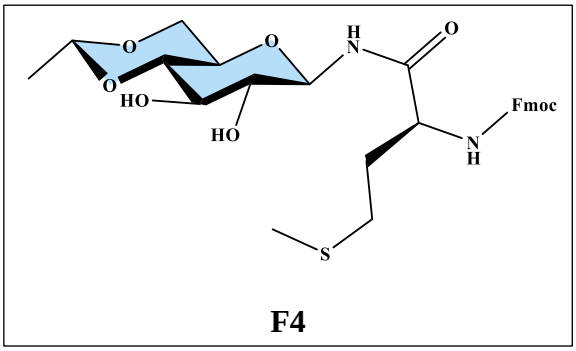

F4

1H), 3.82 – 3.73 (m, 2H), 3.76 – 3.59 (m, 2H), 3.59 (m, 1H), 2.67-2.55 (m, 2H), 2.06 – 1.97 (m, 1H), 1.77 (m, 1H), 1.28 (d, *J* = 4.8 Hz, 3H); ^{13}C NMR (100 MHz, DMSO-d_6) δ 172.86, 156.09, 143.63, 141.22, 127.30, 126.89, 125.14, 120.02, 99.12, 78.32, 77.72, 72.40, 72.24, 71.49, 66.99, 66.47, 52.78, 46.77, 31.72, 30.28, 20.22, 15.11.

2.1.2.7 Synthesis of *N*-Fmoc-L-valinyl-4-6-*O*-ethylidiene-β-D-glucopyranosylamine (**F5**)

This compound was synthesised following the procedure mentioned above (2.1.2.3) but using **EGNH$_2$** (2.05 g, 10 mmol), Fmoc-L-valine (3.39 g, 10 mmol), triethylamine (1.3 mL, 10 mmol) and ethyl chloroformate (0.95 mL, 10 mmol). Yield: 3.5 g (66%), white solid; ^{1}H NMR (400 MHz, DMSO-d_6) δ; 8.94 (1H, d, *J* = 8.8 Hz), 8.66 (1H, d, *J* = 9.1 Hz), 7.83 – 7.78 (m, 2H), 7.66 – 7.61 (m, 2H), 7.54 (m, 2H), 7.45 – 7.38 (m, 2H), 5.08 (d, *J* = 6.2 Hz, 1H), 4.95 (m, 2H), 4.64 (d, *J* = 6.2 Hz, 1H), 4.42 (d, *J* = 4.9 Hz, 2H), 4.29 (t, *J* = 4.9 Hz, 1H), 4.11 – 4.00 (m, 2H), 3.82 – 3.74 (m, 2H), 3.74 – 3.60 (m, 3H), 2.10 – 1.97 (m, 1H), 1.28 (d, *J* = 4.8 Hz, 3H), 0.95 – 0.85 (m, 6H); ^{13}C NMR (100 MHz, DMSO-d_6) δ 172.70, 156.22, 143.63, 141.22, 136.50, 127.30, 127.17, 126.89, 125.14, 123.91, 121.63, 120.02, 119.79, 118.35, 111.94, 110.27, 99.12, 78.41, 77.72, 72.40, 72.24, 71.49, 67.09, 66.99, 59.14, 46.77, 30.52, 20.22, 18.48.

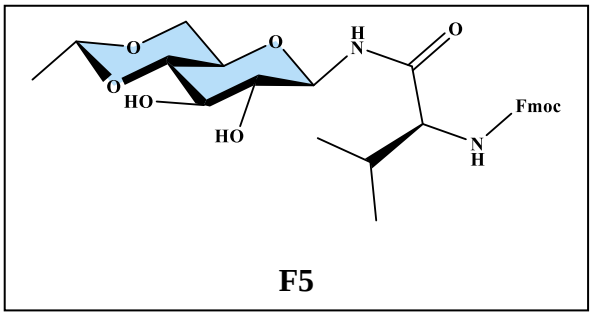

F5

2.1.2.8 Synthesis of *N*-Fmoc-L-isoleucyl-4-6-*O*-ethylidiene-β-D-glucopyranosylamine (**F6**)

This compound was synthesised following the procedure mentioned above (2.1.2.3) but using **EGNH$_2$** (3.62 g, 16.97 mmol), Fmoc-L-isoleucine (6 g, 16.97 mmol), triethylamine (2.35 mL, 16.97 mmol) and ethyl chloroformate (1.62 mL, 16.97 mmol). The characterization details of F4 are as follows: Yield: 5.3 g (58%), ^{1}H NMR (400 MHz, DMSO-d_6) δ; 8.75 (1H, s, NH), 8.40 (1H, s, NH), 7.87 (2H, d, *J* = 7.6 Hz), 7.72 (2H, t, *J* = 7.6 Hz), 7.48-7.35 (2H, m), 7.37-

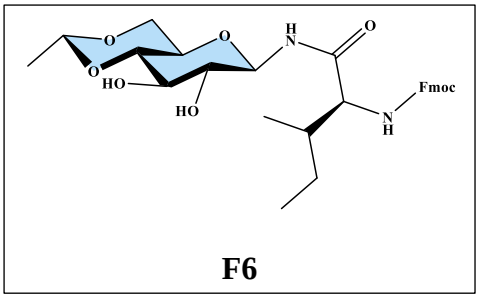

F6

7.27 (2H, m), 5.34 (1H, d, *J* = 5.2 Hz), 5.21 (1H, d, *J* = 5.5 Hz), 4.80 (1H, t, *J*, = 8.9 Hz), 4.69 (1H, q, *J* = 4.8, Hz), 4.29-4.17 (3H, m), 4.03 (1H, m), 3.96 (1H, m), 3.4 – 3.06 (5H, m), 1.68 (1H, m), 1.38 (1H, m), 1.21 (3H, d, *J* = 4.9 Hz), 1.03 (1H, m), 0.80-0.76 (6H, m); ^{13}C NMR (100 MHz, DMSO-d_6) δ 174.27, 143.22, 140.08, 138.08, 129.60, 128.72, 127.97, 122.06, 120.71, 110.47, 99.22, 80.82, 73.95, 68.21, 60.19, 38.82, 37.72, 24.55, 20.97, 16.50, 16.33, 12.14.

2.1.2.9 Synthesis of *N*-Fmoc-L-tryptophanyl-4-6-*O*-ethylidiene-β-D-glucopyranosylamine (**F7**)

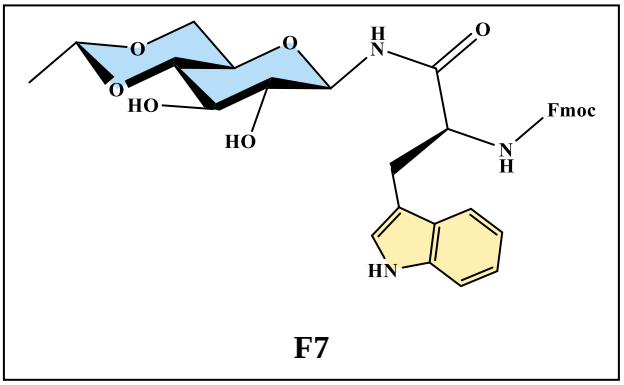

F7

This compound was synthesised following the procedure mentioned above (2.1.2.3) but using **EGNH$_2$** (1.50 g, 7.31 mmol), Fmoc-L-tryptophan (3.12 g, 7.31 mmol), triethylamine (1.02 mL, 7.31 mmol) and ethyl chloroformate (0.70 mL, 7.31 mmol). Yield: 2.10 g (47%), ^{1}H NMR (400 MHz, DMSO-d_6) δ; 10.79 (1H, m), 8.94 (1H, d, *J* = 8.8 Hz), 8.66 (1H, d, *J* = 9.1 Hz), 7.88-7.81 (3H, m), 7.68-7.51 (2H, m), 7.42-7.27 (4H, m), 7.03-6.91 (3H, m), 6.26 (1H, s), 5.41 (1H, d, *J* = 5.2 Hz), 4.82 (1H, d, *J* = 5.5 Hz), 4.69 (1H, m), 4.25 (1H, m), 4.11 (1H, m), 3.98 (1H, m), 3.4-2.85 (7H, m), 1.21 (3H, d, *J* = 4.9 Hz); ^{13}C NMR (100 MHz, DMSO-d_6) δ 172.70, 156.22, 143.63, 141.22, 136.50, 127.30, 127.17, 126.89, 125.14, 123.91, 121.63, 120.02, 119.79, 118.35, 111.94, 110.27, 99.12, 78.32, 77.72, 72.40, 72.24, 71.49, 66.99, 66.78, 54.80, 46.77, 28.20, 20.22.

2.1.2.10 Synthesis of L-phenylalanyl-4-6-*O*-ethylidiene-β-D-glucopyranosylamine (**A1**)

N-Fmoc-L-phenylalanyl-4-6-*O*-ethylidiene-β-D-glucopyranosylamine (**A1**) (2.65 g, 4.62 mmol) was treated with 25% piperidine in DMF (2.65 ml) at room temperature for 10 hours and triturated with ethyl acetate/hexane (3:7) mixture[5]. Yield: 1.05 g (65%), ^{1}H NMR (400 MHz, DMSO-d_6) δ; 8.52 (1H, s), 7.26-7.15 (5H, m), 5.37 (1H, s), 5.30 (1H, s), 4.82(1H, t, *J* = 8.2 Hz), 4.68 (1H, q, *J* = 5.0 Hz), 3.98 (1H, m), 3.41-3.00 (5H, m), 2.90 (1H, m), 2.71-2.51 (2H, m), 1.64 (2H, s), 1.22 (3H, d, *J* = 5.00 Hz); ^{13}C NMR (100 MHz, DMSO-d_6) δ 175.88, 139.50, 130.05, 128.73, 126.70, 99.23, 80.93, 80.89, 74.02, 73.98, 68.24, 68.04, 57.09, 41.46, 21.00.

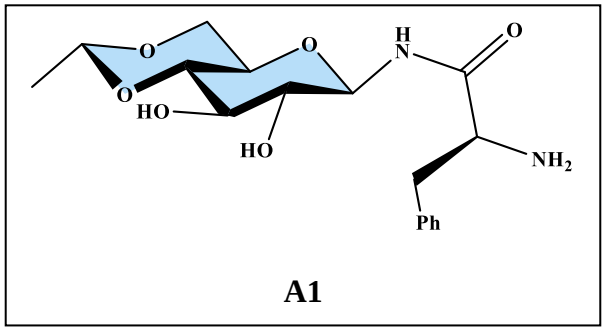

A1

2.1.2.11 Synthesis of L-leucyl-4-6-*O*-ethylidiene-β-D-glucopyranosylamine (**A2**)

This compound was prepared following the procedure adopted for **A1** but using **F2** (2.65 g, 3.7 mmol) 25% piperidine/DMF solution (2.65 mL) Yield: 0.81 g (72%), ^{1}H NMR (400 MHz, DMSO-d_6) δ; 8.44 (1H, s), 5.37 (1H, s), 5.30 (1H, s), 4.76 (1H, q, *J* = 5.0 Hz), 3.95 (1H, m), 3.40-2.87 (7H, m), 1.673 (H, m), 1.34 (1H, m), 1.21 (3H, d, *J* = 4.8), 0.83-0.81 (6H, m); ^{13}C NMR (100 MHz, DMSO-d_6) δ 175.98, 99.20, 80.92, 80.75, 74.09, 73.90, 68.24, 68.03, 60.11, 38.74, 24.35, 21.01, 16.47, 12.14.

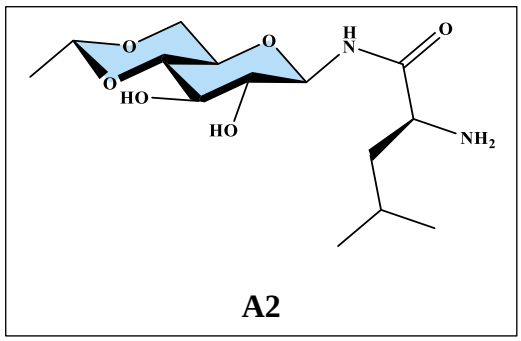

A2

2.1.2.12 Synthesis of L-alanyl-4-6-*O*-ethylidiene-β-D-glucopyranosylamine (**A3**)

This compound was prepared following the procedure adopted for **A1** but using **F3** (3 g, 6 mmol) and 25% piperidine/DMF solution (3 mL) Yield: 1.32 g (80%), ^{1}H NMR (400 MHz,

DMSO-d_6) δ; 8.32 (1H, s), 5.33 (1H, s), 5.31 (1H, s), 4.80 (1H, d, J = 8.0 Hz), 4.70 (1H, q, J = 5.0 Hz), 3.99 (1H, m), 3.36-3.18 (8H, m), 1.23 (3H, d, J = 4.8 Hz), 1.12 (3H, d, J = 6.8 Hz); ^{13}C NMR (100 MHz, DMSO-d_6) δ 176.54, 99.01, 80.69, 80.59, 73.78, 73.72, 68.03, 67.81, 50.60, 21.49, 20.77.

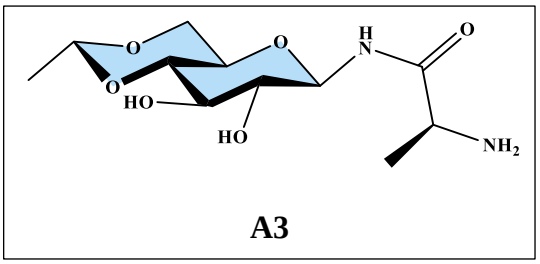

A3

2.1.2.13 Synthesis of L-methionyl-4-6-*O*-ethylidiene-β-D-glucopyranosylamine (**A4**)

This compound was prepared following the procedure adopted for **A1** but using **F4** (1.1 g, 2.0 mmol) 25% piperidine/DMF solution (1 mL) Yield: 0.33 g (50%), ^{1}H NMR (400 MHz, DMSO-d_6) δ ^{1}H NMR (400 MHz, DMSO-d_6) δ; ^{1}H NMR (400 MHz, DMSO-d_6) δ 7.83 (s, 1H), 5.28 (s, 1H), 5.14 (s, 1H), 5.03 (d, J = 5.5 Hz, 2H), 4.94 (m, 2H), 4.03 (m, 1H), 3.84 (m, 1H), 3.81 -3.59 (m, 5H), 2.67 (m, 1H), 2.56 (m, 1H), 2.06 – 1.97 (m, 1H), 1.77 (m, 1H), 1.28 (d, J = 4.8 Hz, 3H), ^{13}C NMR (100 MHz, DMSO-d_6) δ 174.22, 99.12, 78.62, 77.74, 72.40, 72.19, 71.42, 66.99, 52.96, 33.80, 30.56, 20.22, 15.46.

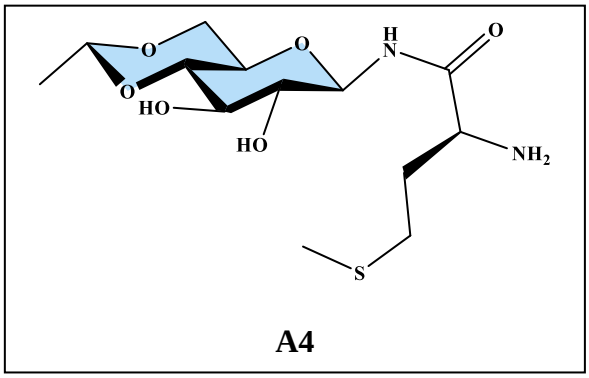

A4

2.1.2.14 Synthesis of L-valinyl-4-6-*O*-ethylidiene-β-D-glucopyranosylamine (**A5**)

This compound was prepared following the procedure adopted for **A1** but using **F5** (5.26 g, 10.0 mmol) 25% piperidine/DMF solution (5.5 mL) Yield: 2 g (66.6 %), ^{1}H NMR (400 MHz, DMSO-d_6) δ ^{1}H NMR (400 MHz, DMSO-d_6) δ; 7.95 (d, J = 8.1 Hz, 1H), 5.68

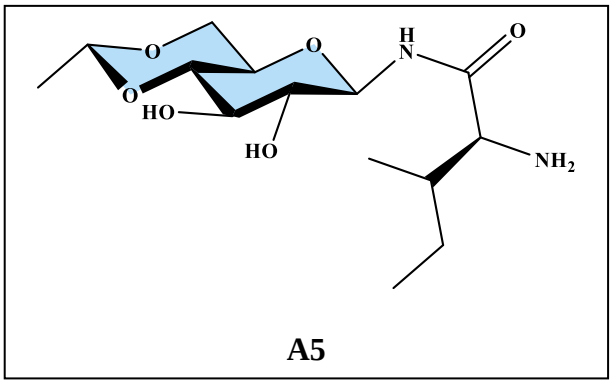

A5

(s, 1H),5.24 (s, 1H), 4.99 – 4.91 (m, 2H), 4.56 (d, J = 6.3 Hz, 2H), 4.03 (m, 1H), 3.82–3.49 (m, 6H), 2.08–1.95 (m, 1H), 1.28 (d, *J* = 4.8 Hz, 3H), 0.96-0.92 (m, 6H), ^{13}C NMR (100 MHz, DMSO-d_6) δ 173.07, 99.12, 78.72, 77.74, 72.40, 72.21, 71.49, 66.99, 58.35, 31.31, 20.22, 18.50.

2.1.2.15 Synthesis of L-isoleucyl-4-6-*O*-ethylidiene-β-D-glucopyranosylamine (**A6**)

This compound was prepared following the procedure
mmol) 25% piperidine/DMF solution (2 mL) The char
Yield: 0.81 g (64%), ^{1}H NMR (400 MHz, DMSO-d_6)
s), 4.80 (1H, s), 4.68 (1H, q, *J* = 5.1 Hz), 3.97-3.94 (
1.42 (1H, m), 1.21 (3H, d, *J* = 4.8), 1.06-0.97 (3H, m),
DMSO-d_6) δ 175.98, 99.20, 80.92, 80.75, 74.09, 73.94, 68.24, 68.03, 60.11, 38.74, 24.35, 20.98, 16.47, 12.14.

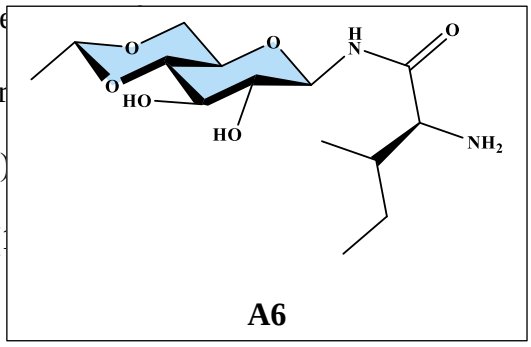

A6

2.1.2.16 Synthesis of L-tryptophanyl-4-6-*O*-ethylidiene-β-D-glucopyranosylamine (**A7**)

This compound was prepared following the procedure adopted for **A1** but using **F7** (2 g, 3.26 mmol) 25% piperidine/DMF solution (2 mL) Yield: 0.80 g (62.7 %), white solid: ^{1}H NMR (400 MHz, DMSO-d_6) δ 10.81 (1H, s), 8.65 (1H, m), 7.93 (1H, s), 7.56 (1H, d, *J* = 7.80), 7.30 (1H, t, *J* = 9.30), 7.14 (1H, s), 7.06-6.87 (2H, m), 5.98 (1H, s), 5.55 (1H, s), 4.83 (1H, m), 4.68 (1H, q, *J* = 4.9), 3.98 (1H, m), 3.50-3.03 (5H, m), 2.85 (1H, m), 2.71-2.57 (2H, m), 1.65 (2H, s), 1.19 (3H, d, *J* = 4.8); ^{13}C NMR (100 MHz, DMSO-d_6) δ 176.03, 162.77, 136.62, 127.89, 124.30, 121.22, 118.99, 118.58, 111.71, 111.06, 98.99, 80.78, 73.81, 73.60, 68.08, 67.88, 55.87, 36.23, 31.36, 20.77.

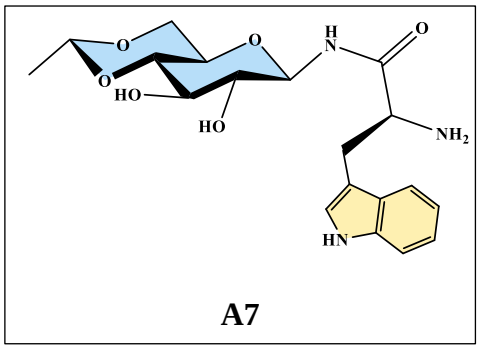

A7

2.1.3 Instrumental techniques and software

Reaction mixture were stirred using IKA magnetic stirrer and solvent evaporation was accomplished by Heidolph rotary evaporator. TLC plates were visualized under Spectroline UV lamp and Pfeiffer Rotary vane vacuum pump was used in compound filtration and drying. The melting points were recorded in open capillary tubes on an EZ-Melt automated melting point apparatus and is uncorrected. X-ray photoelectron spectroscopic (XPS) measurements were performed on a commercial Omicron EA 125 spectrometer with an Al-Kα X-ray electronic source (1486.7 eV). The Quanta FEG 250 instrument was used to record the field emission scanning electron microscopy (FE-SEM) images. Single crystal X-ray diffraction data were recorded on an XtaLAB AFC12 (RINC): Kappa dual home/near diffractometer using Cu (50 mA, 0.6 kV) radiation. The structure was solved using ShelXT[6-7] structure solution program and refined with the ShelXL[8] refinement package. Crystallographic information files were visualized with help of Mercury[9], ORTEP-III[10] and Platon[11] software. Data for Elemental analysis were recorded on elementar Analysensysteme GmbH - vario MICRO Elemental Analyzer.

2.1.3.1 FTIR spectroscopy

FTIR spectra of compounds were recorded on Shimadzu IRAffinity-1S system using KBr pellet and the data was processed on Lab solutions IR software. First a pure KBr pellets were used as the background and then sample containing KBr pellets were scanned in the range of 400–4000 cm^{-1} with a spectral resolution of 4 cm^{-1}. Multipoint method was adopted for base line correction, while peak picking was done in manual mode.

2.1.3.2 NMR spectroscopy

NMR data were recorded on Bruker (400 MHz) spectrometer and acquired using Topspin software. Sample solutions were prepared by dissolving 7-10 mg of analytes in 0.5−0.6 mL of either DMSO-d_6 or $CDCl_3$. Proton decoupled pulse program was used for ^{13}C NMR to simplify the analysis. Software like MestReNova and Topspin was used for data processing. The chemical shifts and coupling constants are presented in δ (ppm) and Hz, respectively.

2.1.3.3 High resolution mass spectrometry (HRMS)

HRMS data were recorded on Agilent 6545 LC-QTOF machine and analyzed by Agilent Masshunter Qualitative Analysis B.07.00 software. Samples were prepared at ppb level concentration using LC-MS grade solvents and Dual AJS ESI source was used for ionization under nitrogen atmosphere with gas flow of 12 L/min at 325 °C. The nebulizer pressure, capillary voltage and nozzle voltage were set at 45 psi, 3500 V and 1500 V, respectively. Abundance of ions as function of m/z ratio was measured in the range 100−1700. Isotope distribution calculator was used to compare the experimental isotope abundance values with theoretical abundances.

2.1.3.4 UV-Visible spectroscopy

UV-Visible spectra of compounds were recorded on Jasco V-650 double beam spectrophotometer using Spectra manager software and processed on OriginPro graphic software. Halogen (330−900 nm) and Deuterium lamps (190−350 nm) were used as UV and visible light sources, respectively. The absorbance data as function of wavelength was measured in the range of 190-900 nm with the scan speed of 200 nm/min.

2.1.3.5 Solid state UV-visible spectroscopy

The solid-state UV visible spectra were recorded on Shimadzu-2450 instrument using barium sulphate as reference. First $BaSO_4$ power was used as the background and then sample containing $BaSO_4$ powers were scanned in the range of 200-800 nm. Visualization and smoothening of the graph was done using OriginPro graphic software.

2.1.3.6 Fluorescence spectra

Fluorescence spectra were recorded on the Fluoromax-4 spectrofluorometer and OriginPro graphic software was used for data collection and processing. The samples are illuminated by continuous out 150 W ozone free xenon lamp and the emission monochromator has a range of 290-850 nm. The FluoroMax 4 has two detectors, which are named as calibrated photodiode reference and R928P red-sensitive PMT. Calibrated photodiode reference detector corrects the intensity and temporal fluctuations in the source during excitation scans, while R928P red-sensitive PMT is used for counting of photon that are originated from the sample.

2.1.3.7 Thermogravimetric analysis (TGA)

Thermal analyses were performed on the TGA-4000 machine from Perkin Elmer, in the temperature range of 30-800 °C with a 10 °C/min heating rate under N_2 atmosphere with a flow rate of 20 mL/min. In pre-tared platinum crucible, well dried powder sample (10 mg) was taken for the analysis and temperature as well as the weight of the sample were recorded as a function of time. The produced data was processed by TRIOS software package and the graphs were smoothened by smoothening tool. In the final TGA data, the graph was plotted between weight% ($\frac{\text{weight}}{\text{weight initial}} \times 100$) values vs temperature.

2.1.3.8 High performance liquid chromatography (HPLC)

HPLC data were recorded on Agilent 1260 Infinity II manual LC system equipped with a VWD (Variable Wavelength Detector) detector and data was acquired and processed using Agilent liquid chromatography software. Instrument was operated in reverse phase using methanol, acetonitrile and water as solvents. Sample were prepared in ppm level and for each run 20 µL of sample was injected. For compound separation Waters Sunfire C18 5 µm 4.6 × 250 mm column was used and chiral chromatography was conducted by Kromasil 5-Amycoat RP 5 µm 4.6 × 250 mm column. VWD detector was set to fixed wavelength between 200−400 nm and confirmation of compounds eluted was obtained by comparing the retention time. Area under curve for the chromatographic peak was calculated by manual integration.

2.1.4 Methods

2.1.4.1 Crystallization techniques

X-Ray suitable single crystals are obtained either by slow evaporation method or by vapour diffusion method. In slow evaporation method, saturated solution of compound was left at the room temperature for slow evaporation to grow crystals. In vapour diffusion method, compound was dissolved in a particular solvent and vapour of a second solvent (which do not solubilize the compound, but miscible with first solvent) was allowed to diffuse into the compound's solution. Slow diffusion of second solvent into the solution reduces the solubility of compound and affords crystals.

2.1.4.2 Yield calculation

Yield of the products were calculated either from the isolated weight of the compound or by HPLC instrument using standard calibration method. For calibration curve, a blank solution and minimum five standard solutions of pure compound with different concentration were prepared and from the area under the curve a linear calibration curve was obtained. This calibration curve was used to calculate the concentration of test sample as shown in *Fig. 2.1*.

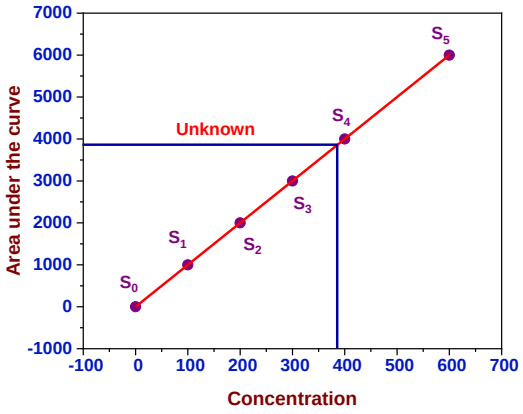

Fig. 2.1 *Calibration curve generated using standards S1-S6*

2.1.5 Theoretical calculation

All the theoretical calculations described in chapter 3 were performed using GAUSSIAN 09 package program,[12] and the obtained results were visualized with the help of Gauss View-5 software.[13] For the structural optimization at the ground state Hartree-Fock (HF) with 6-31G basis set and density functional theory (DFT) with B3LYP (Becke, 3-parameter, Lee-Yang-Parr)[14-15] functional in combination with 6-31G(2d,p) basis set were used. The optimization was performed in both gas and solvent phases. The structural properties, single-point energy, HOMO-LUMO energy in the ground state, vibrational spectra and NBO analysis were determined through the application of HF/6-31G and DFT/B3LYP with 6-31G(2d,p) basis set, respectively. Chemical shifts in ^{1}H and ^{13}C NMR were calculated within gauge-including-atomic-orbital (GIAO)[16-18] approach, which is one of the most common approaches for calculating the nuclear magnetic shielding tensor.

2.1.6 Hirshfeld surface analysis

Hirshfeld surface analyses and 2D fingerprint plots were obtained using Crystal Explorer 17[19]. Hirshfeld surface along with the fingerprint plot provided an exclusive pattern for a particular structure, which involves the interactions between neighbouring molecules.[20] Every point of the Hirshfeld surface is expressed by two distances, d_e (distance from the surface point to the nearest nucleus external to the surface) and d_i (distance from the surface point to the nearest nucleus internal to the surface). The normalized constant distance (d_{norm}) is given by-

$$d_{norm} = \frac{d_i - r_i^{vdW}}{r_i^{vdW}} - \frac{d_e - r_e^{vdW}}{r_e^{vdW}}$$

where r_i^{vdW} and r_e^{vdW} are the van der Waals radii of internal and external atoms respectively. The 2D fingerprint plot was constructed using d_i versus d_e by decomposing the Hirshfeld surface into different intermolecular contacts present in the crystal structure[20].

Reference

1. Barker, R.; MacDonald, D., Some Oxidation and Reduction Products of 2, 4-O-Ethylidene-D-erythrose1. *Journal of the American Chemical Society* 1960, *82*, 2301-2303.

2. Linek, K.; Alfoldi, J.; Durindova, M., Glycosylamines. 3. Preparation, structure, and conformation of some glycosylamines. *Chemical Papers-Chemicke Zvesti* 1993, *47*, 247-250.

3. Sah, A. K.; Rao, C. P.; Saarenketo, P. K.; Rissanen, K., Crystal structure of 4, 6-O-ethylidene-N-(2-hydroxybenzylidene)-β-d-glucopyranosylamine. *Carbohydrate Research* 2002, *337*, 79-82.

4. Nath, R. K.; Sarkar, D. D.; Shankar Rao, D. S.; Nandiraju, V. R., Influence of polar substituents on the mesomorphism of non-symmetrical achiral four-ring bent-core compounds: synthesis and characterisation. *Liquid Crystals* 2012, *39*, 889-902.

5. Sah, A. K.; Soni, K., Synthesis of cupric acetate selective receptor derived from alanyl glycoconjugate and their application in selective oxidation of benzylic alcohols. *Catalysis Communications* 2012, *28*, 120-123.

6. Sheldrick, G. M., SHELXT–Integrated space-group and crystal-structure determination. *Acta Crystallographica Section A: Foundations and Advances* 2015, *71*, 3-8.

7. Dolomanov, O., l. J. Bourhis, RJ Gildea, JAK Howard, H. Puschmann. *J. Appl. Crystallogr* 2009, *42*, 339.

8. Sheldrick, G. M., Crystal structure refinement with SHELXL. *Acta Crystallographica Section C: Structural Chemistry* 2015, *71*, 3-8.

9. Macrae, C. F.; Edgington, P. R.; McCabe, P.; Pidcock, E.; Shields, G. P.; Taylor, R.; Towler, M.; Streek, J., Mercury: visualization and analysis of crystal structures. *Journal of Applied Crystallography* 2006, *39*, 453-457.

10. Farrugia, L. J., WinGX and ORTEP for Windows: an update. *Journal of Applied Crystallography* 2012, *45*, 849-854.

11. Spek, A., Single-crystal structure validation with the program PLATON. *Journal of Applied Crystallography* 2003, *36*, 7-13.

12. Frisch, M.; Trucks, G.; Schlegel, H.; Scuseria, G.; Robb, M.; Cheeseman, J.; Scalmani, G.; Barone, V.; Mennucci, B., Petersson., GA et al. Gaussian09, Rev. C. 01; Gaussian. *Inc.: Wallingford, CT* 2010.

13. Dennington, R.; Keith, T.; Millam, J., GaussView, version 5. 2009.

14. Becke, A. D., A new mixing of Hartree–Fock and local density-functional theories. *The Journal of Chemical Physics* 1993, *98*, 1372-1377.

15. Lee, C.; Yang, W.; Parr, R. G., Development of the Colle-Salvetti correlation-energy formula into a functional of the electron density. *Physical Review B* 1988, *37*, 785.

16. Ditchfield, R., Molecular orbital theory of magnetic shielding and magnetic susceptibility. *The Journal of Chemical Physics* 1972, *56*, 5688-5691.

17. Ditchfield, R., Self-consistent perturbation theory of diamagnetism: I. A gauge-invariant LCAO method for NMR chemical shifts. *Molecular Physics* 1974, *27*, 789-807.

18. Wolinski, K.; Hinton, J. F.; Pulay, P., Efficient implementation of the gauge-independent atomic orbital method for NMR chemical shift calculations. *Journal of the American Chemical Society* 1990, *112*, 8251-8260.

19. Govindarajan, M.; Karabacak, M., Spectroscopic properties, NLO, HOMO–LUMO and NBO analysis of 2, 5-Lutidine. *Spectrochimica Acta Part A: Molecular and Biomolecular Spectroscopy* 2012, *96*, 421-435.

20. Ramalingam, S.; Karabacak, M.; Periandy, S.; Puviarasan, N.; Tanuja, D., Spectroscopic (infrared, Raman, UV and NMR) analysis, Gaussian hybrid computational investigation (MEP maps/HOMO and LUMO) on cyclohexanone oxime. *Spectrochimica Acta Part A: Molecular and Biomolecular Spectroscopy* 2012, *96*, 207-220.

Chapter 3

Synthesis, Crystal Structure of D-Glucose Derived 2-Hydroxy-1-naphthaldehyde Containing Glycopeptides and an Insight from Experimental and Theoretical Calculations

Chapter 3

3.1 Introduction

Glycopeptides are the molecules in which carbohydrates are linked with amino acids or it's polymeric form through a covalent bond. Based on such linkages, they are divided into three categories, *C*-, *O*- and *N*-type glycopeptides. *N*-linked glycopeptides are most common in eukaryotes, archaea and other single-cell organisms. These glycopeptides are well known for their constructive involvement in several biological processes such as brain development[1], endocrine system[1], inflammation,[1-3] immune system,[4] fertilization,[5] cellular communication,[6] etc. Glycopeptide-based antibiotics are often used as the last line of defence, especially against Gram-positive bacterial infections.[7] The *N*-linked glycosylation is a common modification to the peptides that are exposed to an extracellular environment and may exhibit enormous structural diversity.[8] Metal ion-bound glycopeptides facilitate various enzyme-catalyzed biosynthetic reactions in biological systems.[9-10] Due to these wide range applications, several methodologies for the chemical synthesis of *N*-linked glycopeptides have been developed. The most difficult part in the chemical synthesis of *N*-linked glycopeptides is to couple the carbohydrates with amino acids. Coutsogeorgopoulos and Zervas have accomplished the *N*-acylation of 4,6-*O*-benzylidene-D-glucosylamine by coupling it with L-amino acids to form *N*-(α-aminoacyl)-D-glucosylamines.[11] Later our group have adopted this methodology for synthesis of a range of glycopeptides.[12-14] The reaction between of L-alanyl-4,6-*O*-ethylidene-β-D-glucopyranosylamine and salicylic acid in presence of triethylamine (TEA) and ethyl choloroformate (ECF) yielded another amide linkage between glycopeptide and aryl group (*Fig. 3.1*).[12]

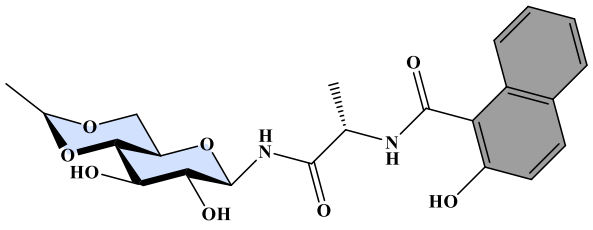

Fig. 3.1 *N-(2-hydroxybenzoyl)-L-alanyl-4,6-O-ethylidene-β-D-glucopyranosylamine*

The synthesized *N*-(2-hydroxybenzoyl)-L-alanyl-4,6-*O*-ethylidene-β-D-glucopyranosylamine

(**L1**) selectively interact with copper acetate and their complex was used for catalytic oxidation of benzylic alcohols. The ligand was also used as receptor, where it interacts with free and protein bound tryptophan through hydrogen bonding.[15] The coupling product of 4,6-*O*-ethylidene-β-D-glucopyranosylamine (**EGNH$_2$**) with different nonpolar natural occurring amino acids had shown a fair amount of antibacterial activity, however the results of glycopeptides containing tryptophan and isoleucine scaffolds are comparable with the standard drug molecule against E. coli and K. pneumoniae bacterial strains, respectively.[13] Later, further arylations of synthesized β-D-glucosylamides at free amine group through amide and imine linkages have been done. The imine derivatives of β-D-glucosylamides were examined for antibacterial activity against Bacillus cereus, Escherichia coli and Klebsiella pneumoniae along with antifungal activity against Fusarium monilliforme, Fusarium graminearum and Aspergillus flavus.[16] D-Glucose derived mefenamic acid containing glycopeptides were also reported with their COX-2 (human) enzyme inhibition abilities.[17] The toxicity analysis of these glycopeptides revealed their minimum oral acute toxicity in comparison to subcutaneous, intravenous and intraperitoneal modes of administration. The molecule with tryptophan moiety has shown the best COX-2 inhibition activity in both in vitro and in silico modes.

The carbohydrate and peptide moieties enrich the glycopeptide with unique structural diversities, which often governs its physical and chemical properties. This structural exclusivity helps them for being selective in several biological processes and hence, the complete structural determination of glycopeptides is an important aspect in biochemistry. Although NMR spectroscopy can provide the configurational information in solution as well as in solid-state, only single-crystal X-ray diffraction studies offer fast and accurate information on the molecular structure at atomic level along with the detailed information regarding intra- and intermolecular interactions. In case of **L1**, the aryl group is attached to glycopeptide through an amide group, was crystalized in mixed solvent (methanol–acetonitrile 1:1) using

slow evaporation technique. The crystal structure revealed the presence of multiple intra and intermolecular hydrogen bonds in the solid state.[15] Due to the intermolecular hydrogen bonds, molecules are assembled in a two-dimensional arrangement where acetonitrile molecules are trapped in between the two layers (*Fig. 3.2*). It was assumed that the intramolecular hydrogen bonds will remain intact in the solution state as well, which govern their metal chelation and amino acids binding abilities. This chapter describes the synthesis of 2-hydroxy-1-naphthaldehyde coupled β-D-glucosylamides, and their structural properties along with the theoretical aspects of their configurations.

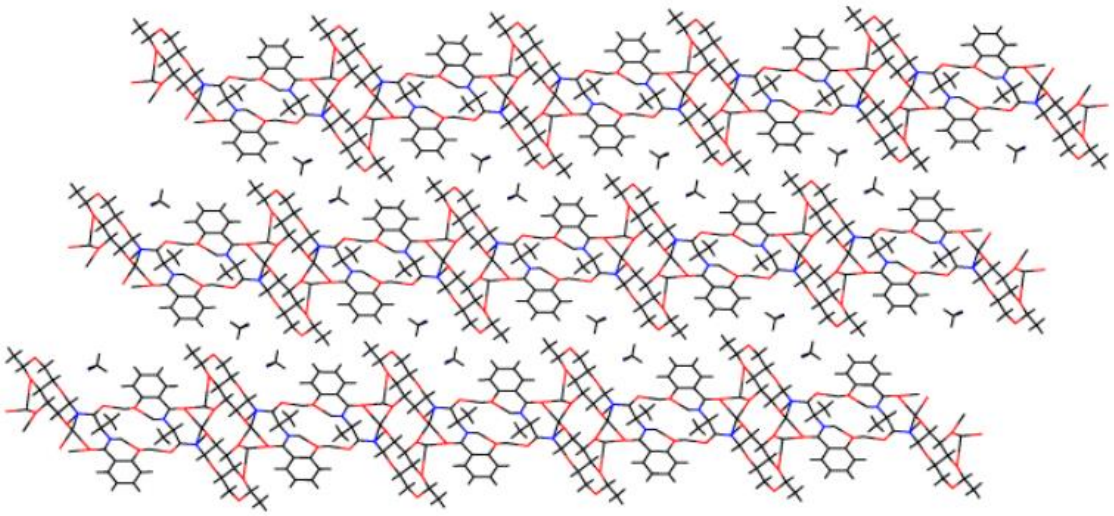

Fig. 3.2 *Packing diagram of N-(2-hydroxybenzoyl)-L-alanyl-4,6-O-ethylidene-β-D-glucopyranosylamine (**L1**) showing the two-dimensional molecular arrangement*[15]

3.2 General procedure for synthesis of glycopeptides

In the second chapter, the targeted coupling of **EGNH$_2$** with *N*-Fmoc protected L-amino acid followed by the deprotection of Fmoc group using the standard methodology (piperidine/DMF) have already been discussed, which results in β-D-glucosylamides. A mixture of β-D-glucosylamides (2 mmol) and 2-hydroxy-1-naphthaldehyde (2.04 mmol) in ethanol (50 mL) was stirred at 80 °C for 8 hrs. The mixture was cooled to room temperature and the resultant

yellow solid product was filtered, washed with cold ethanol and dried. The yields of the products varied in the range of 85-95%. All the compounds were characterized by HRMS and NMR spectroscopy (*Fig. A1.1-A1.21*).

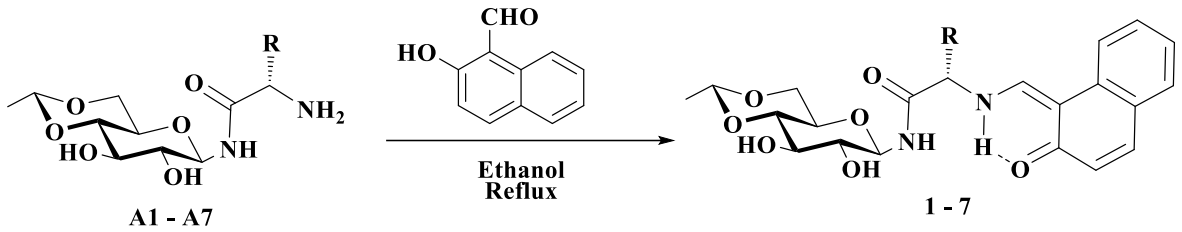

R = CH_2Ph (1), $CH(CH_3)CH_2CH_3$ (2), CH_3 (3), $CH_2CH_2SCH_3$ (4), $CH(CH_3)_2$ (5), $CH_2CH(CH_3)_2$ (6), $CH_2C_8H_6N$ (7)

Scheme 3.1 *Synthesis of glycoconjugate containing amino acid and 2-hydroxy naphthaldehyde.*

Product code 1: Yield = 85%, Melting point: 240-242 °C,^{1}H NMR (400 MHz, DMSO-d_6) δ; 14.11 (dd, *J* = 9.0, 6.6 Hz, 1H, ArOH), 9.05 (d, *J* = 8.9 Hz, 1H, HC=N), 8.68 (d, *J* = 8.7 Hz, 1H, NH), 7.76 (d, *J* = 8.9 Hz, 1H, ArH), 7.74 (d, *J* = 8.9 Hz, 1H, ArH), 7.63 (dd, *J* = 8.0, 1.4 Hz, 1H, ArH), 7.38 (ddd, *J* = 8.4, 7.0, 1.4 Hz, 1H, ArH), 7.30 – 7.17 (m, 6H, ArH), 7.21 – 7.12 (m, 1H, ArH), 6.75 (d, *J* = 9.3 Hz, 1H, ArH), 5.39 (d, *J* = 5.3 Hz, 1H, glucose C3-OH), 5.28 (d, *J* = 5.7 Hz, 1H, glucose C2-OH), 4.94 (t, *J* = 9.0 Hz, 1H, glucose H-1), 4.73 (q, *J* = 5.0 Hz, 1H, ethylidene-CH), 4.56 (dt, *J* = 10.3, 5.0 Hz, 1H, phe-ala-chiral-CH), 4.05 (dd, *J* = 10.1, 4.8 Hz, 1H, glucose H-5), 3.50 – 3.00 (m, 7H), 1.25 (d, *J* = 5.0 Hz, 3H). ^{13}C-NMR (101 MHz, DMSO-d_6) 176.61, 170.44, 158.97, 137.40, 137.02, 134.32, 130.05, 129.34, 128.76, 128.33, 127.12, 125.95, 125.05, 122.92, 118.99, 106.55, 99.05, 80.77, 80.65, 73.89, 73.79, 68.12, 67.79, 66.33, 20.78. HRMS: m/z calcd for $C_{28}H_{30}N_2O_7$ ($[M+H]^+$) = 507.2126, found 507.2197.

Product code 2: Yield = 90%, Melting point: 268-270 °C, ^{1}H NMR (400 MHz, DMSO-d_6) δ; 14.28 (dd, *J* = 9.0, 6.6 Hz, 1H, ArOH), 9.05 (d, *J* = 9.1 Hz, 1H, HC=N), 8.88 (d, *J* = 8.9 Hz,

1H, NH), 8.10 (d, *J* = 8.4 Hz, 1H, ArH), 7.77 (d, *J* = 9.4 Hz, 1H, ArH), 7.67 (dd, *J* = 8.0, 1.4 Hz, 1H, ArH), 7.45 (ddd, *J* = 8.4, 6.9, 1.4 Hz, 1H, ArH), 7.23 (t, *J* = 6.6 Hz, 1H, ArH), 6.77 (d, *J* = 9.3 Hz, 1H, ArH), 5.37 (d, *J* = 5.3 Hz, 1H, glucose C3-OH), 5.22 (d, *J* = 5.8 Hz, 1H, glucose C2-OH), 4.92 (t, *J* = 9.0 Hz, 1H, glucose H-1), 4.71 (q, *J* = 5.0 Hz, 1H, ethylidene-CH), 4.12 (t, *J* = 6.6 Hz, 1H, Ile-chiral-CH), 4.02 (dd, *J* = 10.1, 4.8 Hz, 1H, glucose H-5), 3.42 (m, 2H), 3.26 (tt, *J* = 10.3, 3.5 Hz, 2H), 3.14 (t, *J* = 9.2 Hz, 1H), 2.02 (dtd, *J* = 9.7, 6.1, 3.1 Hz, 1H,Ile-branched-CH), 1.50 (ddq, *J* = 12.6, 8.6, 5.2, 4.4 Hz, 1H, Ile-CH), 1.24 (d, *J* = 5.0 Hz, 3H, ethylidene- CH3), 1.20 – 0.98 (m, 1H, Ile-CH), 0.92 (d, *J* = 5.8 Hz, 3H, Ile-CH3), 0.86 (t, *J* = 9.0 Hz, 3H, Ile-CH3). ^{13}C-NMR (100 MHz, DMSO-*d*$_6$) δ 176.36, 170.63, 159.06, 137.57, 134.46, 129.40, 128.43, 125.94, 125.31, 122.95, 119.17, 106.65, 99.01, 80.73, 80.63, 73.92, 73.59, 70.38, 68.13, 67.79, 38.14, 24.35, 20.17, 15.72, 11.53. HRMS: m/z calcd for $C_{25}H_{32}N_2O_7$ ($[M+H]^+$) = 473.2282, found 473.2268.

Product code 3: Yield = 95%, Melting point: 251-255 °C, ^{1}H NMR (400 MHz, DMSO-*d*$_6$) δ; 14.11 (dd, *J* = 9.0, 6.6 Hz, 1H, ArOH), 9.10 (d, *J* = 9.4 Hz, 1H, HC=N), 8.86 (d, *J* = 8.9 Hz, 1H, NH), 8.09 (d, *J* = 8.4 Hz, 1H, ArH), 7.75 (d, *J* = 9.4 Hz, 1H, ArH), 7.65 (dd, *J* = 7.9, 1.3 Hz, 1H, ArH), 7.44 (ddd, *J* = 8.4, 6.9, 1.4 Hz, 1H, ArH), 7.22 (t, *J* = 7.4 Hz, 1H, ArH), 6.75 (d, *J* = 9.3 Hz, 1H, ArH), 5.34 (d, *J* = 5.2 Hz, 1H, glucose C3-OH), 5.21 (d, *J* = 5.6 Hz, 1H, glucose C2-OH), 4.91 (t, *J* = 9.0 Hz, 1H, glucose H-1), 4.72 (q, *J* = 5.0 Hz, 1H, ethylidene-CH), 4.43 (p, *J* = 6.7 Hz, 1H, ala-chiral-CH), 4.04 (dd, *J* = 10.1, 4.8 Hz, 1H, glucose H-1), 3.47 – 3.36 (m, 2H), 3.31 – 3.20 (m, 2H), 3.13 (t, *J* = 9.3 Hz, 1H), 1.50 (d, *J* = 6.8 Hz, 3H, ala-CH_3), 1.24 (d, *J* = 4.9 Hz, 3H, ethylidene- CH_3). ^{13}C NMR (101 MHz, DMSO-*d*$_6$) δ 176.70, 171.50, 158.39, 137.62, 134.59, 129.36, 128.38, 125.90, 125.49, 122.88, 119.21, 106.70, 99.05, 80.78, 80.66, 73.85, 73.73, 68.18, 67.80, 59.71, 20.80, 20.77. HRMS: m/z calcd for $C_{22}H_{26}N_2O_7$ ($[M+H]^+$) = 431.1813, found 431.1801.

Product code 4: Yield = 88%, Melting point: 218-221 °C, ^{1}H NMR (400 MHz, DMSO-d_6) δ; 14.23 (s, 1H, ArOH), 9.13 (s, 1H, HC=N), 8.96 (d, *J* = 9.0 Hz, 1H, NH), 8.10 (d, *J* = 8.5 Hz, 1H, ArH), 7.79 (d, *J* = 9.3 Hz, 1H, ArH), 7.68 (d, *J* = 7.9 Hz, 1H, ArH), 7.47 (t, *J* = 7.6 Hz, 1H, ArH), 7.24 (t, *J* = 7.4 Hz, 1H, ArH), 6.80 (d, *J* = 9.3 Hz, 1H, ArH), 5.34 (d, *J* = 5.5 Hz, 1H glucose C3-OH), 5.27 (d, *J* = 5.6 Hz, 1H glucose C2-OH), 4.91 (t, *J* = 8.9 Hz, 1H, glucose H-1), 4.71 (q, *J* = 5.5, 5.0 Hz, 1H, ethylidene CH), 4.53 – 4.33 (m, 1H, methionine-chiral-CH), 4.02 (dd, *J* = 10.3, 4.8 Hz, 1H, glucose H-5), 3.5 (q, *J* = 7.9 Hz, 2H), 3.26 (m, *J* = 11.5, 7.6, 6.3 Hz, 2H), 3.13 (t, *J* = 9.2 Hz, 1H), 2.42 (m, 2H, methionine CH_2), 2.14 (m, 2H, methionine CH_2) 2.05 (s, 3H, methionine CH_3), 1.23 (d, *J* = 5.0 Hz, 3H, ethylidene CH_3).^{13}C NMR (101 MHz, DMSO-d_6) δ 177.44, 170.98, 158.77, 138.64, 134.21, 129.53, 128.89, 125.93, 125.17, 123.45, 118.96, 106.52, 99.25, 80.55, 80.14, 73.51, 73.11, 68.11, 67.58, 63.51, 33.16, 29.22, 20.49, 14.87. HRMS: m/z calcd for $C_{24}H_{30}N_2O_7S$ ($[M+H]^+$) = 491.1846, found 491.1815.

Product code 5: Yield = 92%, Melting point: 270-274 °C, ^{1}H NMR (400 MHz, DMSO-d_6) δ; 14.24 (t, *J* = 8.8, 1H, ArOH), (d, *J* = 8.3 Hz, 1H, HC=N), 8.86 (d, *J* = 8.9 Hz, 1H, NH), 8.09 (d, *J* = 8.4 Hz, 1H, ArH), 7.77 (d, *J* = 9.3 Hz, 1H, ArH), 7.66 (d, *J* = 7.8 Hz, 1H, ArH), 7.44 (t, *J* = 7.6 Hz, 1H, ArH), 7.22 (t, *J* = 7.4 Hz, 1H, ArH), 6.77 (d, *J* = 9.3 Hz, 1H, ArH), 5.35 (d, *J* = 5.2 Hz, 1H, 1H glucose C3-OH), 5.20 (d, *J* = 5.7 Hz, 1H, 1H glucose C2-OH), 4.93 (t, *J* = 8.9 Hz, 1H, glucose H-5), 4.71 (q, *J* = 4.9 Hz, 1H, ethylidene CH), 4.10 (t, *J* = 6.0 Hz, 1H, val-chiral-CH), 4.02 (dd, *J* = 10.3, 4.8 Hz, 1H, glucose H-5), 3.5 (q, *J* = 8.0 Hz, 2H), 3.26 (m, 2H), 3.13 (t, *J* = 9.2 Hz, 2H), 2.26 (dt, *J* = 13.9, 6.8 Hz, 1H, val-CH), 1.24 (d, *J* = 5.0 Hz, 3H, ethylidene CH3), 0.91 (dd, *J* = 14.0, 6.7 Hz, 6H, val-CH3). ^{13}C NMR (101 MHz, DMSO-d_6) δ 178.57, 170.79, 158.42, 138.65, 134.44, 129.50, 128.82, 125.73, 123.23, 118.81, 106.17, 99.20, 80.52, 80.22, 73.60, 73.18, 69.74, 68.12, 67.65, 31.88, 20.54, 19.21, 17.50. HRMS: m/z calcd for $C_{24}H_{30}N_2O_7$ ($[M+H]^+$) = 459.2126, found 459.2109.

Product code 6: Yield = 92% Melting point: 268-270, °C ^{1}H NMR (400 MHz, DMSO-d_6) δ; 14.25 (t, *J* = 7.6 Hz, 1H), 9.10 (d, *J* = 8.7 Hz, 1H), 8.92 (d, *J* = 8.9 Hz, 1H), 8.10 (d, *J* = 8.4 Hz, 1H), 7.77 (d, *J* = 9.3 Hz, 1H), 7.67 (d, *J* = 7.9 Hz, 1H), 7.45 (t, *J* = 7.7 Hz, 1H), 7.23 (t, *J* = 7.4 Hz, 1H), 6.77 (d, *J* = 9.3 Hz, 1H), 5.38 (d, *J* = 5.3 Hz, 1H), 5.24 (d, *J* = 5.7 Hz, 1H), 4.91 (t, *J* = 8.9 Hz, 1H), 4.71 (q, *J* = 5.1 Hz, 1H), 4.37 (q, *J* = 6.7 Hz, 1H), 4.02 (dd, *J* = 10.2, 4.8 Hz, 1H), 3.26 (dq, *J* = 12.6, 6.6, 5.3 Hz, 2H), 3.13 (t, *J* = 9.2 Hz, 1H), 1.72 (h, *J* = 7.8 *Hz*, 2H), 1.55 (dt, *J* = 13.4, 6.7 Hz, 1H), 1.24 (d, *J* = 5.0 Hz, 3H), 0.93 (t, *J* = 7.3 Hz, 6H). ^{13}C NMR (101 MHz, DMSO-d_6) δ 175.76, 171.22, 159.07, 137.45, 134.38, 129.38, 128.43, 126.06, 125.06, 123.00, 119.26, 106.82, 99.04, 80.79, 80.69, 73.93, 73.68, 68.18, 67.83, 63.82, 42.50, 24.71, 23.44, 22.05, 20.77. HRMS: m/z calcd for $C_{25}H_{33}N_2O_7$ ($[M+H]^+$) = 473.2288; found 473.2270.

Product code 7: Yield = 88% Melting point: 255-257 °C, ^{1}H NMR (400 MHz, DMSO-d_6) δ; 13.98 (s, 1H), 10.93 – 10.80 (m, 1H), 9.17 (d, *J* = 8.9 Hz, 1H), 8.43 (d, *J* = 8.2 Hz, 1H), 7.78 (d, *J* = 7.9 Hz, 1H), 7.68 (d, *J* = 9.4 Hz, 1H), 7.58 (d, *J* = 7.7 Hz, 1H), 7.40 (d, *J* = 8.4 Hz, 1H), 7.35 – 7.23 (m, 2H), 7.12 (tt, *J* = 15.7, 6.9 Hz, 3H), 7.01 (t, *J* = 7.4 Hz, 1H), 6.68 (d, *J* = 9.4 Hz, 1H), 5.41 (d, *J* = 5.3 Hz, 1H), 5.31 (d, *J* = 5.7 Hz, 1H), 4.98 (t, *J* = 8.9 Hz, 1H), 4.74 (q, *J* = 5.0 Hz, 1H), 4.69 – 4.58 (m, 1H), 4.39 (t, *J* = 5.1 Hz, 1H), 4.06 (dd, *J* = 10.1, 4.9 Hz, 1H), 3.43 (m, 2H), 3.30 (m, 2H), 3.17 (m, 2H), 1.26 (d, *J* = 5.0 Hz, 3H), 1.06 (t, *J* = 7.0 Hz, 2H). ^{13}C NMR (101 MHz, DMSO-d_6) δ 176.71, 170.82, 157.99, 137.50, 136.66, 134.49, 129.30, 128.22, 127.41, 125.77, 125.54, 125.27, 122.73, 121.57, 119.22, 118.95, 118.61, 111.86, 108.98, 106.19, 99.07, 80.82, 80.70, 73.87, 68.19, 67.84, 64.48, 30.59, 20.79. HRMS: m/z calcd for $C_{25}H_{33}N_2O_7$ ($[M+H]^+$) = 546.2235; found 546.2240.

3.3 Results and discussion

The compounds **1**-**7** (Scheme 4.1) were synthesised following the reported procedure[18] and characterized by analytical tools like HRMS, FTIR and NMR spectroscopy. The molecular structures of **1**, **2**, **5** and **6** were established using single crystal X-ray diffraction studies.

3.3.1 FTIR studies

In the FTIR spectra of **1**-**7** (*Fig 3.3*), the appearance of two sharp characteristic peaks in the range of 1004-1018 and 1080-1095 cm^{-1} indicate the presence of pyranose form of glucose residue.[19-20] On the other hand, the spectral peaks in the finger print range of 877-887 and 1257-1271 cm^{-1} support the β-configuration at the anomeric carbon and C-N stretching of anomeric carbon and the nitrogen, respectively.[19] An intense peak observed at around 1678-1695 cm^{-1} can be attributed to the carbonyl (C=O) stretching of the amide fragment.[16] Although FTIR supports the formation of the glycopeptides, it is difficult to distinguish between ketoenamine and phenolimine forms as the stretching vibrations for the C=O (enamine) and C=N (imine) bonds usually overlap.[21] Generally, carbonyl vibrational frequency in a amide linkage appears at about 1640 cm^{-1} due to the hydrogen bonding induced conjugated chelation,[22] while NH bending of amides also occur in the same region (1640-1550 cm^{-1}).[23] In the FTIR spectra of **1**-**7** NH bending for the *trans* configuration of NH and CO groups[23] along with the quinoid C=O stretching frequency are merged together and appeared at around 1622-1631 cm^{-1}.

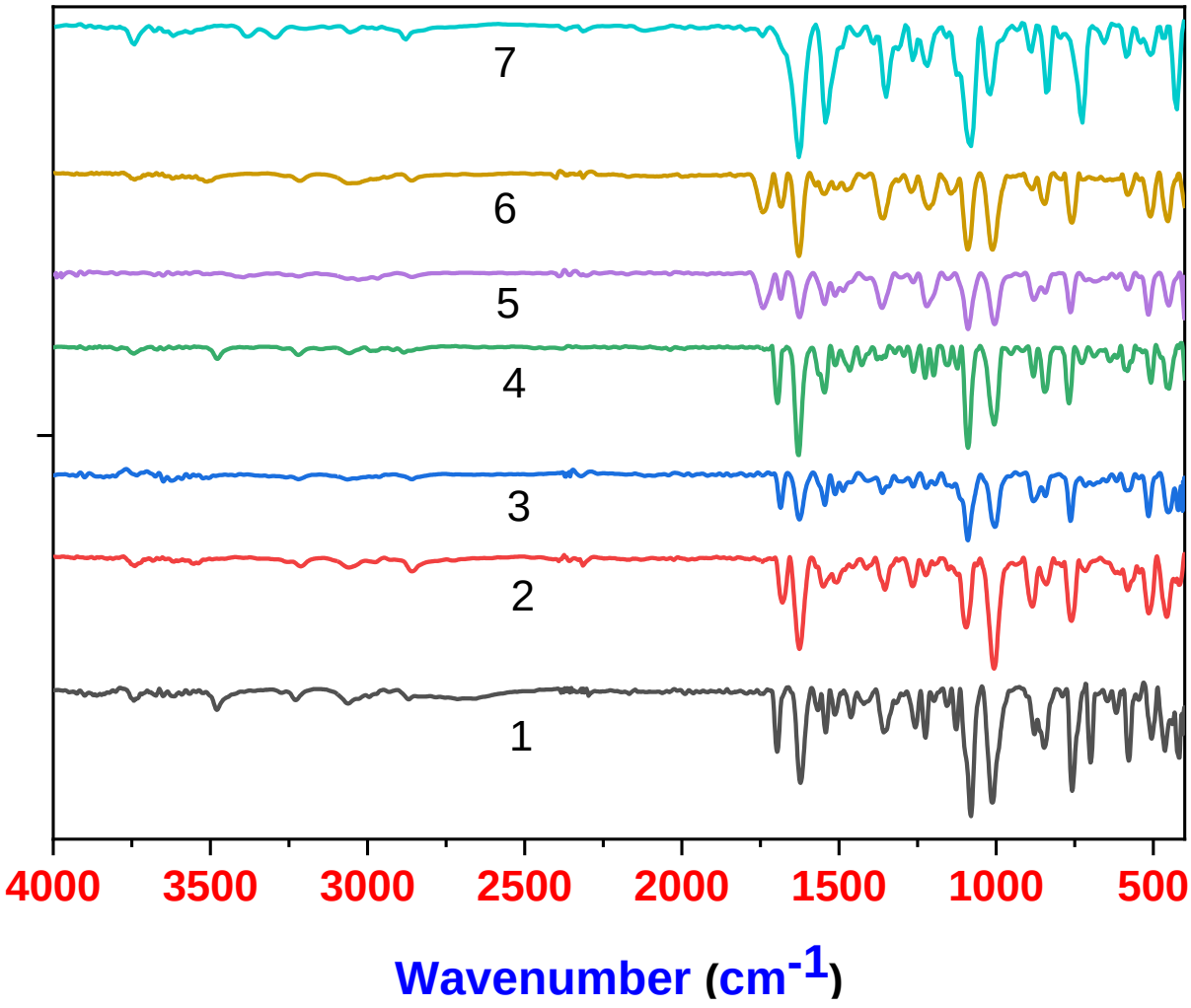

Fig. 3.3 *FTIR spectra of* ***1-7***

3.3.2 NMR studies

In ^{1}H-NMR spectra of compound **1-7**, the doublet (δ 8.6–8.9 ppm) corresponds to amidic N**H** whereas the anomeric C**H** appears as a triplet (δ 4.91-4.98 ppm). The two hydroxyl groups appear as double due to its adjacent CH coupling (C2-O**H** ~ δ 5.20-5.31 ppm and C3-O**H** ~ δ 5.41-5.35 ppm). The appearance of imine C-**H** as a doublet (δ 9.0–9.2 ppm,) and phenolic O**H**/amine N**H** as a triplet or doublet of doublet (δ 14.1–14.4 ppm) supported the shifting of phenolic hydrogen to the imine nitrogen, which resulted in the ketoenamine form of glycopeptides. Such 2-hydroxy-1-naphthaldehydes derived Schiff bases exhibit a dynamic equilibrium between ketoenamine and phenolimine forms in solution state[21] and in both the

tautomeric structures strong intramolecular hydrogen bonding is possible between amine NH and quinoid CO or phenolic OH and imine N, forming a six-membered ring (*Fig. 3.5*), which facilitates the strong deshielding effect of amine/imine N-H and also proton transfer.[24] Further, shifting of naphthalene ring C(2) carbon peak towards highly deshielded region (δ 175.76-178.57 ppm) and C(1) carbon peak towards shielded region (δ 106.17-106.82 ppm) with respect to corresponding carbons of 2–hydroxy-1-naphthaldehyde[25] in ^{13}C NMR spectra indicates the dominance of ketoenamine tautomer.[26]

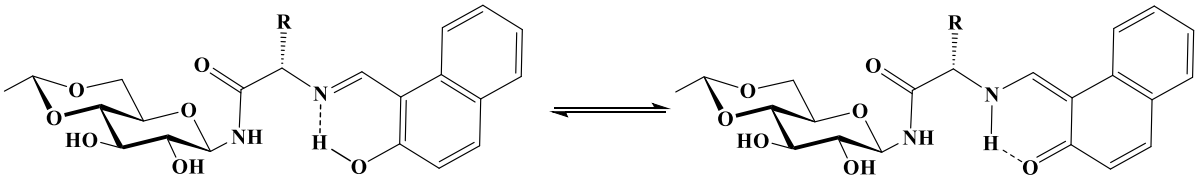

Fig. 3.4 *Tautomeric forms of **1** –**7**, where broken (–) line represents the hydrogen bonding*

Karakaş et al., have reported the appearance of carbonyl carbon for ketoenamine and phenolic carbon for phenolimine at δ ~ 180 and ~ 160 ppm, respectively [27] The tautomerization constant (K_T) and relative Gibbs free energy of such systems can be calculated using the ^{13}C chemical shift of quinoid carbon.[28] The experimental ^{13}C-NMR peak can be regarded as average of chemical shift of ketoenamine (δ_k) and phenolimine (δ_p) forms, such that $\delta_{exp} = n_k\delta_k + n_p\delta_p$, where n_k and n_p represents the molecular populations of ketoenamine and phenolimine structures, respectively. Assuming $n_k + n_p = 1$, the tautomeric population can be expressed as

$$n_p = \frac{\delta_k - \delta_{exp}}{\delta_k - \delta_p} \text{ and } n_k = \frac{\delta_{exp} - \delta_p}{\delta_k - \delta_p} \qquad (1)$$

Further, the tautomerization constant (K_T) and relative Gibbs free energy can be derived as:

$$K_T = \frac{n_k}{n_p} = \frac{\delta_{exp} - \delta_p}{\delta_k - \delta_{exp}} \qquad (2)$$

$$G = -RTlnK_T \qquad (3)$$

To calculate the tautomerization constant, representative ^{13}C chemical shift of quinoid (δ_k) and phenolic carbon (δ_p) is required. Taking ^{13}C chemical shift value reported for similar Schiff bases derived from TRIS (tris(hydroxymethyl)aminomethane) into account[28], the tautomerization constant (K_T) can be expressed by:

$$K_T = \frac{\delta_{exp} - 154.45}{180.18 - \delta_{exp}} \qquad (4)$$

Using equation 6, the tautomerization constant (K_T) values for compound **1-7** were found to be 6.2, 5.7, 6.3, 8.3, 14.9, 4.82 and 6.41, respectively, indicating the solution phase population of ketoenamine form of these compounds lay in between 82 to 93%.

3.3.3 UV-Visible and fluorescence studies

The UV-visible absorption spectra of **1-7** were recorded in DMSO and MeOH in the range of 250 to 500 nm at 20 µM concentration (*Fig. 3.5*). The spectra in both the solvents looks alike with two peaks in the visible region at around 400 and 420 nm, which may be attributed to the zwitterion and ketoenamine form, respectively with some charge redistribution in the hydrogen-bonded pseudo-aromatic ring of these compounds.[29-32] The bands observed at about 300 nm were assignable to the OH attached to the β-carbon of the naphthalene moiety.[33]

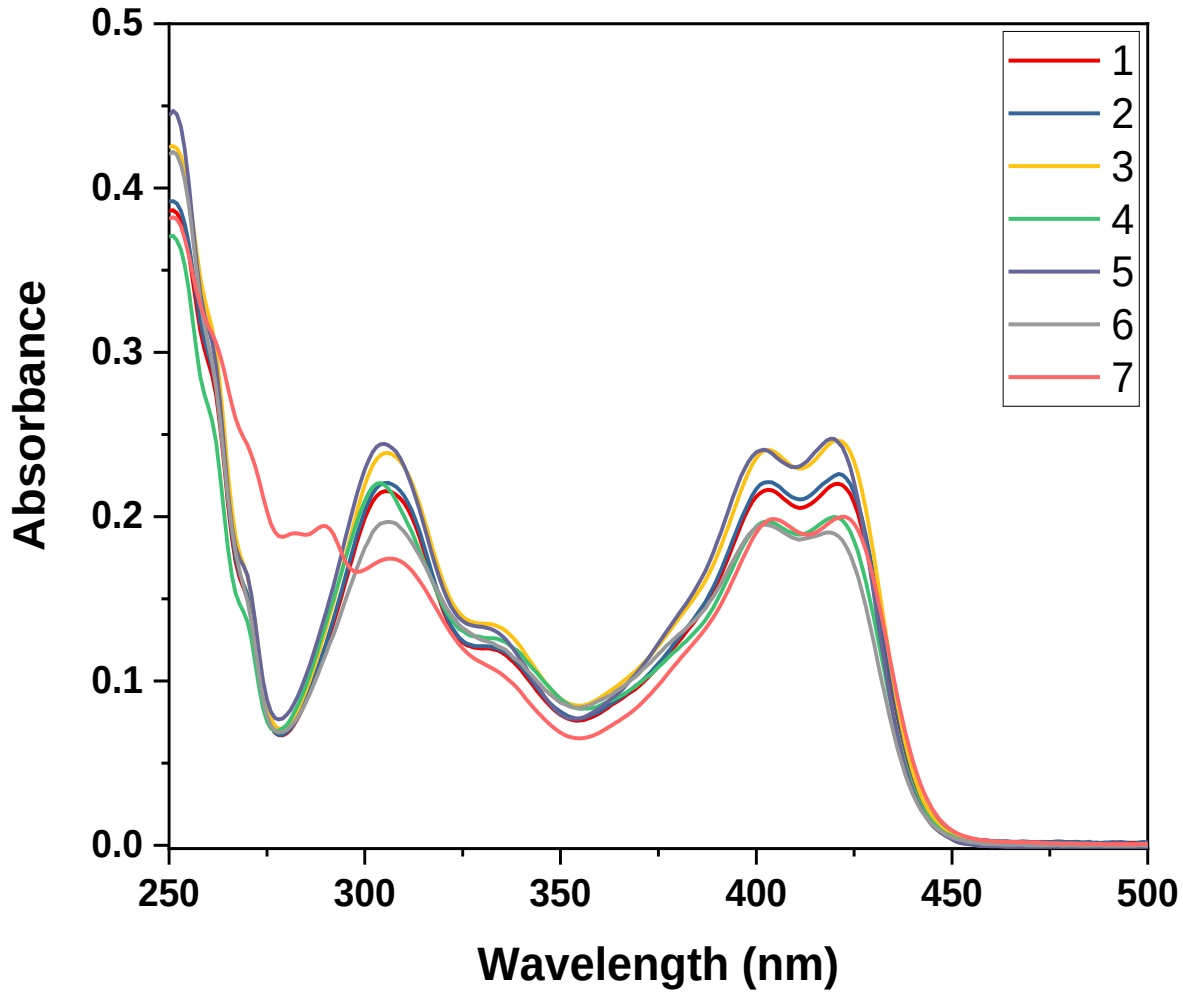

Fig. 3.5 *UV-Visible absorption spectra of* ***1-7***

3.3.4 Crystal structure of glycopeptides

Slow evaporation of concentrated DMSO solution of compounds **1**, **2**, **5** and **6** afforded X-ray suitable single crystals of corresponding glycoconjugates. The compounds **1**, **2** and **6** were crystallized in monoclinic lattice with $P2_1$ space group, while triclinic lattice with P1 space group was noted for **5**. The molecular structures of all these glycopeptides are shown in *Fig. 3.6* as ORTEP diagram and crystallographic data of molecules **1** (CCDC No. 2033083), **2** (CCDC No. 2171119), **5** (CCDC No. 2033084) and **6** (CCDC No. 2120336) are summarized in *Table 3.1*. The crystal structures confirm the pyranose configuration and $^4C_1$ conformation of the sugar moieties. It also reveals the protection at 4- and 6- positions along with β-anomeric

form of the starting glycosylamine, which is supported by the NMR spectra. Both the pyranose rings, caused due to the sugar moiety and it's protecting groups at 4,6-positions are found in chair conformation. The NH and CO groups of amide moiety attached to the sugar in all four molecules are in *trans* configuration, which is reinforced by the FTIR spectra.

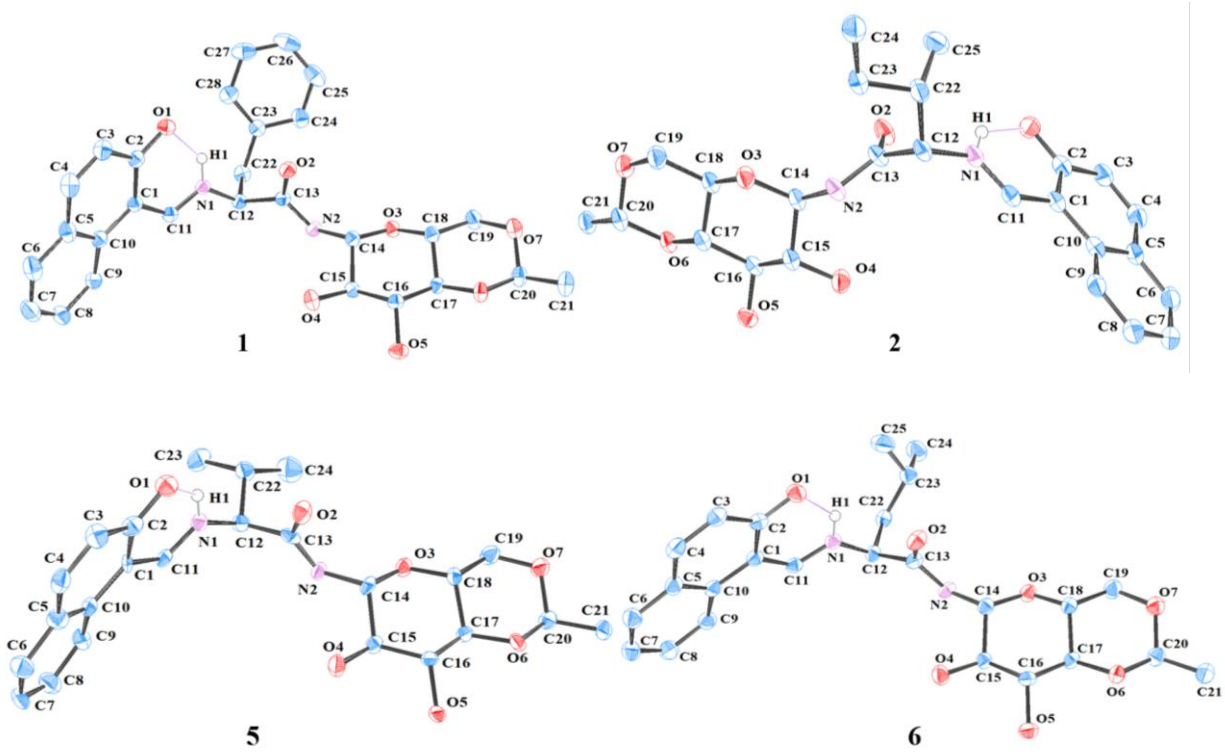

***Fig. 3.6** ORTEP diagram of **1**, **2**, **5** and **6** with thermal ellipsoids drawn at 50 % probability level.*

***Table 3.1** Summary of crystallographic data for **1**, **2**, **5** and **6**.*

Compound	**1**	**2**	**5**	**6**
Empirical formula	$C_{28}H_{30}N_2O_7$	$C_{25}H_{32}N_2O_7$	$C_{24}H_{30}N_2O_7$	$C_{25}H_{32}N_2O_7$
Formula weight	506.54	472.52	458.50	472.52
Temperature/K	93(2)	93(2)	93(2)	93(2)
Crystal system	monoclinic	monoclinic	triclinic	monoclinic
Space group	$P2_1$	$P2_1$	P1	$P2_1$
a/Å	9.9980(2)	9.8166(4)	9.8733(5)	9.9108(2)
b/Å	10.03800(10)	10.7163(5)	10.7594(6)	10.6668(2)
c/Å	13.5001(2)	11.7800(5)	11.4977(4)	23.1660(4)
α/°	90	90	89.697(4)	90
β/°	111.469(2)	103.112(4)	71.490(4)	98.7300(10)

γ/°	90	90	87.554(4)	90
Volume/Å^3	1260.86(4)	1206.92(9)	1157.12(10)	2420.66(8)
Z	2	2	2	4
ρ_{calc}g/cm^3	1.334	1.300	1.316	1.297
μ/mm^{-1}	0.795	0.786	0.804	0.784
F(000)	536.0	504.0	488.0	1008.0
Radiation	Cu Kα (λ = 1.54184)	CuKα (λ = 1.54184)	CuKα (λ = 1.54184)	Cu Kα (λ = 1.54184)
2Θ range for data collection/°	9.506 to 159.012	9.25 to 159.58	8.11 to 159.846	7.722 to 148.61
Index ranges	$-12 \le h \le 11$, $-12 \le k \le 7$, $-16 \le l \le 16$	$-12 \le h \le 12$, $-13 \le k \le 9$, $-14 \le l \le 14$	$-12 \le h \le 11$, $-13 \le k \le 7$, $-14 \le l \le 12$	$-12 \le h \le 11$, $-12 \le k \le 8$, $-26 \le l \le 28$
Reflections collected	7308	6795	6190	13643
Independent reflections	3649 [R_{int} = 0.0263, R_{sigma} = 0.0344]	3389 [R_{int} = 0.0433, R_{sigma} = 0.0515]	4272 [R_{int} = 0.0212, R_{sigma} = 0.0294]	7050 [R_{int} = 0.0306, R_{sigma} = 0.0444]
Data/restraints/parameters	3649/1/337	3389/1/312	4272/3/605	7050/1/623
Goodness-of-fit on F^2	1.058	1.083	1.084	1.068
Final R indexes [I>=2σ (I)]	R_1 = 0.0313, wR_2 = 0.0823	R_1 = 0.0542, wR_2 = 0.1544	R_1 = 0.0772, wR_2 = 0.2354	R_1 = 0.0350, wR_2 = 0.0953
Final R indexes [all data]	R_1 = 0.0322, wR_2 = 0.0832	R_1 = 0.0561, wR_2 = 0.1564	R_1 = 0.0779, wR_2 = 0.2359	R_1 = 0.0369, wR_2 = 0.0966
Largest diff. peak/hole / e Å^{-3}	0.21/-0.23	0.28/-0.27	0.54/-0.39	0.17/-0.20
Flack parameter	0.09(16)	-0.2(2)	-0.2(4)	0.12(11)

Selected bond lengths and bond angles are presented in *Table 3.2*, where O(1)-C(2) and N(1)-C(11) bond lengths indicate higher bond order of phenolic C–O than one and lower bond order of imine C=N than two. Further, a large deviation of C(1)-C(2) from aromatic C=C bond length confirms the existence of compounds **1**, **2**, **5** and **6** in the quinoid form.[34] A similar phenomena was also observed in case of amide bond, where the bond length of O(2)-C(13) and N(2)-C(13) in all the structures suggest their actual bond order is between one and two due to resonance. A slight distortion of naphthyl ring in all the molecules can also be noticed from the crystal structure. Additionally, the plane of naphthyl ring dissect the plane of the carbohydrate ring at 85.70°, 89.06°, 86.71° and 89.42° in molecule **1**, **2**, **5** and **6**, respectively (*Fig. 3.7*), which generate a binding pocket for the analyte molecules. These pockets play a vital role in molecular and metal ion recognition, which will be discussed later.

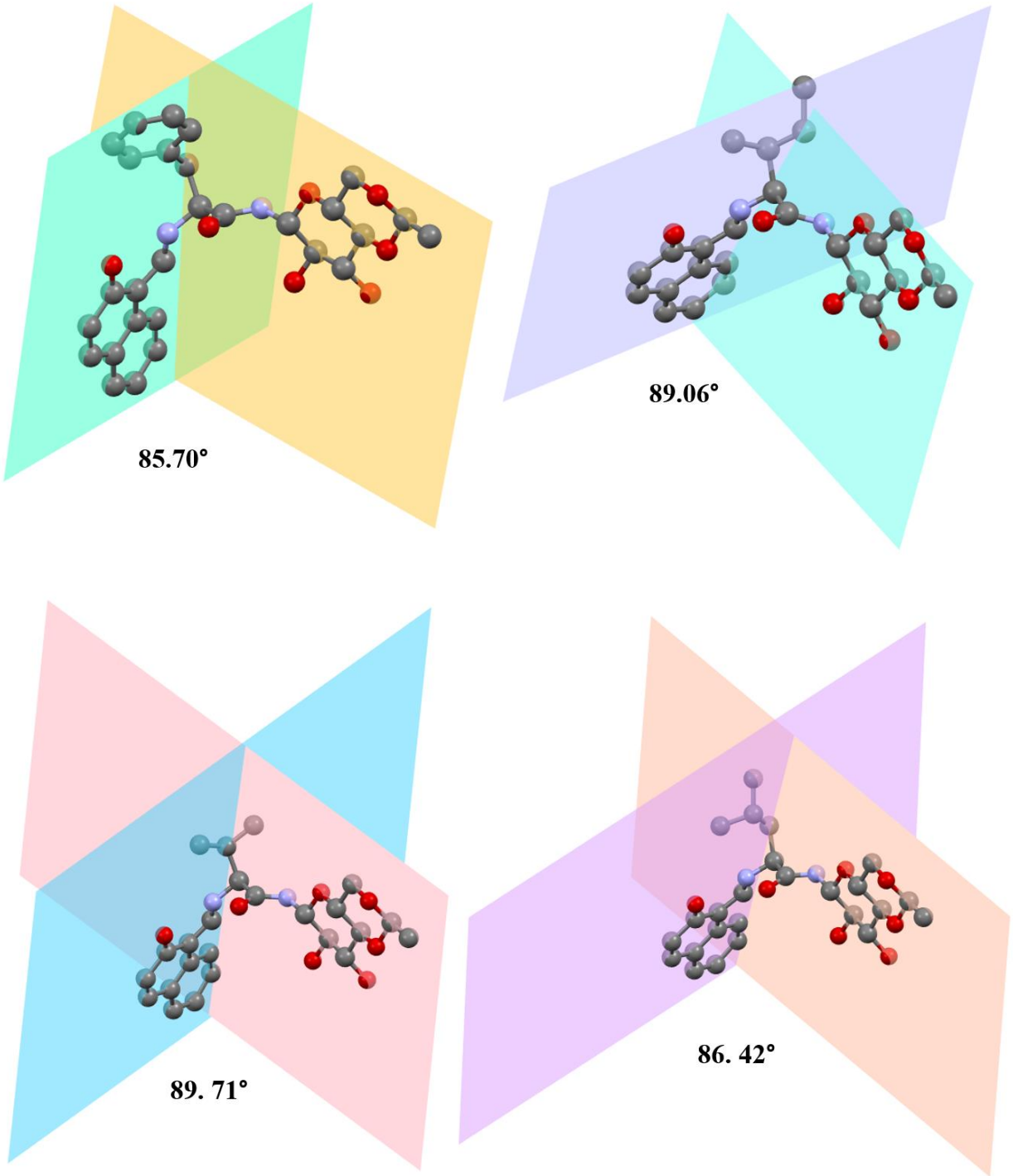

Fig. 3.7 *Angle between naphthyl ring and carbohydrate ring*

Table 3.2 *Selected bond lengths (in Å) and bond angle (˚) of* ***1***, ***2***, ***5*** *and* ***6****.*

Compound **1**			
Atoms	Length/Å	Atoms	Length/Å
C13-C12	1.534(3)	C8-C7	1.404(4)
C16-C17	1.514(3)	C6-C7	1.368(4)
C2-C3	1.445(3)	C5-C4	1.432(3)
C5-C6	1.410(3)	C2-C1	1.433(3)
O7-C19	1.431(3)	C9-C8	1.385(3)
N1-C12	1.461(2)	C16-C15	1.525(3)
N1-C11	1.307(3)	C15-C14	1.533(3)
N2-C14	1.434(3)	C11-C1	1.406(3)
C10-C5	1.424(3)	N2-C13	1.355(2)
C3-C4	1.351(3)	O6-C17	1.434(2)
C10-C9	1.404(3)	O6-C20	1.429(2)
O4-C15	1.418(2)	O1-C2	1.290(2)
O2-C13	1.220(3)	C1-C10	1.456(3)
O5-C16	1.419(2)	C12-C22	1.538(3)
Atom	Angle/˚	Atom	Angle/˚
C11-N1-C12	123.05(16)	O2-C13-N2	124.83(19)
C1-C2-C3	118.31(18)	O1-C2-C1	121.78(18)
N1-C11-C1	124.69(18)	O2-C13-C12	120.78(17)
C13-N2-C14	120.03(17)	O4-C15-C14	109.83(15)
O5-C16-C15	112.26(16)	C9-C10-C1	123.98(19)
C6-C5-C4	120.9(2)	O2-C13-N2	124.83(19)
N1-C12-C22	112.19(16)	C26-C25-C24	120.2(3)
O6-C20-C21	108.10(18)	C9-C8-C7	120.8(2)
Compound **2**			
Atoms	Length/Å	Atoms	Length/Å
C13-C12	1.533(4)	C8-C7	1.397(5)
C16-C17	1.528(4)	C6-C7	1.369(6)
C2-C3	1.438(4)	C5-C4	1.428(5)
C5-C6	1.417(4)	C2-C1	1.432(5)
O7-C19	1.438(4)	C9-C8	1.375(5)
N1-C12	1.442(4)	C16-C15	1.534(4)
N1-C11	1.308(4)	C15-C14	1.537(4)
N2-C14	1.431(4)	C11-C1	1.402(4)
C10-C5	1.417(4)	N2-C13	1.349(4)
C3-C4	1.357(5)	O6-C17	1.434(4)
C10-C9	1.404(5)	O6-C20	1.427(3)
O4-C15	1.416(3)	O1-C2	1.288(4)
O2-C13	1.221(4)	C1-C10	1.465(4)
O5-C16	1.410(3)	C12-C22	1.558(4)
Atom	Angle/˚	Atom	Angle/˚
C11-N1-C12	125.9(3)	O2-C13-N2	119.5(2)
C1-C2-C3	118.4(3)	O1-C2-C1	121.5(3)
N1-C11-C1	123.8(3)	O2-C13-C12	119.5(2)
C13-N2-C14	120.7(3)	O4-C15-C14	110.3(2)
O5-C16-C15	113.3(3)	C9-C10-C1	123.0(3)
C6-C5-C4	120.9(3)	O2-C13-N2	124.7(3)
N1-C12-C22	111.0(2)	C22-C23-C24	113.3(3)
O6-C20-C21	108.1(3)	C9-C8-C7	120.9(4)
Compound **5**			
Atom-Atom	Length/Å	Atom-Atom	Length/Å
C18-C19	1.523(12)	C10-C5	1.416(11)
C16-C15	1.529(12)	C9-C8	1.365(14)
O2-C13	1.226(10)	O6-C20	1.430(10)
O6-C17	1.412(11)	C16-C17	1.525(11)
N2-C13	1.330(11)	N2-C14	1.431(11)

O5-C16	1.420(9)	O4-C15	1.426(11)
C11-C1	1.412(10)	C1-C2	1.444(11)
O1-C2	1.281(11)	C4-C3	1.344(14)
C12-C22	1.560(11)	C13-C12	1.519(13)
C6-C7	1.371(14)	C6-C5	1.416(13)
C14-C15	1.551(10)	C5-C4	1.427(13)
N1-C11	1.292(11)	N1-C12	1.464(10)
C8-C7	1.383(13)	C10-C9	1.420(12)
C2-C3	1.432(11)	C10-C1	1.444(12)
Atom	Angle/˚	Atom	Angle/˚
C11-N1-C12	124.7(7)	O2-C13-N2	123.2(7)
C1-C2-C3	117.3(8)	O1-C2-C1	122.8(7)
C1-C2-C3	117.3(8)	O1-C2-C1	122.8(7)
N1-C11-C1	124.9(8)	O2-C13-C12	118.0(8)
C13-N2-C14	120.9 (7)	O4-C15-C14	111.2(6)
O5-C16-C15	113.0(6)	C9-C10-C1	122.7(7)
C6-C5-C4	120.8(10)	O2-C13-N2	123.2(7)
C11-C1-C2	117.7(8)	C10-C5-C4	118.5(8)
Compound **6**			
Atom-Atom	Length/Å	Atom-Atom	Length/Å
C18-C19	1.511(3)	C10-C5	1.415(3)
C16-C15	1.531(3)	C9-C8	1.372(4)
O2-C13	1.230(3)	O6-C20	1.431(3)
O6-C17	1.433(3)	C16-C17	1.519(3)
N2-C13	1.353(3)	N2-C14	1.436(3)
O5-C16	1.414(2)	O4-C15	1.417(3)
C11-C1	1.410(3)	C1-C2	1.430(3)
O1-C2	1.282(3)	C4-C3	1.351(4)
C12-C22	1.532(3)	C13-C12	1.529(3)
C6-C7	1.369(4)	C6-C5	1.418(3)
C14-C15	1.540(3)	C5-C4	1.434(4)
N1-C11	1.308(3)	N1-C12	1.460(3)
C8-C7	1.405(4)	C10-C9	1.415(4)
C2-C3	1.430(3)	C10-C1	1.452(3)
Atom	Angle/˚	Atom	Angle/˚
C11-N1-C12	123.8(2)	O2-C13-N2	123.8(2)
C1-C2-C3	117.8(2)	O1-C2-C1	121.9(2
C2-C1-C10	120.4(2)	O1-C2-C3	120.2(2)
N1-C11-C1	124.2(2)	O2-C13-C12	120.82(19)
C13-N2-C14	120.8(2)	O4-C15-C14	110.34(18)
O5-C16-C15	113.26(18	C9-C10-C1	123.5(2)
C6-C5-C4	121.0(2)	O2-C13-C12	120.82(19)

In the lattice, **1**, **2**, **5** and **6** possess six intermolecular and one intramolecular hydrogen bonding (*Table 3.3*). Out of six intermolecular hydrogen bonds, there are five O-H···O type and only one N-H···O type interactions. In these molecules, amide NH, amine NH and Glu-OH2 act as hydrogen donors while O-4 and quinoid CO acts as hydrogen acceptors, whereas Glu-OH3 possesses both hydrogen donating and accepting capability. Each molecule is associated with four molecules through intermolecular hydrogen bonds, where three molecules are connected

with the sugar moiety and one is associated with aromatic part. Thus, a two-dimensional multimer is formed through these intermolecular hydrogen bonds (*Fig. 3.8*).

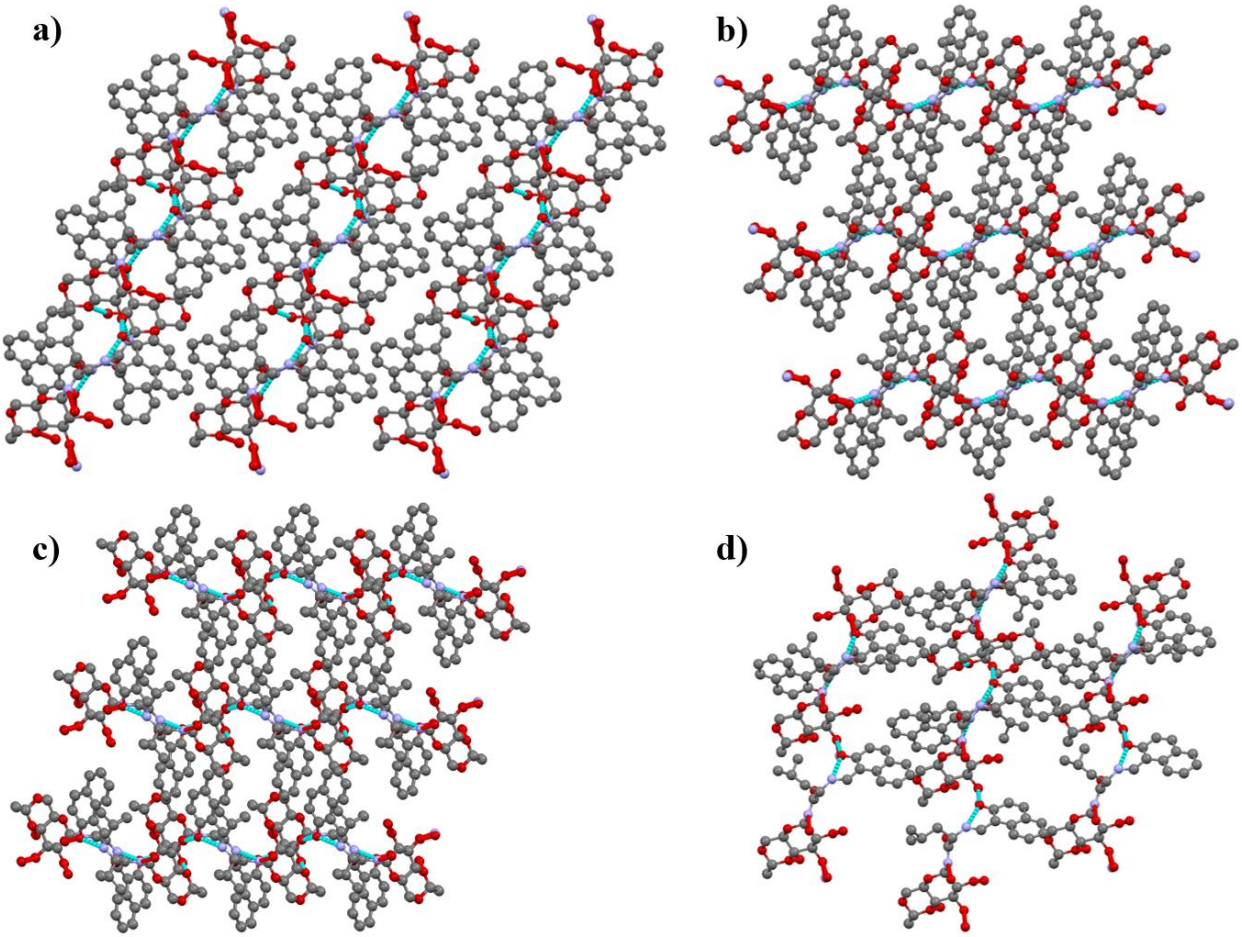

Fig. 3.8 *Packing diagram of* ***1***, ***2***, ***5*** *and* ***6*** *showing two dimensional multimerization (Red and blue dotted lines represent the hydrogen bonds)*

Table 3.3 *Summary of hydrogen bonding data present in the crystal structures of compound* ***1***, ***2***, ***5*** *and* ***6***

Compound	Hydrogen bond	d(D[a]-H) (Å)	d(H-A[b]) (Å)	d(D[a]-A[b]) (Å)	D[a]-H-A[b] (°)
1	O(5) - H(5)···O(1)	0.84	1.77	2.607	174.3
	O(4) - H(4)···O(6)	0.84	2.04	2.868	166.7
	N(2) - H(2)···O(5)	0.88	2.08	2.823	141.7
	N(1) - H(1)···O(1)	0.88	1.91	2.578	131.2

2	O(5) - H(5)···O(1)	0.82	1.79	2.611	176.8
	O(4) - H(4)···O(6)	0.82	2.28	3.091	169.2
	N(2) - H(2)···O(5)	0.86	1.98	2.843(4)	177.2
	N(1) - H(1)···O(1)	0.86	1.87	2.554	134.9
5	O(5) - H(5)···O(1)	0.84	1.82	2.646(5)	168.0
	N(1) - H(1)···O(1)	0.88	1.89	2.559(5)	131.0
	N(2) - H(2)···O(5)	0.88	1.97	2.850(5)	173.0
	O(4) - H(4)···O(6)	0.82	2.186	3.002	174.6
6	O(5) - H(5)···O(1)	0.84	1.80	2.635(2)	177.3
	O(4) - H(4)···O(6)	0.84	2.178	3.014	173.6
	N(2) - H(2)···O(5)	0.88	1.99	2.848(3)	165.2
	N(1) - H(1)···O(1)	0.88	1.92	2.580(2)	130.9

The intramolecular N-H···O type hydrogen bonding interactions between the quinoid CO and amine NH resulted in a six-membered pseudo-aromatic ring, who's planarity is well-aligned with the aromatic ring. These resonance-assisted intramolecular hydrogen bonds increase the electron-withdrawing nature of the carbonyl group which in turn increases the acidity of ring hydrogens and NH (amine).[35] Distance between donor and acceptor atoms ($R_{D\text{-}A}$) can be used to calculate the intramolecular hydrogen bond energy following the empirical formula:

$$E_{HB}\ (\text{kcal/mol}) = -5.554 \times 10^5 \cdot e^{-4.12 \cdot R_{D-A}} \qquad (5)$$

where $R_{D\text{-}A}$ is either theoretically calculated or experimentally measured distance (in Å).[36]

The crystal data provides the distance between donor (N) and acceptor (O) atom, yielding strong intramolecular hydrogen bonding with the energy of -13.54, -14.96, -14.64 and -13.43 kcal/mol for compound **1**, **2**, **5** and **6**, respectively.[37]

3.3.5 Theoretical calculations

In order to ascertain the structural correlation as well as physical and chemical properties, the quantum chemical calculation has been performed for **2**.[38] Computational chemistry helps in rationalizing and understanding the geometrical parameters, IR intensities, electronic transitions as well as charge distribution and natural bond order (NBO) analysis of the

molecules.[38-42] Here, we have discussed the theoretical studies of **2** (for both phenolimine and ketoenamine forms) and the correlation between experimental and theoretical results of single-crystal X-ray data, NMR, and UV-visible spectroscopy. The Mulliken population analysis depicts a clear picture of the net atomic charge of each atom for the ketoenamine form of **2**. The molecular electrostatic potential (MEP) and NBO analysis for both the tautomeric forms of **2** provided additional details like electrophilic/nucleophilic and intramolecular charge transfer sites present in the molecule, respectively.

Although the molecule crystallized in ketoenamine form, the solution studies reveal the existence of equilibrium between its ketoenamine and phenolimine tautomeric forms. In order to understand the energy preferences for ketoenamine form in the solid state, geometrical optimizations of both the tautomeric forms were done using HF/6-31G and DFT/B3LYP/6-31G(2d,p) level of theories, respectively. The theoretical calculations confirmed the higher stability of the quinoid structure by 1.23 Kcal/mol *(Table. 3.4*) and also have higher dipole moment (*Table 3.5*). The theoretically determined geometrical parameters of both the configurations were compared with the XRD data and some selected bond lengths and angles are presented in *Table.3.6*. The theoretical value of bond lengths of ketoenamine form are in good agreement with the experimental data with an average deviation of 0.01 to 0.03 Å for both the basis sets.

Table 3.4 *Comparative single point energy (in a.u.) data for optimized phenolimine and ketoenamine geometry of* ***2***

Entry	HF/6-31G		B3LYP/6-31G(2d,p)	
	Gas Phase	DMSO	Gas Phase	DMSO
Enolimine	-1597.5978	-1597. 668	-1608.496	-1608.681
Ketoenamine	-1597.6013	-1597.671	-1608.499	-1608.690
Energy difference	0.0035	0.003	0.003	0.009

Table 3.5 *Comparative dipole moment (in debye) data for optimized enolimine and ketoenamine geometry of* ***2***

Entry	X-axis	Y-axis	Z-axis	Total
Enolimine	-3.2119	0.6779	-6.5411	7.318595
Ketoenamine	-1.7713	1.4880	-7.5131	7.861191

Table.3.6 *Comparison between crystal and computed geometrical parameters of* ***2***

X-ray parameters	Experimental data	Theoretical							
		HF/6-31G				B3LYP/6-31G (2d, p)			
		Keto		Enol		Keto		Enol	
		Gas phase	DMSO	Gas phase	DMSO	Gas phase	DMSO	Gas phase	DMSO
Bond length									
O6-C17	1.434(4)	1.4266	1.4327	1.4271	1.43237	1.42344	1.42561	1.41992	1.42561
O6-C20	1.427(3)	1.4277	1.4333	1.4269	1.43160	1.42300	1.42529	1.41743	1.42290
C13-C12	1.533(4)	1.5252	1.5200	1.5214	1.52188	1.53605	1.53538	1.53983	1.53765
C9-C8	1.372(4)	1.4061	1.3770	1.3665	1.36677	1.38228	1.38194	1.37569	1.37609
C5-C4	1.428(5)	1.449	1.4449	1.4241	1.42315	1.43906	1.43526	1.42109	1.42086
C5-C6	1.417(4)	1.4003	1.4036	1.4142	1.41669	1.40544	1.40807	1.41303	1.41474
O5-C16	1.410(3)	1.4204	1.4268	1.4208	1.42541	1.41850	1.42396	1.41762	1.42261
O3-C18	1.425(4)	1.4299	1.4297	1.4292	1.42930	1.42262	1.42325	1.42355	1.42288
O3-C14	1.429(4)	1.4384	1.4419	1.4398	1.44361	1.43081	1.43165	1.42984	1.43436
C22-C25	1.528(4)	1.5357	1.5338	1.5337	1.53346	1.5317	1.53158	1.53198	1.53158
C23-C24	1.528(5)	1.5368	1.5326	1.5323	1.53250	1.53092	1.53113	1.53068	1.53101
O0AA -C2	1.288(4)	1.2566	1.2677	1.3471	1.35676	1.25288	1.26492	1.33330	1.34059
C12-C22	1.558(4)	1.5506	1.5616	1.5605	1.56103	1.56158	1.56264	1.55867	1.56093
C4-C3	1.351(4)	1.3372	1.3405	1.35205	1.35490	1.34938	1.35250	1.36191	1.36395
O7-C20	1.404(4)	1.4262	1.4261	1.4264	1.42672	1.41394	1.41754	1.41827	1.41914
C1-C10	1.465(4)	1.4704	1.4662	1.4433	1.44228	1.45972	1.45877	1.44219	1.44166
C1-C2	1.432(5)	1.4530	1.4399	1.38383	1.38261	1.46081	1.45218	1.40504	1.40321
C1-C11	1.402(4)	1.3884	1.3900	1.45978	1.46407	1.38886	1.39871	1.44839	1.45157
C10-C5	1.417(4)	1.4076	1.4088	1.41385	1.41513	1.41996	1.42178	1.42785	1.42878
C10-C9	1.404(5)	1.4052	1.4095	1.42065	1.42199	1.40903	1.41157	1.41726	1.41825
C16-C17	1.528(4)	1.5100	1.5136	1.50997	1.51011	1.51963	1.51863	1.51504	1.51402

C16-C15	1.534(4)	1.5282	1.5235	1.52788	1.52800	1.52752	1.52704	1.53150	1.53162
C17-C18	1.526(4)	1.5257	1.5193	1.52580	1.52574	1.52442	1.52494	1.53078	1.53052
C18-C19	1.507(4)	1.5159	1.5158	1.51590	1.51586	1.52098	1.52155	1.52154	1.52134
O7-C19	1.438(4)	1.4378	1.4450	1.43792	1.44372	1.42644	1.4309	1.42386	1.42952
O2-C13	1.221(4)	1.2218	1.2333	1.22116	1.23148	1.21137	1.22121	1.21123	1.22093
O4-C15	1.416(4)	1.426	1.4254	1.42547	1.42728	1.41543	1.42102	1.42122	1.42376
C14-C15	1.537(4)	1.5261	1.5353	1.52641	1.52852	1.54380	1.54575	1.53693	1.53974
C2-C3	1.438(4)	1.4528	1.4491	1.41592	1.41347	1.45250	1.44837	1.41617	1.41478
N2-C13	1.349(4)	1.3681	1.3479	1.37039	1.35734	1.37936	1.36295	1.38297	1.36749
N2-C14	1.431(4)	1.4299	1.4246	1.42859	1.42525	1.43709	1.43440	1.43599	1.43113
N1-C11	1.308(4)	1.331	1.3175	1.27134	1.27246	1.32729	1.31900	1.28419	1.28467
N1-C12	1.442(4)	1.4453	1.4537	1.44923	1.45271	1.45040	1.45466	1.44982	1.45316
Bond angle									
C20-O6-C17	109.22(17)	113.686	113.430	113.670	113.47691	111.183	110.8771	111.12167	110.87678
C18-O3-C14	109.60(17)	113.60233	113.685	113.569	113.84039	110.3965	110.8656	111.04482	111.20341
C20-O7-C19	111.83(19)	116.56461	116.184	116.54691	116.01959	112.7414	112.5992	112.83888	112.59907
C13-N2-C14	120.8(2)	122.52544	123.062	122.46085	123.08021	123.2815	122.6496	122.15490	123.22331
C11-N1-C12	123.8(2)	123.14750	124.071	121.64693	121.30940	126.6514	125.0548	119.10834	118.77264
O1 -C2-C1	121.9(2)	122.20468	122.577	123.77525	122.72790	122.1032	122.8965	122.67922	122.00763
O0AA -C2-C3	120.2(2)	119.92619	119.444	114.94319	115.64311	122.1032	122.8965	116.62827	117.05397
C1-C2-C3	118.0(2)	117.86267	117.977	121.28080	121.62834	117.553	117.203	120.69210	120.93823
C11-C1-C10	120.3(2)	121.24977	120.667	121.15304	121.23612	121.1495	120.9701	121.63199	121.63849
C11-C1-C2	119.0(2)	118.80679	119.254	119.90205	119.96469	118.1418	118.4309	119.15649	119.23961
C2-C1-C10	120.4(2)	119.91319	120.069	118.94242	118.79706	120.4402	120.599	119.21015	119.12145
O3-C18-C17	109.96(18)	109.44354	107.690	109.47059	109.08588	110.2103	110.1138	110.88576	110.45882
O3-C18-C19	109.59(19)	110.20252	110.570	110.19708	110.09156	110.1845	110.2094	110.03924	110.00128
C19-C18-C17	109.33(18)	109.26370	109.382	109.25624	109.46624	108.5891	108.6241	108.54817	108.75027
N1-C11-C1	124.2(2)	127.14767	126.255	122.90942	122.32824	123.5274	124.1039	122.87936	122.32045
N1-C12-C13	106.03(18)	108.00381	107.111	108.22109	108.01248	108.4913	105.9658	108.14181	108.38564
N1-C12-C22	113.38(18)	111.91353	111.347	110.53759	110.31546	112.8384	110.2458	111.46184	110.92624

C13-C12-C22	111.63(18)	112.41799	112.981	112.07172	112.64905	107.0384	110.7659	112.31366	112.65394
C3-C4-C5	122.1(2)	122.64370	122.381	121.31691	121.19698	122.5618	122.3652	121.61970	121.49868
O4-C15-C16	109.05(18)	105.43139	107.745	105.45902	105.72187	109.4964	107.8732	106.29499	106.19864
O4-C15-C14	110.34(18)	111.02257	108.385	111.03836	110.48834	110.0606	110.2891	111.58550	111.38797
C16-C15-C14	109.25(18)	112.99014	111.897	113.00990	112.39746	111.3116	111.4857	112.34620	111.87455
O3-C14-N2	109.07(18)	107.33525	107.796	107.59512	108.24260	108.7916	107.9612	108.12615	108.38649
O3-C14-C15	110.28(17)	108.41203	110.496	108.27769	108.60524	111.2474	111.3662	110.05446	110.11596
N2-C14-C15	110.53(18)	111.67570	111.179	111.66054	111.67164	109.7419	110.6917	110.75645	111.06582
O2-C13-N2	123.8(2)	122.35118	122.606	121.80431	121.79953	123.9421	123.7375	122.71343	122.81212
O2-C13-C12	120.82(19)	121.41026	120.824	122.81904	122.58306	121.4725	120.6033	122.90102	122.67403
N2-C13-C12	115.4(2)	116.23743	116.568	115.37550	115.61694	114.5846	115.5885	114.35111	114.51026
O5-C16-C17	112.12(18)	108.71919	110.516	108.75052	108.94719	112.9065	113.1225	109.53372	109.66710
O5-C16-C15	113.26(18)	108.94118	107.427	108.98904	109.38051	112.054	112.2316	110.57987	110.56764
C17-C16-C15	106.49(18)	109.73380	107.427	109.68778	109.47495	109.2712	108.8885	108.92935	109.12060
C9-C10-C1	123.5(2)	123.92652	123.894	123.66326	123.52244	123.6775	123.9822	123.79010	123.65424
C5-C10-C1	119.0(2)	118.79466	118.881	119.16410	119.12156	118.7912	118.8144	119.04285	119.01865
C5-C10-C9	117.5(2)	117.27799	117.223	117.17209	117.35563	117.5266	117.2034	117.16688	117.32688
C9-C8-C7	121.0(3)	120.71531	120.926	120.93943	120.99166	120.7403	120.8525	120.90758	120.94945
C6-C7-C8	119.2(2)	118.81193	118.839	119.12618	119.26222	119.1288	118.9782	119.21235	119.31531

The theoretical ^{1}H and ^{13}C-NMR spectra of both the ketoenamine and phenolimine form of **2** in DMSO were generated using B3LYP/6-31G(2d,p) (*Fig. 3.9-3.12*). The chemical shift values show a good agreement between the experimental and calculated NMR of ketoenamine form except for the hydroxyl protons of sugar moiety, which appeared highly upfield in theoretically generated spectrum. OH-2 and OH-3 protons appeared at δ = 5.36 and 5.21 ppm in experimental, while at δ = 1.42 and 2.05 ppm in calculated spectra, respectively. Phenolic proton of phenolimine form appeared downfield (δ = 14.56 ppm) compared to the amine proton of ketoenamine form (δ = 13.3 ppm). The chemical shift values for phenolic carbon (phenolimine form) and quinoid carbon (ketoenamine form) appeared at δ = 169.6 and 188.14 ppm, respectively in simulated ^{13}C NMR spectra.

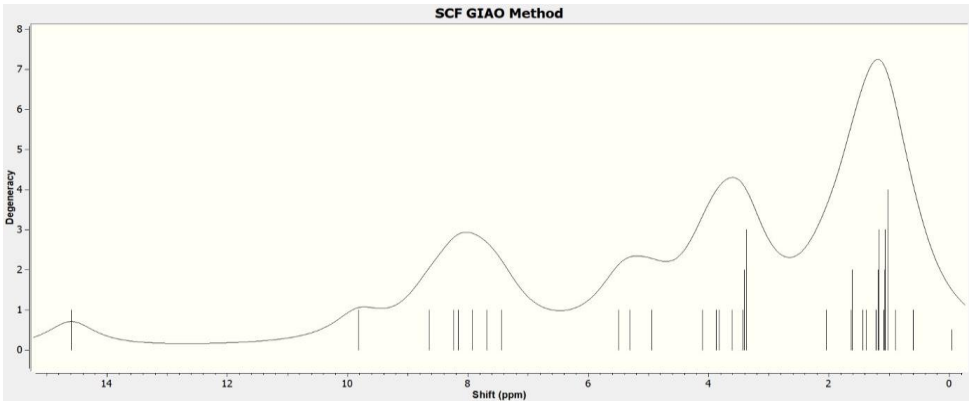

Fig. 3.9 Simulated ^{1}H-NMR of phenolimine form of **2**

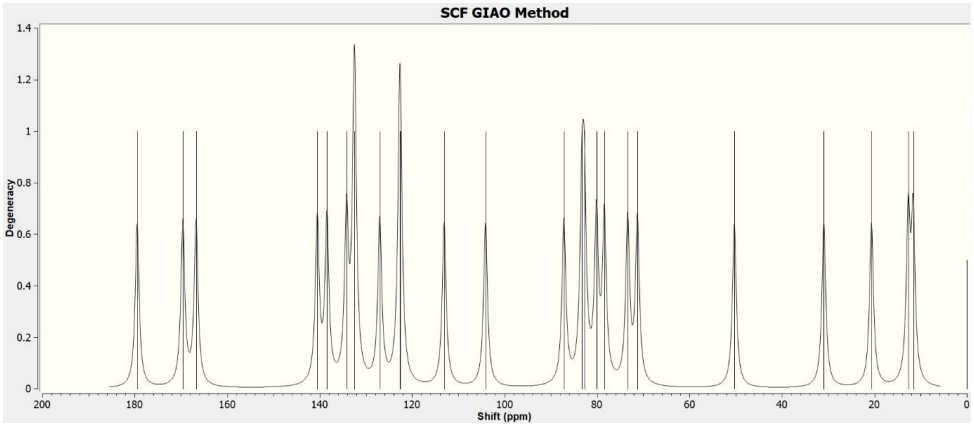

Fig. 3.10 Simulated ^{13}C-NMR of phenolimine form of **2**

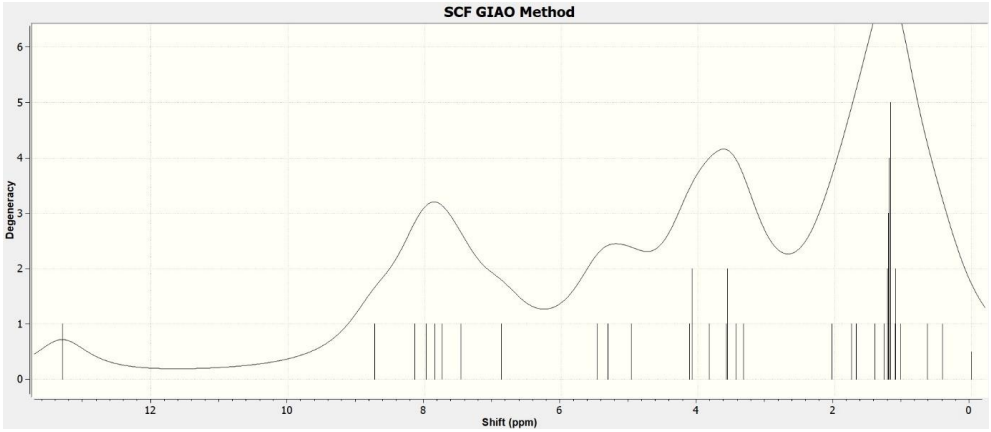

Fig. 3.11 Simulated ^{1}H-NMR of ketoenamine form of **2**

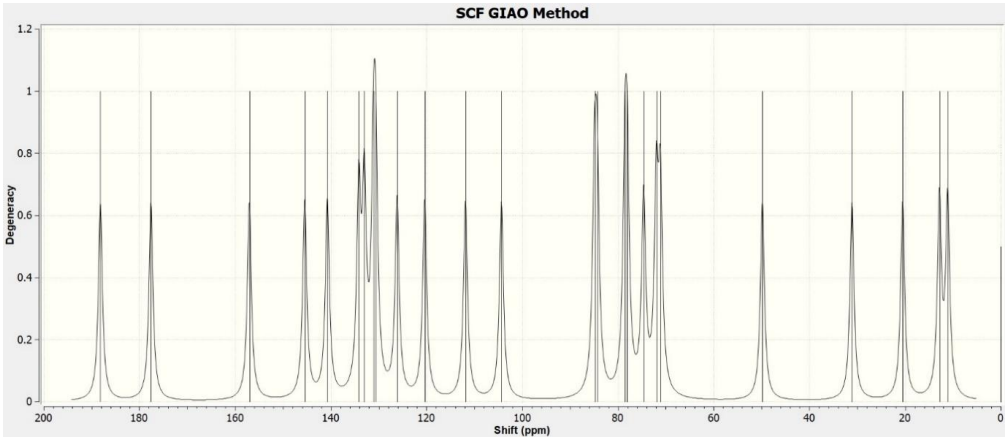

Fig. 3.12 Simulated ^{13}C-NMR of ketoenamine form of **2**

3.3.6 Hirshfeld surface analysis

To investigate the surface environment and intermolecular interactions existing in the crystal lattice, Hirshfeld surface and 2D fingerprint plot has been generated using Crystal Explorer 17.[43] Hirshfeld surface along with the fingerprint plot provides an exclusive pattern for a particular structure, which involves the interactions between neighbouring molecules.[44] Every point of the Hirshfeld surface is expressed by two distances, d_e (distance from the surface point to the nearest nucleus external to the surface) and d_i (distance from the surface point to the nearest nucleus internal to the surface). The normalized constant distance (d_{norm}) is given by-

$$d_{norm} = \frac{d_i - r_i^{vdW}}{r_i^{vdW}} - \frac{d_e - r_e^{vdW}}{r_e^{vdW}} \qquad (6)$$

The Hirshfeld surface of **2** shown in *Fig. 3.13(i)*, illustrate the d_{norm} mapped surface ranging from -0.6 to 1.0 Å. The negative and positive d_{norm} values are illustrated by red and blue colors, respectively, which represent the shorter and longer contacts compare to the van der Waal radii. The areas with zero d_{norm} value stand for the van der Waal contact, which is decorated with white color. The strong intermolecular hydrogen bonding interaction between amide NH and C2 hydroxyl group (denoted by a and b, respectively) is represented as the bright red spots whereas the faint red spot shows the C–H···O type interactions (denoted by c and d).

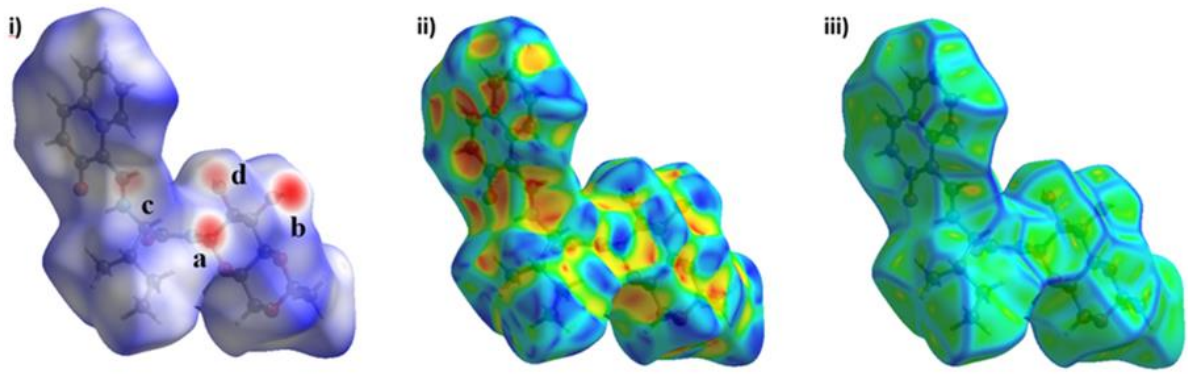

Fig. 3.13 *(i)Hirshfeld surfaces mapped with d_{norm} values ranging from -0.6 Å (red) to 1.0 Å (blue) (ii) shape-index and (iii) curvedness for **2***

Shape index (-1.0 to 1.0 Å) and curvedness (-4.0 to 0.4 Å) mappings are two additional powerful methods used in identifying the crystal packing behaviour and the interaction of nearby molecules with one another. In the shape index of **2**, the acceptor atoms are illustrated by the red concave regions whereas the blue bumps represent the donor atoms on the surface (*Fig. 3.13(ii)*). The curvedness map has been proven to be useful for obtaining information regarding the shape of molecular surface areas. The surface with low value of curvedness is signified by green flat patches, which are divided by dark blue curvature areas representing the

high value of curvedness.[44] The curvedness map (*Fig. 3.13(iii)*) did not show any flat surface patches, which confirms the absence of molecular stacking interactions.

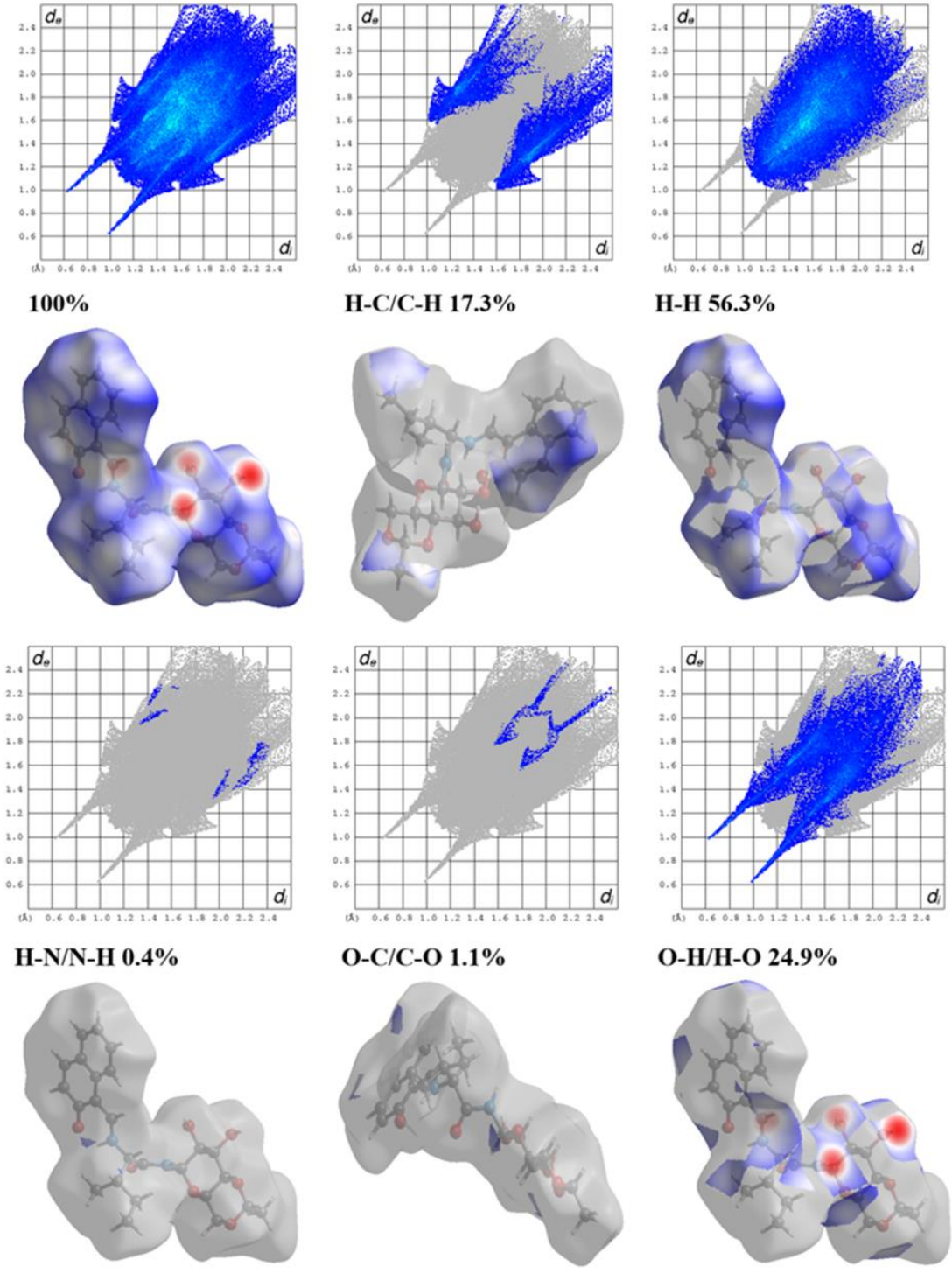

Fig. 3.14 *2D Fingerprint plots of* ***2*** *with d_i and d_e ranging from -0.6 to 1.0 A˚ and atom-based % interaction*

The 2D fingerprint plot was constructed using d_i versus d_e by decomposing the Hirshfeld surface into different intermolecular contacts present in the crystal structure.[44] The fingerprint plot corresponding to significant intermolecular interactions along with their Hirshfeld surface including the reciprocal contacts with their contribution is given in *Fig. 3.14*. The observations clearly reveal that the H···H interaction is the most significant contributor to the total Hirshfeld surface of **2**, which covers 56.3% of all the interactions. The strong hydrogen bonding interactions (H···O/O···H) are accounted to be 24.9%, which is illustrated by two large spikes at the lower end of the fingerprint plot. The contact between carbon and hydrogen (C···H/H···C) is another main contact comprising 17.3% of the total Hirshfeld surface, which corresponds to the C–H···π interaction. The remaining 1.5% of the Hirshfeld surface includes minor interactions C···O (1.1%) and N···H (0.4%).

3.3.7 Molecular electrostatic potential (MEP)

Electrostatic potential surface analysis is a useful tool to visualize the three-dimensional charge distribution of a molecule, which helps in predicting polarity, binding interactions, reactivity, electron density along with nucleophilic and electrophilic sites. Here we have generated the MEP for both the forms of **2** using their optimized structures obtained by DFT/B3LYP with 6-31G(2d,p) basis set. The MEP surface maps of ketoenamine and phenolimine form of **2** in gas phase are shown in *Fig. 3.15*, where red and blue colors represent the negative and positive potential regions, respectively, while the green color stands for the zero electric potential. The MEP surface color code is ranged between -0.062 a.u. (deepest red) to 0.062 a.u. (deepest blue).

The MEP surfaces of both the form of **2** shows a deep blue region over the hydrogen atom of the amide linkage, indicating the most positive electrostatic potential on it. The presence of light red color over the amidic oxygen indicates its electron-withdrawing nature, which might induce positive potential on the hydrogen atom attached with amidic nitrogen. A significant

difference in the MEP surfaces can be seen around the oxygen atom attached with naphthyl ring, where the deep red color appears for ketoenamine form indicating the most negative electrostatic potential. Same region in phenolimine form looks faint red supporting low negative potential on oxygen. Lone pair of electrons associated with most of the saccharide bound oxygen imparts the negative potential, yielding light red region around it. Plenty of light blue regions can be seen over hydrogen atoms attached with aromatic and sugar moieties, signalling positive potential over them. The MEP surfaces of none of the structures exhibited zero electric potential region, indicating the existence of these molecules in polarized form.

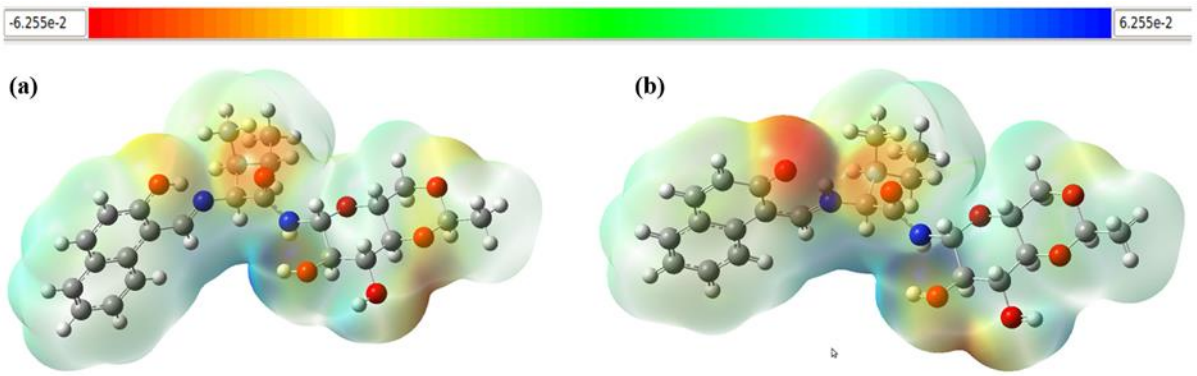

Fig. 3.15 *Molecular electrostatic potential (MEP) mapping for both (a) phenolimine (b) ketoenamine forms of* ***2*** *in gas phase*

3.3.8 Mulliken population analysis

The Mulliken charge distribution is directly linked with the chemical bonds present in the molecule and their vibrational properties. The Mulliken charges not only affect polarizability and dipole moment but also help in quantifying the electronic structure of a molecule.[45] The net atomic charges of ketoenamine form of **2**, obtained by Mulliken population analysis, are summarized in *Table 3.7* and *Fig. 3.16*. The calculations reveal more negative charges on

oxygen and nitrogen atoms, which might be due to their electronegative character,[46-47] whereas all the hydrogen atoms have positive charges. The highest negative charge obtained for amidic nitrogen (N2), while maximum positive charge appeared for the carbonyl carbon (C13).

Table 3.7 *Mulliken charge distribution in keto form of* ***2***

C1	-0.192	C2	0.467	C3	-0.24	C4	-0.093
C5	-0.144	C6	-0.174	C7	-0.215	C8	-0.186
C9	-0.197	C10	0.023	C11	0.271	C12	-0.031
C13	0.818	C14	0.373	C15	0.151	C16	0.171
C17	0.168	C18	0.114	C19	0.032	C20	0.453
C21	-0.439	C22	-0.148	C23	-0.326	C24	-0.454
C25	-0.452	N1	-.0877	N2	-0.910	O1	-0.689
O2	-0.594	O3	-0.727	O4	-0.770	O5	-0.750
O6	-0.714	O7	-0.709	H1	0.482	H2	0.423
H3	0.221	H4	0.440	H4A	0.246	H5	0.426
H6	0.235	H7	0.221	H8	0.223	H9	0.227
H11	0.276	H12	0.242	H14	0.242	H15	0.215
H16	0.210	H17	0.208	H18	0.212	H19 (A, B)	0.192-0.219
H20	0.191	H21 (A, B, C)	0.181	H22	0.194	H23 (A, B)	0.165-0.174
H24 (A, B, C)	0.159-0.168	H25 (A, B, C)	0.166-0.175				

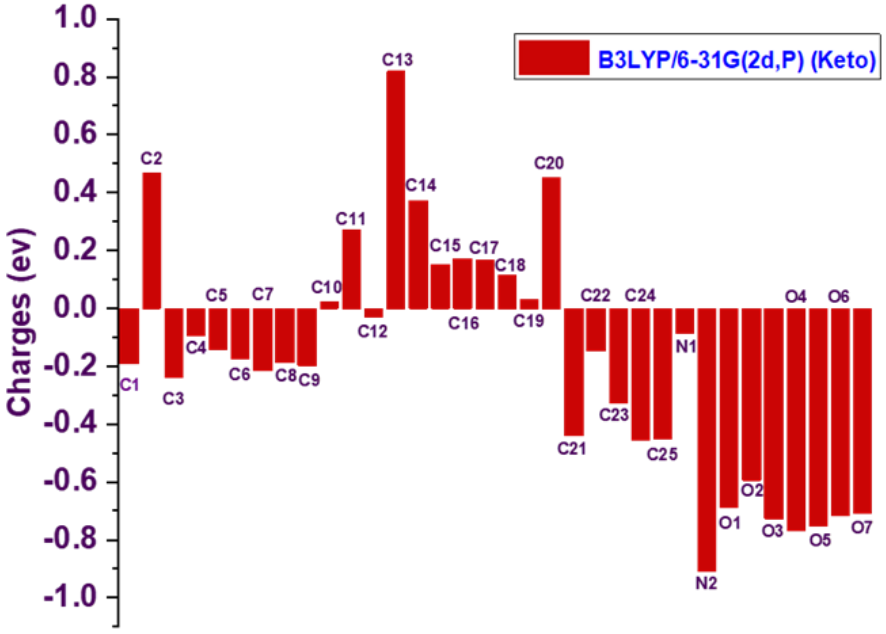

Fig. 3.16 *Mulliken charge distribution in keto form of* ***2*** *(The distributions of hydrogen atoms have been omitted for clarity)*

3.3.9 Natural bond orbital (NBO) analysis

The NBO analysis is an efficient tool to investigate intramolecular charge transfer, which plays a vital role in the molecular stabilization. In this regard, the NBO analysis of **2** for both the tautomeric forms was done by B3LYP/6-31G(2d,p) method to establish their electron-donating and accepting orbitals, electronic structure properties, orbital hybridization along with their stabilization energy ($E^{(2)}$). The quantification of $E^{(2)}$ for the donor(i) and acceptor(j) delocalization can be done with second-order perturbations[48] using the equation-7,

$$E^{(2)} = q_i \frac{F^2(i,j)}{\varepsilon_j - \varepsilon_i} \qquad (7)$$

where q_i denotes the donor orbital occupancy, $F^2(i,j)$ represents the off-diagonal Fock matrix element and $\varepsilon_{i/j}$ stands for the orbital energies. Larger values of $E^{(2)}$ indicate a higher tendency of electron transfer from donor to acceptor.

Selected intramolecular charge transfer processes ($\pi \rightarrow \pi^*$, $n \rightarrow \pi^*$, $n \rightarrow \sigma^*$ and $n \rightarrow RY^*$) occurring in both the tautomeric forms along with their $E^{(2)}$ are summarized in *Table 3.8*. The highest value of $E^{(2)}$ for ketoenamine form obtained as 29.69 KJ/mol for $\pi \rightarrow \pi^*$ transition between C1-C11 (donor) and C2-O1 (acceptor), while 24.48 KJ/mol for phenolimine tautomer corresponding to $\pi_{C1\text{-}C2} \rightarrow \pi^*_{C11\text{-}N1}$ charge transfer. The NBO analysis afforded distinct differences in the delocalization pattern of naphthaldimine π electrons in both the tautomers of **2**.

Table 3.8 *Second-order perturbation theory analysis of Fock matrix on NBO basis for* ***2*** *(obtained from B3LYP/6-31G(2d,p) level)*

NBO analysis for ketoenamine form of **2**								
Donor(i)	Type	ED(e)	Acceptor(j)	Type	ED(e)	$E^{(2)}$ kJ/mol	E_j-E_i a.u.	F(i,j) a.u.
C1-C11	π	1.97626	C2-O1	π*	0.36358	29.69	0.28	0.083
C9-C10	π	1.97547	C7-C8	π*	0.39025	24.02	0.28	0.073
C3-C4	π	1.98233	C2-O1	π*	0.36358	22.99	0.28	0.075
C7-C8	π	1.98012	C5-C6	π*	0.41208	22.62	0.28	0.072
C7-C8	π	1.98012	C9-C10	π*	0.40076	19.51	0.28	0.066
C3-C4	π	1.98233	C5-C6	π*	0.41208	13.43	0.3	0.06
C5-C6	π	1.60826	C9-C10	π*	0.40076	20.61	0.28	0.067
C5-C6	π	1.60826	C3-C4	π*	0.15414	17.94	0.29	0.069
C5-C6	π	1.60826	C7-C8	π*	0.39025	20.37	0.27	0.067
N2	LP (1)	1.72344	C14-O3	σ*	0.05492	12.16	0.56	0.078
O2	LP (1)	1.84951	C13	RY*(1)	0.018	17.18	1.62	0.149
O7	LP (2)	1.90413	C20-O6	σ*	0.06532	13.67	0.59	0.081
O1	LP (2)	1.87148	C1-C2	σ*	0.05829	12.98	0.74	0.089
O1	LP (2)	1.87148	C2-C3	σ*	0.04812	17.69	0.75	0.105
O1	LP (2)	1.87148	N1-H1	σ*	0.07049	18.24	0.71	0.103
O1	LP (1)	1.96531	C2	RY*(1)	0.01365	12.21	1.67	0.128
O6	LP (1)	1.96159	C20-O7	σ*	0.06136	12.49	0.6	0.078
O2	LP (2)	1.84951	C13-N2	σ*	0.0837	28.85	0.7	0.129
O2	LP (2)	1.84951	C12-C13	σ*	0.08053	22.98	0.6	0.106

N1	LP (1)	1.57734	C1-C11	π*	0.34463	62.78	0.28	0.12
N2	LP (1)	1.72344	C12-O2	π*	0.2385	50.69	0.31	0.113
C2-O1	π*	0.36358	C3-C4	π*	0.15414	66.2	0.03	0.079
C1-C11	π*	0.34463	C9-C10	π*	0.40076	119.17	0.02	0.069
C5-C6	π*	0.41208	C3-C4	π*	0.15414	122.31	0.01	0.069
NBO analysis for Phenolimine form of L1								
Donor(i)	Type	ED(e)	Acceptor(j)	Type	ED(e)	$E^{(2)}$ kJ/mol	E_j-E_i a.u.	F(i,j) a.u.
C1-C2	π	1.63953	C11-N1	π*	0.19614	24.48	0.26	0.075
C1-C2	π	1.63953	C5-C10	π*	0.46143	20.09	0.29	0.07
C1-C2	π	1.63953	C3-C4	π*	0.22635	12.06	0.29	0.055
C5-C10	π	1.54788	C1-C2	π*	0.39861	13.8	0.26	0.055
C5-C10	π	1.54788	C8-C9	π*	0.2766	16.27	0.27	0.062
C5-C10	π	1.54788	C3-C4	π*	0.22635	17.58	0.28	0.066
C5-C10	π	1.54788	C6--C7	π*	0.27021	18.19	0.28	0.067
C8-C9	π	1.73719	C5-C10	π*	0.46143	17.28	0.29	0.066
C8-C9	π	1.73719	C6--C7	π*	0.27021	16.52	0.3	0.063
C3-C4	π	1.7607	C1-C2	π*	0.39861	20.45	0.29	0.072
C3-C4	π	1.7607	C5-C10	π*	0.46143	13.42	0.3	0.06
C6--C7	π	1.73169	C5-C10	π*	0.46143	15.92	0.29	0.063
C6--C7	π	1.73169	C8-C9	π*	0.2766	19.4	0.29	0.067
O6	LP (1)	1.90343	C20-O7	σ*	0.06444	13.1	0.59	0.079
O1	LP (1)	1.78417	C1-C2	π*	0.39861	42.84	0.33	0.111
O7	LP (2)	1.90624	C20-O6	σ*	0.06224	13.01	0.6	0.079

O2	LP (1)	1.9739	C13	RY*(1)	0.01841	17.58	1.61	0.15
O2	LP (2)	1.84924	C12-C13	σ*	0.083	23.1	0.59	0.106
N1	LP (1)	1.84678	C11-H1	σ*	0.03961	10.88	0.79	0.085
N2	LP (1)	1.72407	C14-O3	σ*	0.0525	11.42	0.56	0.076
N2	LP (1)	1.72407	C13-O2	π*	0.23368	46.96	0.32	0.111
C11-N1	π*	0.19614	C1-C2	π*	0.39861	97.35	0.02	0.072
C1-C2	π*	0.39861	C3-C4	π*	0.22635	201.2	0.01	0.082

3.3.10 Theorical UV-visible spectra and molecular orbital calculation

The theoretical UV-visible spectra of both the tautomers of **2** were obtained from the respective optimized ground-state structure employing TD-DFT/IEFPCM method in methanol. The simulated absorption excitations along with the observed UV-visible spectra both in solid and solution (methanol and DMSO) state is represented in *Fig. 3.17*. The simulated UV-visible spectra of the ketoenamine form yielded two absorption peaks at 365 and 283 nm. The absorption maxima at 365 nm can be dominated by HOMO-to-LUMO transition and can be attributed to the π→π* character whereas HOMO-to-LUMO+1 transition with π→π* character appears at 283 nm. The theoretical UV-visible spectra of the phenolimine form have shown an absorption peak at about 330 nm which is due to HOMO-to-LUMO transition.

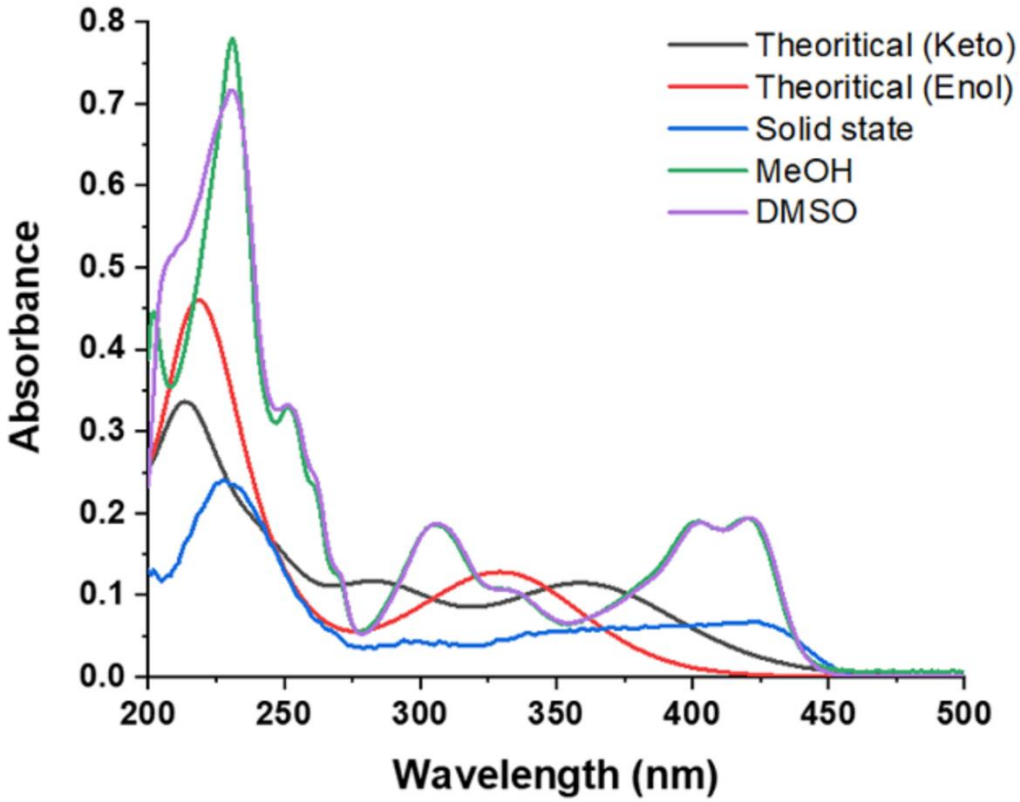

Fig. 3.17 *UV–Visible spectra of* ***2*** *in solid (blue) and in solution state (methanol (green) and DMSO (purple)) along with simulated UV–visible spectra for both ketoenamine (black) and phenolimine (red) form*

The lower HOMO-LUMO energy band gap facilitates the polarizability, conductance and chemical reactivity of molecule, however decrease its kinetic stability.[49-50] The frontier molecular orbital energies for both ketoenamine and phenolimine of **2** were calculated employing TD-DFT/IEFPCM method in methanol. The surface of some important frontier molecular orbitals of ketoenamine and phenolimine form is shown in *Fig. 3.18* and the theoretically calculated energies of these orbitals are summarized in *Table 3.9*. The energy of HOMO and LUMO for ketoenamine obtained as -5.74 and -2.01 eV, while -6.01 and -1.90 eV for phenolimine form, respectively. The HOMO and LUMO is distributed over the naphthalene ring and the amino acid moieties (*Fig. 3.18*). The energy band gaps of ketoenamine and

phenolimine forms obtained as 3.73 eV and 4.11 eV, respectively, which suggests the poor conductivity and high stability for both the configurations.

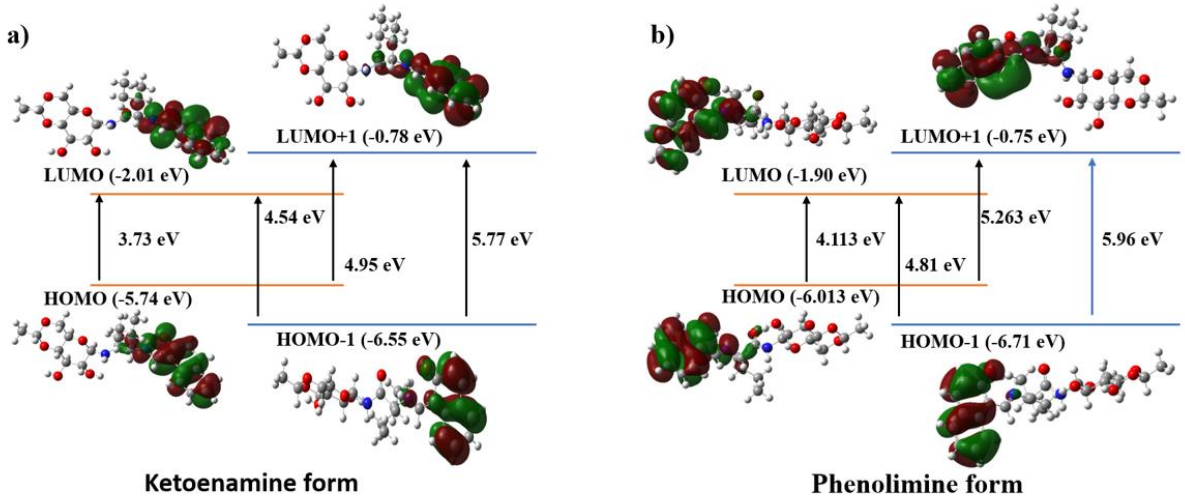

Fig. 3.18 *HOMO and LUMO plot of both ketoenamine (a) and phenolimine (b) form of* ***2***

Table 3.9 *Calculated energies of some important molecular orbitals of both ketoenamine and phenolimine form of* ***2***

Type of molecular orbital	Energy of ketoenamine form in gas phase (eV)[a]	Energy of phenolimine form in gas phase (eV)[a]
HOMO	-5.74 eV	-6.01 eV
LUMO	-2.01 eV	-1.90 eV
HOMO-1	-6.55 eV	-6.71 eV
LUMO+1	-0.78 eV	-0.75 eV
Energy gap (E_{LOMO} - E_{HUMO})	3.73 eV	4.11 eV

[a] Energies were calculated using TD-DFT at the B3LYP/6-31G(2d,p) level.

3.4 Conclusions

The solution phase structural analysis of **1-7** has been explored using NMR and UV-visible absorption spectroscopy, which indicates the dominance of the ketoenamine form. Literature reveals the existence of two tautomeric forms of such molecules (ketoenamine and

phenolimine) in solution and following their approach, NMR studies supported the presence of 82-93% ketoenamine form in DMSO-d_6 solution. The solid-state structural investigations have been done using FTIR and single-crystal X-ray diffraction studies. FTIR studies supported the ketoenamine forms of **1**-**7** and the crystal structures of **1**, **2**, **5** and **6** confirmed the same. The crystal structures also reveal the presence of intramolecular hydrogen bonding between amine NH and quinoid C=O. Using the crystallographic data, the energies of the intramolecular hydrogen bonding were calculated as -13.54, -14.96, -14.64 and 13.43 kcal/mol for compounds **1**, **2**, **5** and **6**, respectively.

The structural parameters of both the tautomeric forms of **2** have been optimized using DFT/B3LYP with 6-31G(2d,p) basis set and the experimental results fit well with the theoretical results of ketoenamine configuration. The Hirshfeld surface analysis data revealed the dominance of intermolecular H···H, H···C and H···O contacts in the crystal lattice of **2**. Potential sites of chemical reactivity and the charge density distribution in the molecular surface have been established using molecular electrostatic potential surface mapping for both the tautomeric forms. Mulliken atomic charges along with thermodynamic zero-point energies and dipole moments have also been tabulated. The difference between the intramolecular charge transfer of both the tautomeric forms has been established using NBO analysis.

Reference

1. Varki, A., Biological roles of oligosaccharides: all of the theories are correct. *Glycobiology* **1993,** *3*, 97-130.

2. Bertozzi, C. R.; Kiessling; L, L., Chemical glycobiology. *Science* **2001,** *291*, 2357-2364.

3. Maverakis, E.; Kim, K.; Shimoda, M.; Gershwin, M. E.; Patel, F.; Wilken, R.; Raychaudhuri, S.; Ruhaak, L. R.; Lebrilla, C. B., Glycans in the immune system and The

Altered Glycan Theory of Autoimmunity: a critical review. *Journal of Autoimmunity* **2015,** *57*, 1-13.

4. Rudd, P. M.; Elliott, T.; Cresswell, P.; Wilson, I. A.; Dwek, R. A., Glycosylation and the immune system. *Science* **2001,** *291*, 2370-2376.

5. Talbot, P.; Shur, B. D.; Myles, D. G., Cell adhesion and fertilization: steps in oocyte transport, sperm-zona pellucida interactions, and sperm-egg fusion. *Biology of Reproduction* **2003,** *68*, 1-9.

6. Lowary, T.; Meldal, M.; Helmboldt, A.; Vasella, A.; Bock, K., Novel Type of Rigid C-Linked Glycosylacetylene− Phenylalanine Building Blocks for Combinatorial Synthesis of C-linked Glycopeptides. *The Journal of Organic Chemistry* **1998,** *63*, 9657-9668.

7. Acharya, Y.; Bhattacharyya, S.; Dhanda, G.; Haldar, J., Emerging Roles of Glycopeptide Antibiotics: Moving beyond Gram-Positive Bacteria. *ACS Infectious Diseases* **2021,** *8*, 1-28.

8. Roth, J., Protein N-glycosylation along the secretory pathway: relationship to organelle topography and function, protein quality control, and cell interactions. *Chemical Reviews* **2002,** *102*, 285-304.

9. Hilvert, D., Design of protein catalysts. *Annual Review of Biochemistry* **2013,** *82*, 447-470.

10. Mechref, Y.; Novotny, M. V., Structural investigations of glycoconjugates at high sensitivity. *Chemical Reviews* **2002,** *102*, 321-370.

11. Coutsogeorgopoulos, C.; Zervas, L., On β-D-Glucosylamides of L-Amino Acids and of Nicotinic Acid. *Journal of the American Chemical Society* **1961,** *83*, 1885-1888.

12. Sah, A. K.; Soni, K., Synthesis of cupric acetate selective receptor derived from alanyl glycoconjugate and their application in selective oxidation of benzylic alcohols. *Catalysis Communications* **2012,** *28*, 120-123.

13. Baig, N.; Singh, R. P.; Chander, S.; Jha, P. N.; Murugesan, S.; Sah, A. K., Synthesis, evaluation and molecular docking studies of amino acid derived N-glycoconjugates as antibacterial agents. *Bioorganic Chemistry* **2015,** *63*, 110-115.

14. Sheppeck II, J. E.; Kar, H.; Hong, H., A convenient and scaleable procedure for removing the Fmoc group in solution. *Tetrahedron Letters* **2000,** *41*, 5329-5333.

15. Soni, K.; Sah, A. K., Alanyl glycoconjugate: a selective receptor for free and protein-bound tryptophan. *RSC Advances* **2013,** *3*, 12096-12099.

16. Baig, N.; Singh, R. P.; Jha, P. N.; Sah, A. K., Synthesis of Glucose-Derived Glycoconjugates and Studies on Their Antimicrobial Activities: Mechanistic Insight. *ChemistrySelect* **2016,** *1*, 5281-5285.

17. Madduluri, V. K.; Sah, A. K., Synthesis of Mefenamic Acid Containing N-Glycoconjugates and Their Evaluation as Human COX-2 Enzyme Inhibitor. *ChemistrySelect* **2020,** *5*, 2197-2200.

18. Dudek, G. O., Nuclear magnetic resonance studies of keto-enol equilibria. IV. Naphthalene derivatives. *Journal of the American Chemical Society* **1963,** *85*, 694-697.

19. Bessonov, D.; Kulakov, I.; Gazaliev, A.; Nurkenov, O., Synthesis of glycoconjugates of physiologically active compounds. *Russian Journal of Applied Chemistry* **2007,** *80*, 506-508.

20. Sah, A. K.; Rao, C. P.; Saarenketo, P. K.; Kolehmainen, E.; Rissanen, K., Synthesis, characterisation and crystal structures of Schiff bases from the reaction of 4, 6-O-ethylidene-β-D-glucopyranosylamine with substituted salicylaldehydes. *Carbohydrate Research* **2001,** *335*, 33-43.

21. Martínez, R. F.; Ávalos, M.; Babiano, R.; Cintas, P.; Jiménez, J. L.; Light, M. E.; Palacios, J. C., Tautomerism in Schiff bases. The cases of 2-hydroxy-1-naphthaldehyde and 1-

hydroxy-2-naphthaldehyde investigated in solution and the solid state. *Organic & Biomolecular Chemistry* **2011,** *9,* 8268-8275.

22. Enchev, V.; Ivanova, G.; Pavlović, G.; Rogojerov, M.; Ahmedova, A.; Mitewa, M., Reaction of 2-acetyl-indane-1, 3-dione with aniline-Schiff base or enamine? *Journal of Molecular Structure* **2003,** *654,* 11-20.

23. Miyazawa, T., Normal vibrations of monosubstituted amides in the cis configuration and infrared spectra of diketopiperazine. *Journal of Molecular Spectroscopy* **1960,** *4,* 155-167.

24. Schilf, W.; Kamieński, B.; Dziembowska, T., Intramolecular hydrogen bond investigations in Schiff bases derivatives of 2-hydroxy-1-naphthaldehyde and 2-hydroxy-1-acetonaphthone in $CDCl_3$ solution and in the solid state by NMR methods. *Journal of Molecular Structure* **2002,** *602,* 41-47.

25. Rażniewska-Lazęcka, G.; Dambska, A.; Janowski, A., ^{13}C NMR spectra of some o-carbonyl derivatives of naphthols. *Magnetic Resonance in Chemistry* **1986,** *24,* 365-367.

26. Zhuo, J. C., NMR of enaminones. part 6-^{17}O and ^{13}C NMR study of tautomerization in Schiff bases. *Magnetic Resonance in Chemistry* **1999,** *37,* 259-268.

27. Karakaş, A.; Elmali, A.; Ünver, H.; Svoboda, I., Nonlinear optical properties of some derivatives of salicylaldimine-based ligands. *Journal of Molecular Structure* **2004,** *702,* 103-110.

28. Salman, S. R.; Kamounah, F. S., Tautomerism in 1-hydroxy-2-naphthaldehyde Schiff bases: Calculation of tautomeric isomers using carbon-13 NMR. *Spectroscopy* **2003,** *17,* 747-752.

29. Dominiak, P. M.; Grech, E.; Barr, G.; Teat, S.; Mallinson, P.; Woźniak, K., Neutral and ionic hydrogen bonding in Schiff bases. *Chemistry–A European Journal* **2003,** *9,* 963-970.

30. Martínez, R. F.; Matamoros, E.; Cintas, P.; Palacios, J. C., Imine or Enamine? Insights and Predictive Guidelines from the electronic Effect of Substituents in H-Bonded Salicylimines. *The Journal of Organic Chemistry* **2020,** *85*, 5838-5862.

31. Mercier, G. M.; Robeyns, K.; Leyssens, T., Altering the photochromic properties of N-salicylideneanilines using a co-crystal engineering approach. *Crystal Growth & Design* **2016,** *16*, 3198-3205.

32. Spackman, M. A.; Jayatilaka, D., Hirshfeld surface analysis. *CrystEngComm* **2009,** *11*, 19-32.

33. Ahuja, R.; Singhal, N. K.; Ramanujam, B.; Ravikumar, M.; Rao, C. P., Experimental and Computational Studies of the Recognition of Amino Acids by Galactosyl-imine and-amine Derivatives: An Attempt to Understand the Lectin− Carbohydrate Interactions. *The Journal of Organic Chemistry* **2007,** *72*, 3430-3442.

34. Blagus, A.; Cinčić, D.; Friščić, T.; Kaitner, B.; Stilinović, V., Schiff bases derived from hydroxyaryl aldehydes: molecular and crystal structure, tautomerism, quinoid effect, coordination compounds. *Macedonian Journal of Chemistry and Chemical Engineering* **2010**, *29*, 117.

35. Huque, F. T.; Platts, J. A., The effect of intramolecular interactions on hydrogen bond acidity. *Organic & Biomolecular Chemistry* **2003,** *1*, 1419-1424.

36. Musin, R. N.; Mariam, Y. H., An integrated approach to the study of intramolecular hydrogen bonds in malonaldehyde enol derivatives and naphthazarin: Trend in energetic versus geometrical consequences. *Journal of Physical Organic Chemistry* **2006,** *19*, 425-444.

37. Matamoros, E.; Cintas, P.; Light, M. E.; Palacios, J. C., Electronic effects in tautomeric equilibria: The case of chiral imines from d-glucamine and 2-hydroxyacetophenones. *Organic & Biomolecular Chemistry* **2019,** *17*, 10209-10222.

38. Kunduracıoğlu, A.; Tamer, Ö.; Avcı, D.; Kani, I.; Atalay, Y.; Çetinkaya, B., 1-Pentamethylbenzyl-3-nbuthylbenzimidazolesilver (I) bromide complex: Synthesis, characterization and DFT calculations. *Spectrochimica Acta Part A: Molecular and Biomolecular Spectroscopy* **2014,** *121*, 35-45.

39. Almutairi, M. S.; Soumya, S.; Al-Wabli, R. I.; Joe, I. H.; Attia, M. I., Density functional theory calculations, vibration spectral analysis and molecular docking of the antimicrobial agent 6-(1, 3-benzodioxol-5-ylmethyl)-5-ethyl-2-{[2-(morpholin-4-yl) ethyl] sulfanyl} pyrimidin-4 (3H)-one. *Open Chemistry* **2018,** *16*, 653-666.

40. Chaudhary, T.; Chaudhary, M. K.; Joshi, B. D.; de Santana, M. S. A.; Ayala, A. P., Spectroscopic (FT-IR, Raman) analysis and computational study on conformational geometry, AIM and biological activity of cephalexin from DFT and molecular docking approach. *Journal of Molecular Structure* **2021,** *1240,* 130594.

41. Erdogdu, Y.; Unsalan, O.; Amalanathan, M.; Joe, I. H., Infrared and Raman spectra, vibrational assignment, NBO analysis and DFT calculations of 6-aminoflavone. *Journal of Molecular Structure* **2010,** *980*, 24-30.

42. Iyasamy, S.; Varadharajan, K.; Sivagnanam, S., Density Functional Theory Calculations, Spectroscopic (FT-IR, FT-RAMAN), Frontier Molecular Orbital, Molecular Electrostatic Potential Analysis of 5-Fluoro-2-Methylbenzaldehyde. *Zeitschrift für Physikalische Chemie* **2016,** *230*, 1681-1710.

43. Govindarajan, M.; Karabacak, M., Spectroscopic properties, NLO, HOMO–LUMO and NBO analysis of 2, 5-Lutidine. *Spectrochimica Acta Part A: Molecular and Biomolecular Spectroscopy* **2012,** *96*, 421-435.

44. Ramalingam, S.; Karabacak, M.; Periandy, S.; Puviarasan, N.; Tanuja, D., Spectroscopic (infrared, Raman, UV and NMR) analysis, Gaussian hybrid computational

investigation (MEP maps/HOMO and LUMO) on cyclohexanone oxime. *Spectrochimica Acta Part A: Molecular and Biomolecular Spectroscopy* **2012,** *96*, 207-220.

45. Ramalingam, S.; Periandy, S.; Govindarajan, M.; Mohan, S., FTIR and FTRaman spectra, assignments, ab initio HF and DFT analysis of 4-nitrotoluene. *Spectrochimica Acta Part A: Molecular and Biomolecular Spectroscopy* **2010,** *75*, 1308-1314.

46. Krygowski, T. M.; Woźniak, K.; Anulewicz, R.; Pawlak, D.; Kolodziejski, W.; Grech, E.; Szady, A., Through-resonance assisted ionic hydrogen bonding in 5-nitro-N-salicylideneethylamine. *The Journal of Physical Chemistry A* **1997,** *101*, 9399-9404.

47. Safin, D. A.; Babashkina, M. G.; Bolte, M.; Ptaszek, A. L.; Kukułka, M.; Mitoraj, M. P., Novel sterically demanding Schiff base dyes: An insight from experimental and theoretical calculations. *Journal of Luminescence* **2021,** *238*, 118264.

48. Demircioğlu, Z.; Albayrak, Ç.; Büyükgüngör, O., Theoretical and experimental investigation of (E)-2-([3, 4-dimethylphenyl) imino] methyl)-3-methoxyphenol: Enol–keto tautomerism, spectroscopic properties, NLO, NBO and NPA analysis. *Journal of Molecular Structure* **2014,** *1065*, 210-222.

49. Ghosh, D. C.; Jana, J., A study of correlation of the order of chemical reactivity of a sequence of binary compounds of nitrogen and oxygen in terms of frontier orbital theory. *Current Science* **1999**, 570-573.

50. Singh, H., A DFT approach for theoretical and experimental study of structure, electronic, Hirshfeld surface and spectroscopic properties of 12-(4-bromophenyl)-2-(prop-2-ynyloxy)-9, 10-dihydro-8H-benzo [a] xanthen-11 (12H)-on single crystal. *Chemical Physics* **2019,** *524*, 1-13.

Chapter 4

N-Glycoconjugates: Selective Colorimetric Chemosensors for Aspartic Acid and Cysteine

Chapter 4

4.1 Introduction

Amino acids are the building blocks of proteins and precursors for several biological molecules such as hormones,[1] vitamins,[2] nucleotides,[3] cell-wall polymers,[4] porphyrins [5] etc., which not only control several cellular processes but also catalyse numerous reactions in the living organisms.[6] Due to increase in attention towards human health, several techniques have been developed for detection and characterization of amino acids.[7] Analytical procedures based on spectroscopic approach are the most elegant approach as they are loaded with features like high sensitivity, easy sample preparation, real time online information, use of simple apparatus, cost efficiency etc.[8] Based on different detection mechanisms, fluorescent and/or colorimetric chemosensors are mainly divided into three categories:

- Metal complex based chemosensors
- Reaction based chemosensors
- Hydrogen bonding and CH-π interactions based chemosensors

4.1.1 Metal complexes based chemosensors

Amino acids detection using organometallic systems is one of the most successful strategies.[7] Here metal centres are either coordinatively flexible/unsaturated or bound with weak ligands, such that amino acids can coordinate with the complex as a signalling subunit[9-11] or displace the weak ligand[12]. However, the special arrangement of carboxyl and amino groups in amino acids, later possess similar properties, which make their selective discrimination a challenging task especially for the chemosensors relying on coordination chemistry.[8] Some of the metal nanoparticles also have attracted considerable interest due to

remarkable changes in their electrical, chemical and optical properties upon interaction with amino acids.[13-15]

4.1.2 Specific reactions between probes and amino acids

Due to the polyfunctionality of amino acids, several reaction-based chemosensors have been developed for their detection. These reaction-based chemosensors can be divided into subclasses according to the mechanism between guest and host such as Michael addition, cleavage of a sulfonate ester or disulfide, imine or thiazinane or thiazolidine formation.[7] Although it is an efficient protocol for amino acid detection, the lack of selectivity is its major drawback.

4.1.3 Hydrogen bonding or CH-π based interactions

Various functionalized side chain present in amino acids facilitate their binding with biological molecules through hydrogen bonding or CH-π interaction. Interaction between biological molecules and amino acids containing aromatic side chains are driven by nonpolar forces like π-π or CH-π interaction whereas polar functional group-containing amino acids are more tilted towards the hydrogen bonding.[16]

Glycoconjugates are well known for discriminative detection of the targeted analyte through hydrogen bonding interactions along with size-specific parameters.[17] During this process, sugar plays vital roles in molecular recognition and hence, researchers focus on scheming sugar derived probes for selective molecular recognition. Rao and co-workers have reported the amino acid-sensing using galactosyl-

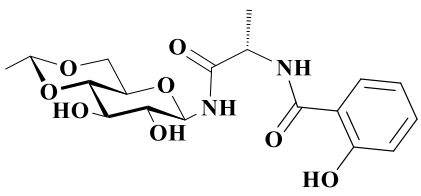

Fig. 4.1 *Structure of N-(2-hydroxybenzoyl)-L-alanyl-4,6-O-ethylidene-β-D-glucopyranosylamine*

naphthyl-imine/amine-based receptors, where the imine derivative interacted with glutamic acid, histidine, leucine and proline, while amine derivative with alanine, cysteine and lysine.[18] They have also reported a glucose-based sensor, which yielded large fluorescence intensity enhancement in presence of aromatic amino acids like phenylalanine, tryptophan, histidine and tyrosine.[19] Our group has reported a glucose-derived probe (*N*-(2-hydroxybenzoyl)-L-alanyl-4,6-*O*-ethylidene-β-D-glucopyranosylamine) (*Fig. 4.1*), which selectively interacts with free as well as protein bounded tryptophan moiety.[20] As a continuation of this work, we have replaced the terminal amide linkage by imine bond (*Fig. 4.2*). Amino acid moieties were changed for molecular discrimination of the receptor, while the terminal component was changed for better photophysical responses. Along this line, totally five receptors were synthesized (*Fig. 4.2*) and tested for interactions with naturally occurring amino acids using UV-visible and NMR spectroscopy. These molecules exhibited selective interaction with either cysteine (**Cys**) or aspartic acid (**Asp**). Previously Rao and co-workers have reported the sensing of **Cys** using a sugar-based probe, however their work lacks the selectivity.[18] Few reports are available on **Asp** recognition by metal complexes,[7-8, 21-23] whereas organic receptors have been developed to interact with the aspartate ion (mainly tetrabutylammonium salts).[24-26]

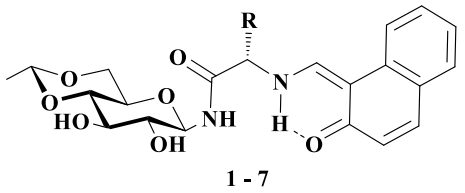

1 - 7

R = CH_2Ph (1), $CH(CH_3)CH_2CH_3$ (2), CH_3 (3), $CH_2CH_2SCH_3$ (4), $CH(CH_3)_2$ (5), $CH_2CH(CH_3)_2$ (6), $CH_2C_8H_6N$ (7)

Fig. 4.2 *Glycoconjugates used for amino acid sensing.*

4.2 Experimental

4.2.1 General procedure of sample preparation for UV-visible spectral measurements

Stock solutions (1 mM) of compounds **1-7** and amino acids were prepared in methanol-water (9:1 v/v) and DMSO. Test solutions for interaction studies were prepared by mixing the probe

and amino acid stock solutions in a suitable ratio as mentioned in the respective figure captions and further diluted with diluent (methanol-water; 9:1 v/v) or DMSO to make the final concentration of probe as 20 μM. Test solutions for UV-visible titration were prepared by mixing 200 μL of the stock probe solution separately with different volumes of the amino acid solution (20–8000 μL) in a series of 10 mL volumetric flasks, followed by dilution up to the mark with diluent. After proper mixing, test solutions were allowed to react for 1 hour and UV-visible spectra were recorded. For competitive selective binding affinity studies, stock solutions of probes **1**-**7** (200 μL) were mixed with amino acid stock solutions (2 mL, 10 equivalents) followed by the addition of **Cys** (2 mL, 10 equivalents) to each solution of **1** and **Asp** (2 mL, 10 equivalents) to each solution of **2**-**5**. The test solutions were mixed properly, and UV-visible spectra were measured after one hour.

4.3 Results and discussion

The synthesis and characterization of ligands **1**-**7** along with the crystal structures of **1**, **2**, **5** and **6** are described in the previous chapter. The presence of multiple hydrogen donor and acceptor sites in these ligands have already been established (Chapter 3). The hydrogen binding sites present in carbohydrate moieties actively participates in amino acid recognition.[24, 27] Inspired from these facts we have screened the interaction of **1**-**7** with natural occurring amino acids using UV-visible and NMR spectral studies.

4.3.1 UV-Visible absorption studies

The UV-visible absorption spectra of **1**–**7** (20 μM) exhibited absorption peaks near 305, 402 and 420 nm. All the naturally occurring amino acids were screened for interactions with the synthesised probes by monitoring these two peaks as the yellow color of the probe solution turned colourless in presence of selected amino acids. Interaction of **Cys** with **1** resulted in a hypochromic shift of these peaks, while no change in the spectral pattern was observed in the

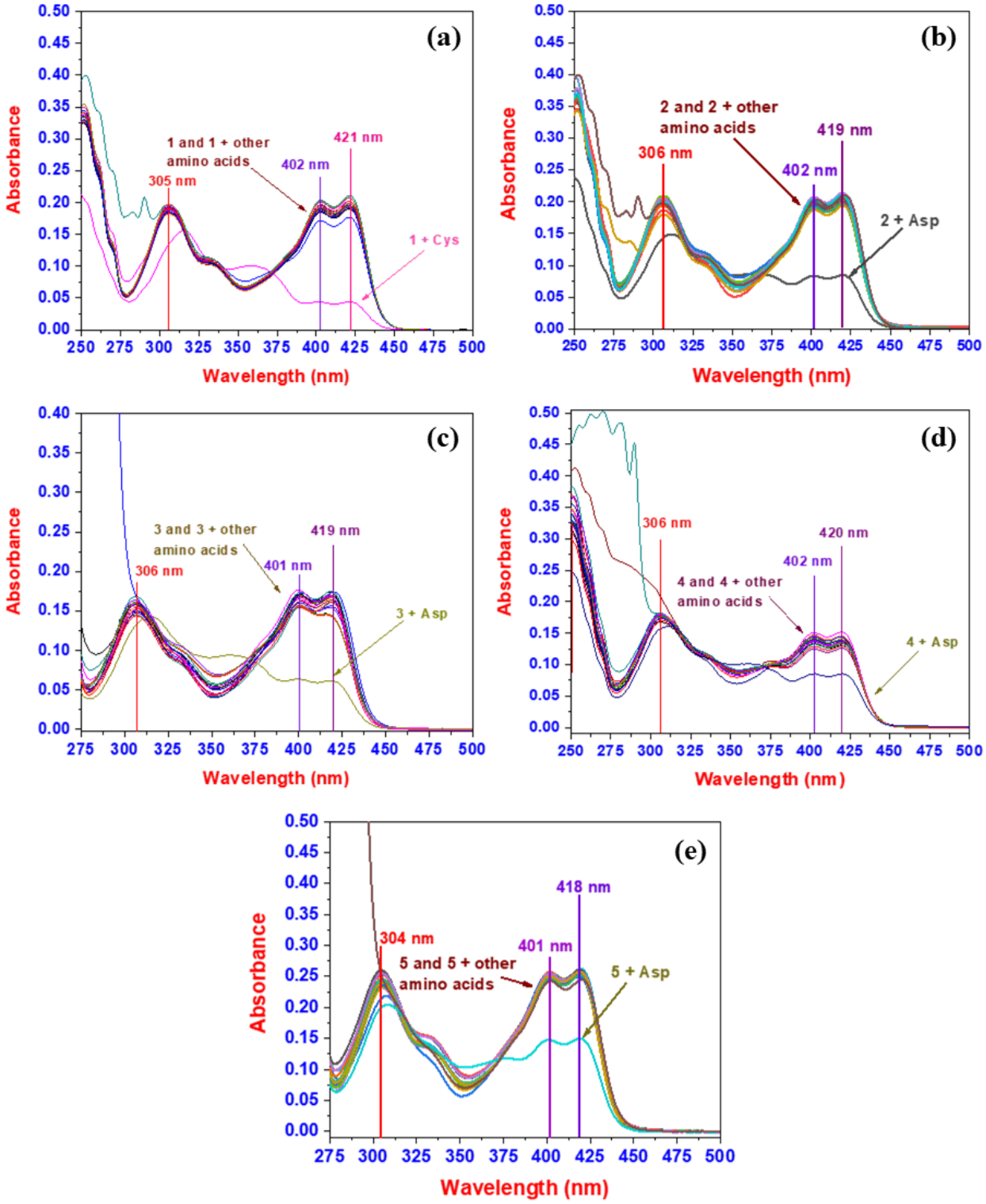

Fig. 4.3 *UV-Visible absorption spectra of (a)* ***1*** *(20 μM), (b)* ***2*** *(20 μM), (c)* ***3*** *(20 μM), (d)* ***4*** *(20 μM) and (e)* ***5*** *(20 μM) in absence and presence of natural amino acids (a) 30 μM, (b) 30, (c) 80 μM, (d) 40 μM and (e) 100 μM recorded in medium*

presence of other amino acids (*Fig. 4.3a*). A redshift of the absorption peaks in the range of 300 –360 nm was also noticed in presence of **Cys**. The yellow solution of the probe was decolorized in presence of **Cys**, while it retained its color in the presence of other amino acids.

Identical studies with **2-5** revealed their selective interaction with **Asp** and the corresponding UV-visible spectra are presented in (*Fig. 4.3b-4.3e*). In these cases, similar spectral behaviour as that of **1** in the presence of **Cys** were also observed. The interaction studies of **6** and **7** with different amino acids were also tested and it was quite evident that even both the ligands show higher degree of association with **Asp**, however the interaction was not selective (*Fig. 4.4*).

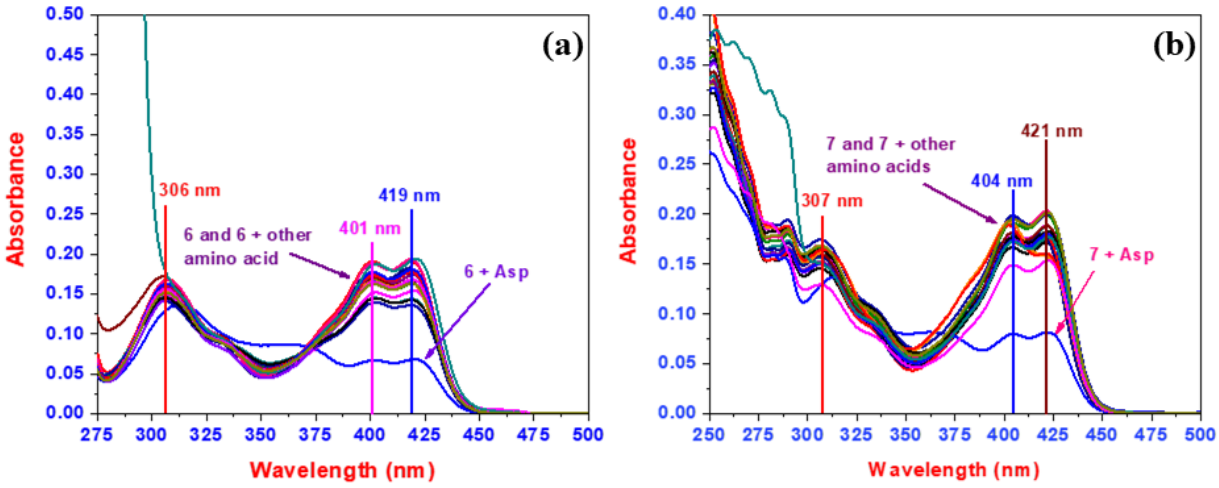

Fig. 4.4 *UV-Visible absorption spectra of (a)* ***6*** *(20 μM) and (b)* ***7*** *(20 μM), in absence and presence of natural amino acids (a) 80 μM and (b) 30, recorded in medium*

The interaction studies between **1-5** and amino acids in DMSO medium was also conducted using UV-visible absorption spectroscopy. This study also revealed the selective interaction of probe-**1** with **Cys** and probe **2-5** with **Asp** (*Fig. 4.5*). Since changing the solvent did not affect the selectivity, it can be concluded that all the ligand and amino acid interactions are independent from the medium interference.

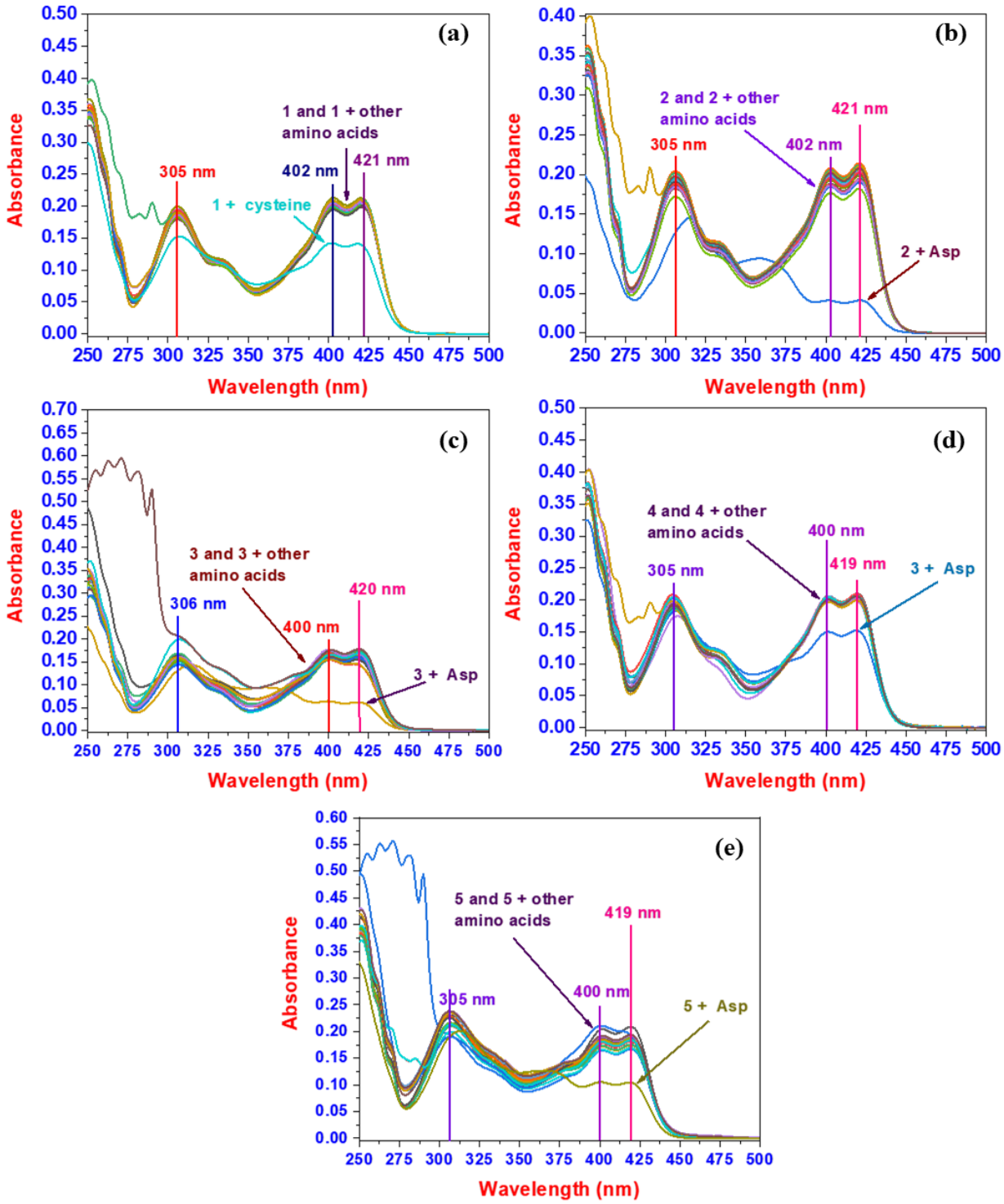

Fig. 4.5 *UV-Visible absorption spectra of (a)* ***1*** *(20 μM), (b)* ***2*** *(20 μM), (c)* ***3*** *(20 μM), (d)* ***4*** *(20 μM) and (e)* ***5*** *(20 μM) in absence and presence of natural amino acids (a) 20 μM and (b) 20 μM, (c) 60 μM, (d) 40 μM and (e) 50 μM recorded in DMSO*

The UV-visible interaction studies demonstrate amino acid binding abilities of the synthesized glycoconjugates. Out of seven, the *N*-glycoconjugates containing phenylalanine moiety selectively interacts with cysteine whereas the glycopeptides with isoleucine, alanine methionine and valine moieties are selectively binds to aspartic acid while remaining two show highest order of interaction towards aspartic acid, although it is not selective (*Fig. 4.6*).

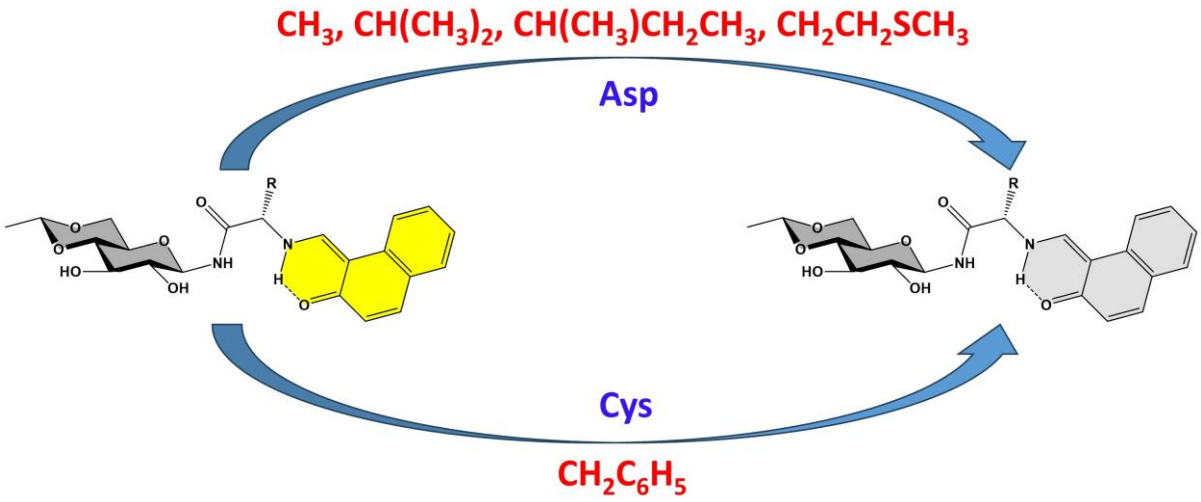

Fig. 4.6 *Selective interactions of different glycoconjugates with aspartic acid and cysteine*

UV-Visible studies were further explored for finding the interference of other amino acids in selective recognition, stoichiometries, association constants, kinetics and detection limits. The data for Job's plot was generated by subtracting the absorbance value of free probe solution from the absorbance value of mixture having same concentration at 420 nm and it was plotted against mole fraction of guest molecule, which revealed the interaction of **1** with **Cys** and **2-5** with **Asp** in 1:1 and 2:3 ratio, respectively (*Fig. 4.7*). The interaction of 1 with Cys and 2-5 with Asp occurs in two different ration due to the interference of side chain of the amino acid moieties.

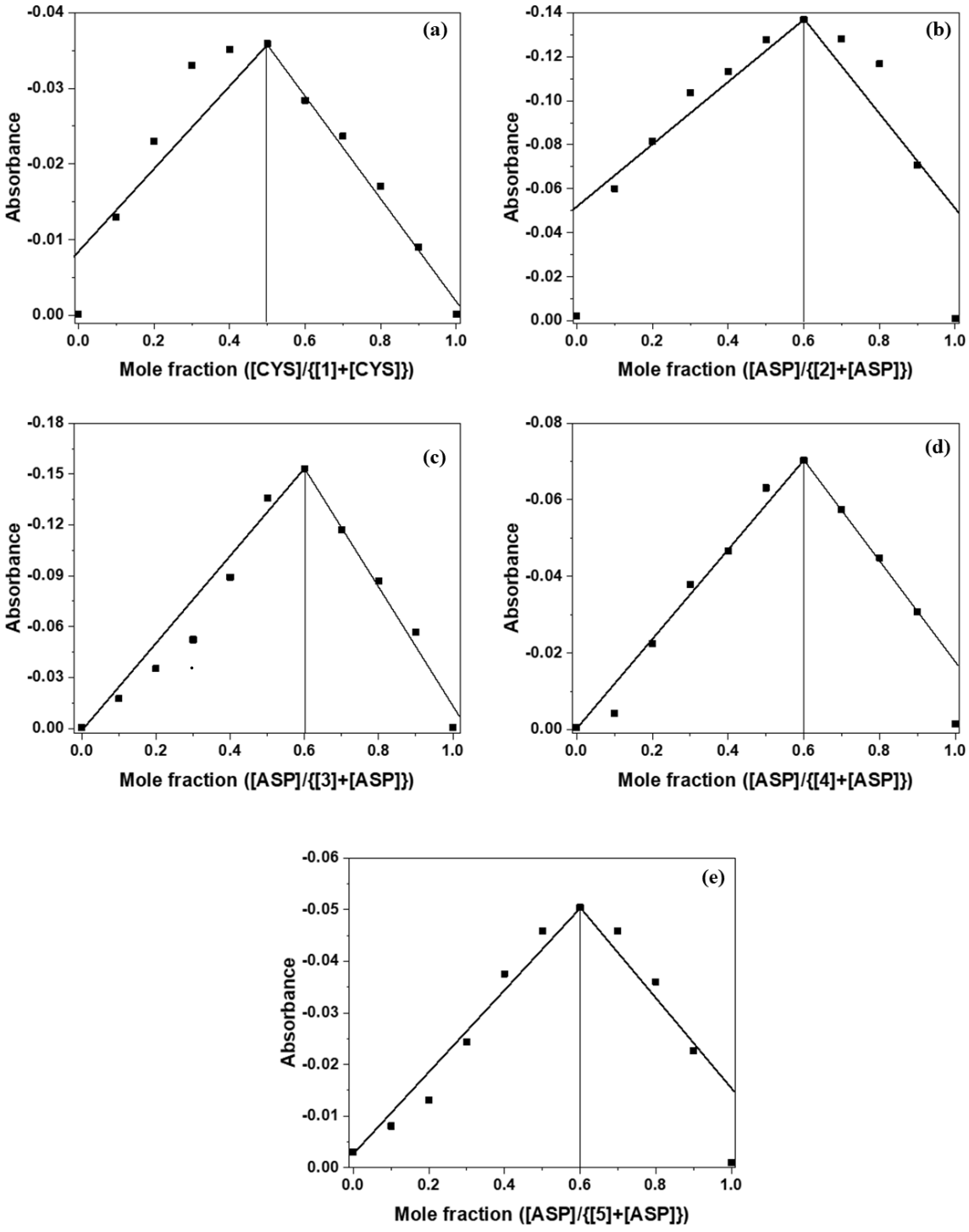

Fig. 4.7 *Job's plot of* ***1*** *(a) and* ***2-5*** *(b-e) showing the stoichiometries of 1:1 and 2:3 respectively with the guest molecule*

UV-Visible spectra for titration of **1** and **2-5** with **Cys** and **Asp** solutions, respectively revealed the gradual decrement of absorbance in the range of 400 –425 nm (*Fig. 4.8*). The appearance

of isosbestic points, supported the formation of unique components. As the absorbance values at 420 nm have shown a hypochromic shift, the association constants (k_a) of ligand and amino acid interactions were calculated by Wolfe-Shimer equation.[28]

$$\frac{A_0}{A - A_0} = \frac{\varepsilon_G}{\varepsilon_{H-G} - \varepsilon_G} + \frac{\varepsilon_G}{\varepsilon_{H-G} - \varepsilon_G} \times \frac{1}{k_a\,[AA]} \qquad \text{(Wolfe-Shimer equation)}$$

Where A and A_0 are the absorbance of ligands in the presence and absence of amino acids whereas ε_{H-G} and ε_G are their extinction coefficients, respectively. The plot between $A_0/(A-A_0)$ versus reciprocal of concentration of amino acids [AA] were linear and hence the association constant (k_a) can be given by the ratio of the intercept to the slope equations.

$$k_a = \frac{Intercept}{slope}$$

The k_a value for **1** and **Cys** interaction was calculated as 1099.98 M^{-1} following the above equation and similarly for **2**–**5** with **Asp** bindings they were calculated as 2732.42, 1102.67, 2045.48 and 2207.14 M^{-1}, respectively (*Fig. 4.9*). These association constant values are well comparable with other hydrogen bond based amino acid sensors.[29] Rao and co-workers have reported the binding constant between galactosyl-naphthyl-amine-based derivative with **Cys** as 1778 M^{-1} using fluorescence spectroscopy.[18]

Limit of detection (LOD) was calculated using the calibration curve method, by plotting the absorbance values of the mixture at 420 nm versus concentration of the analyte (*Fig. 4.10*). During this process, absorbance values were used for the mixtures having a low concentration of analyte while titrating the host with it. Evaluation of 3S/N, where S and N denote the standard deviation of the response and slope of the calibration curve, respectively, yielded the detection limit of **Cys** as 1.89 μM. Similar methodology for **Asp** yielded the detection limit as 2.00, 1.52, 1.88 and 1.36 μM for **2**, **3**, **4** and **5**, respectively.

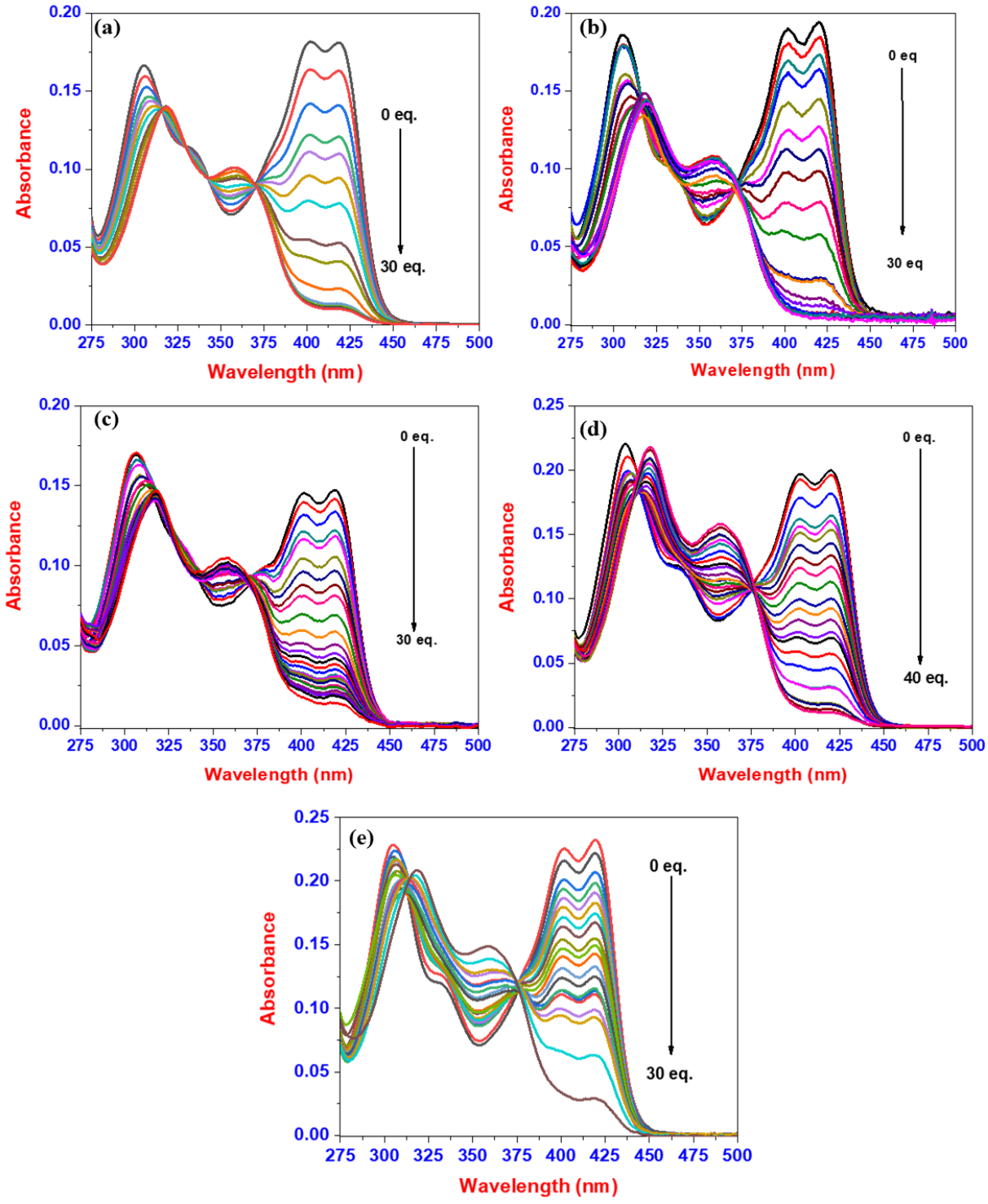

Fig. 4.8 *UV-Visible absorption spectra of (a)* ***1*** *and (b-e)* ***2-5*** *(20 mM) upon titration of* ***Cys*** *and* ***Asp***

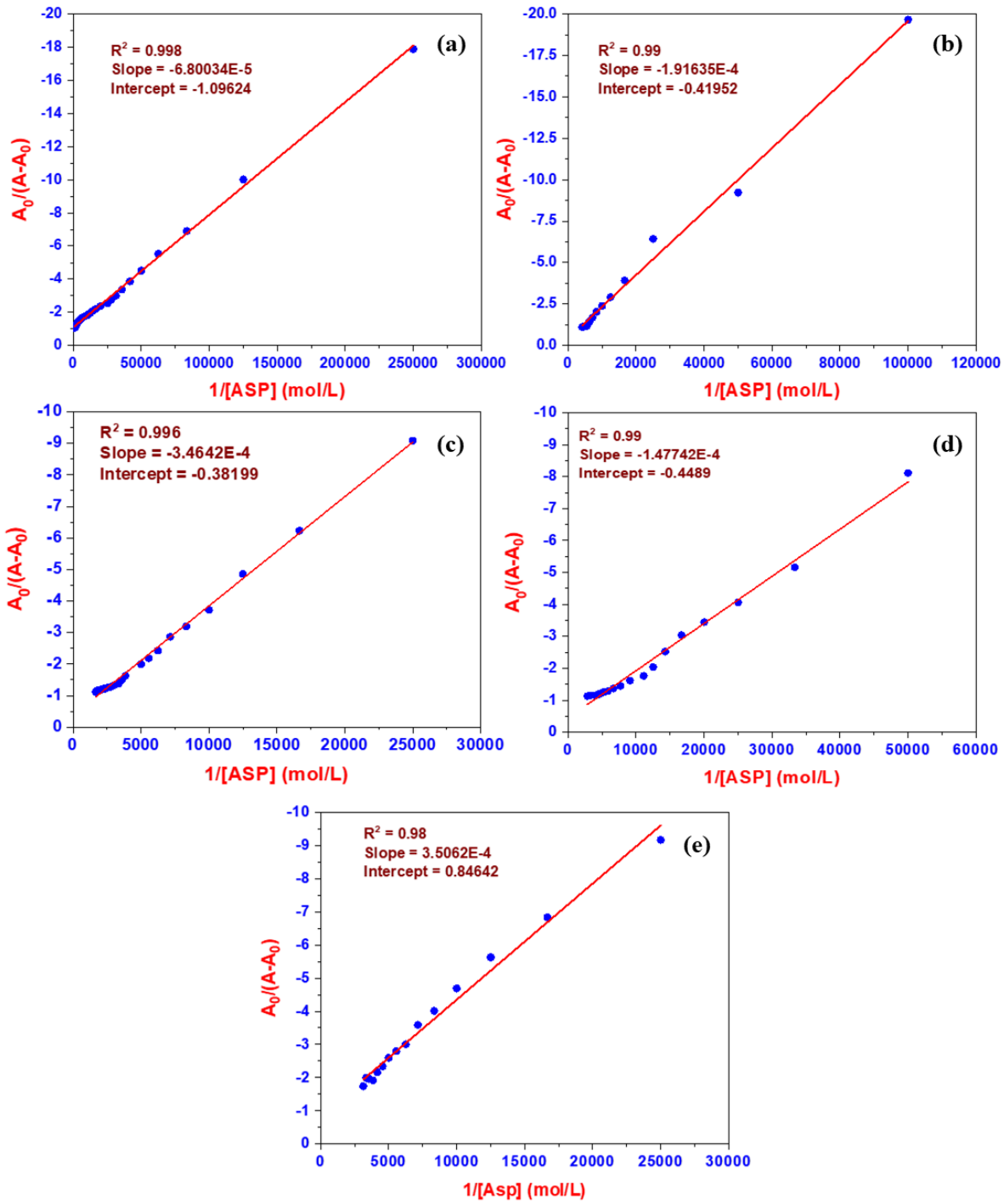

Fig. 4.9 *Plot for the determination of association constant of (a) 1 and (b-e) 2-5 for Cys and Asp, respectively*

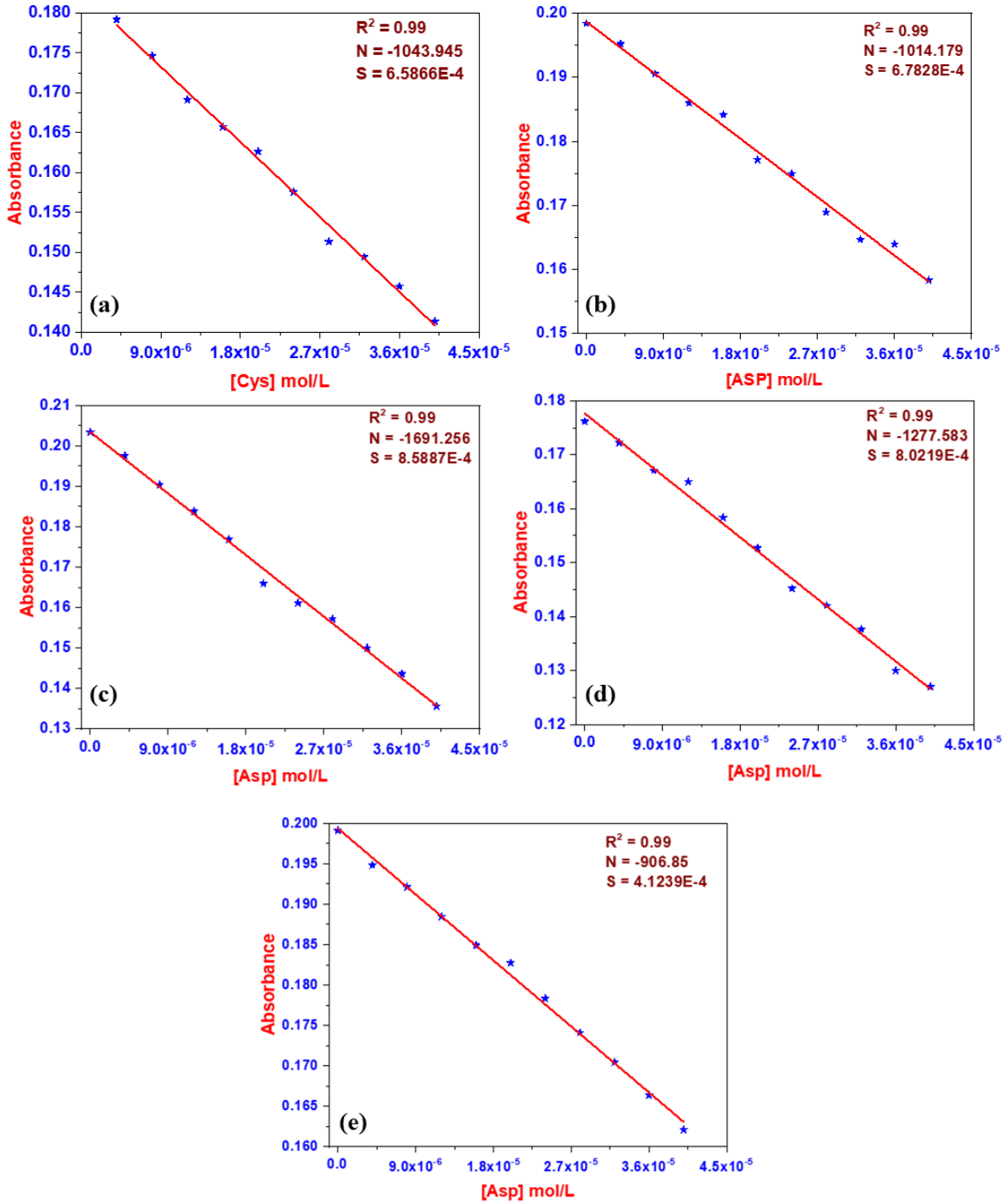

Fig. 4.10 *Plot for the determination of limit of detection of (a)* ***1*** *and (b-e)* ***2-5*** *for* ***Cys*** *and* ***Asp****, respectively*

After establishing the selective interaction of **1-5** with **Cys** and **Asp**, we also explored the possibilities of interference by rest of the naturally occurring amino acids via absorbance competition experiment. During these experiments, excess of amino acids was used to bring

the noticeable change in absorbance, however, the ratio of amino acids in interfering solution was kept the same. A representative plot of absorbance values at 420 nm with respect to added amino acids is shown in *Fig. 4.11a*, which clearly supports the selective recognition ability of **1** without interferences. Similar results were obtained for **2-5** with **Asp** interactions (*Fig. 4.11b-4.11e*), which signify that **1** and **2-5** have an excellent anti-jamming ability for recognition of **Cys** and **Asp** respectively.

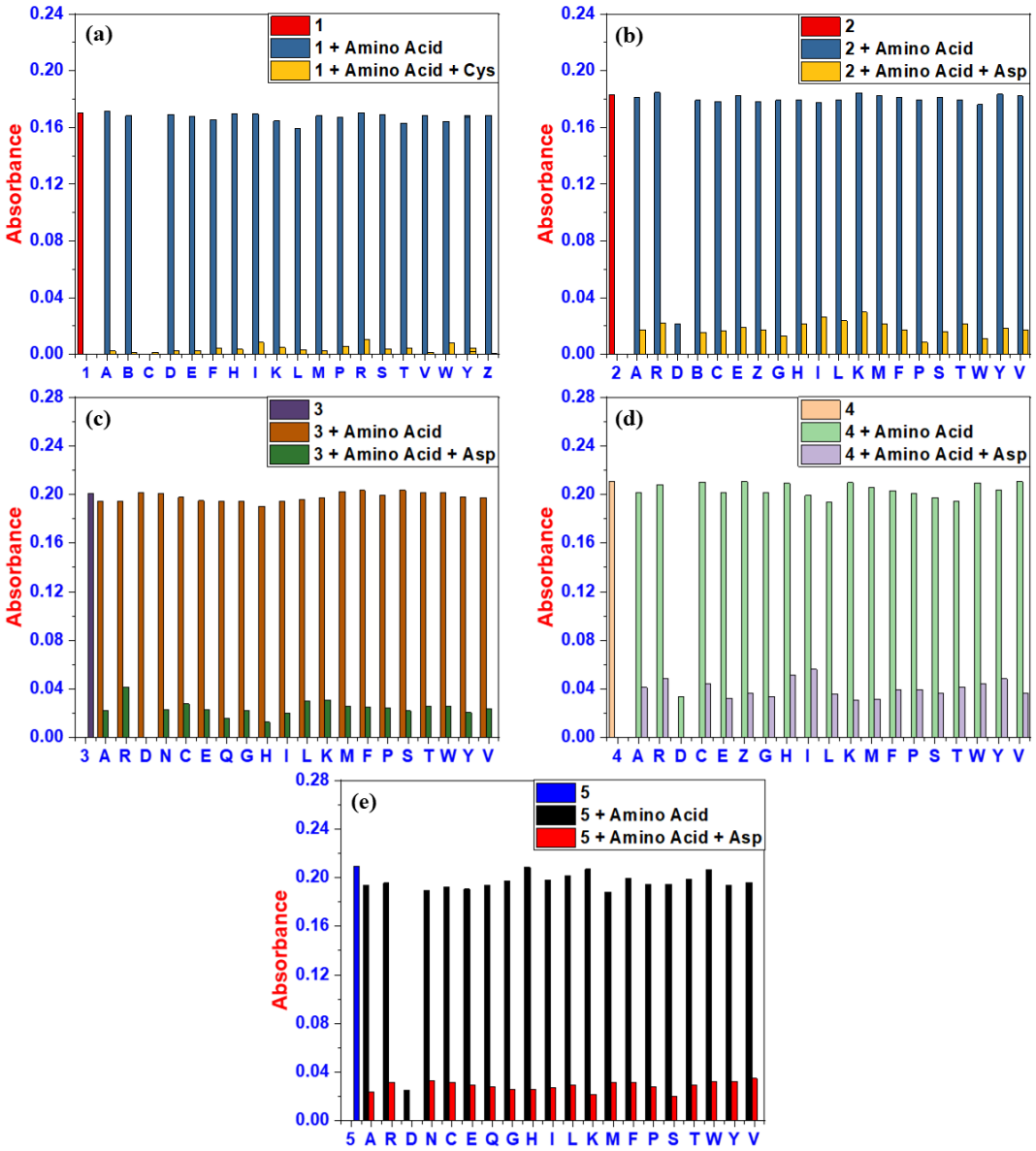

Fig. 4.11 *Competitive selective binding affinity of (a)* ***1*** *and (b-e)* ***2-5*** *(20 μM) toward* ***Cys*** *and* ***Asp****, respectively in the presence of different amino acids in MeOH–H_2O (9 : 1 v/v)*

To know the extent of host-guest interactions, the rates of complexation of the proposed sensing systems could be a decisive factor and hence, the absorption intensities of all five probes at 420 nm were recorded immediately after addition of the amino acid with whom they are interacting. The time-driven absorption at 420 nm of these probes in MeOH–H_2O (9:1 v/v) medium after addition of their selectively interacting amino acids is shown in *Fig. 4.12*. It was quite evident that after the addition of selectively interacting amino acids, the probes displayed a decrease in absorption intensity as a function of time and became constant in an exponential pattern after approaching a minimal intensity. Assuming the guest-host interaction follows first-order kinetics, the rate constant (k) determination in **1**-**5** were done using non-linear curve fitting to the first-order kinetics ($A = A_0e^{-kt}$) over the desired time which are 7.66 x 10^{-3} s^{-1}, 9.12 x 10^{-4} s^{-1}, 1.14 x 10^{-3} s^{-1}, 8.85 x 10^{-4} $s^{-1}$and 1.85 x 10^{-3} s^{-1} respectively.

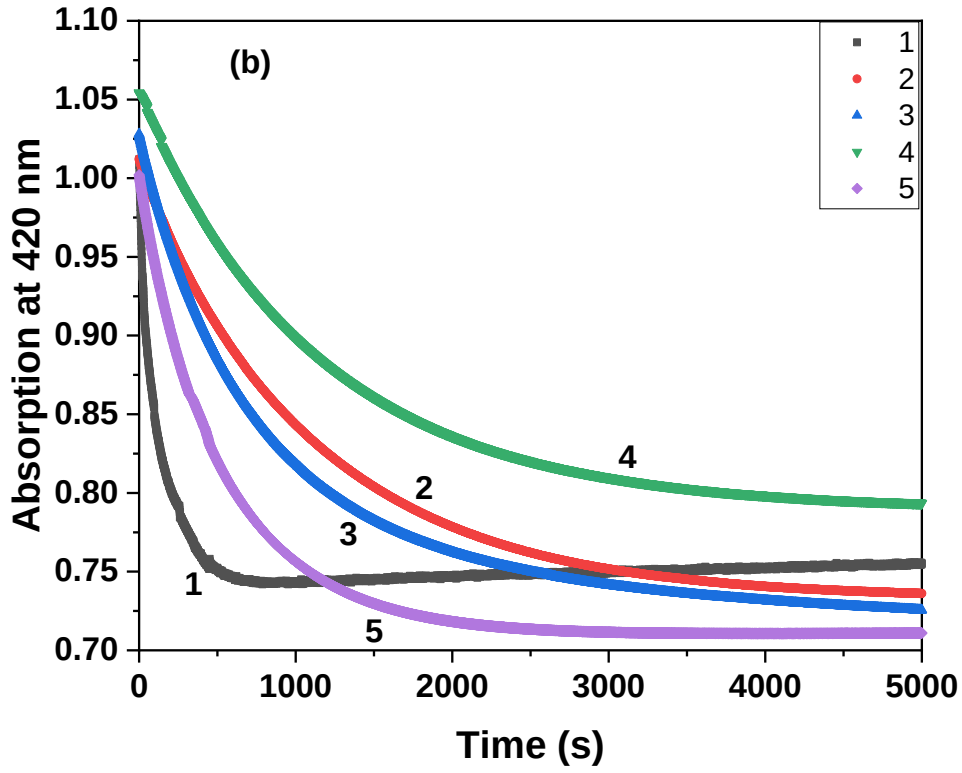

Fig. 4.12 *Absorption spectral responses (λabs = 420 nm) of* ***1****–****5*** *as a function of time (s) on the addition of equimolar* ***Cys*** *(for* ***1****) or* ***Asp*** *(for* ***2****-****5****) ion to the probe solutions*

4.3.2 NMR studies

The host-guest interactions were further investigated by ^{1}H NMR spectroscopy to understand the insight of the molecular recognition process. Due to the low solubility of **Cys** in DMSO-d_6, detailed NMR studies were performed on **Asp** and its specifics with host **3** is presented in *Fig. 4.13*. In ^{1}H NMR spectrum of aspartic acid, chemical shifts (δ) of side-chain CH_2 protons (Asp-H β; 2.74 and 2.43 ppm) and their ^{2}J coupling value (Germinal coupling = 16 Hz) implies that it exists as an anion in the solution state.[30]

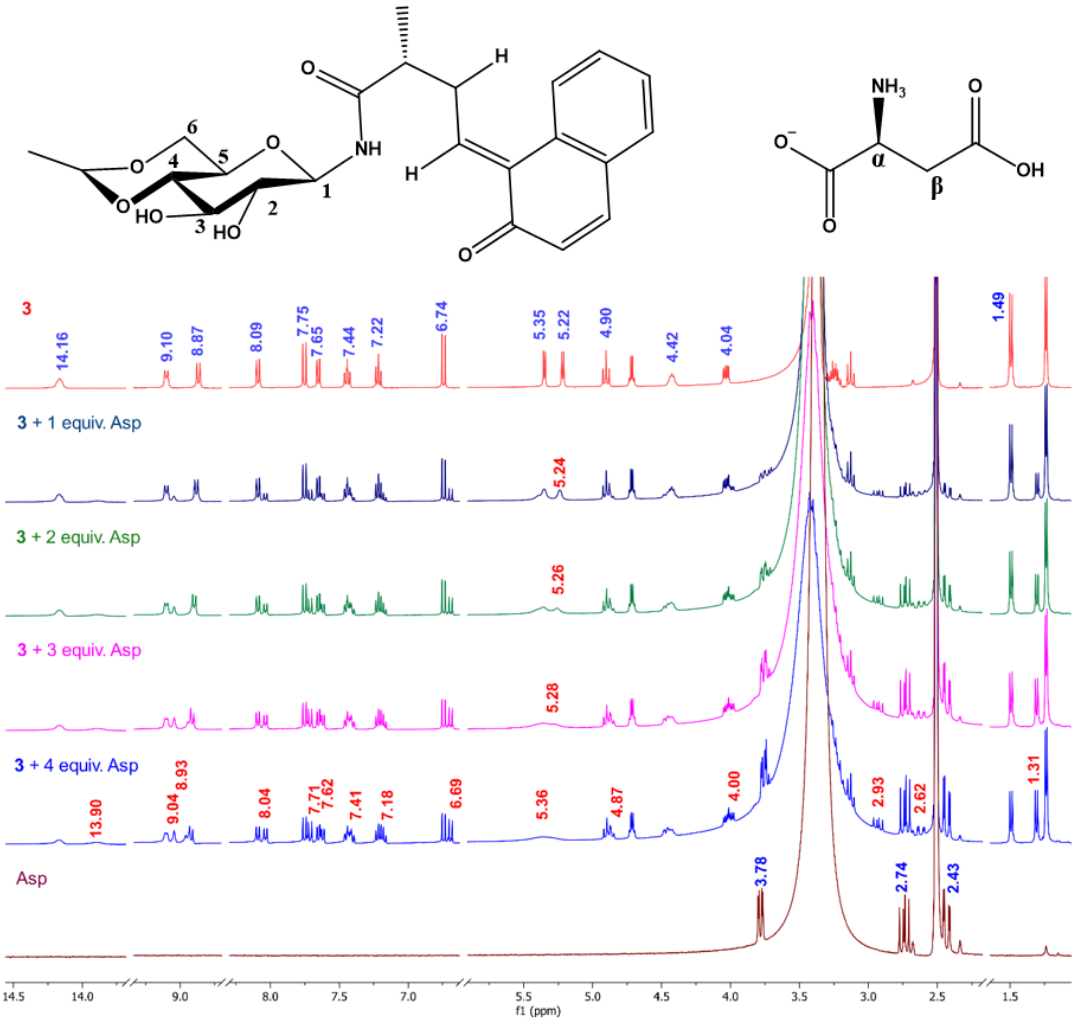

Fig. 4.13 *^{1}H NMR spectra of host **3** with guest **Asp** in different ratios along with chemical shifts (δ) before (blue) and after (red) interaction showing the gradual changes in the spectral pattern; in ppm)*

During the interaction, a downfield shift in the δ values of aspartic acid's CH_2 protons (Asp-H β) were observed whereas upfield shift was detected for N-H (14.16 ppm) of the enaminic tautomer, naphthyl aromatic protons (6.5–8.5 ppm) and methyl protons (1.49 ppm) of alanine moiety, which clearly indicates electron density transfer from the side-chain carboxyl group of aspartic acid to the quinoid part of 3. A minor but steady downfield shift in δ of the Glu-OH2 and amidic proton was observed with increase in the concentration of amino acid, which might be due to the weak interaction of sugar part with either amine or carboxyl groups of aspartic acid forced by excess amino acid. During the interaction, the coupling constant for CH_2 protons of aspartic acid remains unchanged, implying the anionic form of aspartic acid and rules out the possibility of proton transfer.

All these pieces of information suggest the interaction of Asp at the encircled region of the host molecule (*Fig. 4.14*). The interaction might be through the hydrogen bonding of -OH, N-H and Ar=O units of the host with the amine and carboxyl groups of the guest molecule. The upfield shift of methyl proton peak of alanine moiety at 1.31 ppm indicates the possibility of its interaction with the carboxyl group of Asp via C-H ⋯O type hydrogen bonding interaction.

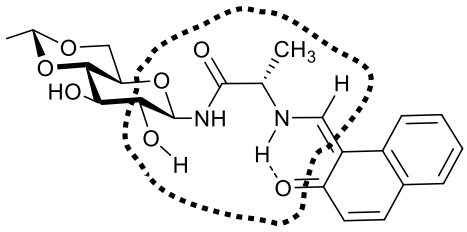

Fig. 4.14 *Probable region of* ***3*** *interacting with* ***Asp***

This assumption is further supported by the appearance of off-diagonal peak (1.30 ppm, 3.70 ppm) in the ^1H–^1H COSY spectrum (*Fig. 4.15*) due to the coupling of alanine CH_3 protons with the chiral proton of aspartic acid. Appearance of another peak at (2.90 ppm, 4.47 ppm) for coupling of aspartic acid's CH_2 proton and alanine chiral proton also supports the involvement of aspartic acid side chain in hydrogen bonding interaction with the host molecule. Selectivity

towards aspartic acid might be due to the involvement of its side chain in the interaction. The interaction between **2**, **4** and **5** with **Asp** was also explored using this methodology and the similar results were obtained (**Appendix** *Fig. A15-A17*), which reinforce our claim.

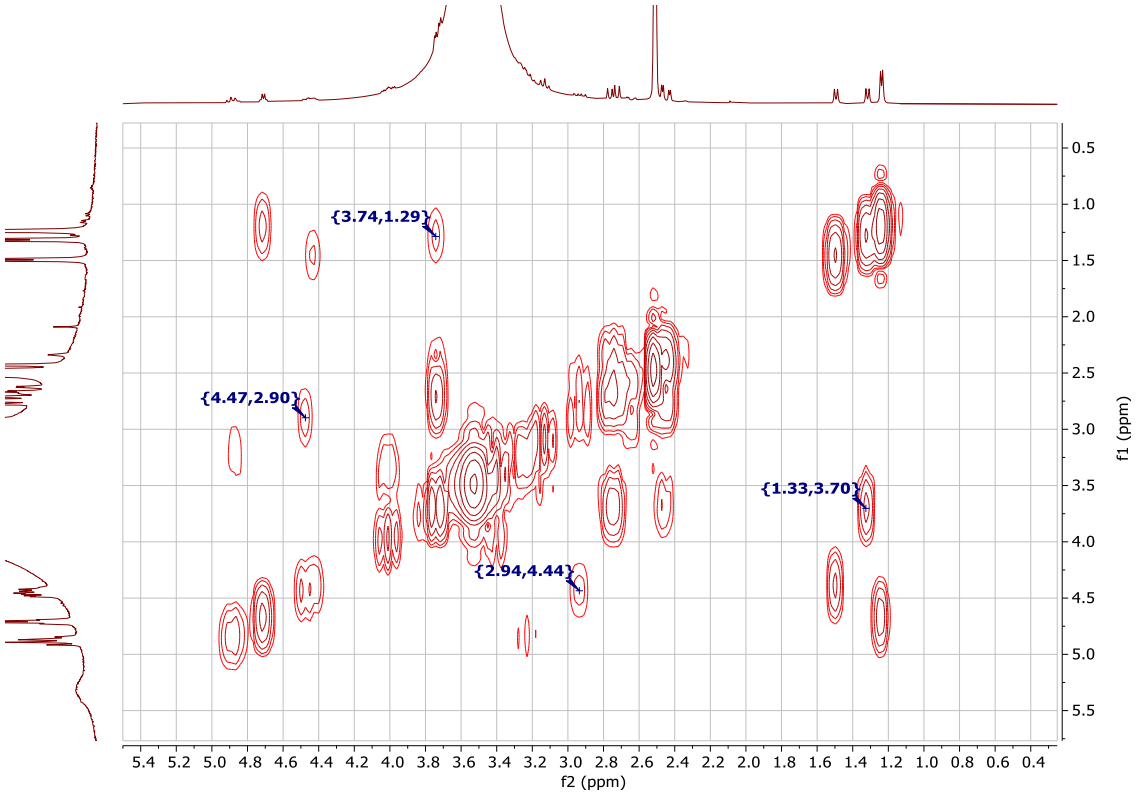

Fig. 4.15 *^{1}H COSY NMR spectrum of host **3** with guest **Asp** (4 equivalents)*

4.4 Conclusions

Seven *N*-glycoconjugates have been explored as colorimetric chemosensors for naturally occurring amino acids. One of the glycoconjugates was highly selective towards **Cys** while the rest four were selective for **Asp**. The interaction studies have been investigated using NMR and UV-visible absorption spectroscopy, however, it can be established via visual changes also. The yellow solution of sensors turns colourless in presence of respective selected amino acid (**Cys** or **Asp**) but retains its original color in presence of any other amino acids. The changes in ^{1}H NMR spectra of receptors after addition of selected amino acid (**Cys** or **Asp**) indicated

the involvement of phenolic oxygen, N–H of the enaminic tautomer and Glu-OH2 in guest recognition. Involvement of the side chain of amino acid moieties has also been noted during the recognition process.

References

1. Mounier, C.; Posner, B. I., Peptide hormones and growth factors: Cellular signaling mechanisms. In *Encyclopedia of Endocrine Diseases*, Martini, L., Ed. Elsevier: New York, 2004; pp 532-539.

2. Miret, J. A.; Munné-Bosch, S., Plant amino acid-derived vitamins: biosynthesis and function. *Amino Acids* **2014,** *46* (4), 809-824.

3. Barbara, A. M.; Hiroshi, A., Purine and pyrimidine nucleotide synthesis and metabolism. *Arabidopsis Book* **2002,** (1).

4. MacGregor, E. A., Biopolymers. In *Encyclopedia of Physical Science and Technology (Third Edition)*, Meyers, R. A., Ed. Academic Press: New York, 2003; pp 207-245.

5. Berg, J. M.; Tymoczko, J. L.; Stryer, L., Amino acids are precursors of many biomolecules. In *Biochemistry*, 5 ed.; W H Freeman: New York:, 2002.

6. Ren, W.; Li, Y.; Yin, Y.; Blachier, F., Structure, metabolism and functions of amino acids: An overview. In *Nutritional and Physiological Functions of Amino Acids in Pigs*, Blachier, F.; Wu, G.; Yin, Y., Eds. Springer Vienna: Vienna, 2013; pp 91-108.

7. Zhou, Y.; Yoon, J., Recent progress in fluorescent and colorimetric chemosensors for detection of amino acids. *Chemical Society Reviews* **2012,** *41* (1), 52-67.

8. Wang, J.; Liu, H.-B.; Tong, Z.; Ha, C.-S., Fluorescent/luminescent detection of natural amino acids by organometallic systems. *Coordination Chemistry Reviews* **2015,** *303*, 139-184.

9. Gunnlaugsson, T.; Glynn, M.; Tocci, G. M.; Kruger, P. E.; Pfeffer, F. M., Anion recognition and sensing in organic and aqueous media using luminescent and colorimetric sensors. *Coordination chemistry reviews* **2006,** *250* (23-24), 3094-3117.

10. Amendola, V.; Esteban-Gómez, D.; Fabbrizzi, L.; Licchelli, M., What anions do to N− H-containing receptors. *Accounts of chemical research* **2006,** *39* (5), 343-353.

11. Gunnlaugsson, T.; Ali, H. D. P.; Glynn, M.; Kruger, P. E.; Hussey, G. M.; Pfeffer, F. M.; dos Santos, C. M.; Tierney, J., Fluorescent photoinduced electron transfer (PET) sensors for anions; from design to potential application. *Journal of Fluorescence* **2005,** *15* (3), 287-299.

12. Li, S.-H.; Yu, C.-W.; Xu, J.-G., A cyclometalated palladium–azo complex as a differential chromogenic probe for amino acids in aqueous solution. *Chemical communications* **2005,** (4), 450-452.

13. Wang, Y.; Wang, J.; Yang, F.; Yang, X., Spectrophotometric determination of cysteine with gold nanoparticles stabilized with single-stranded oligonucleotides. *Analytical Sciences* **2010,** *26* (5), 545-549.

14. Wei, X.; Qi, L.; Tan, J.; Liu, R.; Wang, F., A colorimetric sensor for determination of cysteine by carboxymethyl cellulose-functionalized gold nanoparticles. *Analytica chimica acta* **2010,** *671* (1-2), 80-84.

15. Zhang, Y.; Li, Y.; Yan, X.-P., Photoactivated CdTe/CdSe quantum dots as a near infrared fluorescent probe for detecting biothiols in biological fluids. *Analytical chemistry* **2009,** *81* (12), 5001-5007.

16. Fernández-Alonso, M. d. C.; Cañada, F. J.; Jiménez-Barbero, J.; Cuevas, G., Molecular recognition of saccharides by proteins. Insights on the origin of the carbohydrate− aromatic interactions. *Journal of the American Chemical Society* **2005,** *127* (20), 7379-7386.

17. Davis, B. G., Recent developments in glycoconjugates. *Journal of the Chemical Society, Perkin Transactions 1* **1999,** (22), 3215-3237.

18. Ahuja, R.; Singhal, N. K.; Ramanujam, B.; Ravikumar, M.; Rao, C. P., Experimental and Computational Studies of the Recognition of Amino Acids by Galactosyl-imine and-amine Derivatives: An Attempt to Understand the Lectin− Carbohydrate Interactions. *The Journal of Organic Chemistry* **2007,** *72* (9), 3430-3442.

19. Mitra, A.; Chinta, J. P.; Rao, C. P., 1-(d-Glucopyranosyl-2′-deoxy-2′-iminomethyl)-2-hydroxybenzene as chemosensor for aromatic amino acids by switch-on fluorescence. *Tetrahedron Letters* **2010,** *51* (1), 139-142.

20. Soni, K.; Sah, A. K., Alanyl glycoconjugate: a selective receptor for free and protein-bound tryptophan. *RSC advances* **2013,** *3* (30), 12096-12099.

21. Elamathi, C.; Butcher, R.; Mohankumar, A.; Sundararaj, P.; Madankumar, A.; Kalaivani, P.; Prabhakaran, R., A quinoline-based probe for effective and selective sensing of aspartic acid in aqueous medium: In vitro and in vivo live cell imaging. *Inorganic Chemistry Frontiers* **2019,** *6* (11), 3237-3244.

22. Das, S.; Guha, S.; Banerjee, A.; Lohar, S.; Sahana, A.; Das, D., 2-(2-Pyridyl) benzimidazole based Co (II) complex as an efficient fluorescent probe for trace level determination of aspartic and glutamic acid in aqueous solution: A displacement approach. *Organic & Biomolecular Chemistry* **2011,** *9* (20), 7097-7104.

23. Chen, X.; Zhang, S.; Shan, X.; Chen, Z., Derivative chiral copper (II) complexes as template of an electrochemical molecular imprinting sol-gel sensor for enantiorecognition of aspartic acid. *Analytica Chimica Acta* **2019,** *1072*, 54-60.

24. Liu, S.-Y.; Fang, L.; He, Y.-B.; Chan, W.-H.; Yeung, K.-T.; Cheng, Y.-K.; Yang, R.-H., Cholic-acid-based fluorescent sensor for dicarboxylates and acidic amino acids in aqueous solutions. *Organic Letters* **2005,** *7* (26), 5825-5828.

25. Huang, X.-H.; He, Y.-B.; Chen, Z.-H.; Hu, C.-G.; Qing, G.-Y., Novel chiral fluorescent chemosensors for malate and acidic amino acids based on two-arm thiourea and amide. *Canadian Journal of Chemistry* **2008,** *86* (2), 170-176.

26. Zhou, X.-b.; Yip, Y.-W.; Chan, W.-H.; Lee, A. W., An easy assembled fluorescent sensor for dicarboxylates and acidic amino acids. *Beilstein journal of organic chemistry* **2011,** *7* (1), 75-81.

27. Liu, X.-Y.; Fang, H.-X.; Yu, L.-P., Molecularly imprinted photonic polymer based on β-cyclodextrin for amino acid sensing. *Talanta* **2013,** *116*, 283-289.

28. Hajian, R.; Guan Huat, T., Spectrophotometric studies on the thermodynamics of the ds-DNA interaction with irinotecan for a better understanding of anticancer drug-DNA interactions. *Journal of Spectroscopy* **2013,** *2013*.

29. Mizutani, T.; Ema, T.; Yoshida, T.; Kuroda, Y.; Ogoshi, H., Recognition of. alpha.-amino acid esters by zinc porphyrin derivatives via coordination and hydrogen bonding interactions. Evidence for two-point fixation from thermodynamic and induced circular dichroism spectroscopic studies. *Inorganic Chemistry* **1993,** *32* (10), 2072-2077.

30. Roberts, G.; Jardetzky, O., Nuclear magnetic resonance spectroscopy of amino acids, peptides, and proteins. *Advances in protein chemistry* **1970,** *24*, 447-545

Chapter 5

Development of Glycopeptide Derived Catalyst for One-pot Synthesis of Imidazo[1,2-a]pyridines

Chapter 5

5.1 Introduction

Glycoconjugate derived catalysts are always considered as green biocatalysts because of their biocompatibility, low toxic nature, and their origin from natural resources. The functional form of natural polypeptides covalently bound with carbohydrates are commonly termed as glycoproteins, which play crucial roles in biological processes such as cell-cell recognition, immune response, inflammation, and tumor metastasis.[1-2] Such molecules have unique structural diversity for selective recognition of substrate in bio-catalytic reactions.[3] The facilitation of several catalytic reactions by the metal ion-bound glycoproteins has been explored by in-silico studies.[4] Since the biocatalysts provide regio and stereoselective reactions, researchers are replacing the traditional chemical catalysis with it.[5-6] Unfortunately, the commercial production or isolation of such biocatalysts from natural sources is a challenging task due to their structural flexibility and fragile nature. Hence, functional mimicking of the active site of the biocatalyst is desirable to understand the substrate binding followed by catalysis. Incorporation of biocompatible metal ions can further increase their activity toward a catalytic reaction. Previously we have reported the selective recognition of cupric acetate by *N*-(2-hydroxybenzoyl)-L-alanyl-4,6-*O*-ethylidene-β-D-glucopyranosylamine and used that system as a catalyst in selective oxidation of primary and secondary alcohols into corresponding carbonyl compounds.[7] Currently, we have modified the ligand by replacing the terminal amide group with imine functionality for better metal ion binding and complex stability.

The newly synthesized glycopeptide-based ligand, *N*-(2-hydroxynapthylidene)-L-leucienyl-4,6-*O*-ethylidene-β-D-glucopyranosylamine (**6**), has been tested for metal ion interactions, and positive results have been noted with several transition as well as non-transition metal ions in solution. We explored the stability of interaction in solution at three pH (4.2, 9.2, and 7.2) conditions to choose the suitable catalysts. The interaction of ligand with cupric ion remains

immune toward pH change, supporting the stability of the metal complex in solution. Since copper is the third most abundant transition metal ion in the biological system and controls several biological processes, we focused on cupric complex catalysed reactions.

Heterocyclic compounds are integral part of many natural products, bioactive molecules, and drugs. Among various nitrogen-containing heterocycles, imidazo[1,2-*a*]pyridine is core part of several bioactive molecules which exhibit antitumor, antibacterial, antiviral, antifungal, anti-inflammatory, antiapoptotic, antipyretic, antiprotozoal, analgesic, hypnoselective, and anxioselective activities.[8] Zolpidem, Alpidem, Necopidem, Saripidem, Zolimidine, and Olprinone are some of the commercial available drugs containing this scaffold.[8-9] In addition, imidazo[1,2-*a*]pyridines with 2-hydroxyphenyl substituent are essential in the optoelectronics field due to the intramolecular proton transfer in excited-state (ESIPT).[10-12] Due to the significant role of imidazo[1,2-*a*]pyridines, many strategies, i.e., gold-catalyzed reaction of aminopyridines and propargyl aldehydes (*Scheme 5.1a*),[13-14] heterocyclization between 2-aminopyridines and α-halocarbonyl (*Scheme 5.1b*),[15-17] reactions of 2-chloropyridine with 1,2,3-triazoles and subsequent elimination of nitrogens (*Scheme 5.1c*),[16-18] oxidative coupling between α,β-unsaturated carbonyl compounds, and aminopyridines (*Scheme 5.1d*),[19-20] reaction of 2-aminopyridine, aldehyde, and isonitrile (*Scheme 5.1e*),[21] oxidative cyclization between arylketones and 2-amino-pyridines (*Scheme 5.1f*),[22] tandem amination/cycloisomerization of aryl propargylic alcohols with 2-aminopyridines (*Scheme 5.1g*)[23] are designed to synthesize it. Although many methods are available to synthesize imidazo[1,2-*a*]pyridines, these methods have some drawbacks like preparation of starting material, prefunctionalization of carbonyl group, need of additives, anhydrous conditions, high reaction temperature, etc.

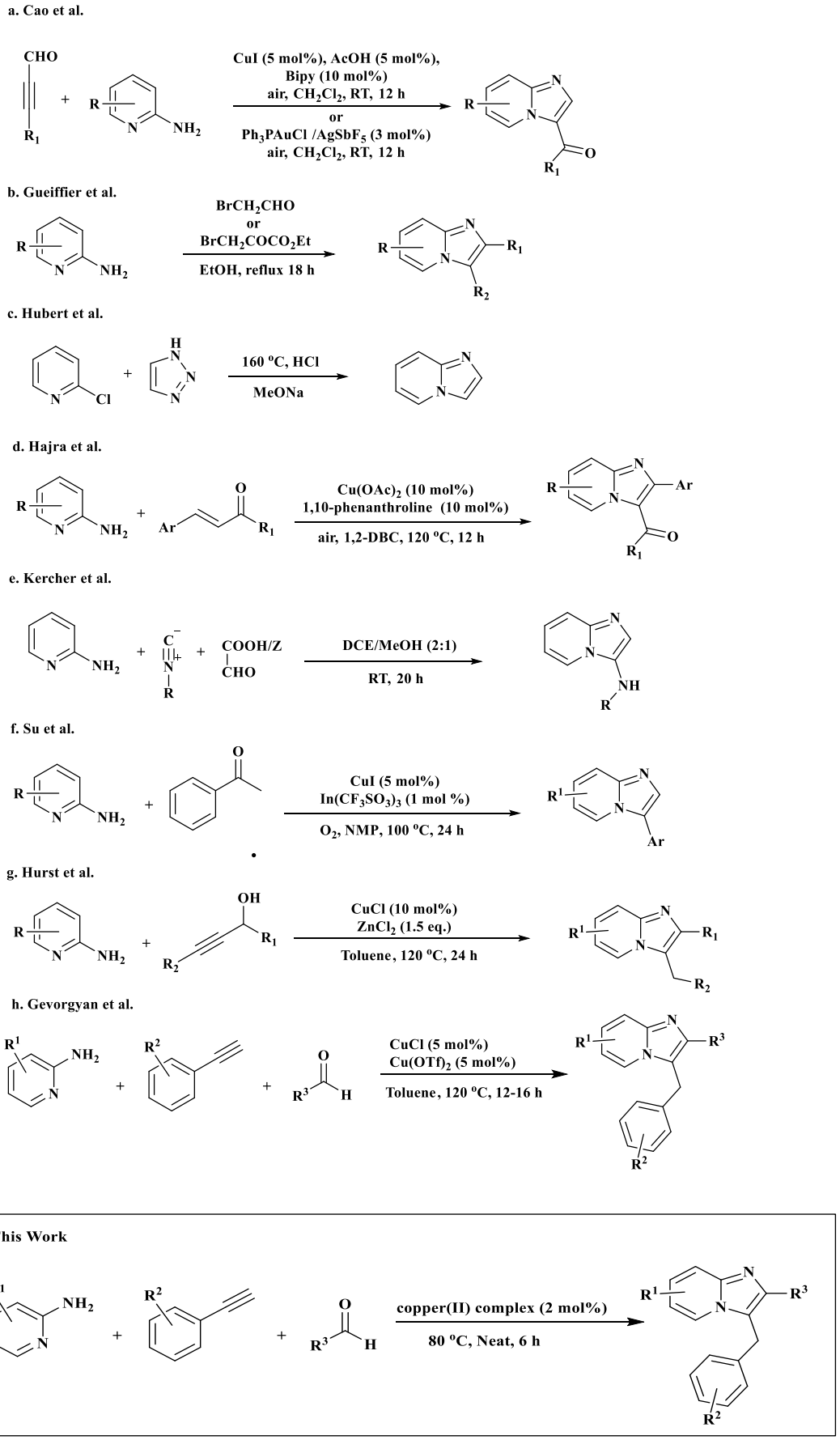

Scheme 5.1 Synthesis of imidazo[1,2-a]pyridines moieties using different methods

In 2010, Gevorgyan et al. have reported one-pot synthesis of imidazo[1,2-*a*]pyridines using aldehydes, 2-aminopyridines, and terminal alkynes (*Scheme 5.1h*).[24] So far several modifications have been done, however, the methodology still have some drawbacks like prolonged reaction time, use of problematic solvent toluene, high Cu(II) salt loading. Inspired by these facts, we explored the application of our catalytic system in the one-pot synthesis of imidazopyridines and produced twenty-three derivatives in good to excellent yields. Hence, we describe the development of new glucose-derived copper catalyst and their application in one-pot synthesis of imidazo[1,2-*a*]pyridines under solvent-free reaction conditions.

5.2 Experimental

5.2.1 General procedure of sample preparation for UV-visible spectral measurements

Stock solutions (1 mM) of compound **6** and metal salts were prepared in a mixed solvent, methanol-water (9:1 v/v). Test solutions for interaction studies were prepared by mixing the probe (200 μL) and metal ion (200 μL) stock solutions in a series of 10 mL volumetric flasks, followed by dilution up to the mark with either buffered solution of three different pH (4.2, 7.2 and 9.2 as mentioned in figure caption) or methanol-water (9:1 v/v).

5.2.2 General procedure for synthesis of Imidazo[1,2-*a*]pyridines

A mixture of 2-aminopyridine derivatives, aldehydes, and terminal alkynes was stirred along with 2 mol% of compound **6** and cupric acetate under the neat condition at 80 °C. The progress of the reaction was monitored by TLC, and after completion of the reaction, the product was purified by column chromatography on neutral alumina/ silica gel (120−200 mesh) eluting with ethyl acetate−hexane.

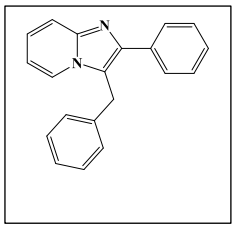

Product code 4a: Off white solid: mp 154-155 °C; 93% yield; ^{1}H NMR (400 MHz, DMSO-d_6) δ 8.15 (d, *J* = 6.9 Hz, 1H), 7.80 (d, *J* = 7.6 Hz, 2H), 7.64 (d, *J* = 9.0 Hz, 1H), 7.46 (t, *J* = 7.5 Hz, 2H), 7.30 (m, *J* = 23.5, 7.2 Hz, 5H), 7.10 (d, *J* = 7.4 Hz, 2H), 6.89 (t, *J* = 6.8 Hz, 1H), 4.58 (s, 2H). ^{13}C NMR (101 MHz, DMSO-d_6) δ 144.38, 142.78, 137.87, 135.05, 129.30, 129.10, 128.02, 127.99, 127.96, 127.07, 124.94, 124.71, 118.79, 117.30, 112.66, 29.16. HRMS: m/z calcd for $C_{20}H_{16}N_2$ $(M+H)^+$ = 285.1386; found 285.1393.

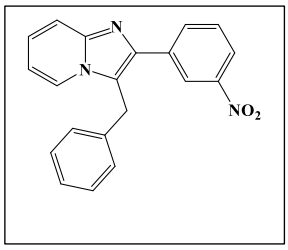

Product code 4b: Off white solid: mp 140-142 °C; 90% yield; ^{1}H NMR (400 MHz, $CDCl_3$) δ 8.69 (t, *J* = 2.0 Hz, 1H), 8.21 (ddd, *J* = 8.2, 2.3, 1.1 Hz, 1H), 8.13 (dt, *J* = 7.7, 1.3 Hz, 1H), 7.81 (dt, *J* = 7.0, 1.2 Hz, 1H), 7.72 (dt, *J* = 9.1, 1.2 Hz, 1H), 7.61 (t, *J* = 8.0 Hz, 1H), 7.39 – 7.23 (m, 4H), 7.20 – 7.12 (m, 2H), 6.80 (td, *J* = 6.8, 1.2 Hz, 1H), 4.55 (s, 2H). ^{13}C NMR (101 MHz, $CDCl_3$) δ 148.62, 145.10, 141.63, 136.45, 136.09, 133.86, 129.56, 129.21, 127.62, 127.22, 124.90, 123.54, 122.96, 122.34, 118.83, 117.84, 112.75, 29.83. HRMS: m/z calcd for $C_{20}H_{15}N_3O_2$ $(M+H)^+$ = 330.1237; found 330.1236.

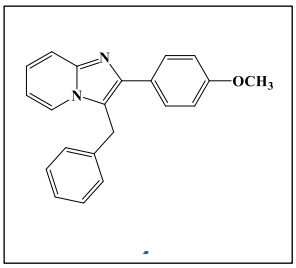

Product code 4c: Off white solid: mp 147-149 °C; 89% yield; ^{1}H NMR (400 MHz, $CDCl_3$) δ 7.78 – 7.65 (m, 4H), 7.31 – 7.23 (m, 3H), 7.23 – 7.12 (m, 3H), 7.03 – 6.95 (m, 2H), 6.71 (td, *J* = 6.8, 1.4 Hz, 1H), 4.49 (s, 2H), 3.86 (s, 3H). ^{13}C NMR (101 MHz, $CDCl_3$) δ 159.36, 144.81, 144.07, 136.92, 129.38, 129.03, 127.71, 127.15, 126.88, 123.97, 123.29, 117.36, 116.99, 114.12, 112.04, 55.30, 29.92. HRMS: m/z calcd for $C_{21}H_{18}N_2O$ $(M+H)^+$ = 315.1492; found 315.1481.

Product code 4d: Off white solid: mp 198-200 °C; 84% yield; ^{1}H NMR (400 MHz, $CDCl_3$) δ 7.80 – 7.68 (m, 2H), 7.68 – 7.54 (m, 3H), 7.38 (t, *J* = 7.6 Hz, 2H), 7.35 – 7.23 (m, 5H), 7.22 –

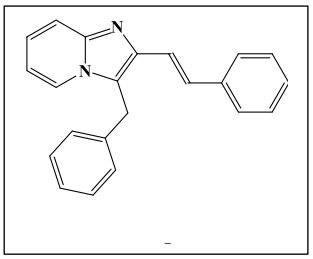

7.14 (m, 3H), 6.69 (td, *J* = 6.8, 1.2 Hz, 1H), 4.43 (s, 2H).^{13}C NMR (101 MHz, $CDCl_3$) δ 137.45, 136.59, 130.76, 128.95, 128.64, 127.99, 127.63, 126.97, 126.64, 124.69, 123.22, 119.88, 118.27, 117.14, 111.90, 29.09. HRMS: m/z calcd for $C_{22}H_{18}N_2$ $(M+H)^+$ = 311.1543; found 311.1541

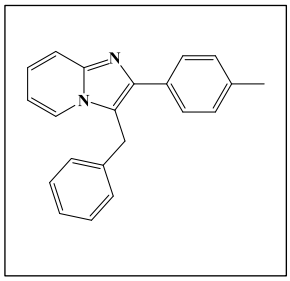

Product code 4e: Off white solid: mp 157-159 °C; 83% yield; ^{1}H NMR (400 MHz, $CDCl_3$) δ 7.78 – 7.66 (m, 4H), 7.38 – 7.23 (m, 6H), 7.23 – 7.14 (m, 3H), 6.71 (t, *J* = 6.7 Hz, 1H), 4.51 (s, 2H), 2.41 (s, 3H). ^{13}C NMR (101 MHz, $CDCl_3$) δ 144.85, 144.29, 137.49, 136.92, 131.68, 129.36, 129.02, 128.08, 127.74, 126.87, 123.99, 123.35, 117.50, 117.40, 112.06, 29.95, 21.28. HRMS: m/z calcd for $C_{21}H_{18}N_2$ $(M+H)^+$ = 299.1543; found 299.1548.

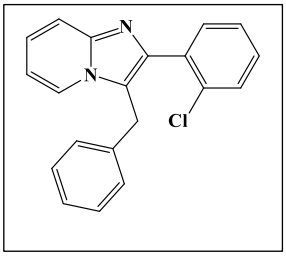

Product code 4f: Off white solid: mp 134-135 °C; 83% yield; ^{1}H NMR (400 MHz, $CDCl_3$) δ 7.78 – 7.65 (m, 2H), 7.63 – 7.47 (m, 2H), 7.42 – 7.32 (m, 2H), 7.31 – 7.16 (m, 4H), 7.15 – 7.01 (m, 2H), 6.80 – 6.66 (m, 1H), 4.31 (s, 2H). ^{13}C NMR (101 MHz, $CDCl_3$) δ 144.74, 142.28, 136.55, 134.09, 133.70, 132.58, 129.78, 129.49, 128.80, 127.93, 126.73, 126.65, 124.05, 123.76, 119.70, 117.84, 112.16, 30.00. HRMS: m/z calcd for $C_{20}H_{15}N_2Cl$ $(M+H)^+$ = 319.0997; found 319.1001.

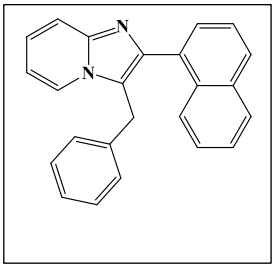

Product code 4g: Off white solid: mp 135-138 °C; 81% yield; ^{1}H NMR (400 MHz, $CDCl_3$) δ 8.24 – 8.15 (m, 1H), 7.93 (dd, *J* = 7.4, 2.1 Hz, 2H), 7.77 (dd, *J* = 11.4, 8.0 Hz, 2H), 7.66 – 7.45 (m, 4H), 7.36 – 7.16 (m, 4H), 7.15 – 7.01 (m, 2H), 6.83 – 6.71 (m, 1H), 4.33 (s, 2H). ^{13}C NMR (101 MHz, $CDCl_3$) δ 144.84, 143.91, 136.87, 133.89, 132.69, 131.90, 128.85, 128.61,

128.15, 128.14, 127.82, 126.71, 126.45, 126.36, 125.83, 125.13, 124.01, 123.74, 119.83, 117.75, 112.08, 29.78. HRMS: m/z calcd for $C_{24}H_{18}N_2$ $(M+H)^+$ = 335.1543; found 335.1489

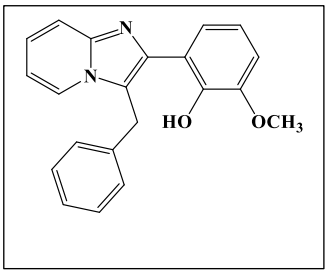

Product code 4h: Off white solid: mp 148-150 °C; 88% yield; ^{1}H NMR (400 MHz, $CDCl_3$) δ 7.80 (d, *J* = 6.8 Hz, 1H), 7.68 (d, *J* = 9.0 Hz, 1H), 7.38 – 7.23 (m, 4H), 7.23 – 7.15 (m, 3H), 6.91 (dd, *J* = 8.1, 1.5 Hz, 1H), 6.86 – 6.76 (m, 2H), 4.59 (s, 2H), 3.97 (s, 3H). ^{13}C NMR (101 MHz, DMSO) δ 144.38, 142.66, 138.11, 137.25, 131.45, 124.37, 122.97, 122.32, 120.15, 118.24, 114.23, 113.82, 112.98, 112.67, 112.13, 108.21, 107.00, 51.42, 25.55. HRMS: m/z calcd for $C_{21}H_{18}N_2O_2$ $(M+H)^+$ = 331.1441; found 331.1387

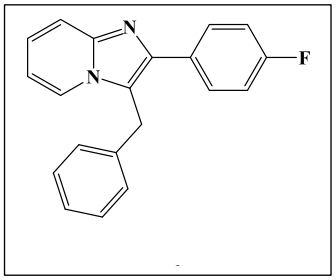

Product code 4i: Yellow liquid; 88% yield; ^{1}H NMR (400 MHz, $CDCl_3$) δ 7.84 – 7.65 (m, 4H), 7.37 – 7.19 (m, 4H), 7.18 – 7.07 (m, 4H), 6.74 (t, *J* = 6.8 Hz, 1H), 4.47 (s, 2H). ^{13}C NMR (101 MHz, $CDCl_3$) δ 163.89, 161.44, 144.60, 142.77, 136.47, 130.25, 130.21, 129.96, 129.88, 129.15, 127.64, 127.08, 124.76, 123.49, 117.59, 117.32, 115.78, 115.57, 112.58, 29.76. HRMS: m/z calcd for $C_{20}H_{15}N_2F$ $(M+H)^+$ = 303.1292; found 303.1241.

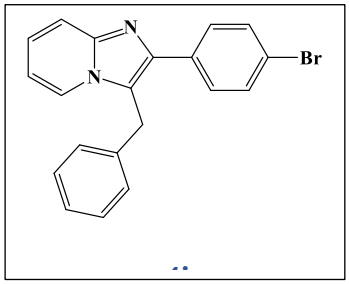

Product code 4j: Yellow solid: mp 174-176 °C; 81% yield; ^{1}H NMR (400 MHz, $CDCl_3$) δ 7.77 – 7.64 (m, 4H), 7.61 – 7.52 (m, 2H), 7.33 (qt, *J* = 7.8, 1.6 Hz, 3H), 7.22 (ddd, *J* = 9.1, 6.7, 1.3 Hz, 1H), 7.19 – 7.09 (m, 2H), 6.75 (td, *J* = 6.8, 1.2 Hz, 1H), 4.49 (s, 2H). ^{13}C NMR (101 MHz, $CDCl_3$) δ 144.97, 143.06, 136.50, 133.53, 131.79, 129.69, 129.12, 127.64, 127.04, 124.42, 123.41, 121.92, 117.87, 117.63, 112.37, 29.87. HRMS: m/z calcd for $C_{20}H_{15}N_2Br$ $(M+H)^+$ = 363.0491; found 363.0440.

Product code 4k: Pale Yellow solid: mp 228-230 °C; 71% yield; ^{1}H NMR (400 MHz, DMSO) δ 11.30 (d, *J* = 2.6 Hz, 1H), 8.38 (d, *J* = 7.9 Hz, 1H), 8.23 – 8.11 (m, 1H), 7.64 (dd, *J* = 8.9, 1.2

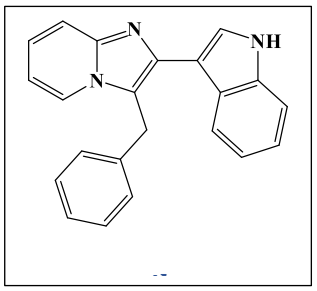

Hz, 1H), 7.56 (d, *J* = 2.6 Hz, 1H), 7.47 – 7.41 (m, 1H), 7.28 (td, *J* = 7.2, 1.4 Hz, 2H), 7.24 – 7.07 (m, 6H), 6.86 (td, *J* = 6.7, 1.1 Hz, 1H), 4.58 (s, 2H). ^{13}C NMR (101 MHz, DMSO) δ 144.38, 140.04, 138.24, 136.68, 129.57, 129.21, 128.27, 128.12, 126.95, 126.92, 124.05, 123.89, 123.64, 122.09, 121.83, 119.75, 117.53, 116.74, 112.20, 111.94, 109.77, 29.19. HRMS: m/z calcd for $C_{22}H_{17}N_3$ $(M+H)^+$ = 324.1495; found 324.1447.

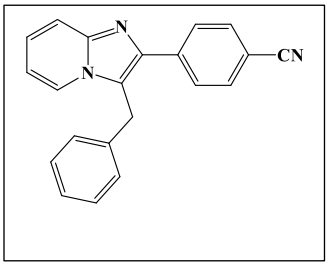

Product code 4l: Off white solid: mp 152-154 °C; 89% yield; ^{1}H NMR (400 MHz, $CDCl_3$) δ 8.01 – 7.89 (m, 2H), 7.81 (dd, *J* = 10.0, 8.2 Hz, 2H), 7.77 – 7.68 (m, 2H), 7.34 (qd, *J* = 6.8, 4.8 Hz, 4H), 7.20 – 7.06 (m, 2H), 6.86 (td, *J* = 6.8, 1.2 Hz, 1H), 4.53 (s, 2H). ^{13}C NMR (101 MHz, $CDCl_3$) δ 144.38, 140.55, 137.73, 135.54, 132.59, 129.35, 128.64, 127.52, 127.42, 126.27, 123.72, 119.26, 118.80, 117.30, 113.61, 111.61, 29.75. HRMS: m/z calcd for $C_{21}H_{15}N_3$ $(M+H)^+$ = 310.1339; found 310.1286.

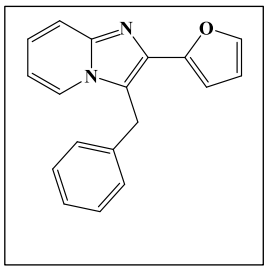

Product code 4m: Off white solid: mp 124-126 °C; 78% yield; ^{1}H NMR (400 MHz, $CDCl_3$) δ 7.77 (dt, *J* = 6.9, 1.2 Hz, 1H), 7.68 (dt, *J* = 9.2, 1.1 Hz, 1H), 7.52 (dd, *J* = 1.8, 0.8 Hz, 1H), 7.33 – 7.17 (m, 6H), 7.00 (dd, *J* = 3.4, 0.8 Hz, 1H), 6.73 (td, *J* = 6.8, 1.2 Hz, 1H), 6.55 (dd, *J* = 3.4, 1.8 Hz, 1H), 4.64 (s, 2H).^{13}C NMR (101 MHz, $CDCl_3$) δ 144.72, 142.41, 136.71, 134.63, 128.90, 127.96, 126.86, 125.05, 123.36, 118.10, 117.09, 112.60, 111.56, 108.22, 29.64. HRMS: m/z calcd for $C_{18}H_{14}N_2O$ $(M+H)^+$ = 275.1179; found 275.1141.

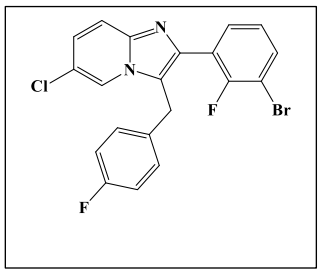

Product code 4n: Pale yellow solid: mp 130-132 °C; 77% yield; ^{1}H NMR (400 MHz, $CDCl_3$) δ 7.70 (dd, *J* = 2.0, 0.9 Hz, 1H), 7.66 – 7.58 (m, 2H), 7.43 (dd, *J* = 8.3, 1.9 Hz, 1H), 7.37 (dd, *J* = 9.7, 1.9 Hz, 1H), 7.19 (dd, *J* = 9.6, 2.0 Hz, 1H), 7.09 – 6.97 (m, 4H), 4.29 (s,

2H). ^{13}C NMR (101 MHz, $CDCl_3$) δ 163.08, 160.80, 160.64, 158.29, 143.66, 139.06, 133.06, 133.02, 131.40, 131.37, 129.30, 129.22, 127.99, 127.96, 125.96, 122.69, 122.60, 121.36, 121.27, 121.12, 120.83, 120.42, 119.78, 119.52, 118.19, 116.05, 115.83, 29.22, 29.16. HRMS: m/z calcd for $C_{20}H_{12}BrClF_2N_2$ $(M+H)^+$ = 332.9913; found 332.9894.

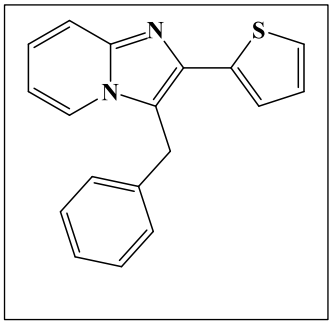

Product code 4o: Off white solid: mp 135-137 °C; 85% yield; ^{1}H NMR (400 MHz, $CDCl_3$) δ 7.75 (dt, *J* = 6.9, 1.2 Hz, 1H), 7.68 (dt, *J* = 9.1, 1.2 Hz, 1H), 7.43 (dd, *J* = 3.6, 1.2 Hz, 1H), 7.38 (dd, *J* = 5.1, 1.2 Hz, 1H), 7.35 – 7.23 (m, 4H), 7.20 (ddd, *J* = 9.2, 6.7, 1.3 Hz, 3H), 7.12 (dd, *J* = 5.1, 3.6 Hz, 1H), 6.74 (td, *J* = 6.8, 1.2 Hz, 1H), 4.58 (s, 2H). ^{13}C NMR (101 MHz, $CDCl_3$) δ 144.82, 138.63, 137.59, 136.39, 129.01, 127.79, 127.72, 126.97, 125.57, 124.53, 124.42, 123.16, 117.42, 117.37, 112.36, 29.92. HRMS: m/z calcd for $C_{18}H_{14}N_2O$ $(M+H)^+$ = 291.0950; found 291.0902.

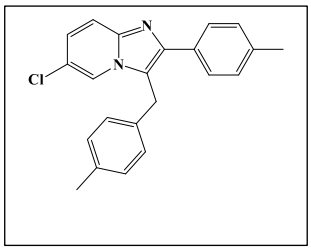

Product code 4p: Off white solid: mp 138-140 °C; 86% yield; ^{1}H NMR (400 MHz, $CDCl_3$) δ 7.75 (d, *J* = 2.0 Hz, 1H), 7.72 – 7.66 (m, 2H), 7.63 (d, *J* = 9.5 Hz, 1H), 7.26 (d, *J* = 7.9 Hz, 2H), 7.15 (dd, *J* = 7.8, 1.6 Hz, 3H), 7.04 (d, *J* = 7.9 Hz, 2H), 4.44 (s, 2H), 2.41 (s, 3H), 2.36 (s, 3H). ^{13}C NMR (101 MHz, $CDCl_3$) δ 145.19, 143.16, 137.82, 136.74, 133.10, 131.21, 129.86, 129.44, 128.00, 127.56, 125.32, 121.17, 120.28, 118.38, 117.79, 29.48, 21.29, 21.05. HRMS: m/z calcd for $C_{22}H_{19}ClN_2$ $(M+H)^+$ = 347.1310; found 347.1303.

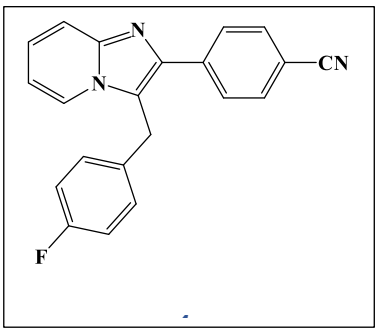

Product code 4q: white solid: mp 167-169 °C; 93% yield; ^{1}H NMR (400 MHz, $CDCl_3$) δ 7.97 – 7.92 (m, 2H), 7.90 (d, *J* = 9.1 Hz, 1H), 7.81 (dd, *J* = 6.9, 1.2 Hz, 1H), 7.78 – 7.74 (m, 2H), 7.41 (ddd, *J* = 9.0, 6.8, 1.2 Hz, 1H), 7.14 – 7.01 (m, 4H), 6.93 (td, *J* = 6.8, 1.1 Hz, 1H), 4.51 (s, 2H). ^{13}C NMR (101 MHz,

$CDCl_3$) δ 163.33, 160.87, 143.98, 139.77, 136.77, 132.71, 130.88, 130.84, 129.06, 128.98, 128.70, 127.12, 123.70, 119.15, 118.63, 117.08, 116.48, 116.26, 114.19, 112.03, 28.95. HRMS: m/z calcd for $C_{21}H_{14}N_3F$ $(M+H)^+$ = 328.1245; found 328.1201.

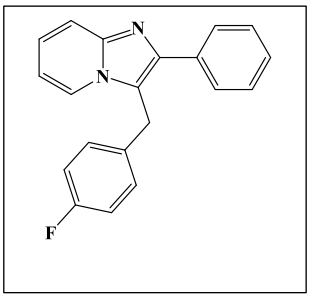

Product code 4r: Yellow semisolid; 82% yield; ^{1}H NMR (400 MHz, $CDCl_3$) δ 7.92 (d, *J* = 9.1 Hz, 1H), 7.87 – 7.71 (m, 3H), 7.52 – 7.32 (m, 4H), 7.12 (dd, *J* = 8.5, 5.3 Hz, 2H), 7.03 (t, *J* = 8.6 Hz, 2H), 6.88 (t, *J* = 6.8 Hz, 1H), 4.51 (s, 2H). ^{13}C NMR (101 MHz, $CDCl_3$) δ 163.21, 160.76, 143.50, 141.51, 131.87, 131.51, 131.47, 129.15, 129.07, 128.99, 128.71, 128.30, 126.56, 123.62, 117.88, 116.74, 116.26, 116.04, 113.82, 28.93. HRMS: m/z calcd for $C_{20}H_{15}N_2F$ $(M+H)^+$ = 303.1292; found 303.1245.

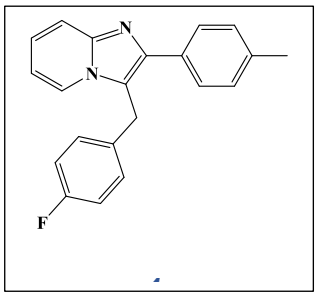

Product code 4s: Off white solid: mp 127-129 °C; 89% yield; ^{1}H NMR (400 MHz, $CDCl_3$) δ 8.06 (d, *J* = 9.0 Hz, 1H), 7.79 (d, *J* = 6.9 Hz, 1H), 7.72 (d, *J* = 8.1 Hz, 2H), 7.44 (t, *J* = 7.9 Hz, 1H), 7.31 (d, *J* = 7.9 Hz, 2H), 7.12 (dd, *J* = 8.6, 5.3 Hz, 2H), 7.08 – 7.01 (m, 2H), 6.95 (t, *J* = 6.8 Hz, 1H), 4.50 (s, 2H), 2.42 (s, 3H). ^{13}C NMR (101 MHz, $CDCl_3$) δ 163.30, 160.86, 142.48, 139.45, 130.99, 129.93, 129.14, 129.06, 128.26, 127.89, 123.74, 117.77, 116.40, 116.18, 116.11, 114.71, 28.82, 21.36. HRMS: m/z calcd for $C_{21}H_{17}N_2F$ $(M+H)^+$ = 317.1449; found 317.1431.

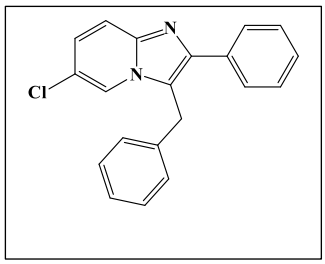

Product code 4t: Pale yellow solid: mp 190-193 °C; 78% yield; ^{1}H NMR (400 MHz, $CDCl_3$) δ 7.83 – 7.77 (m, 3H), 7.74 (dd, *J* = 9.6, 0.8 Hz, 1H), 7.50 – 7.43 (m, 2H), 7.43 – 7.30 (m, 4H), 7.22 (dd, *J* = 9.5, 2.0 Hz, 1H), 7.19 – 7.12 (m, 2H), 4.50 (s, 2H).^{13}C NMR (101 MHz, $CDCl_3$) δ 144.37, 142.79, 135.89, 133.26, 129.26, 128.82, 128.29, 128.19, 127.62,

127.25, 126.22, 121.29, 120.97, 118.50, 117.66, 29.79. HRMS: m/z calcd for $C_{20}H_{15}N_2F$ $(M+H)^+$ = 319.0997; found 319.0952.

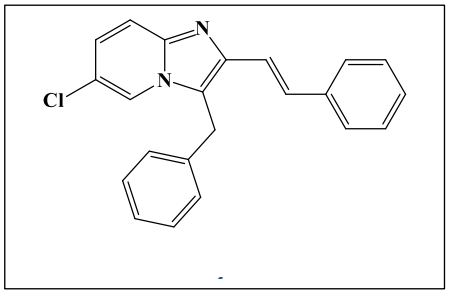

Product code 4u: Pale yellow solid: mp 219-222 °C; 89% yield; ^{1}H NMR (400 MHz, $CDCl_3$) δ 7.75 (dd, *J* = 2.0, 0.9 Hz, 1H), 7.71 (d, *J* = 15.9 Hz, 1H), 7.60 – 7.55 (m, 3H), 7.41 – 7.25 (m, 6H), 7.24 – 7.16 (m, 3H), 7.14 (dd, *J* = 9.5, 2.0 Hz, 1H), 4.40 (s, 2H). ^{13}C NMR (101 MHz, $CDCl_3$) δ 143.67, 142.54, 137.20, 136.00, 131.49, 129.11, 128.69, 127.95, 127.87, 127.21, 126.72, 126.04, 121.00, 120.39, 120.15, 117.83, 117.41, 29.05. HRMS: m/z calcd for $C_{22}H_{17}N_2Cl$ $(M+H)^+$ = 345.1153; found 345.1130.

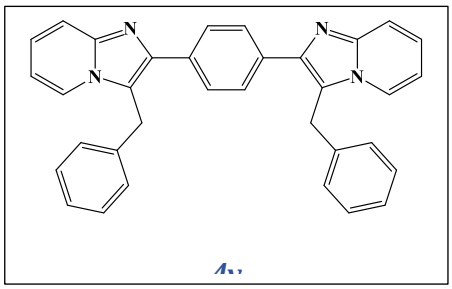

Product code 4v: Pale yellow solid: mp 230-235 °C; 53% yield; ^{1}H NMR (400 MHz, $CDCl_3$) δ 7.89 (s, 4H), 7.73 (t, *J* = 7.1 Hz, 4H), 7.32 (dd, *J* = 8.1, 6.3 Hz, 4H), 7.28 – 7.15 (m, 8H), 6.78 – 6.70 (m, 2H), 4.55 (s, 4H). ^{13}C NMR (101 MHz, $CDCl_3$) δ 145.01, 143.85, 136.76, 133.87, 129.05, 128.44, 127.75, 126.92, 124.20, 123.39, 117.94, 117.57, 112.21, 29.98. HRMS: m/z calcd for $C_{34}H_{26}N_4$ $(M+H)^+$ = 491.2230; found 491.2155.

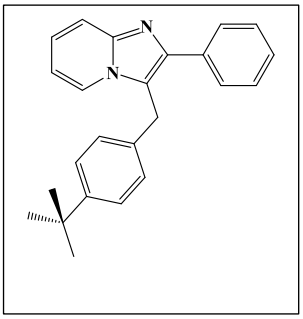

Product code 4w: Sticky orange liquid: mp 154-155 °C; 85% yield; ^{1}H NMR (400 MHz, $CDCl_3$) δ 7.93 – 7.77 (m, 4H), 7.51 – 7.27 (m, 7H), 7.15 – 7.06 (m, 2H), 6.83 (td, *J* = 6.8, 1.2 Hz, 1H), 4.49 (s, 2H), 1.33 (s, 9H). ^{13}C NMR (101 MHz, $CDCl_3$) δ 150.11, 143.79, 142.00, 132.96, 132.66, 129.91, 128.85, 128.33, 127.30, 126.08, 125.82, 123.78, 118.25, 116.84, 113.28, 34.49, 31.33, 29.23. HRMS: m/z calcd for $C_{24}H_{24}N_2$ $(M+H)^+$ = 341.2012; found 341.1965.

5.3 Results and discussion

Synthesis and structural details of *N*-(2-hydroxynapthylidene)-L-leucienyl-4,6-*O*-ethylidene-β-D-glucopyranosylamine (**6**) has already been discussed in chapter 3. The molecule was crystallized in ketoenamine tautomeric forms and dynamic equilibrium between phenolimine and ketoenamine tautomeric forms in solution state of **6** was also established.

5.3.1 Metal ion interaction studies using UV-visible and fluorescence spectroscopy

Compound **6** has been treated with acetates of Na(I), Sn(II), Mg(II), Ca(II), Cr(III), Mn(II), Fe(III), Co(II), Ni(II), Cu(II), Zn(II), Cd(II), Ag(I), Hg(II), Pb(II) and Al(III) in methanol and the interaction has been monitored using UV-visible absorption and fluorescence spectroscopy. Free ligand exhibited three major absorption peaks in near UV to the visible region (305, 403, and 421 nm), while excitation of the molecule at 290 nm yielded emission peaks at 317, 355, and 445 nm, analogous to the previous report on naphthalene derivatives.[25] Similar studies on a 1:1 mixture of **6** (20 μm) and metal acetates (20 μm) exhibited the spectral change in cases of Fe(III), Pb(II), Ni(II), Zn(II), Hg(II), Co(II), Al(III) and Cu(II) precursors (*Fig. 5.1*), supporting the interaction between them.

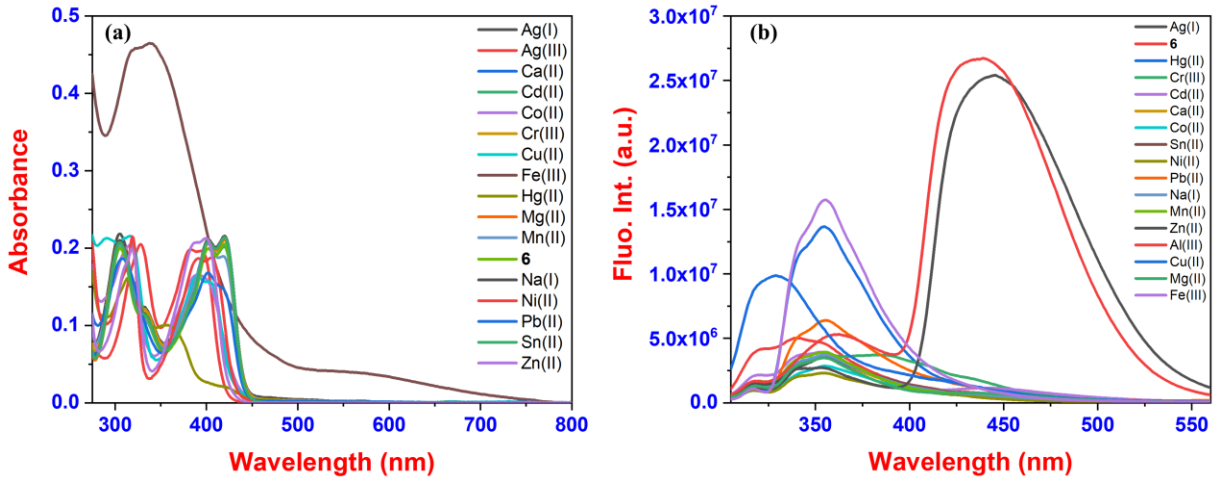

Fig. 5.1 *(a) Absorbance (b) emission spectra of* ***6*** *alone and in presence of various metal ions in MeOH medium*

In order to explore the solution stability of the complexes, absorption and emission spectra of all the above-mentioned systems were recorded at three different pHs (4.2, 9.2 and 7.2) (*Fig. 5.2-5.4*). Generally, the pH of the solution influences the hydrolysis rate of the metal complex and the surface charge of sorbents, which provides a narrow window of 1 to 2 pH units in which the rate of metal ion complexation increases unexpectedly.[26] We also noticed a similar phenomenon, as most of the metal ions exhibited pH-dependent interaction.

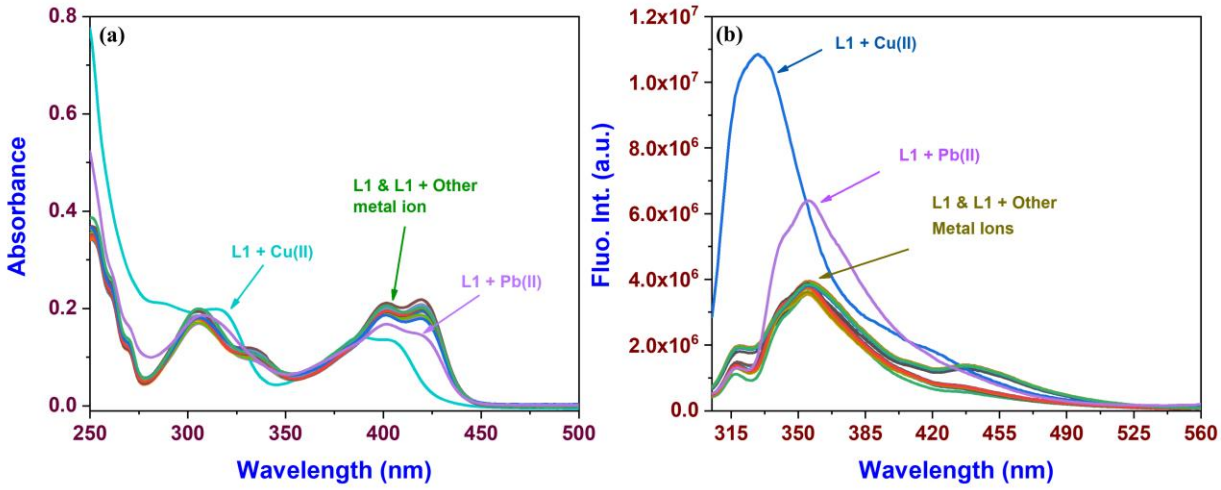

Fig. 5.2 *(a) Absorbance (b) emission spectra of* ***6*** *alone and in presence of various metal ions in buffered MeOH (pH = 4.2)*

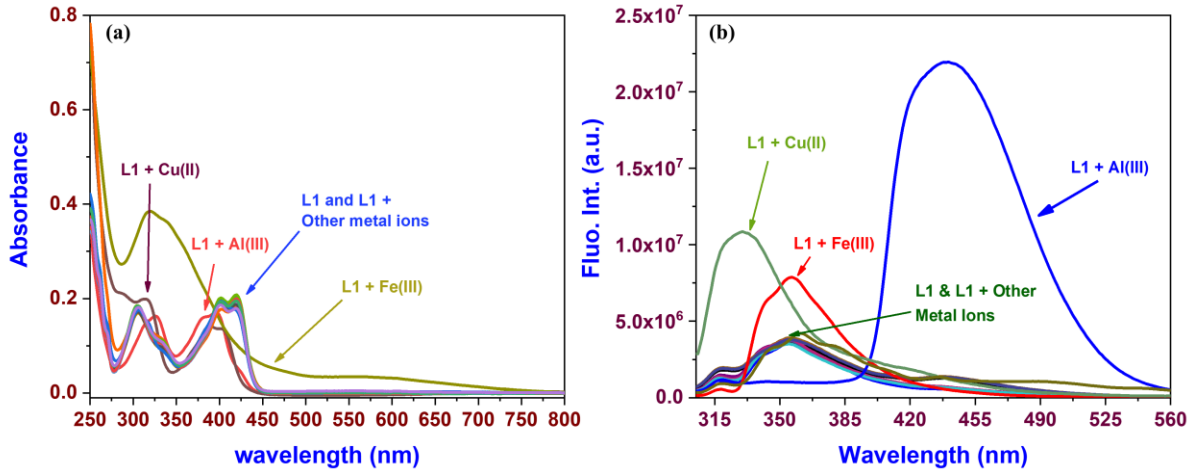

Fig. 5.3 *(a) Absorbance (b) emission spectra of* ***6*** *alone and in presence of various metal ions in buffered MeOH (pH = 7.2)*

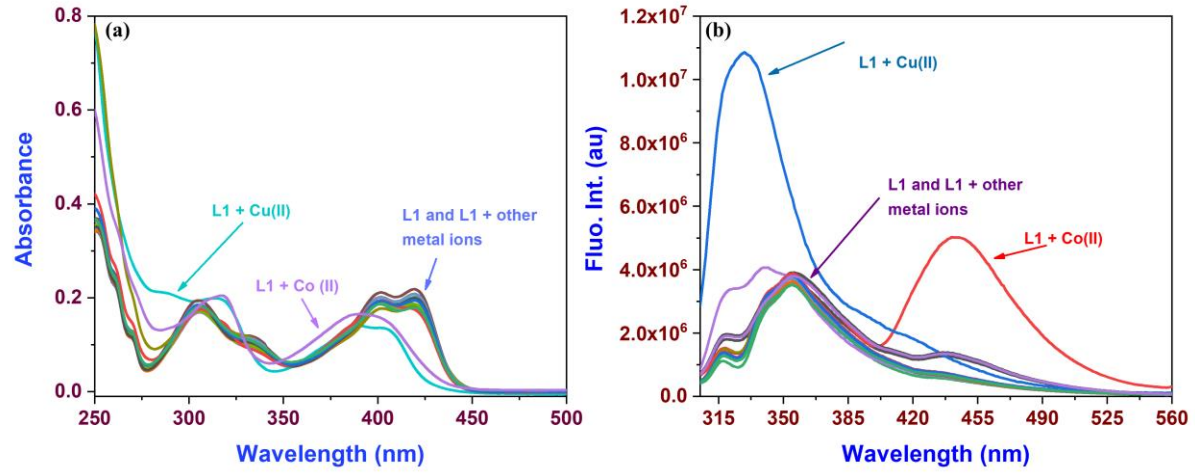

Fig. 5.4 *(a) Absorbance (b) emission spectra of* ***6*** *alone and in presence of various metal ions in buffered MeOH (pH = 9.2) medium*

The complexation with copper(II) ion was uniform at all three pH conditions (*Fig. 5.5*). The ligands absorption peak at 420 nm underwent a hypochromic shift, and a new peak appeared at 379 nm due to cupric ion interaction in the ground state. The emission spectrum of the complex solution afforded a highly intense peak at 329 nm, supporting the retention of metal ion interaction in the excited state. These studies also indicate a higher affinity for metal-ligand interaction than the hydration of metal ions.[27]

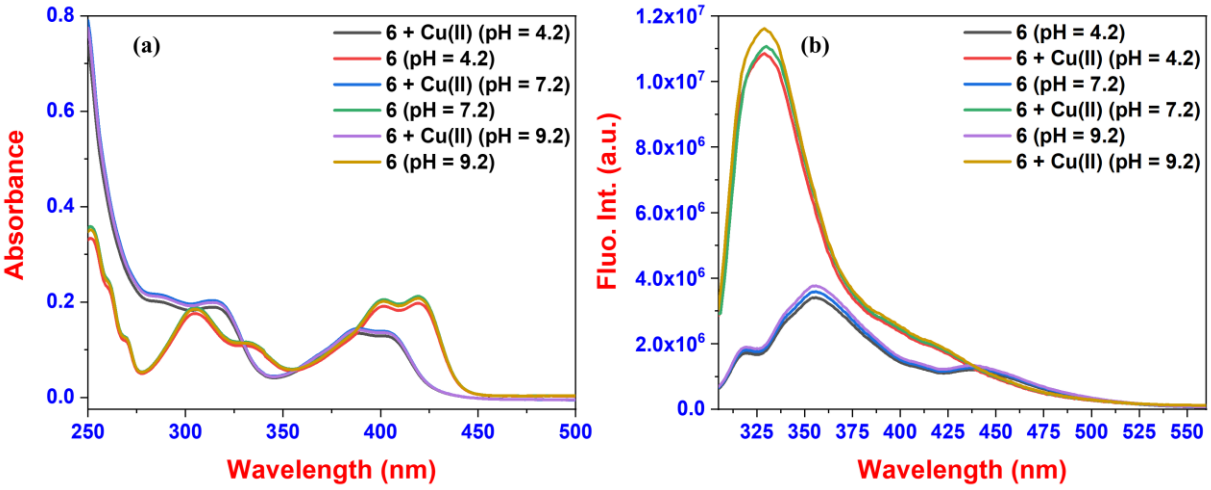

Fig. 5.5 *(a) Absorbance (b) emission spectra for interaction of* ***6*** *with Cu(II) at different pH*

To ascertain the stoichiometry and association constant, the methanolic solution of **6** was titrated with cupric acetate, which revealed a gradual decrement in absorption peak intensity at 421 nm of ligand and the appearance of a new peak at 379 nm (*Fig. 5.6a*). Appearance of the isosbestic point at 330 nm indicates the formation of unique components. The gradual increase in emission spectra at 329 nm in titration study (*Fig. 5.6b*) indicate the stability of copper complex in the excited state as well.

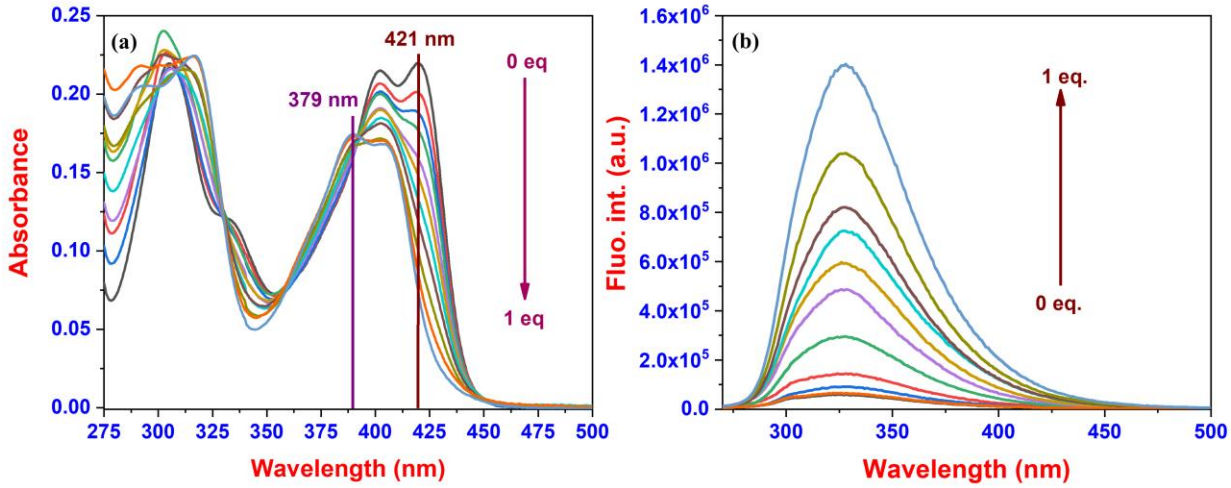

Fig. 5.6 *(a)Absorbance and (b) emission spectra for titration of* ***6*** *with cupric acetate solution*

Stoichiometry of complex formation has been calculated using modified Yoe-Jones method,[28] where the change in absorbance of **6** at 421 nm was plotted against cupric acetate to ligand molar ratio (*Fig. 5.7*). The interception points of tangents to the distal parts of curve yielded the interaction of cupric acetate with ligand in 1:1 ratio, and the same was supported by HRMS studies, where a set peak at m/z value 534.1381 corresponds to $[\mathbf{CuL}+H]^+$ (*Fig. 5.8*). The Association constant (K_a) has been calculated as 9.25×10^5 M^{-1} using the Yoe-Jones method.

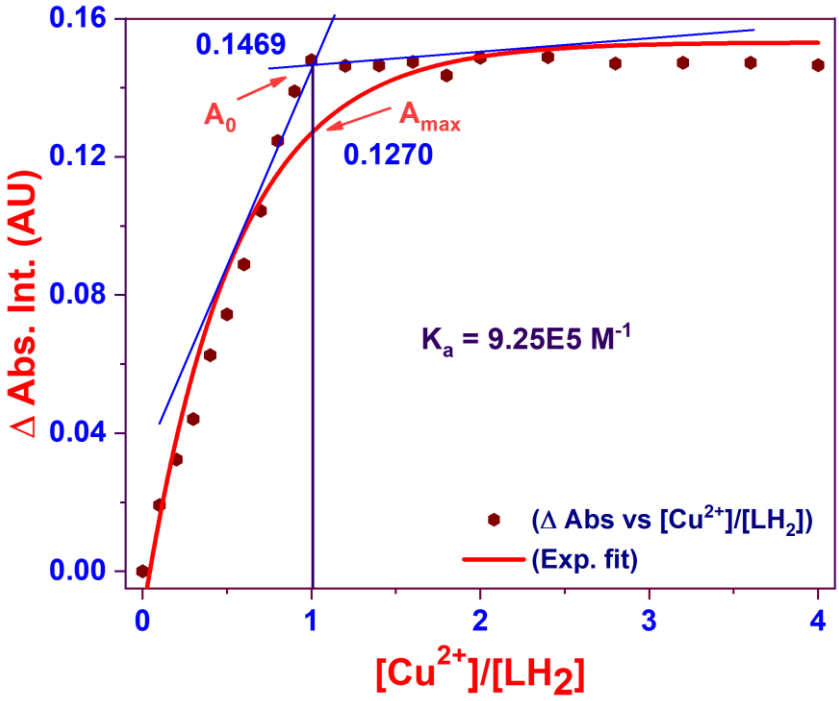

Fig. 5.7 *Exponential fit titration curve between $Cu(CH_3COO)_2$ and* ***6*** *at 420 nm (modified Yoe-Jones method)*

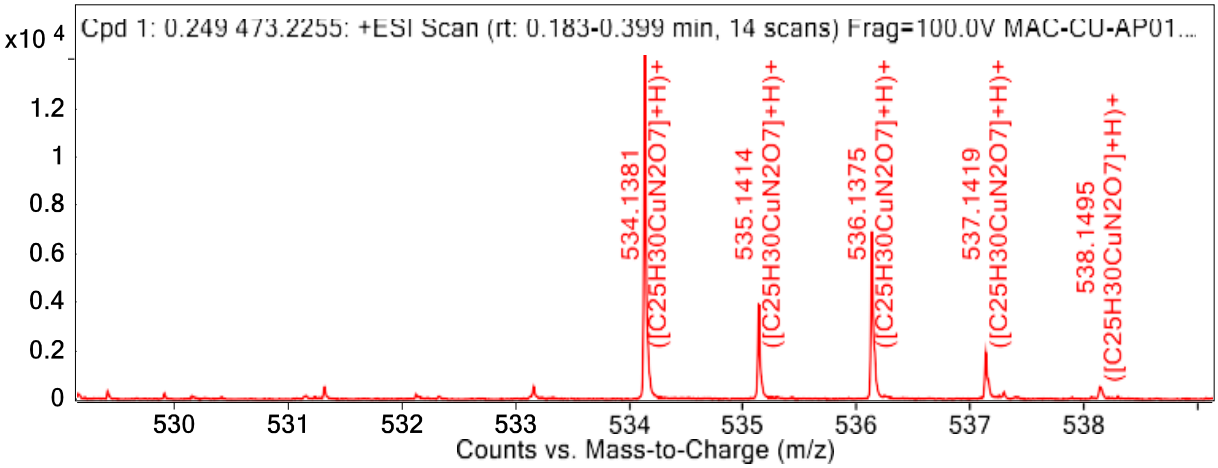

Fig. 5.8 *HRMS of* ***CuL***

5.3.2 Catalytic synthesis of substituted imidazo[1,2-*a*]pyridines

It has been observed that the catalyst may change its entity with the pH of the solution,[29-30] hence the pH immunity of the current copper complex encouraged us to explore its catalytic applications. Limited reactions using metal complexes of glycoconjugates as a catalyst are

available in literature due to the fragile nature of such molecules.[31] Copper complexes have been widely used as a catalyst for the synthesis of imidazo[1,2-*a*]pyridines,[8, 32] Homogeneous catalysis by copper salts is efficient and economical but requires 10-15% catalyst loading and its separation from the reaction mixture is tough.[8, 32] On the other hand, catalyst gets easily separated from the heterogeneous catalytic reactions, but the use of hazardous solvents like toluene becomes major concern.[8, 32] Inspired by these facts, we started exploring the application of our complex system as a catalyst in one-pot synthesis of imidazo[1,2-*a*]pyridine (*Scheme 5.2*).

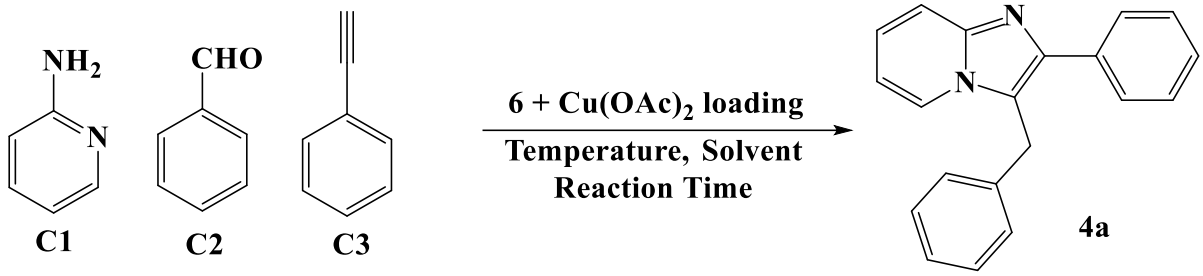

Scheme 5.2 *one-pot synthetic protocol of imidazo[1,2-a]pyridine*

In order to establish the optimum catalytic reaction condition, experiments were carried out for 6 hours using a 5 mol% catalyst; 2-aminopyridine, benzaldehyde, and phenylacetylene as model reactants. The control reactions were executed in ethanol, water, and neat condition at 80 °C, where the solvent-free condition afforded the best yield (*Table 5.1*). Two reports are available on solvent-free such reactions with 12 hours reaction time[33-34] and either high catalyst loading (5-10 mol%) or high temperature (120 °C). After finalizing the reaction media, reactions were repeated with 3.0, 2.0, 1.0, and 0.5 mol% catalyst loading at 80 °C (*Table 5.1*), and optimum yield was considered with 2.0 mol% catalyst because the efficiency is almost as good as that of 3 mol%. A few reports are available with comparable catalyst loading, but reactions require hazardous solvents,[35-36] higher temperature[34-37] and longer reaction time,[34, 36] while the present method provides maximum yield in 6 hours. Replacement of the catalytic system with 5 mol% of cupric acetate only, resulted in 10.7 and 17.9% yield after 24 and 48

hours, respectively. No product formation was noted in the absence of a catalytic system or the presence of **6** (5 mol%; no copper source).

Table 5.1 *Optimization of reaction conditions for* ***CuL****-catalyzed imidazo[1,2-a]pyridine synthesis*

Entry	Catalyst (mol %)	Solvent	Yield (%)[a]	Time (h)	Temp. (^{o}C)
1	**CuL** (5.0)	Ethanol	74.6	6	80
2	**CuL** (5.0)	Water	55.3	6	80
3	**CuL** (5.0)	Neat	95.4	6	80
4	**CuL** (3.0)	Neat	95.7	6	80
5	**CuL** (2.0)	Neat	93.2	6	80
6	**CuL** (1.0)	Neat	82.6	6	80
7	**CuL** (0.5)	Neat	63.2	6	80
8	**CuL** (2.0)	Neat	2.6	0.5	80
9	**CuL** (2.0)	Neat	13	1	80
10	**CuL** (2.0)	Neat	29.3	2	80
11	**CuL** (2.0)	Neat	53.7	3	80
12	**CuL** (2.0)	Neat	76.7	4	80
13	**CuL** (2.0)	Neat	87.4	5	80
14	**CuL** (2.0)	Neat	95.5	8	80
15	**CuL** (2.0)	Neat	15.8	24	RT
16	**CuL** (2.0)	Neat	35.8	48	RT
17	**CuL** (2.0)	Neat	53.8	6	50
18	**CuL** (2.0)	Neat	89.7	15	50
19	**CuL** (2.0)	Neat	79.4	6	70
20	**CuL** (2.0)	Neat	91.3	12	70
21	**6** (2.0)	Neat	-	24	80
22	$Cu(CH_3COO)_2$	Neat	10.7	24	80
23	$Cu(CH_3COO)_2$	Neat	17.9	48	80
24	No Catalyst	Neat	-	24	80

[a] represents the HPLC yield

C1 - 100 mmol, C2 - 100 mmol, C3 - 110 mmol

Under the optimized reaction conditions, twenty-three imidazo[1,2-*a*]pyridine derivatives were synthesized in good to excellent yields (53-93%), including six new molecules (*Table 5.2*). All the molecules were characterized using HRMS and NMR spectroscopy, while molecular structures of **4t** and **4u** have been established via single-crystal X-ray diffraction studies (CCDC no. 2120461 and 2120463, respectively). Both the molecules have monoclinic crystal system and their structures are presented in *Fig. 5.9*, and the summary of crystallographic data is shown in *Table 5.3*.

Table 5.2 *Substrate scope of aldehyde, 2-aminopyridines, and terminal alkynes*

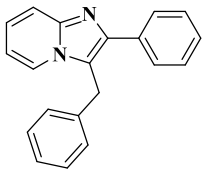

4a, 93% yield

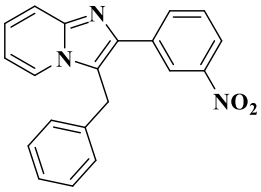

4b, 90% yield

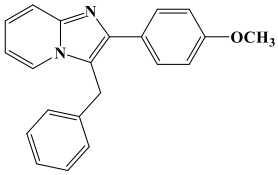

4c, 89% yield

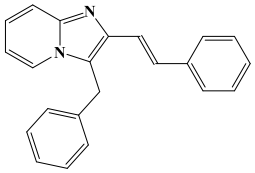

4d, 84% yield

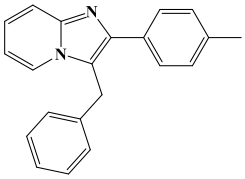

4e, 83% yield

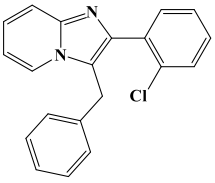

4f, 83% yield

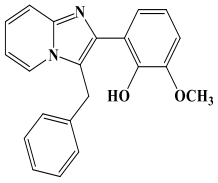

4g, 81% yield

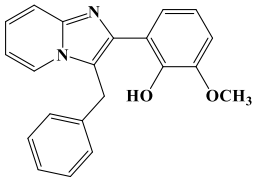

4h, 88% yield

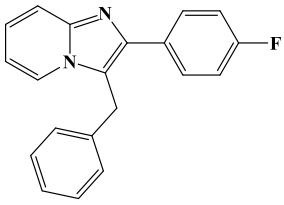

4i, 88% yield

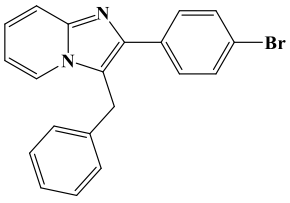

4j, 81% yield

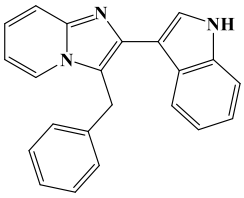

4k, 71% yield

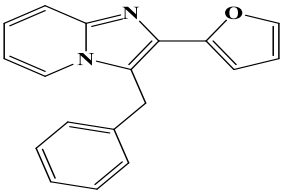

4l, 89% yield

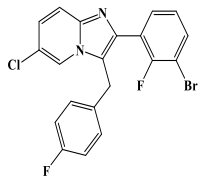

4m, 78% yield

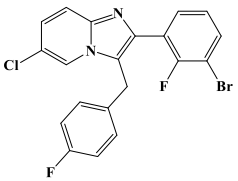

4n, 77% yield

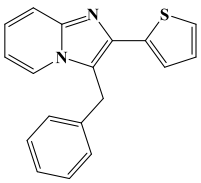

4o, 75% yield

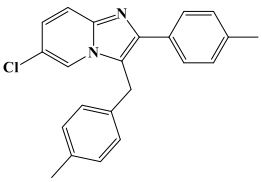

4p, 86% yield

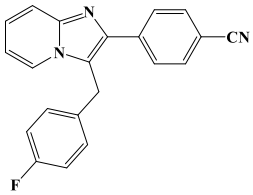

4q, 93% yield

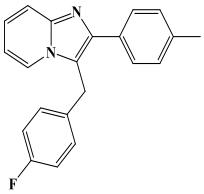

4r, 82% yield

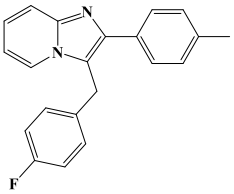

4s, 89% yield

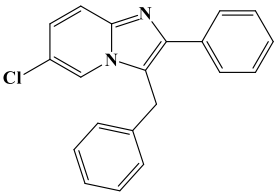

4t, 78% yield

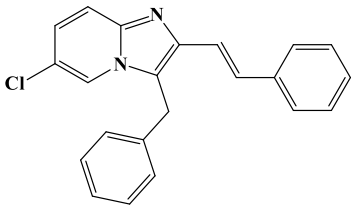

4u, 89% yield

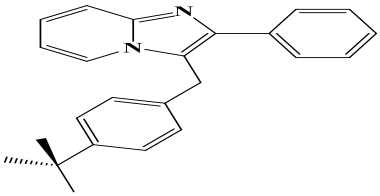

4v, 53% yield

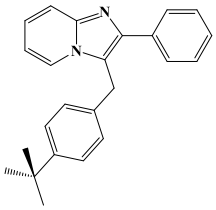

4w, 85% yield

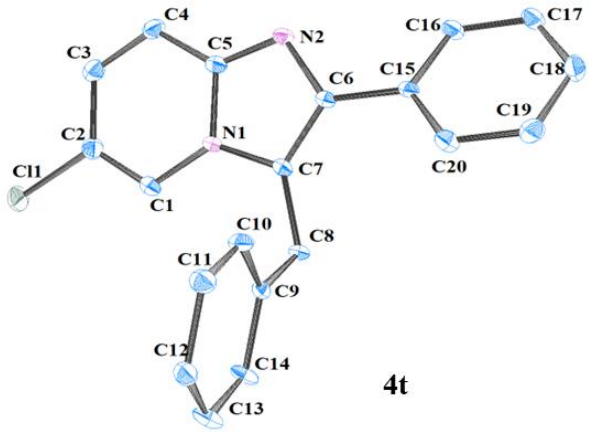

4t

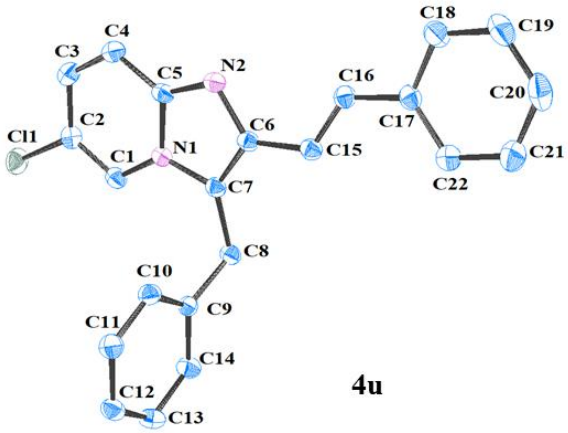

4u

Fig. 5.9 *ORTEP diagrams of* ***4t*** *and* ***4u*** *with thermal ellipsoids drawn at a 50% probability level*

Table 5.3 Crystal data and structure refinement for **4u** and **4t**

Identification code	**4u**	**4t**
Empirical formula	$C_{22}H_{17}ClN_2$	$C_{20}H_{15}ClN_2$
Formula weight	344.82	318.79
Temperature/K	93(2)	93(2)
Crystal system	monoclinic	monoclinic
Space group	$P2_1/n$	$P2_1/c$
a/Å	6.16360(10)	6.42400(10)
b/Å	8.07990(10)	7.9525(2)
c/Å	35.2337(4)	31.2364(7)
β/°	91.2950(10)	93.929(2)

Volume/Å^3	1754.23(4)	1592.02(6)
Z	4	4
ρ_{calc}g/cm^3	1.306	1.330
μ/mm^{-1}	1.955	2.109
F(000)	720.0	664.0
Radiation	Cu Kα (λ = 1.54184)	Cu Kα (λ = 1.54184)
2Θ range for data collection/°	10.044 to 159.586	11.358 to 159.956
Index ranges	-7 ≤ h ≤ 5, -9 ≤ k ≤ 9, -44 ≤ l ≤ 44	-8 ≤ h ≤ 6, -9 ≤ k ≤ 7, -39 ≤ l ≤ 31
Reflections collected	9462	8292
Independent reflections	3679 [R_{int} = 0.0261, R_{sigma} = 0.0317]	3343 [R_{int} = 0.0849, R_{sigma} = 0.0821]
Data/restraints/parameters	3679/0/226	3343/0/208
Goodness-of-fit on F^2	1.064	1.070
Final R indexes [I>=2σ (I)]	R_1 = 0.0390, wR_2 = 0.1058	R_1 = 0.0956, wR_2 = 0.2389
Final R indexes [all data]	R_1 = 0.0404, wR_2 = 0.1069	R_1 = 0.0990, wR_2 = 0.2464
Largest diff. peak/hole / e Å^{-3}	0.25/-0.45	0.62/-1.47

More than dozens of reports are available on mechanistic aspects of one-pot synthesis of imidazo[1,2-*a*]pyridines, where most researchers proposed the formation of Schiff base initially, followed by the reaction with alkynes.[24, 36, 38-41] Only one report is available by Ghosh et al., which deals with two mechanistic pathways for this reaction (*Scheme 5.3*). They used $NaHSO_4.SiO_2$, along with CuI, as catalyst and found the formation of product at a faster rate through prior imine in comparison to the propargyl alcohol formation route.[38] We reacted benzaldehyde and 2-aminopyridine in the presence and absence of **CuL** and noticed the time-independent formation of the Schiff base. The addition of alkyne in the reaction mixture affords the product formation, where the catalyst system was present but not in the other one, supporting the necessity of the catalyst and its utilization in the formation of propargylamine intermediate (7, Scheme 3). A similar reaction setup using benzaldehyde and phenylacetylene did not indicate the formation of propargyl alcohol even after 10 h; however, the addition of 2-

aminopyridine afforded the product formation in the catalyst-containing reaction mixture, supporting the reaction passage through imine formation.

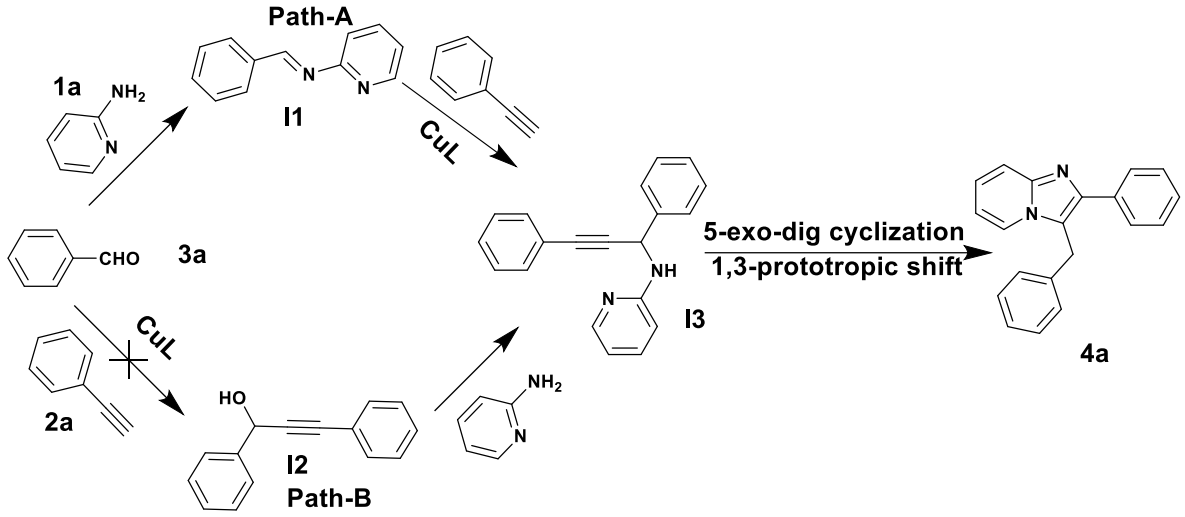

Scheme 5.3 *Multistep reactions to study the reaction mechanism for* ***CuL*** *catalyzed one-pot synthesis of imidazo[1,2-a]pyridine*

The time dependency of imidazo[1,2-*a*]pyridine formation has been explored using 2-aminopyridine, benzaldehyde, and phenylacetylene at 80 °C in the presence of **CuL** (2 mol%). The results have been summarized in *Fig. 5.10*, which reveals slow initiation followed by fast propagation with more than 90% yield within 6 h. The slow initiation time may be attributed to the formation of imine in the beginning, which is independent of the catalyst **CuL**. The boundaries of catalytic efficiency have been explored by varying the substrate-to-catalyst ratio, and the results are summarized in *Table 5.4*. Maximum turnover frequency has been noted as 21.9 using 0.25 mol% of catalyst which is quite comparable with one another report.[42]

The recyclability of the catalyst has been tested using benzaldehyde, 2-aminopyridine, and phenylacetylene as reactants under the optimized reaction condition. After completion of the first cycle, a hexane-ethyl acetate mixture (9:1, v/v) was added to the reaction mixture to solubilize the contents except for the catalyst. The catalyst was filtered and recharged with

fresh reactants for subsequent cycles. During the recycling process, a gradual decrease in product yield was noticed (*Fig. 5.11*), which might be due to the loss of catalyst during the filtration process. The integrity of the catalyst has also been tested at the end of the fifth cycle using HRMS studies, where a set of peaks at an m/z value of 534.1382 (*Fig. 5.12*) supports its stability.

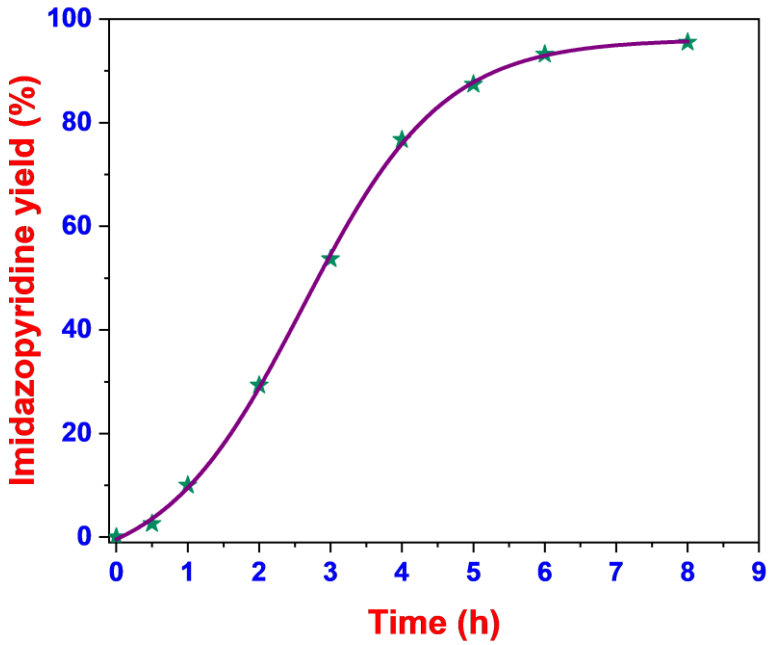

Fig. 5.10 *Formation of imidazo[1,2-a]pyridine concerning time in the presence of* ***CuL*** *as a catalyst*

Table 5.4 *TOF calculation by variation of the substrate-to-catalyst ratio*

Entry	Subs (mmol)	Cat (mmol)	Yield (%)[a]	Time (h)	TOF (h^{-1})
1	1	0.0025	27.3	6	18.2
2	1	0.0025	65.8	12	21.9
3	1	0.005	63.2	6	21.0
4	1	0.005	85.7	12	14.2
5	1	0.01	82.6	6	13.7
6	1	0.02	93.2	6	7.7
7	1	0.03	95.7	6	5.3

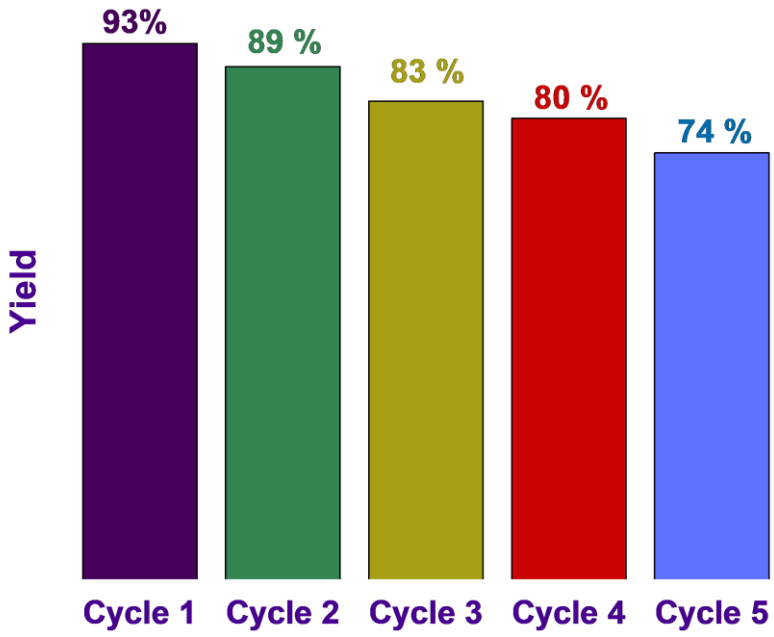

Fig. 5.11 *Recyclability result of* ***CuL*** *catalyzed synthesis of imidazo[1,2-a]pyridine*

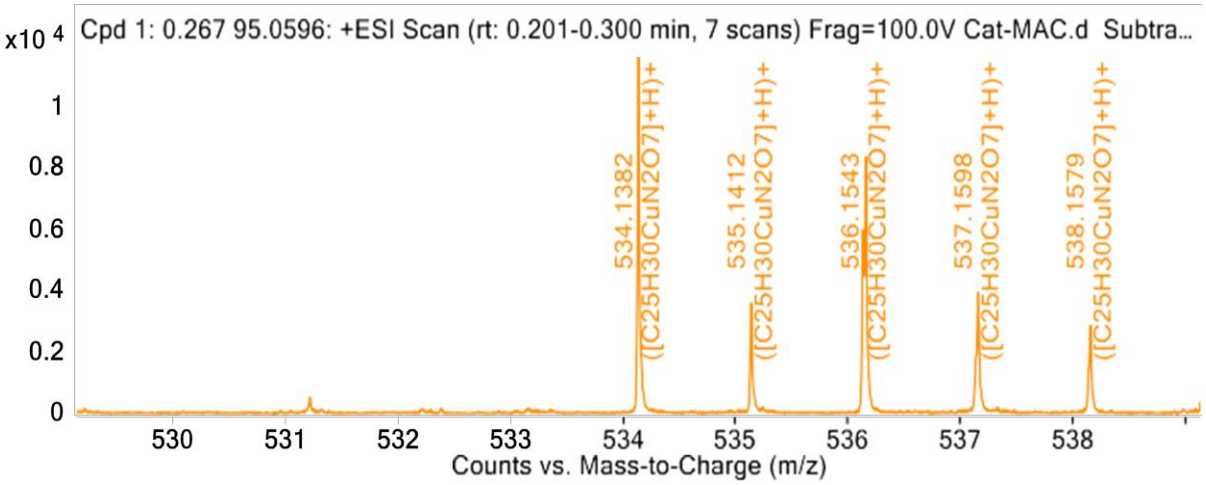

Fig. 5.12 *HRMS of recovered catalyst after fifth cycle*

A comparison of our findings with other reports on the copper complex catalyzed synthesis of imidazo[1,2-*a*]pyridines has been summarized in *Table 5.5*. Generally, researchers have used a mixture of Cu(I)/Cu(II) salts or Cu(II) slat with reducing agents like D-glucose as catalyzing system.[43-47] During the synthesis, 15 mol% of copper salt along with 30 mol% of D-glucose have been used by others,[44-45] while we have utilized 2 mol% of the catalyst system.

Effectively, our catalyst provides advantages in terms of low catalyst loading, shorter reaction time, solvent-free process, and ease of catalyst separation for reusability.

Table 5.5 *Comparison of different copper catalysed imidazo[1,2-a]pyridine synthesis*

Entry	Catalyst (mol %)	Time	Solvent	Temp.	Yield (%)	Reference
1	$Cu(OTf)_2$ (5 mol%)+ CuCl (5 mol%)	16 h	Toluene	120°C	92	24
2	CuI (5 mol%)+ $NaHSO4{\cdot}SiO2(N2)$	12h	Toluene	Reflux	91	38
3	$CuO\text{-}CuAl_2O_4$ (15 mol%)+ D-Glucose (30 mol%)	18 h	Toluene	Reflux	88	44
4	CuI (10 mol%)+ $Cu(OTf)_2$ (10 mol%)	16 h	DMSO	110°C	85	43
5	$CuSO_4{\cdot}H_2O$ (15 mol%)+ D-Glucose (30 mol%)	10 h	EtOH	Reflux	79	45
6	CuL^a (10 mol%)	30 h	Toluene	120°C	97	46
7	L^a-CuCl (5 mol%)+ L^a- $Cu(OTf)_2$ (5 mol%)	16 h	Toluene	120°C	93	47
8	Copper oxide Nanoparticle (1 mol%)	12 h	Neat	120°C	85	34
9	Ionic liquid tagged Cu(II) (5) +,metallic copper(10)	12 h	Neat	80°C	90	33
10	Copper nanoparticle (0.95)	4 h	TBAB-glycerol (1:9)	110°C	93	35
11	Copper nanoparticle (2.8)	6 h	DMSO	110°C	91	37
12	**CuL** (2 mol%)	6h	Neat	80°C	93	This report

L^a represents the ligand used in the respective reference

5.4 Conclusions

N-(2-Hydroxynapthylidene)-L-leucienyl-4,6-*O*-ethylidene-β-D-glucopyranosylamine has been synthesized, and its metal ion binding abilities have been explored at three pH (4.2, 9.2 and 7.1) conditions. Cupric acetate interacted with the glycoconjugate at all three pH conditions, and hence, this system has been used as a catalyst for the synthesis of imidazo[1,2-*a*]pyridines. After several controlled reactions, the optimized reaction conditions have been finalized as 2 mol% catalyst loading under the neat condition at 80 °C, and twenty-three derivatives have been synthesized in good to excellent yields (53–93%). All the molecules have been

characterized using NMR and HRMS studies, while the molecular structure of the glycoconjugate and two of the imidazo[1,2-*a*]pyridine derivatives have been established using single-crystal X-ray diffraction studies. The reusability of the catalyst has been achieved up to five cycles with marginal loss in efficiency due to the handling errors of catalyst separation.

References

1. Herzner, H.; Reipen, T.; Schultz, M.; Kunz, H., Synthesis of glycopeptides containing carbohydrate and peptide recognition motifs. *Chemical Reviews* **2000,** *100*, 4495-4538.

2. Matsushita, T.; Handa, S.; Naruchi, K.; Garcia-Martin, F.; Hinou, H.; Nishimura, S.-I., A novel approach for the parallel synthesis of glycopeptides by combining solid-phase peptide synthesis and dendrimer-supported enzymatic modifications. *Polymer Journal* **2013,** *45*, 854-862.

3. Kunz, H., Synthesis of glycopeptides, partial structures of biological recognition components [New synthetic methods (67)]. *Angewandte Chemie International Edition in English* **1987,** *26*, 294-308.

4. Hilvert, D., Design of protein catalysts. *Annual Review of Biochemistry* **2013,** *82*, 447-470.

5. Schmid, A.; Dordick, J.; Hauer, B.; Kiener, A.; Wubbolts, M.; Witholt, B., Industrial biocatalysis today and tomorrow. *Nature* **2001,** *409*, 258-268.

6. Schoemaker, H. E.; Mink, D.; Wubbolts, M. G., Dispelling the myths-biocatalysis in industrial synthesis. *Science* **2003,** *299*, 1694-1697.

7. Sah, A. K.; Soni, K., Synthesis of cupric acetate selective receptor derived from alanyl glycoconjugate and their application in selective oxidation of benzylic alcohols. *Catalysis Communications* **2012,** *28*, 120-123.

8. Bagdi, A. K.; Santra, S.; Monir, K.; Hajra, A., Synthesis of imidazo [1, 2-*a*] pyridines: a decade update. *Chemical Communications* **2015,** *51*, 1555-1575.

9. Trapani, G.; Franco, M.; Ricciardi, L.; Latrofa, A.; Genchi, G.; Sanna, E.; Tuveri, F.; Cagetti, E.; Biggio, G.; Liso, G., Synthesis and binding affinity of 2-phenylimidazo [1, 2-*a*] pyridine derivatives for both central and peripheral benzodiazepine receptors. A new series of high-affinity and selective ligands for the peripheral type. *Journal of Medicinal Chemistry* **1997,** *40*, 3109-3118.

10. Douhal, A.; Amat-Guerri, F.; Acuna, A. U., Photoinduced intramolecular proton transfer and charge redistribution in imidazopyridines. *The Journal of Physical Chemistry* **1995,** *99*, 76-80.

11. Douhal, A.; Amat-Guerri, F.; Acuña, A. U., Probing Nanocavities with Proton-Transfer Fluorescence. *Angewandte Chemie International Edition in English* **1997,** *36*, 1514-1516.

12. Douhal, A., The involvement of rotational processes in the intramolecular proton-transfer cycle. *Berichte der Bunsengesellschaft für physikalische Chemie* **1998,** *102*, 448-451.

13. Cao, H.; Liu, X.; Liao, J.; Huang, J.; Qiu, H.; Chen, Q.; Chen, Y., Transition Metal-Mediated C-O and C-C Bond-Forming Reactions: A Regioselective Strategy for the Synthesis of Imidazo [1, 2-*a*] pyridines and Imidazo [1, 2-*a*] pyrazines. *The Journal of Organic Chemistry* **2014,** *79*, 11209-11214.

14. Zhan, H.; Zhao, L.; Liao, J.; Li, N.; Chen, Q.; Qiu, S.; Cao, H., Gold-Catalyzed Synthesis of 3-Acylimidazo [1, 2-*a*] pyridines via Carbene Oxidation. *Advanced Synthesis & Catalysis* **2015,** *357*, 46-50.

15. Denora, N.; Laquintana, V.; Pisu, M. G.; Dore, R.; Murru, L.; Latrofa, A.; Trapani, G.; Sanna, E., 2-Phenyl-imidazo [1, 2-*a*] pyridine compounds containing hydrophilic groups as potent and selective ligands for peripheral benzodiazepine receptors: synthesis, binding affinity and electrophysiological studies. *Journal of Medicinal Chemistry* **2008,** *51*, 6876-6888.

16. Katritzky, A. R.; Xu, Y.-J.; Tu, H., Regiospecific synthesis of 3-substituted imidazo [1, 2-*a*] pyridines, imidazo [1, 2-*a*] pyrimidines, and imidazo [1, 2-*c*] pyrimidine. *The Journal of Organic Chemistry* **2003,** *68*, 4935-4937.

17. Gueiffier, A.; Lhassani, M.; Elhakmaoui, A.; Snoeck, R.; Andrei, G.; Chavignon, O.; Teulade, J.-C.; Kerbal, A.; Essassi, E. M.; Debouzy, J.-C., Synthesis of acyclo-C-nucleosides in the imidazo [1, 2-*a*] pyridine and pyrimidine series as antiviral agents. *Journal of Medicinal Chemistry* **1996,** *39*, 2856-2859.

18. Hubert, A. J.; Reimlinger, H., Thermolyse von ν-Triazoly-Derivaten. *Chemische Berichte* **1970,** *103*, 3811-3816.

19. Monir, K.; Kumar Bagdi, A.; Mishra, S.; Majee, A.; Hajra, A., Copper(II)-Catalyzed Aerobic Oxidative Coupling between Chalcone and 2-Aminopyridine via C-H Amination: An Expedient Synthesis of 3-Aroylimidazo [1, 2-*a*] pyridines. *Advanced Synthesis & Catalysis* **2014,** *356*, 1105-1112.

20. Kaswan, P.; Pericherla, K.; Kumar, A., Synthesis of 3-aroylimidazo [1, 2-*a*] pyridines via CuCl2 catalyzed tandem dual carbon–nitrogen bonding. *Tetrahedron* **2014,** *70*, 8539-8544.

21. Lyon, M. A.; Kercher, T. S., Glyoxylic acid and MP-glyoxylate: efficient formaldehyde equivalents in the 3-CC of 2-aminoazines, aldehydes, and isonitriles. *Organic Letters* **2004,** *6*, 4989-4992.

22. Zhang, Y.; Chen, Z.; Wu, W.; Zhang, Y.; Su, W., CuI-catalyzed aerobic oxidative α-aminaton cyclization of ketones to access aryl or alkenyl-substituted imidazoheterocycles. *The Journal of Organic Chemistry* **2013,** *78*, 12494-12504.

23. Snieckus, V.; Hurst, T., A Tandem Amination–Cycloisomerization Approach to Imidazo [1, 2-*a*] pyridines. *Synfacts* **2012,** *8*, 0134-0134.

24. Chernyak, N.; Gevorgyan, V., General and Efficient Copper-Catalyzed Three-Component Coupling Reaction towards Imidazoheterocycles: One-Pot Synthesis of Alpidem and Zolpidem. *Angewandte Chemie* **2010,** *122*, 2803-2806.

25. Mishra, S. K.; Madduluri, V. K.; Rangan, K.; Sah, A. K., *N*-Glycoconjugates: Selective colorimetric chemosensors for aspartic acid and cysteine. *Journal of Molecular Structure* **2021,** *1241*, 130644.

26. Joly, N.; Ghemati, D.; Aliouche, D.; Martin, P., Interaction of metal ions with mono- and polysaccharides for wastewater treatment: A review. *Natural Products Chemistry & Research* **2020,** *8*, 373.

27. Mishra, S. K.; Dehuri, S.; Bag, B., Effect of n-alkyl substitution on Cu(ii)-selective chemosensing of rhodamine B derivatives. *Organic & Biomolecular Chemistry* **2020,** *18*, 316-332.

28. Knez, D.; Sosič, I.; Mitrović, A.; Pišlar, A.; Kos, J.; Gobec, S., 8-Hydroxyquinoline-based anti-Alzheimer multimodal agents. *Monatshefte für Chemie-Chemical Monthly* **2020,** *151*, 1111-1120.

29. Tang, S.; Sun, J.; Li, Y.; Xia, D.; Qi, T.; Liu, K.; Deng, H.; Shen, W.; Lee, H. K., pH-dependent selective ion exchange based on (ethylenediamintetraacetic acid-nickel)-layered double hydroxide to catalyze the polymerization of aniline for detection of Cu^{2+} and Fe^{3+}. *Talanta* **2018,** *187*, 287-294.

30. Chang, C. A.; Twu, J.; Bartsch, R. A., pH-Dependent metal ion selectivity by a crown ether carboxylic acid. *Inorganic Chemistry* **1986,** *25*, 396-398.

31. Madduluri, V. K.; Sah, A. K., Metal complexes of 4,6-*O*-ethylidene-β-D-glucopyranosylamine derivatives and their application in organic synthesis. *Carbohydrate Research* **2019,** *485*, 107798.

32. Panda, J.; Raiguru, B. P.; Mishra, M.; Mohapatra, S.; Nayak, S., Recent advances in the synthesis of imidazo [1, 2-*a*] pyridines: A brief review. *ChemistrySelect* **2022,** *7*, e202103987.

33. Ghosh, S.; Kundu, D.; Dey, A.; Majee, A.; Hajra, A., Functionalized ionic liquid tagged Cu (II) catalyst: Design, characterization, and application in synthesis of imidazo [1, 2-*a*] pyridine. *Journal of the Indian Chemical Society* **2020,** *97*, 2533-2539.

34. Zong, C.; Zeng, R.; Zou, J., One-pot copper nanoparticle-catalyzed synthesis of imidazo [1, 2-*a*] pyridines under solvent-free conditions. *Chemical Research in Chinese Universities* **2014,** *30*, 632-638.

35. Salamatmanesh, A.; Heydari, A., Magnetic nanostructure-anchored mixed-donor ligand system based on carboxamide and *N*-heterocyclic thiones: An efficient support of CuI catalyst for synthesis of imidazo [1, 2-*a*] pyridines in eutectic medium. *Applied Catalysis A: General* **2021,** *624*, 118306.

36. Salles, H. D. d.; Silva, T. L. d.; Radatz, C. S.; Affeldt, R. F.; Benvenutti, E. V.; Schneider, P. H., Imidazo [1, 2-a] pyridine A^3-Coupling Catalyzed by a Cu/SiO_2 Material. *Journal of the Brazilian Chemical Society* **2019,** *30*, 1825-1833.

37. Hussain, N.; Gogoi, P.; Das, M. R.; Sengupta, P.; Fedorov, V. E.; Asanov, I. P.; Kozlova, M. N.; Artemkina, S. B., Development of novel efficient 2D nanocomposite catalyst towards the three-component coupling reaction for the synthesis of imidazo [1, 2-*a*] pyridines. *Applied Catalysis A: General* **2017,** *542*, 368-379.

38. Mishra, S.; Ghosh, R., Mechanistic studies on a new catalyst system (CuI-$NaHSO_4$× SiO_2) leading to the one-pot synthesis of imidazo [1, 2-*a*] pyridines from reactions of 2-aminopyridines, aldehydes, and terminal alkynes. *Synthesis* **2011,** *2011*, 3463-3470.

39. Purohit, G.; Kharkwal, A.; Rawat, D. S., CuIn-ethylxanthate, a "Versatile Precursor" for Photosensitization of Graphene-Quantum Dots and Nanocatalyzed Synthesis of

Imidazopyridines with Ideal Green Chemistry Metrics. *ACS Sustainable Chemistry & Engineering* **2020,** *8*, 5544-5557.

40. Geedkar, D.; Kumar, A.; Kumar, K.; Sharma, P., Hydromagnesite sheets impregnated with cobalt–ferrite magnetic nanoparticles as heterogeneous catalytic system for the synthesis of imidazo [1, 2-*a*] pyridine scaffolds. *RSC Advances* **2021,** *11*, 23207-23220.

41. Hamidi Dastjerdi, F.; Ghorbani-Vaghei, R.; Alavinia, S., Copper Iodide Nanoparticles Immobolized Porous Polysulfonamide: An Effective Nanocatalyst for Synthesis of Imidazo [1, 2-*a*] Pyridines. *Catalysis Letters* **2020,** *150*, 3514-3522.

42. Tajbakhsh, M.; Farhang, M.; Hosseinzadeh, R.; Sarrafi, Y., Nano Fe_3O_4 supported biimidazole Cu(i) complex as a retrievable catalyst for the synthesis of imidazo [1, 2-*a*] pyridines in aqueous medium. *RSC Advances* **2014,** *4*, 23116-23124.

43. Palani, T.; Park, K.; Kumar, M. R.; Jung, H. M.; Lee, S., Copper-Catalyzed Decarboxylative Three-Component Reactions for the Synthesis of Imidazo [1, 2-*a*] pyridines. *European Journal of Organic Chemistry* **2012,** *2012*, 5038-5047.

44. Balijapalli, U.; Iyer, S. K., CuO–$CuAl_2O_4$ and D-glucose catalyzed synthesis of a family of excited state intramolecular proton transfer imidazo [1, 2-*a*] pyridine analogues and their optical properties. *Dyes and Pigments* **2015,** *121*, 88-98.

45. Guchhait, S. K.; Chandgude, A. L.; Priyadarshani, G., $CuSO_4$–glucose for in situ generation of controlled Cu(I)–Cu(II) bicatalysts: multicomponent reaction of heterocyclic azine and aldehyde with alkyne, and cycloisomerization toward synthesis of *N*-fused Imidazoles. *The Journal of Organic Chemistry* **2012,** *77*, 4438-4444.

46. Luz, I.; i Xamena, F. L.; Corma, A., Bridging homogeneous and heterogeneous catalysis with MOFs: Cu-MOFs as solid catalysts for three-component coupling and cyclization reactions for the synthesis of propargylamines, indoles and imidazopyridines. *Journal of Catalysis* **2012,** *285*, 285-291.

47. Liao, Y.; Huang, B.; Huang, X.; Cai, M., Heterogeneous Copper-Catalyzed Cascade Three-Component Reaction Towards Imidazo [1, 2-*a*] pyridines: Efficient and Practical One-Pot Synthesis of Alpidem. *ChemistrySelect* **2019,** *4*, 2320-2326.

Chapter 6

Glycoconjugate-derived Dinuclear Copper(II) Complex Catalyzed Solvent-free A^3 Coupling Reactions for Stereoselective Synthesis of Trisubstituted Propargylamines

Chapter 6

6.1 Introduction

Propargylamines are important precursors for the synthesis of natural products and organic compounds, which are important from pharmaceutical point of view.[1-2] Many propargylamine-derived drugs like Pargyline,[3] Rasagyline,[4] Selegiline[5] etc., are used in treating the neurodegeneration problems such as Alzheimer's and Parkinson's diseases. Bioactive molecules like (indol-2-yl)methanamines are synthesized using chiral propargylamines as an intermediate.[6] Several protocols for enantioselective synthesis of propargylamines from primary amines have been developed, predominantly catalyzed by pybox-based ligands and copper salts.[7-11] Traditionally, the most elegant approach includes chiral metal complexes as homogeneous catalysts in the enantioselective synthesis of propargylamines.[12] Use of secondary instead of primary amines, dramatically changes the mechanism of the reaction as it follows the formation of an iminium ion intermediate, which in turn changes the mode of asymmetric catalysis.[13] Due to this additional obstacle, only a handful of articles are available on Cu(I) catalyzed enantioselective A^3 reactions of secondary amines.[2, 13-23] These procedures require harsh reaction conditions, hazardous catalysts and harmful solvents like toluene, dimethyl chloride etc., which is a major concern from the environmental point of view.[23] Although few Cu(II) catalyzed greener protocols have also been developed in recent years, they lack enantioselectivity.[24-27]

The copper(II) complexes of D-glucose derived ligands have great importance in biological and bioinorganic fields due to their non-toxic nature.[28] Presence of the multiple chiral centers in the carbohydrate-based ligands drive its metal complexes towards the asymmetric synthesis.[29-30] We are exploring the catalytic activity of metal complexes containing 4,6-*O*-ethylidene-β-D-glucopyranosylamine derived ligands.[28,31] Herein, we have developed an amphiphilic ligand using D-glucose and its copper(II) complex to tune the solubility of

compounds in less polar solvents. The molecular structure of the complex has been established using single-crystal X-ray diffraction study, which reveals a one-dimensional hydrogen-bonded network in the lattice. This complex has been used in the catalytic synthesis of asymmetric trisubstituted propargylamines using cyclic amines under solvent-free condition.

6.2 Experimental

6.2.1 Synthesis of 4,6-*O*-ethylidene-*N*-(2-hydroxy-4-(octyloxy)benzylidene)-β-D-glucopyranosylamine (ALH_2):

2-Hydroxy-4-(octyloxy)benzaldehyde was condensed with 4,6-*O*-ethylidene-β-D-glucopyranosylamine in methanol at 80 °C for 6 hours. The reaction mixture was cooled to 0 °C, and the resultant yellow solid product was filtered, washed with cold hexane and dried.

Product code ALH_2: Yield, 88% (0.184 g); Yellow solid; mp, 109-111 °C; FTIR (KBr matrix, cm^{-1}): 2854-2924 (ν_{C-H}), 1620 ($\nu_{C=N}$), 1573 ($\nu_{C=C}$), ^{1}H-NMR (400 MHz, DMSO-d_6) δ; 13.36 (s, 1H), 8.47 (s, 1H), 7.39 (d, J = 8.6 Hz, 1H), 6.47 (dd, J = 8.6, 2.4 Hz, 1H), 6.40 (d, J = 2.4 Hz, 1H), 5.52 (d, J = 5.8 Hz, 1H), 5.36 (d, J = 5.5 Hz, 1H), 4.75 (q, J = 5.0 Hz, 1H), 4.48 (d, J = 8.3 Hz, 1H), 4.05 (dd, J = 10.0, 4.8 Hz, 1H), 3.98 (t, J = 6.5 Hz, 2H), 3.62 – 3.25 (m, 6H), 3.10 (td, J = 8.5, 5.7 Hz, 1H), 1.78 – 1.62 (m, 2H), 1.40 (d, J = 8.6 Hz, 2H), 1.27 (t, J = 8.2 Hz, 9H), 0.95 – 0.83 (m, 3H). ^{13}C-NMR (101 MHz, DMSO-d_6) δ; 165.27, 163.79, 163.30, 134.26, 112.36, 107.16, 101.68, 99.06, 95.78, 80.59, 75.26, 73.74, 68.35, 68.18, 67.77, 31.70, 29.17, 29.12, 28.98, 25.92, 22.55, 20.80, 14.43.

6.2.2 Synthesis of copper(II) complex (CuAL)

To the stirring solution of **ALH_2** (0.438 g, 1 mmol) in methanol, copper(II) acetate (0.218 g, 1.1 mmol) was added at room temperature. The reaction mixture was stirred for 2 hours and resultant solid product was filtered, washed with ethanol and dried under vacuum.

Product code CuAL: Yield, 93% (0.521 g); greenish-blue (cyan colored) solid; mp, 185-190 °C; FTIR (KBr matrix, cm^{-1}): 2854-2924 (ν_{C-H}), 1604 ($\nu_{C=N}$), 1527 ($\nu_{C=C}$), 1087-1141 (ν_{C-O}), 678 and 624 (ν_{Cu-O}): Elemental analysis (weight %): CHN calculated for $[Cu(C_{23}H_{33}NO_7)(CH_3OH)_2]_2$, C(53.32), H(7.34), N(2.49), found C(53.73), H(6.93), N(2.23); solid state UV–visible peaks: 300 ($\pi \rightarrow \pi^*$) and 361 ($\pi \rightarrow \pi^*$) nm.[33]

6.2.3 General procedure for the synthesis of propargylamines

Secondary amine (1.1 mmol), aromatic aldehyde (1 mmol) and phenylacetylene derivative (1.1 mmol) were stirred at 80 °C in the presence of **CuAL** (2 mol% as per empirical formula) under neat conditions and the progress of reaction was monitored by thin layer chromatography (TLC). The reaction mixture was diluted with methanol (3–5 mL) on completion and filtered to isolate the solid catalyst. The filtrate was dried, and the product was purified using column chromatography in a hexane-ethylacetate mixture (v/v = 9:1).

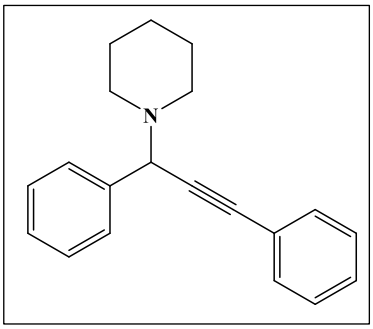

Product code P1: 91% Yield (0.25 g), 98% ee; Brown solid; mp, 65-67 °C;^{1}H-NMR (400 MHz, $CDCl_3$) δ; 7.71 – 7.64 (m, 2H), 7.58 – 7.53 (m, 2H), 7.43 – 7.30 (m, 6H), 4.83 (s, 1H), 2.60 (t, *J* = 5.4 Hz, 4H), 1.69 – 1.57 (m, 4H), 1.48 (p, *J* = 6.1 Hz, 2H). ^{13}C-NMR (101 MHz, $CDCl_3$) δ 138.69, 131.83, 128.53, 128.29, 128.07, 128.05, 127.44, 123.40, 87.85, 86.14, 62.42, 50.74, 26.24, 24.48. HRMS (ESI) m/z calcd for $[M+H]^+$ requires 276.1747, found 276.1753 HPLC (acetonitrile/water) = 25:75, flow rate = 0.35 mL/min, λ = 300 nm minor isomer: t_R = 62.1 min, major isomer: t_R = 71.9 min.

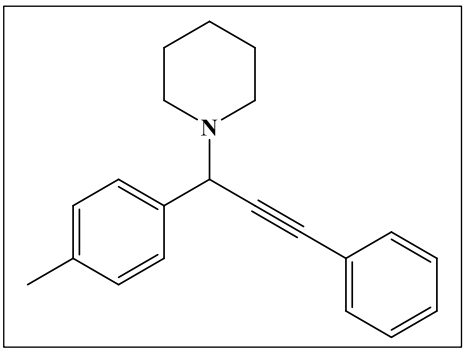

Product code P2: 93% Yield (0.26 g), 96% ee; Brown solid; mp, 58-60 °C ^{1}H-NMR (400 MHz, $CDCl_3$) δ; 7.58 – 7.51 (m, 4H), 7.35 (dd, *J* = 5.0, 2.0 Hz, 3H), 7.23 – 7.17 (m, 2H), 4.78 (s, 1H), 2.58 (d, *J* = 5.5 Hz, 4H), 2.39 (s, 3H), 1.62 (h, *J* = 5.7 Hz, 4H), 1.52 – 1.43 (m, 2H). ^{13}C-NMR (101 MHz, $CDCl_3$) δ 137.08, 135.65, 131.82, 128.76, 128.47, 128.26, 127.99, 123.47, 87.60, 86.44, 62.16, 50.70, 26.23, 24.50, 21.13. HRMS (ESI) m/z calcd for $[M+H]^+$ requires 290.1903, found 290.1913. HPLC (acetonitrile/water) = 25:75, flow rate = 0.2 mL/min, λ = 295 nm minor isomer: t_R = 100.8 min, major isomer: t_R = 110.5 min.

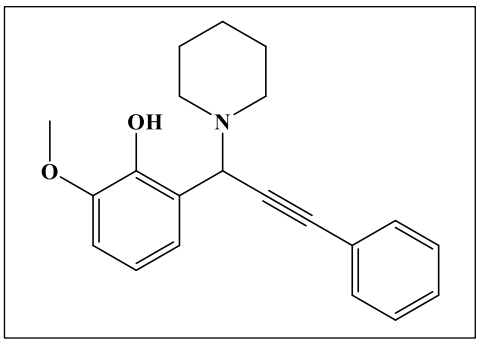

Product code P3: 95% Yield (0.30 g), 97% ee; off white solid; mp, 129-131 °C ^{1}H-NMR (400 MHz, $CDCl_3$) δ; 7.57 (dtd, *J* = 5.5, 4.7, 3.2 Hz, 2H), 7.39 (tt, *J* = 3.9, 2.6 Hz, 3H), 7.21 (ddd, *J* = 7.7, 1.6, 1.0 Hz, 1H), 6.90 (dd, *J* = 8.2, 1.6 Hz, 1H), 6.83 (t, *J* = 7.9 Hz, 1H), 5.13 (s, 1H), 3.92 (s, 3H), 2.76 (s, 4H), 1.75 – 1.66 (m, 4H), 1.53 (s, 2H). ^{13}C-NMR (101 MHz, $CDCl_3$) δ 148.07, 147.19, 131.89, 128.55, 128.40, 122.65, 121.57, 120.43, 118.34, 111.74, 89.58, 82.44, 61.06, 56.03, 25.97, 24.01. HRMS (ESI) m/z calcd for $[M+H]^+$ requires 322.1802, found 322.1819 HPLC (acetonitrile/water) = 1:1, flow rate = 0.3 mL/min, λ = 272 nm major isomer: t_R = 38.7 min, minor isomer: t_R = 48.8 min.

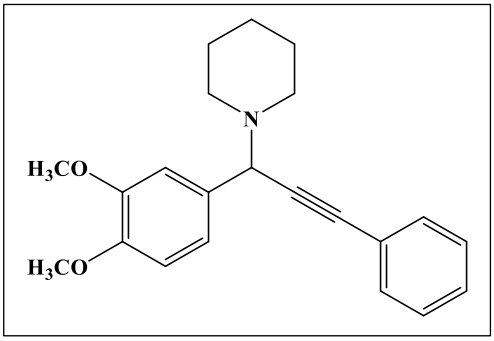

Product code P4: 95% Yield (0.31 g), 90% ee; brown oil ^{1}H-NMR (400 MHz, $CDCl_3$) δ; 7.57 – 7.50 (m, 2H), 7.38 – 7.31 (m, 3H), 7.25 – 7.19 (m, 2H), 6.87 (d, *J* = 8.0 Hz, 1H), 4.76 (s, 1H), 3.94 (s, 3H), 3.91 (s, 3H), 2.60 (tq, *J* = 13.6, 4.5 Hz, 4H), 1.62 (tdd, *J* = 13.2,

6.8, 3.6 Hz, 4H), 1.51 – 1.44 (m, 2H). ^{13}C-NMR (101 MHz, $CDCl_3$) δ 148.75, 148.43, 131.78, 131.33, 128.30, 128.05, 123.39, 120.70, 111.69, 110.58, 87.72, 86.37, 62.08, 55.93, 55.92, 50.72, 26.22, 24.50. HRMS (ESI) m/z calcd for $[M+H]^+$ requires 336.1958, found 336.1967 HPLC (acetonitrile/water) = 1:1, flow rate = 0.35 mL/min, λ = 290 nm major isomer: t_R = 27.1 min, minor isomer: t_R = 30.6 min.

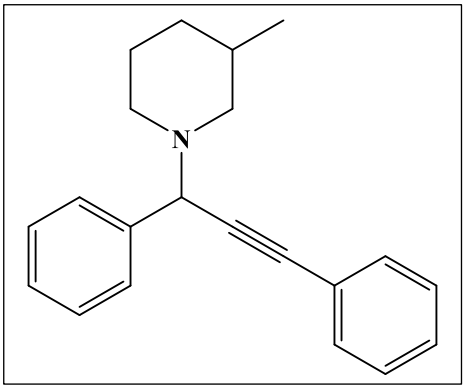

Product code P5: 88% Yield (0.25 g), 98% ee; brown oil; ^{1}H-NMR (400 MHz, $CDCl_3$) δ; 7.66 (ddt, *J* = 7.7, 2.3, 1.2 Hz, 2H), 7.59 – 7.50 (m, 2H), 7.43 – 7.29 (m, 6H), 4.85 (s, 1H), 2.98 – 2.86 (m, 1H), 2.69 – 2.57 (m, 1H), 2.24 – 2.06 (m, 1H), 1.90 – 1.44 (m, 5H), 0.99 – 0.80 (m, 4H). ^{13}C-NMR (101 MHz, Chloroform-*d*) δ 138.72, 138.66, 131.84, 128.51, 128.48, 128.28, 128.08, 128.05, 127.43, 123.39, 87.90, 87.85, 86.07, 86.02, 62.18, 62.12, 60.52, 55.61, 52.63, 47.75, 33.07, 31.61, 31.18, 25.87, 25.49, 19.78, 19.74. HRMS: m/z calcd for $C_{21}H_{23}N$ $(M+H)^+$ 290.1903; found 290.1915. HPLC (acetonitrile/methanol) = 1:1, flow rate = 0.35 mL/min, λ = 290 nm major isomer: t_R = 29.48 and 37.56 min, minor isomer: t_R = 33.04 and 41.15 min.

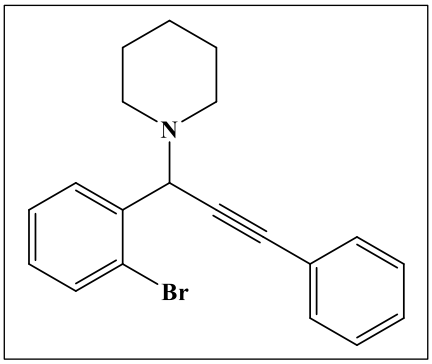

Product code P6: 93% Yield (0.33 g), 95% ee; orange oil; ^{1}H-NMR (400 MHz, $CDCl_3$) δ; 7.78 (dd, *J* = 7.7, 1.7 Hz, 1H), 7.61 (dd, *J* = 7.9, 1.3 Hz, 1H), 7.56 – 7.50 (m, 2H), 7.38 – 7.31 (m, 4H), 7.22 – 7.15 (m, 1H), 5.07 (s, 1H), 2.63 (t, *J* = 5.4 Hz, 4H), 1.58 (tq, *J* = 12.7, 6.0 Hz, 4H), 1.47 (q, *J* = 5.7 Hz, 2H). ^{13}C-NMR (101 MHz, $CDCl_3$) δ 138.10, 133.18, 131.81, 130.68, 129.02, 128.30, 128.15, 126.79, 125.30, 123.20, 88.00, 85.72, 61.71, 50.67, 26.17, 24.51. HRMS (ESI)

m/z calcd for $[M+H]^+$ requires 354.0852, found 354.0863 HPLC (acetonitrile/water) = 1:1, flow rate = 0.35 mL/min, λ = 290 nm minor isomer: t_R = 38.4 min, major isomer: t_R = 42.5 min

Product code P7: 91% Yield (0.28 g), 95% ee; orange oil; ^{1}H-NMR (400 MHz, $CDCl_3$) δ; 7.66 – 7.57 (m, 2H), 7.57 – 7.51 (m, 2H), 7.41 – 7.32 (m, 5H), 4.78 (s, 1H), 2.56 (t, J = 5.4 Hz, 4H), 1.67 – 1.55 (m, 4H), 1.48 (q, J = 5.9 Hz, 2H). ^{13}C-NMR (101 MHz, $CDCl_3$) δ 137.37, 133.18, 131.82, 129.81, 128.33, 128.25, 128.20, 123.12, 88.24, 85.41, 61.75, 50.66, 26.19, 24.40. HRMS (ESI) m/z calcd for $[M+H]^+$ requires 310.1357, found 310.1365. HPLC (acetonitrile/water) = 1:1, flow rate = 0.3 mL/min, λ = 290 nm minor isomer: t_R = 48.4 min, major isomer: t_R = 54.4 min

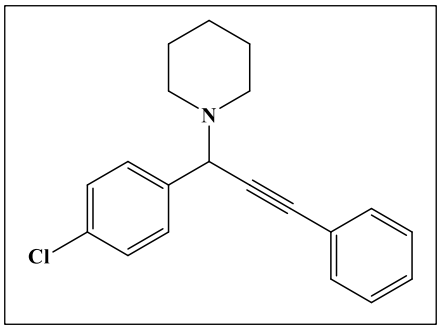

Product code P8: 84% Yield (0.27 g), 94% ee; off white solid, mp, 65-67 °C ;^{1}H-NMR (400 MHz, $CDCl_3$) δ; 8.57 (t, J = 2.2 Hz, 1H), 8.18 (ddt, J = 8.1, 2.1, 0.9 Hz, 1H), 8.04 (ddt, J = 7.7, 1.8, 1.0 Hz, 1H), 7.60 – 7.53 (m, 3H), 7.42 – 7.34 (m, 3H), 4.90 (s, 1H), 2.57 (qd, J = 11.1, 5.0 Hz, 4H), 1.64 (dtt, J = 15.2, 9.3, 3.8 Hz, 4H), 1.49 (p, J = 6.0 Hz, 2H). ^{13}C-NMR (101 MHz, $CDCl_3$) δ 148.35, 141.41, 134.47, 131.90, 128.98, 128.48, 128.41, 123.41, 122.74, 122.61, 89.14, 84.17, 61.72, 50.73, 26.13, 24.29. HRMS (ESI) m/z calcd for $[M+H]^+$ requires 321.1598, found 321.1608 HPLC (acetonitrile/water) = 1:1, flow rate = 0.5 mL/min, λ = 290 nm minor isomer: t_R = 48.9 min, major isomer: t_R = 51.0 min

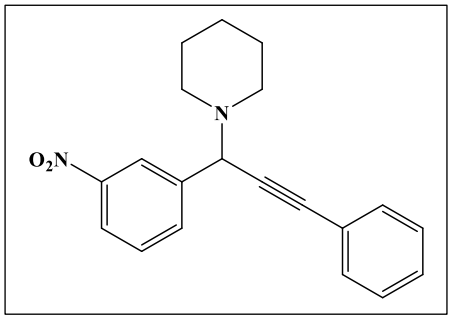

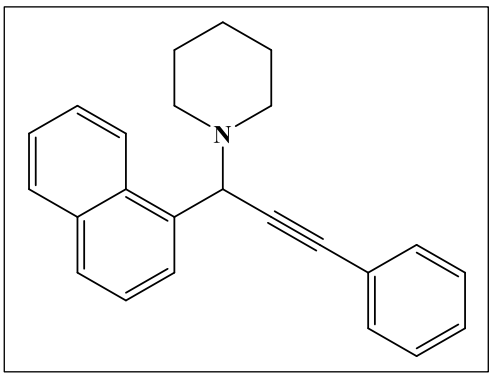

Product code P9: 94% Yield (0.30 g), 93% ee; off white solid, mp, 109-111 °C ^{1}H-NMR (400 MHz, $CDCl_3$) δ; 8.45 (dd, J = 8.5, 1.3 Hz, 1H), 7.97 (dt, J = 7.1, 1.0 Hz, 1H), 7.90 (dd, J = 7.8, 1.7 Hz, 1H), 7.85 (d, J = 8.2 Hz, 1H), 7.63 – 7.46 (m, 5H), 7.43 – 7.32 (m, 3H), 5.47 (s, 1H), 2.82 – 2.56 (m, 4H), 1.66 – 1.45 (m, 6H). ^{13}C-NMR (101 MHz, $CDCl_3$) δ 134.29, 134.05, 131.96, 131.85, 128.55, 128.40, 128.33, 128.06, 126.87, 125.75, 125.56, 125.06, 124.79, 123.49, 88.55, 85.95, 60.52, 50.72, 26.31, 24.63. HRMS (ESI) m/z calcd for $[M+H]^+$ requires 326.1903, found 326.1915. HPLC (acetonitrile/water) = 75:25, flow rate = 0.3 mL/min, λ = 290 nm minor isomer: t_R = 68.0 min, major isomer: t_R = 74.2 min

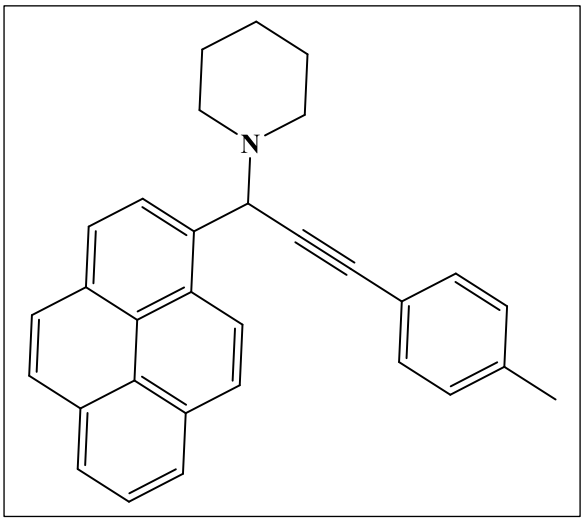

Product code P10: 95% Yield (0.39 g), 87% ee; pale yellow solid, mp, 135-137 °C ^{1}H-NMR (400 MHz, $CDCl_3$) δ; 8.66 (d, J = 9.3 Hz, 1H), 8.53 – 8.48 (m, 1H), 8.26 – 8.15 (m, 4H), 8.09 (s, 2H), 8.03 (t, J = 7.6 Hz, 1H), 7.52 (dd, J = 8.1, 1.3 Hz, 2H), 7.20 (d, J = 7.9 Hz, 2H), 5.72 (s, 1H), 2.85 – 2.64 (m, 4H), 2.41 (s, 3H), 1.65 – 1.57 (m, 3H), 1.48 (dd, J = 10.5, 4.8 Hz, 3H). ^{13}C-NMR (101 MHz, $CDCl_3$) δ 138.17, 132.32, 131.76, 131.31, 131.08, 130.87, 129.51, 129.09, 127.47, 127.33, 127.12, 127.09, 125.86, 125.21, 125.12, 125.06, 124.78, 124.40, 124.02, 120.39, 88.81, 85.53, 60.68, 50.88, 26.32, 24.62, 21.51. HRMS (ESI) m/z calcd for $[M+H]^+$ requires 414.2216, found 414.2222. HPLC (acetonitrile/water) = 75:25, flow rate = 0.25 mL/min, λ = 290 nm minor isomer: t_R = 100.2 min, major isomer: t_R = 110.9 min

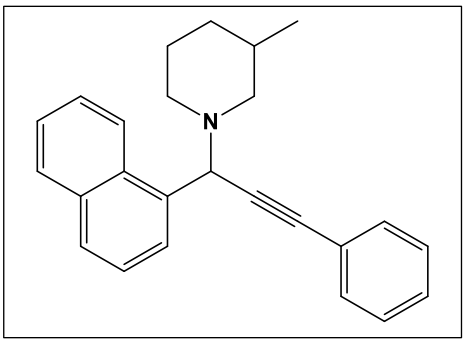

Product code P11: 89% Yield (0.30 g), 90% ee; brown oil,^{1}H-NMR (400 MHz, $CDCl_3$) δ; 8.46 (dt, *J* = 8.7, 1.2 Hz, 1H), 8.00 (ddt, *J* = 7.1, 3.1, 1.0 Hz, 1H), 7.95 – 7.83 (m, 2H), 7.65 – 7.47 (m, 5H), 7.45 – 7.35 (m, 3H), 5.51 (s, 1H), 3.12 – 3.00 (m, 1H), 2.63 (td, *J* = 9.7, 6.0 Hz, 1H), 2.38 – 2.24 (m, 1H), 2.03 (t, *J* = 10.4 Hz, 1H), 1.90 – 1.63 (m, 3H), 1.61 – 1.43 (m, 1H), 1.41 – 1.29 (m, 1H), 1.02 – 0.80 (m, 4H). ^{13}C-NMR (101 MHz, $CDCl_3$) δ 134.35, 134.29, 134.07, 132.00, 131.97, 131.89, 128.56, 128.41, 128.34, 128.07, 126.93, 126.83, 125.74, 125.58, 125.57, 125.11, 124.84, 124.80, 123.51, 88.65, 88.63, 85.85, 61.01, 60.36, 60.32, 55.26, 52.92, 47.25, 33.23, 33.09, 31.73, 31.02, 25.85, 25.47, 19.79, 19.65. HRMS (ESI) m/z calcd for $[M+H]^+$ requires 340.2060, found 340.2065. HPLC (acetonitrile/methanol) = 1:1, flow rate = 0.35 mL/min, λ = 290 nm major isomer: t_R = 34.40 and 43.19 min, minor isomer: t_R = 38.48 and 47.34 min.

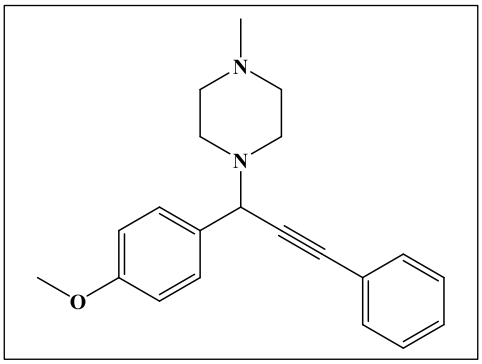

Product code P12: 94% Yield (0.3 g), 99% ee; brown oil, ^{1}H-NMR (400 MHz, $CDCl_3$) δ; 7.60 – 7.45 (m, 4H), 7.36 – 7.28 (m, 3H), 6.96 – 6.87 (m, 2H), 4.79 (s, 1H), 3.84 (s, 3H), 2.69 (s, 4H), 2.51 (s, 3H), 2.31 (s, 3H). ^{13}C-NMR (101 MHz, $CDCl_3$) δ 159.13, 131.83, 130.39, 129.67, 128.21, 128.08, 123.16, 113.51, 88.11, 85.66, 61.03, 55.30, 45.99. HRMS (ESI) m/z calcd for $[M+H]^+$ requires 321.1961, found 321.1966. HPLC (acetonitrile/water) = 1:1, flow rate = 0.35 mL/min, λ = 290 nm minor isomer: t_R = 18.1 min, major isomer: t_R = 21.3 min.

Product code P13: 92% Yield (0.32 g), 96% ee; pale yellow solid 115-117 °C; ^{1}H-NMR (400 MHz, $CDCl_3$) δ; 8.40 (d, J = 8.3 Hz, 1H), 7.97 (d, J = 7.1 Hz, 1H), 7.92 – 7.81 (m, 2H), 7.59 –

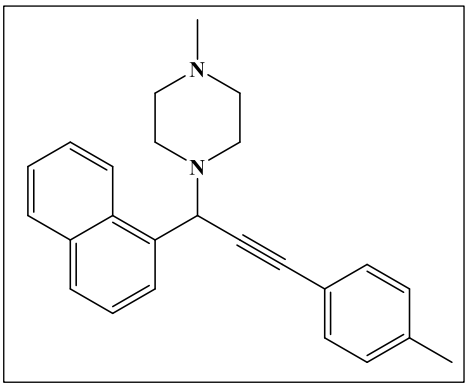

7.43 (m, 5H), 7.15 (d, J = 7.9 Hz, 2H), 5.49 (s, 1H), 2.78 (s, 4H), 2.39 (s, 7H), 2.29 (s, 3H). ^{13}C-NMR (101 MHz, $CDCl_3$) δ 138.18, 134.05, 133.88, 131.80, 131.76, 129.00, 128.72, 128.45, 127.02, 125.80, 125.61, 124.91, 124.85, 120.12, 89.01, 84.42, 59.74, 55.36, 45.97, 21.49. HRMS (ESI) m/z calcd for $[M+H]^+$ requires 355.2 169, found 355.2175. HPLC (acetonitrile/water) = 1:1, flow rate = 0.35 mL/min, λ = 290 nm minor isomer: t_R = 28.9 min, major isomer: t_R = 32.1 min.

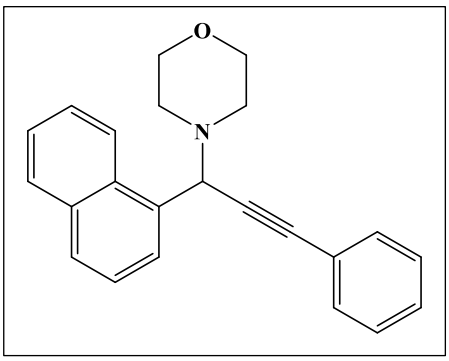

Product code P14: 91% Yield (0.29 g), 99% ee; yellow oil 132-134 °C; ^{1}H-NMR (400 MHz, $CDCl_3$) δ; 8.42 (dd, *J* = 8.5, 1.4 Hz, 1H), 7.97 – 7.84 (m, 3H), 7.61 – 7.48 (m, 5H), 7.40 – 7.35 (m, 3H), 5.47 (s, 1H), 3.73 (tdd, *J* = 14.8, 6.0, 3.2 Hz, 4H), 2.75 (dtd, *J* = 19.2, 11.9, 11.4, 5.3 Hz, 4H).^{13}C-NMR (101 MHz, $CDCl_3$) δ 134.11, 133.24, 131.86, 131.72, 128.93, 128.53, 128.36, 128.27, 127.14, 125.93, 125.72, 124.82, 124.77, 123.10, 89.07, 85.04, 67.24, 60.22, 29.73..HRMS: m/z calcd for $C_{23}H_{21}NO$ $(M+H)^+$ 328.1696; found 328.1689. HPLC (acetonitrile/water) = 1:1, flow rate = 0.35 mL/min, λ = 290 nm minor isomer: t_R = 27.1 min, major isomer: t_R = 32.1 min.

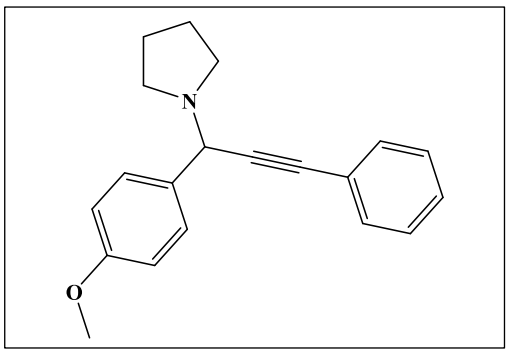

Product code P15: 89% Yield (0.26 g), 96% ee; yellow oil; ^{1}H-NMR (400 MHz, Chloroform-*d)* δ; 7.61 – 7.45 (m, 4H), 7.40 – 7.29 (m, 3H), 6.92 (d, *J* = 8.7 Hz, 2H), 4.86 (s, 1H), 3.84 (s, 3H), 2.71 (dt, *J* = 6.9, 4.2 Hz, 4H), 1.94 – 1.71 (m, 4H).^{13}C-NMR (101 MHz, Chloroform-*d*) δ 159.07, 131.79, 131.64, 129.44, 128.27, 128.08, 123.26, 113.61,

86.95, 86.72, 77.37, 77.05, 76.73, 58.52, 55.31, 50.26, 23.47.HRMS: m/z calcd for $C_{20}H_{21}NO$ $(M+H)^+$ 292.1696; found 292.1695. HPLC (acetonitrile/water) = 1:1, flow rate = 0.35 mL/min, λ = 290 nm minor isomer: t_R = 32.2 min, major isomer: t_R = 27.9 min.

Product code P16: 86% Yield (0.23 g), 93% ee; brown oil; ^{1}H-NMR (400 MHz, $CDCl_3$) δ; 7.60 – 7.52 (m, 2H), 7.37 (dp, *J* = 5.9, 1.7 Hz, 3H), 7.31 (dd, *J* = 5.1, 1.3 Hz, 1H), 7.27 (dt, *J* = 3.5, 1.2 Hz, 1H), 7.01 (dd, *J* = 5.1, 3.5 Hz, 1H), 5.24 (d, *J* = 1.2 Hz, 1H), 2.86 – 2.78 (m, 4H), 1.93 – 1.83 (m, 4H). ^{13}C-NMR (101 MHz, $CDCl_3$) δ 144.35, 131.90, 128.35, 128.31, 126.24, 125.46, 125.32, 122.99, 86.46, 85.89, 54.43, 49.86, 23.70. HRMS (ESI) m/z calcd for $[M+H]^+$ requires 268.1154, found 268.1157. HPLC (acetonitrile/water) = 1:1, flow rate = 0.35 mL/min, λ = 290 nm minor isomer: t_R = 28.9 min, major isomer: t_R = 32.1 min.

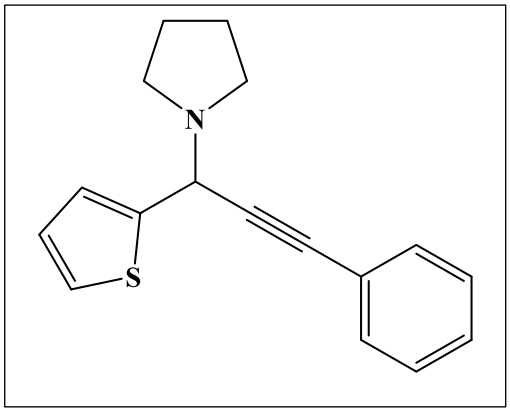

Product code P17: 90% Yield (0.28 g), 99% ee; brown oil; ^{1}H-NMR (400 MHz, $CDCl_3$) δ; 8.47 (d, *J* = 8.4 Hz, 1H), 7.97 (d, *J* = 7.1 Hz, 1H), 7.91 (dd, *J* = 8.0, 1.5 Hz, 1H), 7.86 (d, *J* = 8.2 Hz, 1H), 7.55 (dddt, *J* = 11.8, 10.6, 8.3, 6.3 Hz, 6H), 7.37 (dd, *J* = 5.0, 2.0 Hz, 3H), 5.64 (s, 1H), 2.91 – 2.82 (m, 2H), 2.78 – 2.69 (m, 2H), 1.91 – 1.75 (m, 4H). ^{13}C-NMR (101 MHz, $CDCl_3$) δ 135.38, 134.01, 131.86, 131.57, 128.53, 128.51, 128.33, 128.10, 126.00, 125.97, 125.63, 125.09, 124.52, 123.41, 87.45, 86.82, 56.72, 50.25, 23.76. HRMS (ESI) m/z calcd for $[M+H]^+$ requires 312.1747, found 312.1748. HPLC (acetonitrile/water) = 1:1, flow rate = 0.35 mL/min, λ = 290 nm minor isomer: t_R = 29.6 min, major isomer: t_R = 32.6 min.

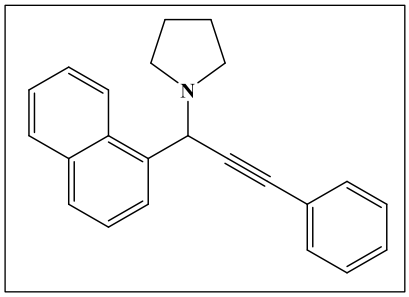

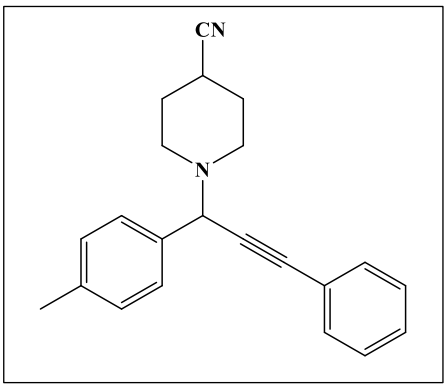

Product code P18: 91% Yield (0.28 g), 97% ee; brown oil; ^{1}H-NMR (400 MHz, $CDCl_3$) δ; 7.59 – 7.49 (m, 4H), 7.41 – 7.33 (m, 3H), 7.25 – 7.17 (m, 2H), 4.83 (s, 1H), 2.89 (dd, *J* = 11.5, 5.9 Hz, 1H), 2.79 (ddd, *J* = 11.1, 6.5, 4.0 Hz, 1H), 2.61 (ddt, *J* = 11.8, 8.3, 4.2 Hz, 2H), 2.39 (m, 4H), 2.02 – 1.85 (m, 4H). ^{13}C-NMR (101 MHz, $CDCl_3$) δ 137.55, 134.89, 131.84, 128.97, 128.37, 128.33, 128.30, 122.96, 121.88, 88.41, 84.93, 61.65, 47.08, 29.14, 29.03, 26.35, 21.15. HRMS (ESI) m/z calcd for $[M+H]^+$ requires 315.1856, found 315.1853. HPLC (acetonitrile/methanol) = 1:1, flow rate = 0.5 mL/min, λ = 290 nm minor isomer: t_R = 20.77 and 24.19 min, major isomer: t_R = 28.57 and 32.06 min.

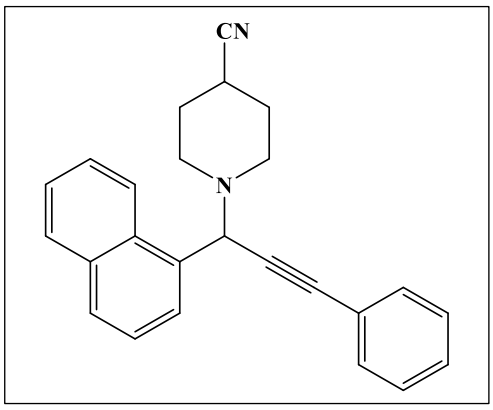

Product code P19: 90% Yield (0.31 g), 99% ee; brown oil; ^{1}H-NMR (400 MHz, CDCl3) δ; 8.36 (dd, *J* = 8.2, 1.6 Hz, 1H), 7.99 (d, J = 7.1 Hz, 1H), 7.96 – 7.86 (m, 2H), 7.66 – 7.49 (m, 5H), 7.41 (dd, J = 5.0, 2.0 Hz, 3H), 5.54 (s, 1H), 3.04 (dt, J = 10.9, 4.9 Hz, 1H), 2.87 (ddd, J = 11.2, 6.9, 3.6 Hz, 1H), 2.78 – 2.53 (m, 3H), 1.94 (ddq, J = 10.7, 7.0, 3.0 Hz, 3H), 1.78 (qd, J = 8.7, 4.4 Hz, 1H). ^{13}C-NMR (101 MHz, $CDCl_3$) δ 134.13, 133.29, 131.92, 131.72, 129.04, 128.62, 128.51, 128.47, 128.41, 127.12, 126.05, 125.81, 124.88, 124.68, 123.02, 121.89, 89.30, 84.63, 60.12, 47.11, 29.18, 29.04, 26.42. HRMS (ESI) m/z calcd for $[M+H]^+$ requires 351.1856, found 351.1861. HPLC (acetonitrile/methanol) = 1:1, flow rate = 0.4 mL/min, λ = 290 nm minor isomer: t_R = 17.90 and 22.73 min, major isomer: t_R = 29.00 and 33.92 min.

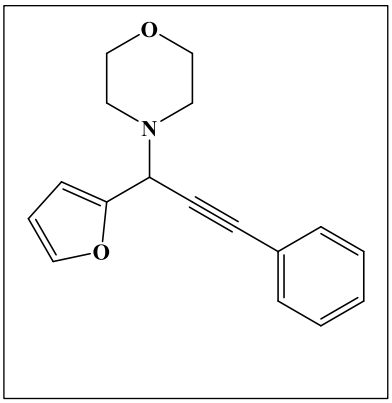

Product code P20: 82% Yield (0.22 g), 93% ee; brown oil; ^{1}H-NMR (400 MHz, $CDCl_3$) δ; 7.54 – 7.50 (m, 2H), 7.47 (dd, *J* = 1.9, 0.9 Hz, 1H), 7.37 – 7.34 (m, 3H), 6.54 (dt, *J* = 3.2, 0.9 Hz, 1H), 6.39 (dd, *J* = 3.2, 1.9 Hz, 1H), 4.91 (d, *J* = 0.9 Hz, 1H), 3.83 – 3.77 (m, 4H), 2.71 – 2.66 (m, 4H).^{13}C-NMR (101 MHz, $CDCl_3$) δ 150.76, 142.89, 131.88, 128.50, 128.35, 122.56, 110.13, 109.78, 87.02, 82.81, 77.37, 77.25, 77.05, 76.73, 66.96, 56.12, 49.63. HRMS: m/z calcd for $C_{17}H_{17}NO_2$ $(M+H)^+$ 268.1332; found 268.1334. HPLC (acetonitrile/water) = 3:1, flow rate = 0.2 mL/min, λ = 295 nm minor isomer: t_R = 83.9 min, major isomer: t_R = 98.3 min.

6.3 Results and discussion

6.3.1 Synthesis and characterization

The alkoxy appended 4,6-*O*-ethylidene-*N*-(2-hydroxy-4-(octyloxy)benzylidene)-β-D-glucopyranosylamine (**ALH2**) was synthesized by condensing 2-hydroxy-4-octyloxy-benzaldehyde (**1**) with 4,6-*O*-ethylidene-β-D-glucopyranosylamine (**2**) (Scheme 6.1). The product formation was confirmed by noting the singlet peaks at δ, 13.36 and 8.43 ppm (Figure S1) for Ar-OH and azomethine (CH=N), respectively in the ^{1}H-NMR spectrum. In the FTIR spectrum of **ALH2**, the broad bands at 3456 and 3379 cm^{-1} were assigned to the O-H stretches (Figure S4). Two intense peaks at around 1620 and 1226 cm^{-1} can be attributed to the imine bond (C=N) and C–N stretching at the anomeric carbon, respectively. The two peaks at 1010 and 1087 cm^{-1} support the C-O stretches of pyranose form for carbohydrate residue whereas the peak at 879 cm^{-1} belongs to its β-configuration.[32]

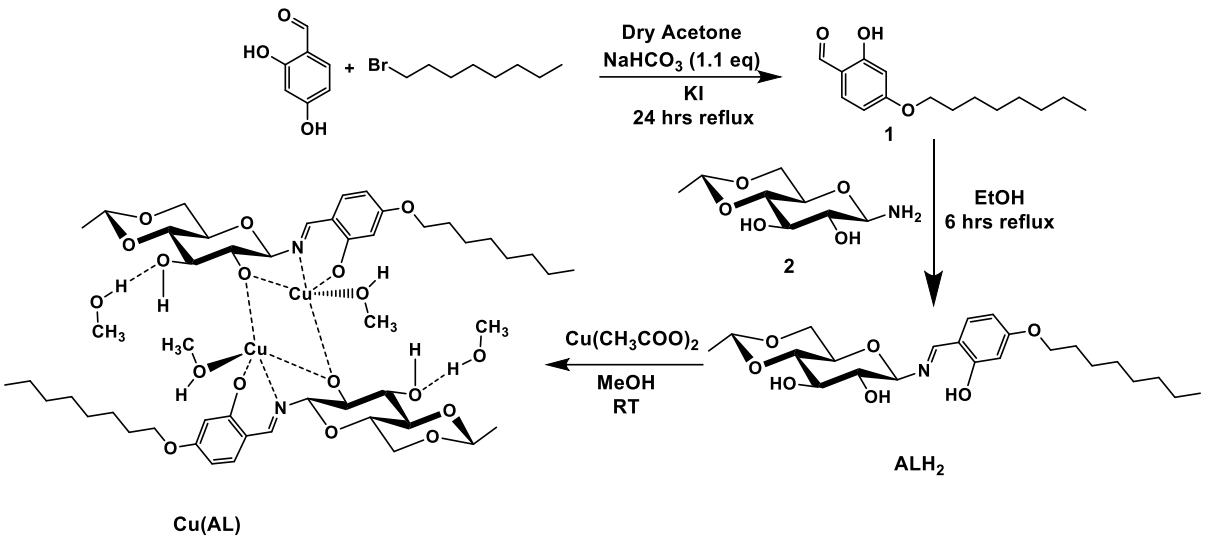

Scheme 6.1. *Synthetic protocol of* ***ALH₂*** *and* ***CuAL***

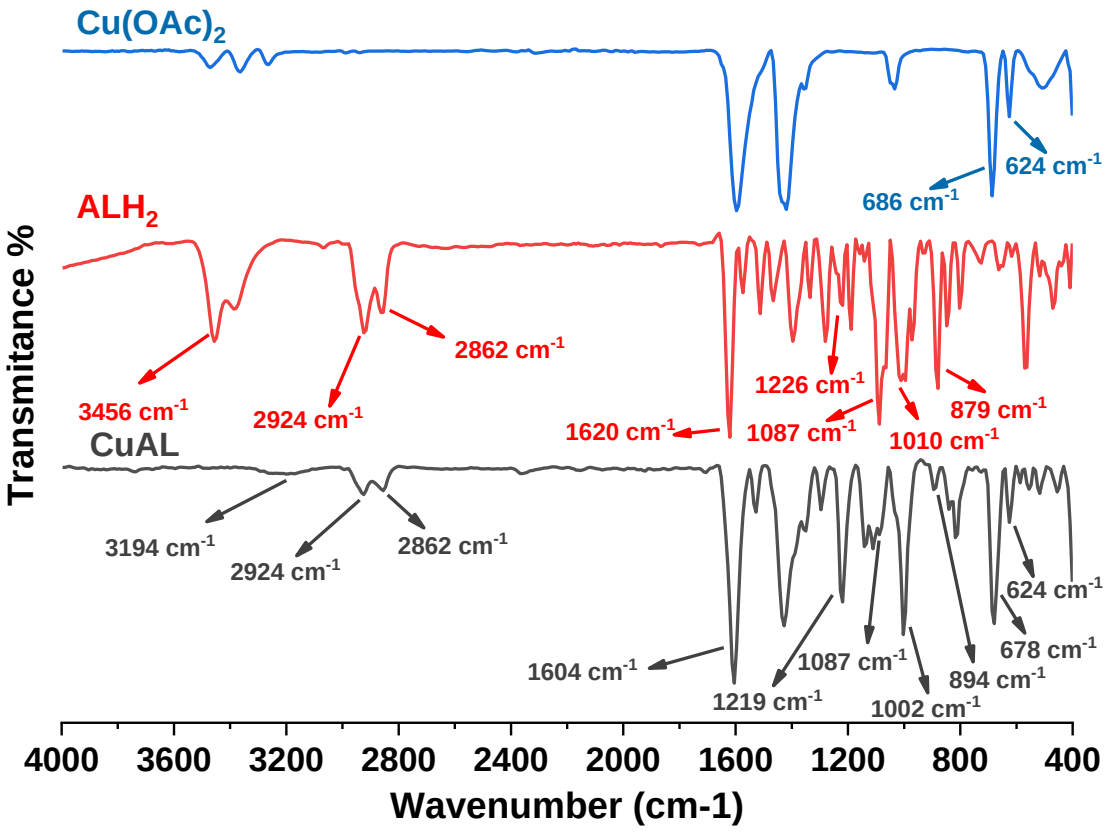

Fig. 6.1 *FTIR spectra of cupric acetate,* ***ALH₂*** *and* ***CuAL***

The reaction of **ALH$_2$** with copper(II) acetate in 1:1.1 molar ratio in methanol led to the formation of a greenish-blue (cyan) colored dinuclear copper complex [Cu($C_{23}H_{33}NO_7$)($CH_3OH)_2$]$_2$. The CHN analysis supported the association of four methanol molecules with each dinuclear complex. The FTIR spectra of **CuAL** exhibited red shift of the C=N stretching by 16 cm^{-1} with respect to the free ligand, supporting the participation of imine nitrogen in metal-ion interaction (*Fig. 6.1*). The appearance of peaks at 678 and 624 cm^{-1} might be due to the metal-oxygen vibrations,[33] which supports the complexation between glycoconjugate and copper(II) ion.

The structural morphology of **CuAL** was examined by field emission scanning electron microscopy (FE-SEM), which reveals the nearly spherical shape of the complex (*Fig. 6.2*). The energy-dispersive X-ray spectroscopy (EDS) confirms the presence of the main elements (copper, carbon, oxygen and nitrogen) and elemental mapping shows their uniform distribution all over the surface (*Fig. 6.3*). Solid-state UV–visible spectrum of **ALH$_2$** shows three major bands at 224 (n→π*), 300 (π→π*) and 361 (π→π*) nm,[34] and a similar pattern persisted in the spectrum of **CuAL** (*Fig. 6.4*). A very broad peak with λ_{max} at 719 nm also appeared for the d-d electronic transition of Cu(II) ion in the complex.

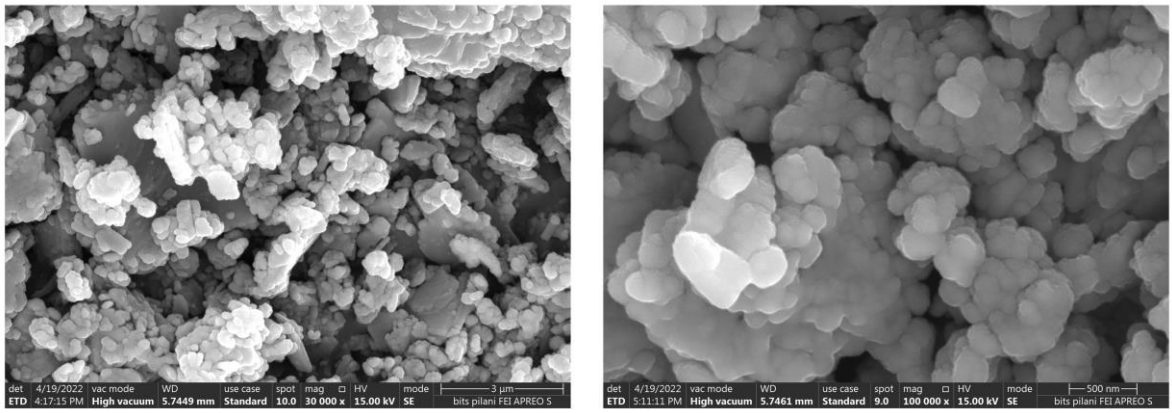

Fig. 2** SEM image of **CuAL

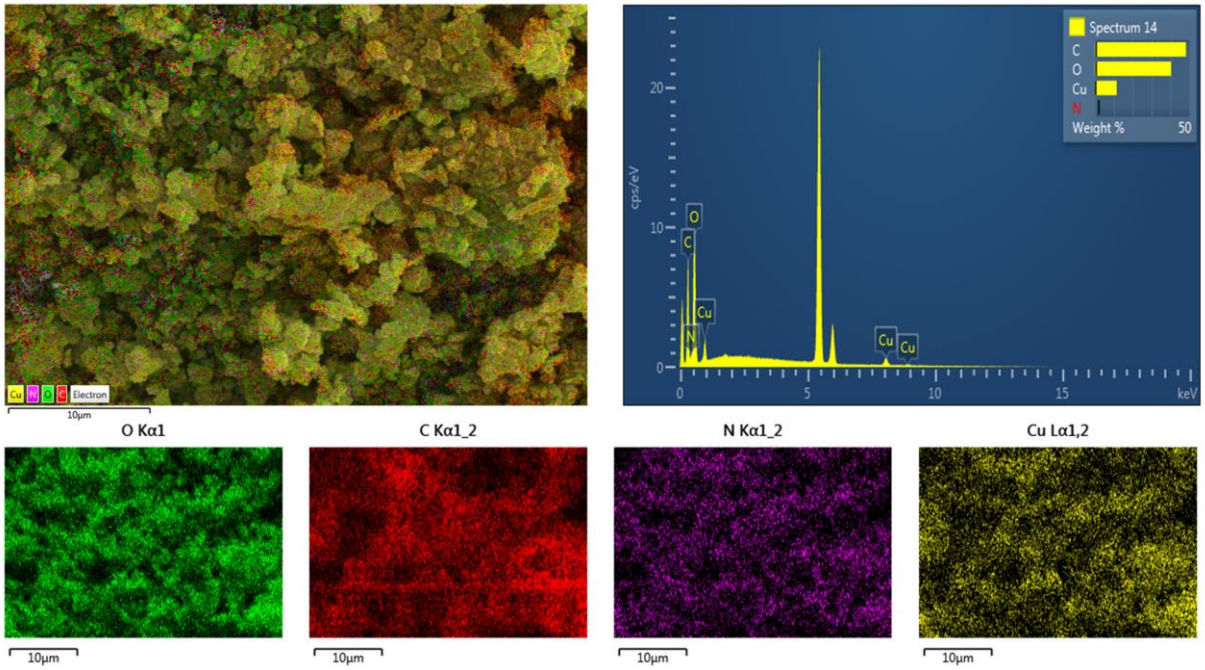

Fig. 3 *EDS Layered image of* ***CuAL***

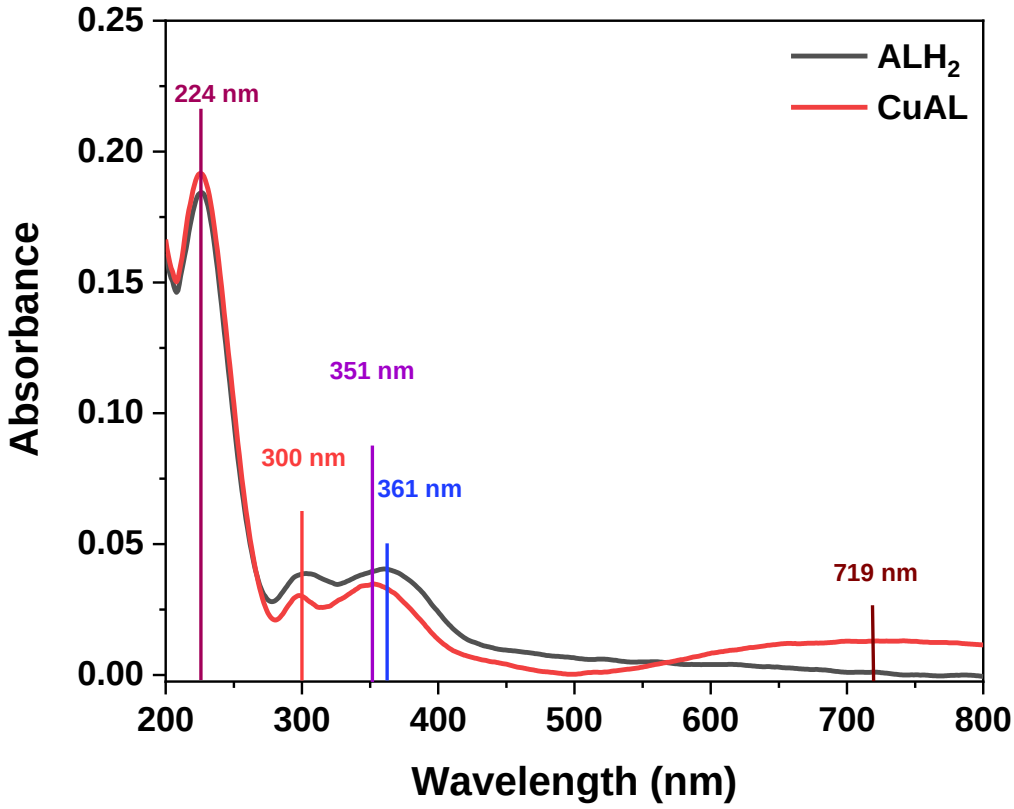

Fig. 6.4 *UV-visible spectra of* ***ALH_2*** *and* ***CuAL***

To determine the thermal resistance of the **ALH₂** and its copper complex, the thermogravimetric analysis (TGA) was performed under the nitrogen atmosphere in the temperature range of 30-800 °C (*Fig. 6.5*). The compound **ALH₂** was thermally stable up to 160 °C, whereas the complex shows thermal resistance over 200 °C. In each case, there is a marginal weight loss due to the removal of adsorbed moisture or residual solvent in the temperature range of 50-150 °C. Both the ligand and complex exhibited a three-stage decomposition process with overall mass losses of 100% (in the temperature range 160-500 °C) and 62.34% (between 200-350 °C), respectively.

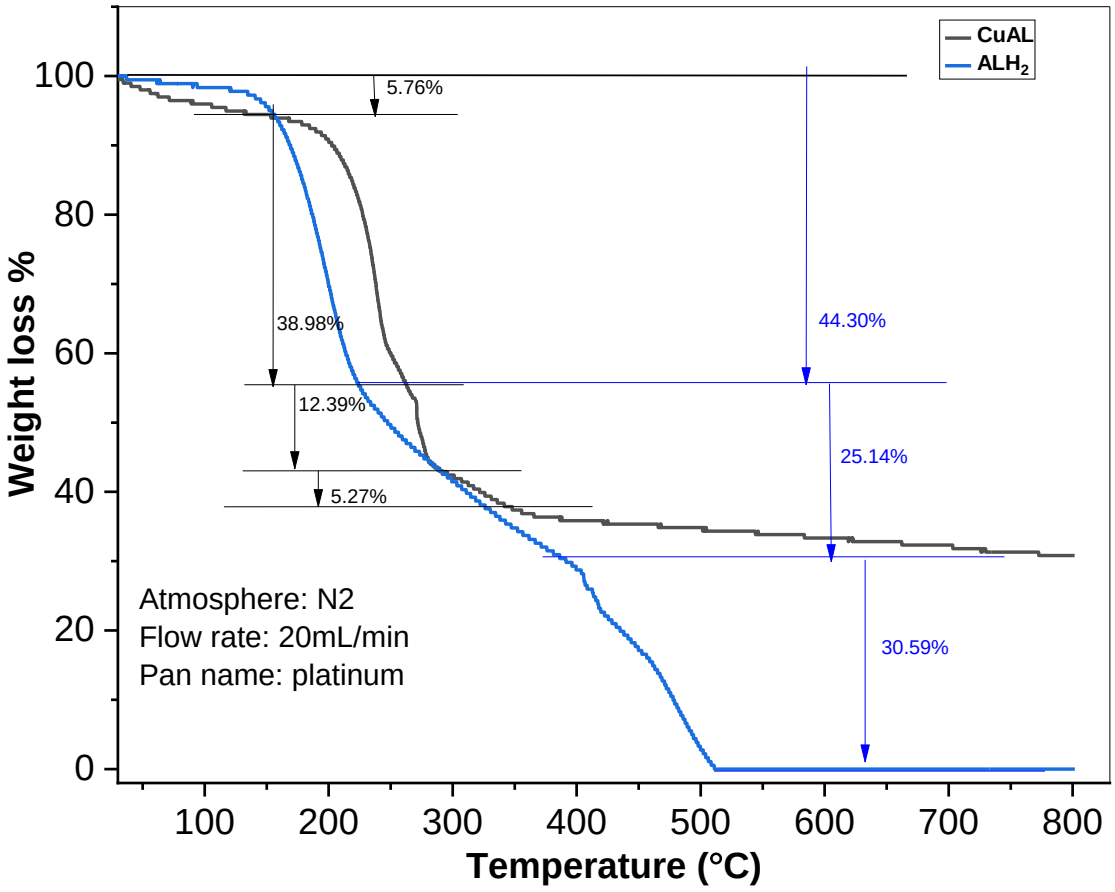

Fig. 6.5** TGA plot of **ALH₂** and **CuAL

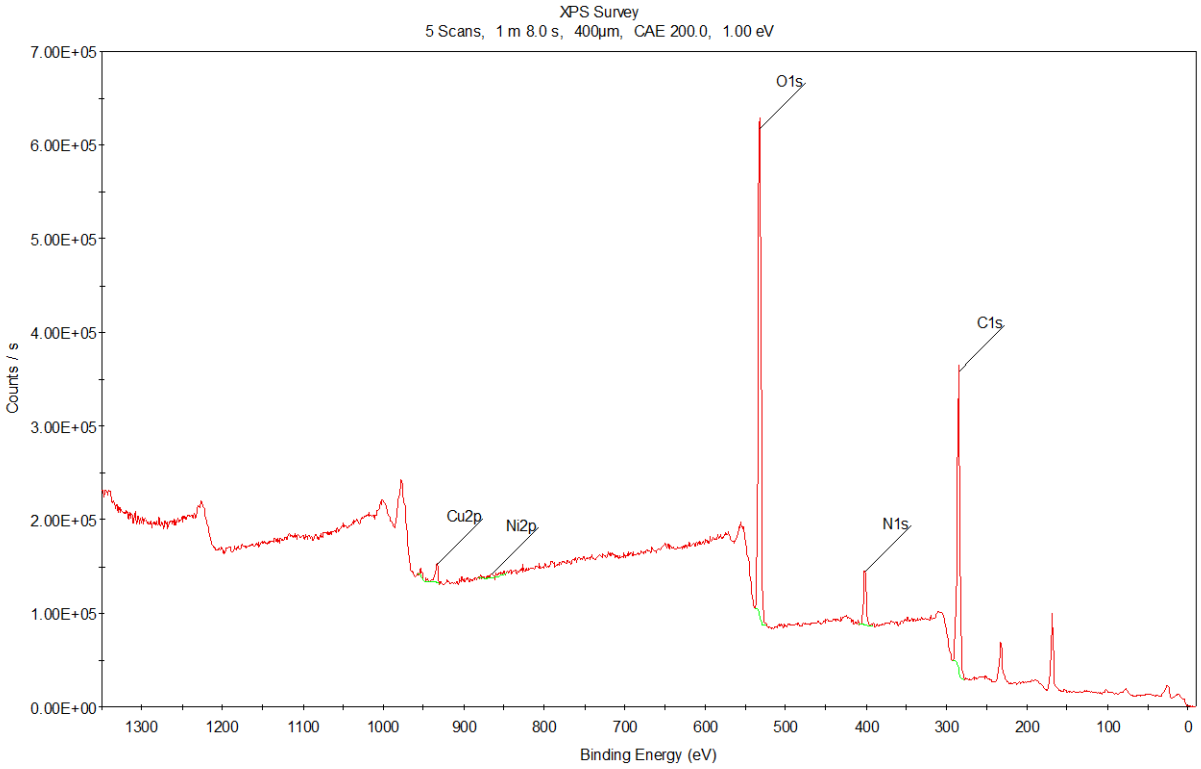

Fig. 6.6** XPS survey spectra of **CuAL

The complex formation was further supported by an X-ray photoelectron spectroscopy (XPS) elemental survey (*Fig. 6.6*), where peaks of core level electrons appeared at 285 (C1s), 401 (N1s), 532 (O1s), 934 ($Cu2p_{3/2}$) and 954 ($Cu2p_{1/2)}$ eV.[35-36] The deconvolution of XPS peak of C1s using Gaussian function revealed three different states of carbon, including C-C/C=C, C-O/C-N and C=O/C=N with the binding energy of 284.5, 286.26 and 288.2 eV respectively.[37] Each of the Cu2p peaks in the XPS spectrum of **CuAL** was fitted into two Gaussian peaks with the energies of 932.6 and 934.34 eV for $Cu2p_{3/2}$, and 952.5 and 954.4 eV for $Cu2p_{1/2}$ (*Fig. 6.7*).[35] The peaks at 934.34 and 954.4 eV (~ 10%) belongs to Cu(II) ions while the peaks at 932.6 and 952.5 eV (~ 90%) appears due to the change in the electronic confirmation ($2p^63d^9 \rightarrow 2p^53d^{10}$).[38]

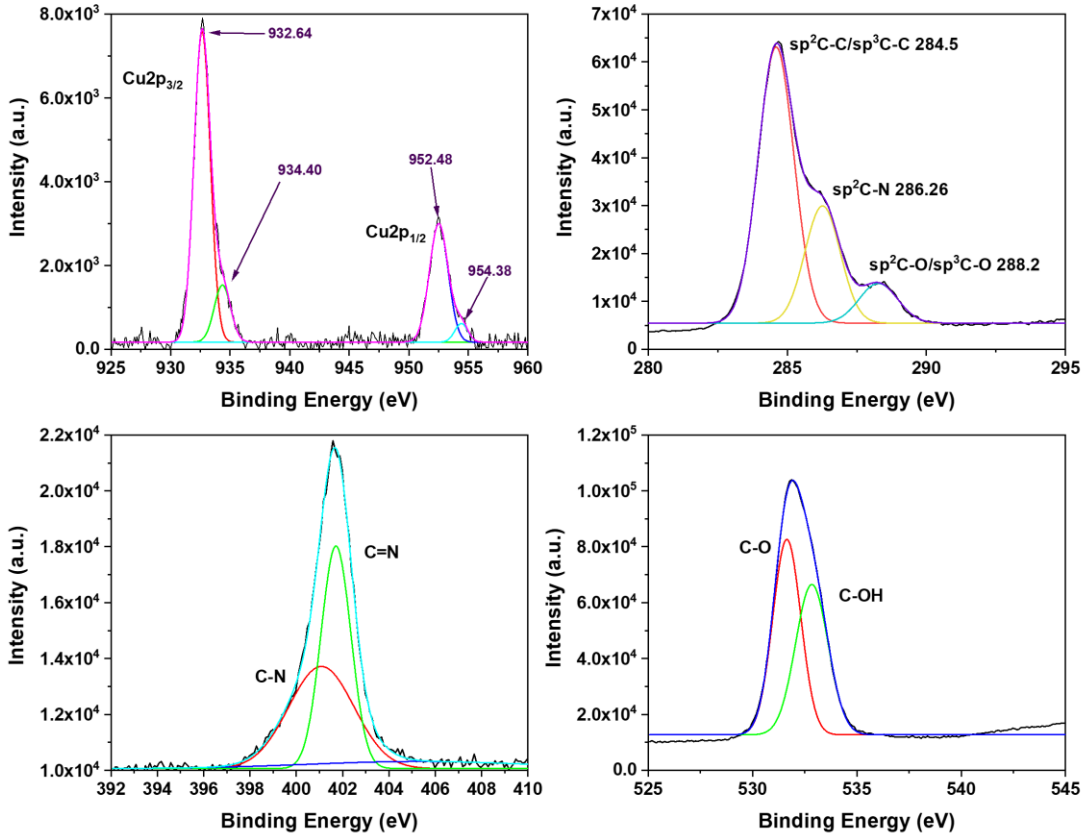

Fig. 6.7 *High resolution Cu2p, C1s, N1s and O1s XPS spectra present in* ***CuAL***

6.3.2 Crystal structure of copper complex

Recrystallization of **CuAL** from hot DMSO yielded a greenish-blue (cyan) needle-shaped X-ray suitable triclinic crystal system with P1 space group (CCDC 2219842). The single-crystal X-ray diffraction studies revealed the formation of a dinuclear complex with a stoichiometry of 1:1 for metal and ligand. The crystal structure with atomic labelling is displayed in *Fig. 6.8*, and the crystallographic data is summarized in *Table 1*. Both the metal centers of the **CuAL** are separated by 2.968 Å, which confirms the absence of metallic bond between them. Each copper atom has five-coordination sites [$CuNO_4$], with slightly distorted square-pyramidal geometry ($\tau = 0.053$, where τ = difference between the two most considerable angles/60; $\tau = 0$ is ideal for square-pyramidal geometry and $\tau = 1$ is perfect for trigonal-bipyramidal).[39-41] The Glu-OH2 of carbohydrate moieties bridges the two copper centers to

form a Cu_2O_2 rhomb. The axial positions are occupied by methanol (solvent) molecules with trans-orientation about the Cu_2O_2 rhomb.

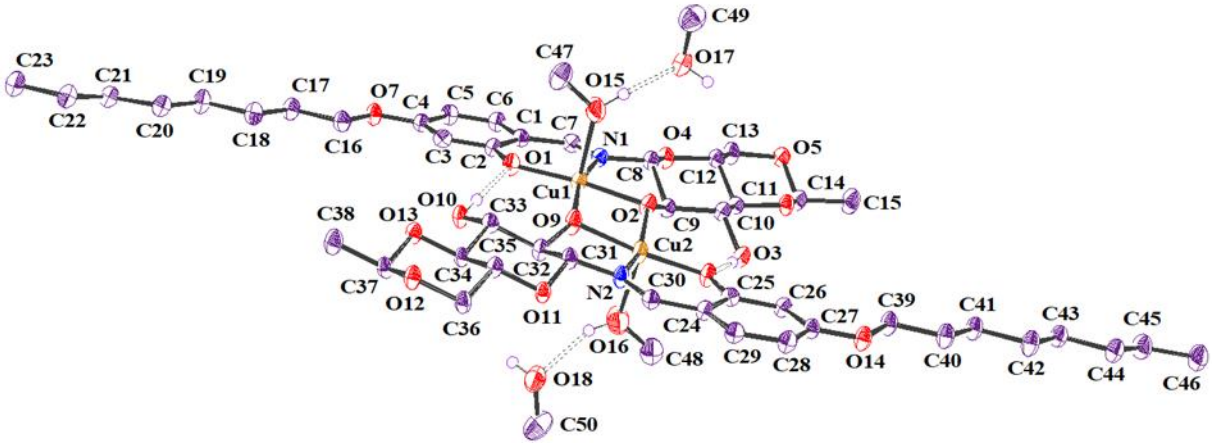

Fig. 6.8. *ORTEP diagram of* ***CuAL*** *(with 50% probability level)*

Table 6.1 *Crystal data and structure refinement for* ***CuAL***

Identification code	**CuAL**
Empirical formula	$C_{50}H_{82}Cu_2N_2O_{18}$
Formula weight	1126.25
Temperature/K	93(2)
Crystal system	triclinic
Space group	P1
a/Å	8.8485(2)
b/Å	12.3590(2)
c/Å	12.6692(3)
α/°	92.829(2)
β/°	99.740(2)
γ/°	98.879(2)
Volume/Å^3	1345.09(5)
Z	1
ρ_{calc}g/cm^3	1.390
μ/mm^{-1}	1.584
F(000)	598.0
Radiation	Cu Kα (λ = 1.54184)
2Θ range for data collection/°	9.76 to 159.516
Index ranges	$-6 \le h \le 11$, $-15 \le k \le 15$, $-15 \le l \le 16$
Reflections collected	14488
Independent reflections	7356 [R_{int} = 0.0258, R_{sigma} = 0.0360]
Data/restraints/parameters	7356/6/665
Goodness-of-fit on F^2	1.093

Final R indexes [I>=2σ (I)]	R_1 = 0.0411, wR_2 = 0.1167
Final R indexes [all data]	R_1 = 0.0417, wR_2 = 0.1174
Largest diff. peak/hole / e Å^{-3}	0.71/-0.61
Flack parameter	-0.05(2)

In the lattice, **CuAL** possesses four inter-molecular and two intra-molecular hydrogen bonding interactions. The intramolecular hydrogen bonding interaction is of O-H···O type occurring between the phenolate oxygen and Glu-OH3. The oxygen atom of the coordinated methanol molecule forms O-H…O type hydrogen bond with an adjacent free methanol molecule which further interacts with the Glu-OH3 through O-H···O type hydrogen bonding. Thus, the inter-complex hydrogen bonds (O-H···O) link each complex with two different molecules forming a supramolecular 1-D chain along 'a' axis (*Fig.6. 9*).

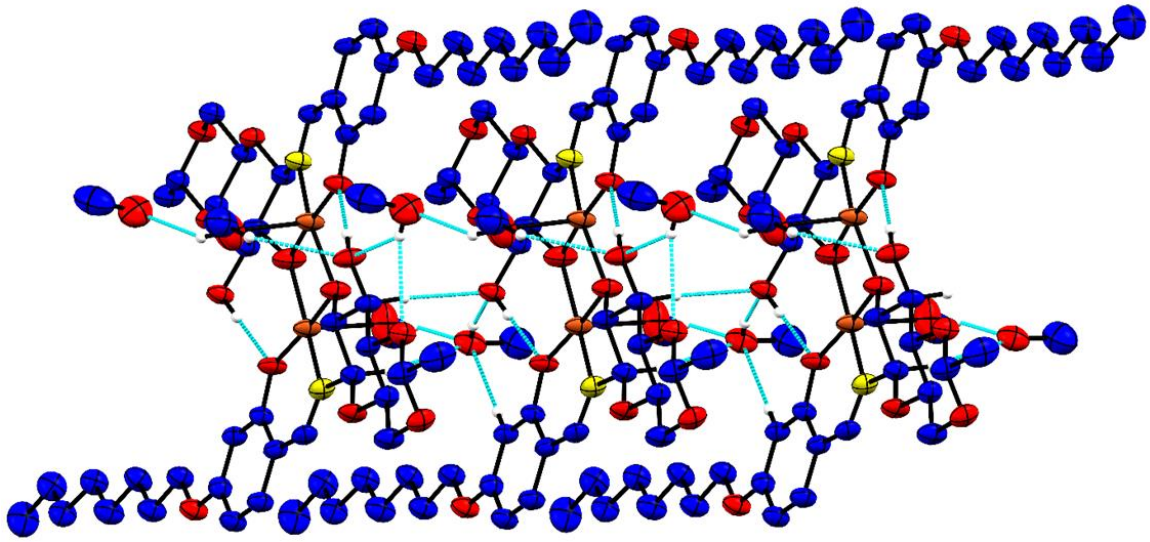

***Fig. 6.9** 1-D chain structure of **CuAL** (dashed lines represent the hydrogen bonding)*

6.3.3 Hirshfeld surface analysis

The surface environment and intermolecular interactions responsible for packing in the crystal lattice have been investigated using Hirshfeld surface (HS) analysis (*Fig. 6.10(i)*). This study reveals a symmetric HS and 2D fingerprint plot of **CuAL** due to the presence of identical interaction on both metal centers. The bright red spots were observed due to the trimming of

hydrogen bonds between Glu-OH3 and methanol molecules while other faint red spots correspond to the C–H···O interactions.

The 2D fingerprint plots with contributions of significant intermolecular interactions for **CuAL** are represented in *Fig. 6.10(ii)* and *Fig. 6.11*. The H···H contacts are accounted to be the highest contributor to the total HS of **CuAL**, which includes 70.9% of all the interactions. Another major contributor to the whole HS of **CuAL** is O···H /H···O (16.4%), which is represented by two lower-end large spikes in the fingerprint plot. The interaction between carbon and hydrogen (C···H/H···C) contributes 10.6% to the total Hirshfeld surface. Some other minor interactions like Cu···H, O···O, N···H, O···C etc., comprise the remaining 2.1% of the total HS. The donor and acceptor atoms present on the surface of the **CuAL** are illustrated by blue bumps and red concaves, respectively (*Fig. 6.10(iii)*) in the shape index. The presence of flat green areas in curvedness plot (*Fig. 6.10(iv)*) suggests the stacking of **CuAL** molecules.

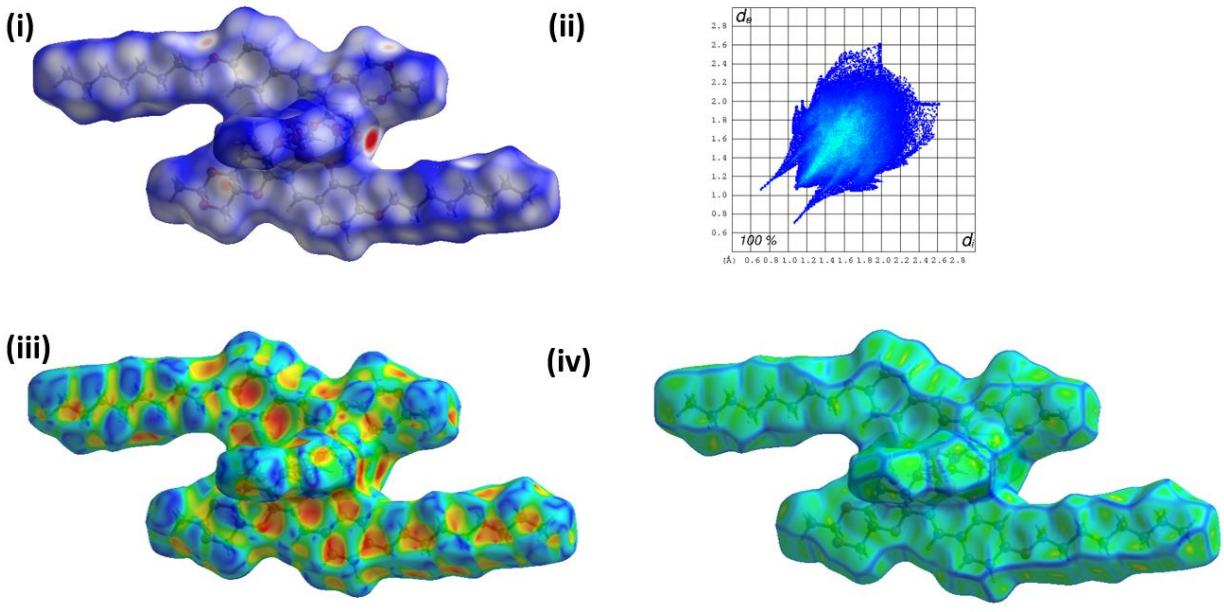

Fig. 6.10. *(i) 3D Hirshfeld surface of* **CuAL** *mapped over* d_{norm} *from -0.50 Å (red) to 1.0 Å (blue), (ii) 2D Finger print plot for 100% Hirshfeld surface, (iii) The shape-index curve (-1.0 to 1.0 Å) plot, (iv) The curvedness plot (-4.00 Å to 0.40 Å)*

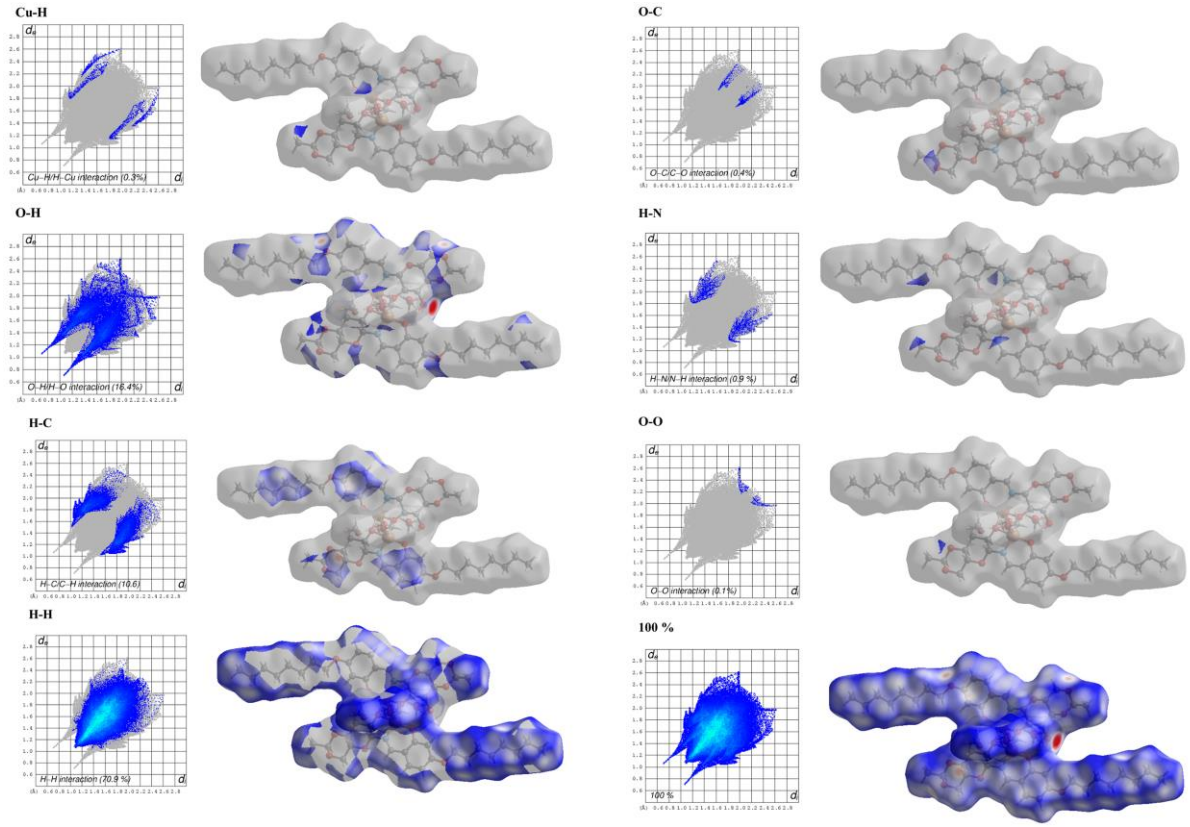

Fig. 6.11 *2D fingerprint of* ***CuAL***

6.3.4 Catalytic activity

Metal complexes of 4,6-*O*-ethylidene-*N*-(2-hydroxybenzylidene)-β-D-glucopyranosylamine have been used as catalysts in several organic transformations.[28, 42] Its dinuclear Cu(II) complex has been reported for the selective oxidation of aromatic alcohols to corresponding carbonyl compounds.[28] Several literatures are available on Cu(I) catalyzed enantioselective A^3 coupling reactions, whereas Cu(II) complexes are widely used for KA^2 coupling transformations.[2, 23] Despite the advantages like lower cost and higher stability to air oxidation over Cu(I),[2] to the best of our knowledge no Cu(II) catalyzed asymmetric synthesis of trisubstituted propargylamines has been reported. These facts inspired us to explore the catalytic application of our complex in one-pot synthesis of trisubstituted propargylamines. Primarily, to establish the optimum reaction condition, piperidine (1.1 eq), benzaldehyde (1.0 eq) and phenylacetylene (1.1 eq) were used as model reactants (*Scheme 6.2*). The controlled

reactions were conducted at different temperatures, catalyst loading and solvent systems like dioxane, ethanol, dimethylformamide (DMF), acetonitrile (ACN), dichloromethane (DCM), water and neat condition (*Table 2*). The reaction conditions were optimized using quantitative high-performance liquid chromatography (HPLC) separation and the product yields are presented in *Table 2*, which validates the best suited condition as 2 mol % catalyst loading under the solvent-free condition at 80 °C with a reaction time of five hours and 91% yield. Although, slightly higher yield was observed in some cases, the above condition has been chosen as optimized protocol considering the reaction time and catalyst loading

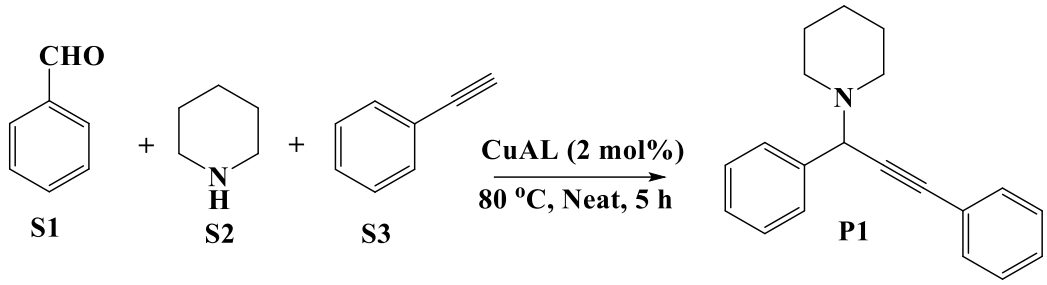

Scheme 6.2. *Optimized reaction condition for catalytic synthesis of propargylamine*

Table 6.2. *Optimization of reaction conditions for* ***CuAL*** *catalyzed propargylamine synthesis*

Entry	Catalyst (mol %)	Solvent	Yield (%)[a]	Time (h)	Temperature (°C)
1	**CuAL** (5.0)	ACN	55.7	6	reflux
2	**CuAL** (5.0)	DCM	38.2	6	reflux
3	**CuAL** (5.0)	Ethanol	60.4	6	reflux
4	**CuAL** (5.0)	DMF	38.2	6	80
5	**CuAL** (5.0)	Water	15.4	6	80
6	**CuAL** (5.0)	Dioxane	65.6	6	80
7	**CuAL** (5.0)	Neat	92.3	6	80
8	**CuAL** (3.0)	Neat	92.7	6	80
9	**CuAL** (2.0)	Neat	92.1	6	80
10	**CuAL** (1.0)	Neat	81.9	6	80
11	**CuAL** (0.5)	Neat	35.3	6	80

12	**CuAL** (2.0)	Neat	3.9	0.5	80
13	**CuAL** (2.0)	Neat	9.1	1	80
14	**CuAL** (2.0)	Neat	35.4	2	80
15	**CuAL** (2.0)	Neat	55.6	3	80
16	**CuAL** (2.0)	Neat	80.1	4	80
17	**CuAL** (2.0)	Neat	91.3	5	80
18	**CuAL** (2.0)	Neat	96.5	8	80
19	**CuAL** (2.0)	Neat	TRACE	24	RT
20	**CuAL** (2.0)	Neat	35.6	6	50
21	**CuAL** (2.0)	Neat	89.4	6	70
22	**CuAL** (2.0)	Neat	95.3	12	70
23	**ALH_2** (2.0)	Neat	-	24	80
24	$Cu(CH_3COO)_2$	Neat	12.1	24	80
25	No Catalyst	Neat	-	24	80

[a] represents the HPLC yield
S1 – 100 mmol, S2 – 100 mmol, S3 – 110 mmol

Under the optimized reaction conditions, the universality of aromatic aldehydes, cyclic amines, and phenylacetylenes were investigated, which afforded twenty trisubstituted propargylamines derivatives (*Table 6.3*) in good to excellent yields (82-95%), including six new molecules. All the molecules were characterized by NMR and HRMS analysis and their enantiomeric excess (ee; 87-99%) was confirmed by chiral HPLC. HPLC. During the catalytic process, four compounds with two chiral centers (P5, P11, P18, P19) were also developed using optically inactive molecules. The reactions with achiral 4-cyanopiperidine and racemic mixture of 3-methylpiperidene yielded the mixture of corresponding diastereomers due to the formation of stereoselective chiral methyl center. The reaction mixture of cupric bromide catalyzed reactions afforded four sets of HPLC signals for the products (*Fig. A103, A126, A154 and A158*), while that of **CuAL** catalyzed reactions yielded majorly two sets (*Fig. A104, A127, A155 and A159* confirming the stereoselective synthesis. The molecular structures of P10 (CCDC 2237442) and P13 (CCDC 2237441) were established by single crystal X-ray

diffraction studies (*Fig. 6.12*) and their structural details are summarized in *Table 6.4*. Aryl aldehydes containing electron donating groups (CH_3, OMe) efficiently decrease the reaction time (4.5 h), while electron withdrawing substituents (Cl, Br, NO_2) and heterocyclic aldehydes follow the opposite trend (6 h). The fused aromatic aldehydes (1-naphthaldehyde and 1-pyrenecarboxaldehyde) also afforded good yield (89-95 %).

Table 6.3. *Scope of the A^3 coupling reaction between cyclic amines, aldehydes, and alkynes, to form the corresponding propargylamine*

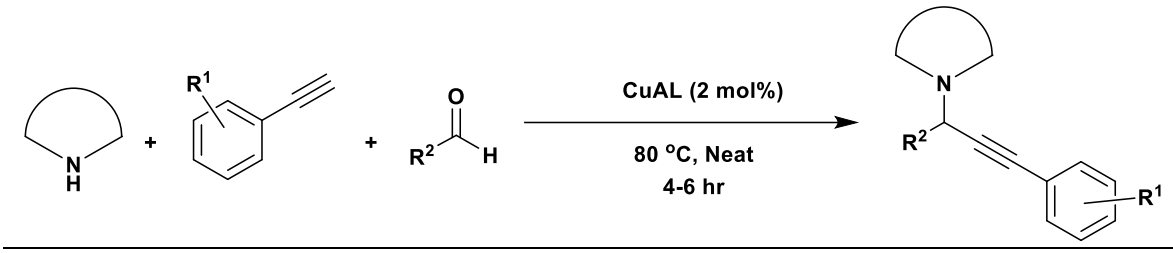

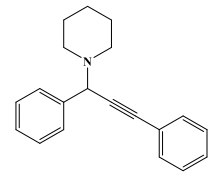

P1, 91% yield[a], 98% ee

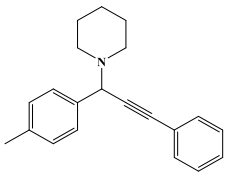

P2, 93% yield[b], 93% ee

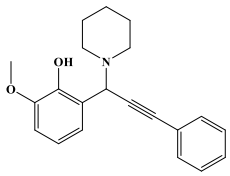

P3, 95% yield[b], 97% ee

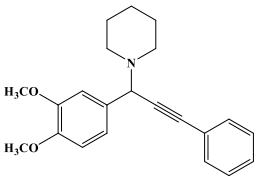

P4, 95% yield[b], 90% ee

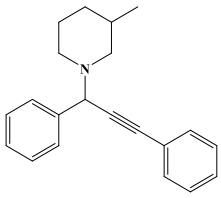

P5*[d], 88% yield[b], 98% ee

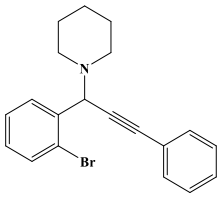

P6, 93% yield[b], 95% ee

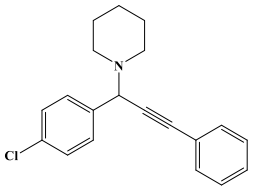

P7, 91% yield[b], 95% ee

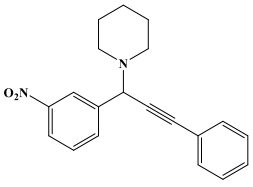

P8, 84% yield[b], 94% ee

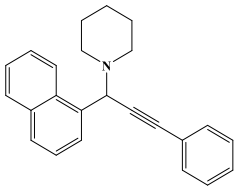

P9, 94% yield[b], 93% ee

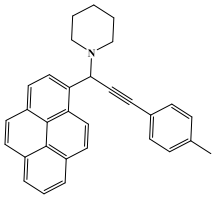

P10*, 95% yield[b], 87% ee

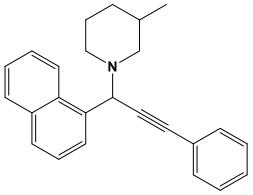

P11*[d], 89% yield[b], 90% ee

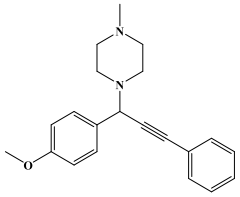

P12, 94% yield[b], 99% ee

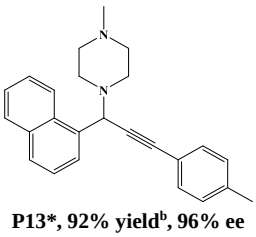

P13*, 92% yield[b], 96% ee

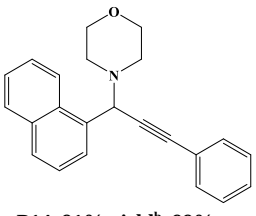

P14, 91% yield[b], 99% ee

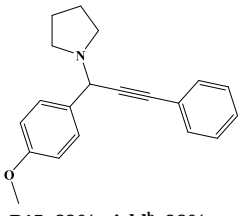

P15, 89% yield[b], 96% ee

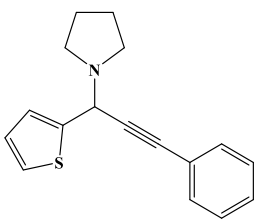

P16, 86% yield[b], 93% ee

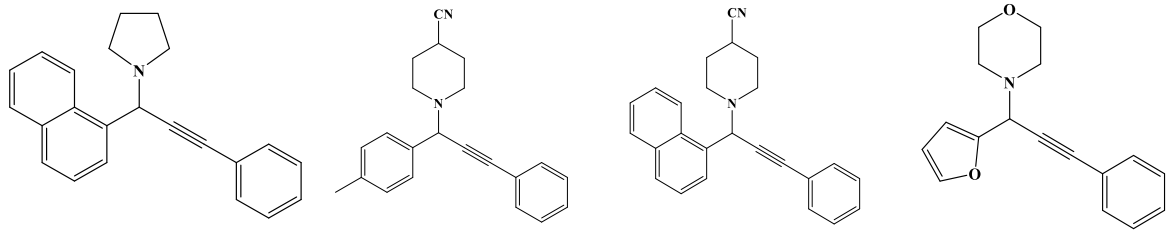

P17, 90% yield[b], 99% ee **P17, 90% yield[b], 99% ee** **P19*[d], 90% yield[b], 99% ee** **P20, 82% yield[b], 93% ee**

[a] represents HPLC yield, [b] represents isolated yields, * newly synthesized compounds, [d] diastereomers

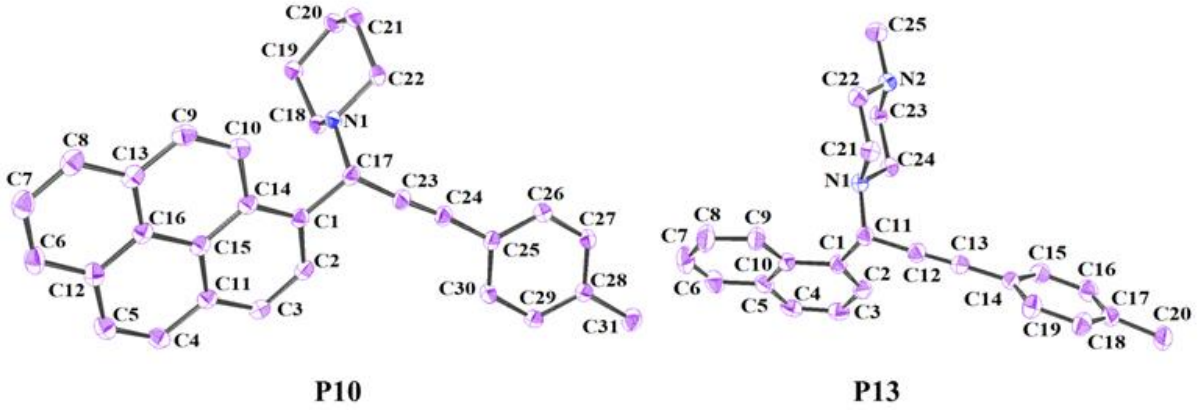

Fig. 6.12 ORTEP diagram of P10 and P13 (with 50% probability level)

Table 6.4. *Crystal data and structure refinement for P10 and P13*

Identification code	**P10**	**P13**
Empirical formula	$C_{31}H_{27}N$	$C_{25}H_{26}N_2$
Formula weight	413.53	354.48
Temperature/K	93(2)	93(2)
Crystal system	orthorhombic	monoclinic
Space group	$P2_12_12_1$	$P2_1/n$
a/Å	5.87110(10)	13.8215(3)
b/Å	18.2584(3)	5.87010(10)
c/Å	20.1596(3)	24.6855(5)
α/°	90	90
β/°	90	92.512(2)
γ/°	90	90

Volume/Å^3	2161.05(6)	2000.90(7)
Z	4	4
ρ_{calc}g/cm^3	1.271	1.177
μ/mm^{-1}	0.551	0.522
F(000)	880.0	760.0
Radiation	Cu Kα (λ = 1.54184)	Cu Kα (λ = 1.54184)
2Θ range for data collection/°	8.772 to 159.054	12.286 to 159.562
Index ranges	-7 ≤ h ≤ 3, -21 ≤ k ≤ 23, -25 ≤ l ≤ 22	-17 ≤ h ≤ 15, -7 ≤ k ≤ 3, -21 ≤ l ≤ 31
Reflections collected	7834	10382
Independent reflections	4206 [R_{int} = 0.0410, R_{sigma} = 0.0492]	4196 [R_{int} = 0.0476, R_{sigma} = 0.0561]
Data/restraints/parameters	4206/0/290	4196/0/246
Goodness-of-fit on F^2	1.065	1.114
Final R indexes [I>=2σ (I)]	R_1 = 0.0413, wR_2 = 0.1062	R_1 = 0.0518, wR_2 = 0.1480
Final R indexes [all data]	R_1 = 0.0436, wR_2 = 0.1079	R_1 = 0.0556, wR_2 = 0.1513
Largest diff. peak/hole / e Å^{-3}	0.14/-0.23	0.18/-0.28

Based on previous literature reports[43-45] and our findings, the plausible mechanism for **CuAL** catalyzed A^3-coupling reaction is presented in *Scheme 6.3*. The reaction is initiated by the activation of C-H bond of terminal alkyne by copper complex followed by mild base (piperidine) assisted deprotonation resulting in the formation of the copper-acetylide complex (**CuAL**-C_8H_5). The reaction between benzaldehyde and piperidine affords the 1,1'-(phenylmethylene)dipiperidine (**M2**), which can be isolated and purified from the reaction mixture. The isolated **M2** was characterized by NMR studies (*Fig. A164*) and the molecular structure was confirmed by X-ray crystallography (CCDC 2235550) and their structural details are summarized in *Table 6.5*. The reaction between benzaldehyde and piperidine in the presence and absence of **CuAL** confirms the time-independent formation of **M2**, which indicates this conversion is independent of the catalyst. Additionally, the HRMS analysis of

the reaction mixture establishes the generation of iminium ion (**M1**) during the reaction (Figure S122), which inspires to conclude that there must be an equilibrium between these two intermediates during the reaction. The **CuAL**-C_8H_5 reacts with *in situ* generated iminium ion to produce the corresponding propargylamine. The use of sugar-derived chiral ligand imparted excellent stereoselectivity with 98% ee. The maximum turnover frequency (TOF) for the A^3 coupling reaction was found to be 16.6 h^{-1}, which is significantly higher compared to other reports.[46]

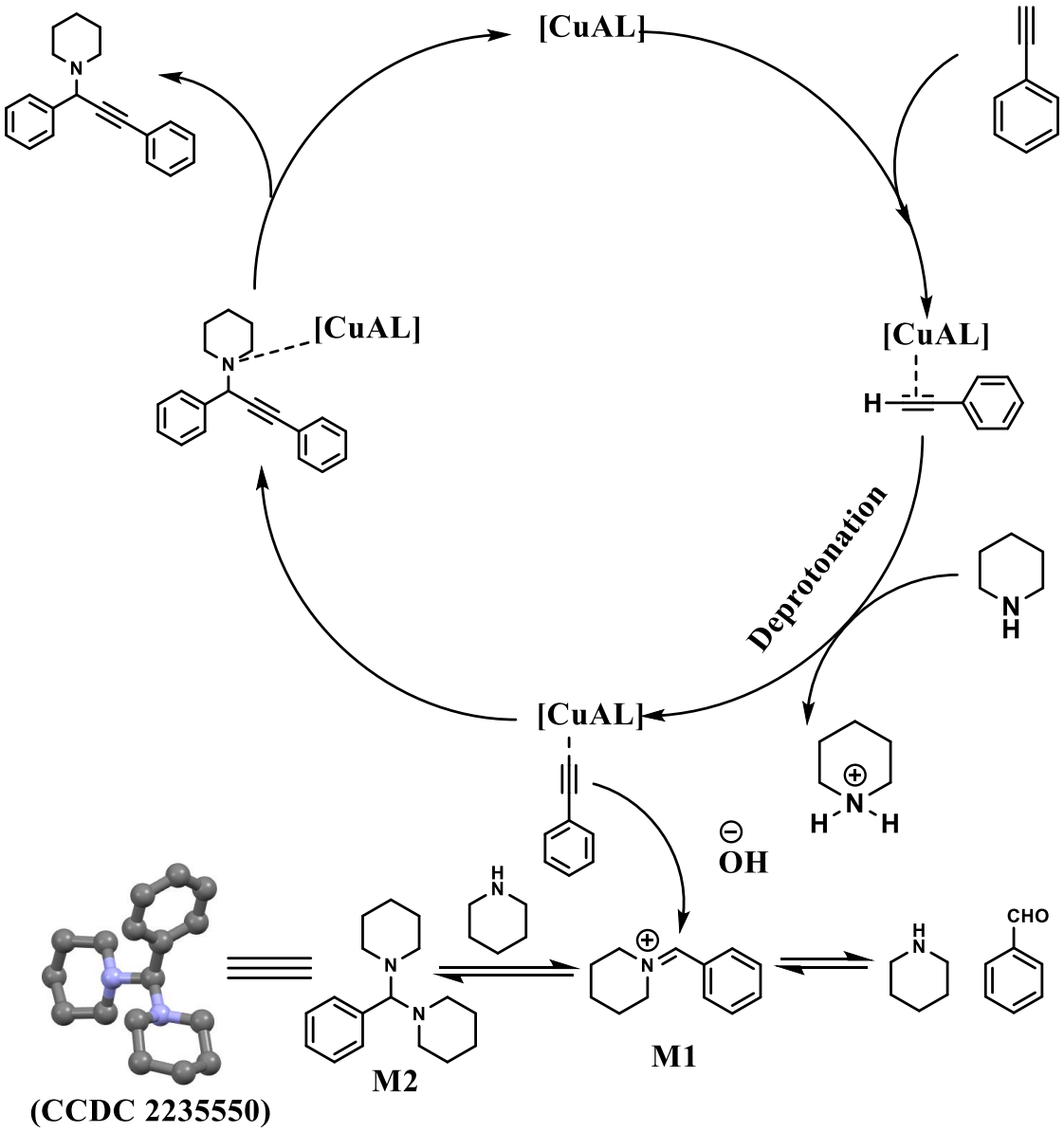

Scheme 6.3. *Plausible reaction mechanism for* ***CuAL*** *catalyzed synthesis of propargylamine*

Table 6.5 *Crystal data and structure refinement for* ***M2***

Identification code	**M2**
Empirical formula	$C_{17}H_{26}N_2$
Formula weight	258.40
Temperature/K	133(2)
Crystal system	monoclinic
Space group	$P2_1/c$
a/Å	15.8550(4)
b/Å	6.25900(10)
c/Å	16.9146(4)
α/°	90
β/°	117.118(3)
γ/°	90
Volume/Å^3	1494.02(7)
Z	4
ρ_{calc}g/cm^3	1.149
μ/mm^{-1}	0.506
F(000)	568.0
Radiation	Cu Kα (λ = 1.54184)
2Θ range for data collection/°	10.5 to 159.5
Index ranges	$-19 \leq h \leq 19$, $-7 \leq k \leq 6$, $-13 \leq l \leq 21$
Reflections collected	8509
Independent reflections	3132 [R_{int} = 0.0247, R_{sigma} = 0.0307]
Data/restraints/parameters	3132/0/172
Goodness-of-fit on F^2	1.082
Final R indexes [I>=2σ (I)]	R_1 = 0.0397, wR_2 = 0.1033
Final R indexes [all data]	R_1 = 0.0430, wR_2 = 0.1058
Largest diff. peak/hole / e Å^{-3}	0.23/-0.22

The order of reaction with respect to individual constituent has been established by changing the mol % of each reagents (benzaldehyde, piperidine, phenylacetylene and the catalyst) at a

time during the experiment and monitoring the product formation using HPLC. Rate of product formation at different catalyst loading (0.5, 1, 2, 3 and 5 mol%) was calculated by plotting the concentration of product against the time (*Fig. 6.13*), which yielded a linear plot with $R^2 > 0.99$, supporting the reliability. When the rate of product formation is plotted against the mol% of **CuAL**, the resulting straight line ($R^2 = 0.996$) indicated that the A^3 reaction is first order with respect to the catalyst.[47] Similar protocol was followed for the remaining starting materials (*Fig. 6.14-6.16*), and first-order reaction was established with respect to each substrate.

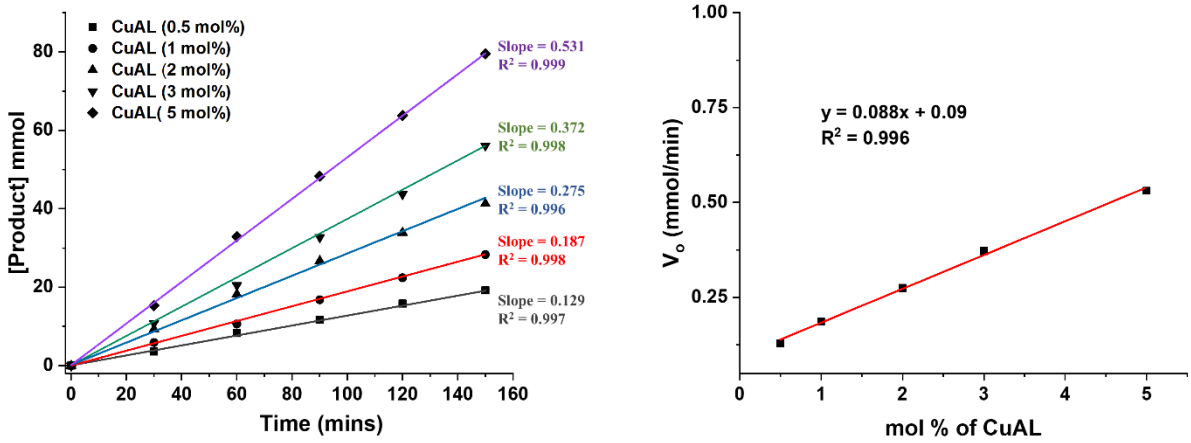

Fig. 6.13 *(i) Rate of product formation at catalyst loading of 0.5 to 5 mol% (ii) Linear plot indicates first order dependence on catalyst*

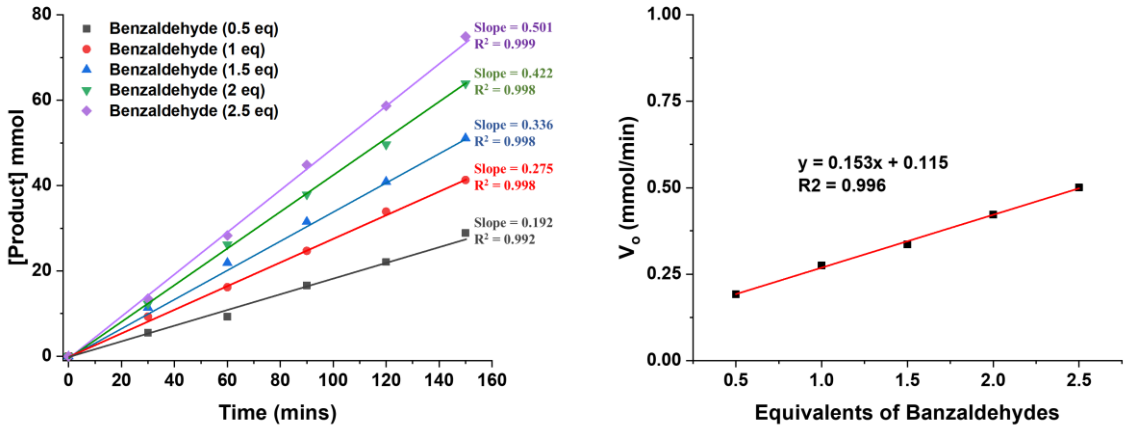

Fig. 6.14 *(i) Rate of product formation in presence of 0.5 to 2.5 equivalent of benzaldehyde (ii) Linear plot indicates first order dependence on benzaldehyde*

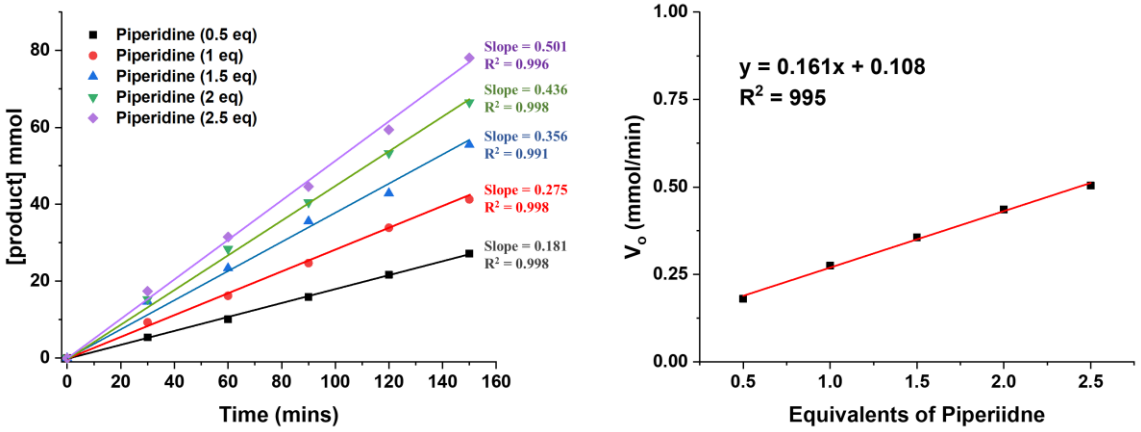

Fig. 6.15 *(i) Rate of product formation in presence of 0.5 to 2.5 equivalent of piperidine (ii) Linear plot indicates first order dependence on piperidine*

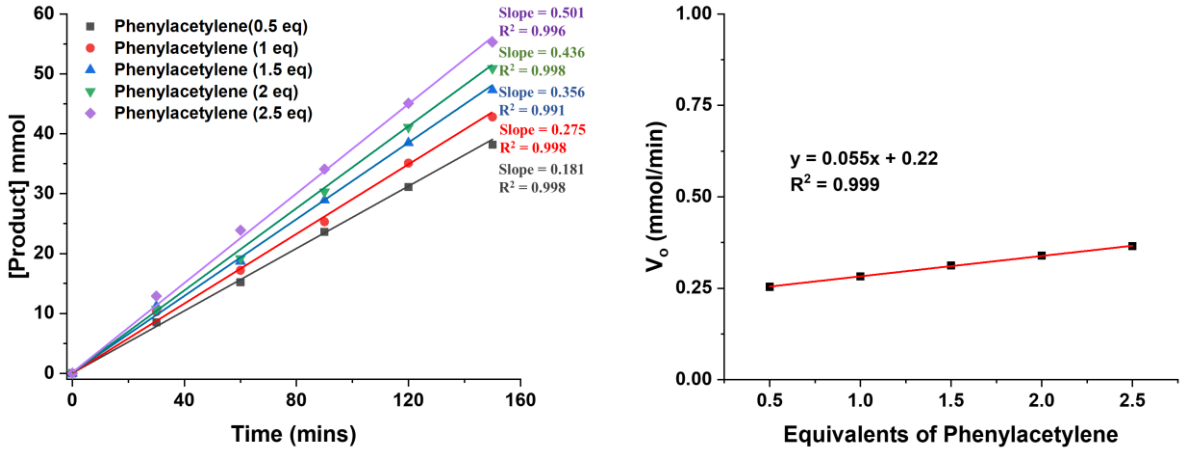

Fig. 6.16 *(i) Rate of product formation in presence of 0.5 to 2.5 equivalent of phenylacetylene (ii) Linear plot indicates first order dependence on phenylacetylene*

The reusability of the catalyst, under the optimized reaction condition was explored using benzaldehyde, piperidine, and phenylacetylene as the model reactants. After completion of reaction, the catalyst was recovered by simple filtration (yellow solid) and used for subsequent runs. Marginal change in the yield and enantioselectivity was noticed during the five cycles of reaction (*Fig. 6.17*). The identity of the recovered catalyst was established by FTIR, UV-visible, XPS and CHN analysis.

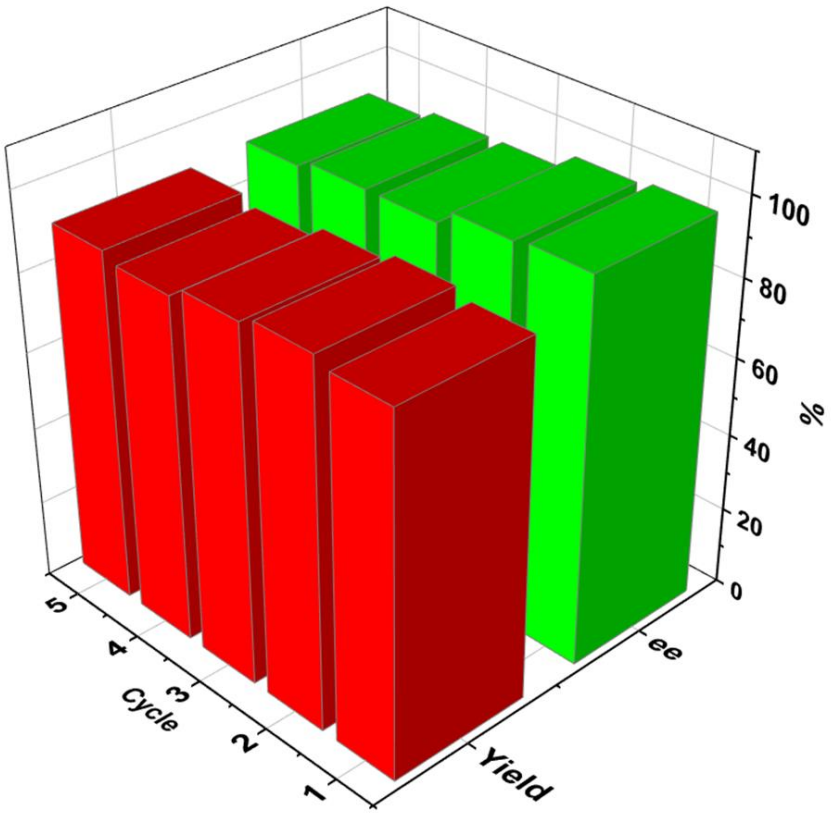

Fig. 6.17 *Recyclability result of* ***CuAL*** *catalyzed synthesis of propargylamine*

The FTIR spectra of the recovered catalyst has been compared with that of **CuAL** and phenylacetylene (*Fig. 6.18*). There is 8 cm^{-1} shift in stretching frequency of imine bond towards the higher wavenumber compared to the parent complex which indicate weakening of the copper-nitrogen bond. This weakening might occur due to the addition of phenylethyn-1-ide ion into the coordination sphere of **CuAL** and resulting the copper-acetylide complex (**CuAL-C_8H_5**). The absence of intense peak at about 3300 cm^{-1} (attributed to C≡C−H stretching) confirms the elimination of acidic proton from phenylacetylene molecule. The stretching frequency of C≡C bond, appearing in the range of 2200 to 2400 cm^{-1}, also indicates that the isolated copper complex is **CuAL-**C_8H_5. The solid-state UV-visible spectra of **CuAL-**C_8H_5 is similar to that of **CuAL** except for an additional peak at 461 nm, which might appear due to the charge transfer between metal and phenylethyn-1-ide ion (*Fig. 6.19*). The CHN analysis confirms the formation of copper-acetylide complex along with the presence of methanol

molecules $[Cu_2(C_{23}H_{33}NO_7)_2(C_8H_5)_2(CH_3OH)_3]$ (calculated, C(60.22), H(6.84), N(2.16), found C(59.88), H(6.51), N(2.48). The XPS analysis of the recovered complex exhibited very intense peaks at 932 and 934 eV ($Cu2p_{3/2}$) along with 952 and 954 eV (Cu $2p_{1/2}$) supporting the conservation of cupric ion (*Fig. 6.20 and 6.21*).

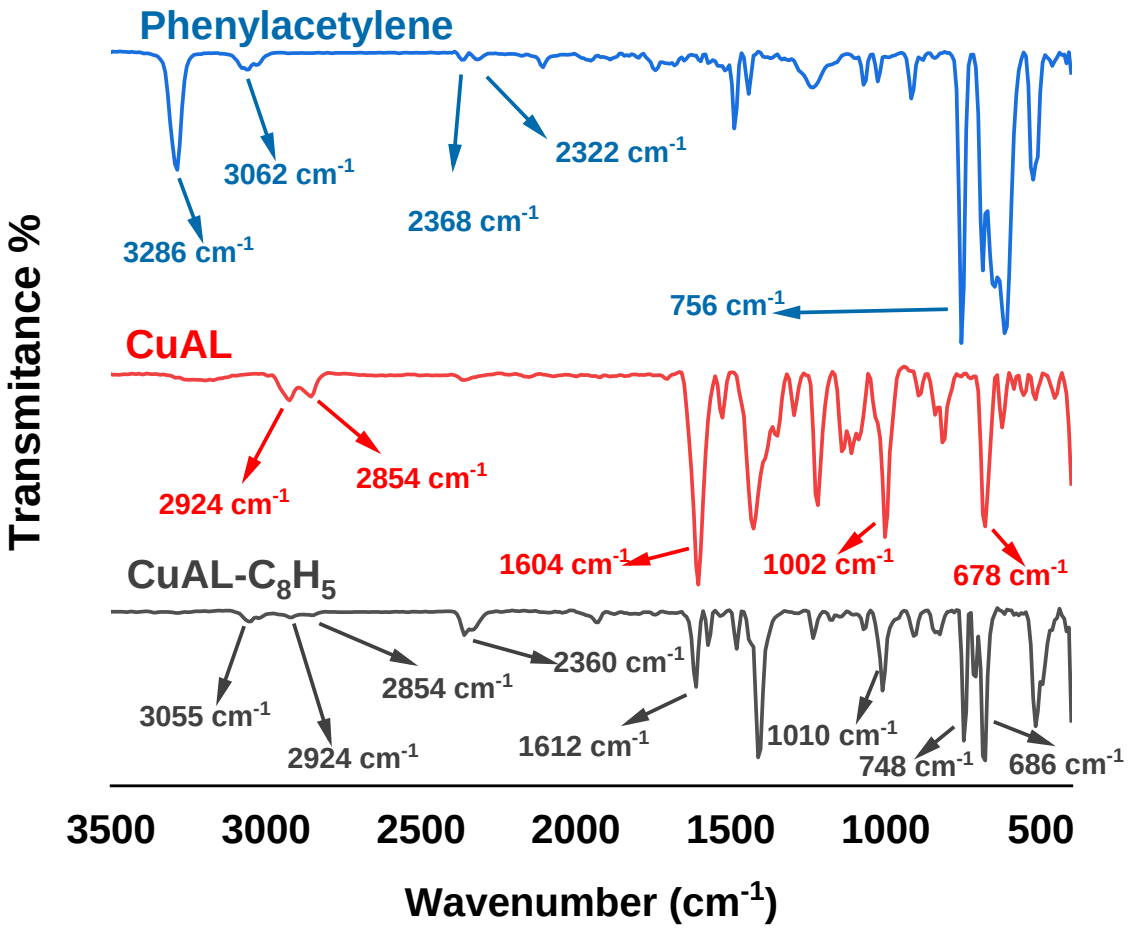

Fig. 6.18 *FTIR spectra of phenylacetylene,* ***CuAL*** *and* ***CuAL-C_8H_5***

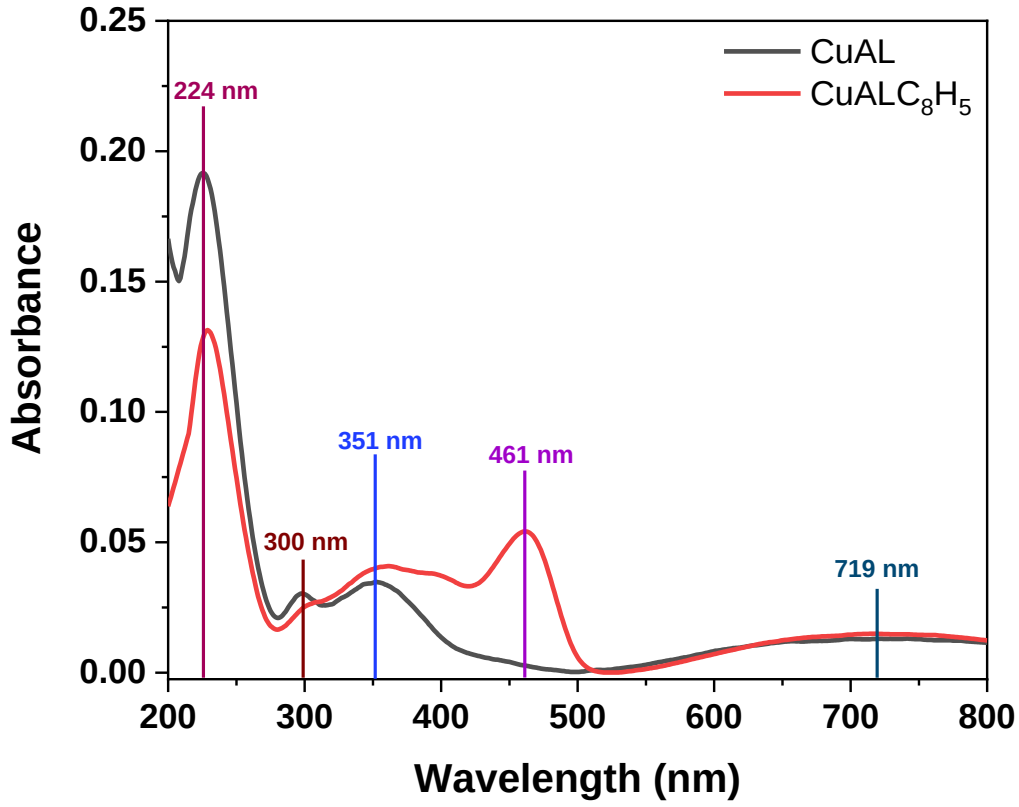

Fig. 6.19 *UV-visible spectra of* ***CuAL*** *and* ***CuAL-C$_8$H$_5$***

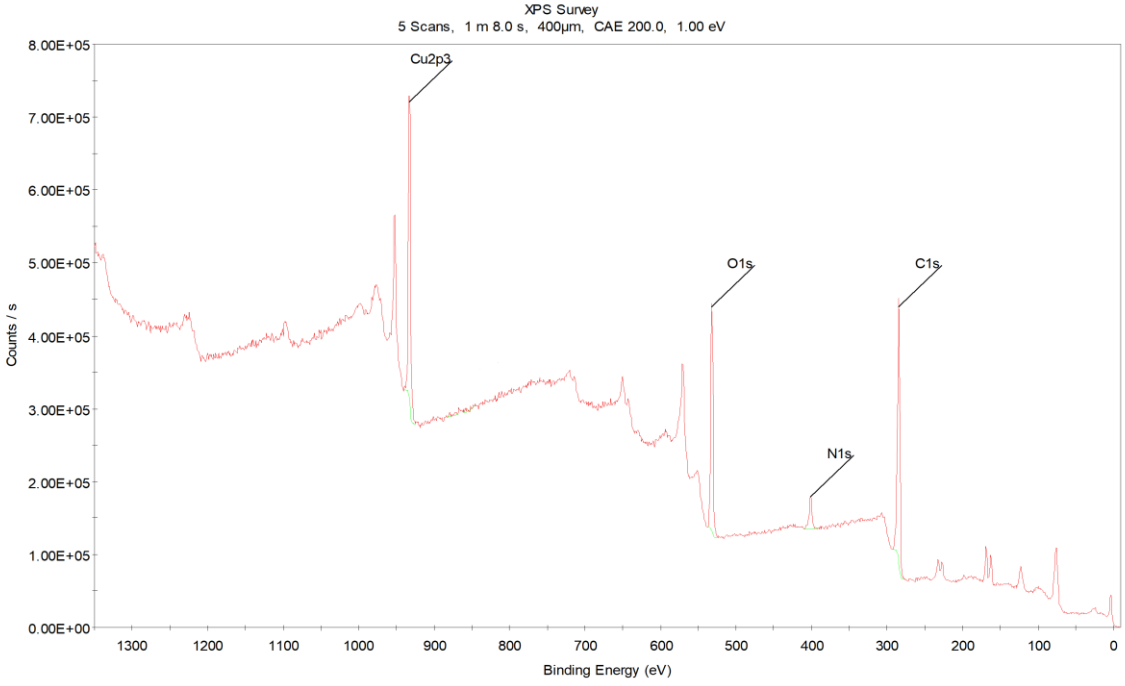

Fig. 6.20 *XPS survey spectra of* ***CuAL-C$_8$H$_5$***

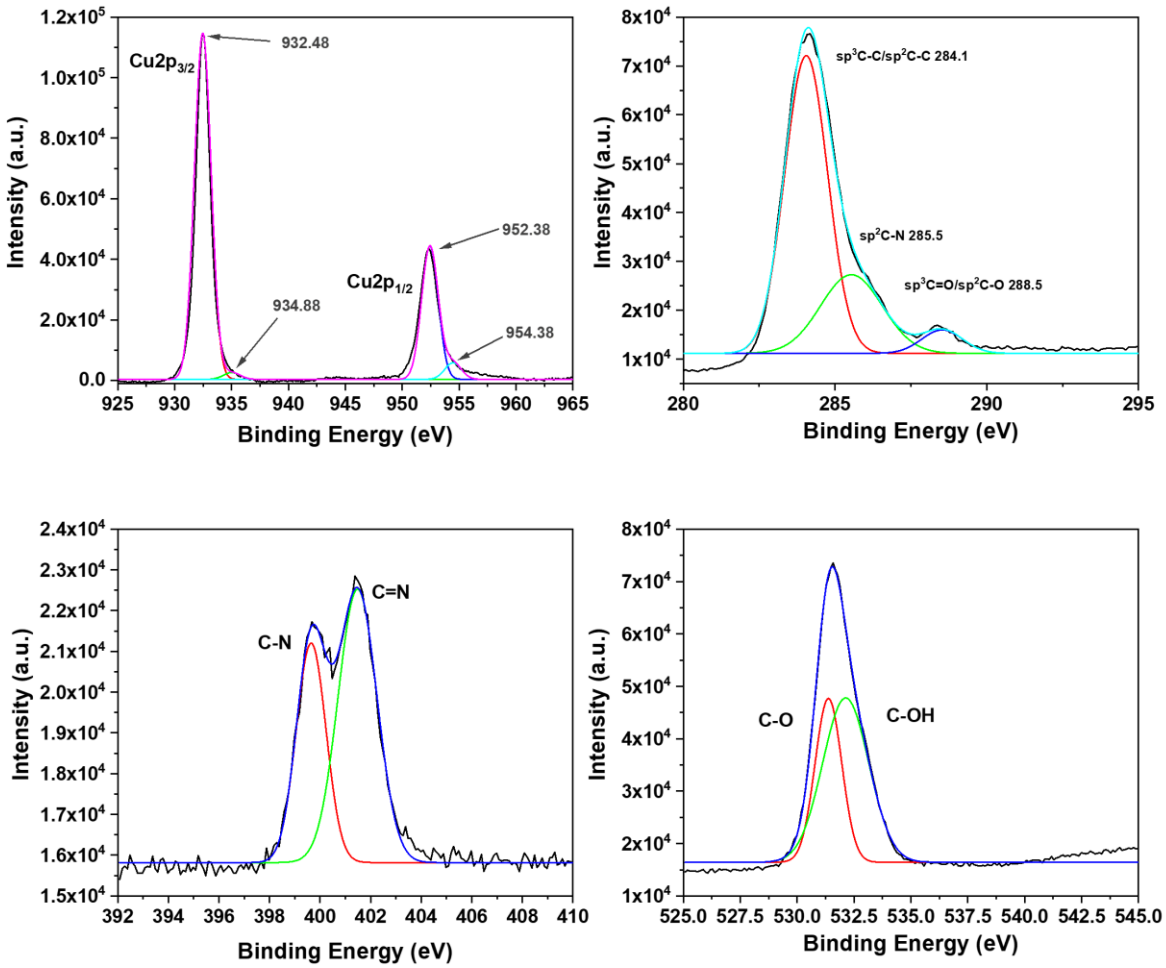

Fig. 6.21 *High resolution Cu2p, C1s, N1s and O1s XPS spectra present in* ***CuAL-C$_8$H$_5$***

6.4 Conclusion

In conclusion, we have synthesized an octyloxy group containing glycoconjugate and its dinuclear cupric complex. Crystal structure of the complex confirmed the dinuclear arrangement of copper in 1:1 stoichiometry with ligand. The metal complexes are arranged in a 1-D array via intermolecular hydrogen bonding among free and coordinated methanol molecules along with the ligand unit. Further, the complex has been used in catalytic synthesis of asymmetric propargylamines with a faster rate and higher yield under solvent-free condition using A^3 coupling reaction. Twenty derivatives of propargylamines including six new compounds has been synthesized in good to excellent yield (82-95%) and enantiomeric excess (87-99%). During the mechanistic studies, formation of aminals (1,1'-

(phenylmethylene)dipiperidine) as an intermediate was established by ^{1}H-NMR and X-ray crystallography whereas the presence of iminium ion in the reaction mixture was confirmed by HRMS studies. The coupling reaction was found to be the first order with respect to each component like catalyst, aldehydes, cyclic amines and alkynes. The copper-acetylide complex was isolated from the reaction mixture and reused for another four cycles, without any appreciable change in enantioselectivity and product yield.

References

1. Koradin, C.; Polborn, K.; Knochel, P., Enantioselektive Synthese von Propargylaminen durch Kupfer-katalysierte Addition von Alkinen an Enamine. Angewandte Chemie 2002, 114, 2651-2654.

2. Lauder, K.; Toscani, A.; Scalacci, N.; Castagnolo, D., Synthesis and reactivity of propargylamines in organic chemistry. Chemical reviews 2017, 117, 14091-14200.

3. Langston, J. W.; Irwin, I.; Langston, E. B.; Forno, L. S., Pargyline prevents MPTP-induced parkinsonism in primates. Science 1984, 225, 1480-1482.

4. Chen, J. J.; Swope, D. M., Clinical pharmacology of rasagiline: a novel, second-generation propargylamine for the treatment of Parkinson disease. The journal of clinical pharmacology 2005, 45, 878-894.

5. Birks, J.; Flicker, L., Selegiline for Alzheimer's disease. Cochrane Database of Systematic Reviews 2003, 1, 1-32.

6. Dhanasekaran, S.; Kannaujiya, V. K.; Biswas, R. G.; Singh, V. K., Enantioselective A3-Coupling Reaction Employing Chiral CuI-i PrpyboxdiPh/N-Boc-(L)-Proline Complex under Cooperative Catalysis: Application in the Synthesis of (Indol-2-yl) methanamines. The Journal of Organic Chemistry 2019, 84, 3275-3292.

7. Wei, C.; Li, C.-J., Enantioselective direct-addition of terminal alkynes to imines catalyzed by copper (I) pybox complex in water and in toluene. Journal of the American Chemical Society 2002, 124, 5638-5639.

8. Wei, C.; Mague, J. T.; Li, C.-J., Cu(I)-catalyzed direct addition and asymmetric addition of terminal alkynes to imines. Proceedings of the National Academy of Sciences 2004, 101, 5749-5754.

9. Bisai, A.; Singh, V. K., Enantioselective one-pot three-component synthesis of propargylamines. Organic letters 2006, 8, 2405-2408.

10. Nakamura, S.; Ohara, M.; Nakamura, Y.; Shibata, N.; Toru, T., Copper-Catalyzed Enantioselective Three-Component Synthesis of Optically Active Propargylamines from Aldehydes, Amines, and Aliphatic Alkynes. Chemistry–A European Journal 2010, 16, 2360-2362.

11. Ohara, M.; Hara, Y.; Ohnuki, T.; Nakamura, S., Direct enantioselective three-component synthesis of optically active propargylamines in water. Chemistry–A European Journal 2014, 20, 8848-8851.

12. Steiner, I.; Aufdenblatten, R.; Togni, A.; Blaser, H.-U.; Pugin, B. t., Novel silica gel supported chiral biaryl-diphosphine ligands for enantioselective hydrogenation. Tetrahedron: Asymmetry 2004, 15, 2307-2311.

13. Zhao, C.; Seidel, D., Enantioselective A3 reactions of secondary amines with a Cu (I)/acid–thiourea catalyst combination. Journal of the American Chemical Society 2015, 137, 4650-4653.

14. Gommermann, N.; Koradin, C.; Polborn, K.; Knochel, P., Enantioselective, Copper (i)-Catalyzed Three-Component Reaction for the Preparation of Propargylamines. Angewandte Chemie International Edition 2003, 42, 5763-5766.

15. Gommermann, N.; Knochel, P., Practical highly enantioselective synthesis of terminal propargylamines. An expeditious synthesis of (S)-(+)-coniine. Chemical communications 2004, 20, 2324-2325.

16. Gommermann, N.; Knochel, P., 2-Phenallyl as a versatile protecting group for the asymmetric one-pot three-component synthesis of propargylamines. Chemical communications 2005, 33, 4175-4177.

17. Gommermann, N.; Knochel, P., Practical highly enantioselective synthesis of propargylamines through a copper-catalyzed one-pot three-component condensation reaction. Chemistry–A European Journal 2006, 12, 4380-4392.

18. Knöpfel, T. F.; Aschwanden, P.; Ichikawa, T.; Watanabe, T.; Carreira, E. M., Readily available biaryl P, N ligands for asymmetric catalysis. Angewandte Chemie International Edition 2004, 43, 5971-5973.

19. Aschwanden, P.; Stephenson, C. R.; Carreira, E. M., Highly enantioselective access to primary propargylamines: 4-piperidinone as a convenient protecting group. Organic Letters 2006, 8, 2437-2440.

20. Fan, W.; Ma, S., An easily removable stereo-dictating group for enantioselective synthesis of propargylic amines. Chemical Communications 2013, 49, 10175-10177.

21. Cardoso, F. S.; Abboud, K. A.; Aponick, A., Design, preparation, and implementation of an imidazole-based chiral biaryl P, N-ligand for asymmetric catalysis. Journal of the American Chemical Society 2013, 135, 14548-14551.

22. Naeimi, H.; Moradian, M., Thioether-based copper (I) Schiff base complex as a catalyst for a direct and asymmetric A3-coupling reaction. Tetrahedron: Asymmetry 2014, 25, 429-434.

23. Rokade, B. V.; Barker, J.; Guiry, P. J., Development of and recent advances in asymmetric A3 coupling. Chemical Society Reviews 2019, 48, 4766-4790.

24. Tajbaksh, M.; Farhang, M.; Mardani, H. R.; Hosseinzadeh, R.; Sarrafi, Y., Cu (II) salen complex catalyzed synthesis of propargylamines by a three-component coupling reaction. Chinese Journal of Catalysis 2013, 34, 2217-2222.

25. Kumari, S.; Shekhar, A.; Pathak, D. D., Synthesis and characterization of a Cu (II) Schiff base complex immobilized on graphene oxide and its catalytic application in the green synthesis of propargylamines. RSC Advances 2016, 6, 15340-15344.

26. Shouli, A.; Menati, S.; Sayyahi, S., Copper(II) chelate-bonded magnetite nanoparticles: A new magnetically retrievable catalyst for the synthesis of propargylamines. Comptes Rendus Chimie 2017, 20, 765-772.

27. Sharghi, H.; Khoshnood, A.; Khalifeh, R., Three-component synthesis of propargylamine derivatives via 1, 4-dihydroxyanthraquinone-copper(II) complexes as an efficient catalyst under solvent-free conditions. Iranian Journal of Science and Technology (Sciences) 2012, 36, 25-35.

28. Madduluri, V. K.; Sah, A. K., Metal complexes of 4, 6-O-ethylidene-β-D-glucopyranosylamine derivatives and their application in organic synthesis. Carbohydrate Research 2019, 485, 107798.

29. Mishra, Santosh K., Parikh, Anuvasita. Rangan, Krishnan. Sah, A. K. Synthesis of Catalyst Using Bio-benign Precursors and Its Application in One-Pot Catalytic Synthesis of Imidazo[1,2-a]pyridines, ChemistrySelect., 2023, 8, e202300129.

30. Diéguez, M.; Pàmies, O.; Ruiz, A.; Díaz, Y.; Castillón, S.; Claver, C., Carbohydrate derivative ligands in asymmetric catalysis. Coordination chemistry reviews 2004, 248, 2165-2192.

31. Diéguez, M.; Claver, C.; Pàmies, O., Recent Progress in Asymmetric Catalysis Using Chiral Carbohydrate-Based Ligands. European Journal of Organic Chemistry 2007, 2007, 4621-4634.

32. Mishra, S. K.; Parikh, A.; Rangan, K.; Sah, A. K., Crystal Structure of N-(2-hydroxynapthylidene)-L-isoleucinyl-4, 6-O-ethylidene-β-D-glucopyranosylamine and an Insight from Experimental and Theoretical Calculations. Crystal Research and Technology 2007, 58, 2200209.

33. Nakamoto, K.; Martell, A. E., Infrared Spectra of Metal-Chelate Compounds. I. A Normal Coordinate Treatment on Bis-(Acetylacetonato)-Cu(II). The Journal of Chemical Physics 1960, 32, 588-597.

34. Seliskar, C. J., Spectroscopy of pyridoxal analogs. 2. N-Ethylsalicylaldimines. The Journal of Physical Chemistry 1977, 81, 1331-1334.

35. Li, H.; Wang, L.; Yan, S.; Chen, J.; Zhang, M.; Zhao, R.; Niu, X.; Wang, K., Fusiform-like metal-organic framework for enantioselective discrimination of tryptophan enantiomers. Electrochimica Acta 2022, 419, 140409.

36. Zakeri, M.; Moghadam, M.; Mirkhani, V.; Tangestaninejad, S.; Mohammadpoor-Baltork, I.; Pahlevanneshan, Z., Copper containing nanosilica thioalated dendritic material: A

recyclable catalyst for synthesis of benzimidazoles and benzothiazoles. Applied Organometallic Chemistry 2018, 32, e3937.

37. Okpalugo, T.; Papakonstantinou, P.; Murphy, H.; McLaughlin, J.; Brown, N., High resolution XPS characterization of chemical functionalised MWCNTs and SWCNTs. Carbon 2005, 43, 153-161.

38. Abbate, M.; Sacchi, M.; Wnuk, J.; Schreurs, L.; Wang, Y.; Lof, R.; Fuggle, J., Polarization dependence of the Cu 2p absorption spectra in (Bi 0.84 Pb 0.16)2Sr2CaCu2O8. Physical Review B 1990, 42, 7914.

39. Bikas, R.; Ajormal, F.; Emami, M.; Noshiranzadeh, N.; Kozakiewicz, A., Catalytic oxidation of benzyl alcohols by new Cu(II) complexes of 1, 3-oxazolidine based ligand obtained from a solvent free reaction. Inorganica Chimica Acta 2018, 478, 77-87.

40. Bikas, R.; Krawczyk, M. S.; Lis, T., Catalytic Activity of Azido-Bridged Dinuclear Cu(II)-Hydrazone Coordination Compound in Green Click Synthesis of 1, 2, 3-Triazoles. ChemistrySelect 2020, 5, 6759-6764.

41. Aslkhademi, S.; Noshiranzadeh, N.; Sadjadi, M. S.; Mehrani, K.; Farhadyar, N., Synthesis, crystal structure and investigation of the catalytic and spectroscopic properties of a Zn (II) complex with coumarin-hydrazone ligand. Polyhedron 2019, 160, 115-122.

42. Madduluri, V. K.; Mishra, S. K.; Sah, A. K., Synthesis and catalytic application of d-glucose derived ytterbium(III) complex in Biginelli reaction. Inorganic Chemistry Communications 2020, 120, 108165.

43. Liu, X.; Lin, B.; Zhang, Z.; Lei, H.; Li, Y., Copper(ii) carboxymethylcellulose (CMC-CuII) as an efficient catalyst for aldehyde–alkyne–amine coupling under solvent-free conditions. RSC Advances 2016, 6, 94399-94407.

44. Bukowska, A.; Bukowski, W.; Bester, K.; Hus, K., Polymer supported copper(II) amine-imine complexes in the C-N and A3 coupling reactions. Applied Organometallic Chemistry 2017, 31, e3847.

45. Daryanavard, M.; Ataei, A.; Sheykhabadi, P. G.; Rafiee, E.; Joshaghani, M., A Novel Recyclable Ni/Cu/Fe Termetallic Nanocatalyst for the Synthesis of Propargylamines through the A3-Coupling Reactions. ChemistrySelect 2020, 5, 18-27.

46. Marquez, C.; Cirujano, F. G.; Van Goethem, C.; Vankelecom, I.; De Vos, D.; De Baerdemaeker, T., Tunable Prussian blue analogues for the selective synthesis of propargylamines through A3 coupling. Catalysis Science & Technology 2018, 8, 2061-2065.

47. Palchak, Z. L.; Lussier, D. J.; Pierce, C. J.; Larsen, C. H., Synthesis of tetrasubstituted propargylamines from cyclohexanone by solvent-free copper(II) catalysis. Green Chemistry 2015, 17, 1802-1810.

Chapter 7

Conclusion and Future Scope

Chapter 7

7.1 General conclusion

Glycoconjugates are involved in various biological events like cell-cell interaction, fertilization, embryonic development, pathogenesis, etc. They are also used in synthetic chemistry due to their metal binding abilities and multiple chiral centers, however, carbohydrate derivatives offer problems like mutarotation, hydrolysis and low solubilities in organic solvents. These hurdles can be overcome by applying the protection at 4- and 6-positions and derivatizing the C-1 position. The compound 4,6-*O*-ethylidene-β-D-glucosylamine (**EGNH$_2$**) is soluble in DMSO as well as in hot alcohols and offers stability in the β-anomeric from. By further derivatizing **EGNH$_2$** with imine and amide bonds increase the number of binding sites as well. The synthesis of glycopeptides and the theoretical as well as experimental aspects of their configurational isomers have been explored. The synthesized glycoconjugates have been used for selective detection of aspartic acid or cysteine and their copper(II) complexes have been used for catalytic synthesis of imidazo[1,2-*a*]pyridines. The synthesis of amphiphilic glycoconjugates along with its copper(II) complex have also been reported and they are applied for the asymmetric synthesis of propargylamines.

7.2 Specific conclusions

The thesis has been divided into seven chapters, where first chapter includes brief introduction about carbohydrates and different protocols for the synthesis of *N*-glycoconjugates. This chapter also contains applications of glycoconjugates in the field of amino acid sensing and the catalytic activities of their metal complexes.

Second chapter provides the details of commercially available chemicals, synthesized starting materials, instruments, software and experimental methods used during the entire thesis work.

Chapter 3 elaborates the synthesis of *N*-glycopeptides containing alanine, phenyl alanine, valine, leucine, isoleucine, methionine and tryptophan along with their characterization

methods like Fourier transform infrared, UV–visible absorption and nuclear magnetic resonance spectroscopy. The crystal structures of *N*-glycopeptides confirmed their existence in ketoenamine form in the solid state. The noncovalent intermolecular interactions present in *N*-(2-hydroxynapthylidene)-L-isoleucinyl-4,6-*O*-ethylidene-β-D-glucopyranosylamine have been explored by Hirshfeld surface analysis and 2D fingerprint plots generated using crystallographic data. The structural parameters of one of the glycoconjugate in both the tautomeric forms (ketoenamine and phenolimine) at ground states have been optimized using Hartree–Fock and density functional theory calculations in gaseous and solution phases. Additionally, Mulliken population analysis, molecular electrostatic potential, and natural bond order analysis provide a better understanding of charge distribution, presence of electrophilic/nucleophilic sites, and intramolecular charge transfer, respectively, in the molecule.

Chapter 4 explains the interactions of synthesized *N*-glycopeptide with naturally occurring amino acids using UV-visible absorption and ^{1}H NMR spectroscopy. The receptors containing alanine, valine, isoleucine and methionine moieties interact selectively with aspartic acid, while phenylalanine derivative with cysteine.

Chapter 5 summarizes an efficient method for the synthesis of imidazo[1,2-*a*]pyridines using Cu(II)-complex of *N*-(2-hydroxynapthylidene)-L-leucienyl-4,6-*O*-ethylidene-β-D-glucopyranosylamine, under solvent-free conditions. The complexation between Cu(II) and glycopeptide has been established using HRMS, UV-visible and fluorescence spectroscopy. Further, the stoichiometry and association constant of the glycopeptide with Cu(II) ion have also been calculated. The synthesized catalytic products have been characterized by analytical techniques like NMR and HRMS. The molecular structure of two imidazo[1,2-*a*]pyridines derivatives have been established using single-crystal X-ray diffraction studies. The reusability

of the catalyst up to five cycles have also been explored and the results have shown a marginal loss in its activity which might be due to the handling errors.

Chapter 6 elaborates the synthesis of D-glucose derived amphiphilic glycoconjugate and its copper (II) complex. The structural details of the metal complex have been established by X-ray crystallography and we have also explored its catalytic application in solvent-free one-pot synthesis of chiral propargylamines. This is the first report, where glucopyranosylamine containing Cu(II)-complex has been used as a catalyst for the chiral synthesis of propargylamines. Our method provides a greener route for the synthesis of propargylamines and holds good in the presence of both electron-withdrawing and donating substitutions. We have synthesized twenty trisubstituted propargylamine derivatives in good to excellent yields (82-95%), including six new molecules. All the molecules were characterized by NMR and HRMS analysis and their enantiomeric excess (ee; 87-99%) was confirmed by chiral HPLC. The molecular structure of two propargylamines derivatives have been established using single-crystal X-ray diffraction studies.

7.3 Future scope of this thesis

During the thesis work we have explored the catalytic activity of copper complex of 4,6-*O*-ethylidene-*N*-(2-hydroxy-4-(octyloxy)benzylidene)-β-D-glucopyranosylamine for chiral synthesis of propargylamines. As a continuation of this work, the synthesis of amphiphilic glycoconjugates with longer alkyl chains and their metal binding abilities with other metal ions can be explored. Micellization properties of carbohydrate derived amphiphilic molecules has already been explored. Such molecules are practically useful for drug delivery, chemosensing, catalysis, etc. Trail reaction has been performed to synthesize such ligands along with their Co(II) and Lu(III) complexes. The next step will be to characterize such compounds and test their abilities towards molecular detection as well as catalysis. This work can be further

extended towards exploring the micellization properties of alkylated glycoconjugates and discovering their drug delivering activities.

Appendix A

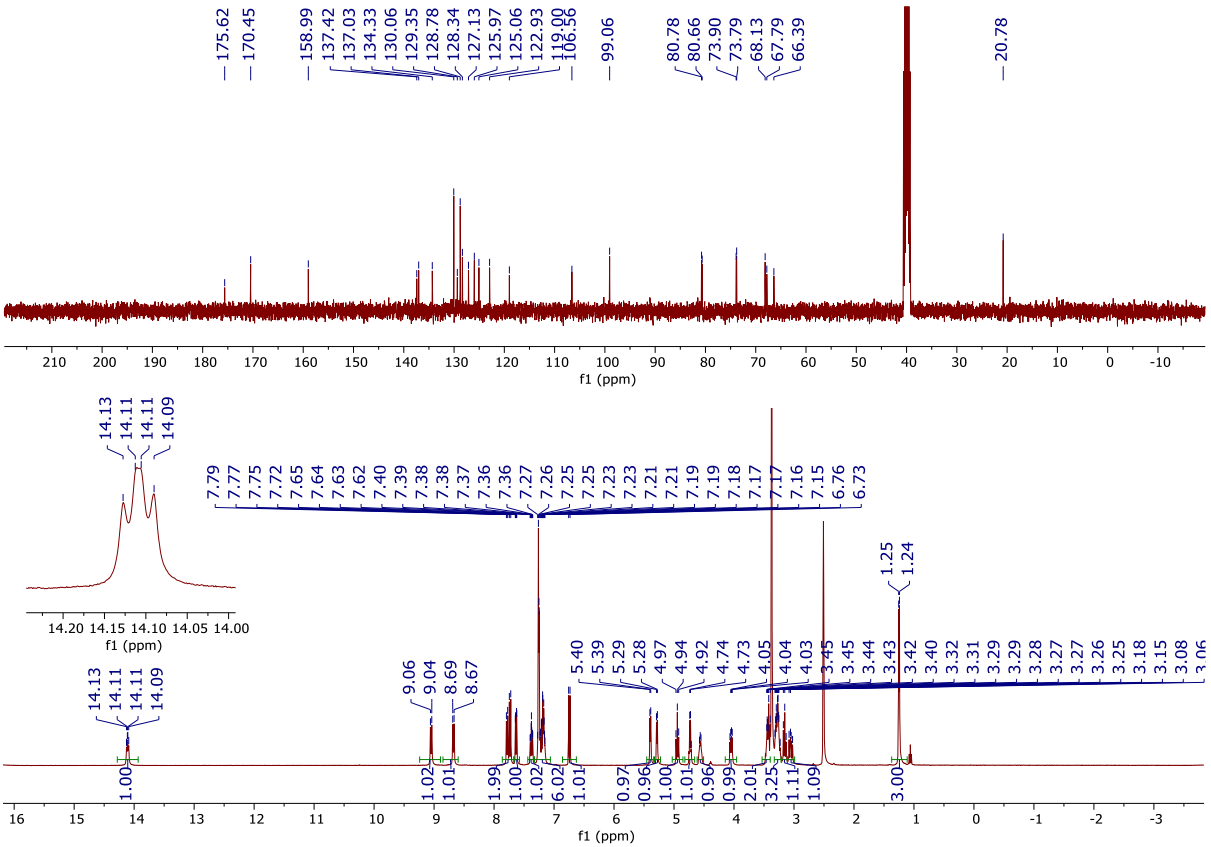

Fig. A1 *^{1}H and ^{13}C-NMR spectrum of **1** (in DMSO-d_6)*

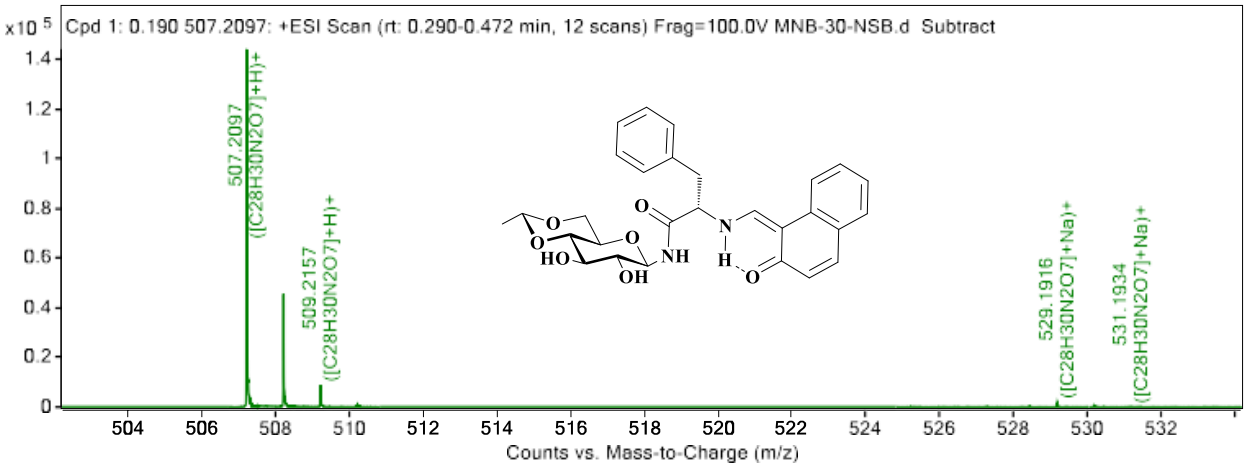

Fig. A2 *HRMS of **1***

Appendix A

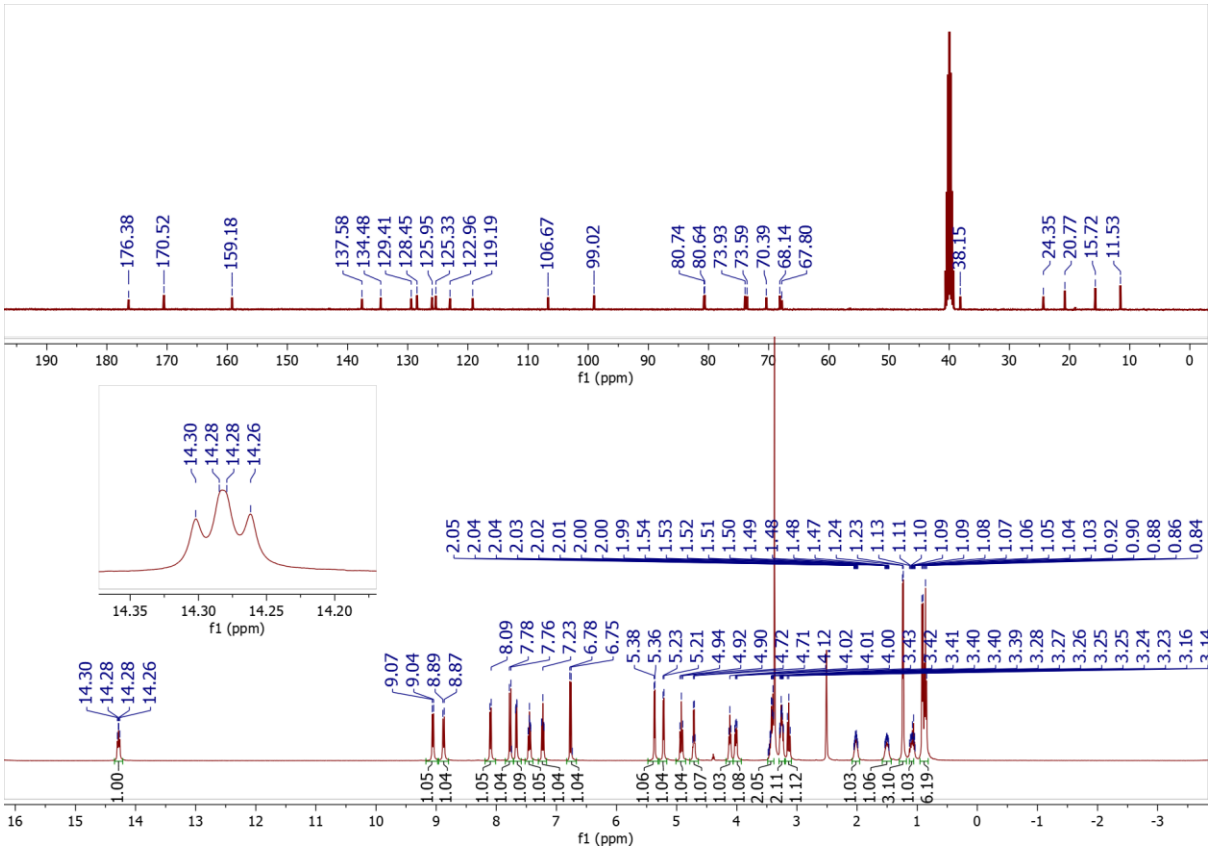

Fig. A3 *^{1}H and ^{13}C-NMR spectrum of **2** (in DMSO-d_6)*

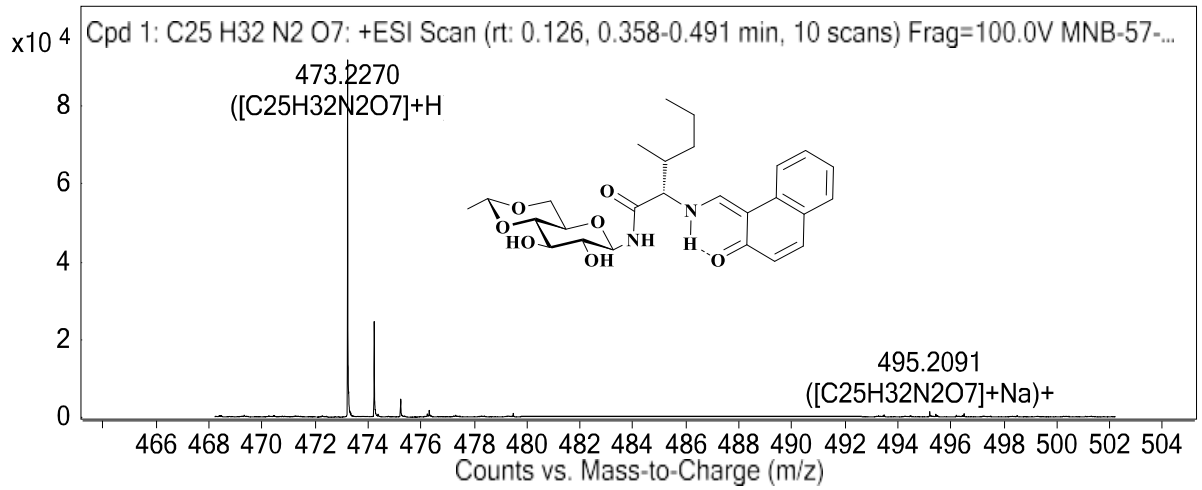

Fig. A4 *HRMS of **2***

Appendix A

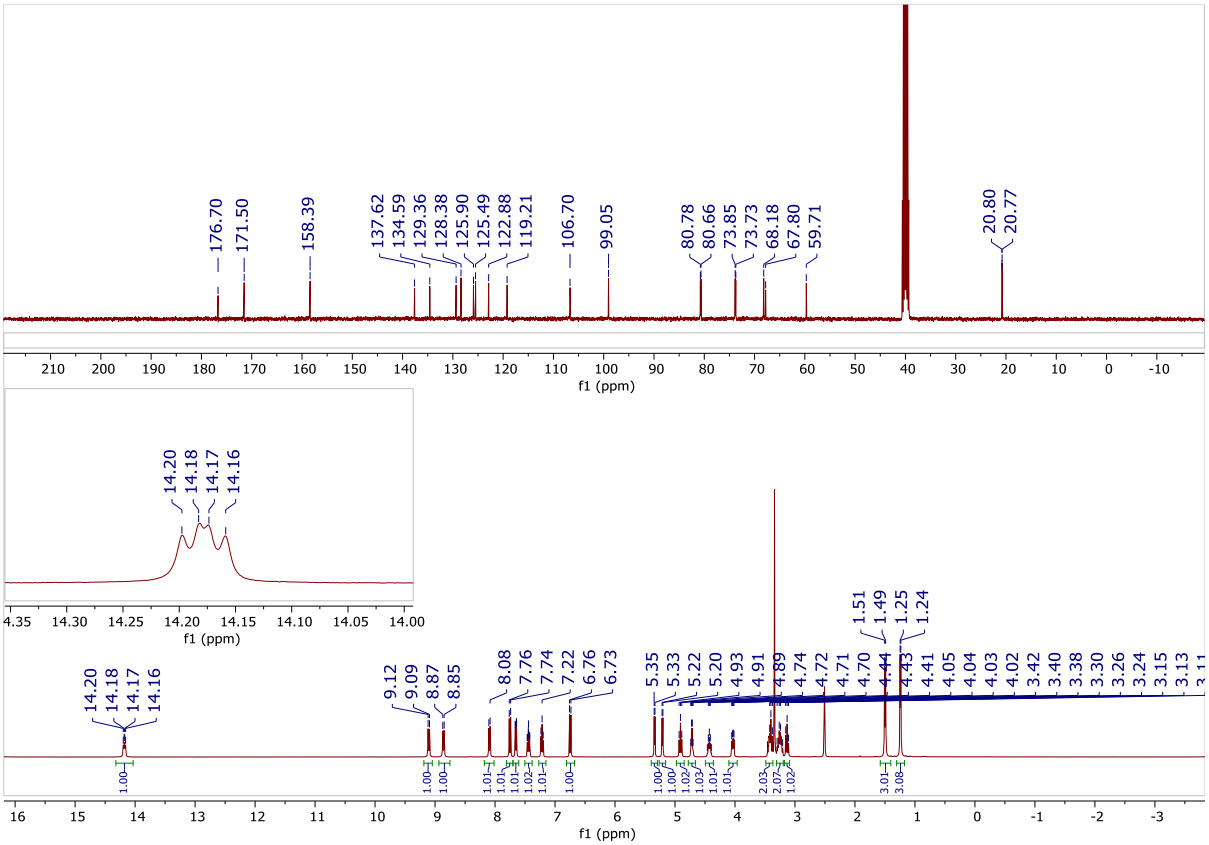

Fig. A5 *^{1}H and ^{13}C-NMR spectrum of **3** (in DMSO-d_6)*

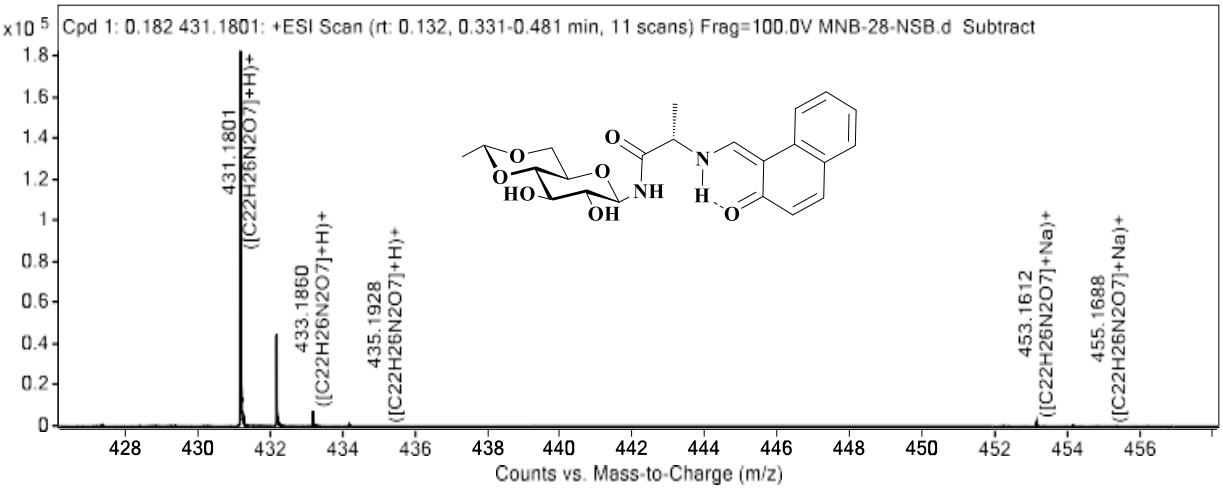

Fig. A6 *HRMS of **3***

Appendix A

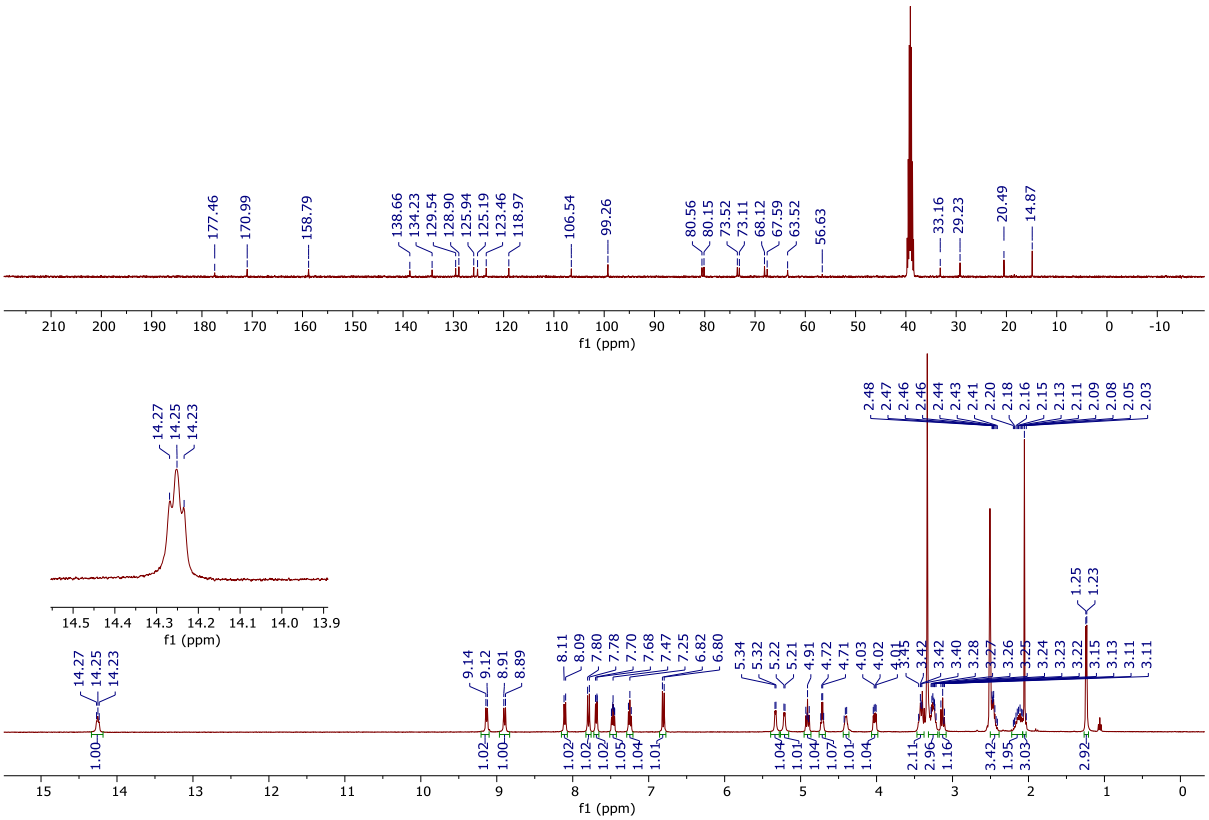

Fig. A7 *^{1}H and ^{13}C-NMR spectrum of **4** (in DMSO-d_6)*

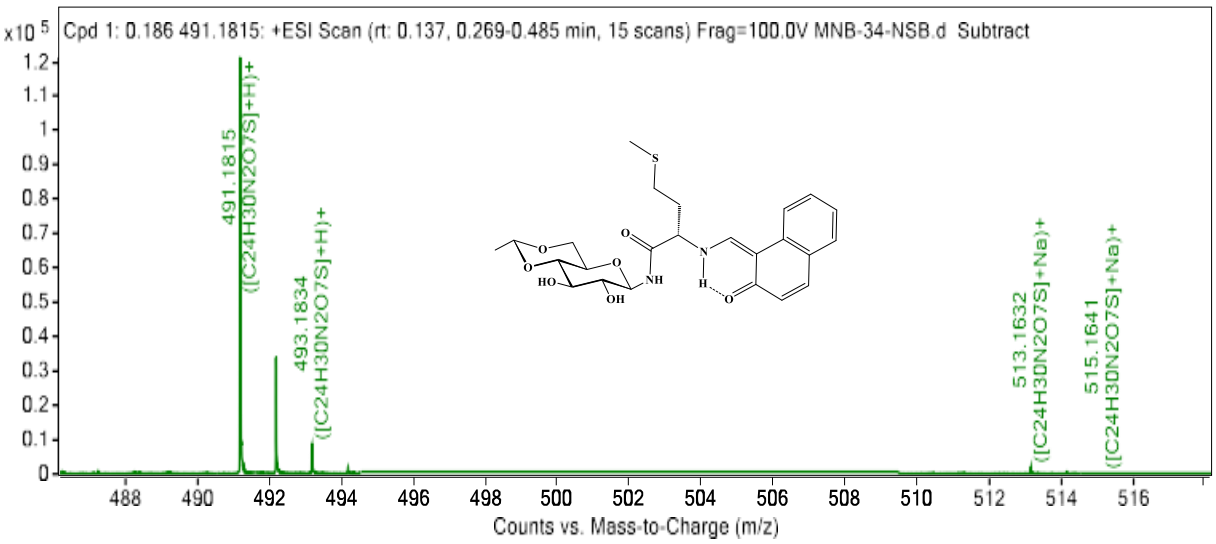

Fig. A8 *HRMS of **4***

Appendix A

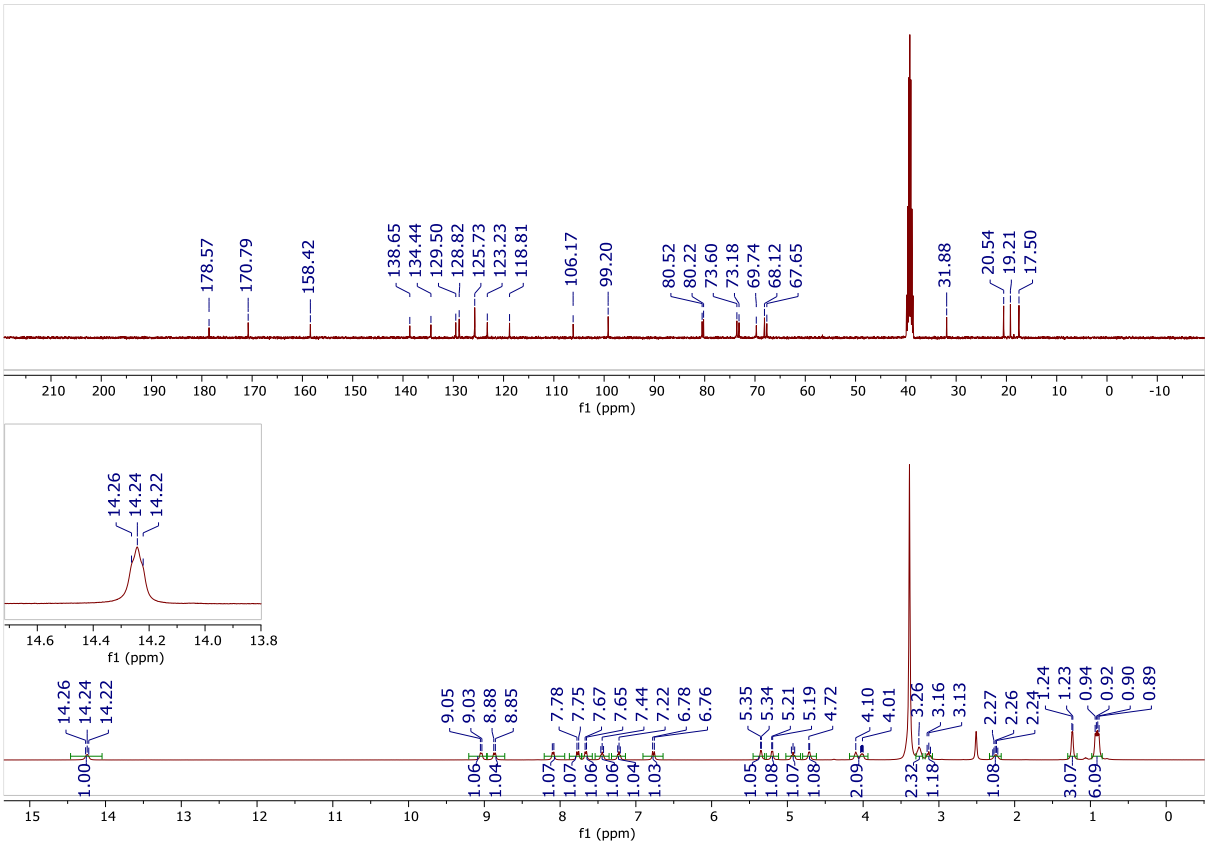

Fig. A9 *^{1}H and ^{13}C-NMR spectrum of **5** (in DMSO-d_6)*

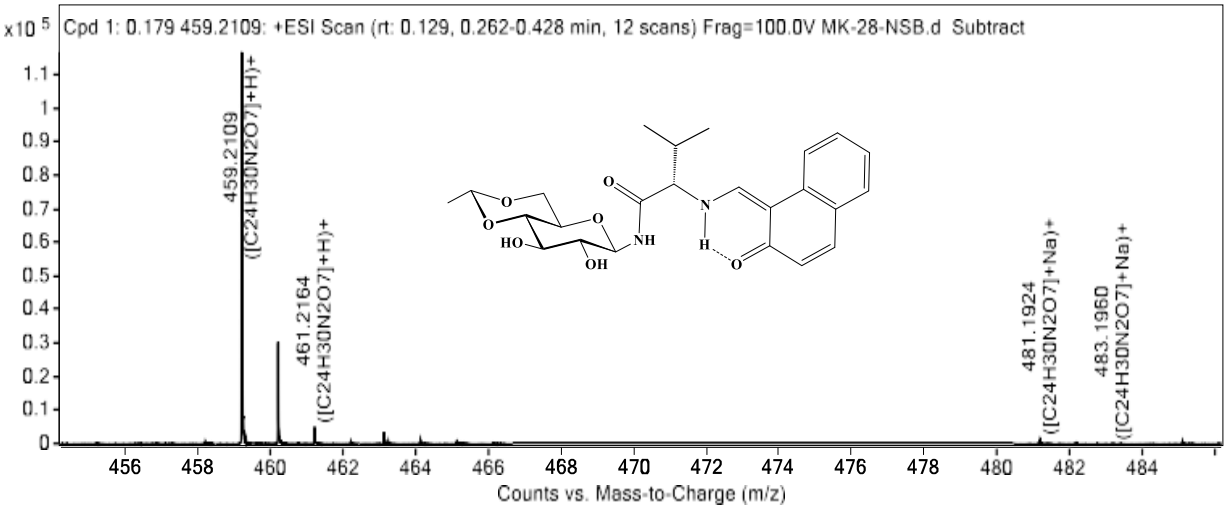

Fig. A10 *HRMS of **5***

Appendix A

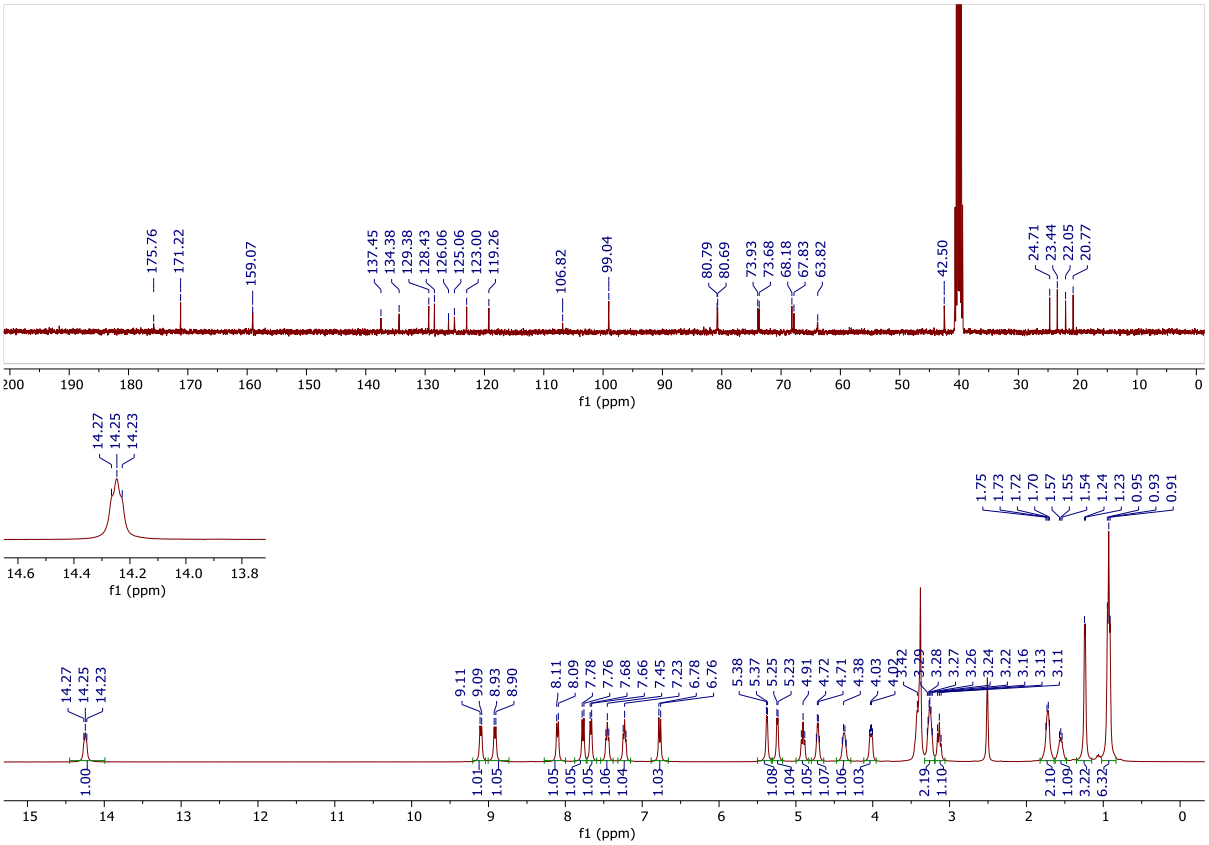

Fig. A11 *^{1}H and ^{13}C-NMR spectrum of **6** (in DMSO-d_6).*

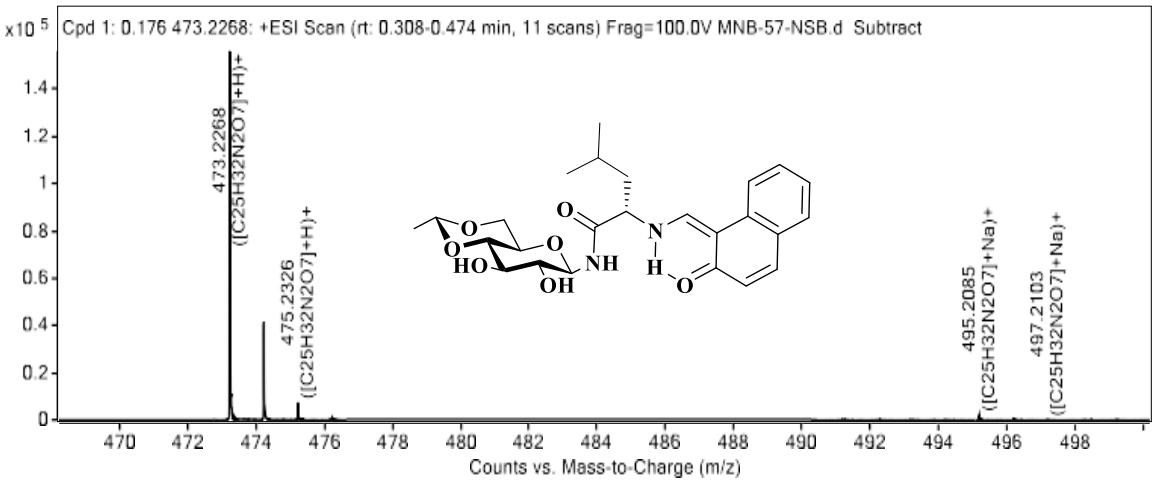

Fig. A12 *HRMS of **6**.*

Appendix A

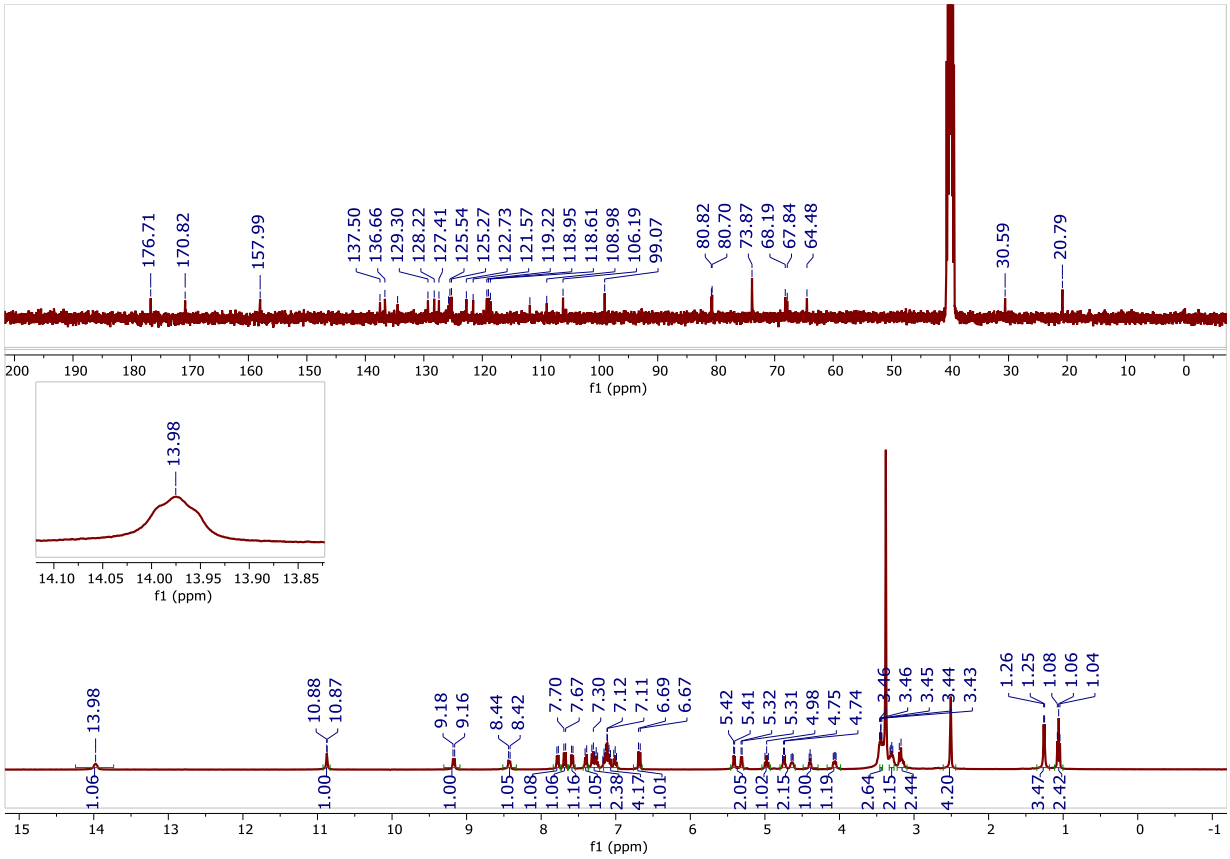

Fig. A13 *^{13}C-NMR spectrum of **7** (in DMSO-d_6).*

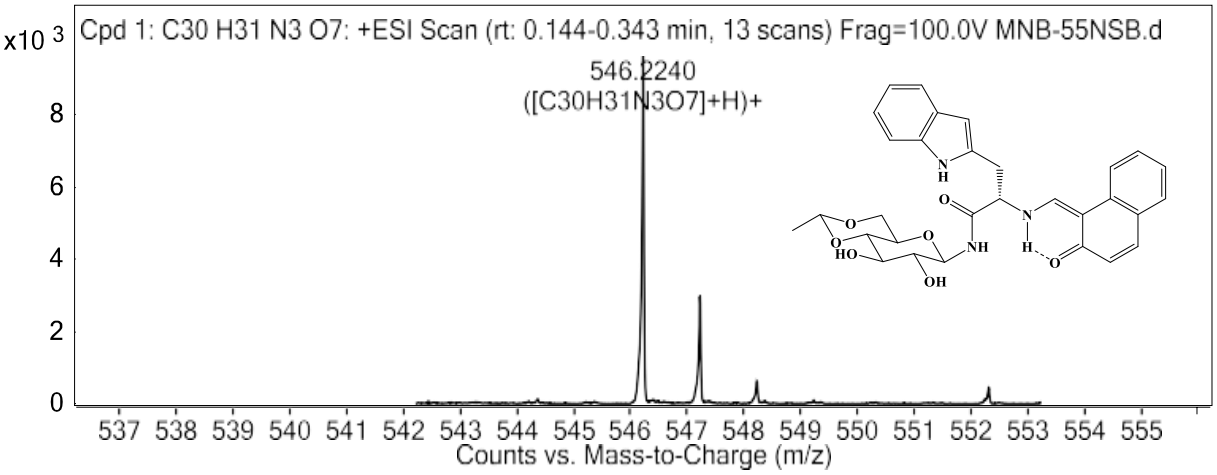

Fig. A14 *HRMS of **7**.*

Appendix A

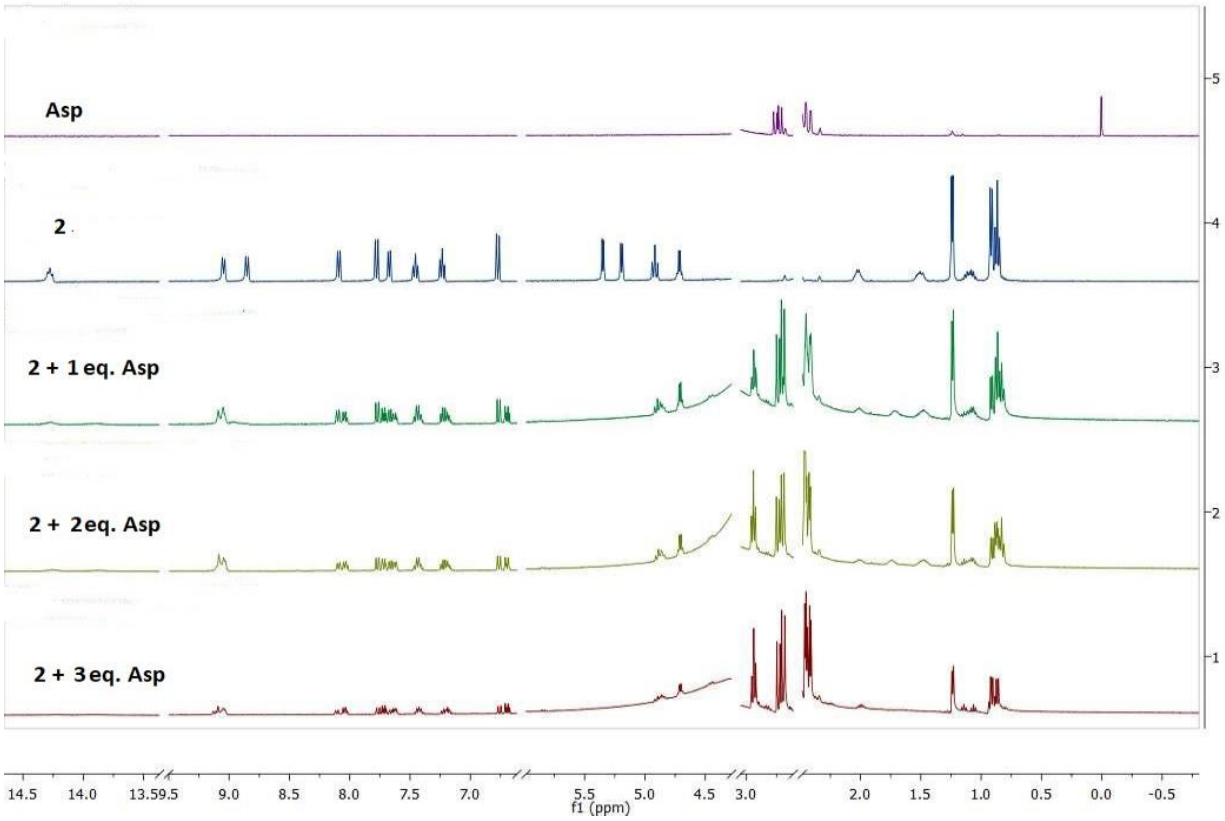

Fig. A15 *^{1}H NMR spectra of host **2** with guest Asp in different ratios showing gradual changes in the spectral pattern; eq. represents equivalent.*

Appendix A

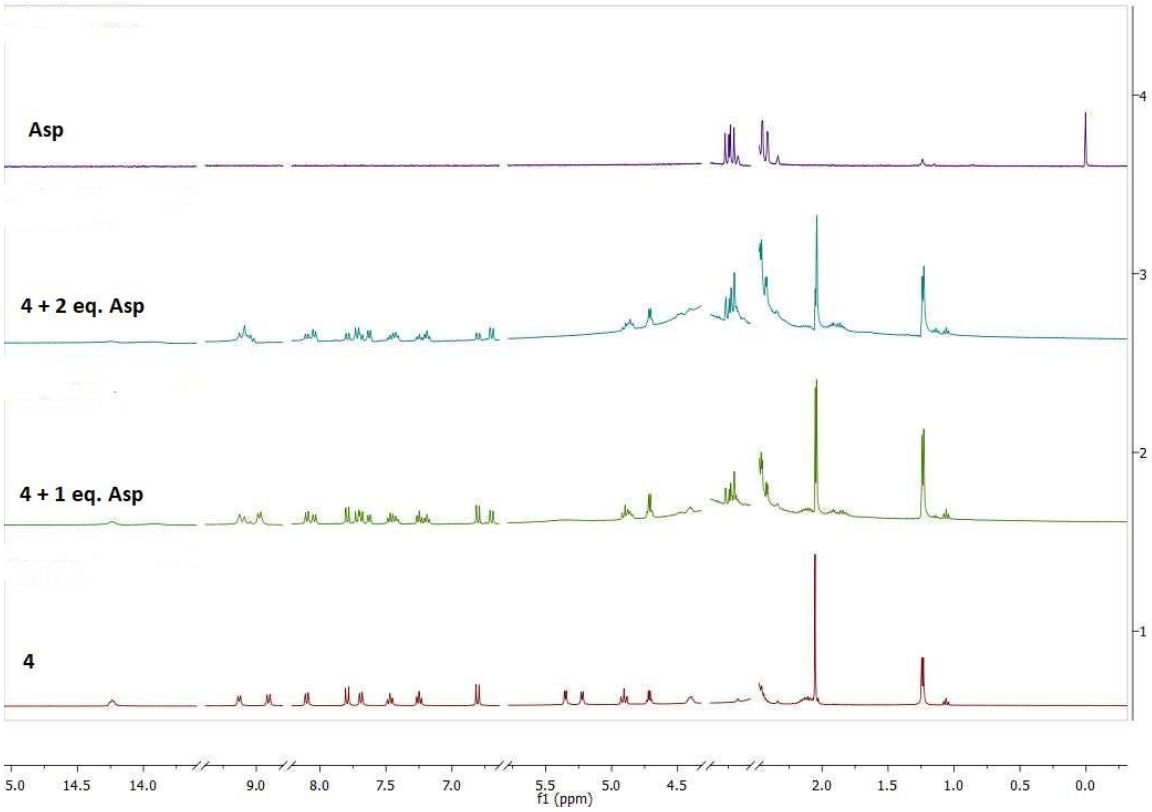

Fig. 16 *^{1}H NMR spectra of host **4** with guest Asp in different ratios showing gradual changes in the spectral pattern; eq. represents equivalent.*

Appendix A

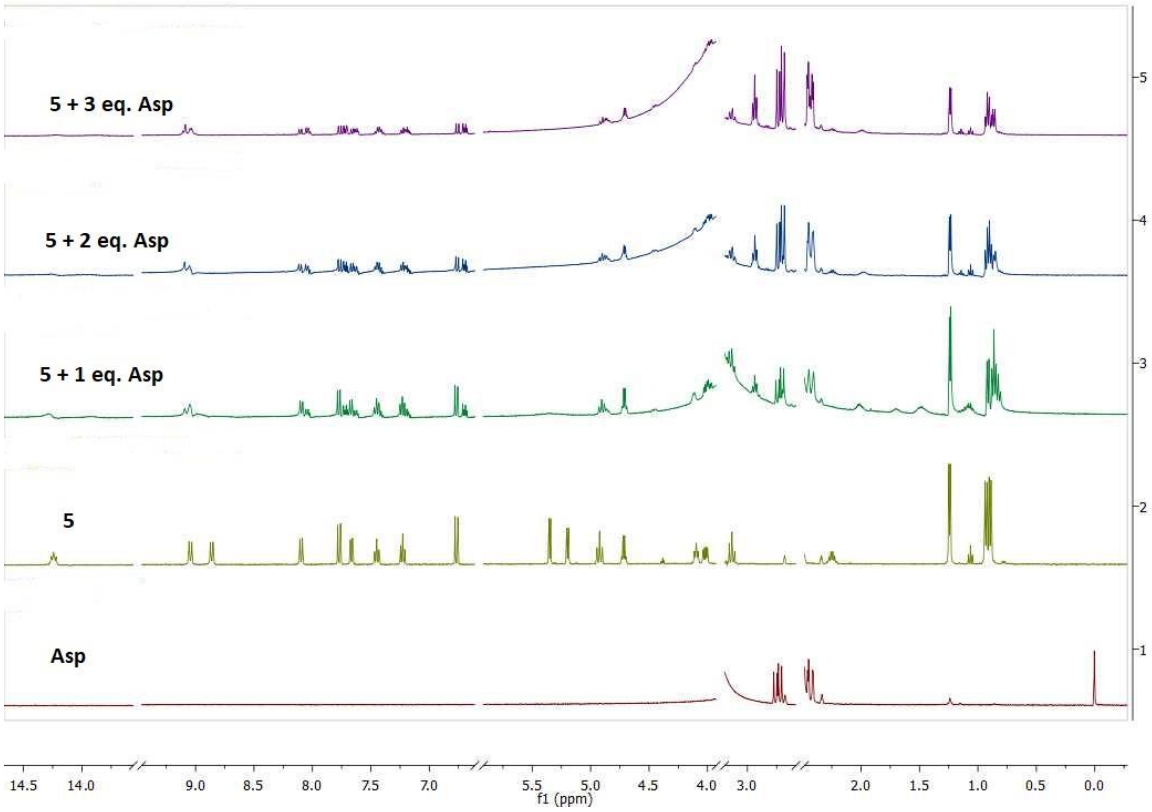

Fig. 17 *^{1}H NMR spectra of host **5** with guest Asp in different ratios showing gradual changes in the spectral pattern; eq. represents equivalent.*

Appendix A

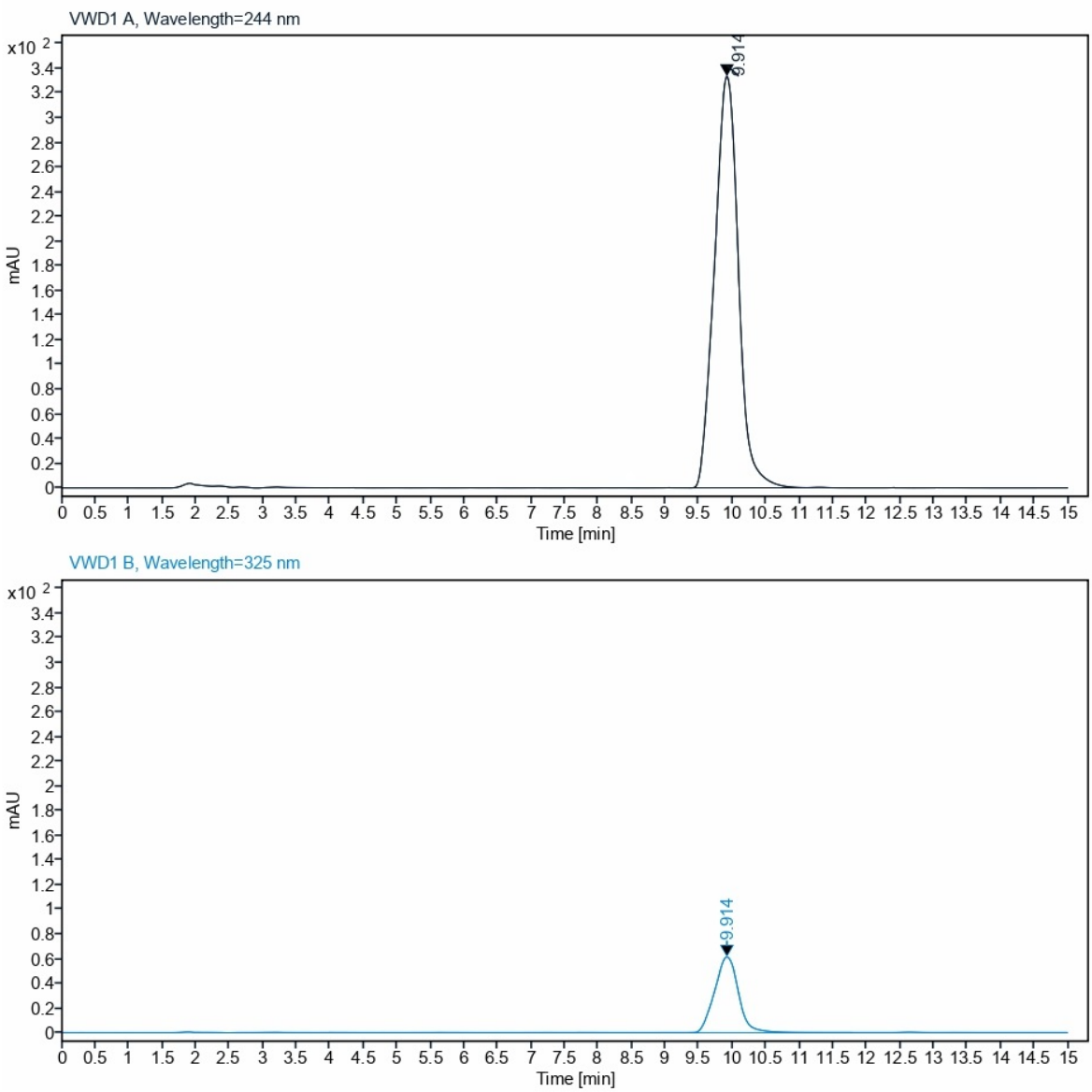

Fig. A.18 *HPLC specta of* ***4a*** *at 244 nm and 325 nm after purification (collected on Agilent 1260 Infinity II instrument with Sunfire C18 5µm 4.6×250 mm column; Elution method, isocratic; Mobile phase, water and acetonitrile (v/v) in the ratio 6: 4; flow rate, 0.5 mL/min)*

Appendix A

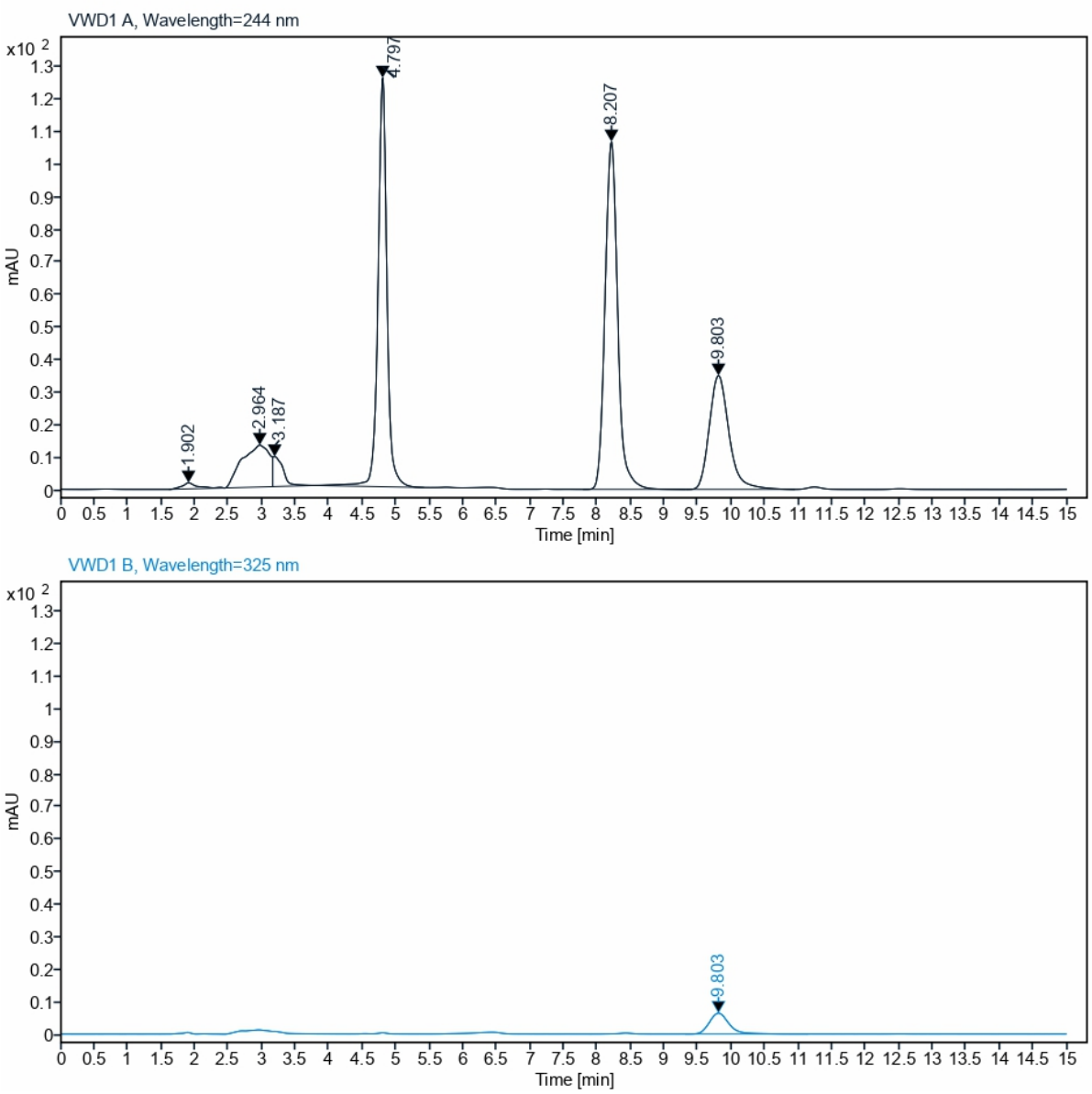

Fig. A.19 *HPLC specta of reaction mixture of* ***4a*** *at 244 nm and 325 nm after 3 hrs. (collected on Agilent 1260 Infinity II instrument with Sunfire C18 5μm 4.6×250 mm column; Elution method, isocratic; Mobile phase, water and acetonitrile (v/v) in the ratio 6: 4; flow rate, 0.5 mL/min)*

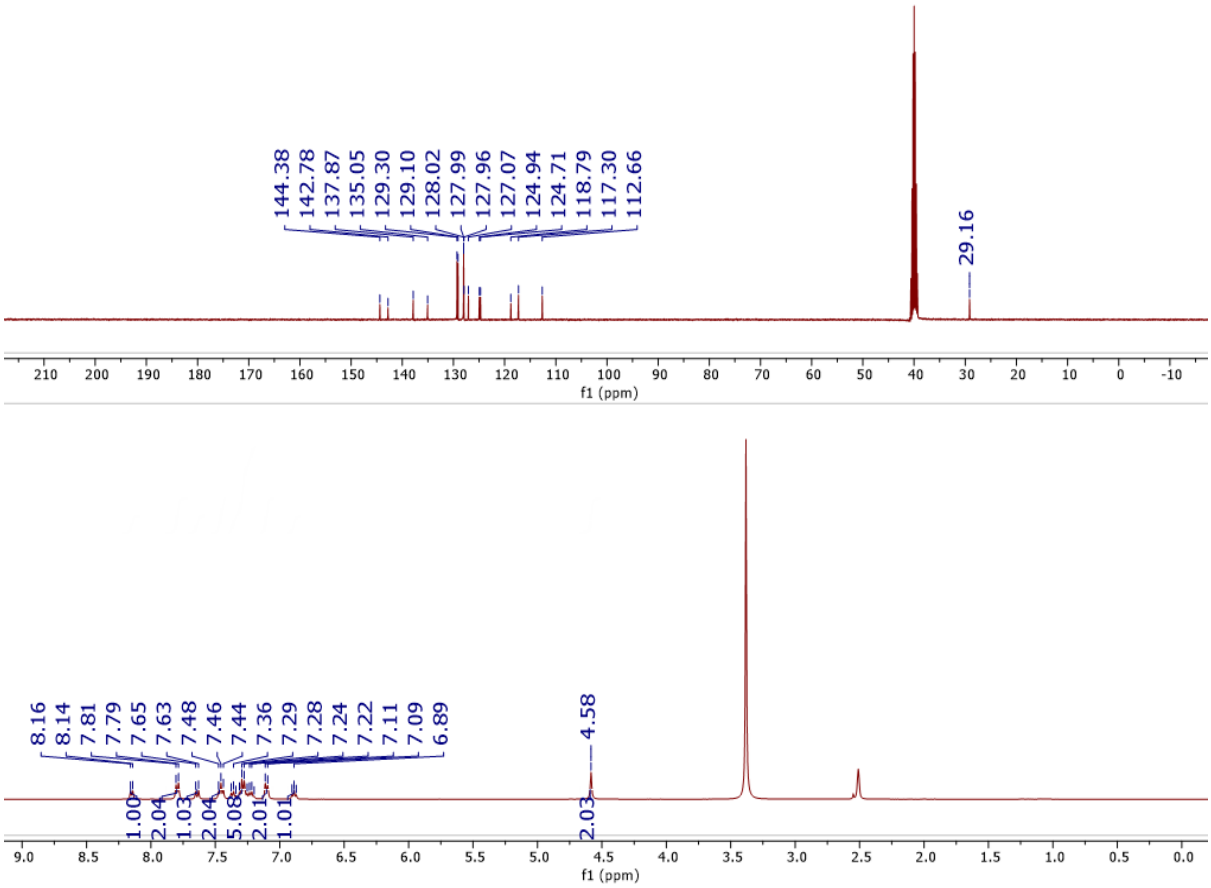

Fig. A.20 *^{1}H and ^{13}C-NMR spectrum of* ***4a*** *recorded in $CDCl_3$.*

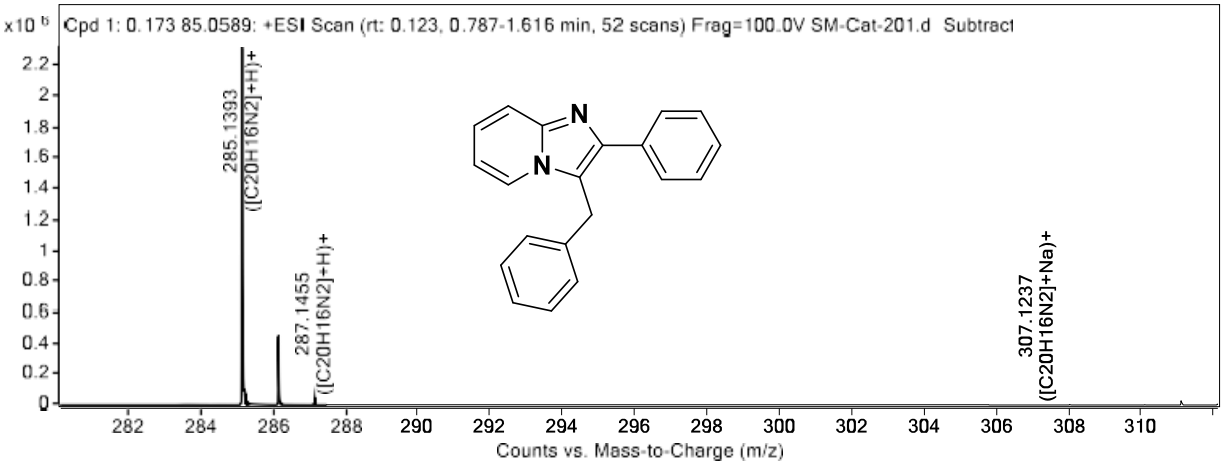

Fig. A.21 *HRMS of* ***4a****.*

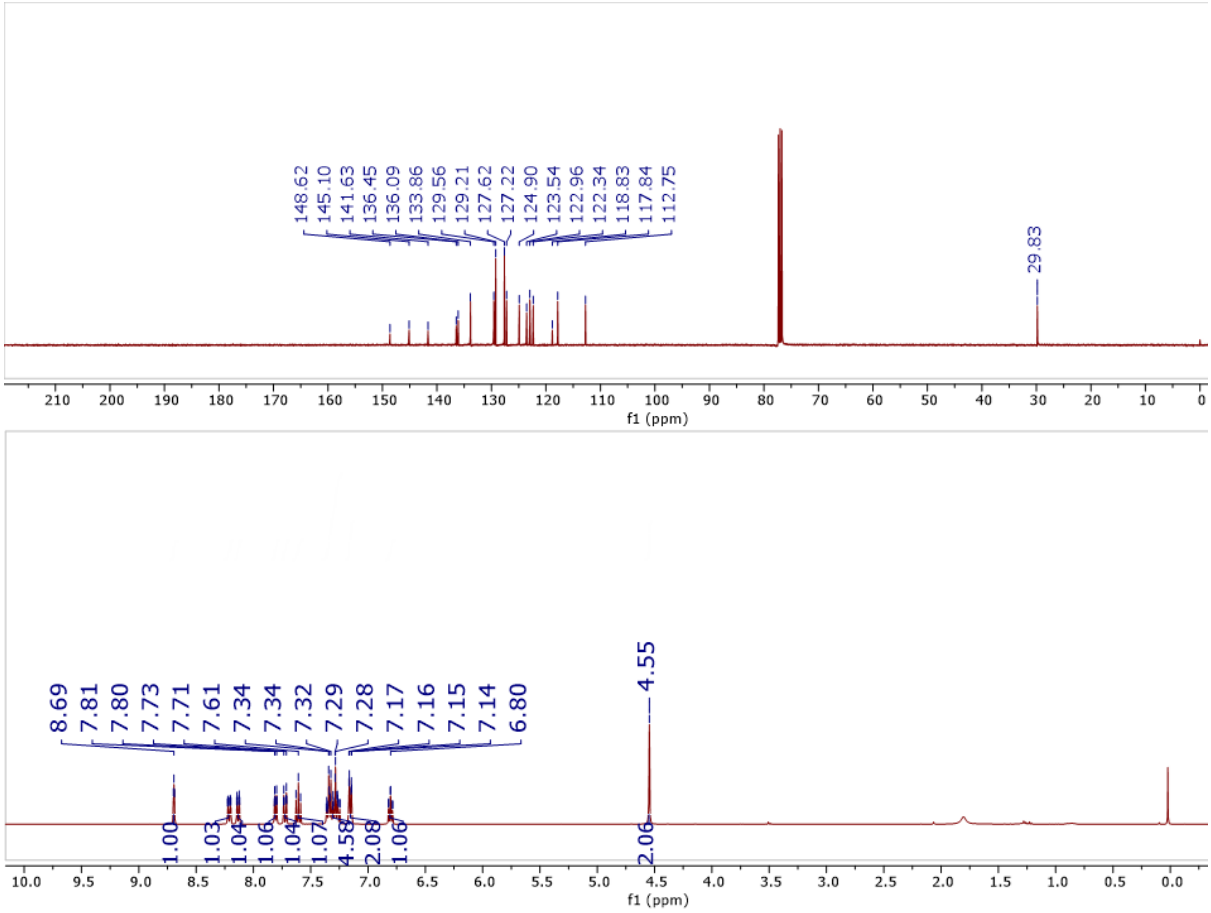

Fig. A.22 *^{1}H and ^{13}C-NMR spectrum of* ***4b*** *recorded in* ***$CDCl_3$.***

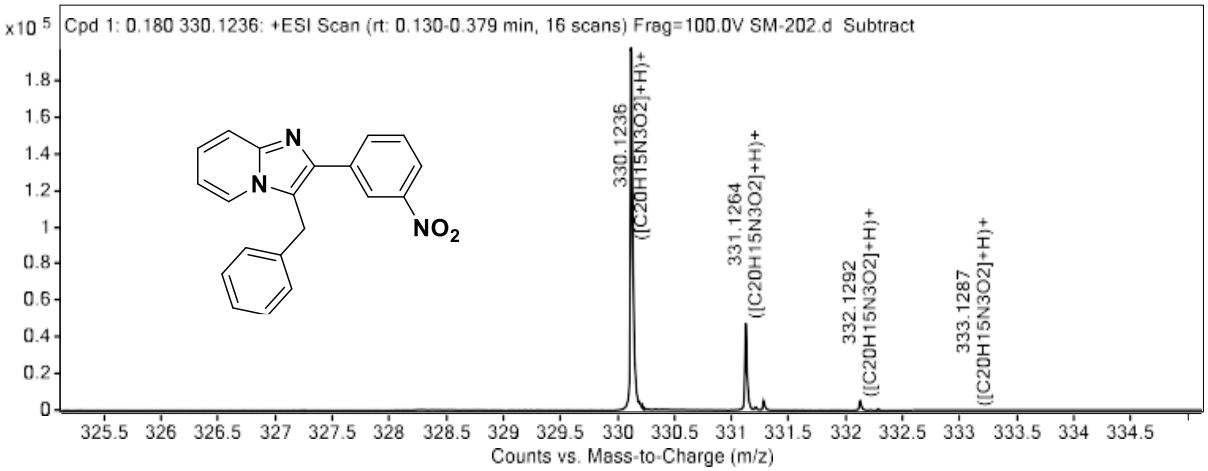

Fig. A.23 *HRMS of* ***4b****.*

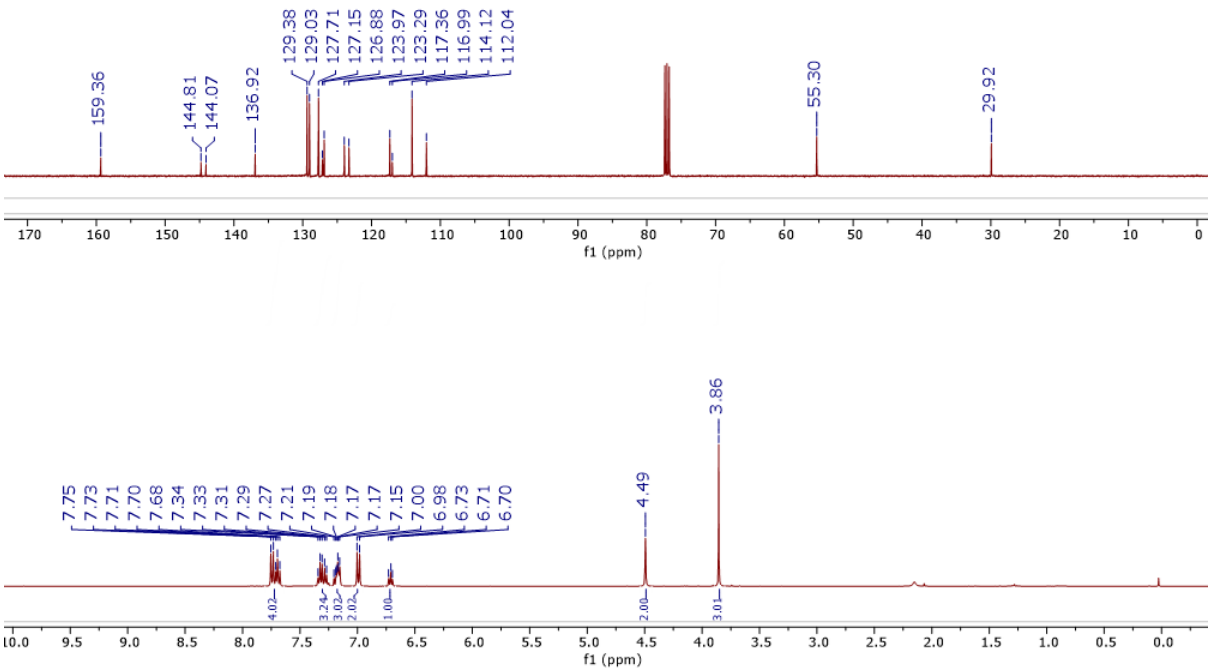

Fig. A.24 *^{1}H and ^{13}C-NMR spectrum of* ***4c*** *recorded in* ***$CDCl_3$.***

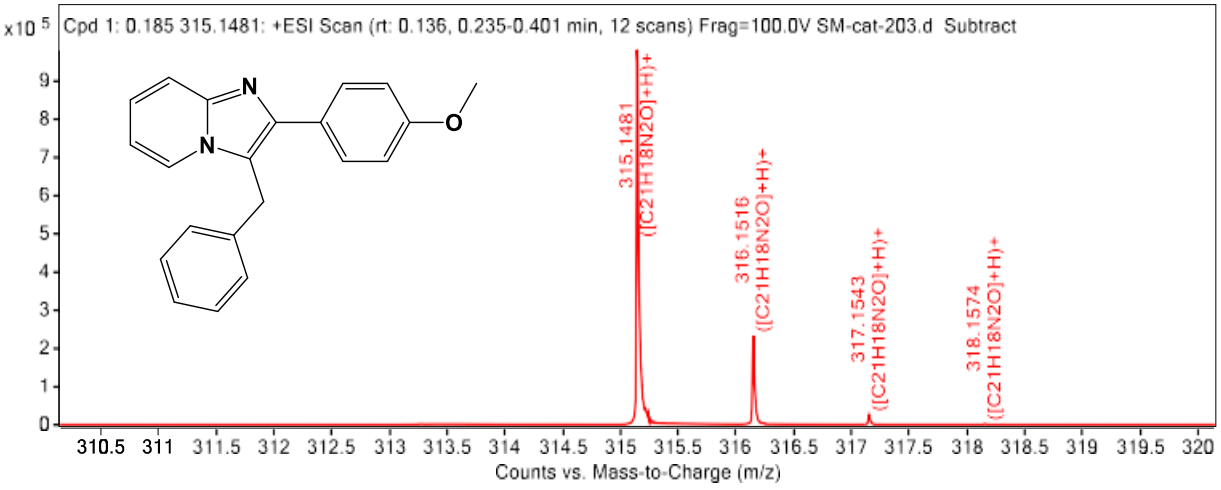

Fig. A.25 *HRMS of* ***4c****.*

Appendix A

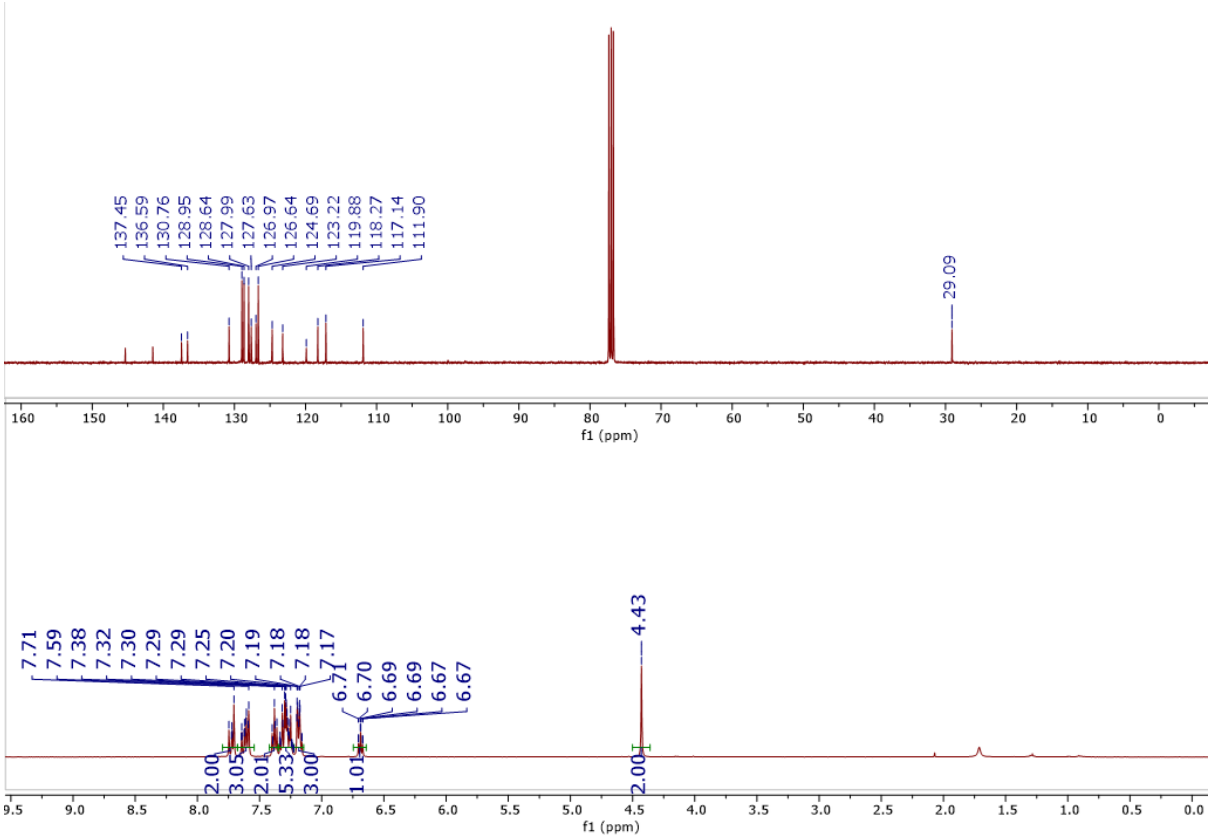

Fig. A.26 *^{1}H and ^{13}C-NMR spectrum of* ***4d*** *recorded in* ***$CDCl_3$****.*

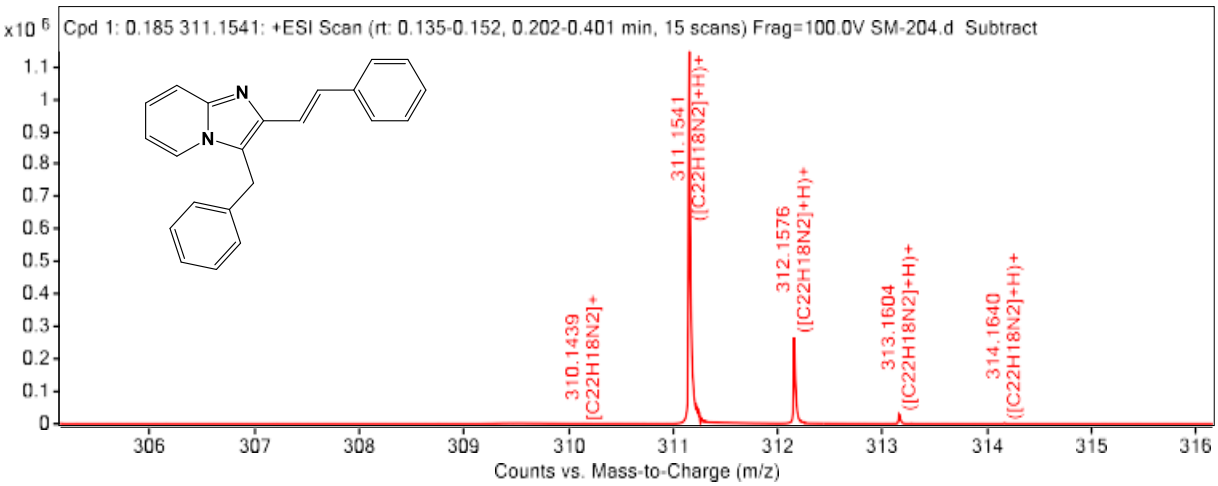

Fig. A.27 *HRMS of* ***4d****.*

Appendix A

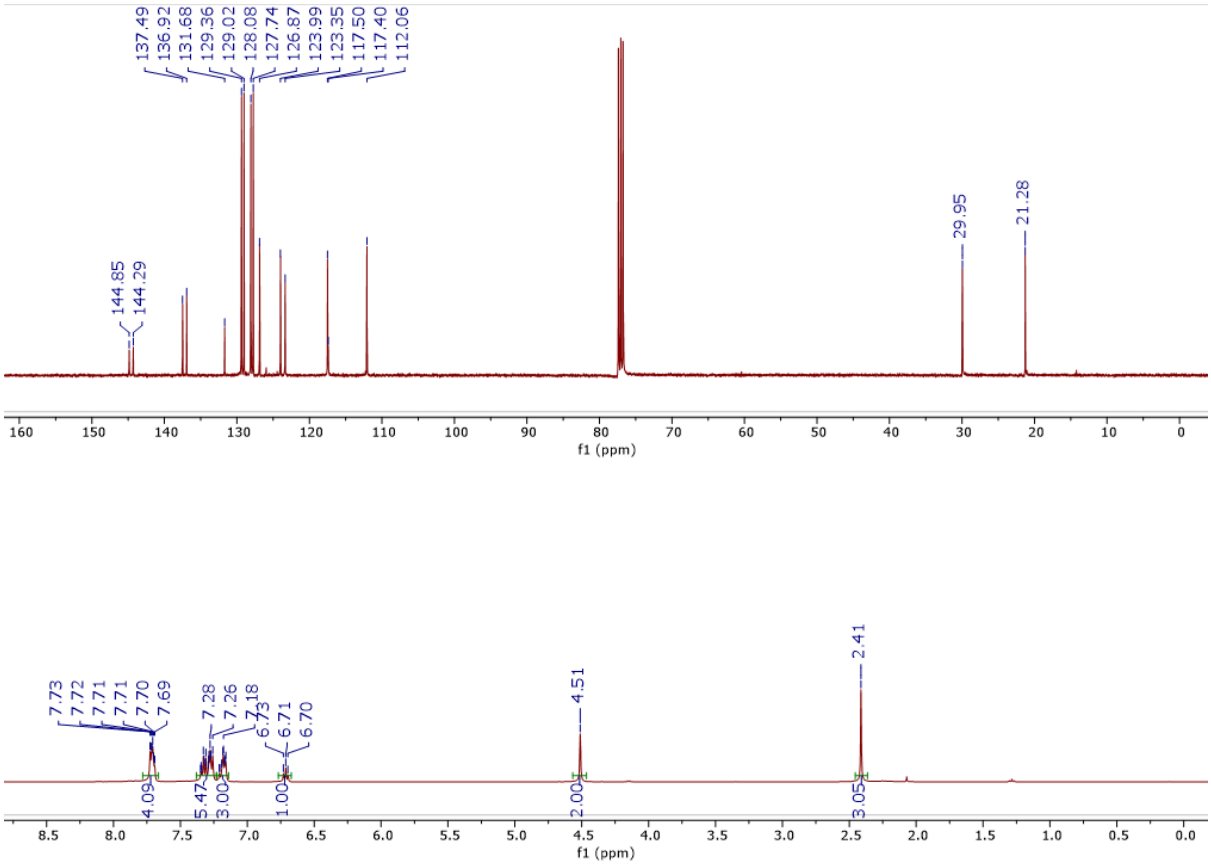

Fig. A.28 *^{1}H and ^{13}C-NMR spectrum of* ***4e*** *recorded in* ***$CDCl_3$.***

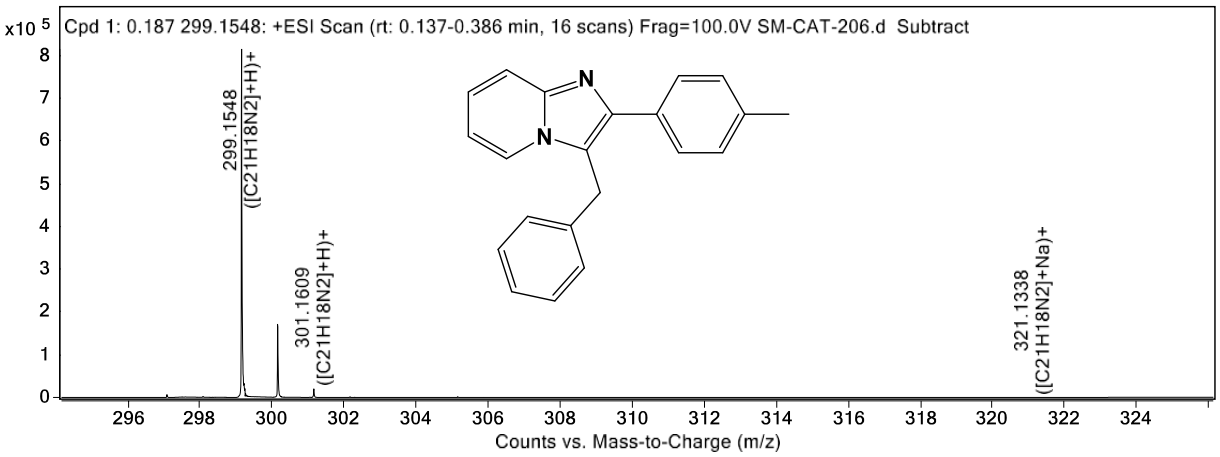

Fig. A.29 *HRMS of* ***4e****.*

Appendix A

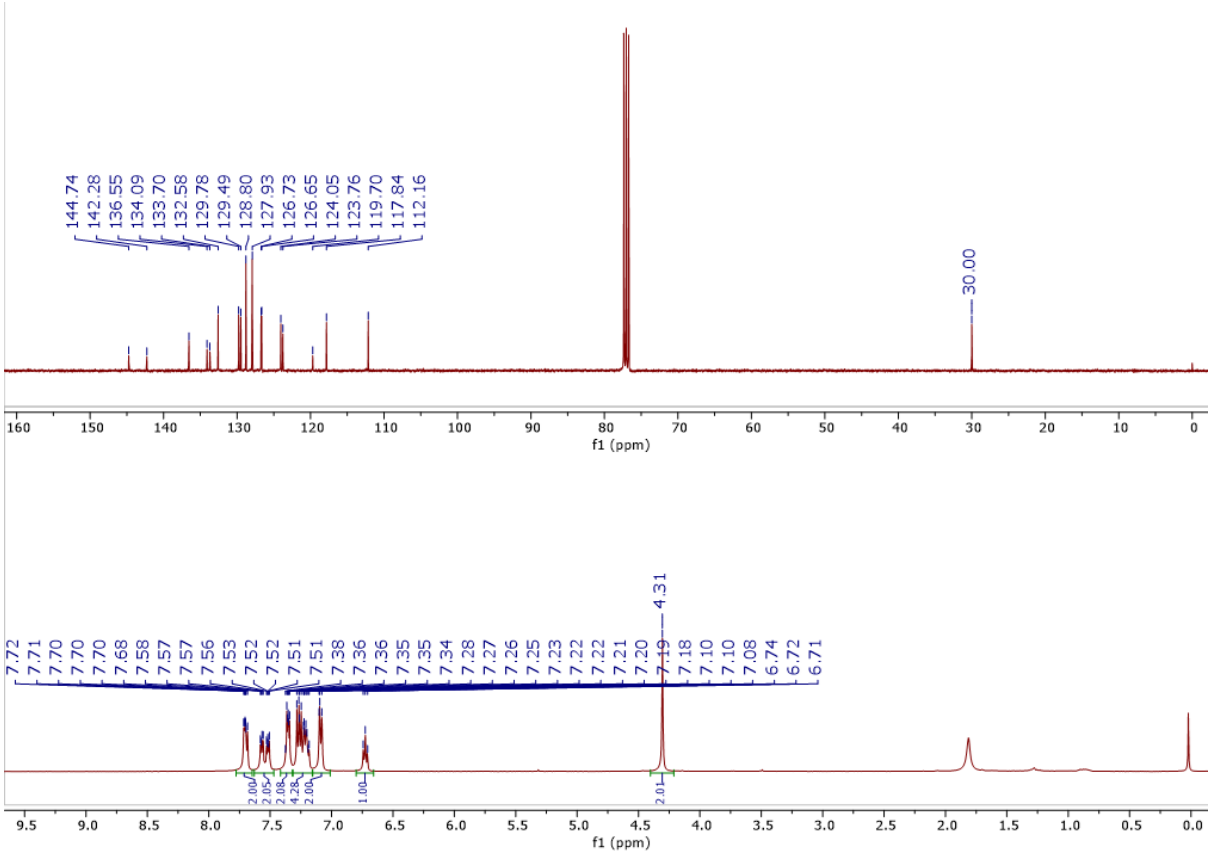

Fig. A.30 *^{1}H and ^{13}C-NMR spectrum of* ***4f*** *recorded in* ***$CDCl_3$.***

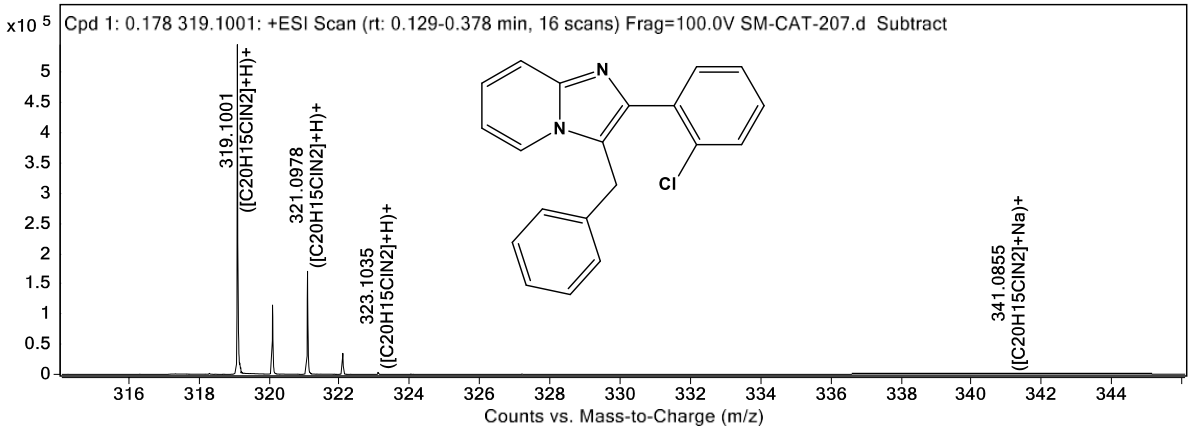

Fig. A.31 *HRMS of* ***4f*****.**

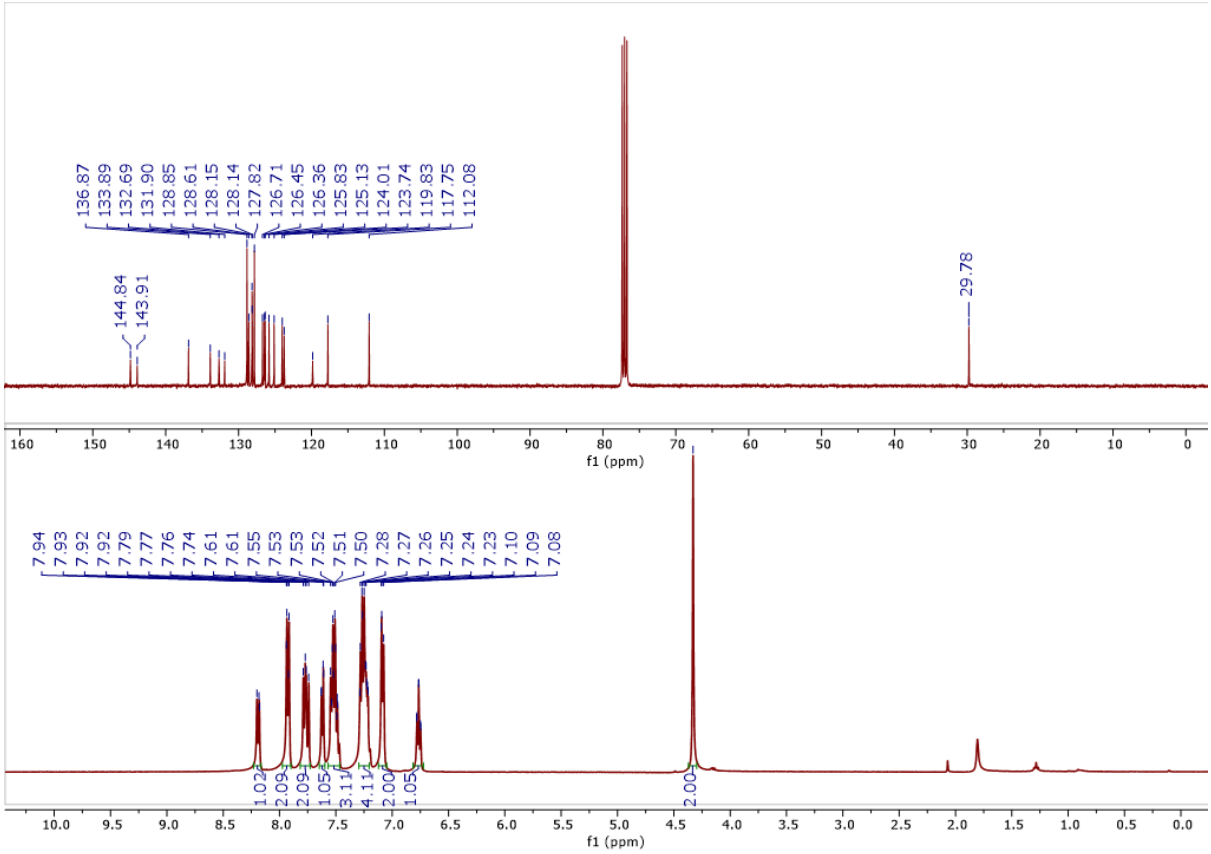

Fig. A.32 *^{1}H and ^{13}C-NMR spectrum of* ***4g*** *recorded in* ***$CDCl_3$.***

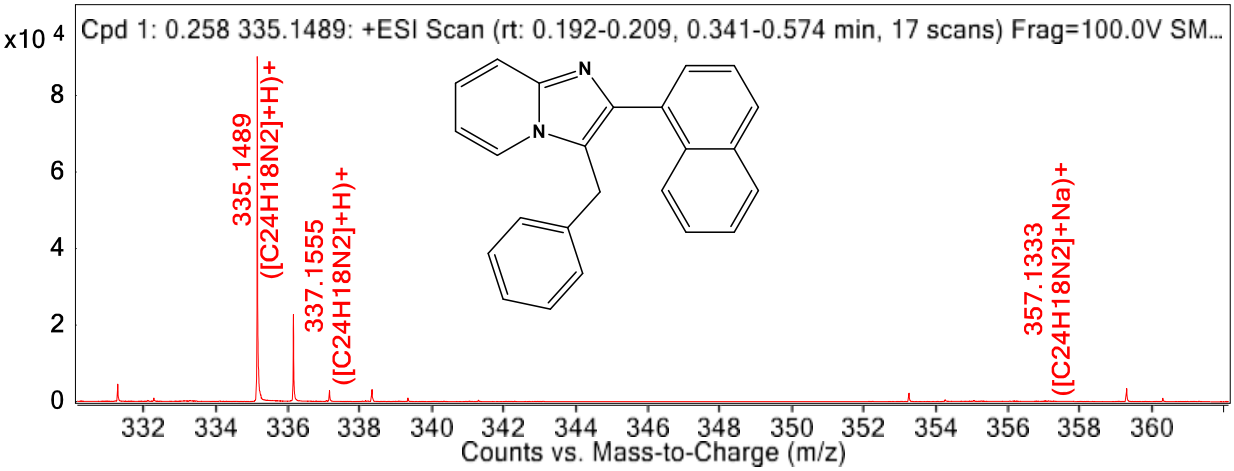

Fig. A.33 *HRMS of* ***4g*****.**

Appendix A

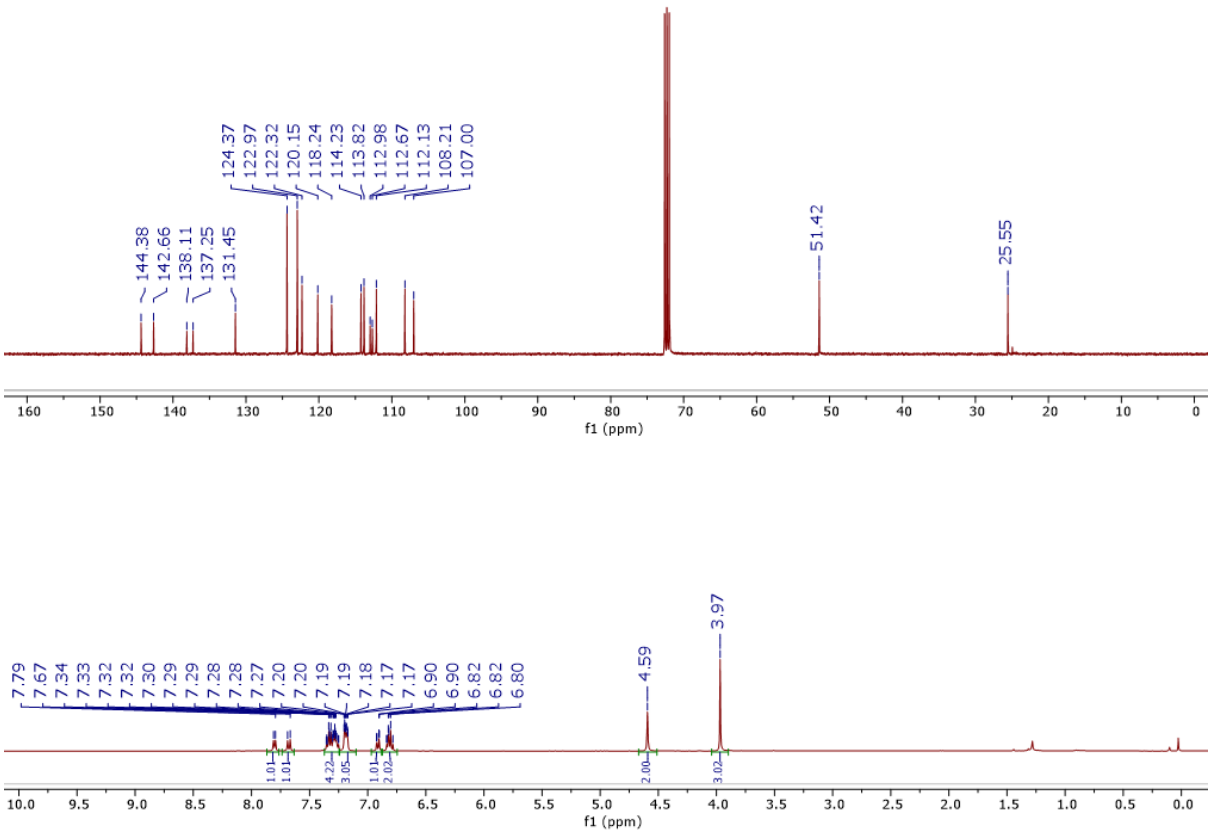

Fig. A.34 *^{1}H and ^{13}C-NMR spectrum of* ***4h*** *recorded in* ***$CDCl_3$.***

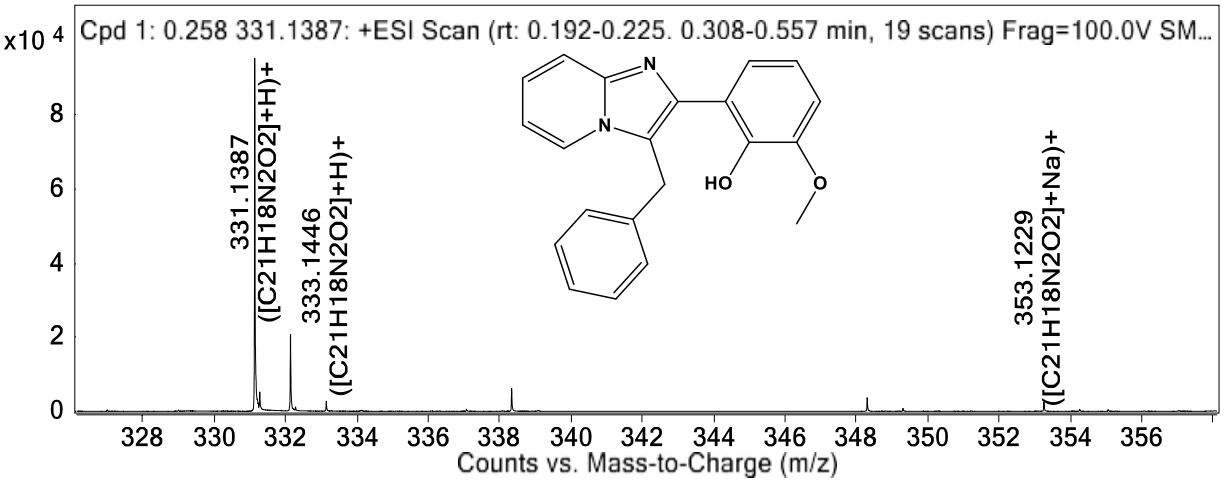

Fig. A.35 *HRMS of* ***4h*****.**

Appendix A

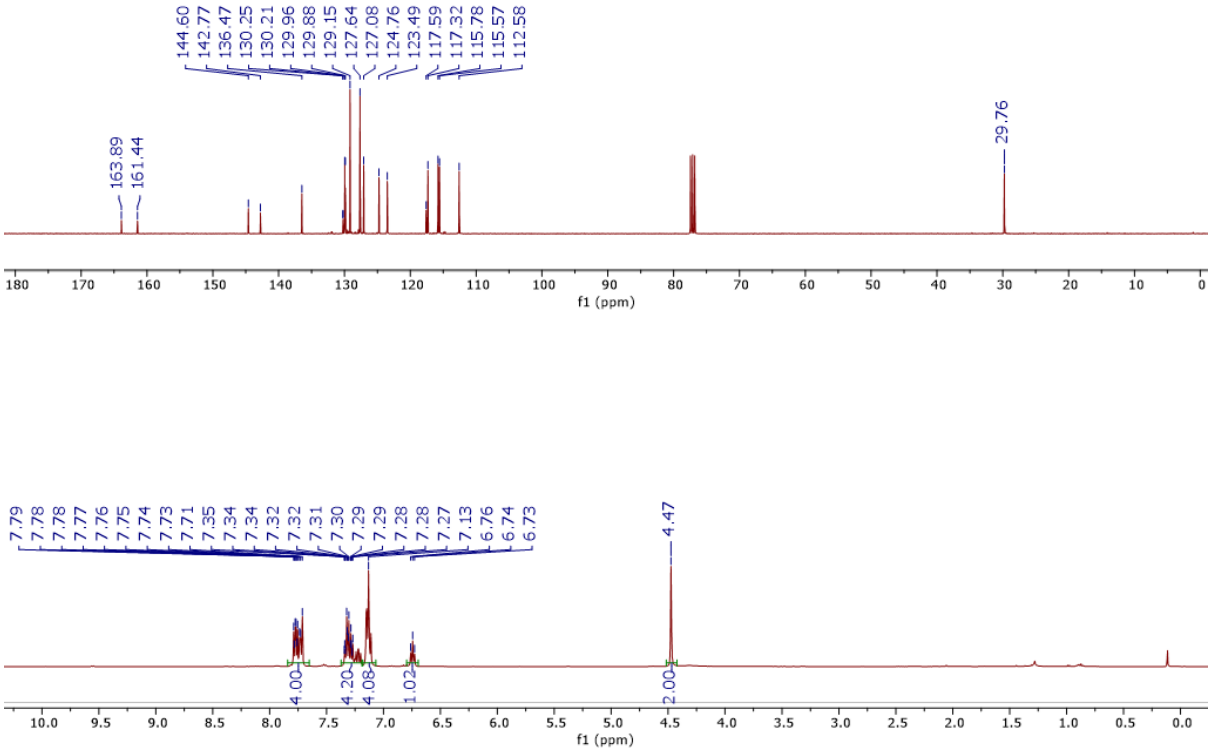

Fig. A.36 *^{1}H and ^{13}C-NMR spectrum of* ***4i*** *recorded in* ***$CDCl_3$.***

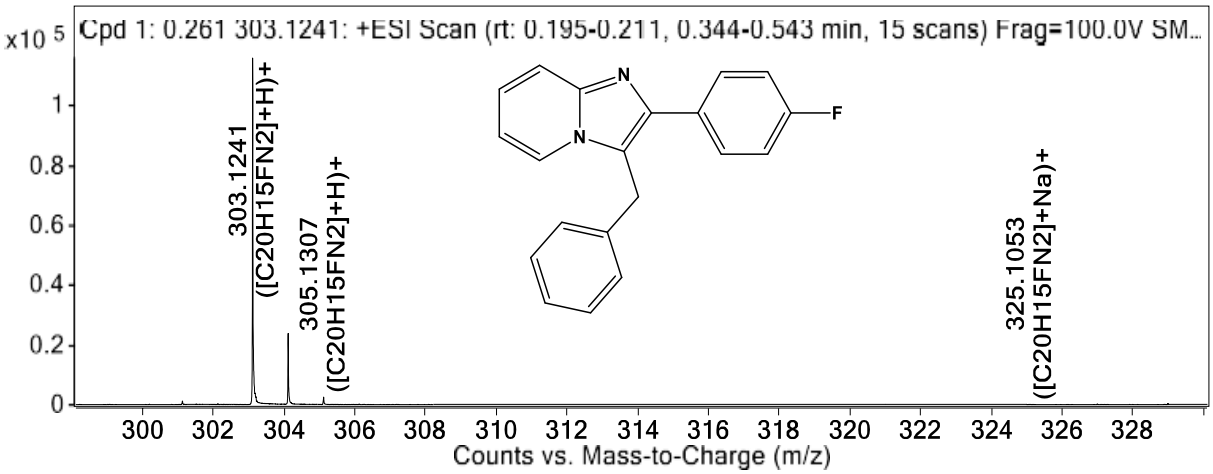

Fig. A.37 *HRMS of* ***4i*****.**

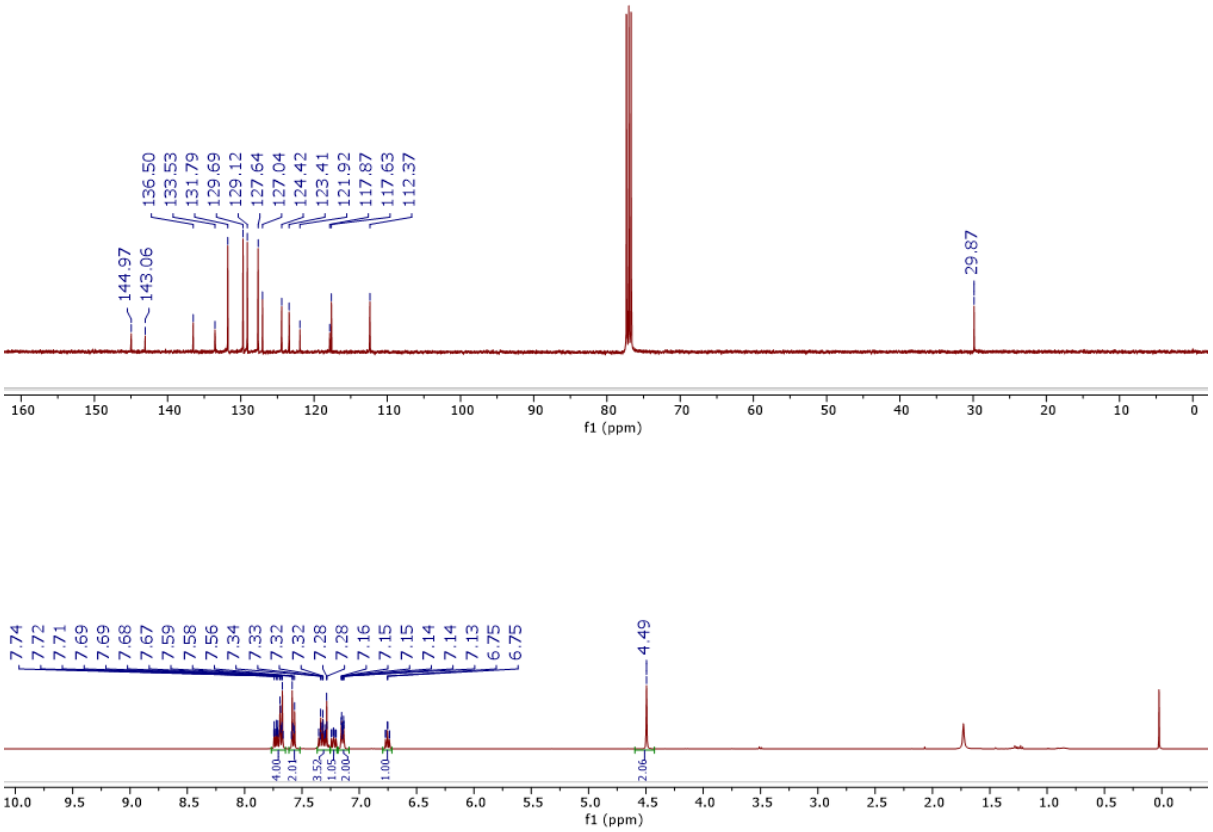

Fig. A.38 *^{1}H and ^{13}C-NMR spectrum of* ***4j*** *recorded in* ***$CDCl_3$.***

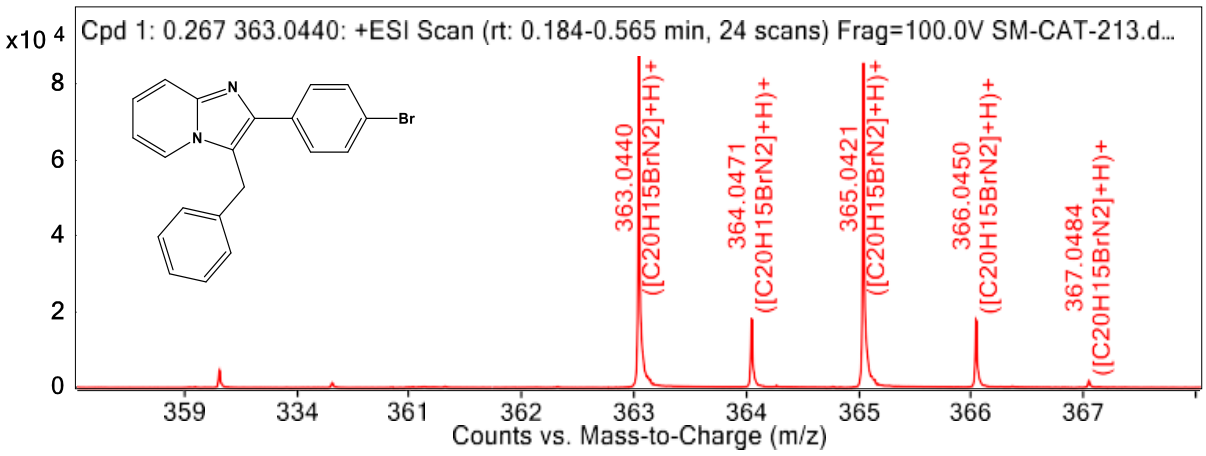

Fig. A.37 *HRMS of* ***4j*****.**

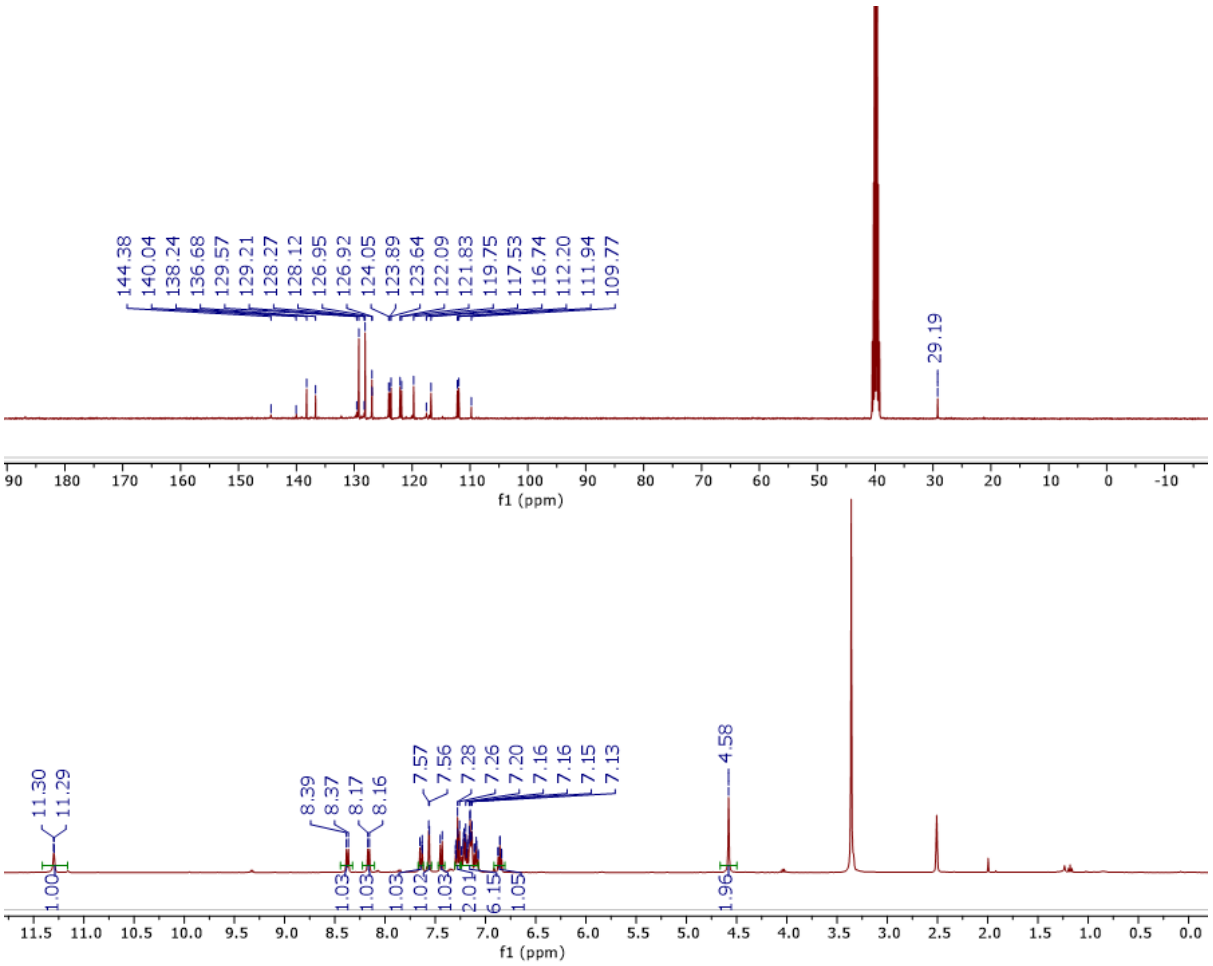

Fig. A.38 *^{1}H and ^{13}C-NMR spectrum of* ***4k*** *recorded in* ***DMSO-d$_6$.***

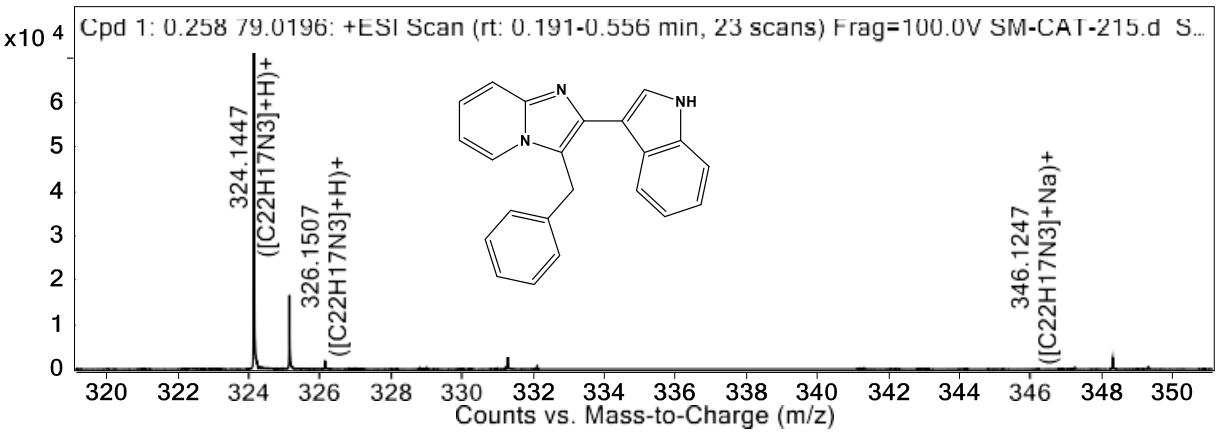

Fig. A.39 *HRMS of* ***4k.***

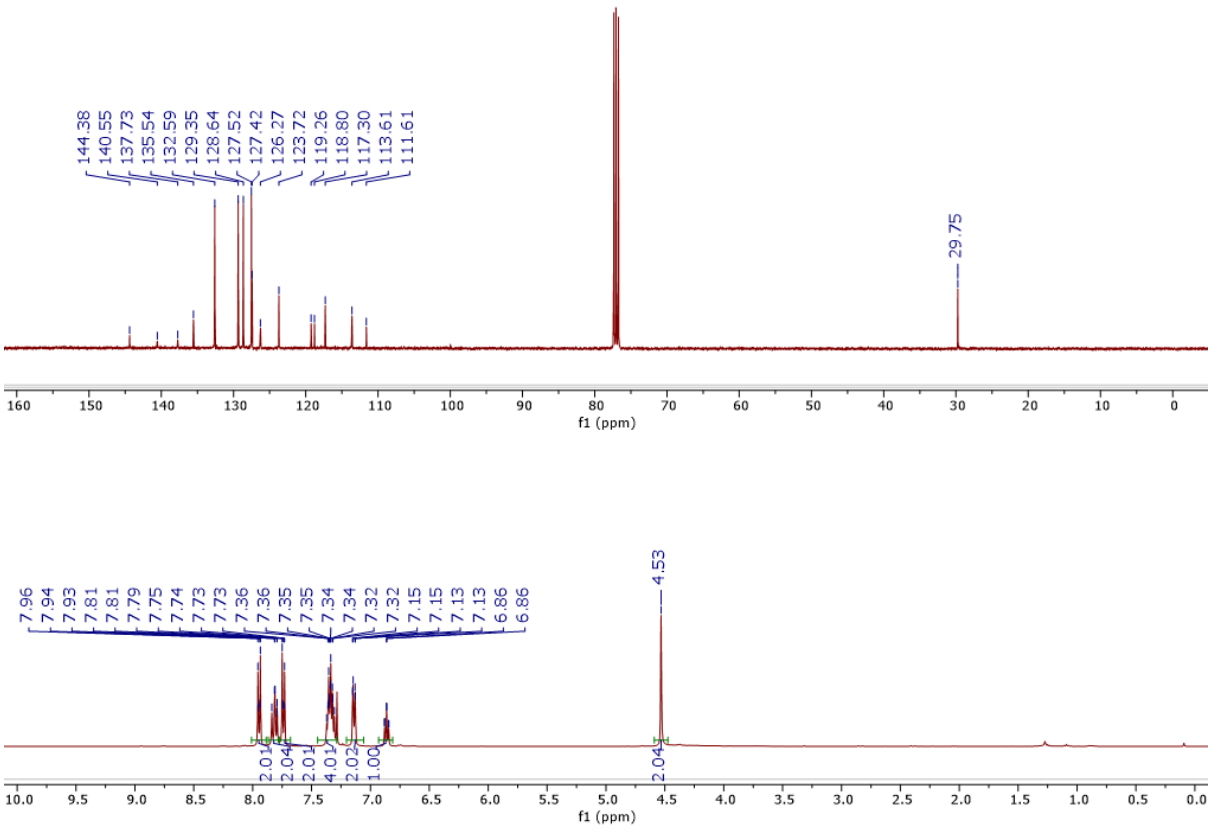

Fig. A.40 *^{1}H and ^{13}C-NMR spectrum of* ***4l*** *recorded in* ***$CDCl_3$.***

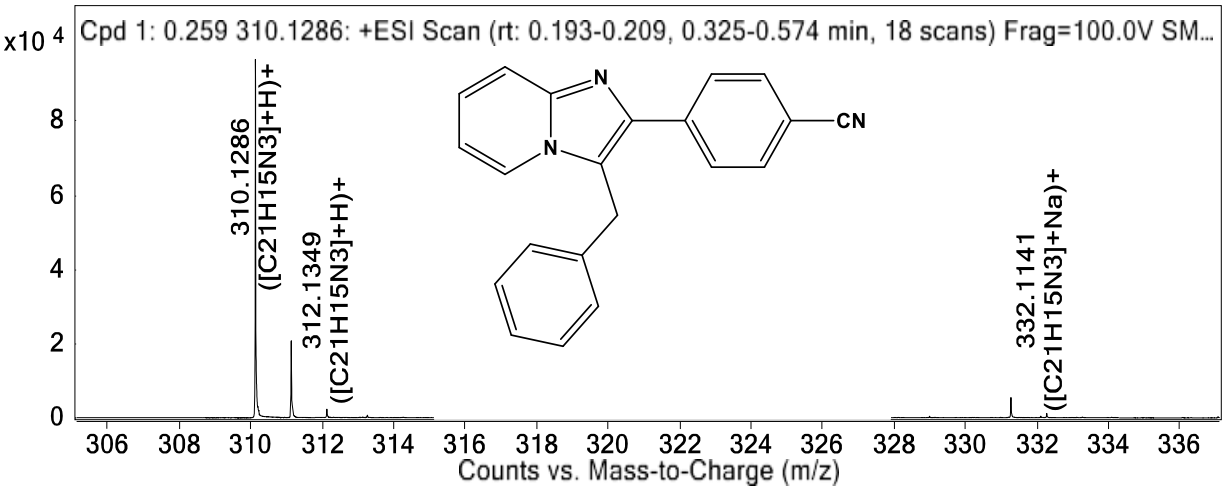

Fig. A.51 *HRMS of* ***4l.***

Appendix A

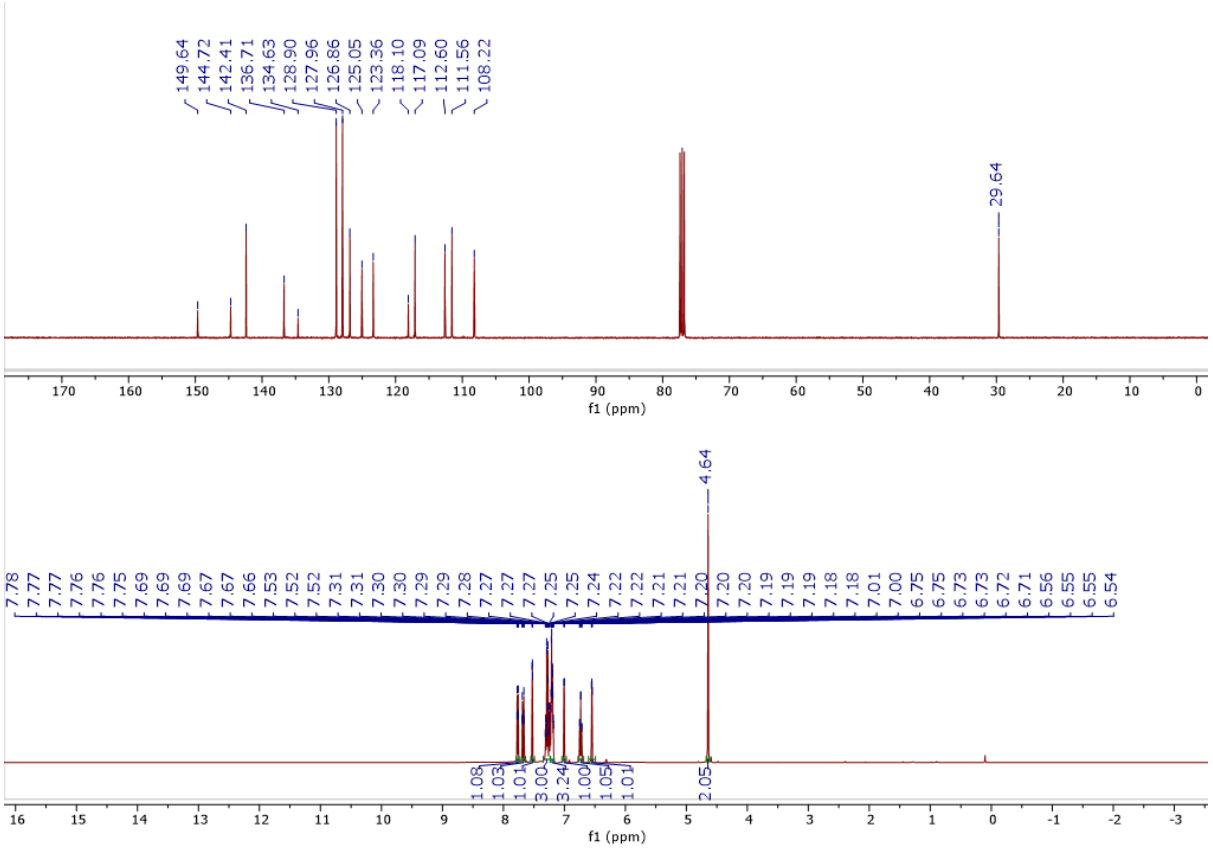

Fig. A.52 *^{1}H and ^{13}C-NMR spectrum of* ***4m*** *recorded in* ***$CDCl_3$.***

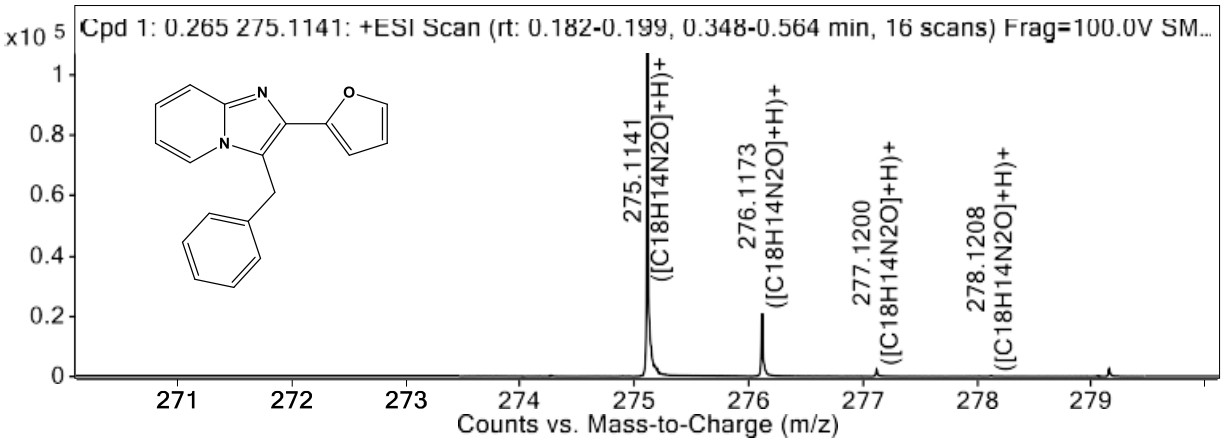

Fig. A.53 *HRMS of* ***4m*****.**

Appendix A

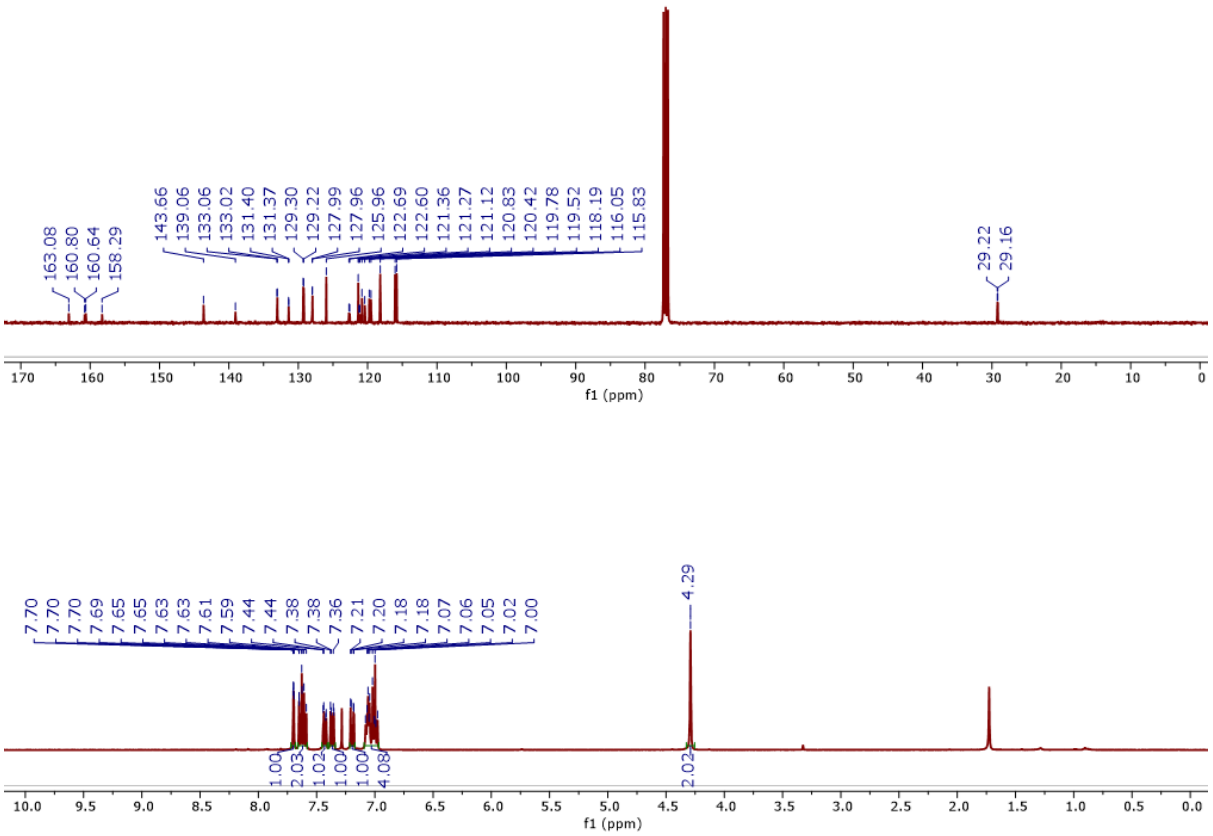

Fig. A.54 *^{1}H and ^{13}C-NMR spectrum of* ***4n*** *recorded in* ***$CDCl_3$.***

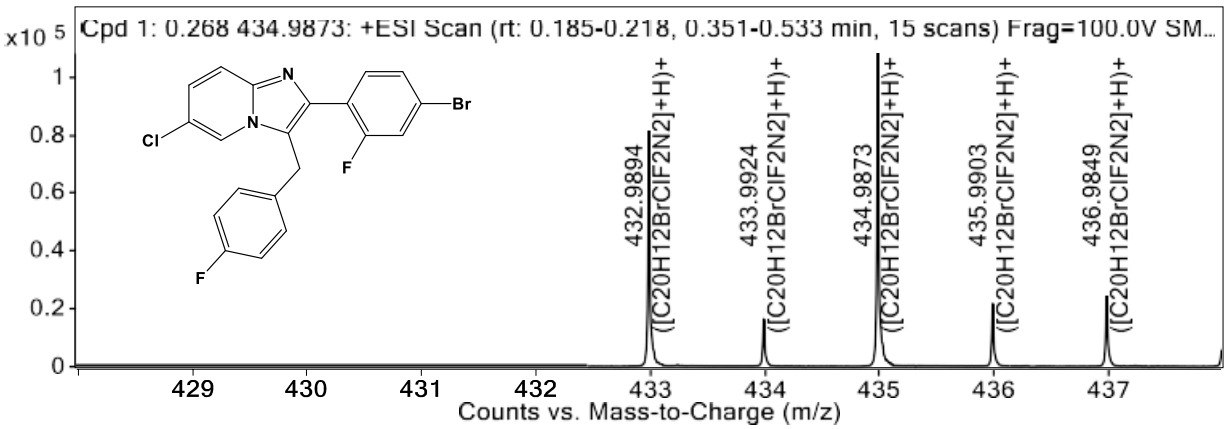

Fig. A.55 *HRMS of* ***4n*****.**

Appendix A

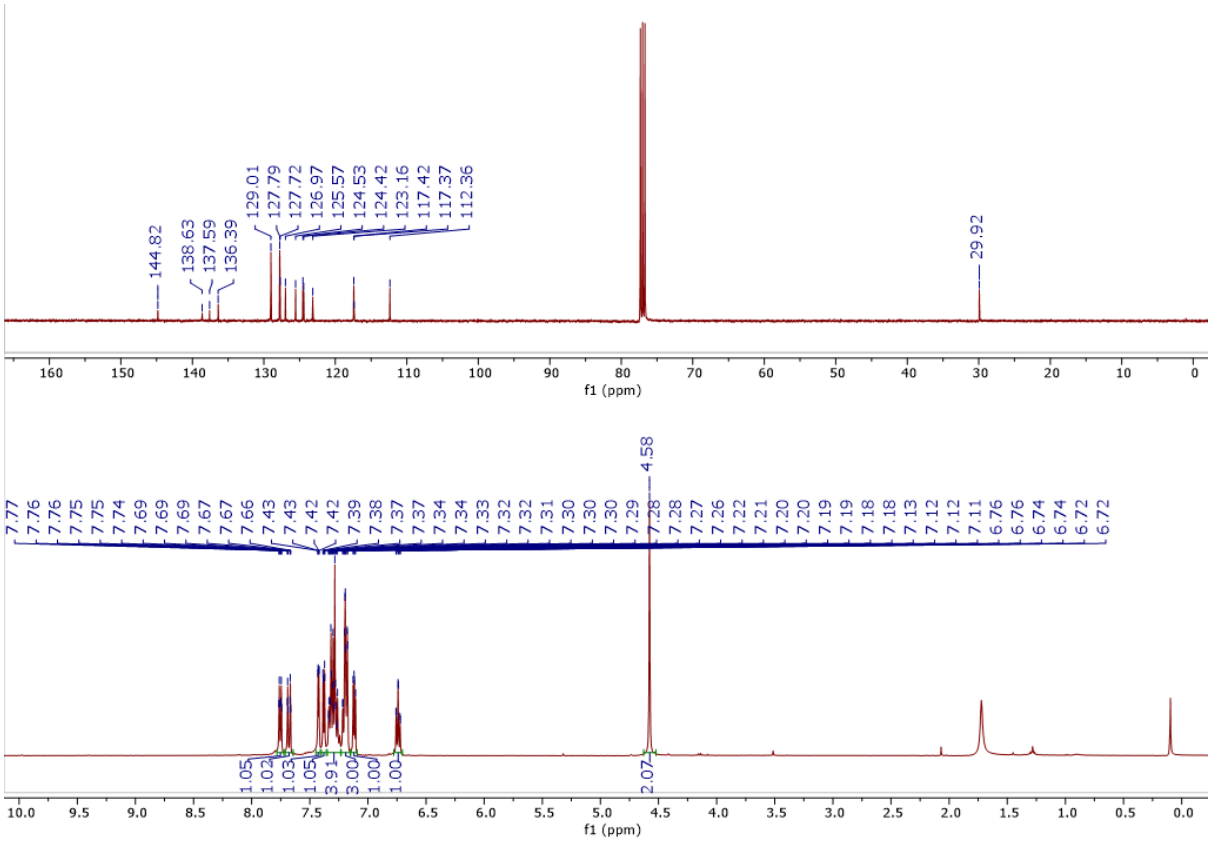

Fig. A.56 *^{1}H and ^{13}C-NMR spectrum of* ***4o*** *recorded in* ***$CDCl_3$.***

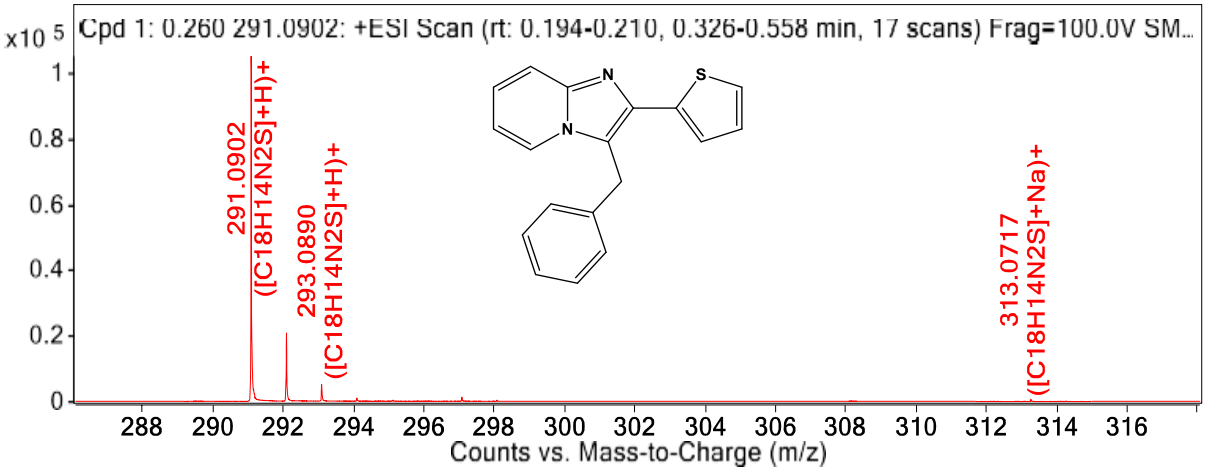

Fig. A.57 *HRMS of* ***4o*****.**

Appendix A

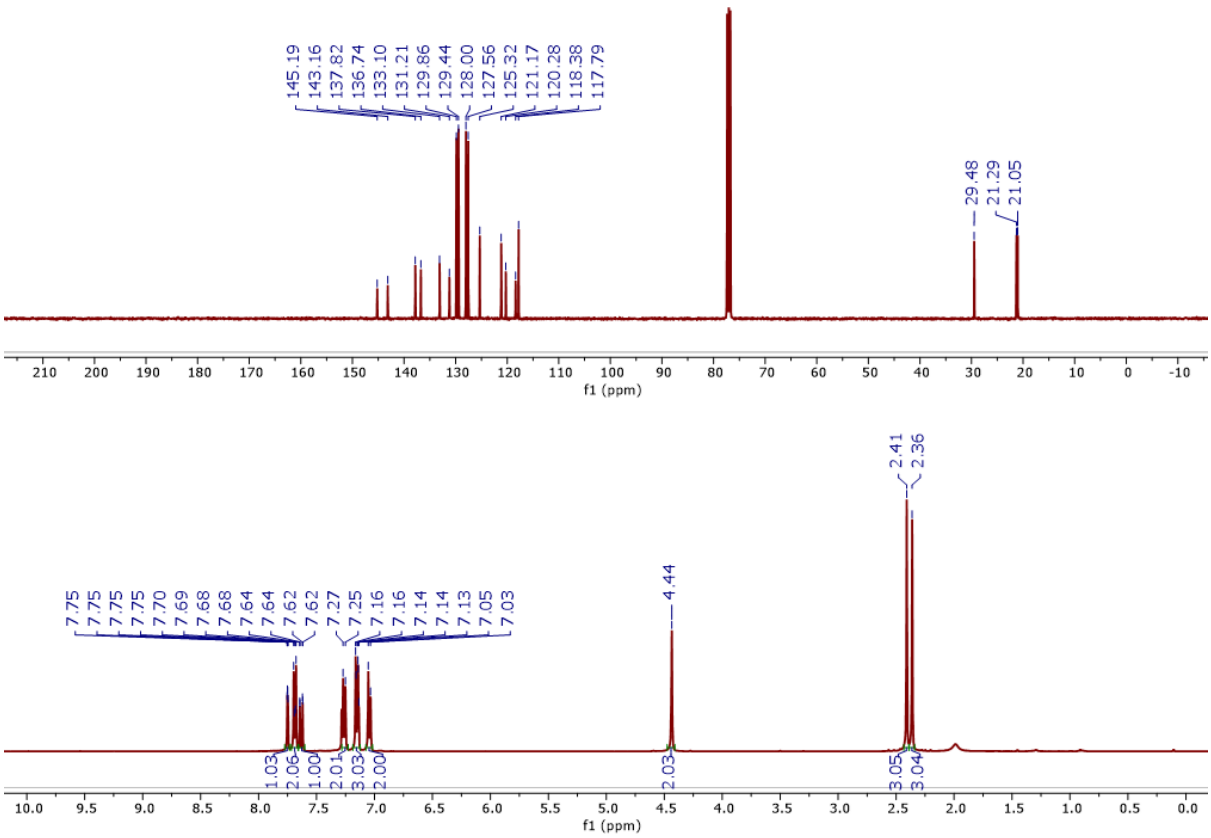

Fig. A.58 *^{1}H and ^{13}C-NMR spectrum of* ***4p*** *recorded in* ***$CDCl_3$.***

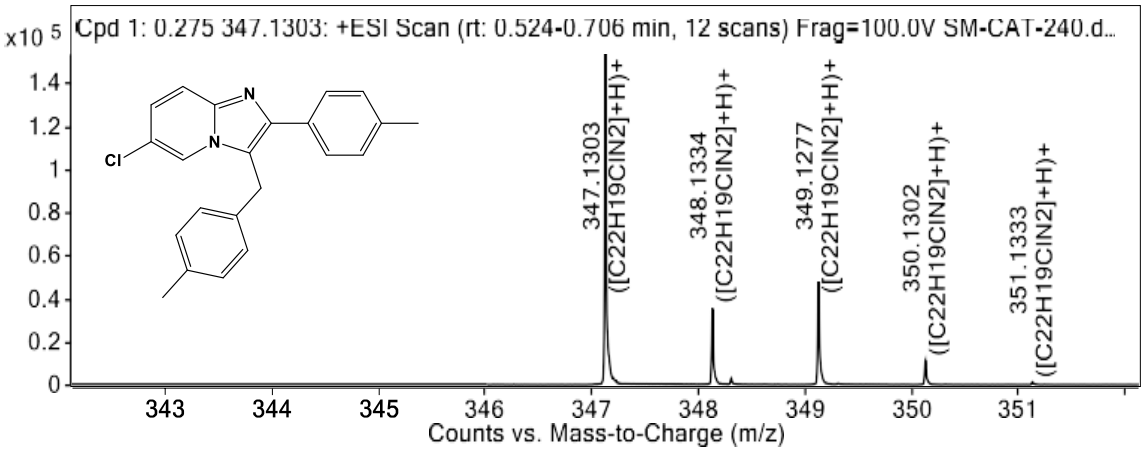

Fig. A.59 *HRMS of* ***4p****.*

Appendix A

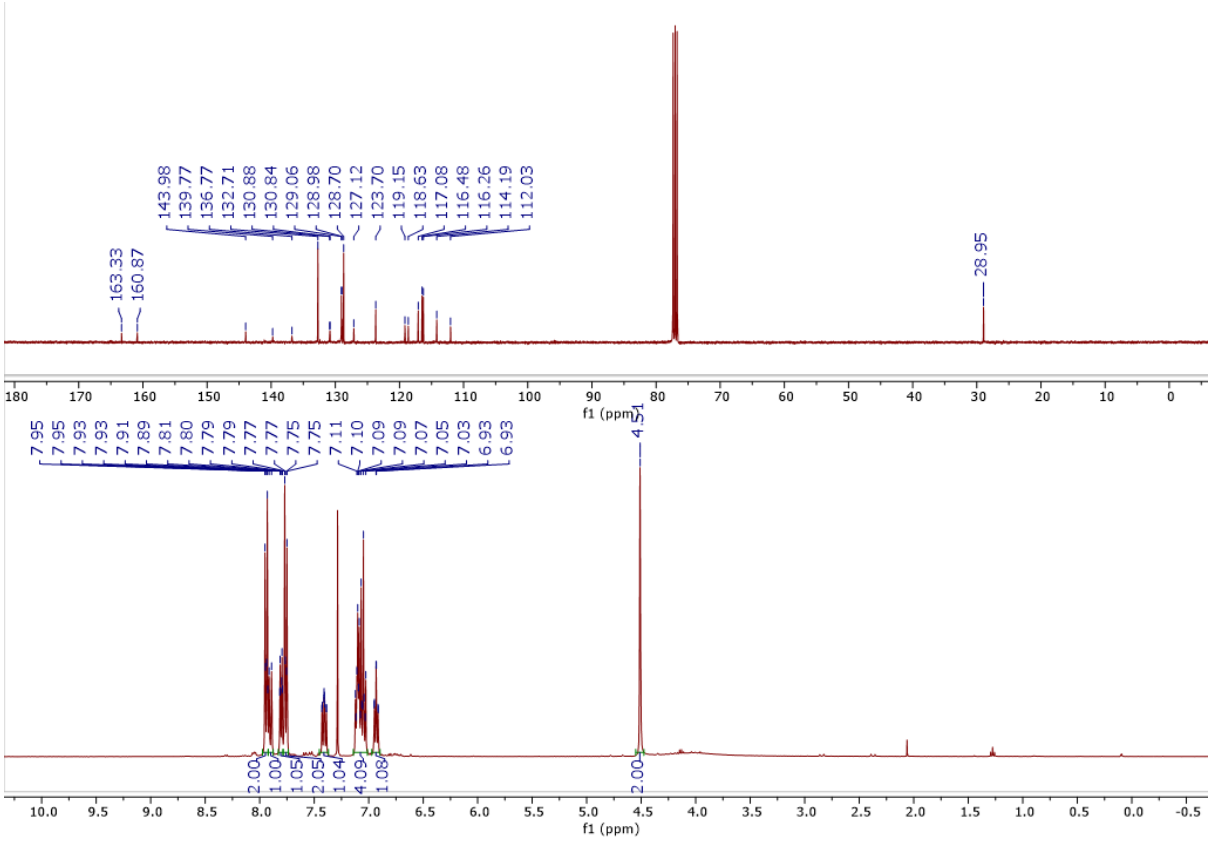

Fig. A.60 *^{1}H and ^{13}C-NMR spectrum of* ***4q*** *recorded in* ***$CDCl_3$.***

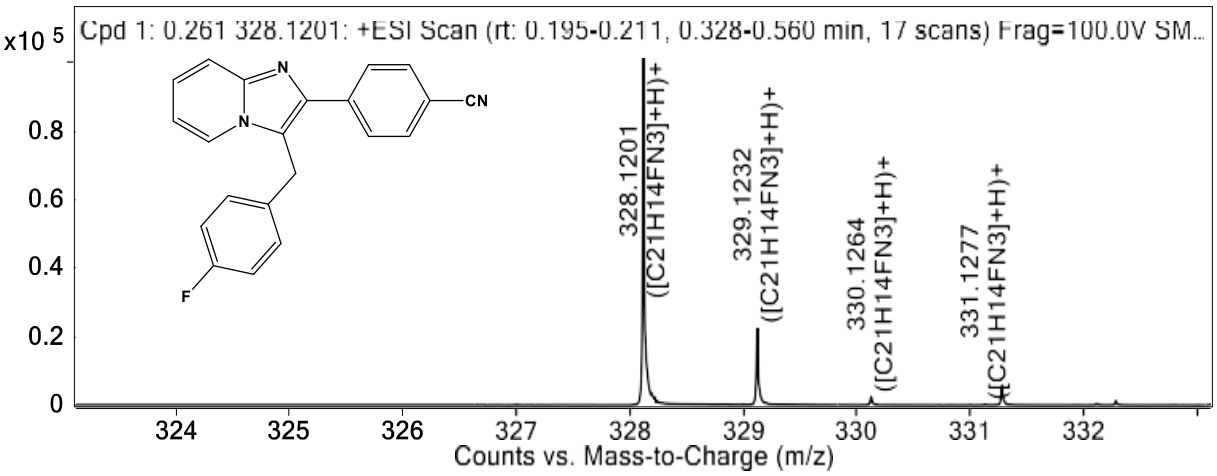

Fig. A.61 *HRMS of* ***4q*****.**

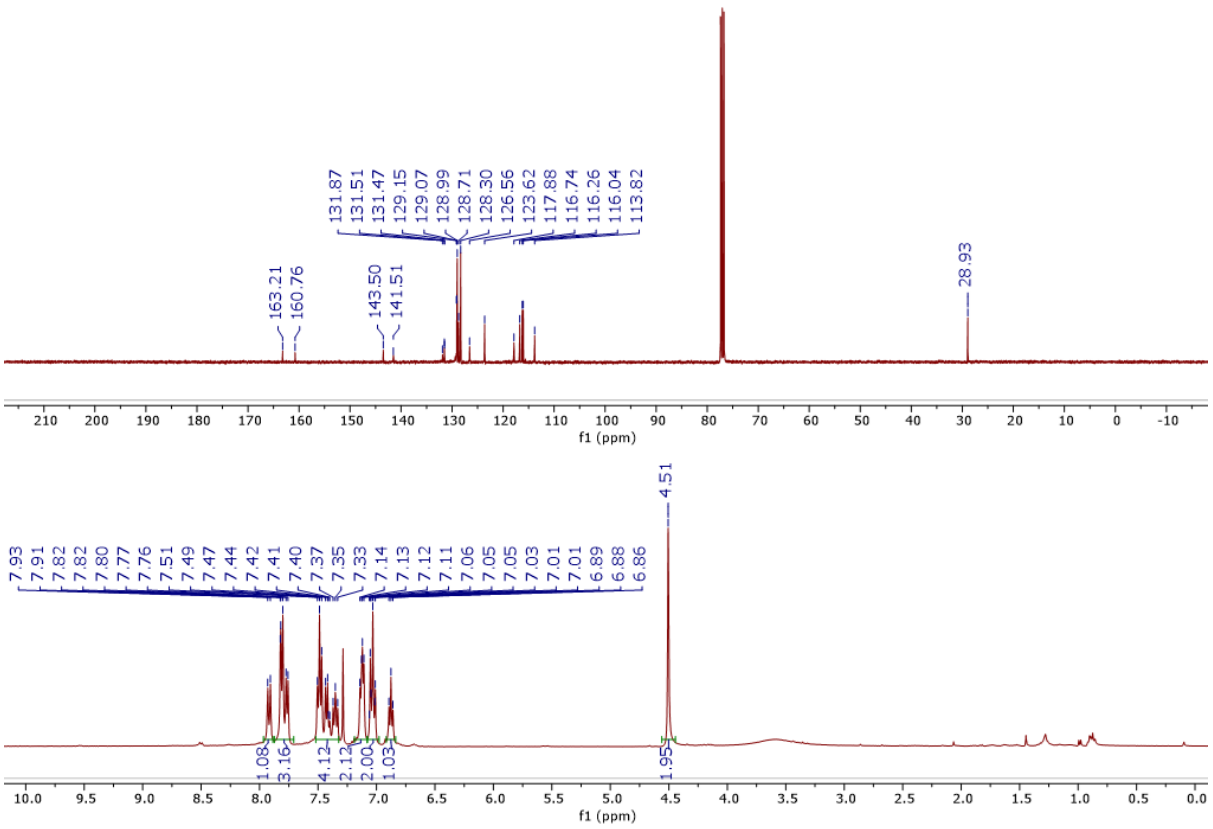

Fig. A.62 *^{1}H and ^{13}C-NMR spectrum of* ***4r*** *recorded in* ***$CDCl_3$.***

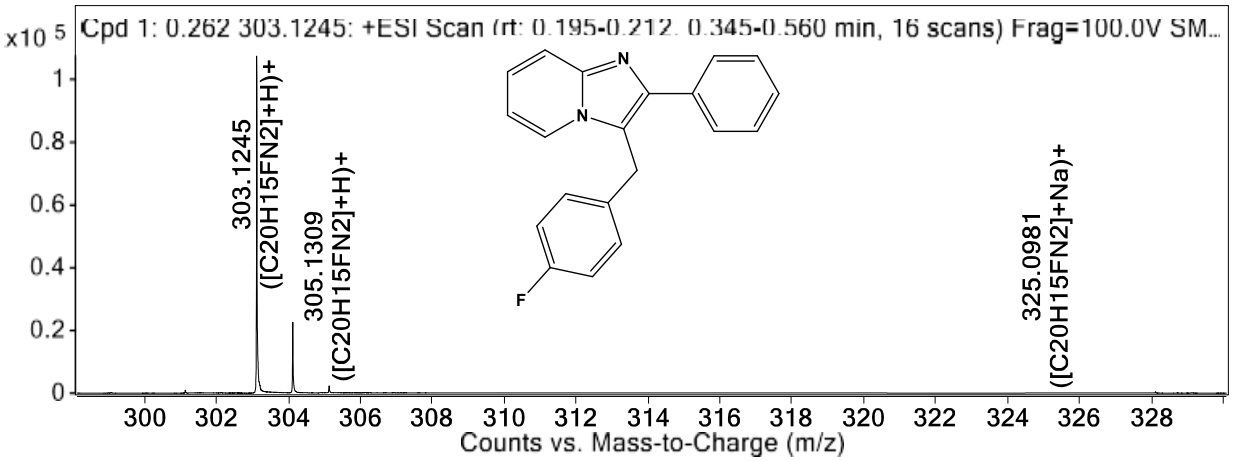

Fig. A.63 *HRMS of* ***4r*****.**

Appendix A

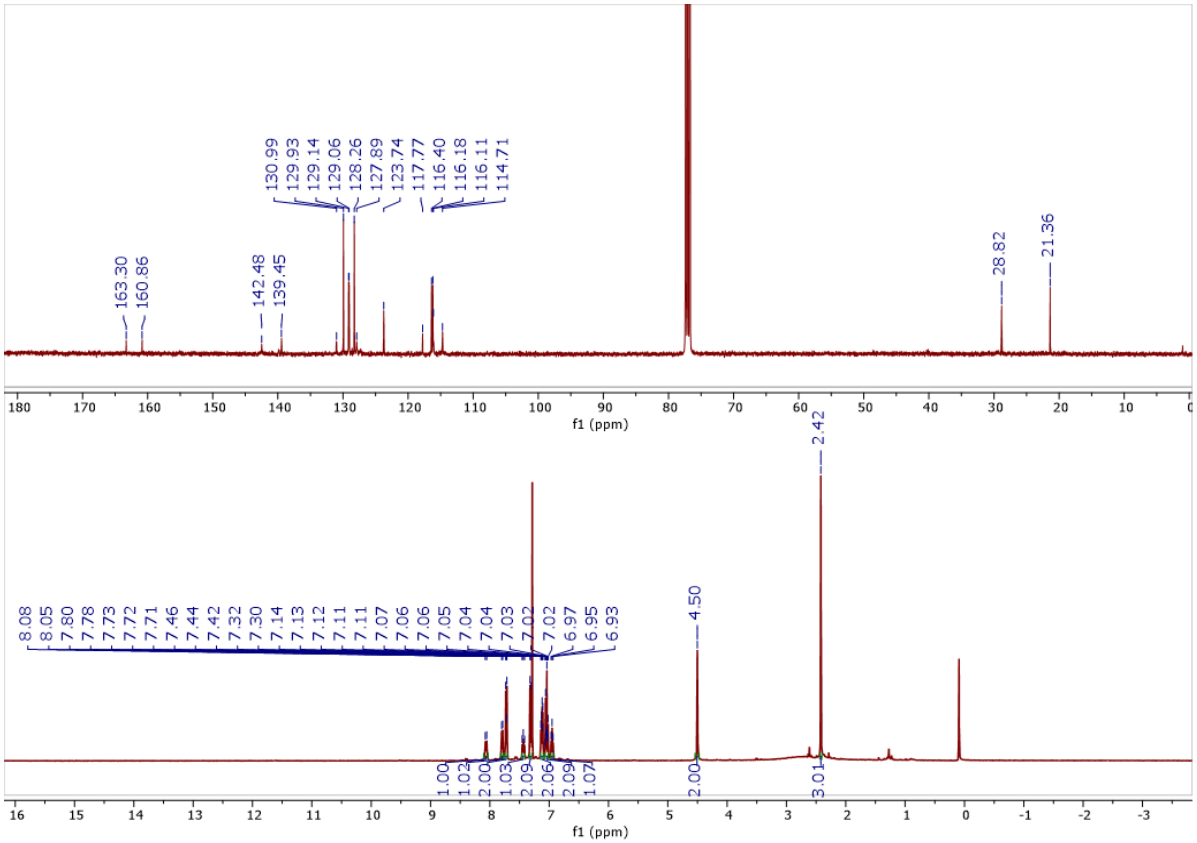

Fig. A.64 *^{1}H-NMR and ^{13}C-NMR spectrum of* ***4s*** *recorded in* ***$CDCl_3$.***

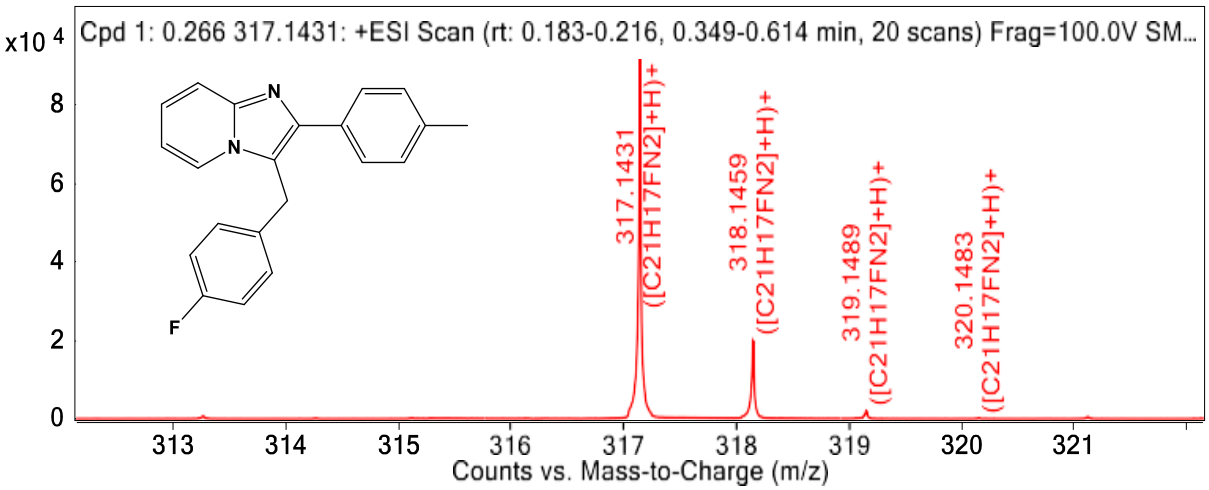

Fig. A.65 *HRMS of* ***4s*****.**

Appendix A

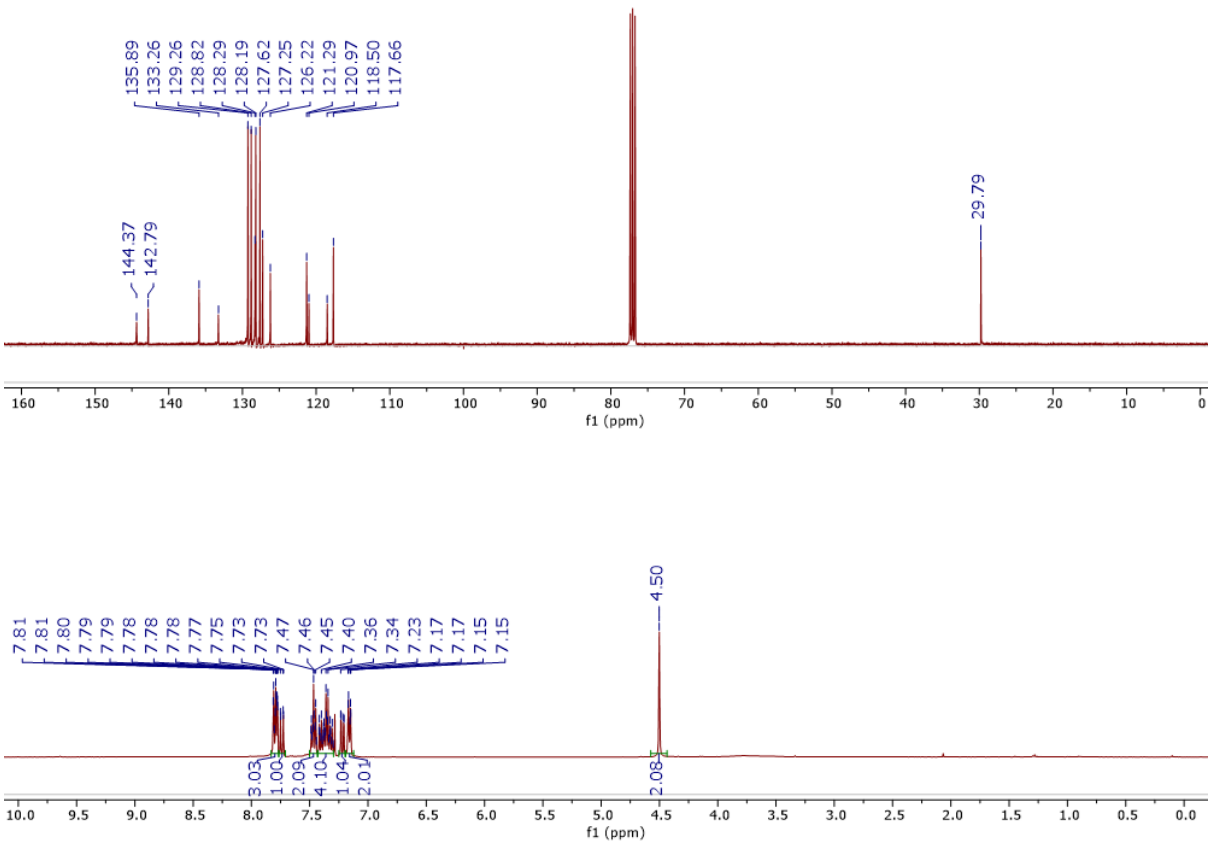

Fig. A.66 *^{1}H-NMR and ^{13}C-NMR spectrum of* ***4t*** *recorded in* ***$CDCl_3$.***

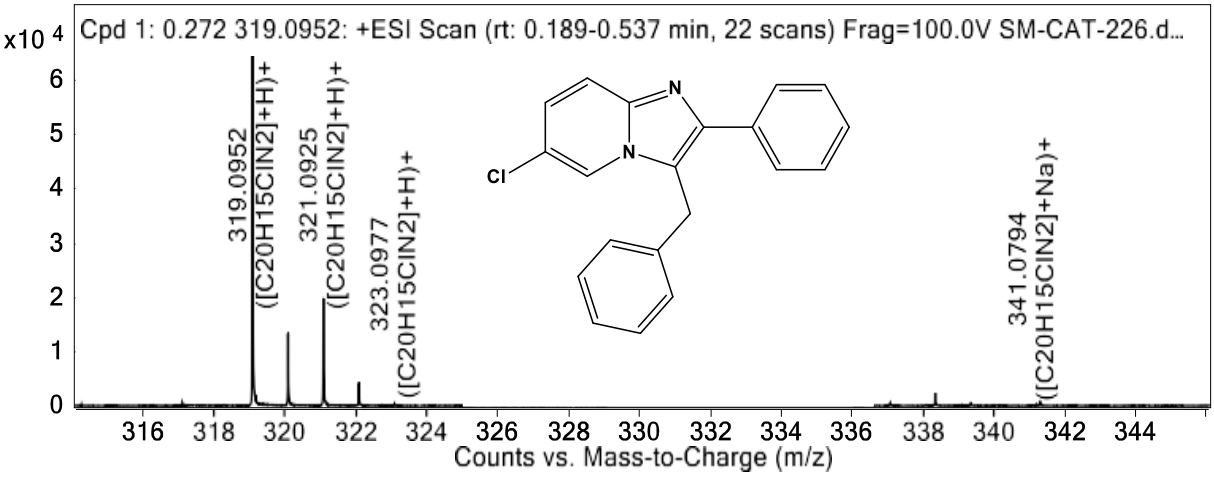

Fig. A.67 *HRMS of* ***4t****.*

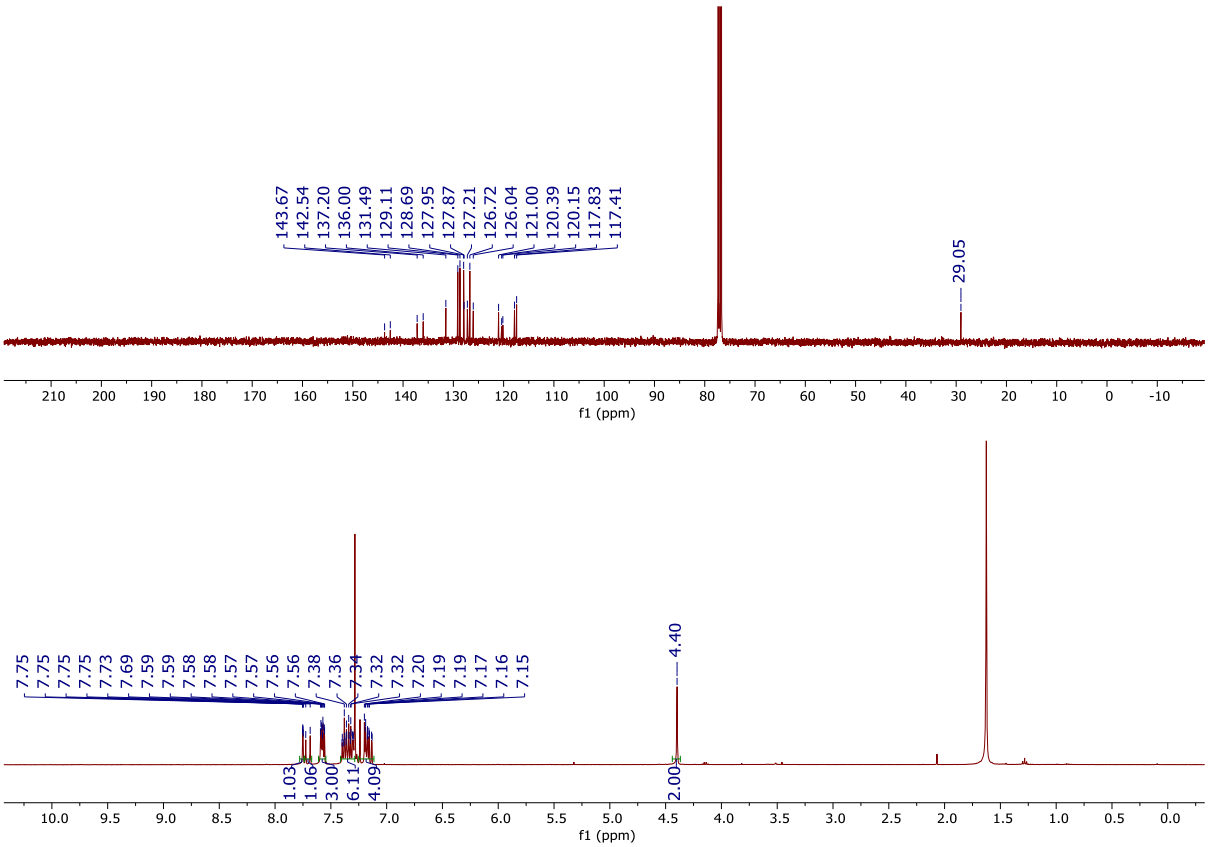

Fig. A.68 *^{1}H and ^{13}C-NMR spectrum of* ***4u*** *recorded in* ***$CDCl_3$.***

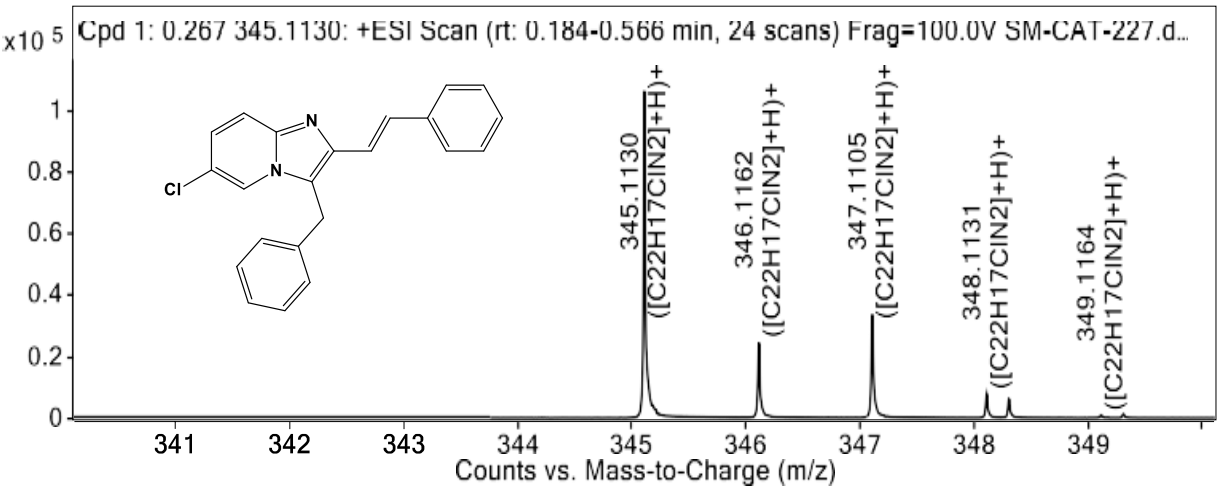

Fig. A.69 *HRMS of* ***4u*****.**

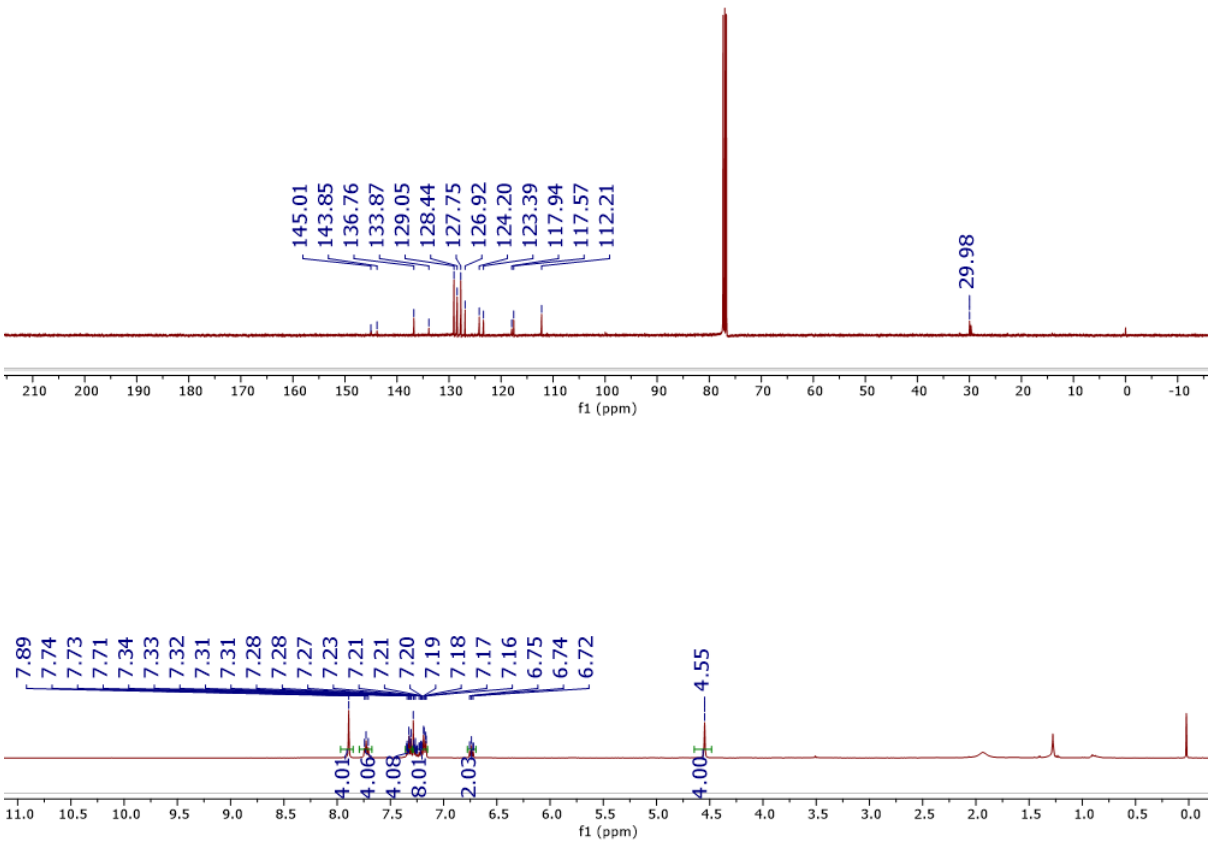

Fig. A.70 *^{1}H-NMR and ^{13}C-NMR spectrum of* ***4v*** *recorded in* ***$CDCl_3$.***

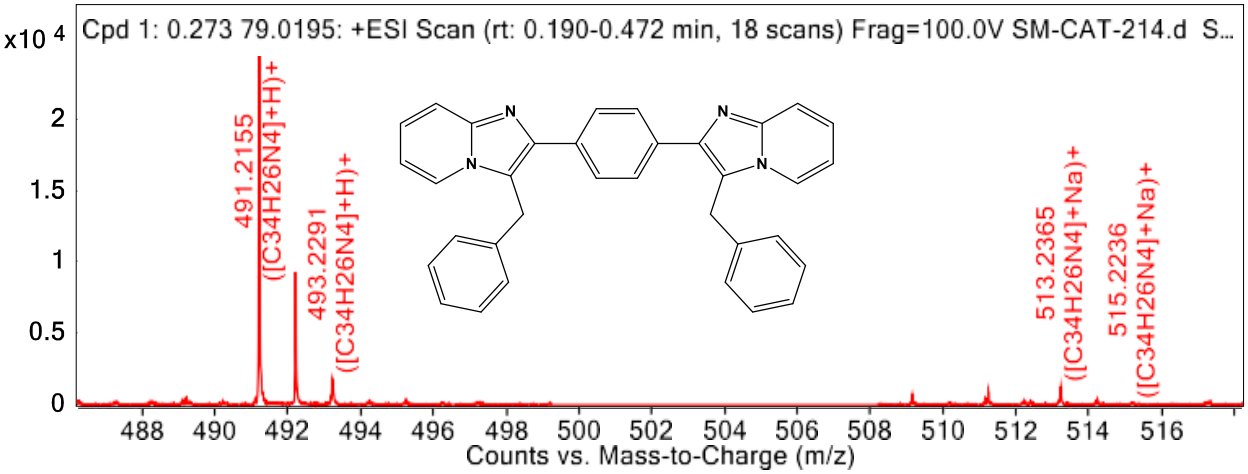

Fig. A.71 *HRMS of* ***4v.***

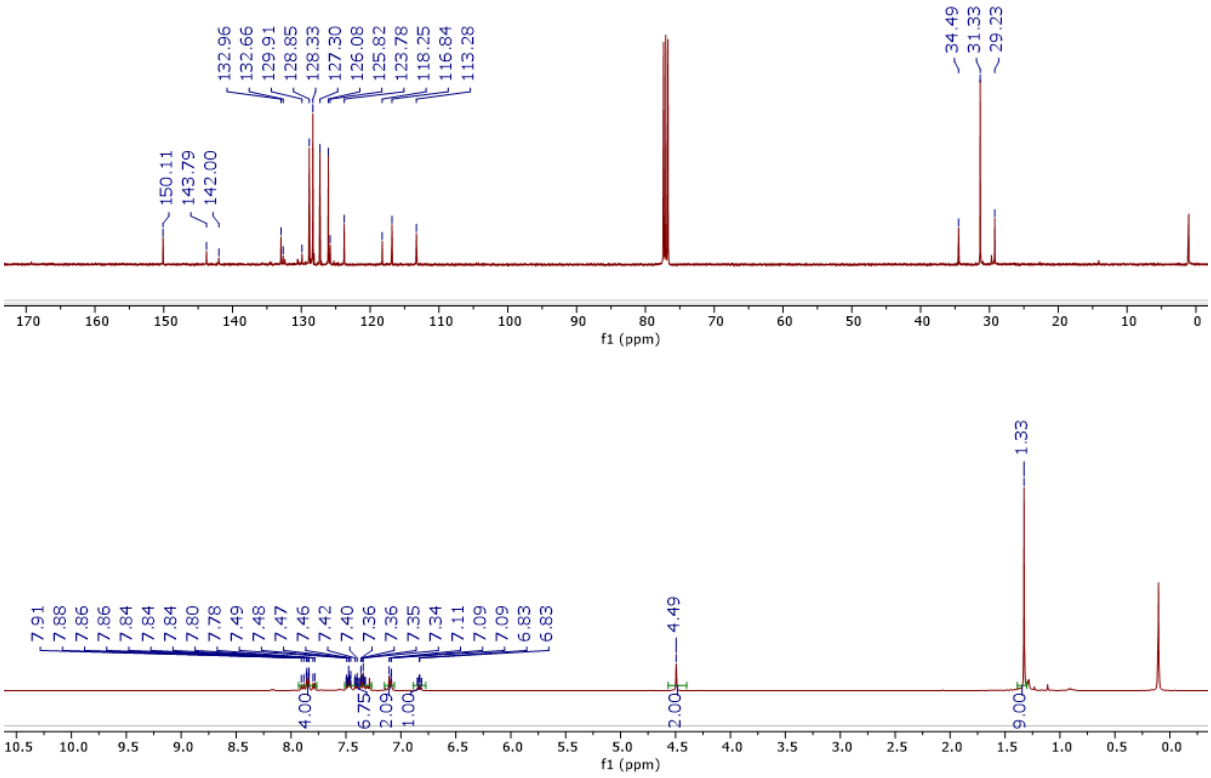

Fig. A.72 *^{1}H-NMR and ^{13}C-NMR spectrum of* ***4w*** *recorded in* ***$CDCl_3$****.*

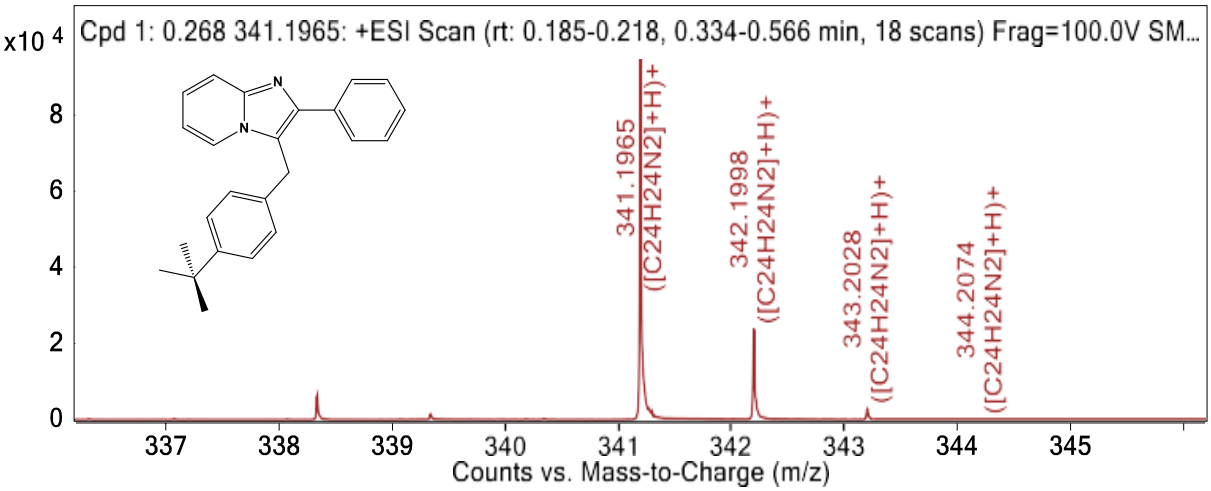

Fig. A.73 *HRMS of* ***4w****.*

Appendix A

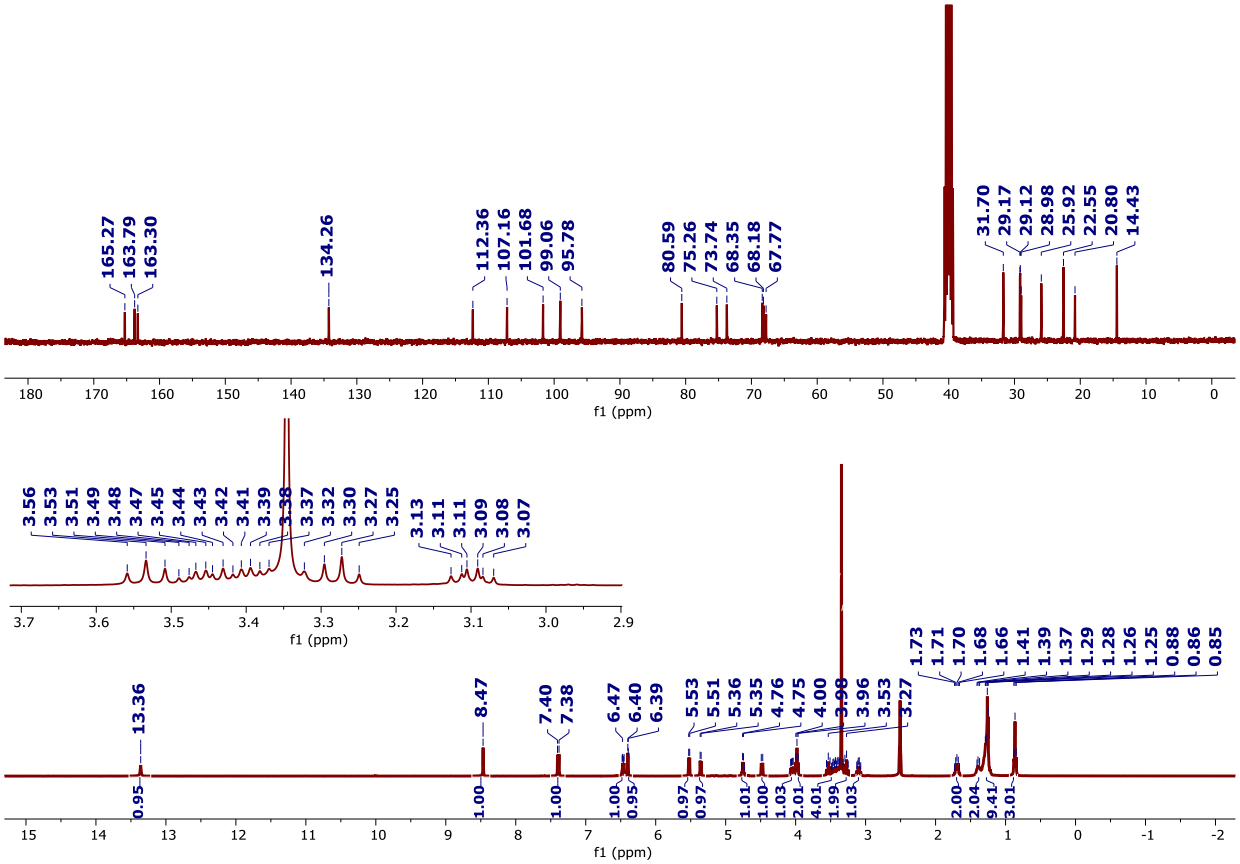

Fig. A.74 *^{1}H-NMR and ^{13}C-NMR spectrum of* ***4w*** *recorded in* ***DMSO-d6****.*

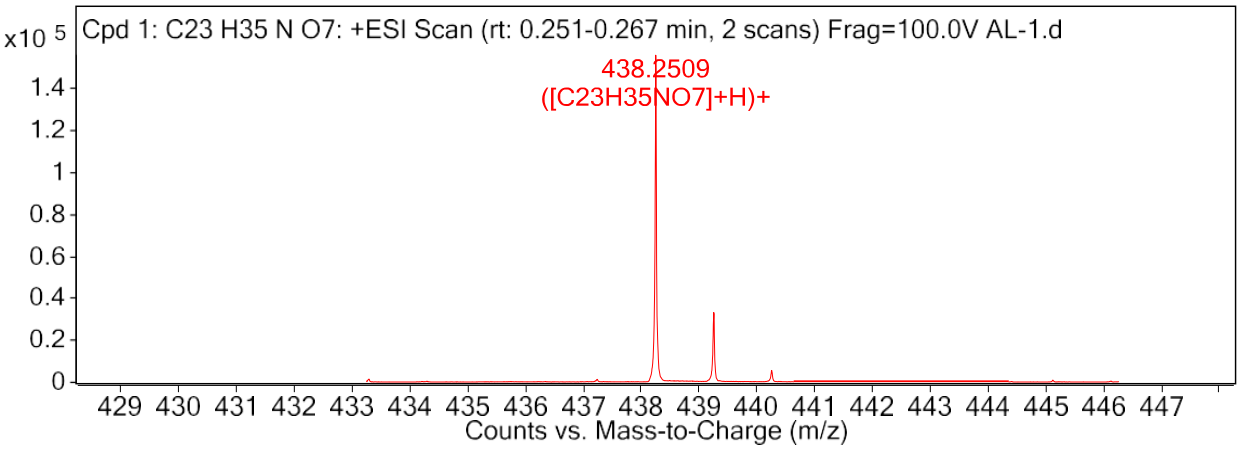

Fig. A.75 *HRMS of* ***ALH$_2$****.*

Appendix A

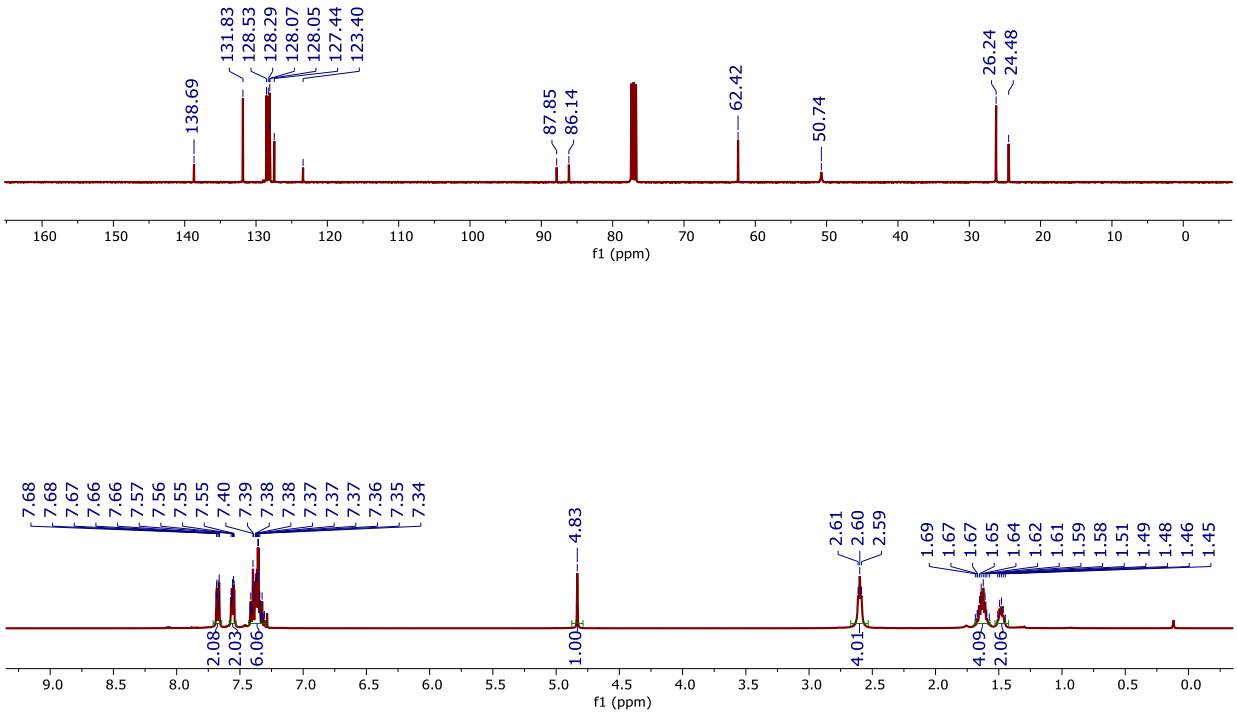

Fig. A76 *^{1}H-NMR and ^{13}C-NMR spectrum of* ***P1*** *recorded in* ***$CDCl_3$.***

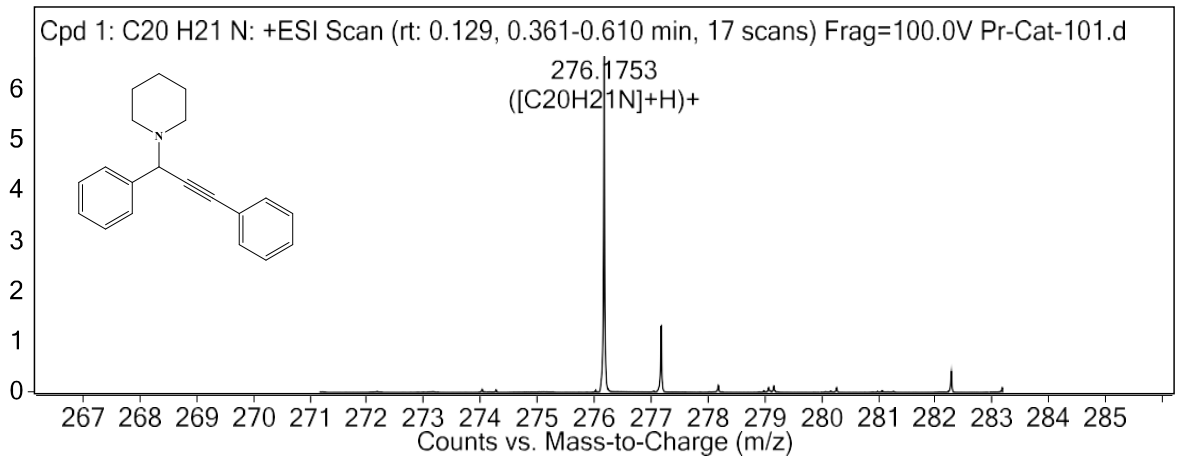

Fig. A77 *HRMS of* ***P1***

Appendix A

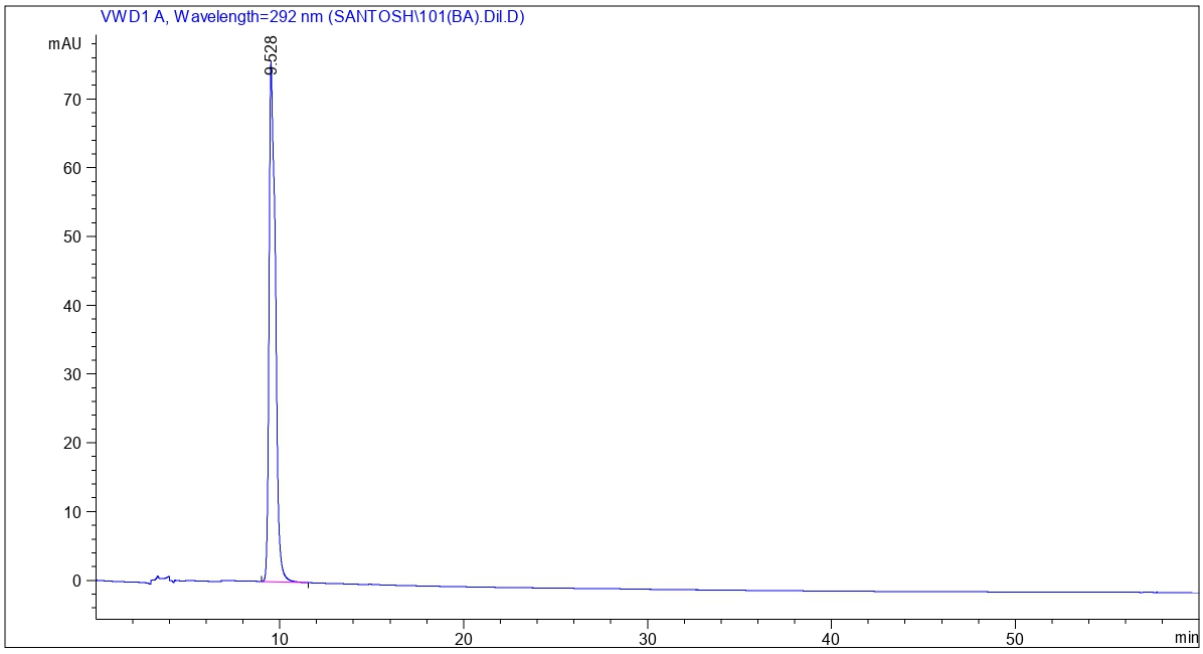

Fig. A78 *HPLC of Benzaldehyde*

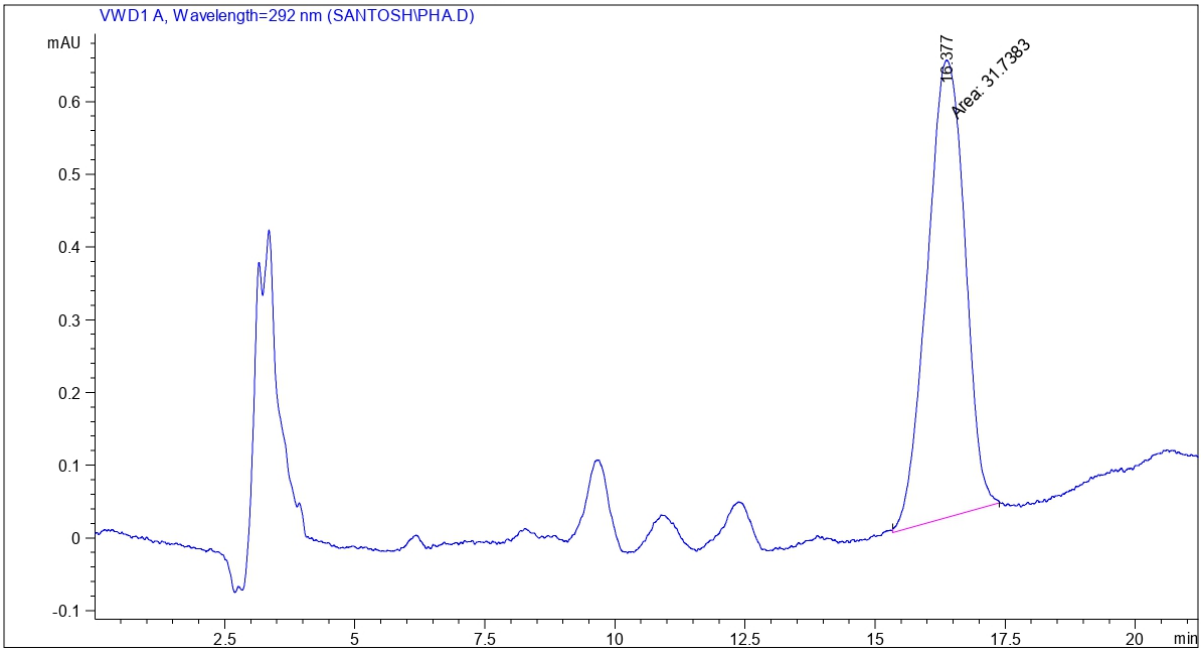

Fig. A79 *HPLC of Phenylacetylene*

Appendix A

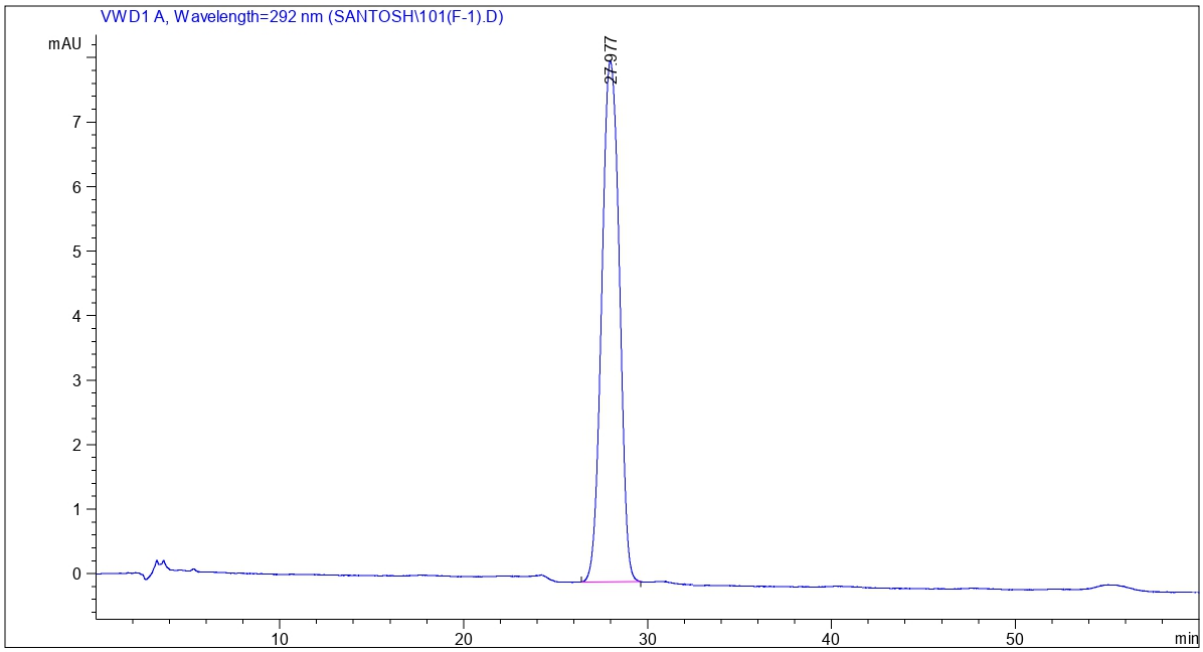

Fig. A80 *HPLC of* ***P1***

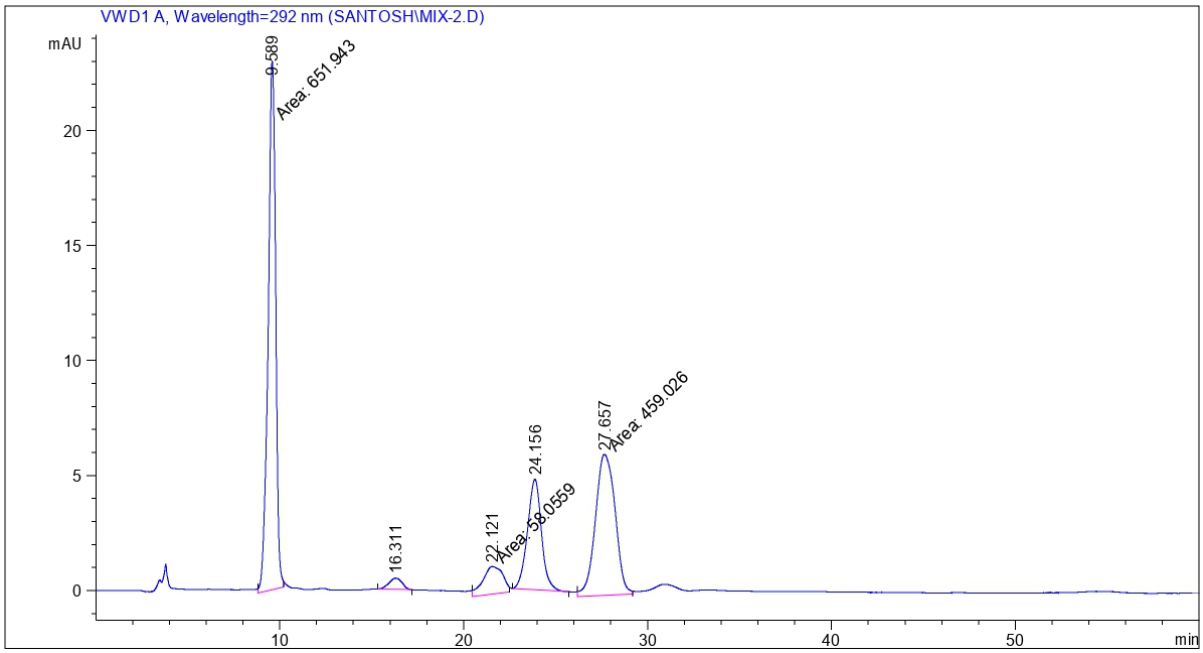

Fig. A81 *HPLC of reaction mixture (****P1****) after 2 hours*

Appendix A

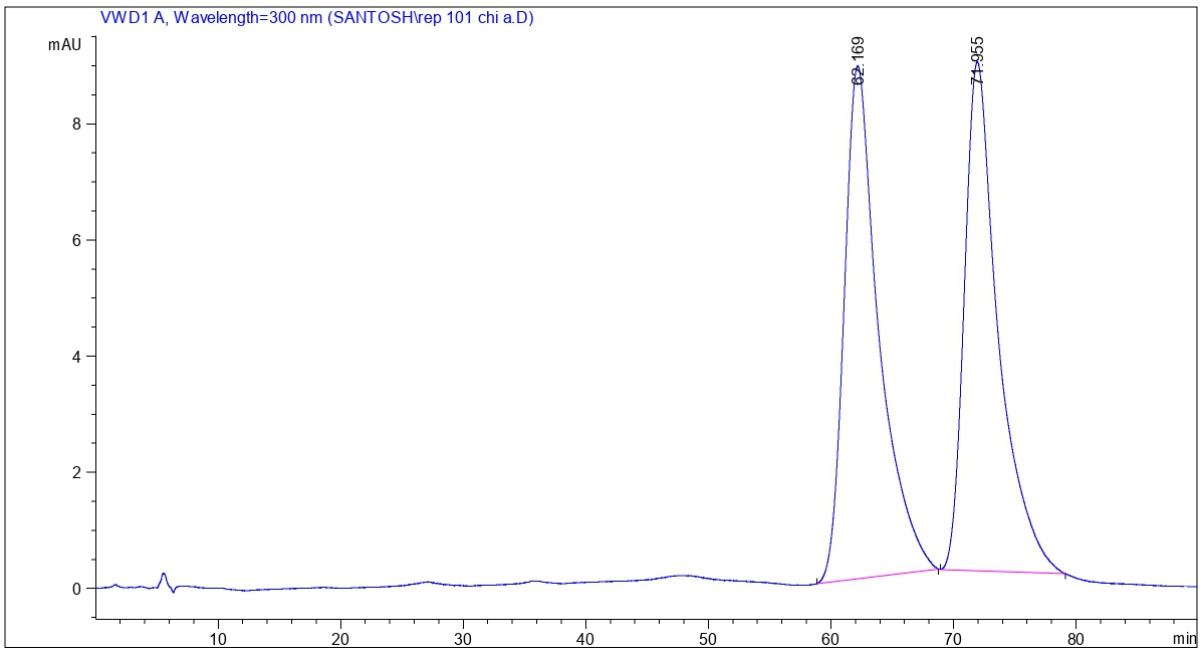

Signal 1: VWD1 A, Wavelength=300 nm

Peak #	RetTime [min]	Type	Width [min]	Area [mAU*s]	Height [mAU]	Area %
1	62.169	BB	2.3111	1738.28857	8.83248	50.7981
2	71.955	BB	2.2610	1683.66443	8.76136	49.2019
Totals :				3421.95300	17.59384	

Fig. A82 *HPLC of racemic* ***P1***

Appendix A

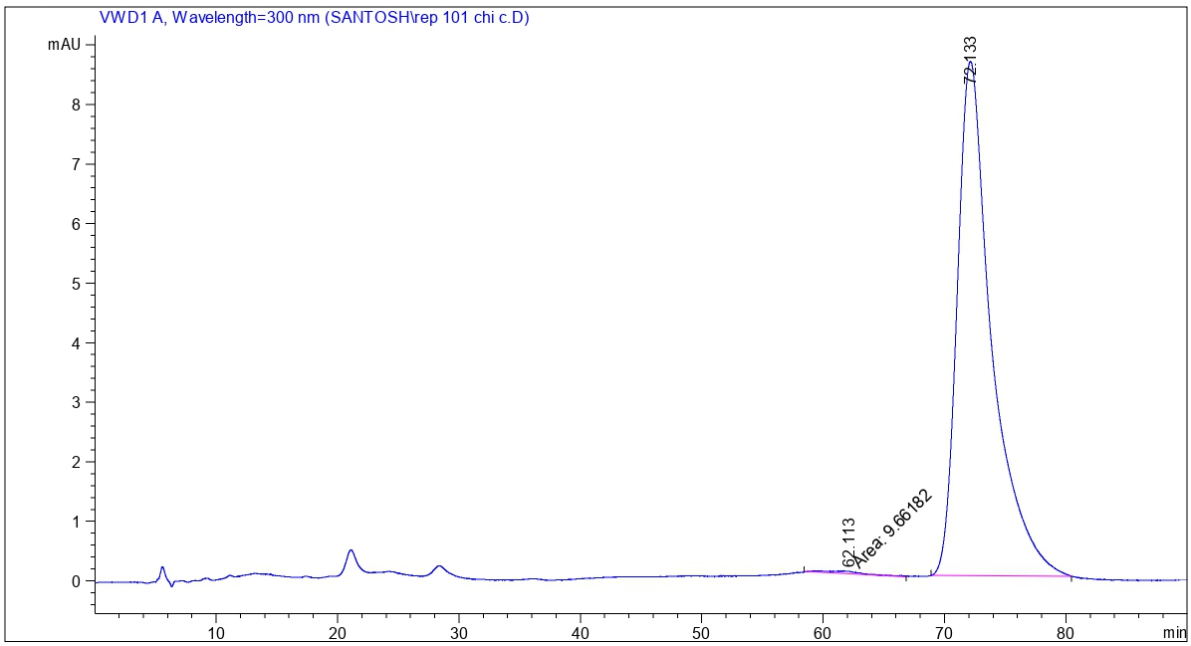

Signal 1: VWD1 A, Wavelength=300 nm

Peak #	RetTime [min]	Type	Width [min]	Area [mAU*s]	Height [mAU]	Area %
1	62.113	MM	3.5238	9.66182	4.56979e-2	0.5633
2	72.133	BB	2.3431	1705.62769	8.63651	99.4367
Totals :				1715.28950	8.68220	

Fig. A83 *HPLC of chiral* ***P1*** *isolated from first run*

Appendix A

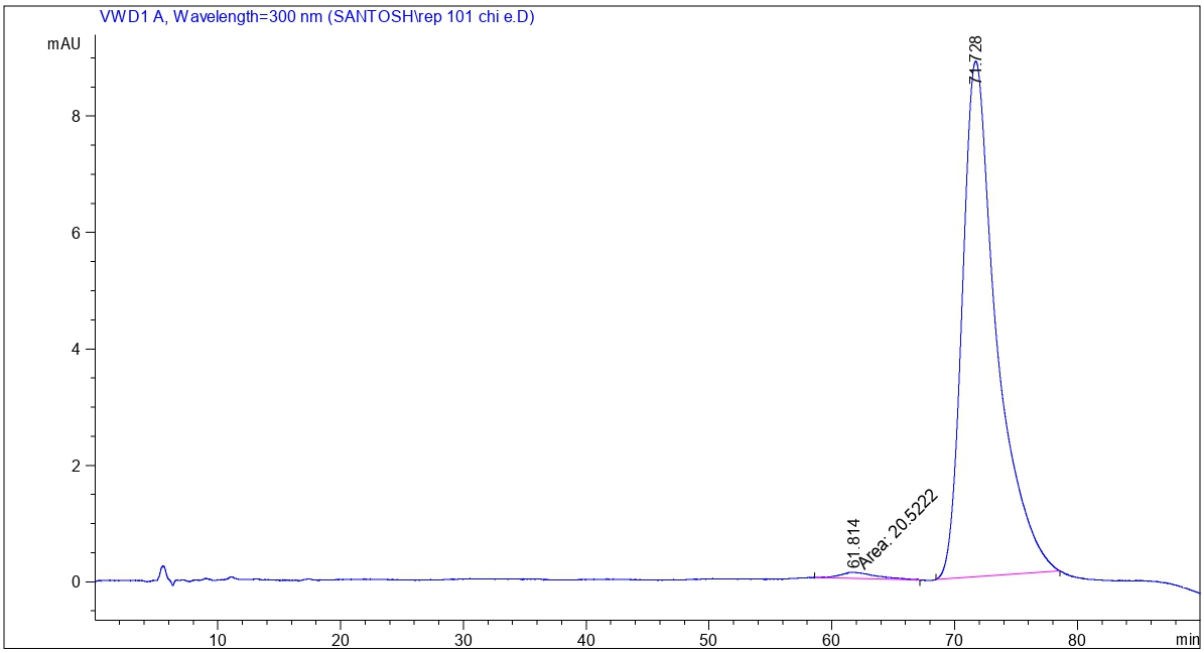

Signal 1: VWD1 A, Wavelength=300 nm

Peak #	RetTime [min]	Type	Width [min]	Area [mAU*s]	Height [mAU]	Area %
1	61.814	MM	3.2562	20.52224	1.05043e-1	1.1829
2	71.728	BB	2.2695	1714.40100	8.85584	98.8171
Totals :				1734.92324	8.96089	

Fig. A84 *HPLC of chiral* ***P1*** *isolated from second run*

Appendix A

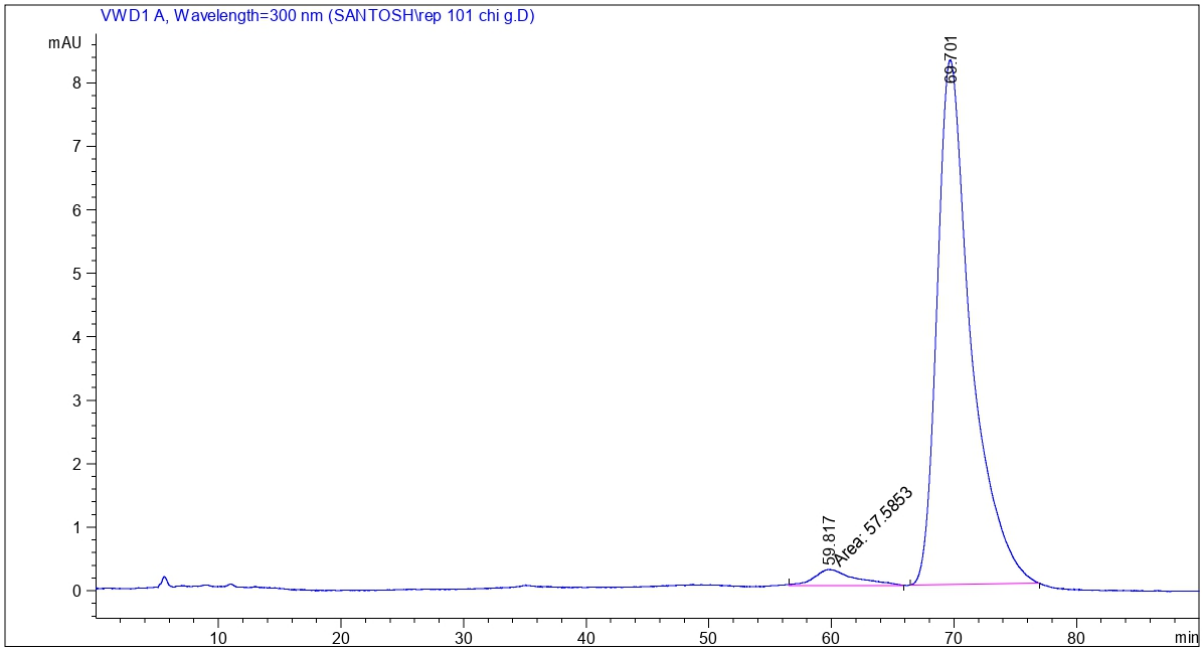

Signal 1: VWD1 A, Wavelength=300 nm

Peak #	RetTime [min]	Type	Width [min]	Area [mAU*s]	Height [mAU]	Area %
1	59.817	MM	3.8238	57.58528	2.50993e-1	3.4968
2	69.701	BB	2.2503	1589.21387	8.26513	96.5032
Totals :				1646.79914	8.51612	

Fig. A85 *HPLC of chiral* ***P1*** *isolated from third run*

Appendix A

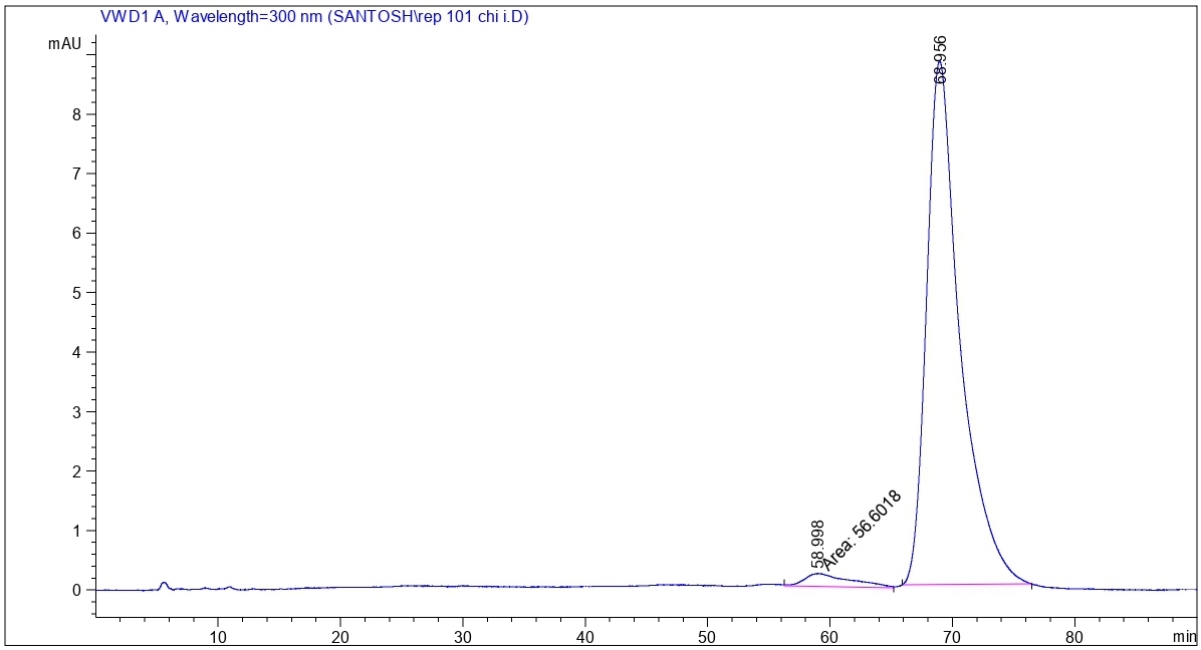

Signal 1: VWD1 A, Wavelength=300 nm

Peak #	RetTime [min]	Type	Width [min]	Area [mAU*s]	Height [mAU]	Area %
1	58.998	MM	4.3126	56.60182	2.18744e-1	3.2518
2	68.956	BB	2.2414	1684.04565	8.80890	96.7482
Totals :				1740.64747	9.02764	

Fig. A86 *HPLC of chiral* ***P1*** *isolated from forth run*

Appendix A

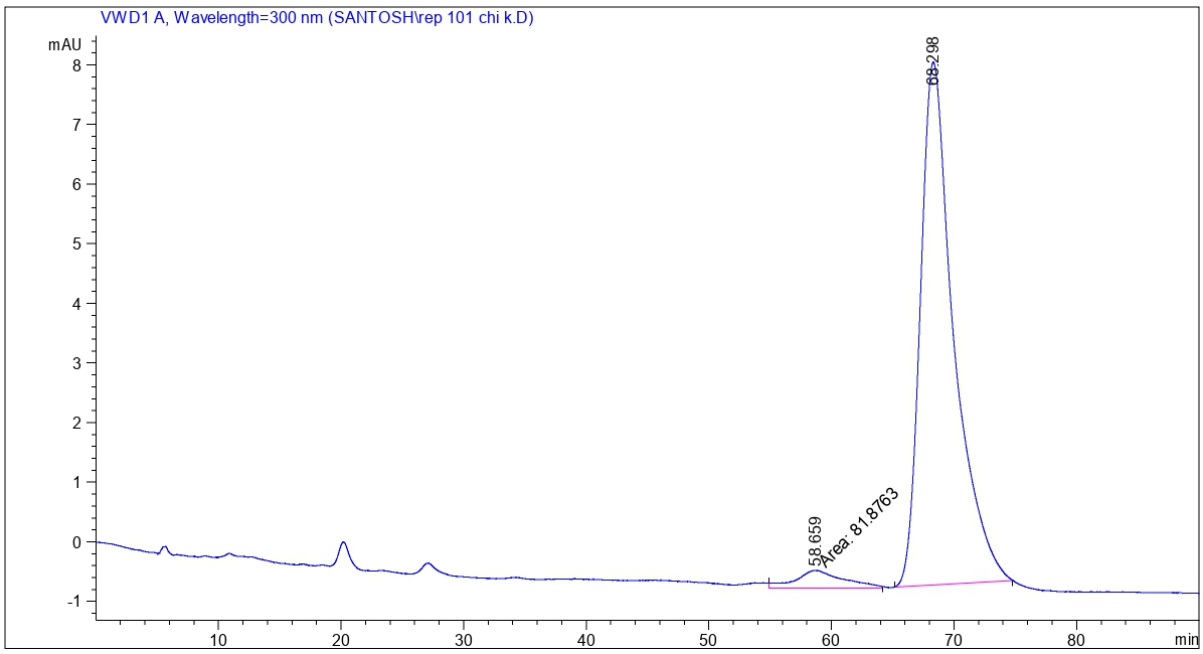

Signal 1: VWD1 A, Wavelength=300 nm

Peak #	RetTime [min]	Type	Width [min]	Area [mAU*s]	Height [mAU]	Area %
1	58.659	MM	4.5754	81.87632	2.98248e-1	4.7152
2	68.298	BB	2.2272	1654.57178	8.76927	95.2848
Totals :				1736.44810	9.06752	

Fig. A87 *HPLC of chiral* ***P1*** *isolated from fifth run*

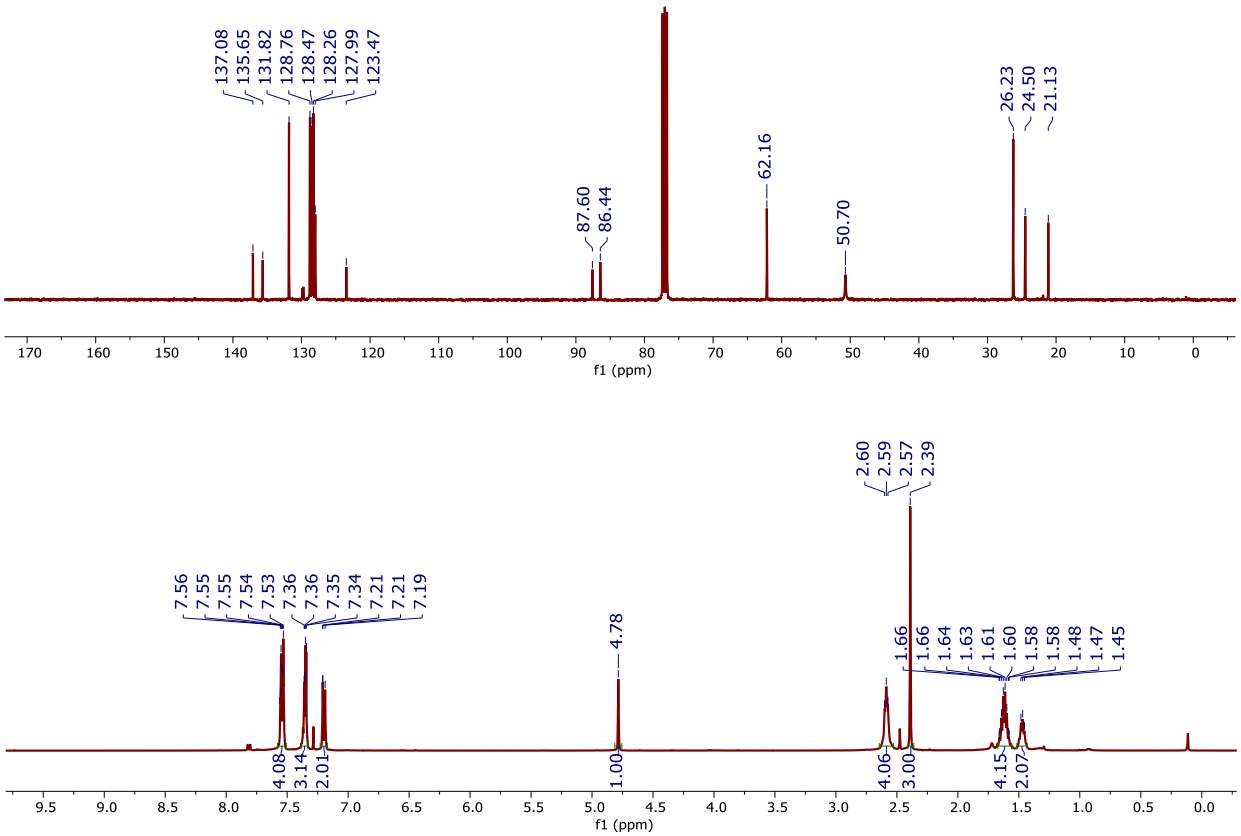

Fig. A88 *^{1}H-NMR and ^{13}C-NMR spectrum of* ***P2*** *recorded in* ***$CDCl_3$***

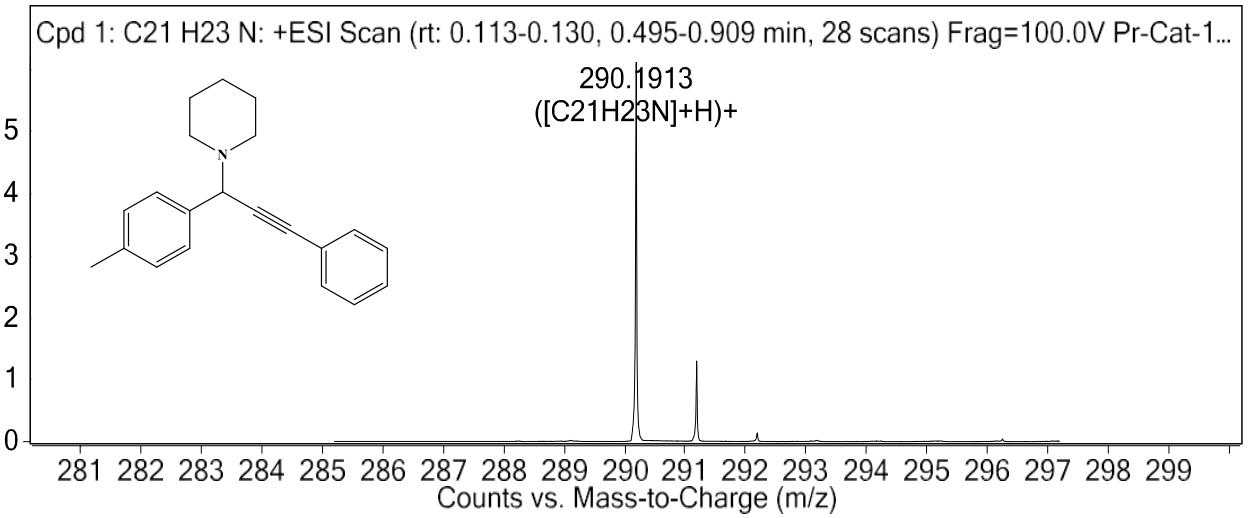

Fig. A89 *HRMS of* ***P2***

Appendix A

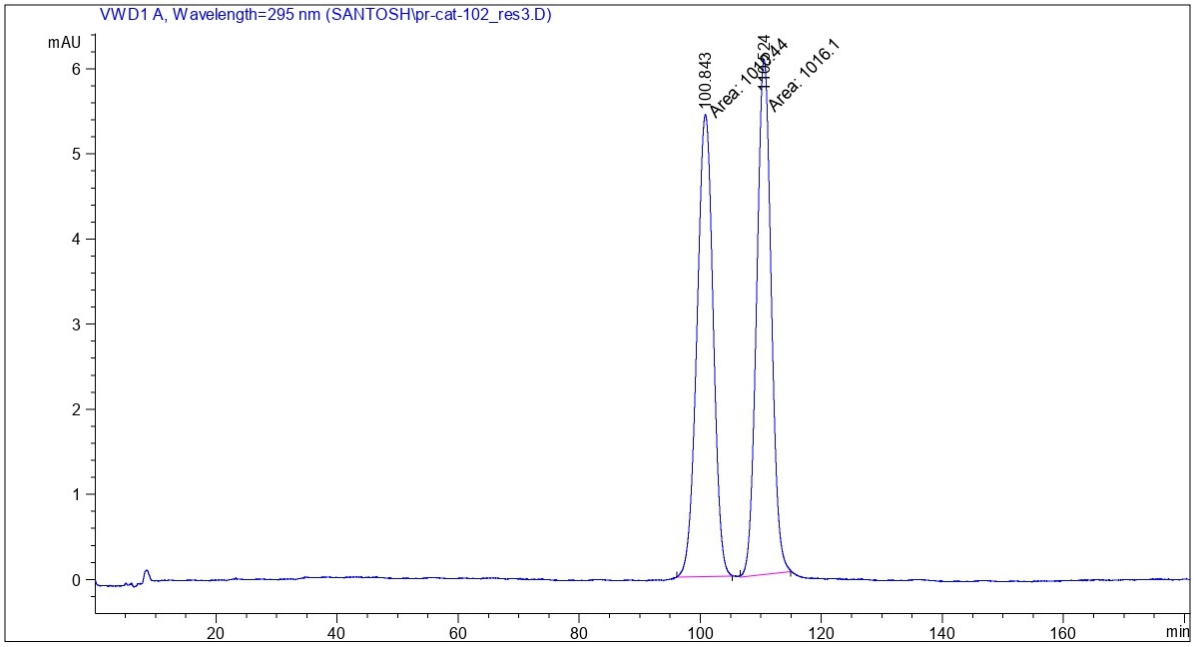

Signal 1: VWD1 A, Wavelength=295 nm

Peak #	RetTime [min]	Type	Width [min]	Area [mAU*s]	Height [mAU]	Area %
1	100.843	MM	3.1025	1010.43732	5.42805	49.8602
2	110.524	MM	2.7995	1016.10425	6.04937	50.1398
Totals :				2026.54156	11.47743	

Fig. A90 *HPLC of racemic* ***P2***

Appendix A

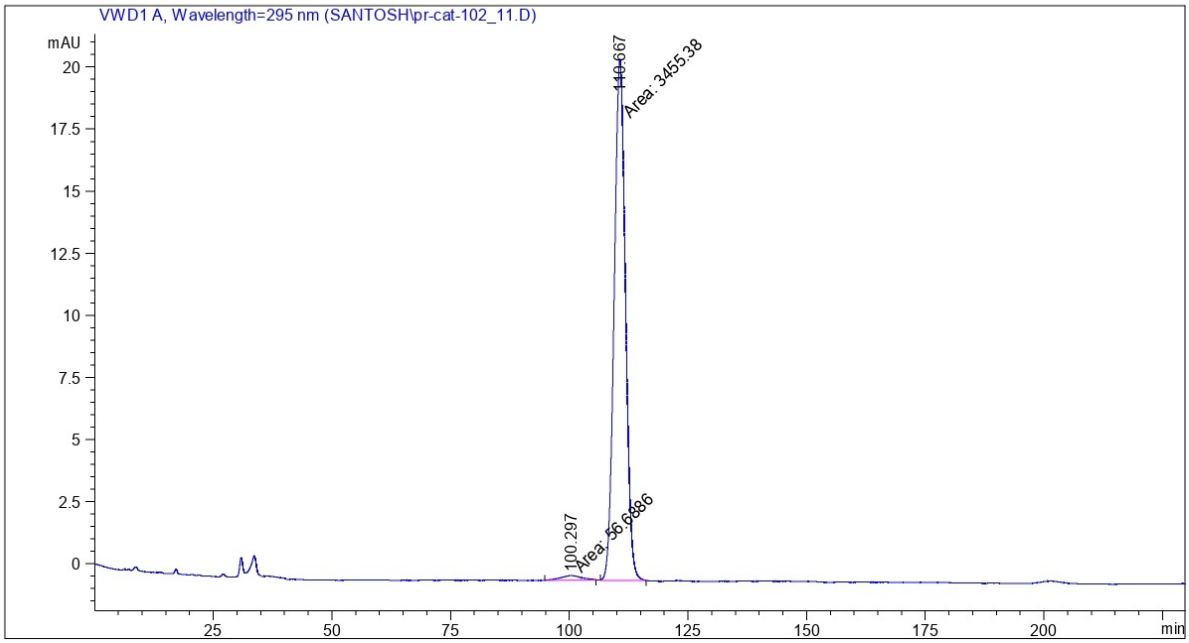

Signal 1: VWD1 A, Wavelength=295 nm

Peak #	RetTime [min]	Type	Width [min]	Area [mAU*s]	Height [mAU]	Area %
1	100.297	MM	5.0900	56.68857	1.85622e-1	1.6141
2	110.667	MM	2.7492	3455.38110	20.94757	98.3859
Totals :				3512.06967	21.13319	

Fig. A91 *HPLC of chiral* ***P2***

Appendix A

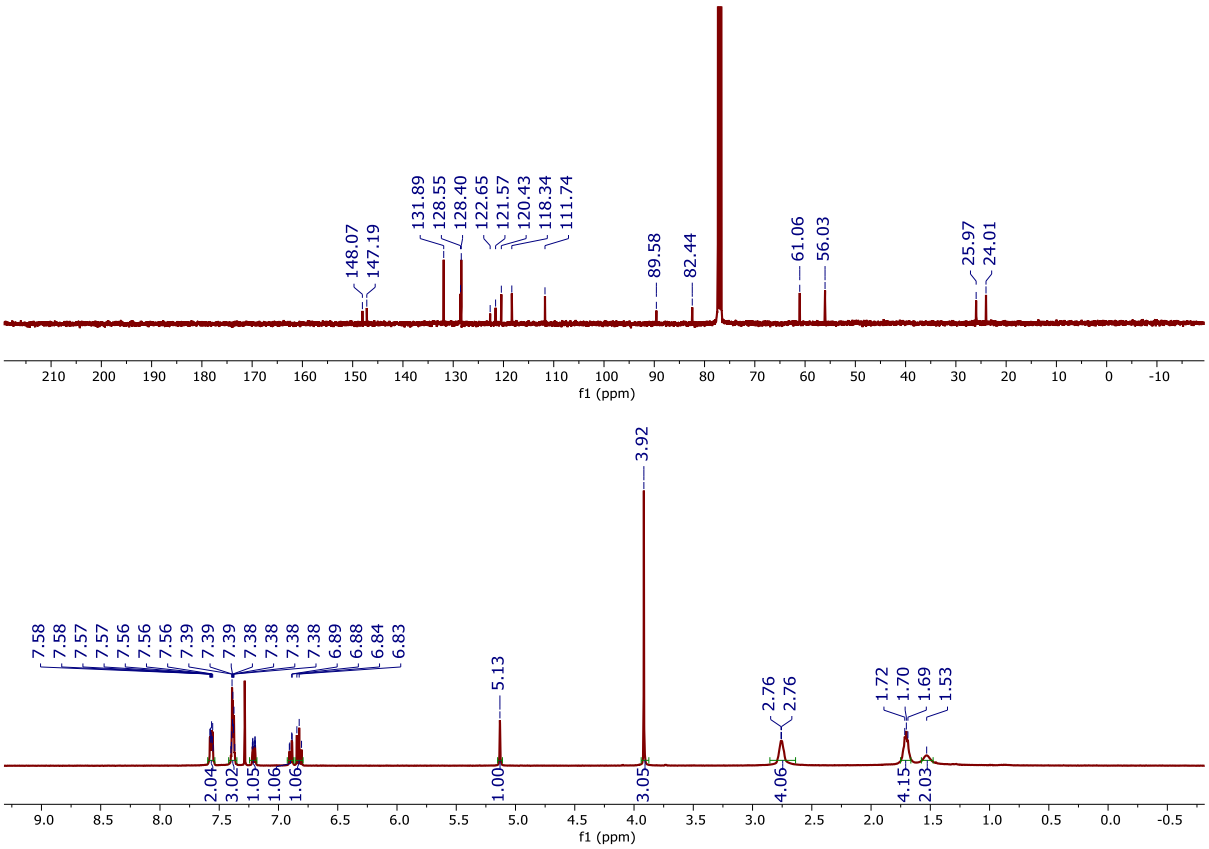

Fig. A92 *^{1}H-NMR and ^{13}C-NMR spectrum of* ***P3*** *recorded in* ***$CDCl_3$***

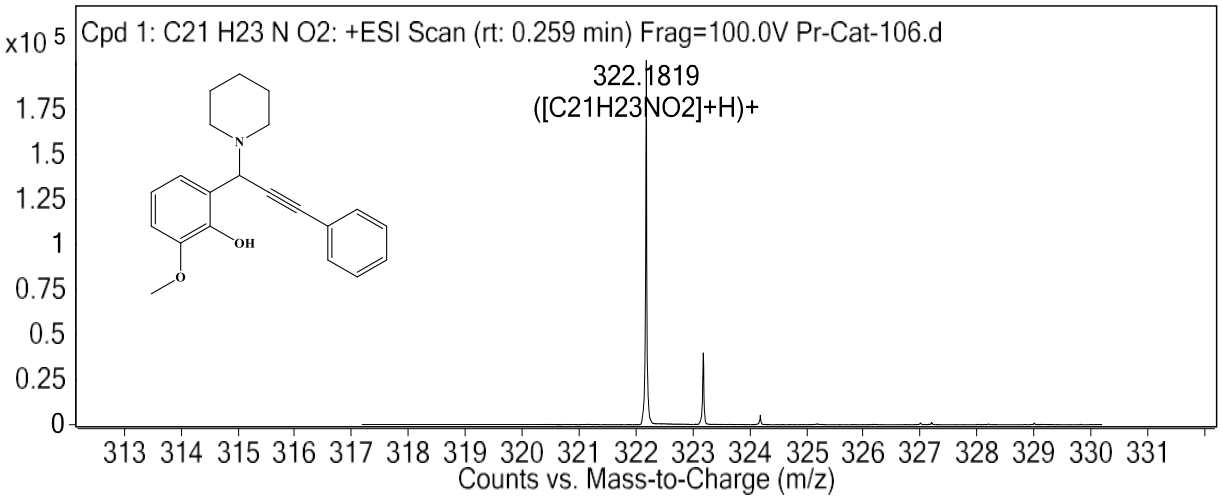

Fig. A93 *HRMS of* ***P3***

Appendix A

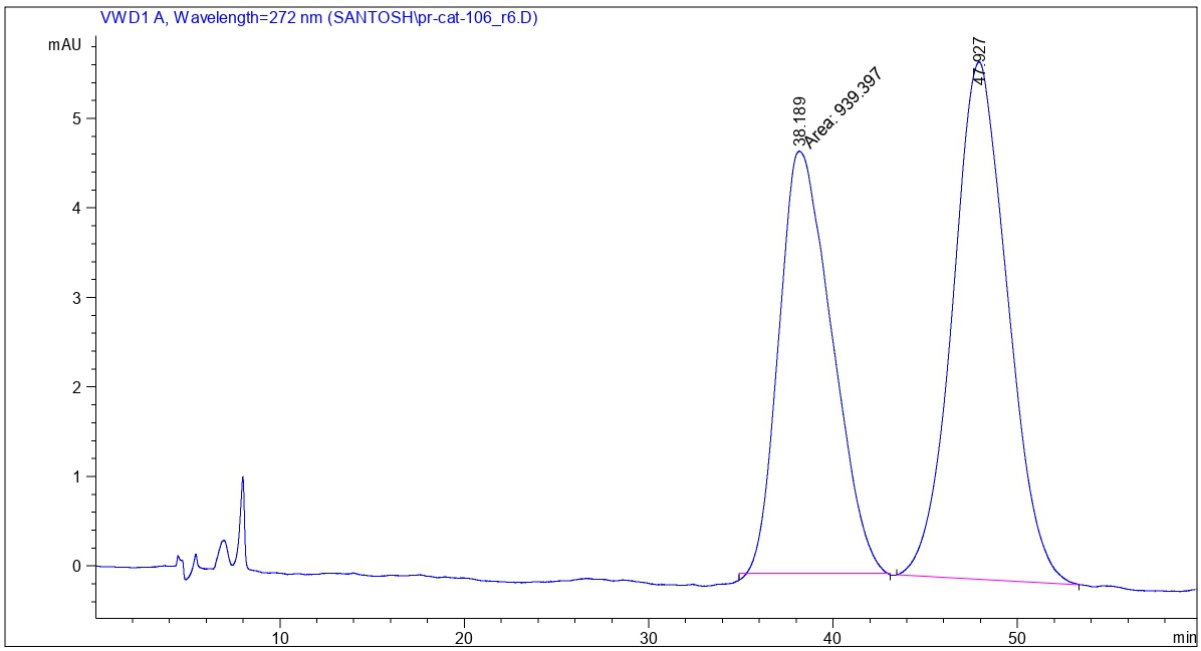

Signal 1: VWD1 A, Wavelength=272 nm

Peak #	RetTime [min]	Type	Width [min]	Area [mAU*s]	Height [mAU]	Area %
1	38.189	MM	3.3199	939.39667	4.71593	44.0343
2	47.927	BB	2.4134	1193.93469	5.77886	55.9657
Totals :				2133.33136	10.49478	

Fig. A94 *HPLC of racemic* ***P3***

Appendix A

Additional Info : Peak(s) manually integrated

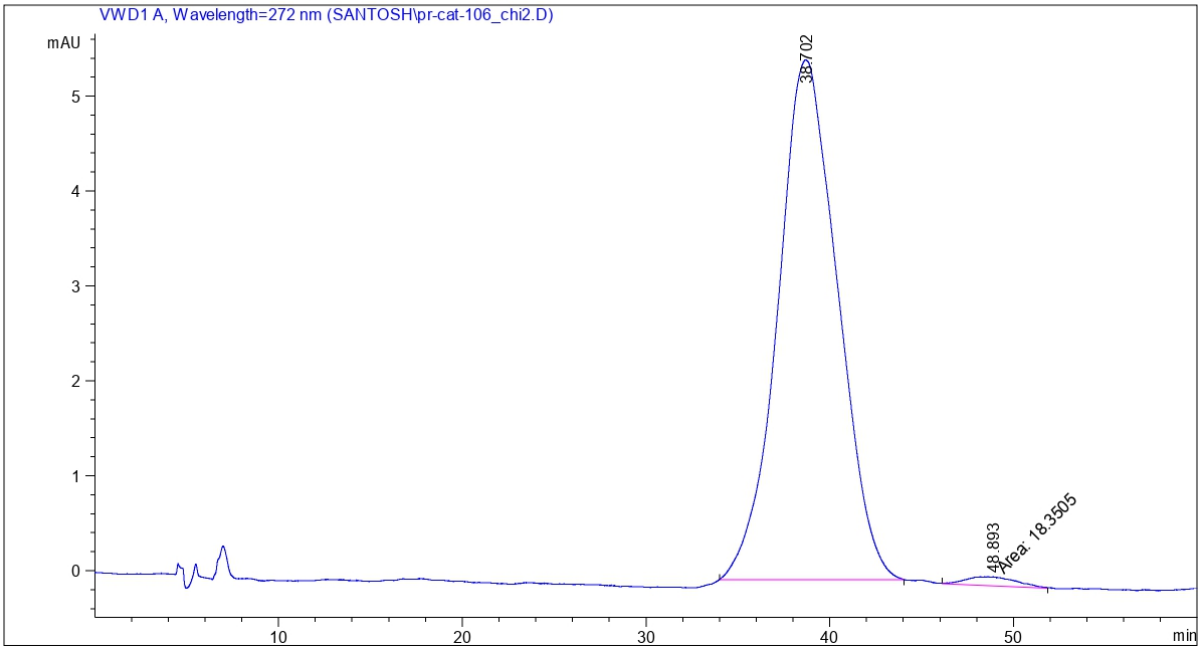

Signal 1: VWD1 A, Wavelength=272 nm

Peak #	RetTime [min]	Type	Width [min]	Area [mAU*s]	Height [mAU]	Area %
1	38.702	BB	2.6394	1236.63428	5.47453	98.5378
2	48.893	MM	3.1927	18.35048	9.57953e-2	1.4622
Totals :				1254.98476	5.57033	

Fig. A95 *HPLC of chiral* ***P3***

Appendix A

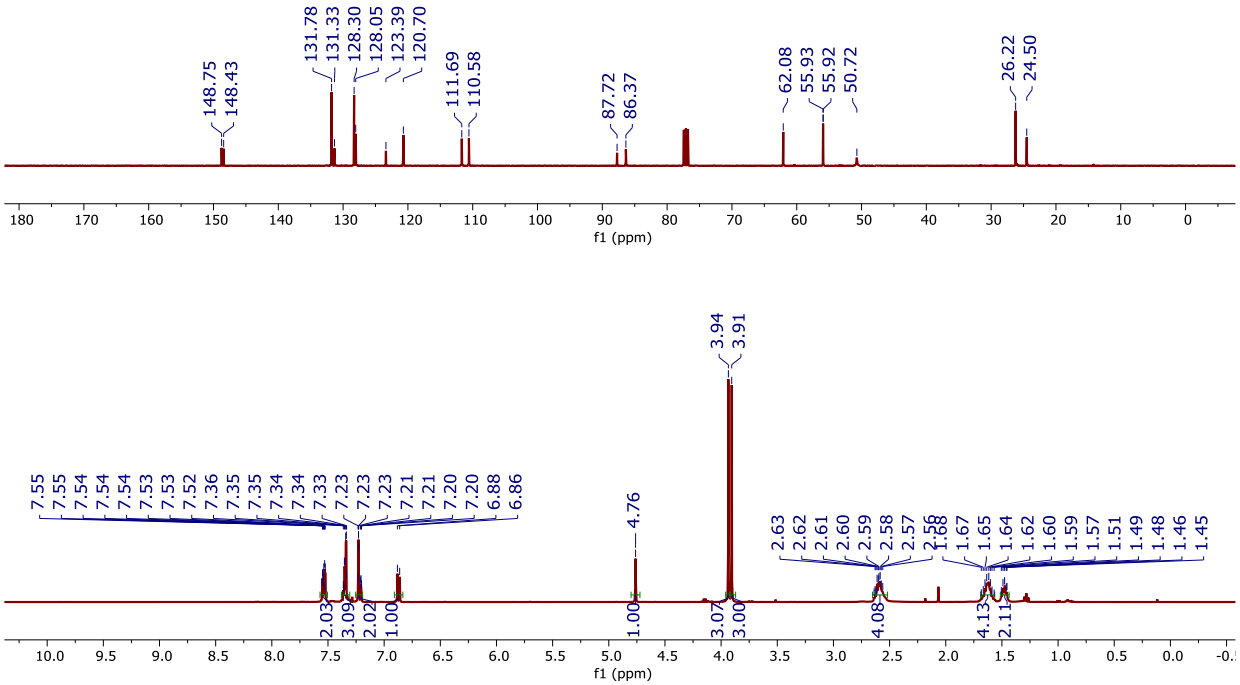

Fig. A96 *^{1}H-NMR and ^{13}C-NMR spectrum of* ***P4*** *recorded in* ***$CDCl_3$***

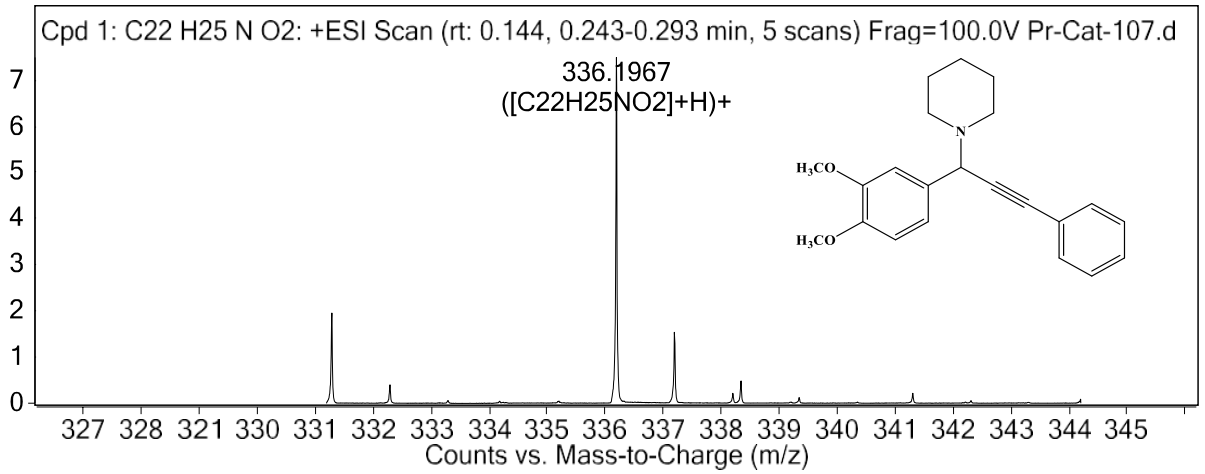

Fig. A97 *HRMS of* ***P4***

Appendix A

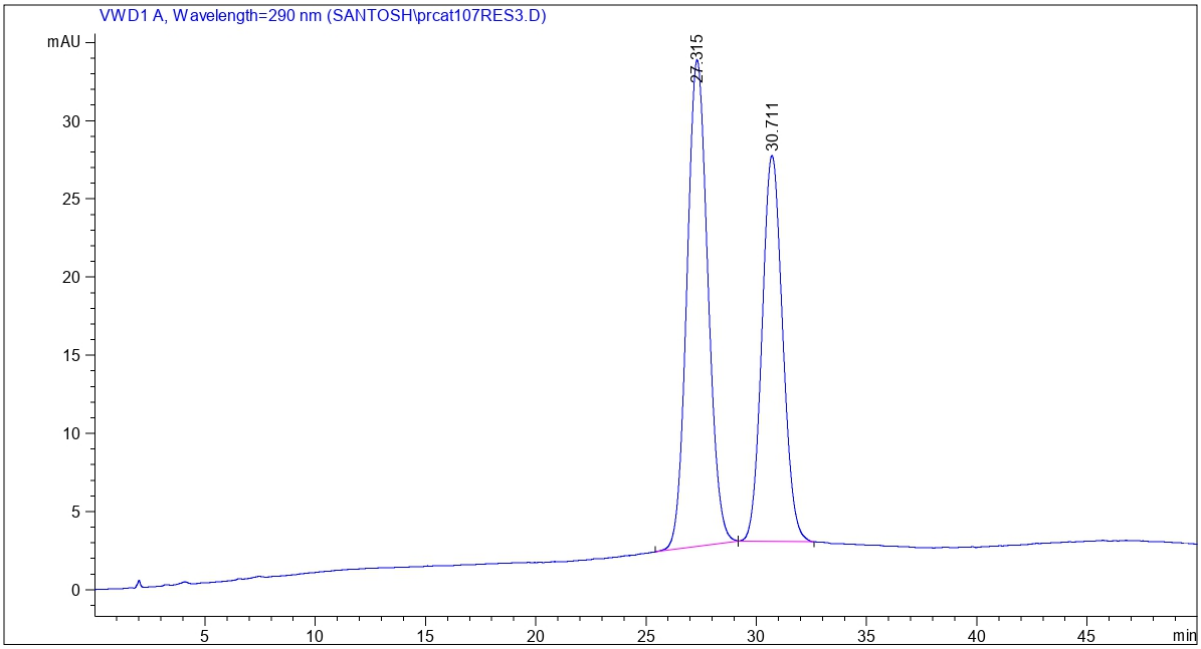

Signal 1: VWD1 A, Wavelength=290 nm

Peak #	RetTime [min]	Type	Width [min]	Area [mAU*s]	Height [mAU]	Area %
1	27.315	BB	1.0244	2058.27197	31.12779	56.2072
2	30.711	BB	1.0000	1603.66187	24.68325	43.7928
Totals :				3661.93384	55.81104	

Fig. A98 *HPLC of racemic* ***P4***

Appendix A

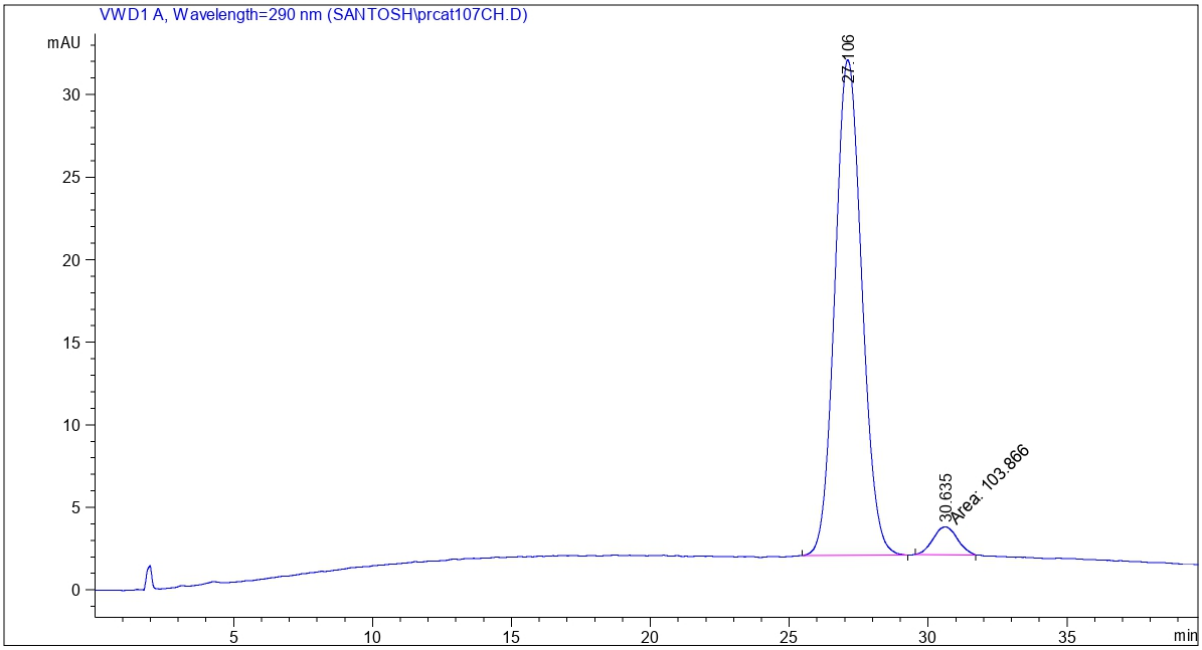

Signal 1: VWD1 A, Wavelength=290 nm

Peak #	RetTime [min]	Type	Width [min]	Area [mAU*s]	Height [mAU]	Area %
1	27.106	BB	1.0401	2025.23633	30.01692	95.1216
2	30.635	MM	1.0185	103.86600	1.69972	4.8784
Totals :				2129.10233	31.71665	

Fig. A99 *HPLC of chiral* ***P4***

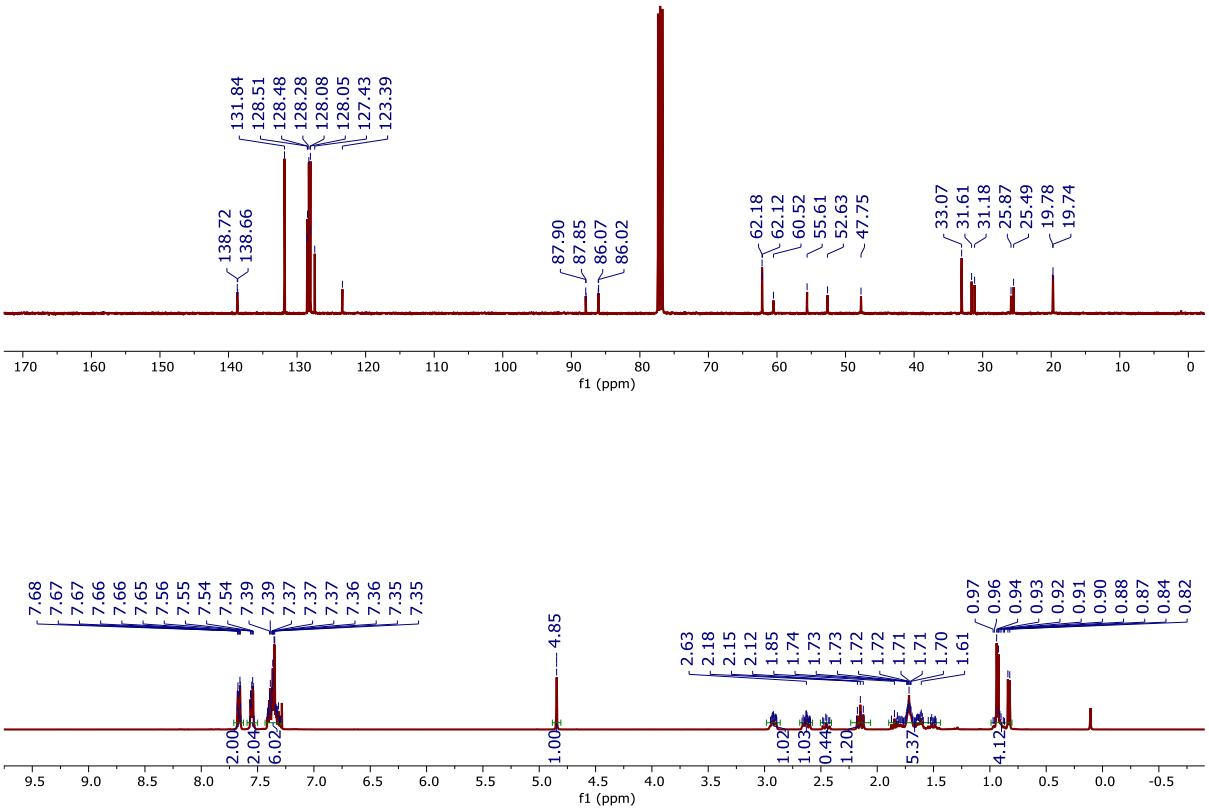

Fig. A100 *^{1}H-NMR and ^{13}C-NMR spectrum of* ***P5*** *recorded in* ***$CDCl_3$***

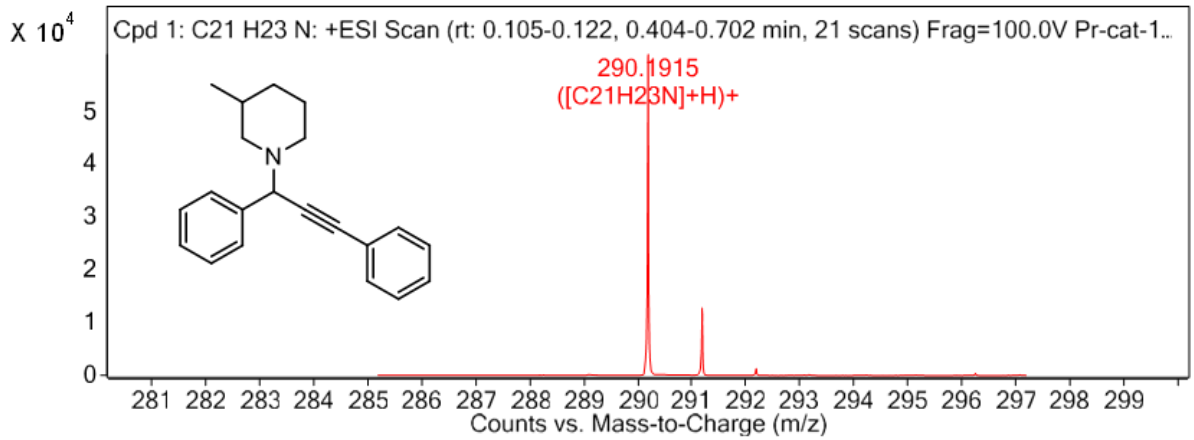

Fig. A101 *HRMS of* ***P5***

Appendix A

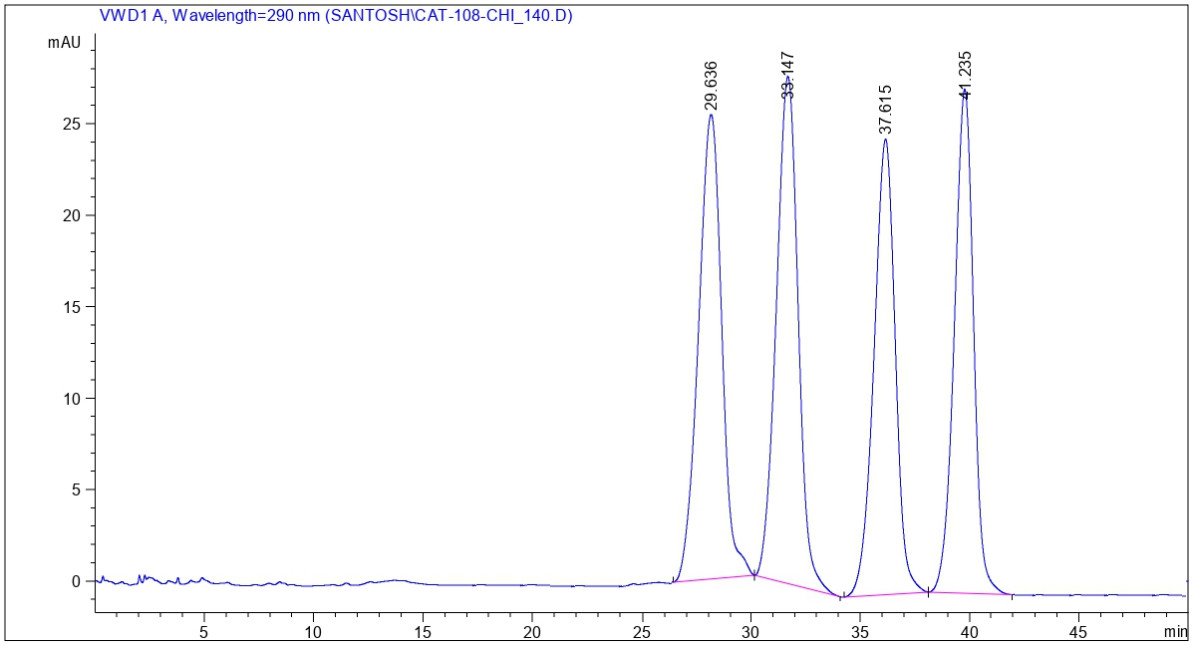

Signal 1: VWD1 A, Wavelength=290 nm

Peak #	RetTime [min]	Type	Width [min]	Area [mAU*s]	Height [mAU]	Area %
1	29.636	BB	1.1330	1878.49500	25.39462	26.2321
2	33.147	BB	1.0726	1922.37463	27.73810	26.8448
3	37.615	BB	1.0405	1684.75989	24.89728	23.5267
4	41.235	BB	0.9426	1675.43616	27.54593	23.3965
Totals :				7161.06567	105.57592	

Fig. A102 *HPLC of racemic* ***P5***

Appendix A

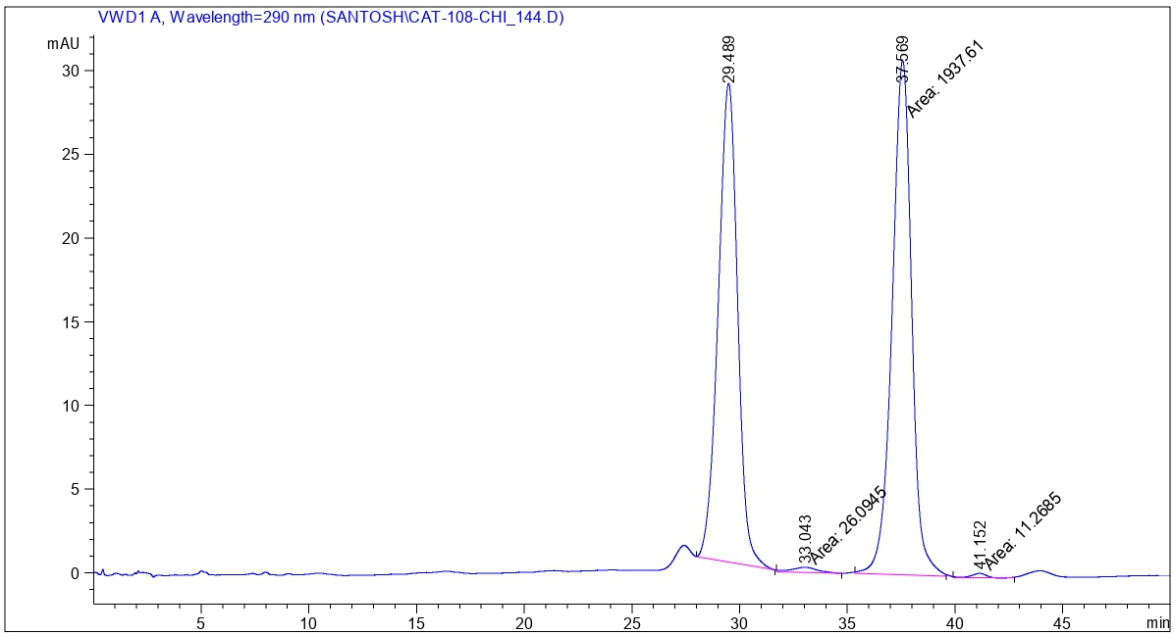

Signal 1: VWD1 A, Wavelength=290 nm

Peak #	RetTime [min]	Type	Width [min]	Area [mAU*s]	Height [mAU]	Area %
1	29.489	BB	0.9466	1790.91858	28.60022	47.5562
2	33.043	MM	1.3848	26.09446	3.14060e-1	0.6929
3	37.569	MM	1.0512	1937.61499	30.71970	51.4516
4	41.152	MM	0.7538	11.26849	2.49135e-1	0.2992
Totals :				3765.89652	59.88311	

Fig. A103 *HPLC of chiral* ***P5***

Appendix A

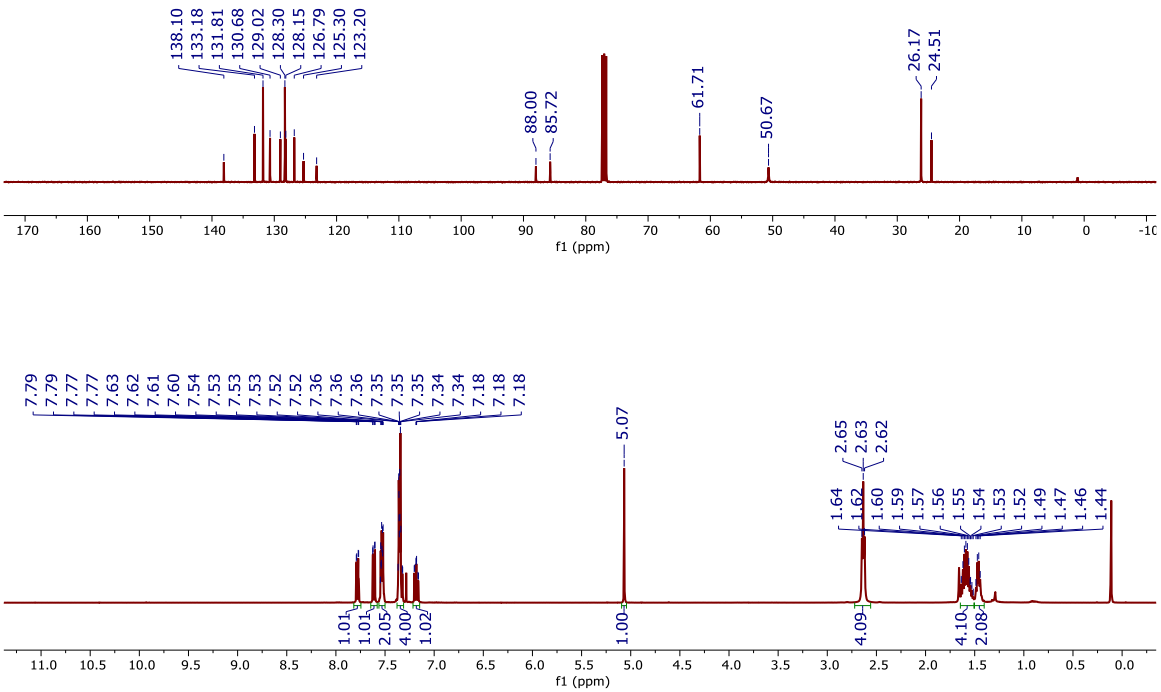

Fig. A104 *^{1}H-NMR and ^{13}C-NMR ^{1}H-NMR spectrum of* ***P6*** *recorded in* ***$CDCl_3$***

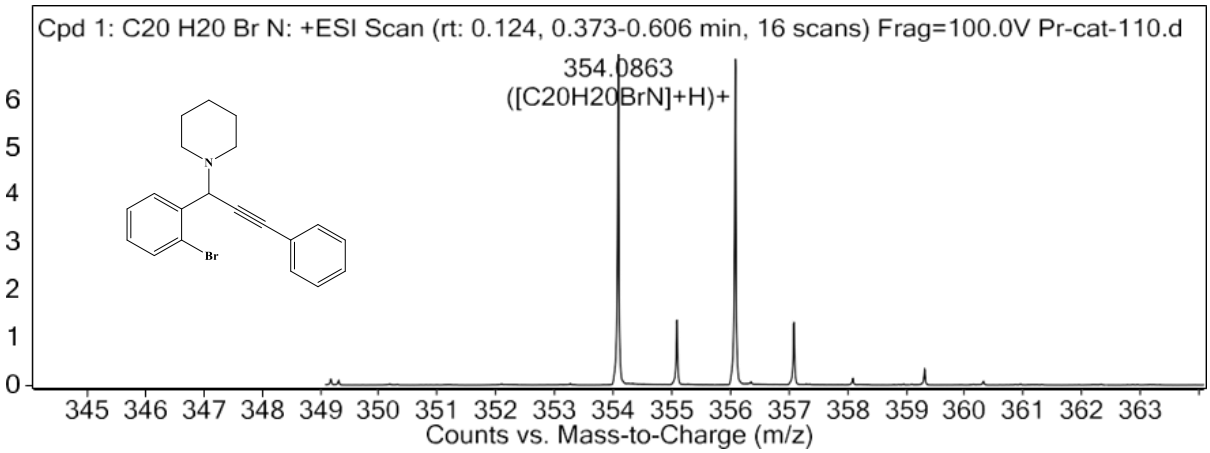

Fig. A105 *HRMS of* ***P6***

Appendix A

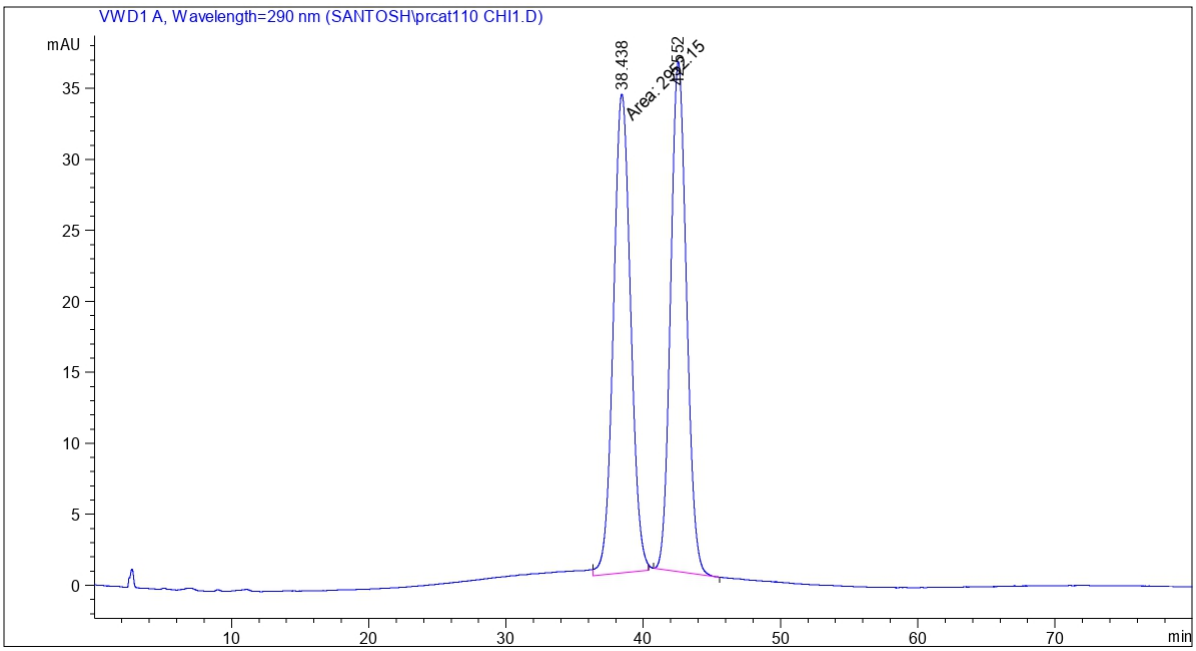

Signal 1: VWD1 A, Wavelength=290 nm

Peak #	RetTime [min]	Type	Width [min]	Area [mAU*s]	Height [mAU]	Area %
1	38.438	MM	1.4583	2952.14917	33.73915	50.5115
2	42.552	BB	1.2307	2892.36499	35.90923	49.4885
Totals :				5844.51416	69.64839	

Fig. A106 *HPLC of racemic* ***P6***

Appendix A

Additional Info : Peak(s) manually integrated

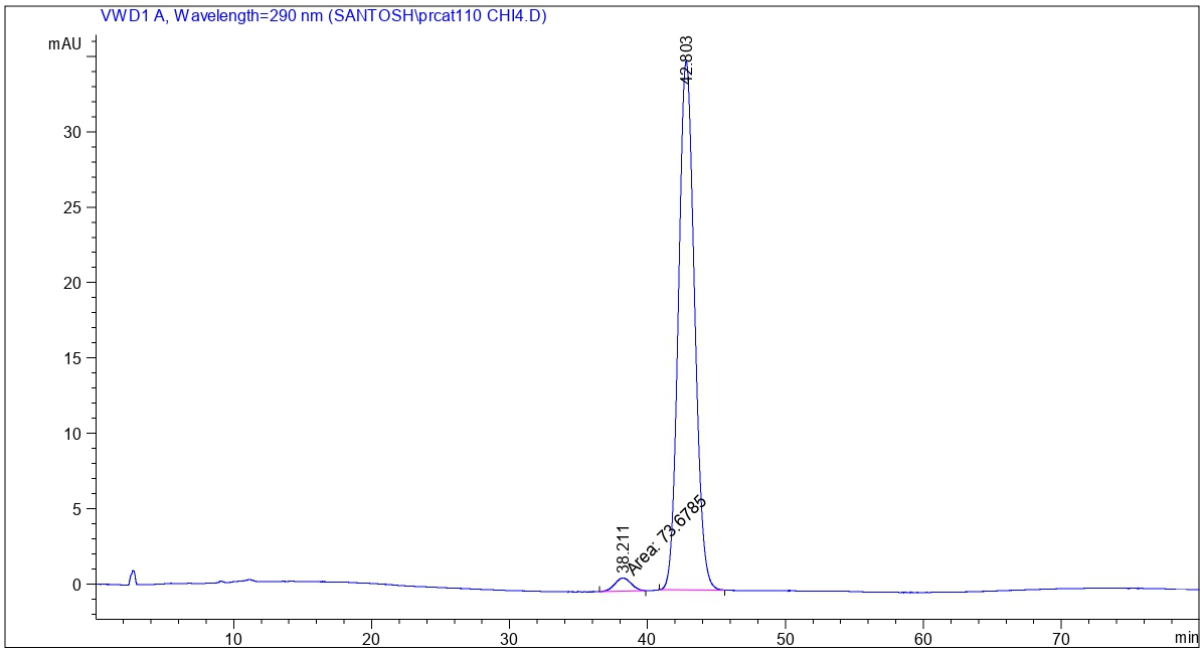

Signal 1: VWD1 A, Wavelength=290 nm

Peak #	RetTime [min]	Type	Width [min]	Area [mAU*s]	Height [mAU]	Area %
1	38.211	MM	1.3973	73.67847	8.78796e-1	2.5251
2	42.803	BB	1.2435	2844.17822	35.05753	97.4749
Totals :				2917.85670	35.93633	

Fig. A107 *HPLC of chiral* ***P6***

Appendix A

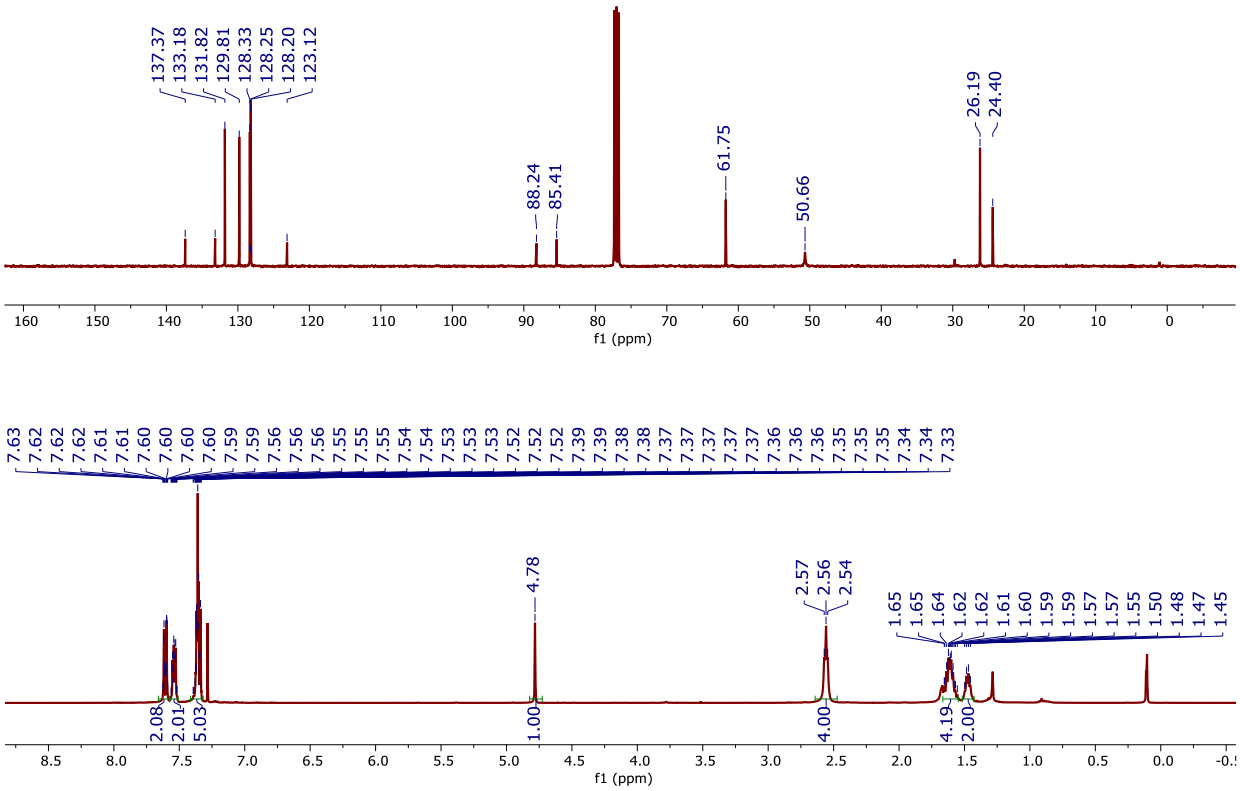

Fig. A108 *^{1}H-NMR and ^{13}C-NMR spectrum of* ***P7*** *recorded in* ***$CDCl_3$***

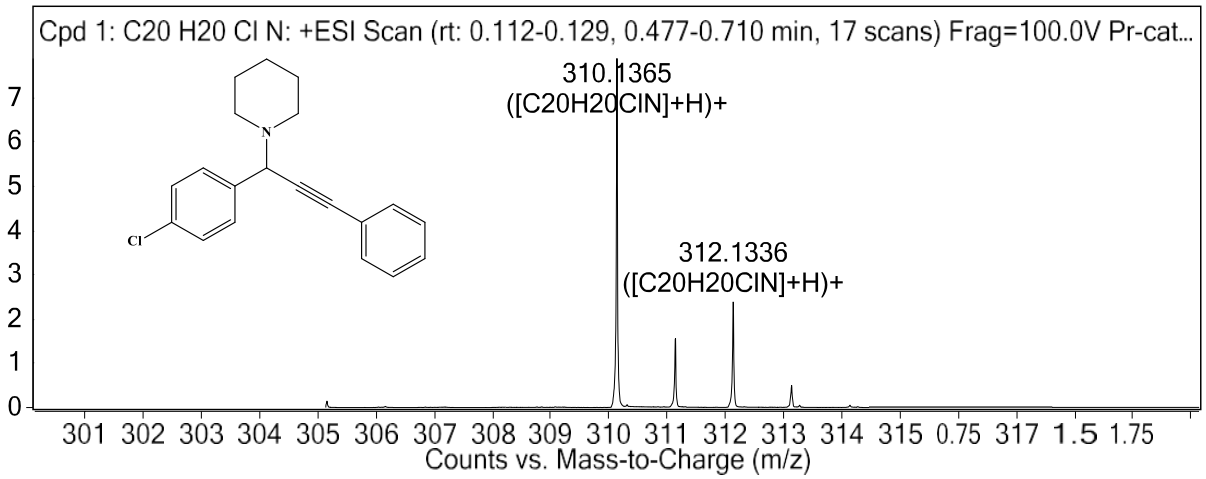

Fig. A109 *HRMS of* ***P7***

Appendix A

Additional Info : Peak(s) manually integrated

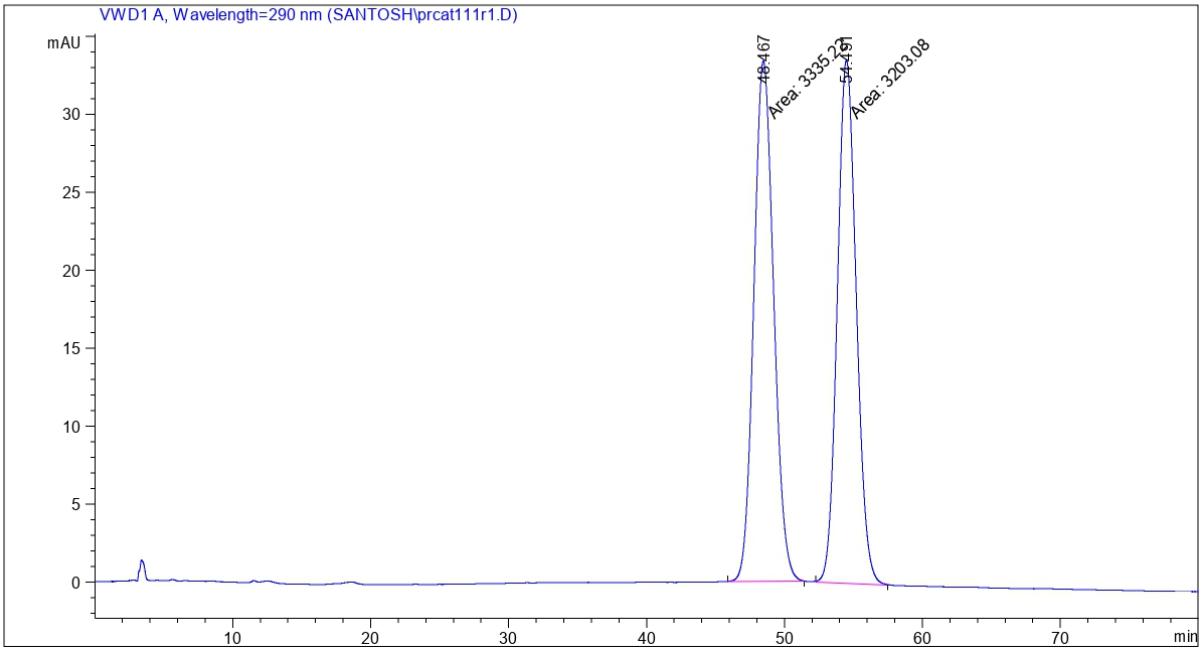

Signal 1: VWD1 A, Wavelength=290 nm

Peak #	RetTime [min]	Type	Width [min]	Area [mAU*s]	Height [mAU]	Area %
1	48.467	MM	1.6662	3335.21777	33.36098	51.0105
2	54.491	MM	1.5922	3203.07959	33.52966	48.9895
Totals :				6538.29736	66.89064	

Fig. A110 *HPLC of racemic* ***P7***

Appendix A

Additional Info : Peak(s) manually integrated

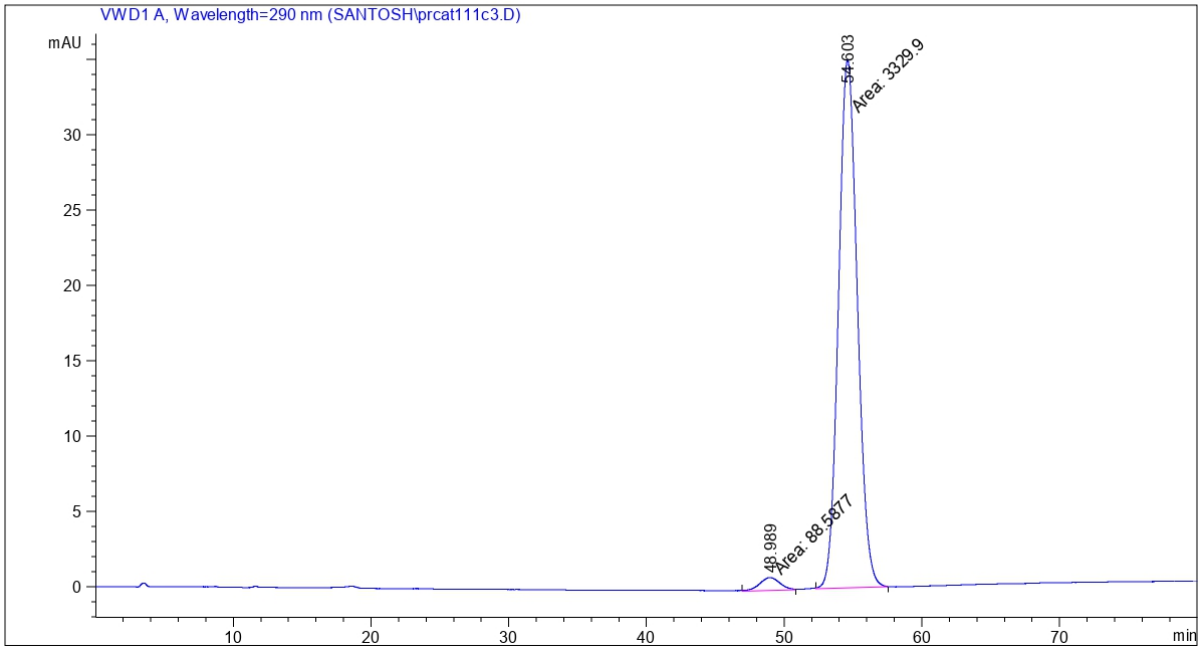

Signal 1: VWD1 A, Wavelength=290 nm

Peak #	RetTime [min]	Type	Width [min]	Area [mAU*s]	Height [mAU]	Area %
1	48.989	MM	1.7220	88.58774	8.57408e-1	2.5914
2	54.603	MM	1.5851	3329.90234	35.01332	97.4086
Totals :				3418.49008	35.87073	

Fig. A111 *HPLC of chiral* ***P7***

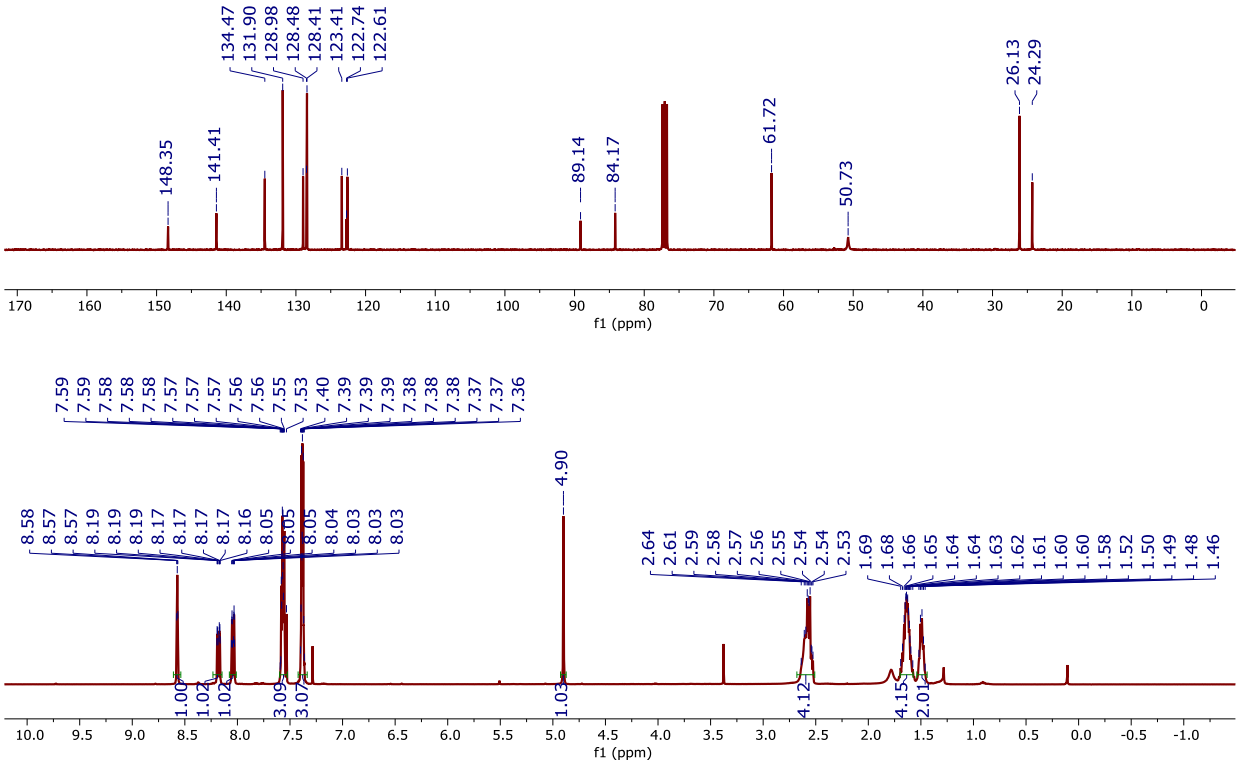

Fig. A112 *^{1}H-NMR and ^{13}C-NMR spectrum of* ***P8*** *recorded in* ***$CDCl_3$***

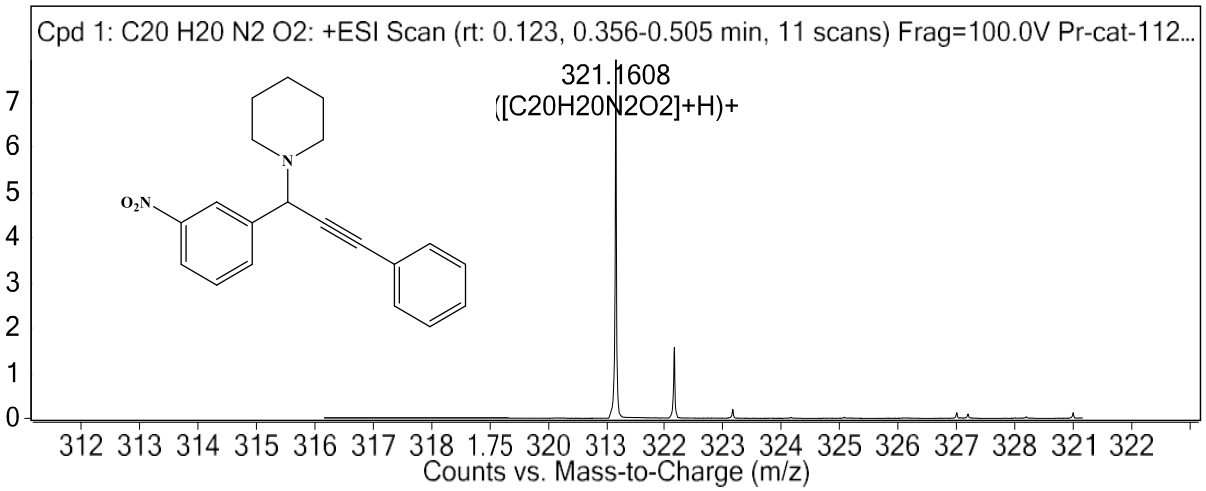

Fig. A113 *HRMS of* ***P8***

Appendix A

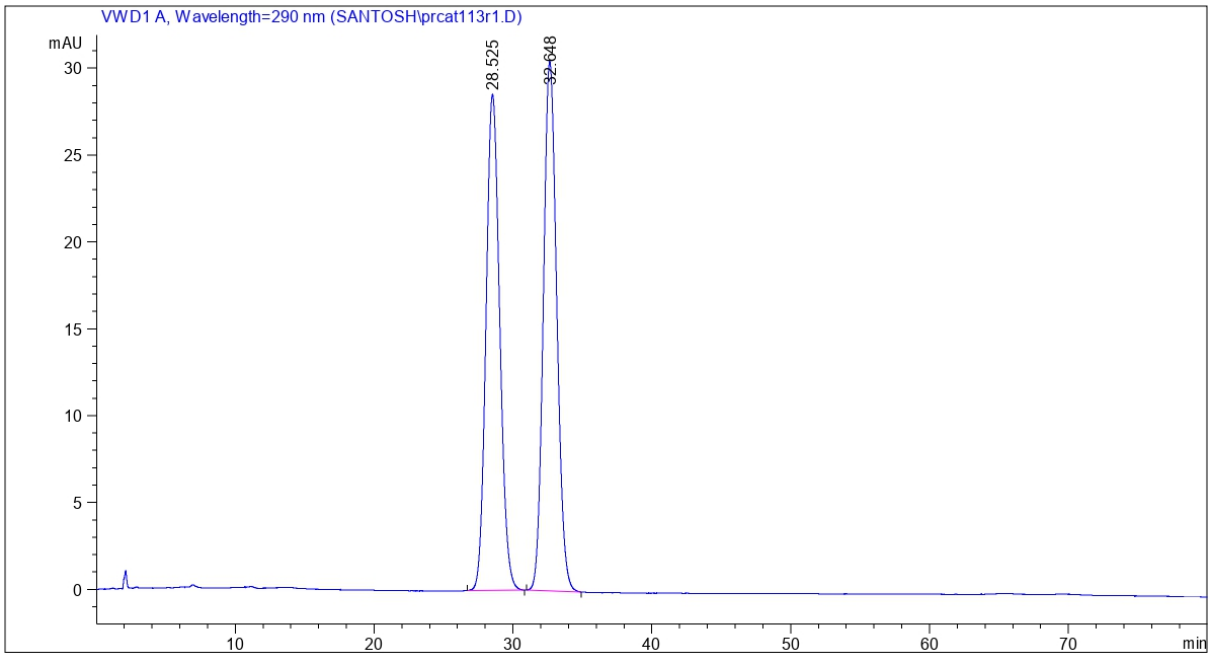

Signal 1: VWD1 A, Wavelength=290 nm

Peak #	RetTime [min]	Type	Width [min]	Area [mAU*s]	Height [mAU]	Area %
1	28.525	BB	1.0535	1956.00806	28.54211	48.9392
2	32.648	BB	1.0384	2040.80359	30.46917	51.0608
Totals :				3996.81165	59.01128	

Fig. A114 *HPLC of racemic* ***P8***

Appendix A

Additional Info : Peak(s) manually integrated

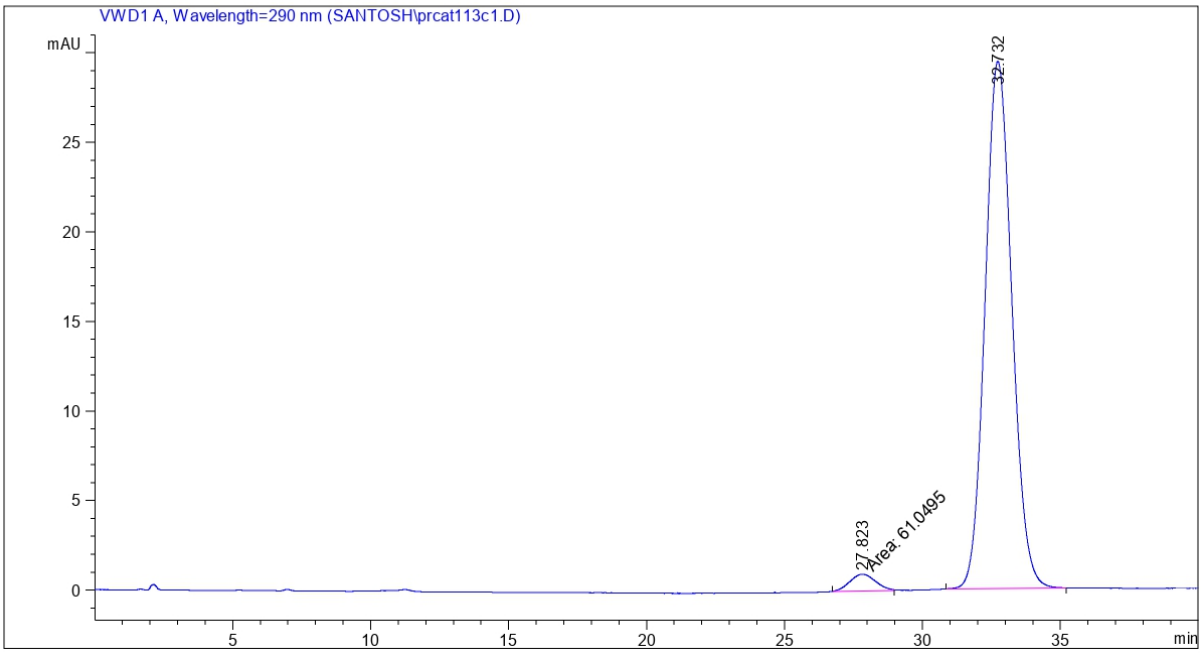

Signal 1: VWD1 A, Wavelength=290 nm

Peak #	RetTime [min]	Type	Width [min]	Area [mAU*s]	Height [mAU]	Area %
1	27.823	MM	1.0833	61.04951	9.39268e-1	2.9856
2	32.732	BB	1.0204	1983.76514	29.43149	97.0144
Totals :				2044.81465	30.37075	

Fig. A115 *HPLC of chiral* ***P8***

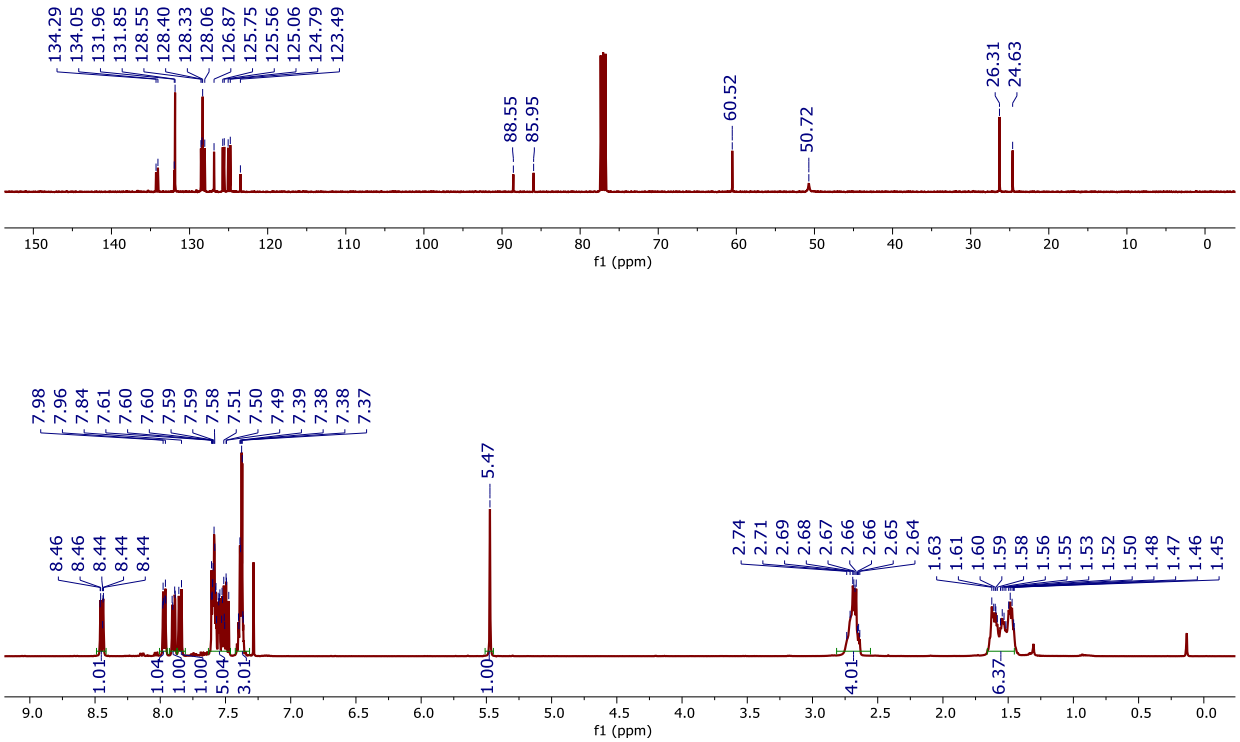

Fig. A116 *^{1}H-NMR and ^{13}C-NMR spectrum of* ***P9*** *recorded in* ***$CDCl_3$***

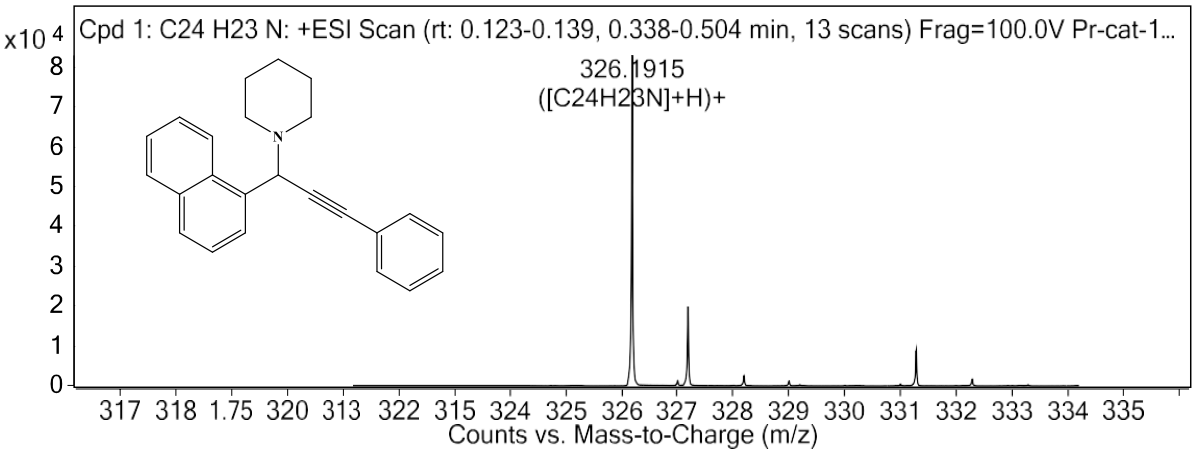

Fig. A117 *HRMS of* ***P9***

Appendix A

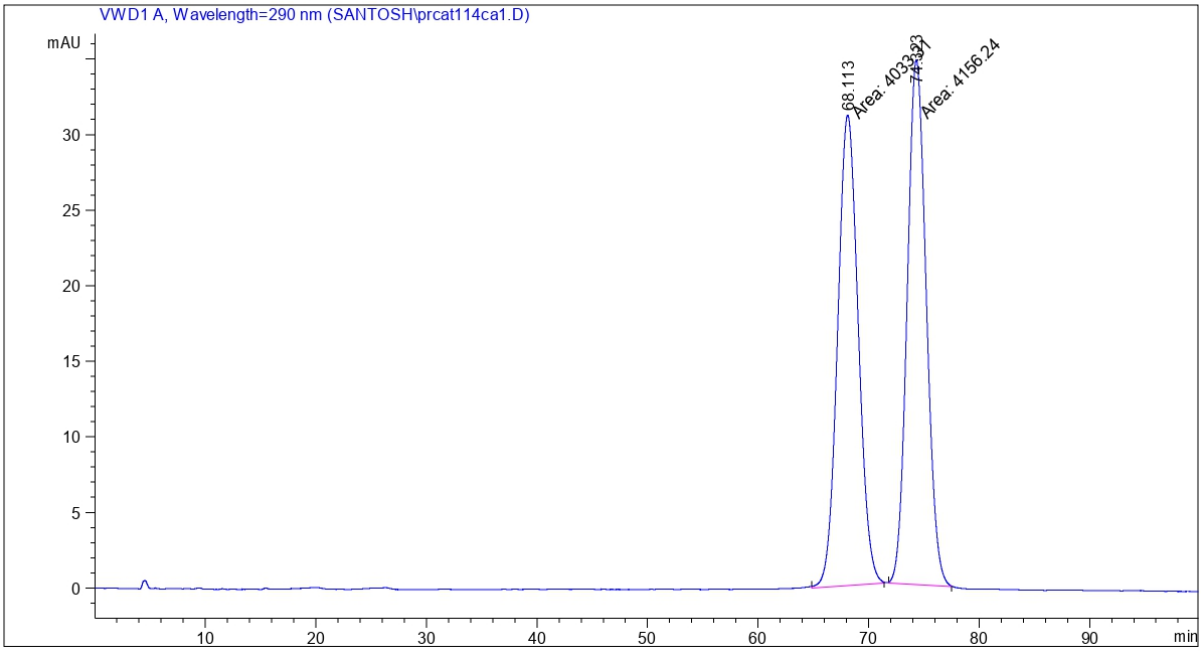

Signal 1: VWD1 A, Wavelength=290 nm

Peak #	RetTime [min]	Type	Width [min]	Area [mAU*s]	Height [mAU]	Area %
1	68.113	MM	2.1587	4033.31128	31.13952	49.2495
2	74.323	MM	1.9949	4156.24365	34.72390	50.7505
Totals :				8189.55493	65.86342	

Fig. A118 *HPLC of racemic* ***P9***

Appendix A

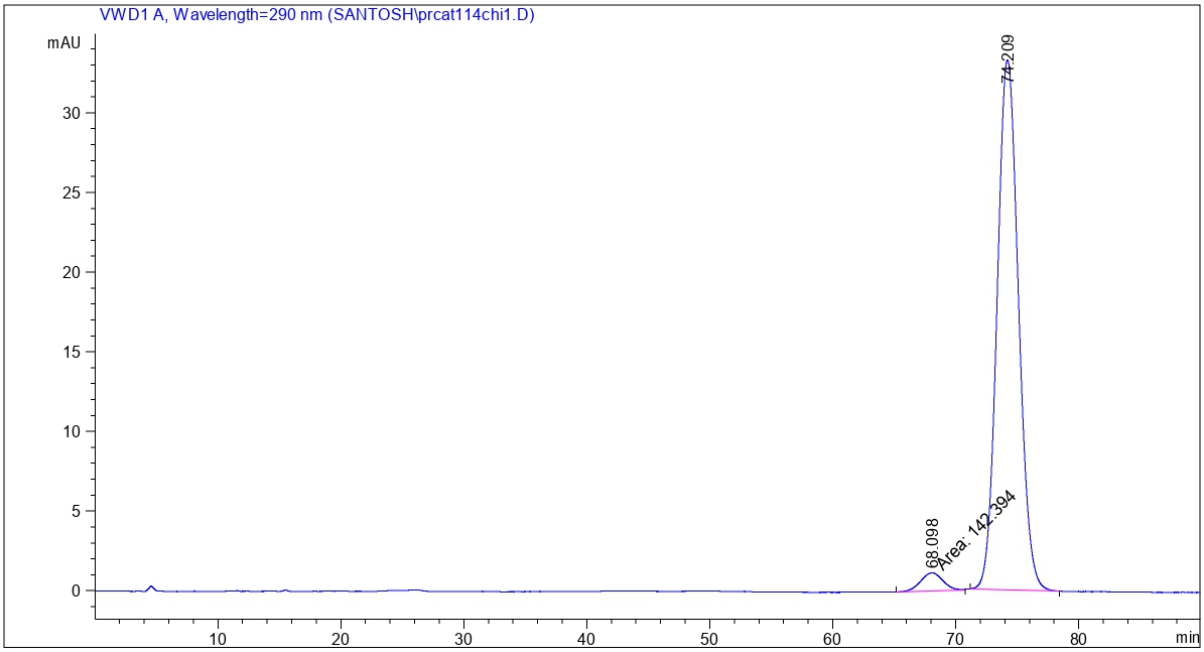

Signal 1: VWD1 A, Wavelength=290 nm

Peak #	RetTime [min]	Type	Width [min]	Area [mAU*s]	Height [mAU]	Area %
1	68.098	MM	2.1033	142.39447	1.12835	3.4234
2	74.209	BB	1.7905	4017.06396	33.24884	96.5766
Totals :				4159.45844	34.37719	

Fig. A119 *HPLC of chiral* ***P9***

Appendix A

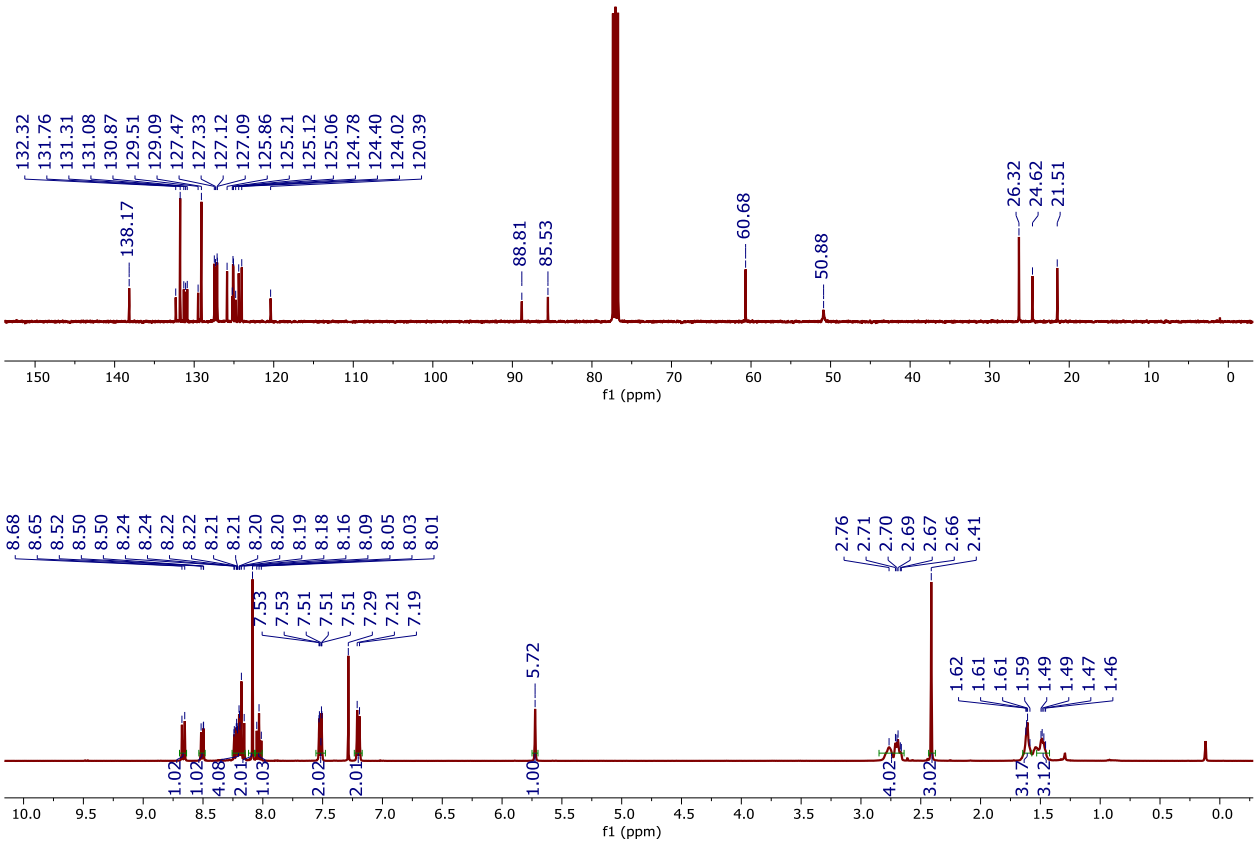

Fig. A120 *^{1}H-NMR and ^{13}C-NMR spectrum of* ***P10*** *recorded in* ***$CDCl_3$***

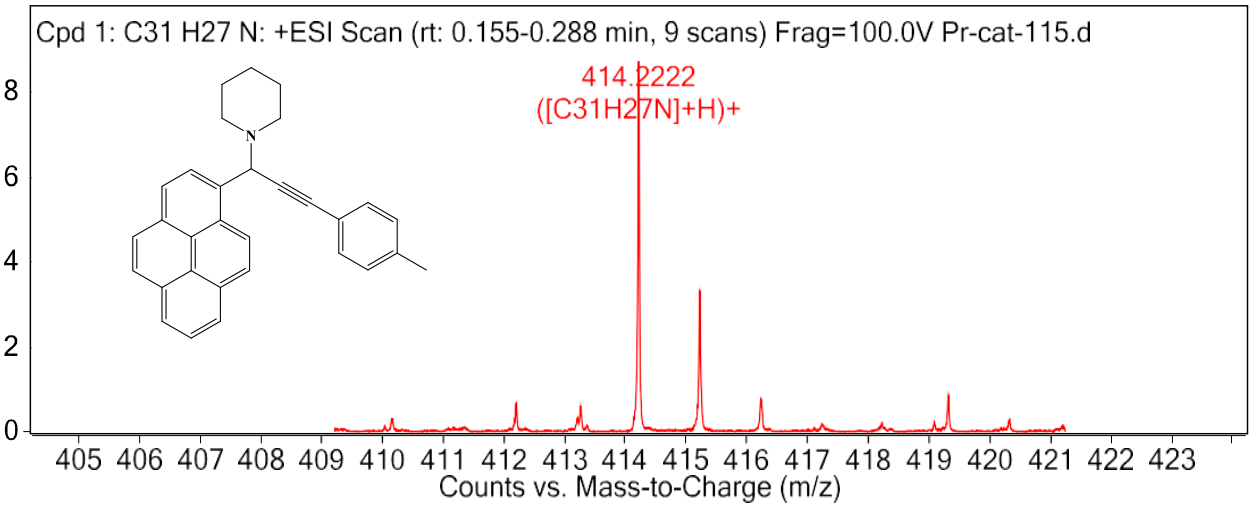

Fig. A121 *HRMS of* ***P10***

Appendix A

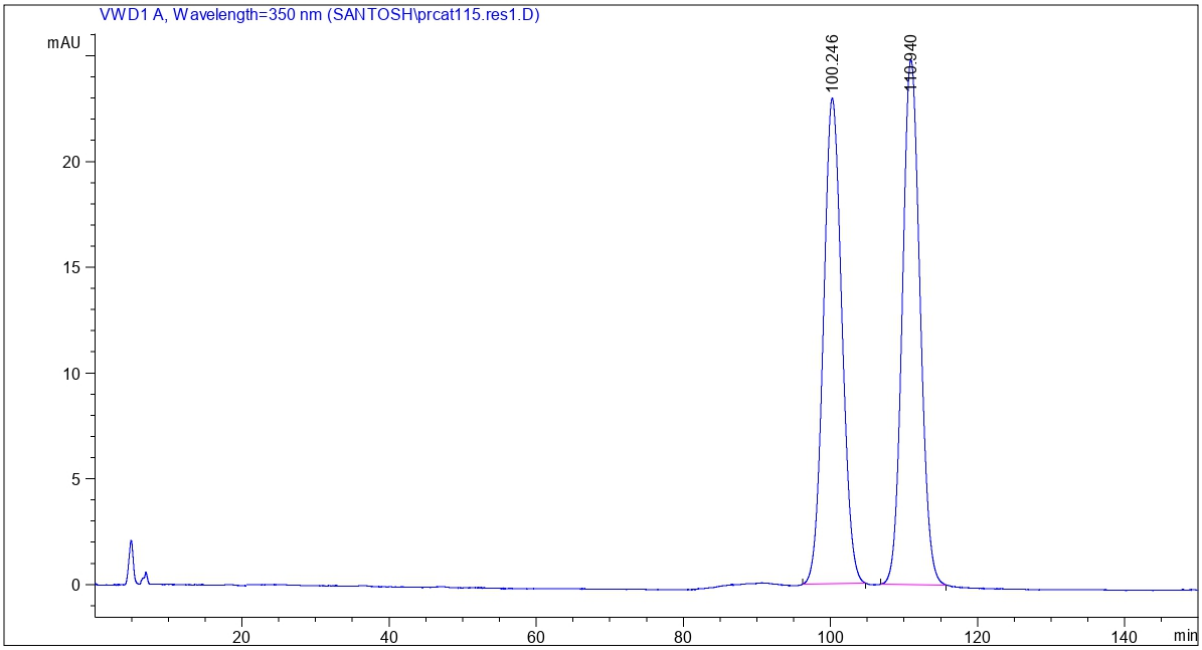

Signal 1: VWD1 A, Wavelength=350 nm

Peak #	RetTime [min]	Type	Width [min]	Area [mAU*s]	Height [mAU]	Area %
1	100.246	BB	2.0768	3991.66357	22.96500	49.0275
2	110.940	BB	2.0202	4150.01709	24.81340	50.9725
Totals :				8141.68066	47.77840	

Fig. A122 *HPLC of racemic* ***P10***

Appendix A

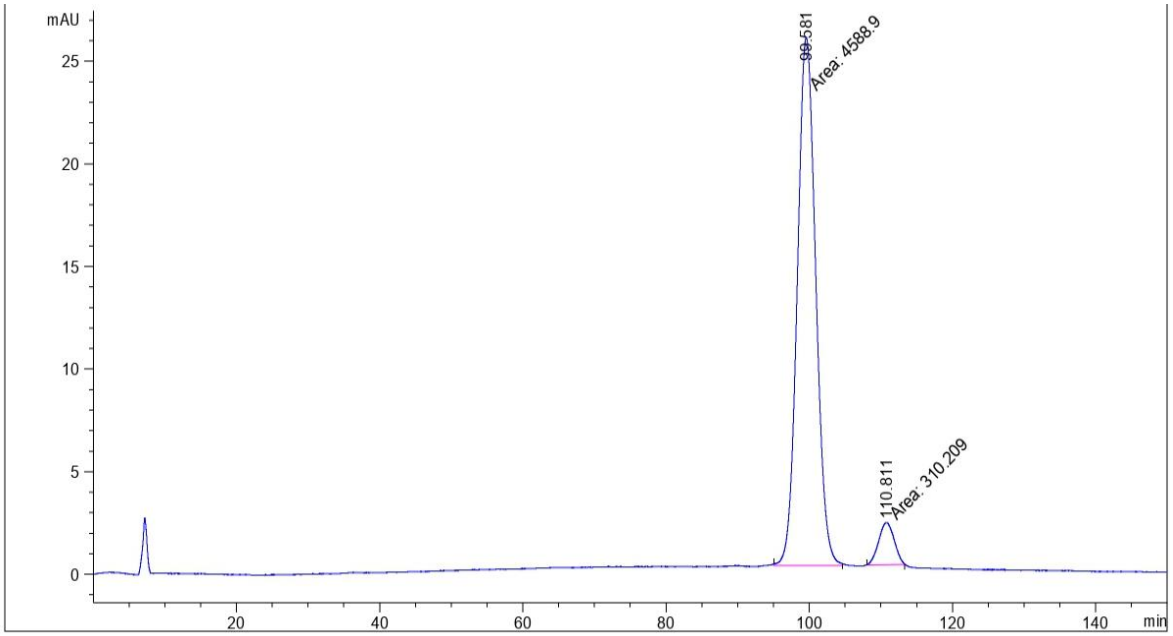

Signal 1: VWD1 A, Wavelength=350 nm

Peak #	RetTime [min]	Type	Width [min]	Area [mAU*s]	Height [mAU]	Area %
1	99.581	MM	2.9726	4588.89844	25.72922	93.6680
2	110.811	MM	2.5140	310.20929	2.05658	6.3320
Totals :				4899.10773	27.78580	

Fig. A123 *HPLC of chiral* ***P10***

Appendix A

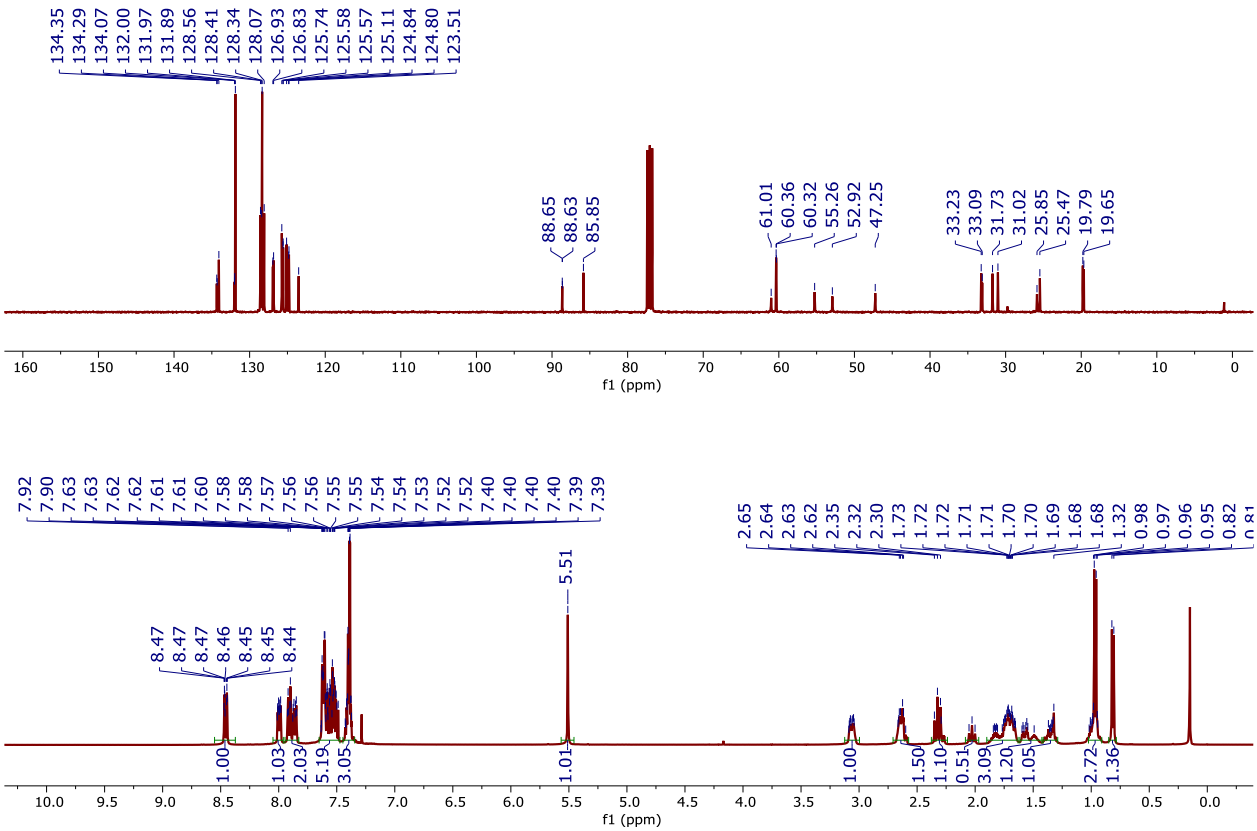

Fig. A124 *^{1}H-NMR and ^{13}C-NMR spectrum of* ***P11*** *recorded in* ***$CDCl_3$***

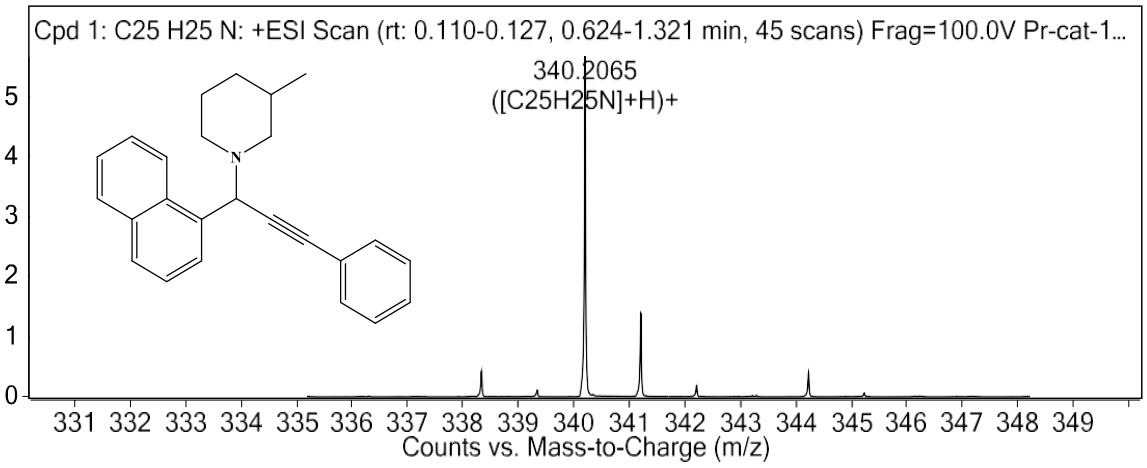

Fig. A125 *HRMS of* ***P11***

Appendix A

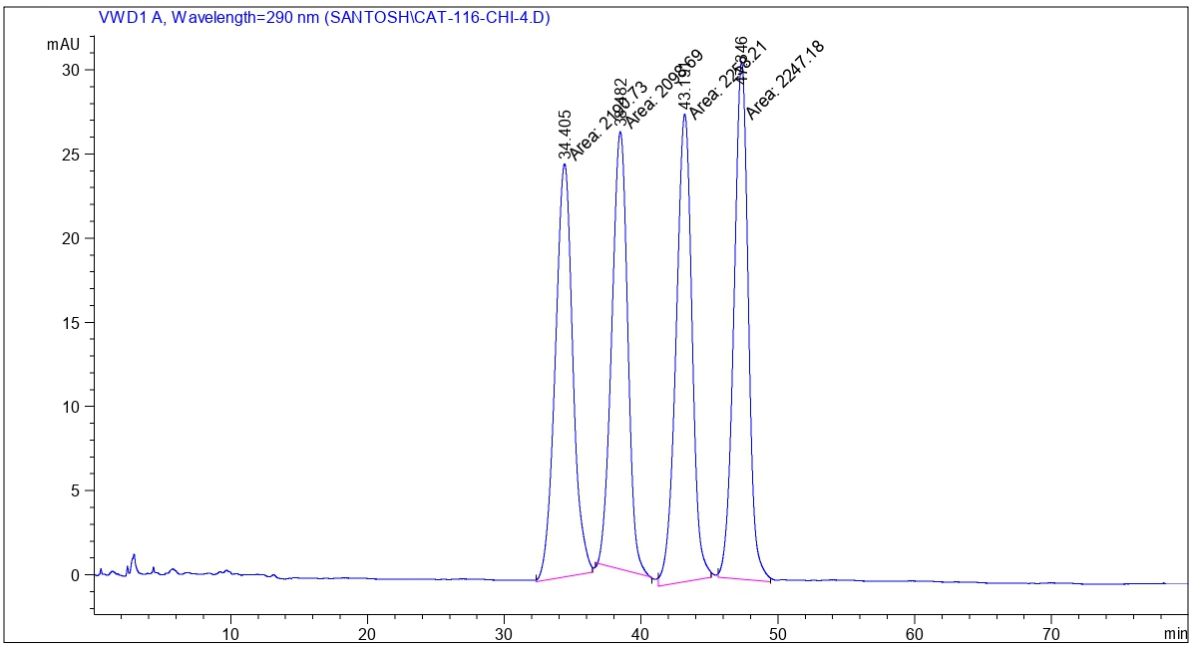

Signal 1: VWD1 A, Wavelength=290 nm

Peak #	RetTime [min]	Type	Width [min]	Area [mAU*s]	Height [mAU]	Area %
1	34.405	MM	1.4870	2190.73438	24.55388	24.9094
2	38.482	MM	1.3462	2098.69409	25.98293	23.8628
3	43.191	MM	1.3546	2258.21094	27.78526	25.6766
4	47.346	MM	1.2178	2247.18262	30.75375	25.5512
Totals :				8794.82202	109.07582	

Fig. A126 *HPLC of racemic* ***P11***

Appendix A

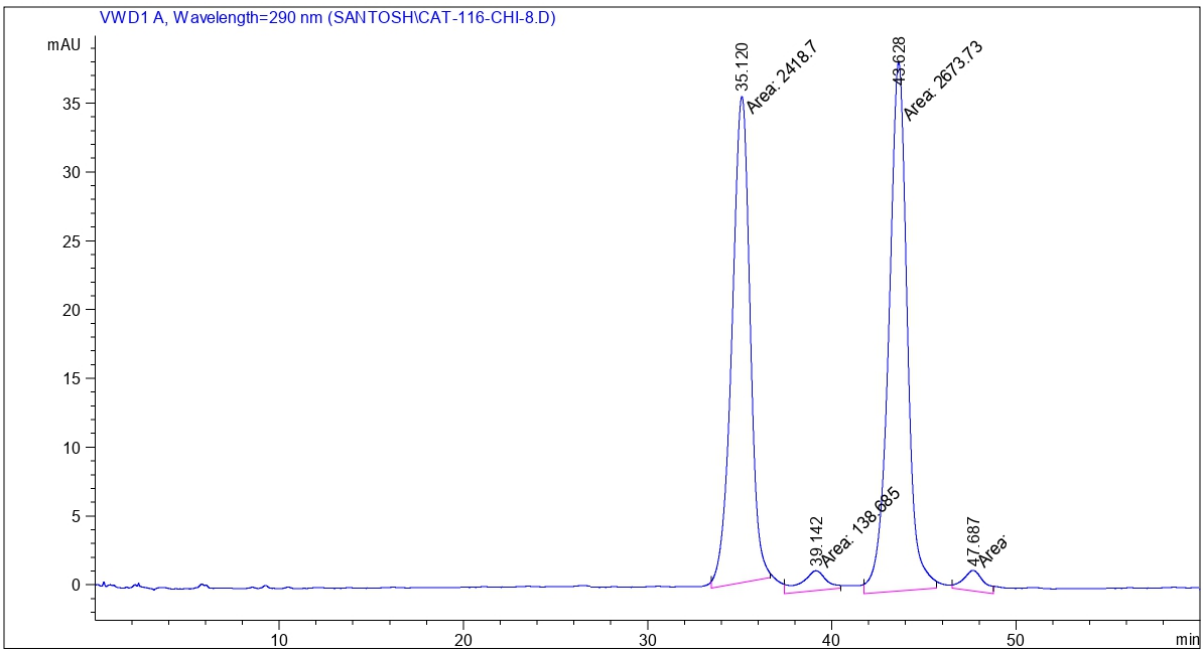

Signal 1: VWD1 A, Wavelength=290 nm

Peak #	RetTime [min]	Type	Width [min]	Area [mAU*s]	Height [mAU]	Area %
1	35.120	MM	1.1407	2418.70020	35.34011	45.2507
2	39.142	MM	1.6079	138.68489	1.43756	2.5946
3	43.628	MM	1.1594	2673.72778	38.43689	50.0219
4	47.687	MM	1.2744	113.99998	1.49090	2.1328
Totals :				5345.11285	76.70545	

Fig. A127 *HPLC of chiral* ***P11***

Appendix A

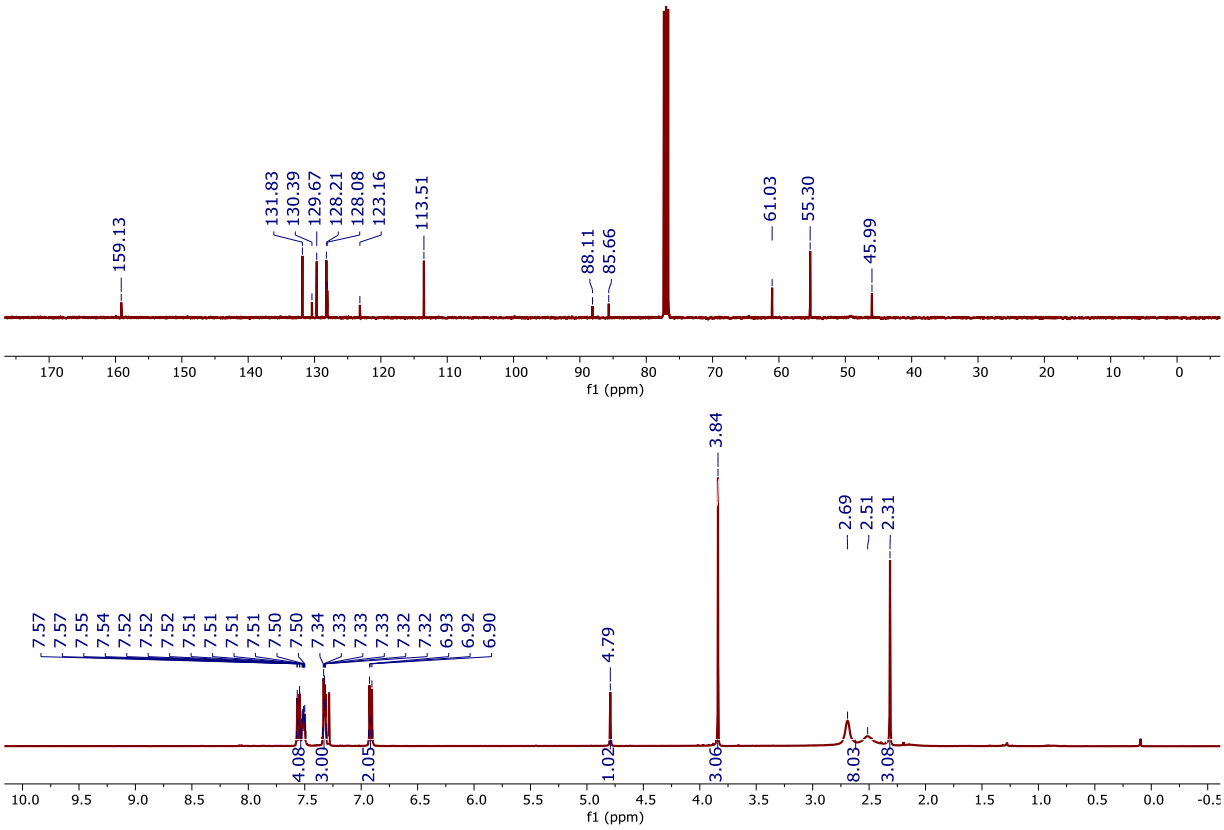

Fig. A128 *^{1}H-NMR and ^{13}C-NMR spectrum of* ***P12*** *recorded in* ***$CDCl_3$***

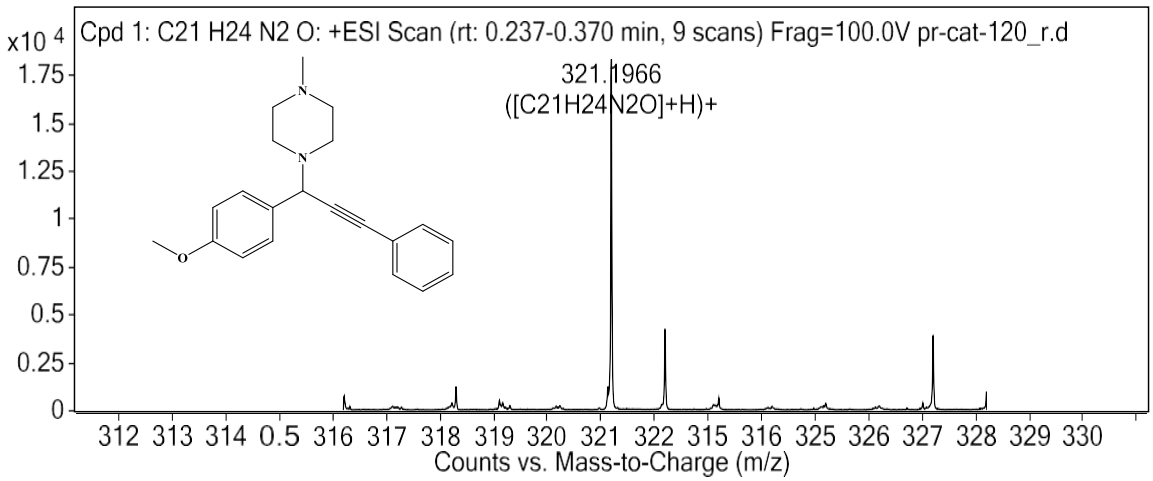

Fig. A129 *HRMS of* ***P12***

Appendix A

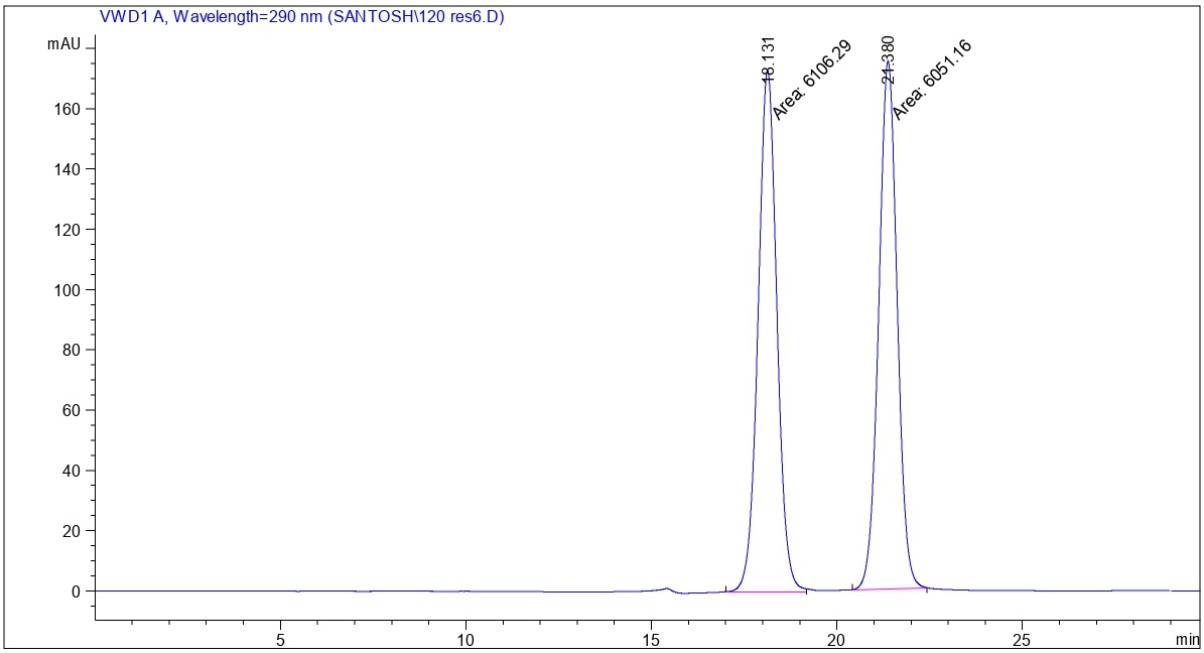

Signal 1: VWD1 A, Wavelength=290 nm

Peak #	RetTime [min]	Type	Width [min]	Area [mAU*s]	Height [mAU]	Area %
1	18.131	MM	0.5882	6106.28857	173.03003	50.2267
2	21.380	MM	0.5759	6051.15625	175.11908	49.7733
Totals :				1.21574e4	348.14911	

Fig. A130 *HPLC of racemic* ***P12***

Appendix A

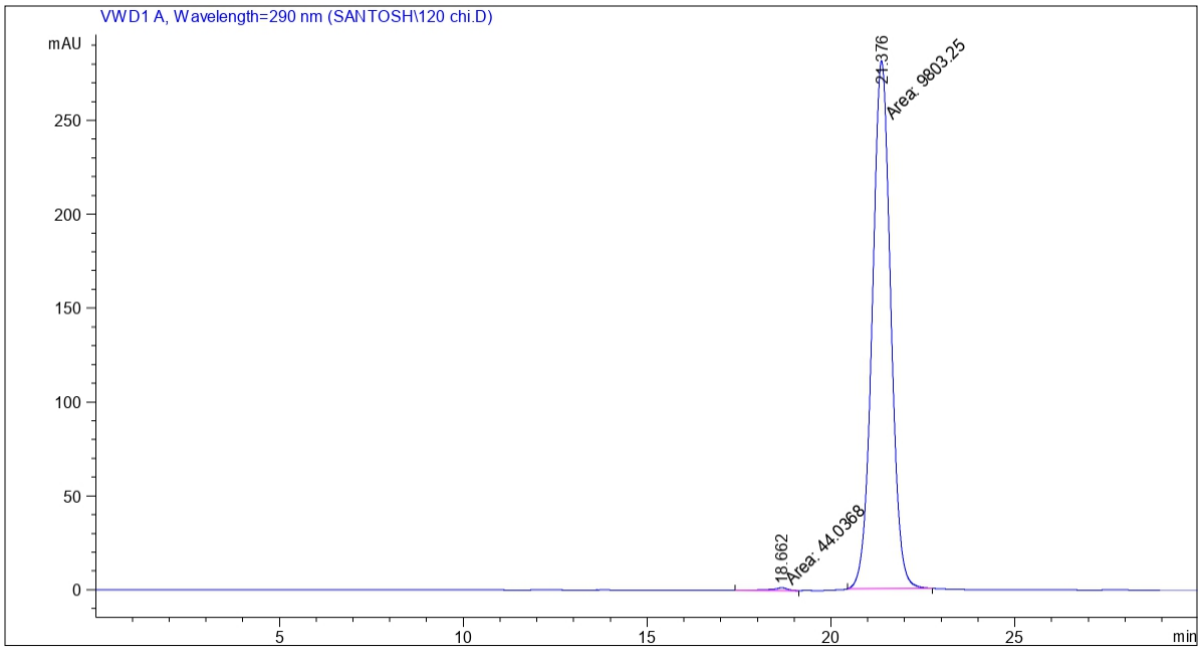

Signal 1: VWD1 A, Wavelength=290 nm

Peak #	RetTime [min]	Type	Width [min]	Area [mAU*s]	Height [mAU]	Area %
1	18.662	MM	0.4896	44.03681	1.49903	0.4472
2	21.376	MM	0.5813	9803.25293	281.09558	99.5528
Totals :				9847.28974	282.59461	

Fig. A131 *HPLC of chiral* ***P12***

Appendix A

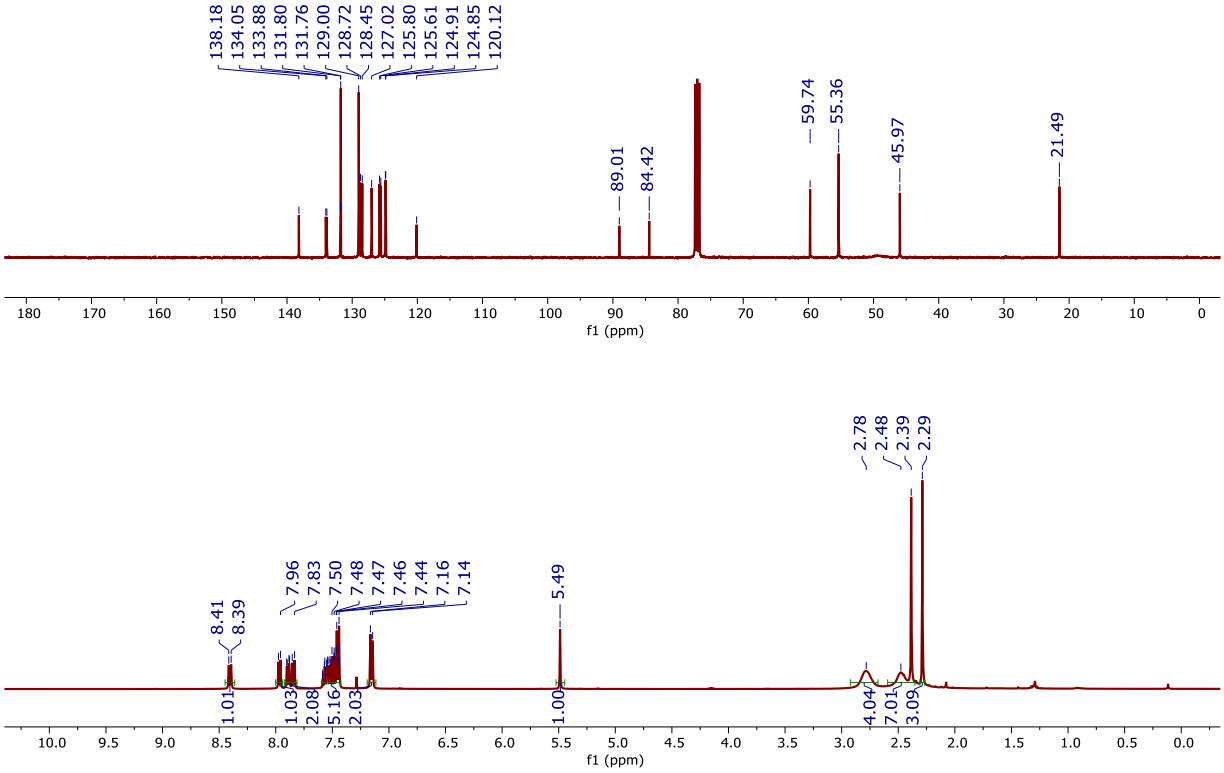

Fig. A132 *^{1}H-NMR and ^{13}C-NMR spectrum of* ***P13*** *recorded in* ***$CDCl_3$***

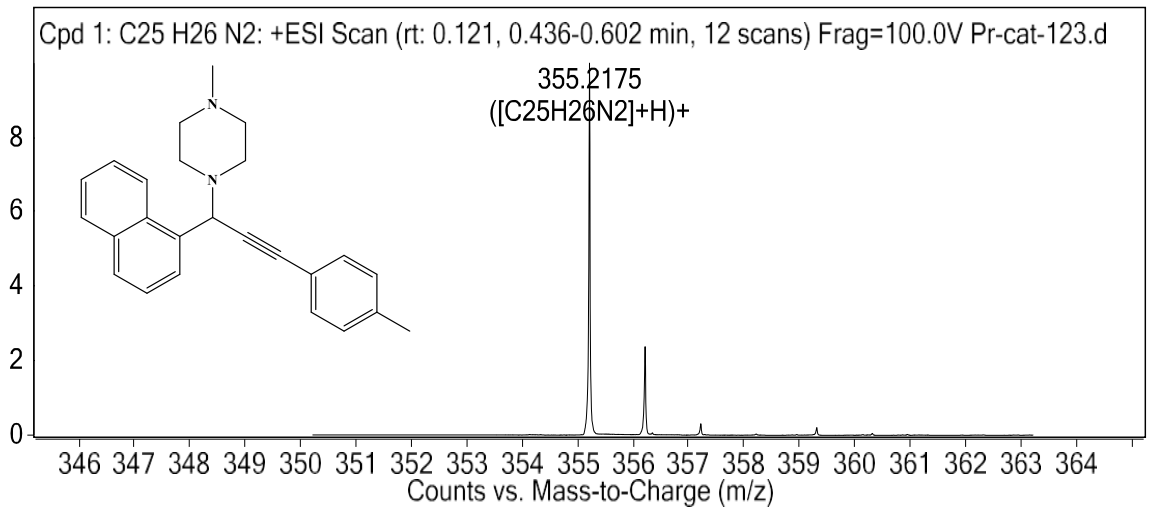

Fig. A133 *HRMS of* ***P13***

Appendix A

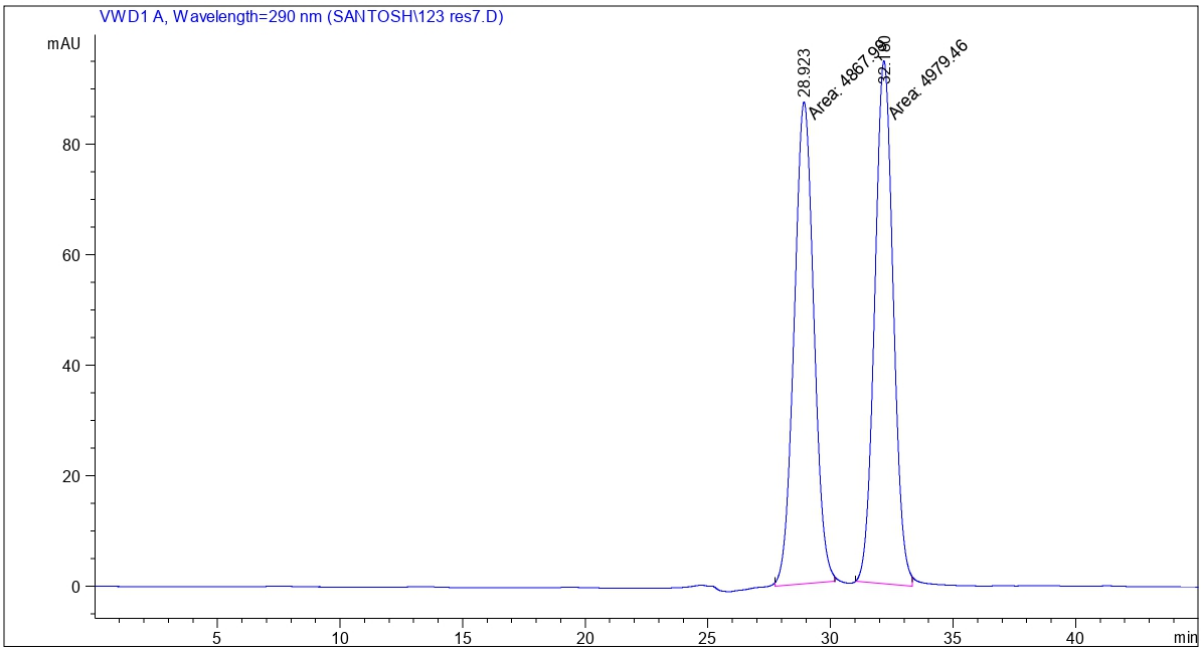

Signal 1: VWD1 A, Wavelength=290 nm

Peak #	RetTime [min]	Type	Width [min]	Area [mAU*s]	Height [mAU]	Area %
1	28.923	MM	0.9303	4867.99316	87.21054	49.4340
2	32.180	MM	0.8773	4979.45703	94.59606	50.5660
Totals :				9847.45020	181.80660	

Fig. A134 *HPLC of racemic* ***P13***

Appendix A

Additional Info : Peak(s) manually integrated

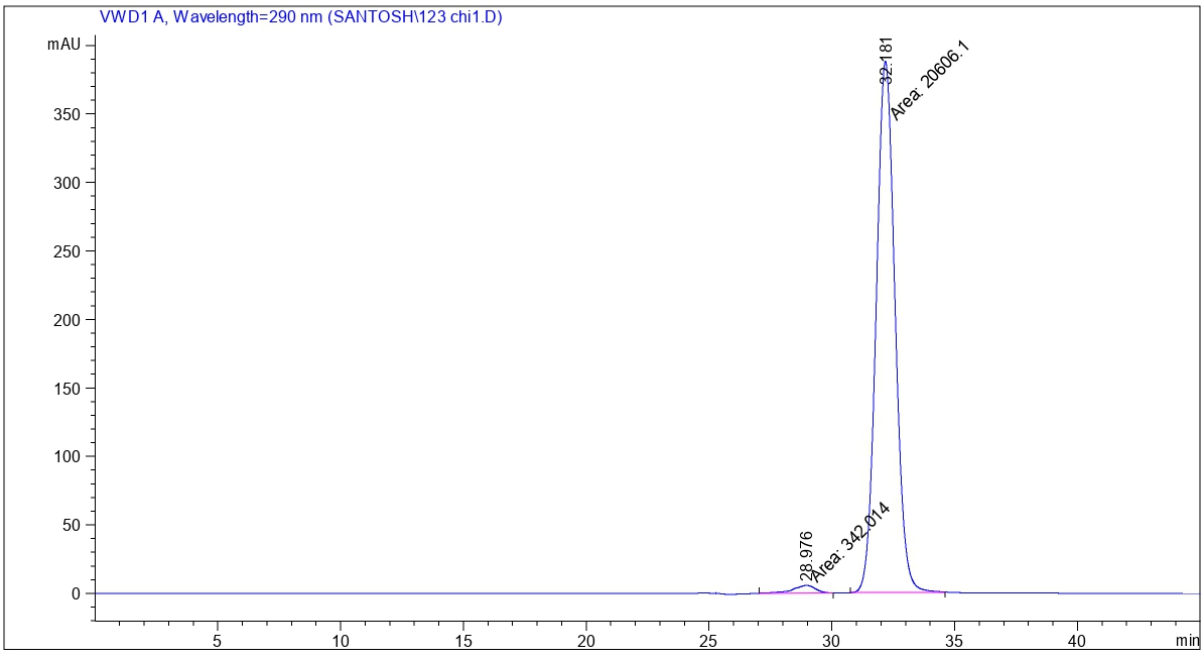

Signal 1: VWD1 A, Wavelength=290 nm

Peak #	RetTime [min]	Type	Width [min]	Area [mAU*s]	Height [mAU]	Area %
1	28.976	MM	1.0320	342.01410	5.52323	1.6327
2	32.181	MM	0.8860	2.06061e4	387.64209	98.3673
Totals :				2.09481e4	393.16532	

Fig. A135 *HPLC of chiral* ***P13***

Appendix A

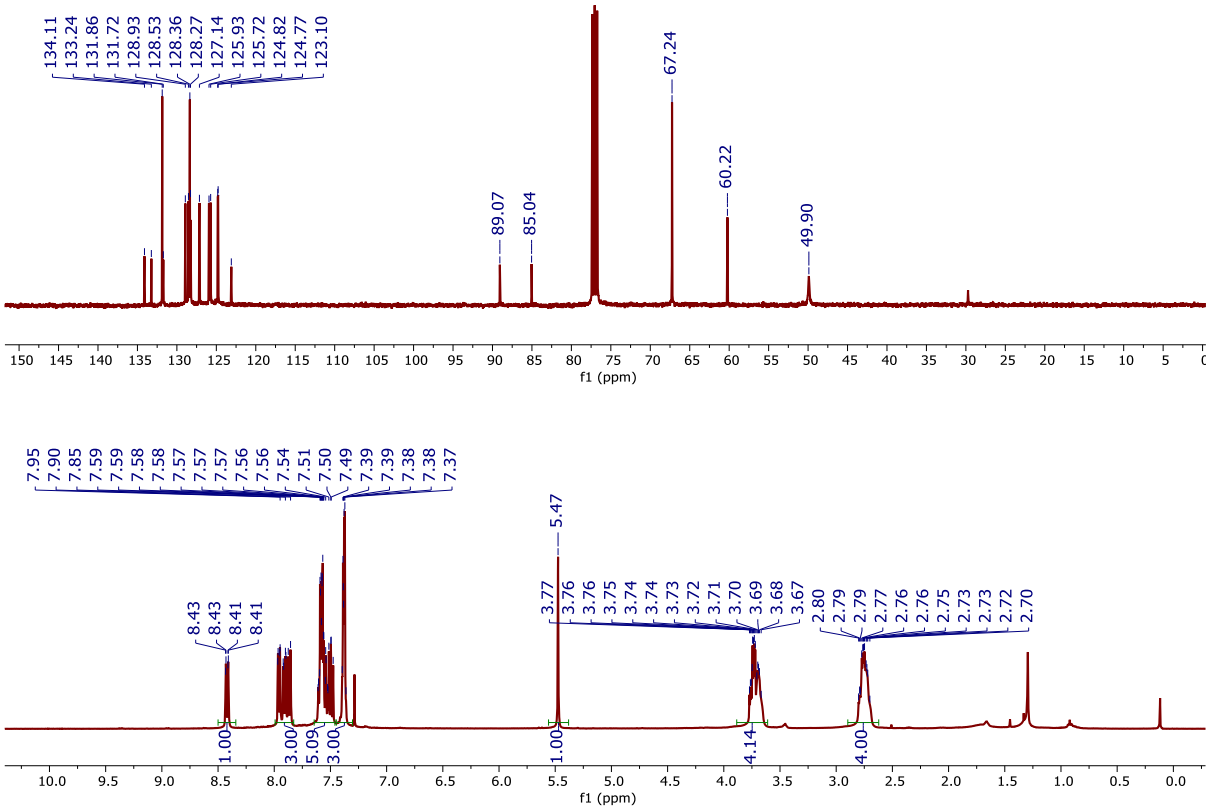

Fig. A136 *^{1}H-NMR and ^{13}C-NMR spectrum of* ***P14*** *recorded in* ***$CDCl_3$***

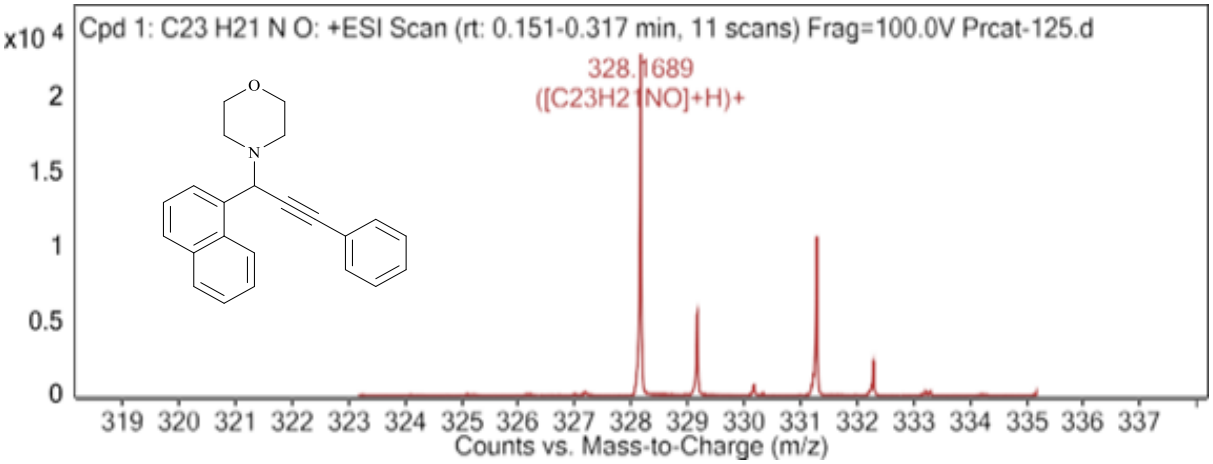

Fig. A137 *HRMS of* ***P14***

Appendix A

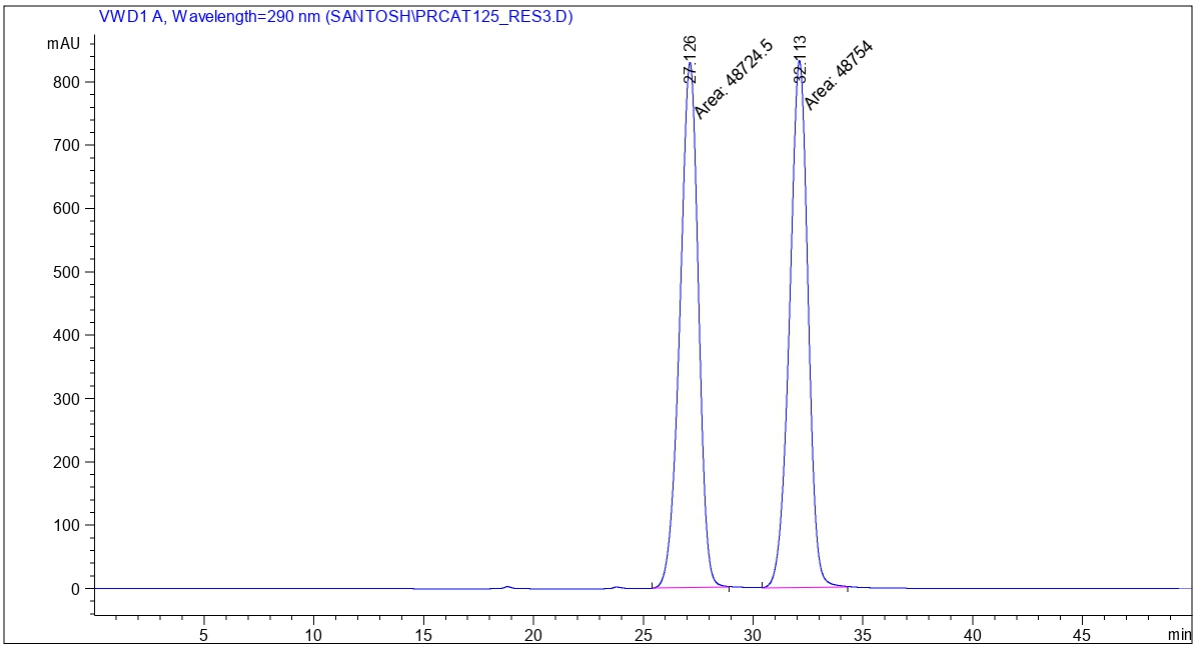

Signal 1: VWD1 A, Wavelength=290 nm

Peak #	RetTime [min]	Type	Width [min]	Area [mAU*s]	Height [mAU]	Area %
1	27.126	MM	0.9796	4.87245e4	829.01172	49.9849
2	32.113	MM	0.9765	4.87540e4	832.15131	50.0151
Totals :				9.74786e4	1661.16302	

Fig. A138 HPLC of racemic **P14**

Additional Info : Peak(s) manually integrated

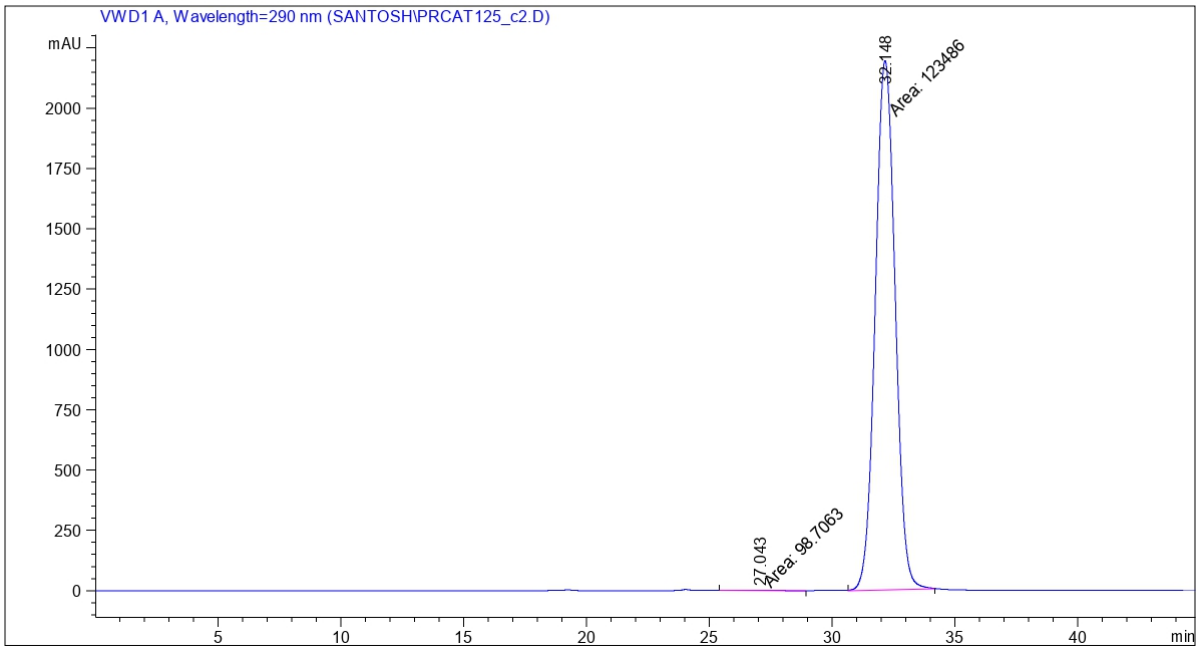

Signal 1: VWD1 A, Wavelength=290 nm

Peak #	RetTime [min]	Type	Width [min]	Area [mAU*s]	Height [mAU]	Area %
1	27.043	MM	1.1758	98.70634	1.39915	0.0799
2	32.148	MM	0.9384	1.23486e5	2193.08691	99.9201
Totals :				1.23585e5	2194.48606	

Fig. A139 *HPLC of chiral* ***P14***

Appendix A

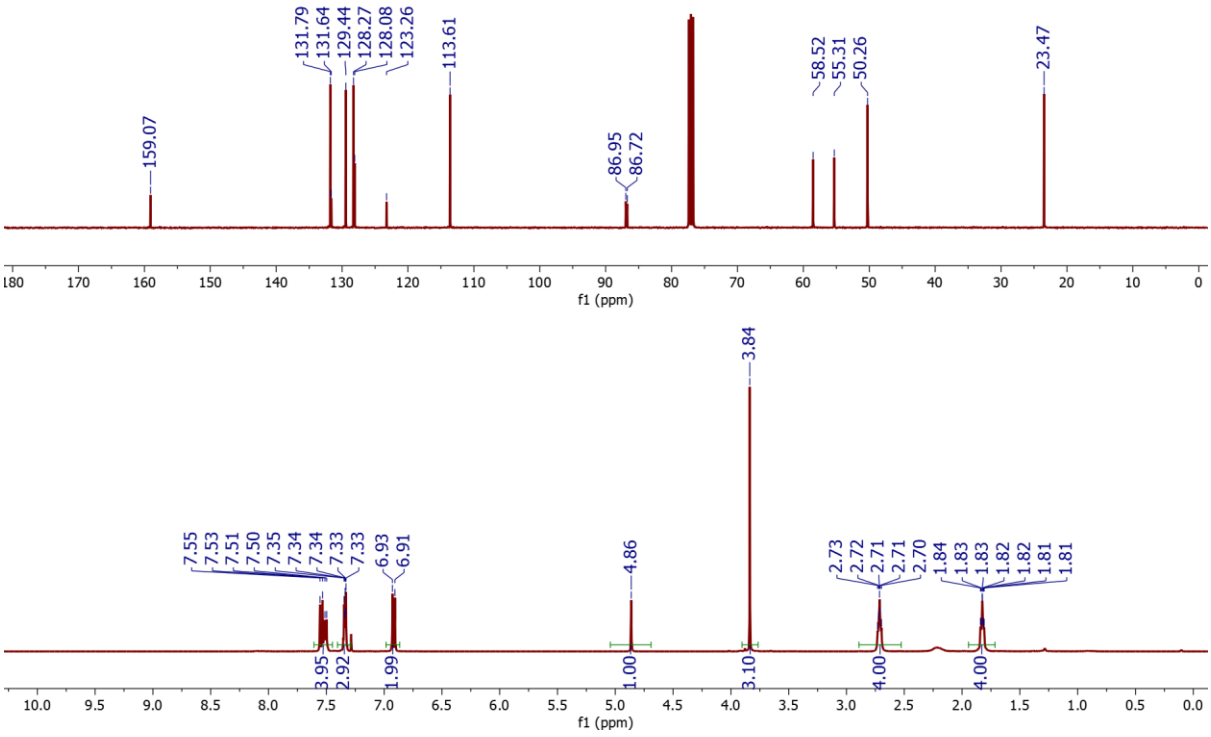

Fig. A140 *^{1}H-NMR and ^{13}C-NMR spectrum of* ***P15*** *recorded in* ***$CDCl_3$***

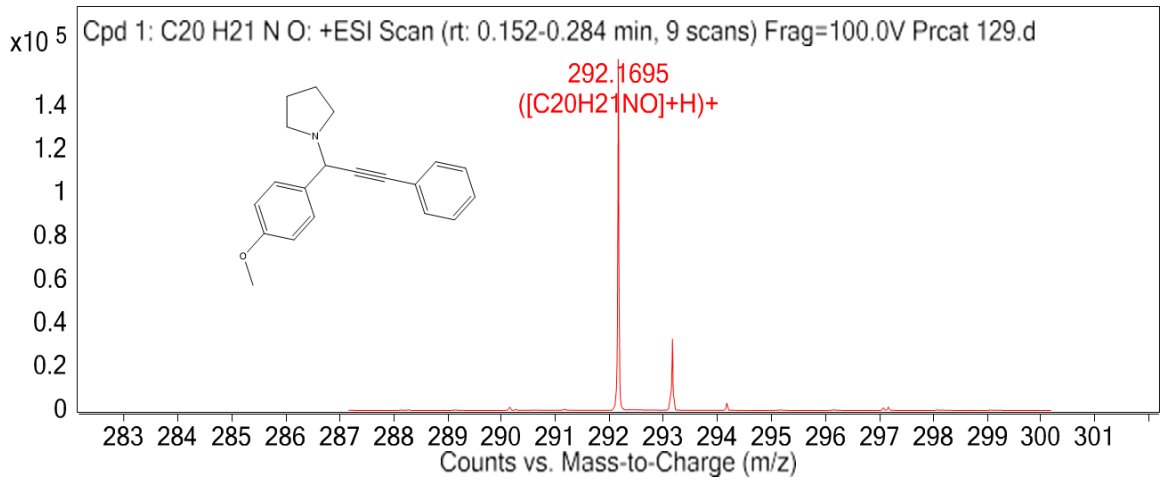

Fig. A141 *HRMS of* ***P15***

Appendix A

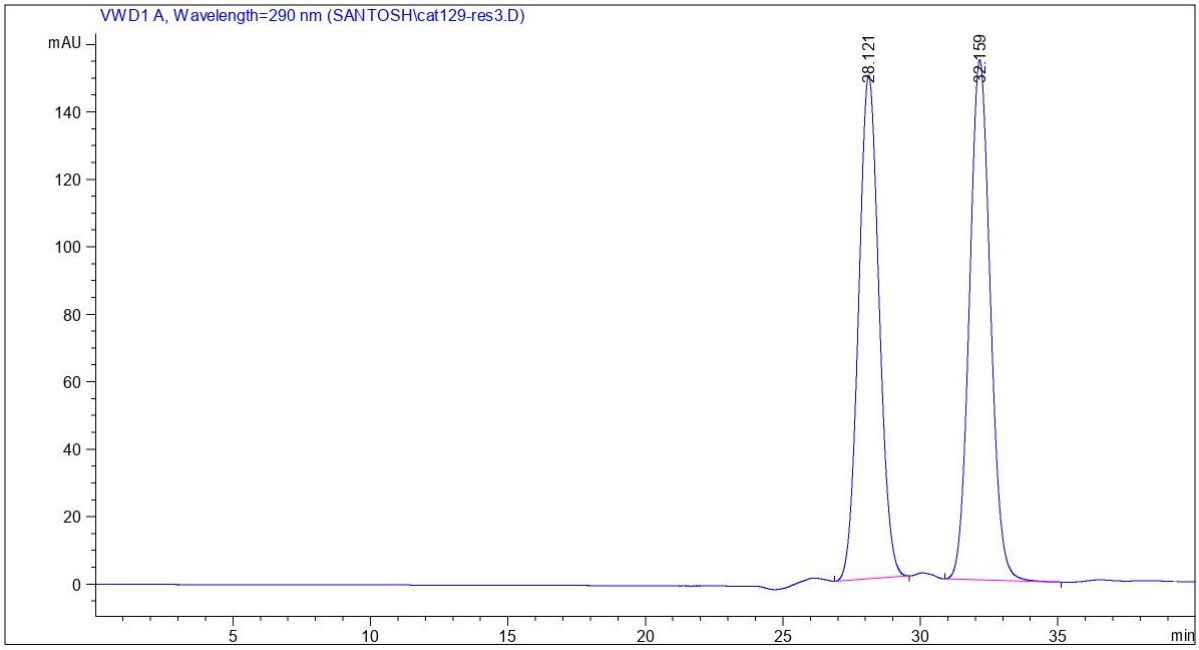

Signal 1: VWD1 A, Wavelength=290 nm

Peak #	RetTime [min]	Type	Width [min]	Area [mAU*s]	Height [mAU]	Area %
1	28.121	BB	0.8049	7731.99414	149.37242	48.7657
2	32.159	BB	0.8078	8123.40283	154.16287	51.2343
Totals :				1.58554e4	303.53529	

Fig. A142 *HPLC of racemic* ***P15***

Appendix A

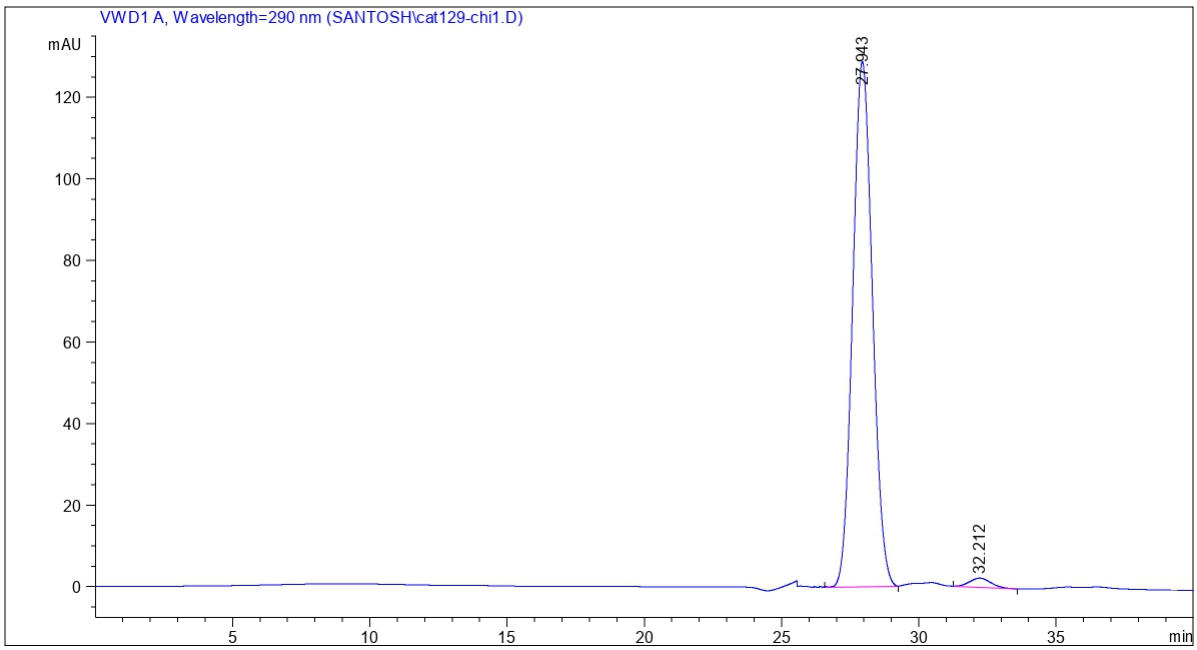

Signal 1: VWD1 A, Wavelength=290 nm

Peak #	RetTime [min]	Type	Width [min]	Area [mAU*s]	Height [mAU]	Area %
1	27.943	VB R	0.7796	6419.67432	128.77101	98.1450
2	32.212	BB	0.7247	121.33817	2.25870	1.8550
Totals :				6541.01248	131.02971	

Fig. A143 *HPLC of chiral* ***P15***

Appendix A

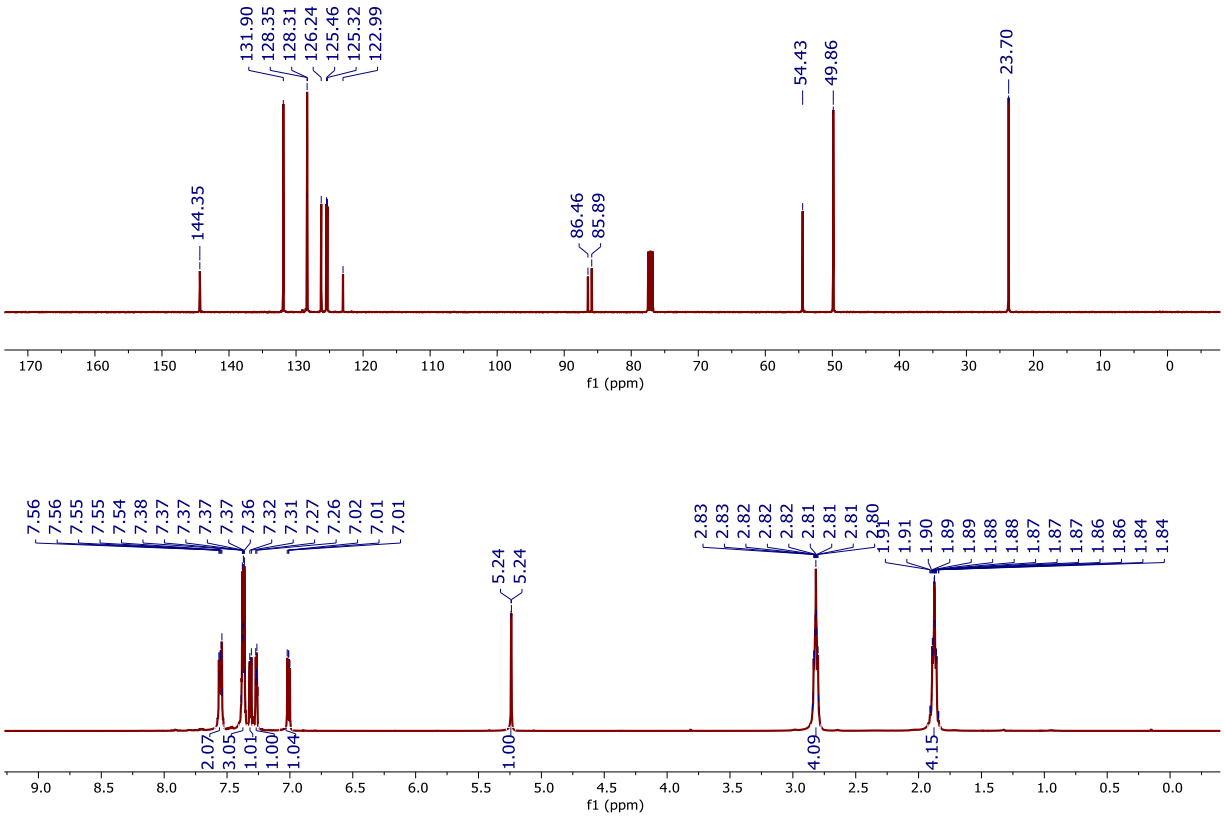

Fig. A144 ^{1}H-NMR and ^{13}C-NMR spectrum of P16 recorded in $CDCl_3$

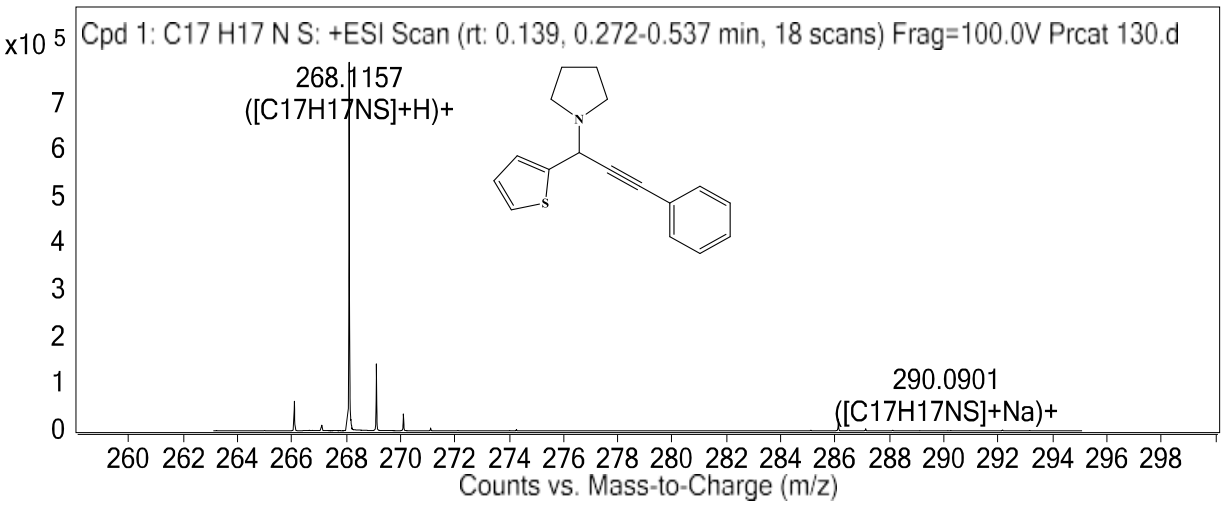

Fig. A145** HRMS of **P16

Appendix A

Additional Info : Peak(s) manually integrated

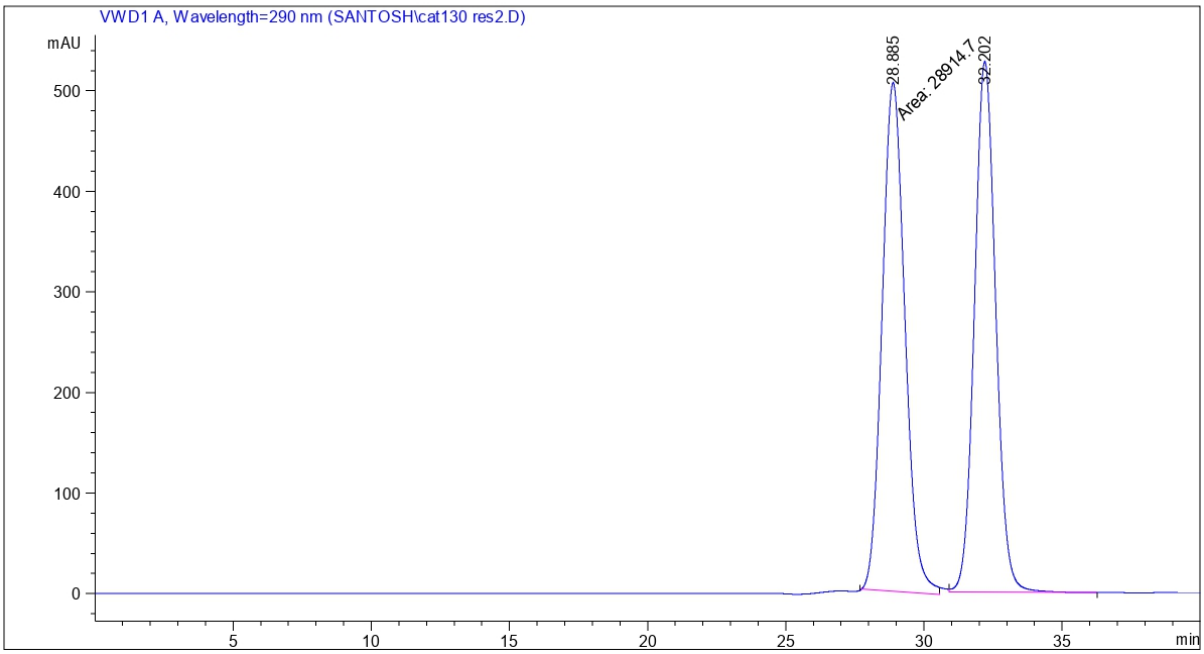

Signal 1: VWD1 A, Wavelength=290 nm

Peak #	RetTime [min]	Type	Width [min]	Area [mAU*s]	Height [mAU]	Area %
1	28.885	MM	0.9530	2.89147e4	505.68588	50.6247
2	32.202	VB	0.8196	2.82011e4	527.61792	49.3753
Totals :				5.71158e4	1033.30380	

Fig. A146 *HPLC of racemic* ***P16***

Appendix A

Additional Info : Peak(s) manually integrated

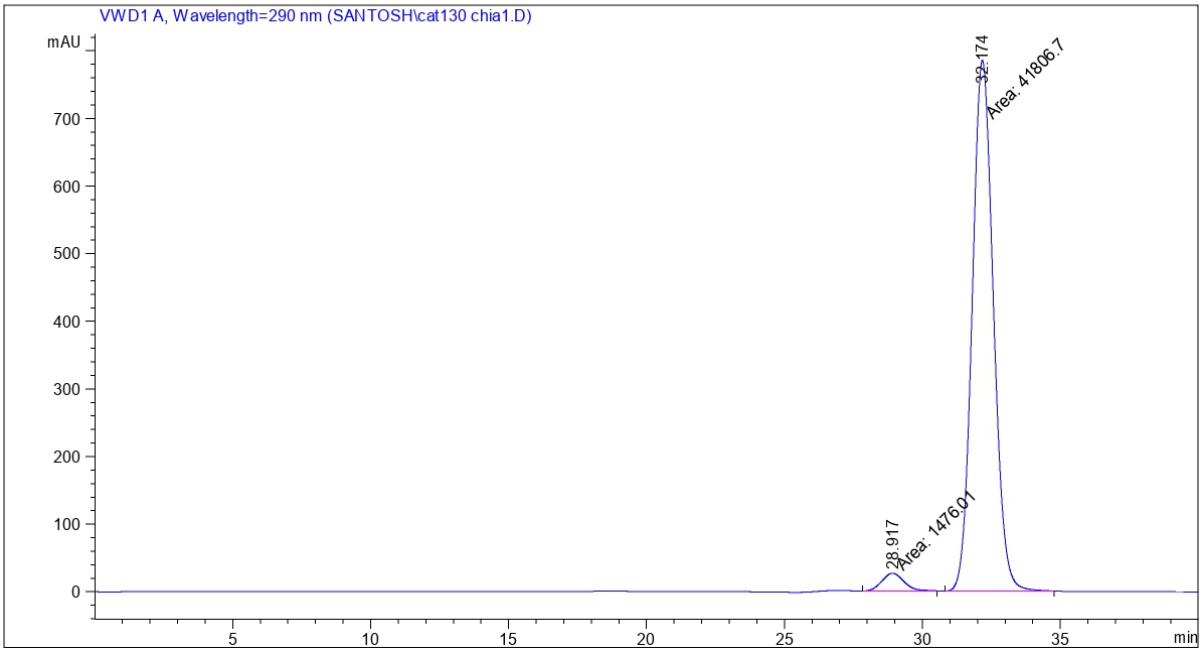

Signal 1: VWD1 A, Wavelength=290 nm

Peak #	RetTime [min]	Type	Width [min]	Area [mAU*s]	Height [mAU]	Area %
1	28.917	MM	0.9341	1476.01074	26.33522	3.4102
2	32.174	MM	0.8876	4.18067e4	785.03680	96.5898
Totals :				4.32827e4	811.37202	

Fig. A147 *HPLC of chiral* ***P16***

Appendix A

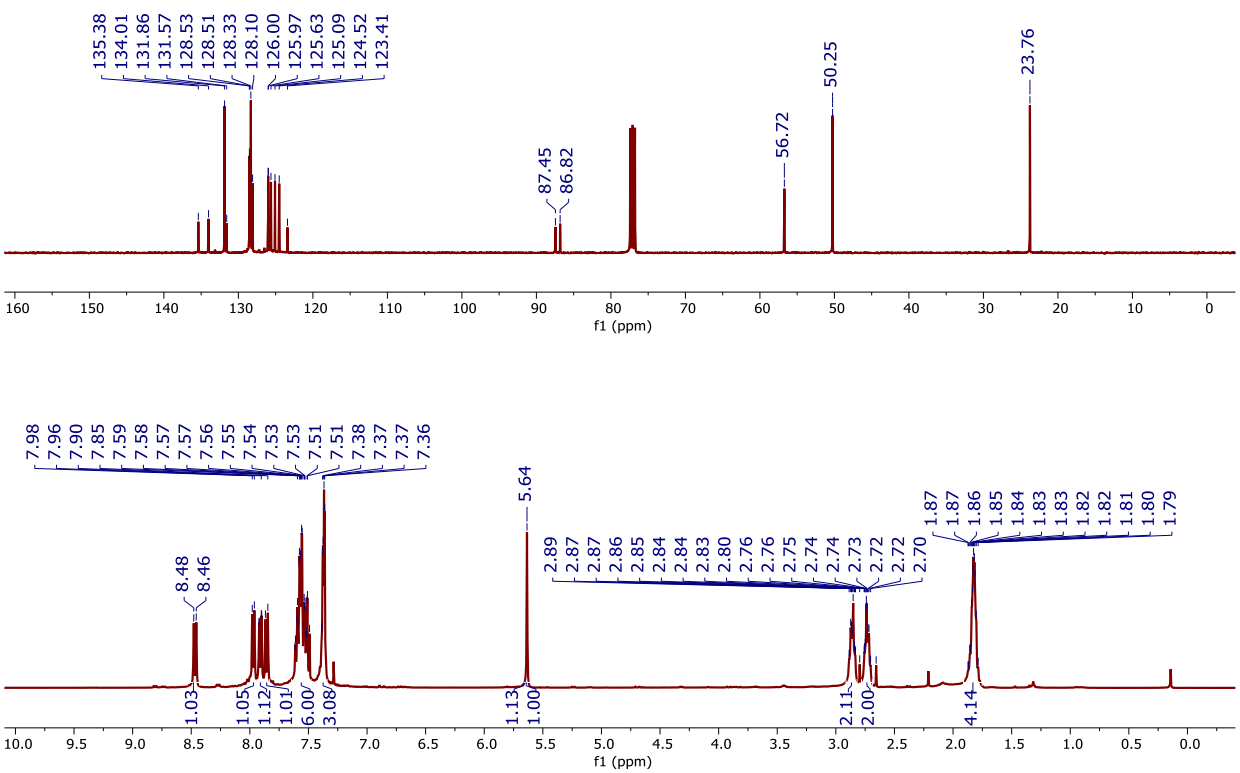

Fig. A148 *^{1}H-NMR and ^{13}C-NMR spectrum of* ***P17*** *recorded in* ***$CDCl_3$***

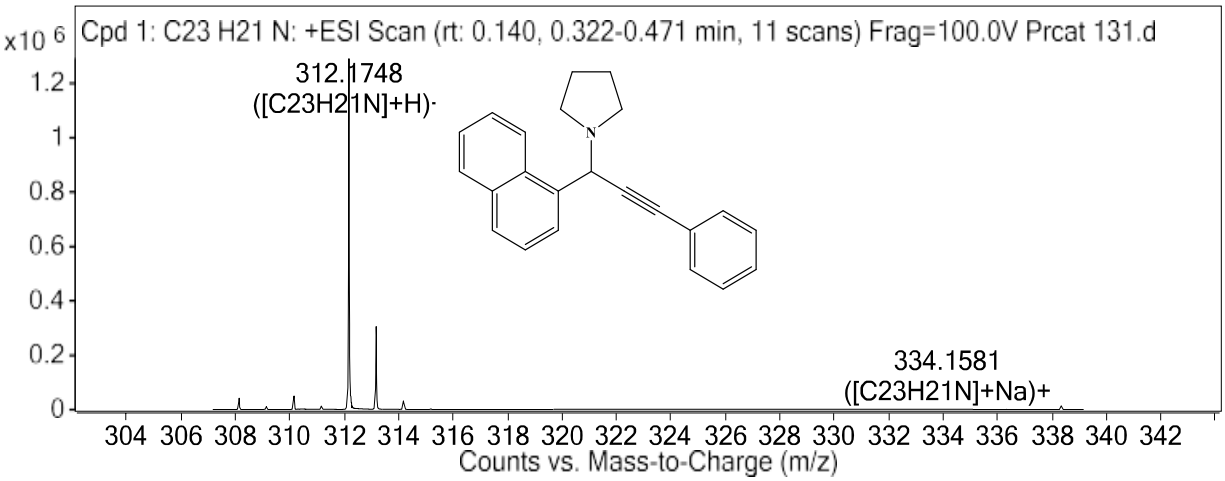

Fig. A149 *HRMS of* ***P17***

Appendix A

Additional Info : Peak(s) manually integrated

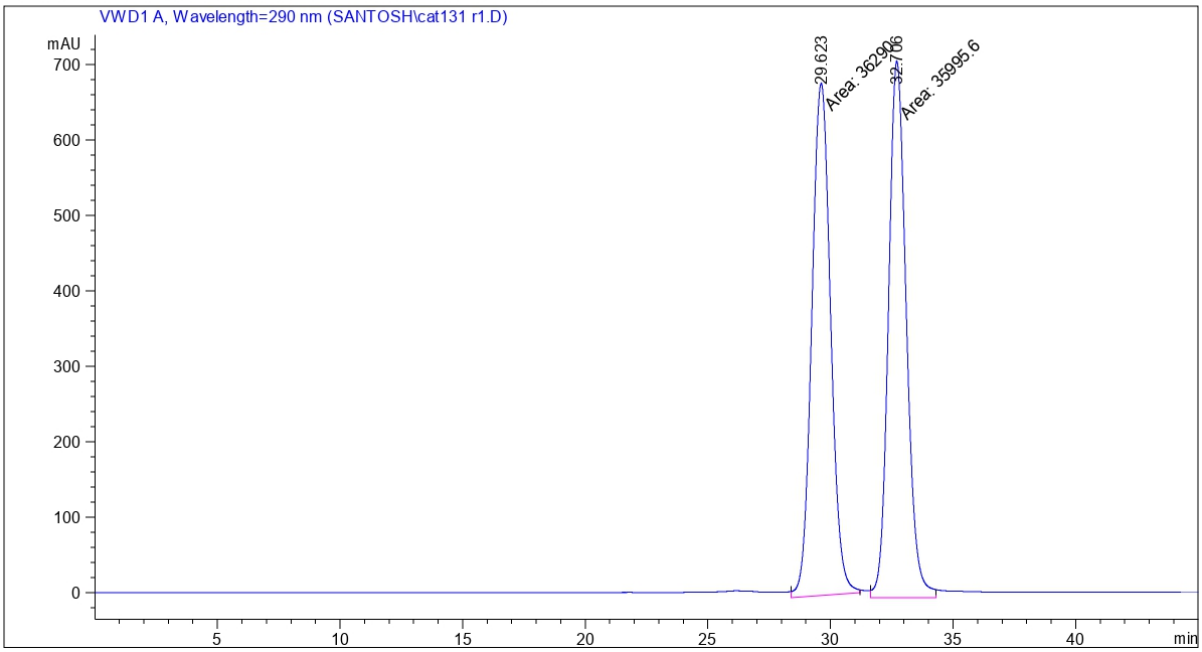

Signal 1: VWD1 A, Wavelength=290 nm

Peak #	RetTime [min]	Type	Width [min]	Area [mAU*s]	Height [mAU]	Area %
1	29.623	MM	0.8907	3.62900e4	679.02502	50.2036
2	32.706	MM	0.8432	3.59956e4	711.46283	49.7964
Totals :				7.22856e4	1390.48785	

Fig. A150 *HPLC of racemic* ***P17***

Appendix A

Additional Info : Peak(s) manually integrated

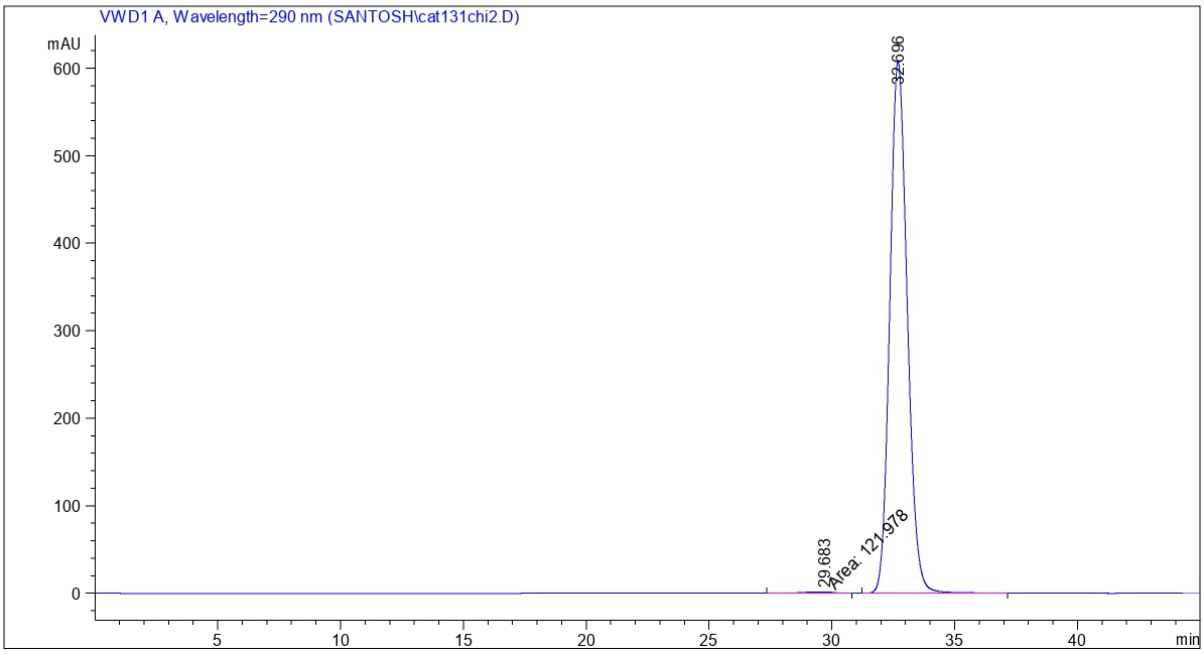

Signal 1: VWD1 A, Wavelength=290 nm

Peak #	RetTime [min]	Type	Width [min]	Area [mAU*s]	Height [mAU]	Area %
1	29.683	MM	1.3459	121.97787	1.51050	0.4053
2	32.696	BB	0.7665	2.99764e4	607.68213	99.5947
Totals :				3.00984e4	609.19263	

Fig. A151 *HPLC of chiral* ***P17***

Appendix A

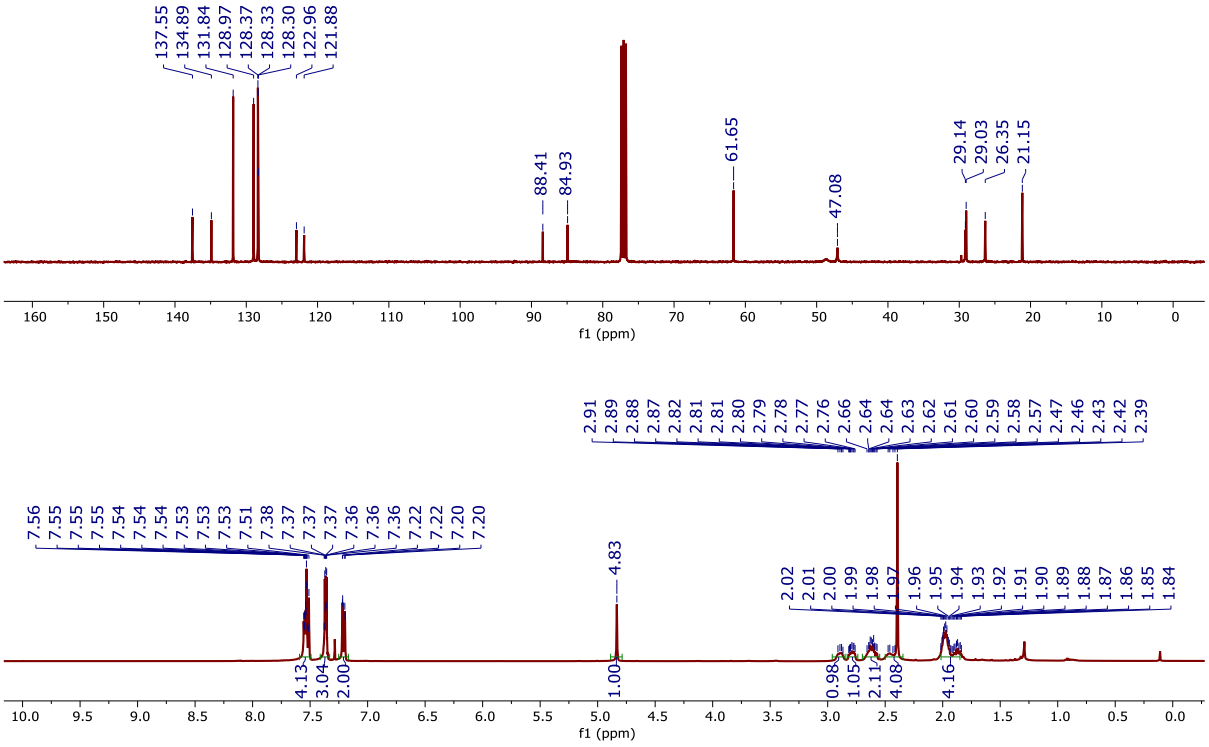

Fig. A152 *^{1}H-NMR and ^{13}C-NMR spectrum of* ***P18*** *recorded in* ***$CDCl_3$***

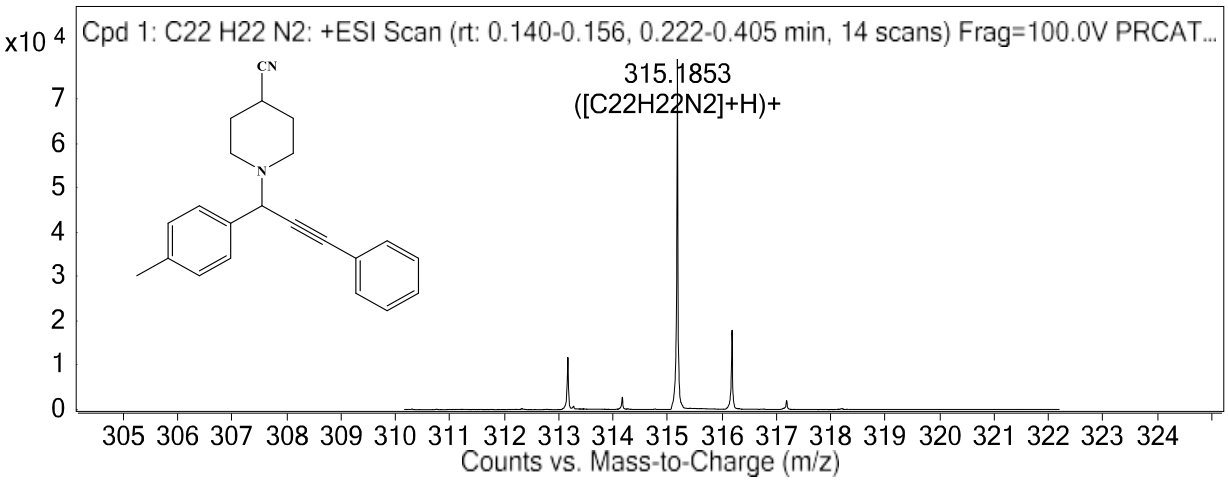

Fig. A153 *HRMS of* ***P18***

Appendix A

Additional Info : Peak(s) manually integrated

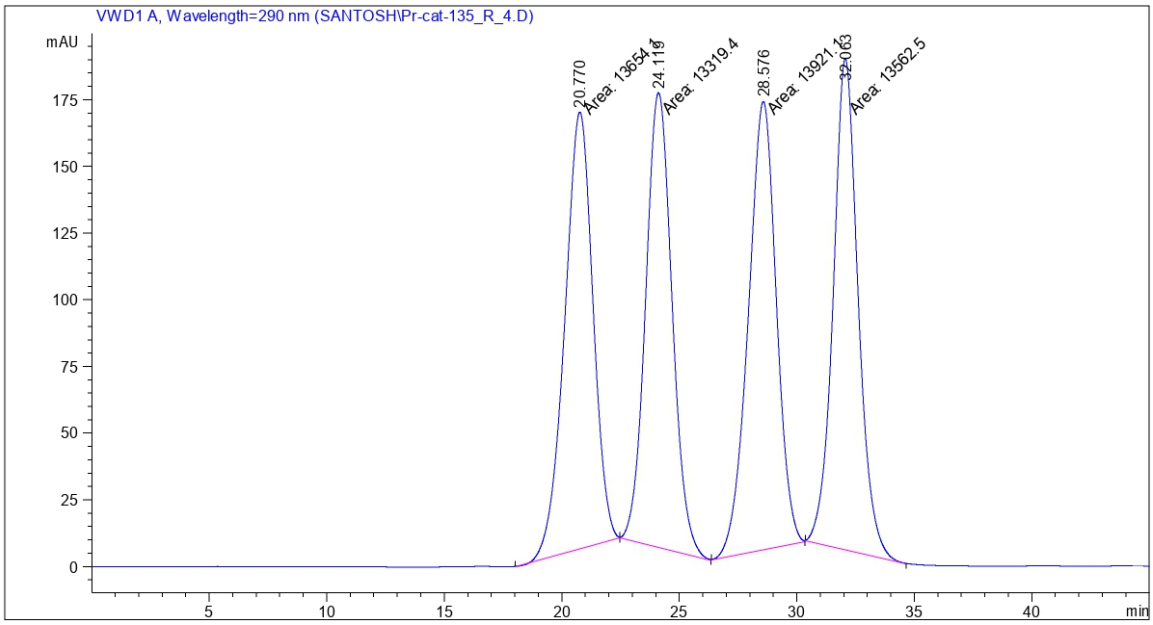

Signal 1: VWD1 A, Wavelength=290 nm

Peak #	RetTime [min]	Type	Width [min]	Area [mAU*s]	Height [mAU]	Area %
1	20.770	MM	1.3897	1.36541e4	163.75276	25.0731
2	24.119	MM	1.3026	1.33194e4	170.42360	24.4586
3	28.576	MM	1.3806	1.39211e4	168.05676	25.5634
4	32.063	MM	1.2268	1.35625e4	184.24829	24.9050
Totals :				5.44571e4	686.48141	

Fig. A154 *HPLC of r racemic* ***P18***

Appendix A

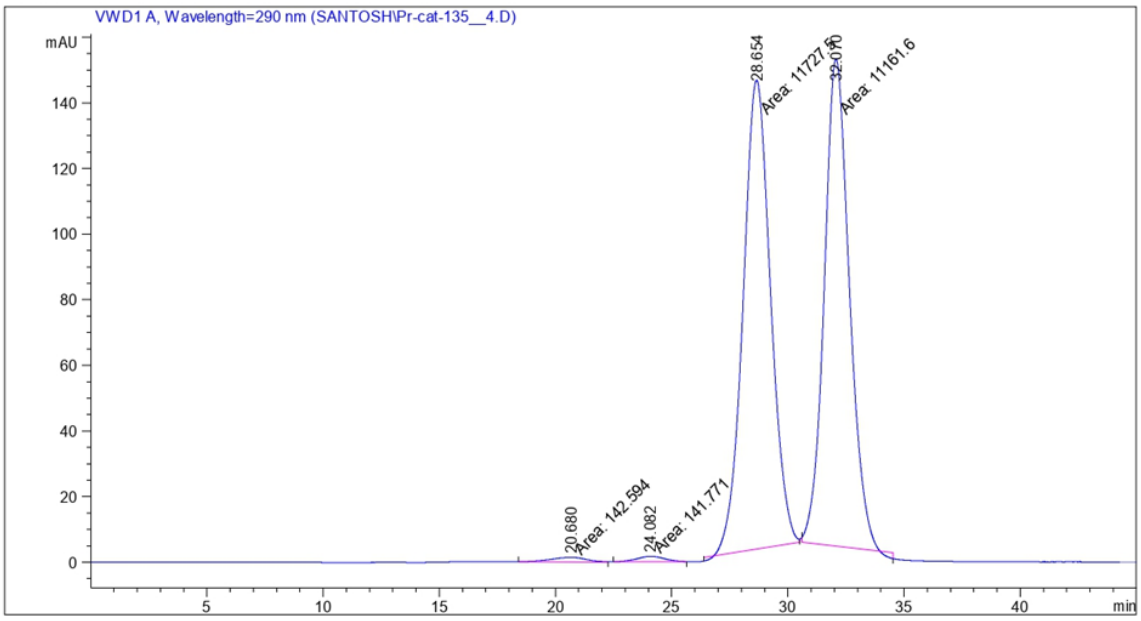

Signal 1: VWD1 A, Wavelength=290 nm

Peak #	RetTime [min]	Type	Width [min]	Area [mAU*s]	Height [mAU]	Area %
1	20.680	MM	1.7102	142.59392	1.38966	0.6153
2	24.082	MM	1.4263	141.77121	1.65665	0.6118
3	28.654	MM	1.3669	1.17275e4	142.99507	50.6073
4	32.070	MM	1.2527	1.11616e4	148.49825	48.1655
Totals :				2.31735e4	294.53962	

Fig. A155 *HPLC of chiral* ***P18***

Appendix A

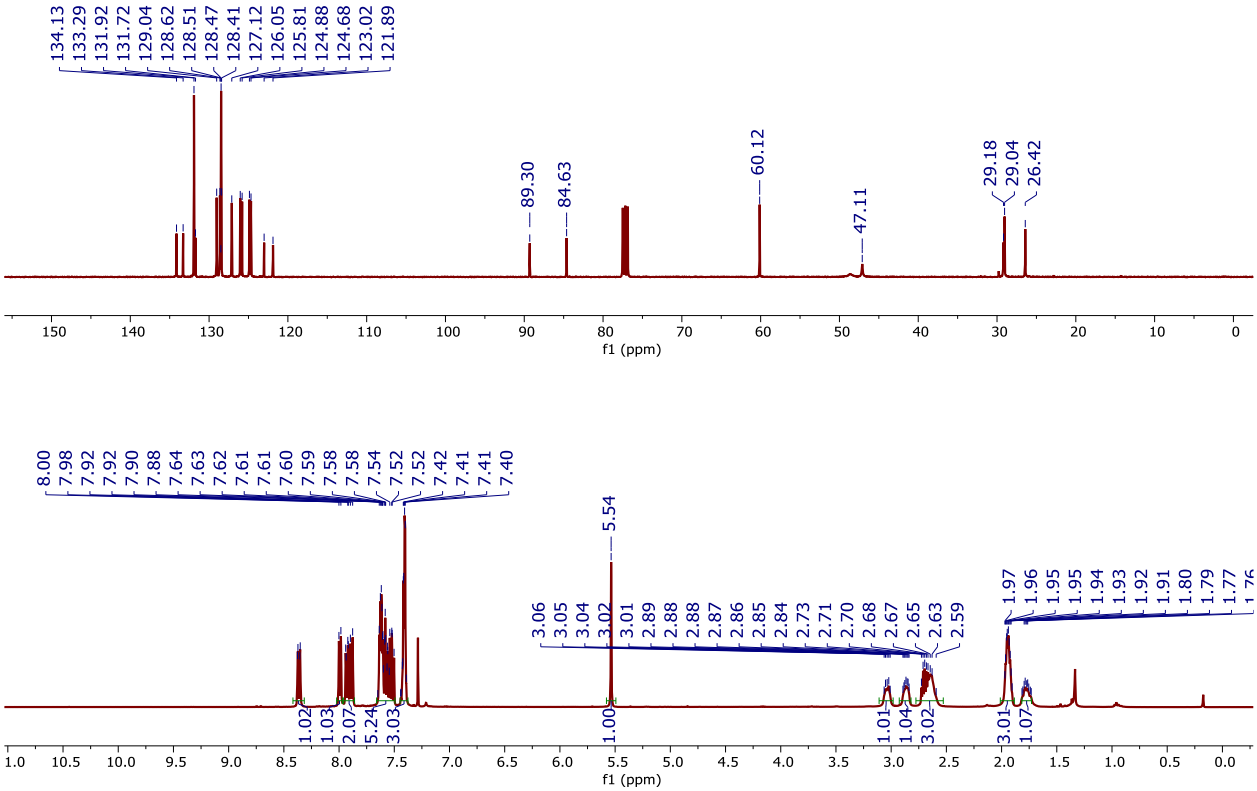

Fig. A156 *^{1}H-NMR and ^{13}C-NMR spectrum of* ***P19*** *recorded in* ***$CDCl_3$***

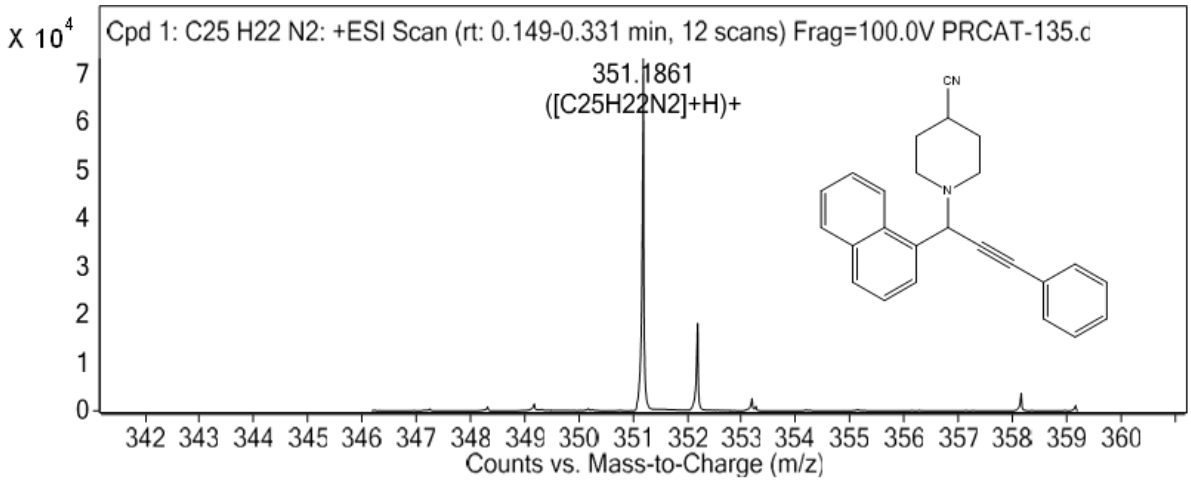

Fig. A157 *HRMS of* ***P19***

Appendix A

Additional Info : Peak(s) manually integrated

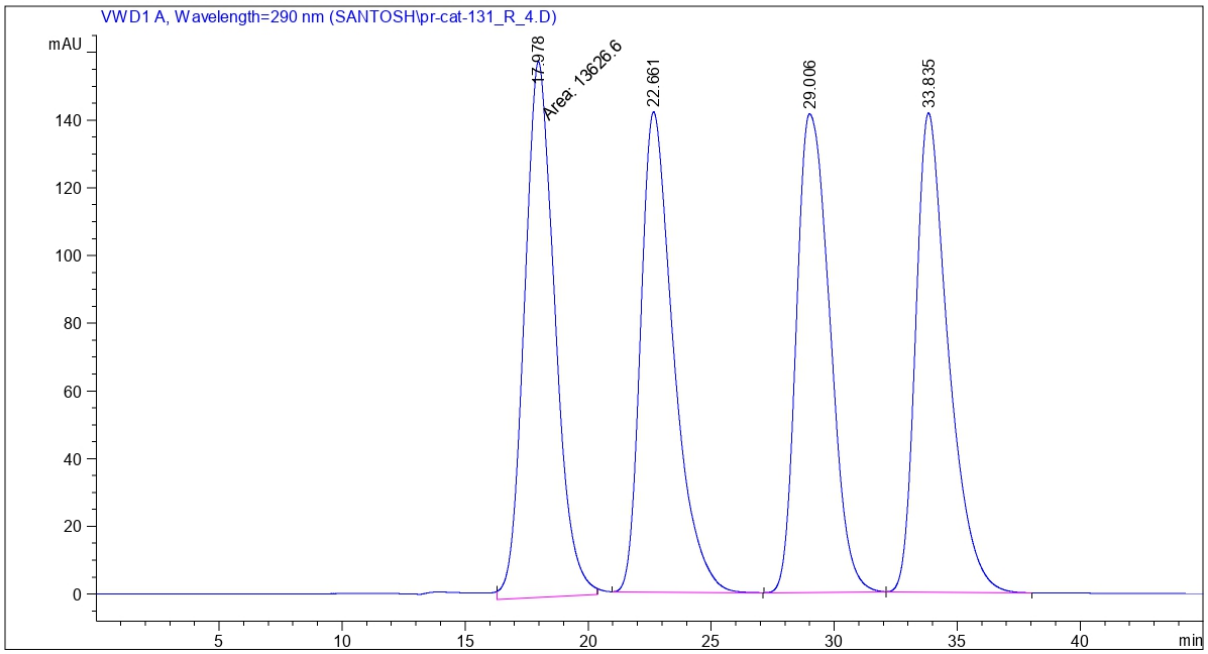

Signal 1: VWD1 A, Wavelength=290 nm

Peak #	RetTime [min]	Type	Width [min]	Area [mAU*s]	Height [mAU]	Area %
1	17.978	MM	1.4342	1.36266e4	158.35332	25.6380
2	22.661	BB	1.3858	1.31436e4	141.87172	24.7291
3	29.006	BB	1.4605	1.33112e4	141.37318	25.0445
4	33.835	BB	1.3722	1.30688e4	141.53831	24.5884
Totals :				5.31502e4	583.13654	

Fig. A158 *HPLC of racemic* ***P19***

Appendix A

Additional Info : Peak(s) manually integrated

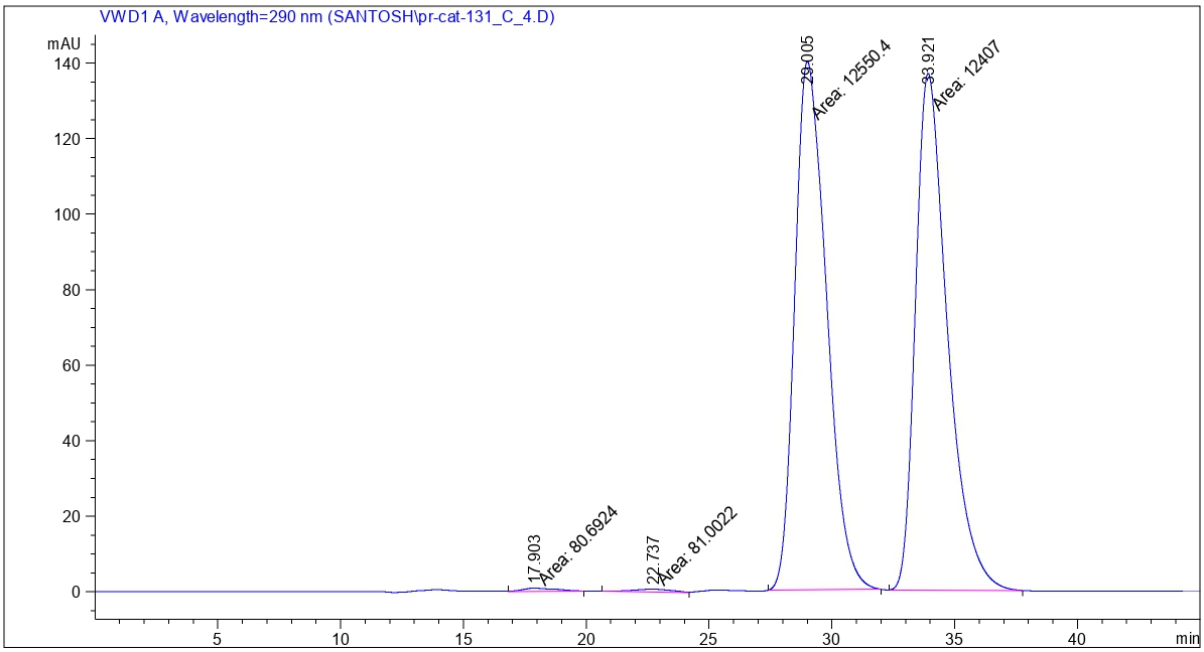

Signal 1: VWD1 A, Wavelength=290 nm

Peak #	RetTime [min]	Type	Width [min]	Area [mAU*s]	Height [mAU]	Area %
1	17.903	MM	1.5773	80.69237	8.52644e-1	0.3212
2	22.737	MM	1.7862	81.00220	7.55805e-1	0.3225
3	29.005	MM	1.4939	1.25504e4	140.02138	49.9636
4	33.921	MM	1.5110	1.24070e4	136.85434	49.3927
Totals :				2.51192e4	278.48417	

Fig. A159 *HPLC of chiral* ***P19***

Appendix A

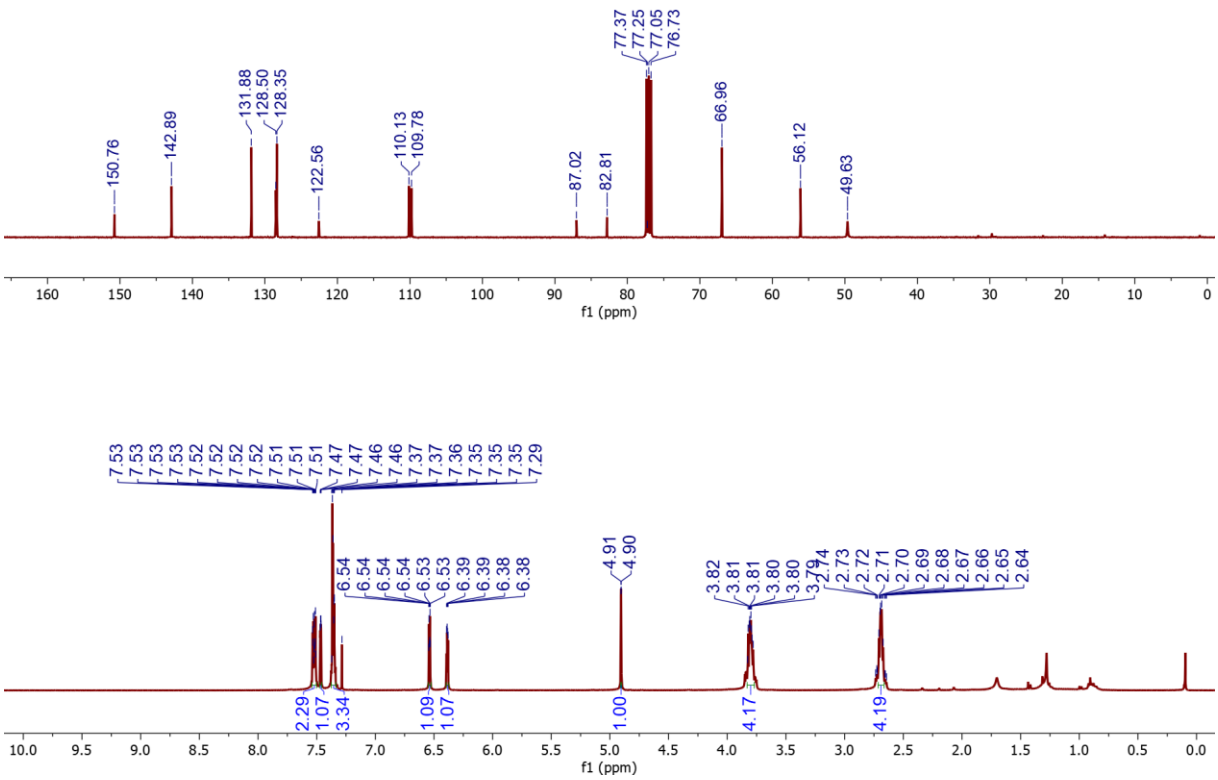

Fig. A160 *^{1}H-NMR and ^{13}C-NMR spectrum of* ***P20*** *recorded in* ***$CDCl_3$***

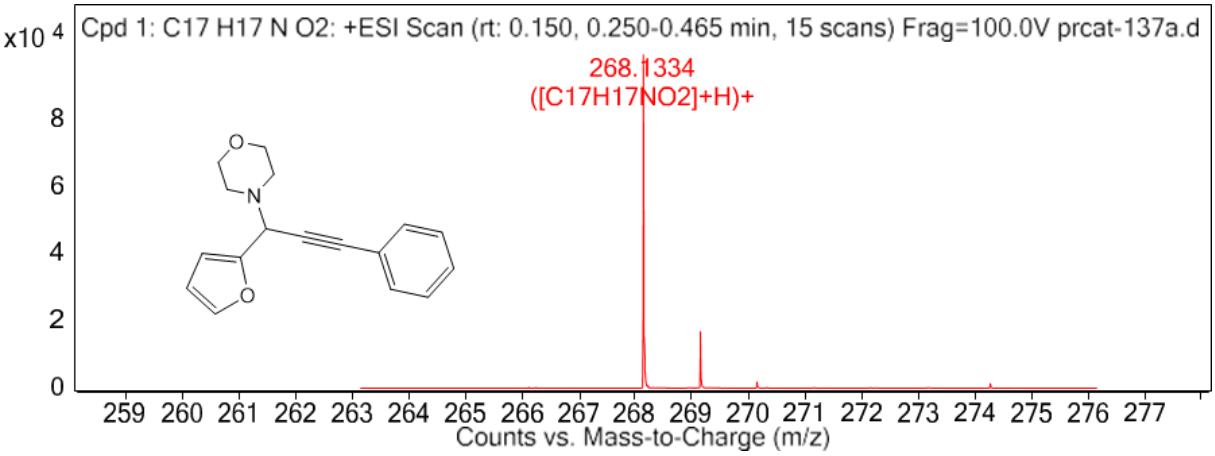

Fig. A161 *HRMS of* ***P20***

Appendix A

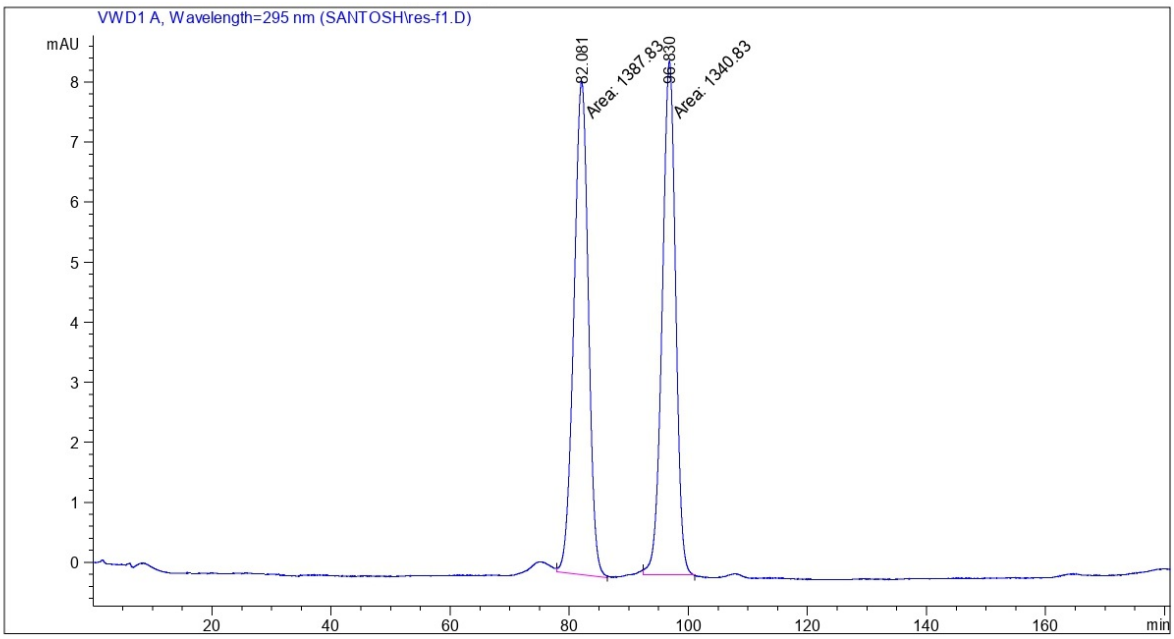

Signal 1: VWD1 A, Wavelength=295 nm

Peak #	RetTime [min]	Type	Width [min]	Area [mAU*s]	Height [mAU]	Area %
1	82.081	MM	2.8145	1387.82690	8.21842	50.8612
2	96.830	MM	2.6118	1340.82813	8.55619	49.1388
Totals :				2728.65503	16.77461	

Fig. A162 *HPLC of chiral* ***P20***

Appendix A

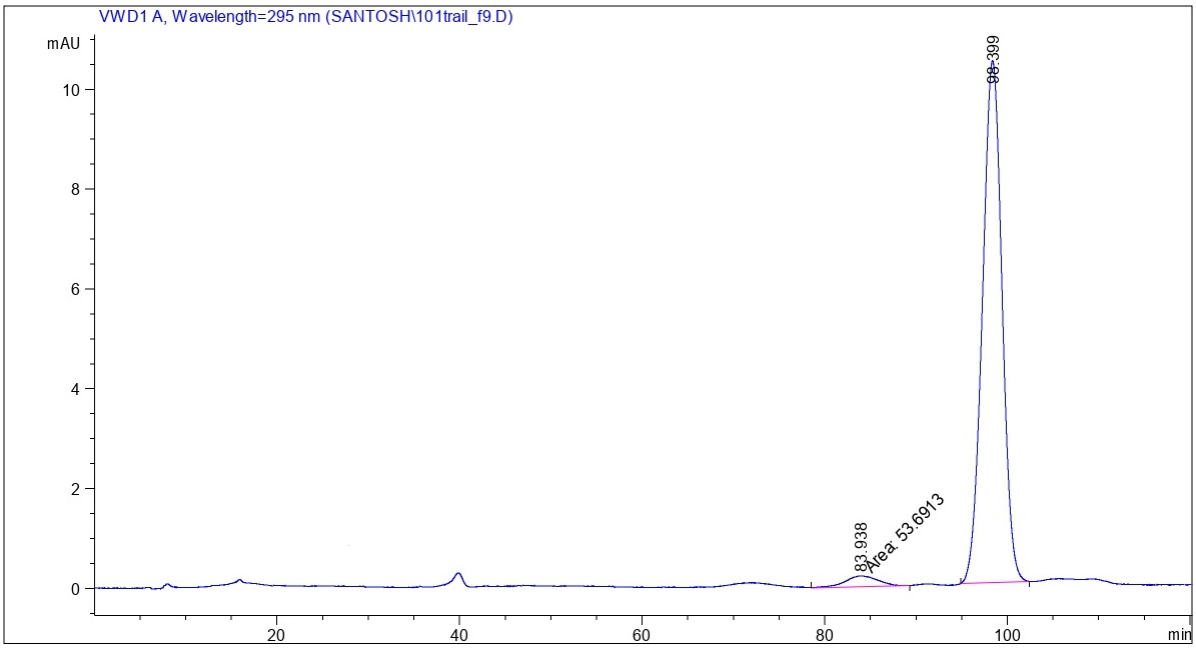

Signal 1: VWD1 A, Wavelength=295 nm

Peak #	RetTime [min]	Type	Width [min]	Area [mAU*s]	Height [mAU]	Area %
1	83.938	MM	4.1789	53.69134	2.14136e-1	3.3377
2	98.399	BB	1.7488	1554.92444	10.45685	96.6623
Totals :				1608.61578	10.67099	

Fig. A163 *HPLC of racemic* ***P20***

Product code M2: White solid; ^{1}H-NMR (400 MHz, $CDCl_3$) δ 7.37– 7.31 (m, 2H), 7.30 – 7.25 (m, 1H), 7.24 – 7.2 (m, 2H), 3.58 (s, 1H), 2.4 – 2.3 (m, 8H), 1.6 – 1.5 (m, 8H) 1.45 – 1.3 (m, 4H). ^{13}C-NMR (101 MHz, $CDCl_3$) δ 129.01, 128.66, 127.27, 126.98, 89.77, 50.19, 47.46, 27.21,26.28, 25.36.

Appendix A

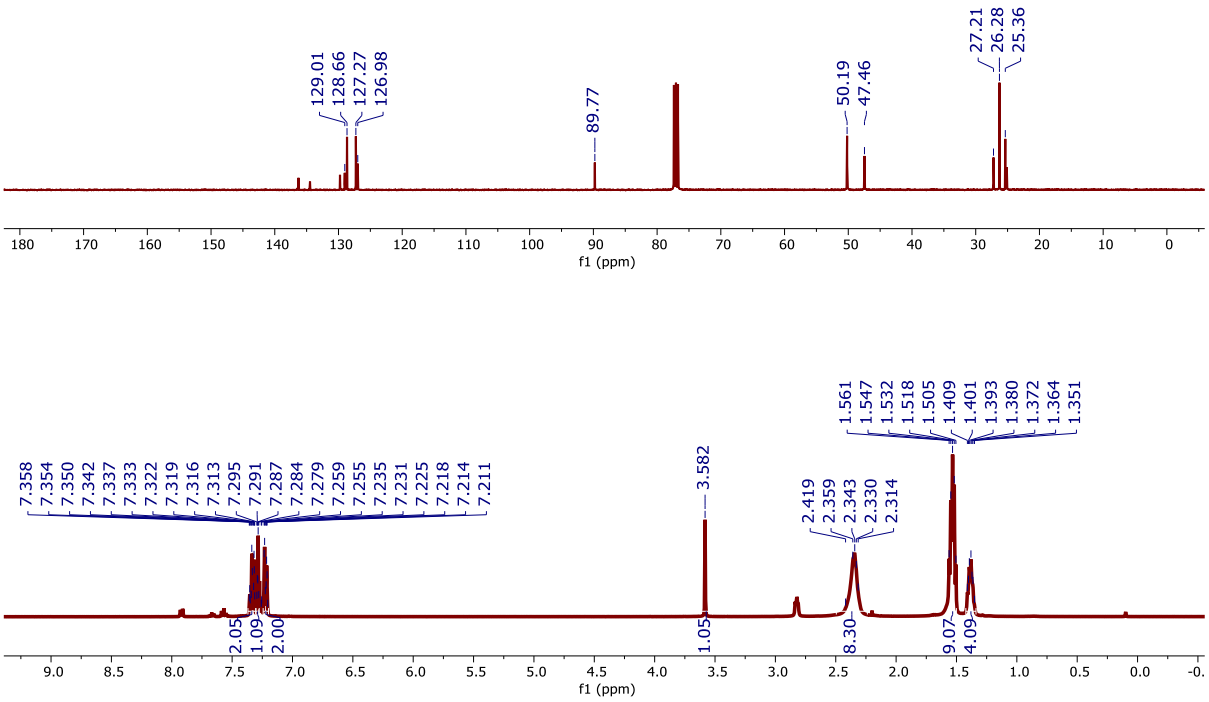

Fig. A164 *^{1}H-NMR spectrum of* ***M2*** *recorded in* ***$CDCl_3$***

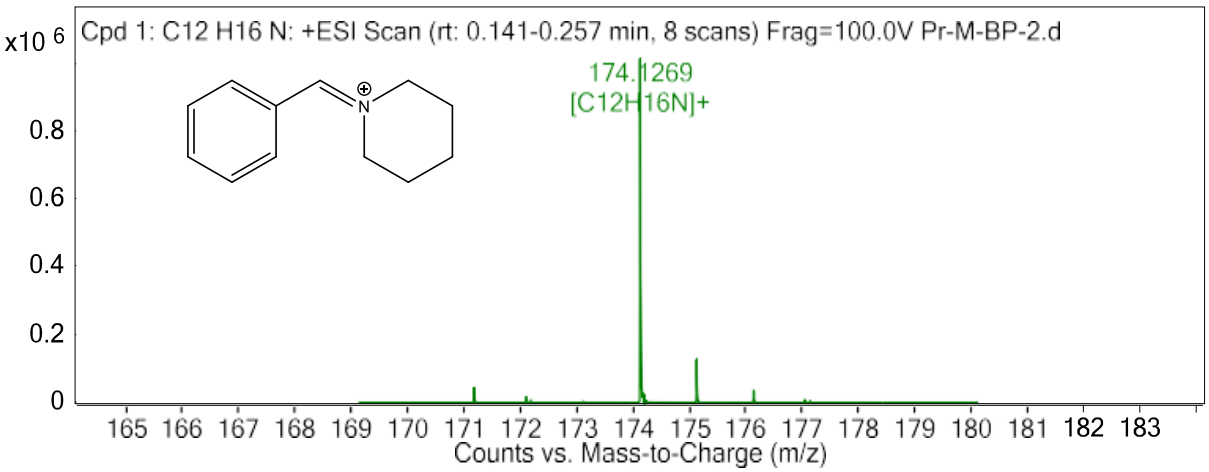

Fig. A165 *HRMS of* ***M1***

Appendix A

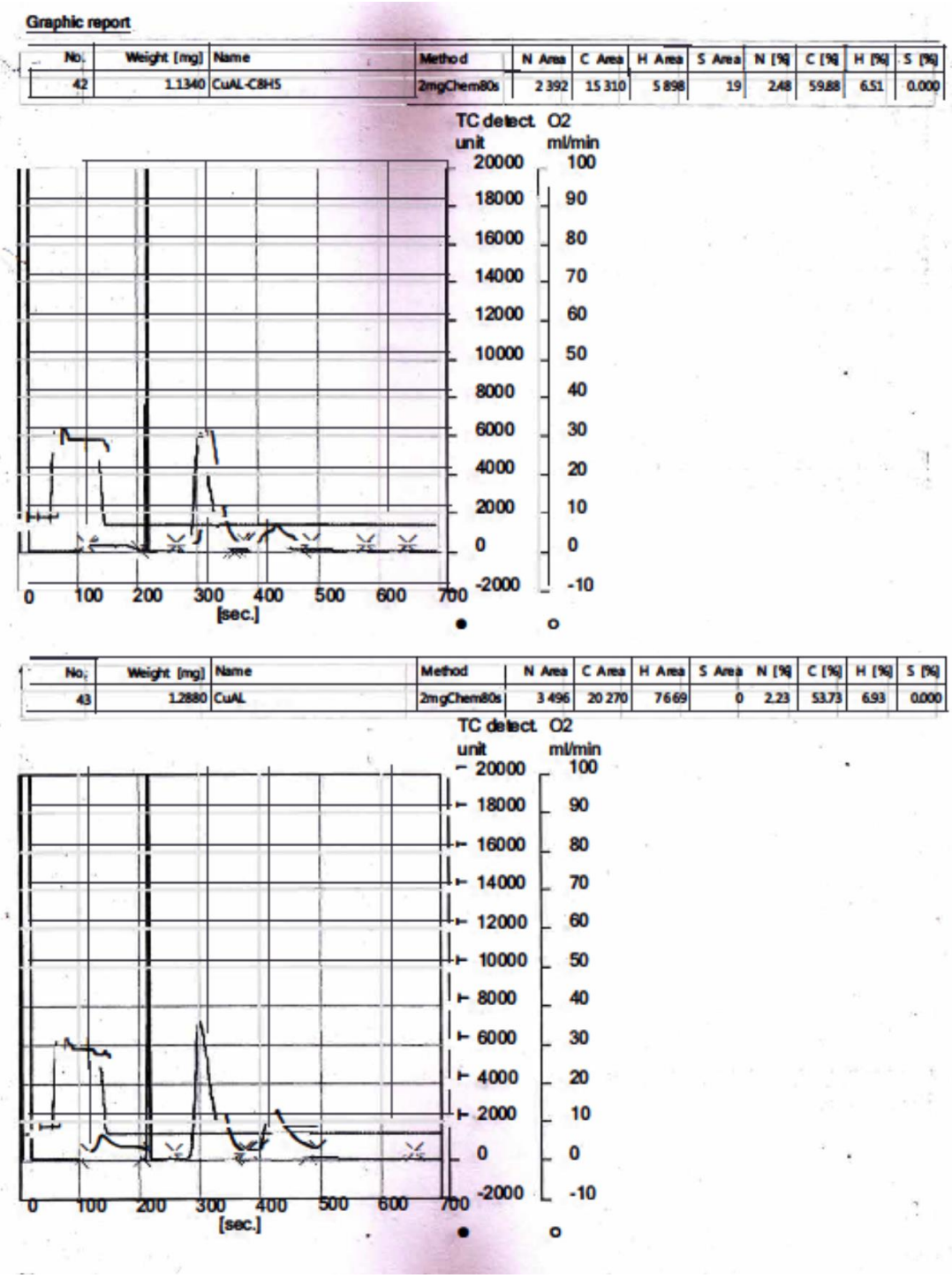

Fig. A166 *CHN analysis report of* ***CuAL*** *and* ***CuAL-C_8H_5***

Appendix B

List of Publications

1. Effect of N-alkyl substitution on Cu(II)-selective chemosensing of rhodamine B derivatives, Santosh Kumar Mishra, Suryakanta Dehuri, and Bamaprasad Bag*, J. Org. Chem. 2020, 18, 316.

2. N-Glycoconjugates: Selective colorimetric chemosensors for aspartic acid and cysteine, Santosh Kumar Mishra, Vimal Kumar Madduluri, Krishnan Rangan, Ajay K. Sah *, J. Mol. Struct. 2021, 1241, 130644.

3. Crystal Structure of N-(2-Hydroxynapthylidene)-L-isoleucinyl-4,6-O-ethylidene-***β***-D-glucopyranosylamine and an Insight from Experimental and Theoretical Calculations, Santosh K. Mishra, Anuvasita Parikh, Krishnan Rangan, and Ajay K. Sah*, Cryst. Res. Technol. 2022, 58, 2200209.

4. Synthesis of Catalyst Using Bio-benign Precursors and Its Application in One-Pot Catalytic Synthesis of Imidazo[1,2-a]pyridines, Santosh Kumar Mishra, Anuvasita Parikh, Krishnan Rangan, and Ajay K. Sah*, ChemistrySelect. 2023, 8, e202300129.

5. Chain length effect of spiro-ring N-alkylation onphotophysical signalling parameters in Fe(III) selective rhodamine probes, Suryakanta Dehuri, Santosh Kumar Mishra and Bamaprasad Bag *, J. Org. Chem. 2022, 20, 3967.

6. Synthesis and catalytic application of D-glucose derived ytterbium(III) complex in Biginelli reaction, Vimal Kumar Madduluri, Santosh Kumar Mishra, Ajay K. Sah*, Inorg. Chem. Commun. 2020, 120, 108165.

Appendix B

List of attended workshops and conferences

- Sweet'18: Glycochemistry, Biology and Technology (SGBT-2018), December 19-21, 2018, Indian Institute of Science Education and Research Kolkata, Kolkata, India (poster presented).

- New Frontiers in Chemistry - From Fundamentals to Applications-III (NFCFA-2019), December 20-22, 2019, Birla Institute of Technology and Science-Pilani K K Birla Goa Campus, Goa, India (poster presented).

- Software and Applications of Single Crystal X-Ray Diffraction 2019 (National Workshop), Smt. S. S. Patel Nootan Science & Commerce College Visnagar, Gujarat, India (participated)

- International Conference on Advances in Chemistry and Biology of Carbohydrates (ICACBC-2021), December 04-05, 2021, Forest Research Institute Dehradun, Uttarakhand, India (poster presented).

Appendix B

BRIEF BIOGRAPHY OF THE CANDIDATE

Santosh Kumar Mishra completed his M.Phil. in chemistry from Utkal University, Bhubaneswar, Odisha, in 2015. In 2017, he joined in BITS-Pilani, Pilani Campus, for his doctoral studies under the supervision of Dr. Ajay Kumar Sah. During his doctorial tenure, he worked as a Project Fellow in DST sponsored project on 'Synthesis of D-glucose derived glycoconjugates and their application in molecular recognition and catalysis' (December 2017 – November 2020). He has published research articles in well renowned international journals and presented papers in conferences/symposium.

Appendix B

BRIEF BIOGRAPHY OF THE SUPERVISOR

Dr. Ajay Kumar Sah is an Professor at Department of Chemistry, Birla Institute of Technology and Science, Pilani, Pilani campus. He received his Ph.D. degree from IIT, Mumbai, Maharashtra in 2002. For his doctoral degree, he worked with Prof. C. P. Rao in the research area of Bioinorganic chemistry. After his doctorate, he worked as a post-doctoral fellow (March 2002-December 2002) with Prof. M. Ravikanth of Department of Chemistry, IIT Bombay, India. In second post doctorate, he worked with Prof. Michael J. Scott of Department of Chemistry, University of Florida (USA), under the project entitled "Synthesis of Ligands for the Selective Binding of Actinides" (January 2003-October 2003). After these two he got selected as a JSPS postdoctoral fellow and worked with Prof. Tomoaki Tanase of Department of Chemistry, Nara Women's University, Japan, under the project entitled "Catalytic Functions of Transition Metal-Sugar Complex". Fourth Postdoctoral Work (Nov 2005 – Oct 2006) was carried out with Prof. Yoichi Habata of Department of Chemistry, Toho University, Japan, under the project entitled "The Silver Vorous Molecules: Design, Synthesis and Kinetic Studies of the Supramolecular Systems". He worked at Syngene International Pvt. Ltd. (BIOCON Group) for six months (Nov 2006 – May 2007) as Associate Scientific Manager. It is a Contract Research Organization (CRO) in Bangalore. He is the Life Member for Association of Carbohydrate Chemists and Technologist (India). From May 2007 – till date, he is working at Department of Chemistry, BITS Pilani, Pilani campus. His area of research is 'synthesis of metal complexes of ligands derived from carbohydrates and to study their structure biological as well as catalytic activity'. He has guided two PhD students and presently three students are working under his supervision. He has successfully completed four research projects as PI, (sponsored by DST, SERB, CSIR and UGC) .